A story about difluoromethyl-1,3,4-oxadiazoles: Synthesis and biochemical evaluation of an enigmatic novel zinc binding group for the highly selective inhibition and degradation of histone deacetylase 6

Dissertation

zur

Erlangung des Doktorgrades (Dr. rer. nat.)

der

Mathematisch-Naturwissenschaftlichen Fakultät

der

Rheinischen Friedrich-Wilhelms-Universität Bonn

vorgelegt von

Beate König

aus

Erlangen

Bonn 2024

Angefertigt mit Genehmigung der Mathematisch-Naturwissenschaftlichen Fakultät

der Rheinischen Friedrich-Wilhelms-Universität Bonn

Gutachter und Betreuer: Prof. Dr. Finn K. Hansen

Gutachter: Prof. Dr. Gerd Bendas

Tag der Promotion: 10.07.2024

Erscheinungsjahr: 2024

Table of Contents

Eidesstattliche Erklärung

Die vorliegende Arbeit wurde in der Zeit von September 2020 bis April 2024 unter der Leitung von Herrn Prof. Dr. Finn K. Hansen am Pharmazeutischen Institut der Rheinischen Friedrich-Wilhelms-Universität Bonn angefertigt.

Ich versichere an Eides statt, dass ich die vorliegende Dissertation „A story about difluoromethyl-1,3,4-oxadiazoles: Synthesis and biochemical evaluation of an enigmatic novel zinc binding group for the highly selective inhibition and degradation of histone deacetylase 6" selbstständig, ohne unzulässige Hilfe Dritter und ohne Benutzung anderer als der von mir angegebenen Hilfsmittel angefertigt habe. Alle aus fremden Quellen direkt oder indirekt übernommenen Gedanken wurden in der vorliegenden Arbeit als solche kenntlich gemacht. Weiterhin versichere ich, dass ich nicht die Hilfe eines Promotionsberaters in Anspruch genommen habe und, dass Dritte von mir weder unmittelbar noch mittelbar geldwerte Leistungen für Arbeiten erhalten haben, die im Zusammenhang mit dem Inhalt der vorgelegten Dissertation stehen. Ich versichere, dass die vorliegende Dissertation in gleicher oder in ähnlicher Form an keiner anderen wissenschaftlichen Einrichtung im In- oder Ausland zum Zwecke einer Promotion oder eines anderen Prüfungsverfahrens vorgelegt und veröffentlicht wurde. Ich habe bisher keine Promotionsversuche unternommen.

Ich bestätige die Richtigkeit der vorstehenden Erklärung und versichere, dass ich nach bestem Wissen die Wahrheit erklärt und nichts verschwiegen habe.

_____   _____

(Ort, Datum)   (Unterschrift)

Beate König

List of Abbreviations

A

Å   Ångström

Acetyl-CoA   acetyl coenzyme A

B

BAX   BCL2-associated X protein

C

CD   catalytic domain

CRBN   cereblon

CTCL   cutaneous T-cell
                     lymphoma

D

DC_{50} half maximal degradation
                     concentration

DFMO   difluoromethyl-1,3,4-
                     oxadiazole

DMB   dynein motor binding

DNA   deoxyribonucleic acid

DNMT   DNA methyl transferase

E

elogD   experimental partition
                     coefficient

F

FDA   U.S. Food and Drug
                     Administration

G

GI_{50} half maximal inhibitory
                     concentrations of cell
                     proliferation

H

HAT   histone acetyl transferase

*h*CD2   catalytic domain 2 from
                     homo sapiens HDAC6

HDAC   histone deacetylase

HFpEF   heart failure with
                     preserved ejection fraction

*h*HDAC6   *homo sapiens* HDAC6

HK   histone kinase

HMT   histone methyltransferase

HPLC   high performance liquid
                     chromatography

HPOB   *N*-Hydroxy-4-(2-[(2-
                     hydroxyethyl)(phenyl)amin
                     o]-2-oxoethyl)benzamide

HPT   hydroxypyridine-2-thione

HSF1   heat shock factor 1

HSP   heat shock protein

I

IAP   inhibitor of apoptosis
                     protein

IC_{50} half maximal inhibitory
                     concentration

K

KDM — lysine demethylases

L

LSD — lysine-specific demethylase

M

MBD — methyl-CpG binding domain

MCF7 — human breast cancer cell line

MM.1S — human multiple myeloma cell line

MT — microtubule

MTOC — microtubule organization center

N

NAD$^+$ — nicotinamide adenine dinucleotide

NES — nuclear export signal

NLS — nuclear localization signal

P

PEG — polyethylene glycol

PHD — plant homeodomain

POI — protein of interest

PP — histone phosphatase

PPB — plasma protein binding

PRMT — arginine methyltransferase

PROTAC — proteolysis targeting chimera

PTCL — peripheral T-cell lymphoma

PTM — post translational modification

S

SE14 — Ser-Glu tetradecapeptide repeat

SI — selectivity index

Sirt — sirtuine

SUMO — small ubiquitin-like modifiers

T

TFMO — trifluoromethyl-1,3,4-oxadiazole

TPD — targeted protein degradation

U

Ub — ubiquitin

Ubp — ubiquitin-specific protease

UPS — ubiquitin proteasome system

V

VHL — von Hippel-Lindau

Z

ZBG — zinc binding group

zCD2 — catalytic domain 2 of *Danio rerio* HDAC6

zHDAC6 — *Danio rerio* HDAC6

ZnF — zinc finger

ZnF-UBD zinc finger ubiquitin-

     binding domain

Amino

acids

A   alanine

D   apartic acid

F   phenylalanine

G   glycine

H   histidine

K   lysine

L   leucine

M   methionine

N   asparagine

P   proline

Q   glutamine

S   serine

W   tryptophan

Y   tyrosine

List of Appendices

1 Introduction

1.1 Epigenetics – an introduction

In the early 1940s, Conrad Waddington introduced *epigenetics*, the branch of biology that studies the causal interactions between genes and their products that lead to the phenotype.[1,2] Today, the term is narrowed down to changes in gene expression that do not affect the deoxyribonucleic acid (DNA) sequence.[3]

The human genome encodes all the relevant information for a living system to grow, develop, function, and reproduce. This knowledge is stored in the double helices of the DNA strands. The genetic information is organized in different layers of packaging. First, the double helix is wrapped around histones to form the nucleosome.[4] This involves the wrapping of 146 base pairs around an octamer of the four histone proteins H2A, H2B, H3, and H4.[5] Second, the nucleosomes are organized into a more compact and dense structure called chromatin.[6] In the highly condensed structure of the chromosome, the third layer of organization, the chromatin is coiled and even more tightly packed. To be accessible for transcription, followed by translation for protein biosynthesis, the chromatin must be less compact. Relaxed euchromatin has acetylated histone
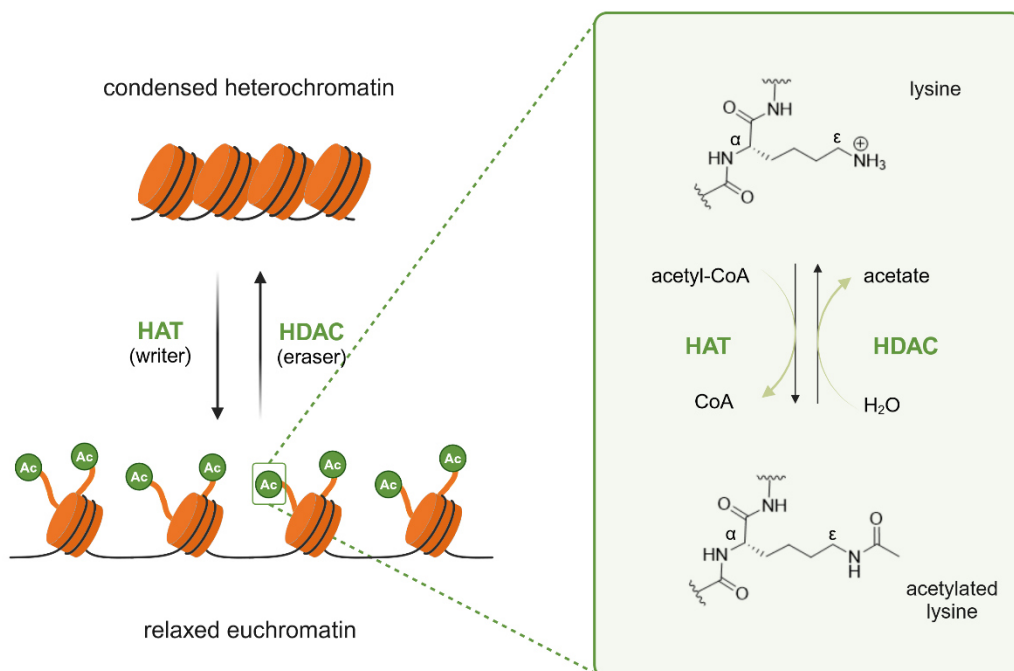
Figure 1. Regulation of the chromatin structure by HATs and HDACs. Figure was created with Biorender.com.

tails, whereas the condensed heterochromatin lacks them, resulting in positively charged lysine residues that interact with the negatively charged DNA backbone.[7] These reactions are catalyzed by histone acetyltransferases (HATs), which add the acetyl group to the lysine residues of the histone tail and histone deacetylases (HDACs), which reverse histone acetylation.[8] In addition to acetylation and deacetylation certain side chains can undergo other post translational modifications (PTMs).[9] Other PTMs include the addition and removal of phosphate groups by histone kinases (HKs) and histone phosphatases (PPs) or the introduction of methyl groups mediated by histone methyltransferases (HMTs), DNA methyltransferases (DNMTs), and arginine methyltransferases (PRMTs).[10] Demethylation, on the other hand, is catalyzed by lysine demethylases (KDMs). In addition to the transfer of chemical moieties, small proteins such as ubiquitin can be shifted by small ubiquitin-like modifiers (SUMOs) and removed by ubiquitin-specific proteases (Ubps).[11] The enzymes responsible for introducing a functional group are called "writers", while the "erasers" control their removal. "Readers" are enzymes that recognize these modification patterns to initiate cellular responses such as the activation of transcription factors.[12]
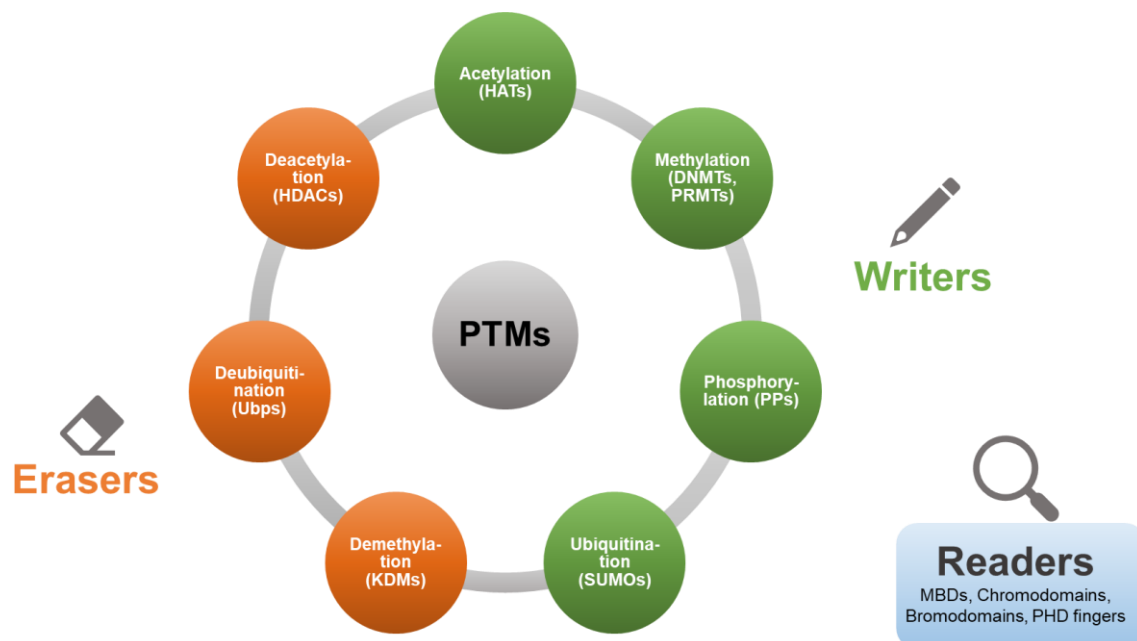
Figure 2. Overview of selected post translational modifications (PTMs) and classification. Histone acetyltransferases (HATs); DNA methyltransferases (DNMTs); arginine methyltransferases (PRMTs); histone phosphatases (PPs); small ubiquitin-like modifiers (SUMOs); lysine demethylases (KDMs); ubiquitin-specific proteases (Ubps); histone deacetylases (HDACs); methyl-CpG binding domains (MBDs); plant homeodomain (PHD) fingers.

1.2 Classification of Histone Deacetylases

Among others, HDACs are known to remove acetyl groups from ε-*N*-lysine residues of histone and non-histone proteins.[13] In 1996, Taunton et *al.* discovered the first human HDAC isoform.[14] To date, 18 mammalian HDAC isoforms have been identified and grouped according to their sequence homology to yeast proteins from *Saccharomyces cerevisiae*.[15] Further, they are classified by their cellular localization and dependency on certain cofactors. In total, there are four classes. Class I, II, and IV depend on a Zn^{2+} ion in their catalytic center, whereas class III, the so-called sirtuins, depend on NAD^+. An overview of the zinc dependent HDAC isoforms is shown in Table 1.

Table 1. Summary of the eleven human Zn^{2+}-dependent HDAC isoforms, according to their classes, main localization, number of amino acids and substrates. Adapted in a modified version from Ho et *al.* 2020.[16]

Class	Isoform	Localisation	Amino acids	Substrates
I	HDAC1	nucleus	481	histones, transcriptional regulators
	HDAC2	nucleus	488	
	HDAC3	nucleus	428	
	HDAC8	nucleus, cytoplasm	377	longer chain acyllysine residues
IIa	HDAC4	nucleus, cytoplasm	1084	none; recruit substrates for HDAC3
	HDAC5	nucleus, cytoplasm	1121	
	HDAC7	nucleus, cytoplasm	952	
	HDAC9	nucleus, cytoplasm	1011	
IIb	HDAC6	cytoplasm	1215	α-tubulin, cortactin, tau, HSP90
	HDAC10	cytoplasm	669	acetylpolyamines
IV	HDAC11	nucleus, cytoplasm	347	longer chain acyllysine residues

Class I includes the isoforms HDAC1, 2, 3, and 8. All isoforms of this class consist of less than 500 amino acids and are mainly located in the cell nucleus, with the exception of HDAC8 which is predominantly located in the cytoplasm.[17] The main function of HDAC1, 2 and 3, according to the family name, is the post-translational modification of histone lysine deacetylation. Class II is further subdivided into class IIa, consisting of HDAC4, 5, 7, and 9, and class IIb, containing HDAC6 and 10.[18] Due to an exchange of a tyrosine with a histidine residue, near the catalytic active site, class IIa enzymes exhibit an approximately 1000-fold weaker catalytic activity than other isoforms and are often considered as pseudo enzymes.[19,20] HDAC10 is highly distinguished to other isoforms, through a glutamate gatekeeper at the entrance to its catalytic center. The substitution allows HDAC10 to act as a polyamine deacetylase and selectively hydrolyze polyamines such as N^8-acetylspermidine.[21] In 1999, HDAC6 was first described in mouse models.[22] Despite its potential

to act on important nuclear proteins like the DNA repair factor Ku70, the main localization of HDAC6 is in the cytoplasm.[23,24] There it exhibits its influence on non-histone targets like α-tubulin,[25] heat shock protein 90 (HSP90),[26] and tau protein.[27] The class III includes the sirtuins Sirt1-7. By a NAD$^+$ dependent mechanism, they catalyze the deacetylation reaction by transferring the acetyl group to the C2 position of the ribose sugar.[28] Class IV contains only one isoform, HDAC11. It is the smallest isoform, located primarily in the nucleus, and has weak catalytic activity towards acetyllysine substrates. Interestingly, it acts as a fatty acid deacylase and prefers longer chain substrates such as dodecanoyllysine (C$_{12}$) and myristoyllysine (C$_{14}$).[29,30]

1.3 HDAC6 relevance in pathological and non-pathological conditions

HDAC6 is involved in several cell signaling pathways and is playing a crucial role in cellular processes, such as cell proliferation, cell motility, apoptosis, aggresome degradation, and the heat shock response.[31]

The key regulators of cellular motility are microtubules (MTs), which are composed of α- and β-tubulin. α-Tubulin was identified as the first physiological substrate of HDAC6.[32–34] Deacetylation of α-tubulin leads to the destabilization of the MTs, resulting in an increase in cellular movement.[33] Similarly, the deacetylation of cortactin by HDAC6 leads to its association with F-actin, enhancing cell motility and division.[35] Conversely, hyperacetylation of cortactin via inhibition of HDAC6 leads to impaired cell motility, which is implicated in several diseases, including chronic inflammation, tumor metastasis, and vascular disease.[35–38]

Due to the deacetylation of the DNA repair factor Ku70, HDAC6 is directly influencing cell apoptosis and has since been described as an anti-apoptotic protein.[24,39] Acetylated Ku70 is unable to bind the pro-apoptotic BCL2-associated X protein (BAX), which induces apoptosis in its free form. On the other hand, deacetylated Ku70 binds BAX and inhibits apoptosis.[40] The oncogenic protein survivin is another HDAC6 substrate involved in the prevention of apoptosis.[41,42] Deacetylation of survivin by HDAC6 leads to a translocation of survivin from the nucleus to the cytoplasm where it inhibits the activity of different caspases, thereby inhibiting apoptosis and activating carcinogenesis.[41,43] The wide spreading influence of HDAC6 in multiple cellular pathways makes it a valuable drug target in cancer treatment. Malfunction of HDAC6 has been associated with altered motility and invasive properties in e.g. neuroblastoma[44] and breast cancer.[45]
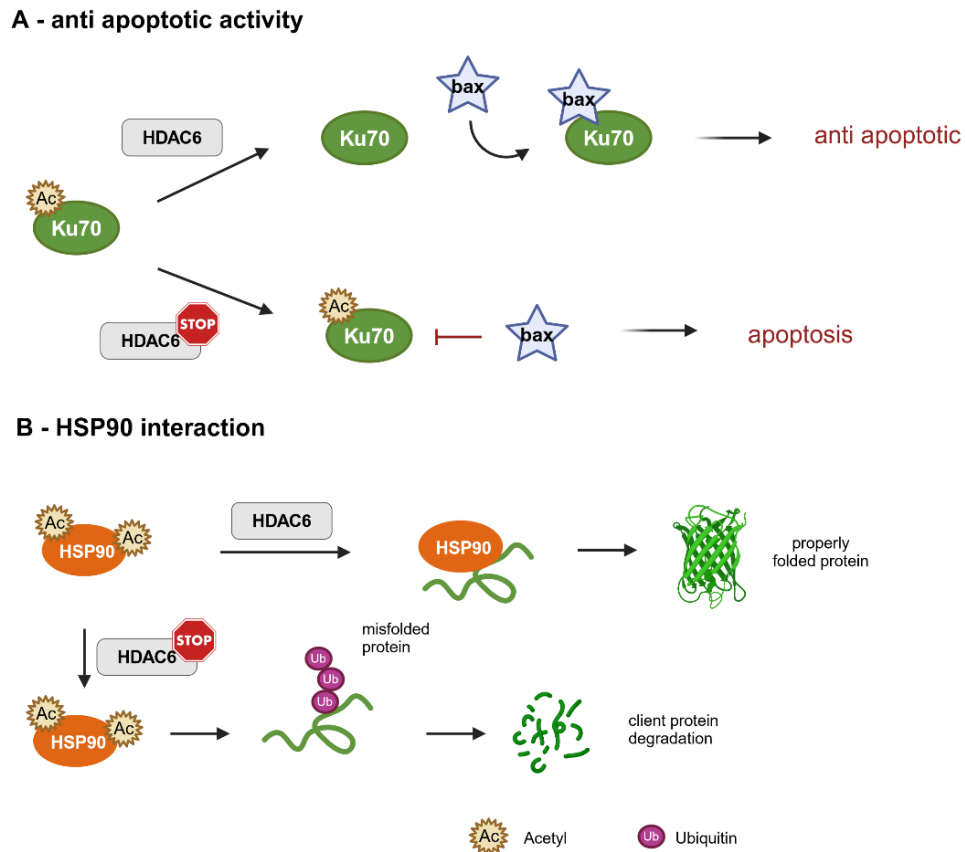
Figure 3. Selected HDAC6 interactions in specific cellular pathways. **A)** Influence of HDAC6 on the pro-apoptotic protein Ku70. **B)** HDAC6 inhibition results in hyperacetylated HSP90 followed by the accumulation and subsequent degradation of polyubiquitinated misfolded proteins. Figure was created with BioRender.com.

Additionally, HDAC6 is involved in the aggresomal degradation of misfolded proteins through the ubiquitin proteasome system (UPS).[46] Under normal conditions, misfolded proteins are getting ubiquitinated by an E3 ligase and further degraded by the proteasome. When this pathway fails, ubiquitinated proteins accumulate in the cell. HDAC6 can bind these proteins via its ZnF ubiquitin-binding domain (ZnF-UBD) and transfers them to the motor binding protein dynein.[47] The cargo is subsequently shuttled along MTs to the microtubule organizing center (MTOC), where HDAC6 deacetylates cortactin. This leads to the formation of aggresomes around the misfolded proteins, which are then cleared by autophagy.[48,49] Furthermore, the dual inhibition of the proteasome and aggresome pathways results in synergistic effects. By inhibiting of the proteasome, the misfolded ubiquitinated proteins are redirected to the aggresome pathway by HDAC6 for degradation. The additional inhibition of HDAC6 leads to the failure of the aggresome pathway, leading to the accumulation of misfolded proteins, thereby demonstrating the synergistic effect of blocking both the proteasome and HDAC6.[50] Moreover, HDAC6 has been implicated in the autophagic clearance

of proteins associated with neurodegenerative diseases like Huntington's and Parkinson's disease.[51,52]

Furthermore, upon the failure of the UPS, HDAC6 is activating the heat shock response.[53] This occurs in two different cascades. On one side, the binding of HDAC6 to the ubiquitinated proteins via the ZnF-UBD leads to the dissociation of the basal complex, which includes among others HDAC6, heat shock factor 1 (HSF1) and HSP90. The release of HSF1, after the translocation from the cytoplasm to the nucleus, enables the transcription of several heat shock proteins such as HSP27, HSP70 and HSP90. The overexpression of these chaperones helps the cell to reduce the toxicity of protein aggregates by reassembling misfolded proteins. Inhibition of HDAC6 prevents this cascade and leads to cell death.[47] On another side, HDAC6 is directly involved in the chaperone activity of HSP90 via its deacetylation.[54] While acetylated HSP90 is unable to recruit misfolded client proteins for reassembly, leading to proteasomal degradation of these proteins, deacetylated HSP90 can reassemble the misfolded clients, resulting in the active proteins.[26]

HDAC6 and its inhibition have been linked to several rare disorders such as Rett syndrome, Charcot-Marie-Tooth disease, inherited retinal diseases, and idiopathic pulmonary fibrosis.[55–57] It has also been implicated in viral infections, inflammatory diseases, and neurodegenerative diseases such as Alzheimer's.[27,57,58] Taken together, the broad range of substrates that HDAC6 is involved in pathological and non-pathological conditions makes it a valuable pharmaceutical target.

1.4 HDAC6 structure and catalytic mode of action

HDAC6 is the largest Zn^{2+}-dependent isoform containing 1215 amino acids. It is unique in the class of HDACs because of its two functional catalytic domains (CD1 & CD2). In 2016 Christianson and co-workers[59] solved the first crystal structure of CD2 from human (*Homo sapiens*) HDAC6 (*h*HDAC6). By comparing the crystal structures of CD2 from zebrafish (*Danio rerio*) HDAC6 (*z*HDAC6) with the human ortholog, it was shown that the zebrafish enzyme is a valid and robust model of human HDAC6.[59,60] The sequence of *h*HDAC6 is depicted in Figure 4 and shows high similarity in the catalytic regions compared to *z*HDAC6. Only two amino acids at the outer rim of the active site in CD2, distant from the catalytic Zn^{2+} ion, are not conserved, so N530 and N645 in *z*CD2 appear as D567 and M682 in *h*CD2.[59]

Both domains are capable of catalyzing the hydrolysis reaction of acetyllysine side chains of non-histone proteins to generate deacetylated lysines.[59] While the endogenous substrates of CD2 are cytosolic protein substrates, such as α-tubulin[32] and tau,[61] the full biological function of CD1 is still

unclear.[62] CD1 shows a narrow substrate range with a preference for peptide substrates bearing a C-terminal acetyllysine residue.[62] Both domains are composed of 356 amino acids, with one of the major differences being the gatekeeper amino acid at the entrance to the catalytic tunnel in CD1, lysine K330, whereas in CD2, leucine L712 is located at the same position.[59,62] This lysine is crucial for the preference of CD1 for substrates bearing a free α-carboxylate group, resulting in maximal catalytic activity compared to other substrates.[59,62] The surface of the entrance to the active site of CD2 is defined by the loops L1 (H463, P464, F583, and L712) and L2 (most important for H-bond interactions with S531), capable of interacting with bulky or bifurcated capping groups of selective HDAC6 inhibitors.[63,64] In general, the active site cleft of CD1 is wider than that of CD2, which is due to slight differences in the aromatic cleft.[62] In detail, the amino acid residues K330, W261, and Q235 in CD1 are changed to L712, F643, and N617 in CD2, respectively.[65] Aromatic linkers of inhibitors can bind in this crevice and form π-π interactions (F583 and F643 in CD2).[62] The co-crystal structures of the pan inhibitor trichostatin A in complex with CD1 and CD2 revealed the same binding mode in both domains.[60] The Zn^{2+} binding site as well as the catalytic residues are identical in both, suggesting that the molecular mechanism of the deacetylation must be the same.[62,66]
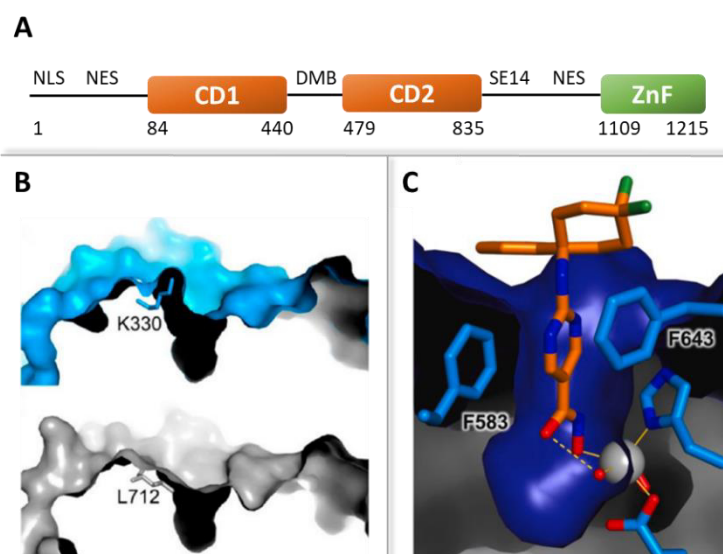
Figure 4. A) Schematic structure of human HDAC6 with the following domain organization: nuclear localization signal (NLS); nuclear export signal (NES); catalytic domain 1 (CD1); dynein motor binding (DMB) domain; catalytic domain 2 (CD2); Ser-Glu tetradecapeptide repeat (SE14); zinc-finger domain (ZnF). Adapted in a modified version from Osko & Christianson 2019.[67]

B) Top: molecular surface of HDAC6 CD1 (blue), bottom: molecular surface of HDAC6 CD2 (gray). Reprinted with permission from Osko, J. D.; and Christianson, D. W. Structural Basis of Catalysis and Inhibition of HDAC6 CD1, the Enigmatic Catalytic Domain of Histone Deacetylase 6. *Biochemistry* **2019**, *58* (49), 4912-4924. Copyright 2019 American Chemical Society.

C) Molecular surface of CD2 HDAC6 with the linker region of the inhibitor ACY1083 stacked between F583 and F643. Reprinted with permission from Porter, N. J.; Mahendran, A.; Breslow, R. and Christianson, D. W. Unusual zinc-binding mode of HDAC6-seelctive hydroxamate inhibitors. Proc. Natl. Acad. Sci. **2017**, *114* (51), 13459-13464. Copyright 2017 National Academy of Sciences.

The Christianson's group was able to reconstruct the mode of action of the deacetylation of lysine residues along snapshots provided by crystal structures of zHDAC6 CD2 (see Figure 5).[59] The Zn^{2+} ion is located in a 10 Å deep tunnel, liganded by D612, H614, D705, and a water molecule, thereby resulting in a distorted tetrahedral coordination geometry. The water molecule forms H-bonds with H573 and H574 (see Figure 5A). The vacant Zn^{2+} coordination site can be occupied by the acetyllysine residue, where the carbonyl is coordinated between Zn^{2+} and Y745, resulting in a pentacoordinated metal ion (see Figure 5B). The scissile carbonyl undergoes a nucleophilic attack by the zinc bound water molecule, which is activated by H573, leading to a tetrahedral intermediate (see Figure 5C). Via the regeneration of the carbonyl function, the nitrogen is protonated by H574, resulting in the cleavage of the amide bond. The formed acetate anion exhibits symmetric coordination to the Zn^{2+} (see Figure 5D). After dissociation of the lysine from
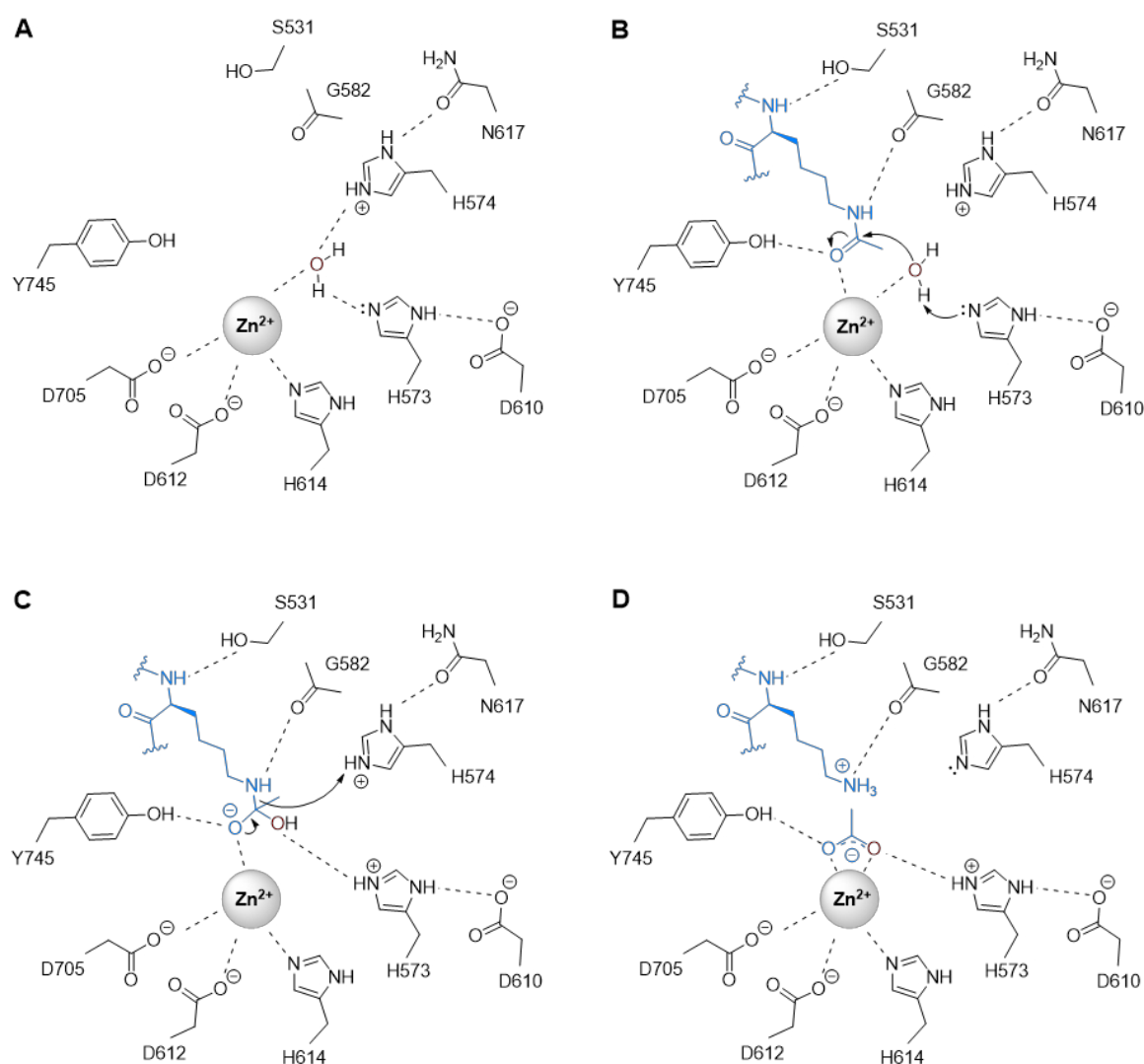
Figure 5. Catalytical mechanism of the deacetylation of acetyllysine residues in the catalytic domain 2 of HDAC6. The acetyllysine substrate is displayed in blue. Adapted in a modified version from Hai & Christianson 2016.[59]

the active site, the acetate can exit the catalytic tunnel to restore the enzyme. In addition, the group of Christianson performed experiments with mutants zHDAC6 CD2 (Y745F and H574A) and revealed that Y745 is necessary for the substrate activation, while H574 is crucial for the protonation of the ε-amino group of the lysine side chain.[59]

In addition to the catalytic domains, HDAC6 possesses a ZnF-UBD. This active site contains three zinc ions that can recruit polyubiquitinated protein aggregates and shuttle misfolded proteins along the MTs to the lysosome for degradation, providing an alternative to the proteasomal degradation of misfolded proteins.[68–70]

1.5 HDAC inhibitors

Trichostatin A was described in 1990 as the first potent HDAC inhibitor (structure is shown in Figure 6A).[71] It was isolated from *Streptomyces platensis* and caused the accumulation of acetylated histones both *in vitro* and *in vivo.* Furthermore, this efficient inhibition of HDAC activity was linked to effects on cell differentiation and proliferation.[71] In 2006, the first HDAC inhibitor, vorinostat, was approved by the U.S. Food and Drug Administration (FDA) for the treatment of cutaneous T-cell lymphoma (CTCL).[72] To date, only four other HDAC inhibitors have been approved by the FDA: belinostat, panobinostat, romidepsin, and givinostat (see Figure 6B).[72,a] While belinostat is used in the therapy of peripheral T-cell lymphoma (PTCL), panobinostat is approved for the treatment of multiple myeloma in combination with the proteasome inhibitor bortezomib and the corticosteroid dexamethasone.[73–75] Vorinostat, belinostat and panobinostat function as non-selective, so called pan inhibitors.[72] In contrast, romidepsin is a natural product HDAC inhibitor, a cyclic depsipeptide acting as a prodrug. It releases the zinc binding thiol by cleavage of the disulfide bridge inside the cell.[66,76] Unlike pan inhibitors, romidepsin is a class I selective HDAC inhibitor and approved for the treatment of CTCL.[77] In March 2024, the latest inhibitor, givinostat, was approved for the treatment of Duchenne muscular dystrophy.[a]

In general, most HDAC inhibitors follow the same pharmacophore model. Inspired by the natural substrate of most HDACs, ε-*N*-acetyl-*L*-lysine, the structure is divided into three distinct motifs (see Figure 6A).[78] First, the cap group can interact and recognize the surface of the different enzyme isoforms. Second, the linker dives deep into the catalytic tunnel connecting the cap to the zinc binding group (ZBG). Third, the ZBG coordinates the Zn^{2+}, mimicking the tetrahedral oxyanion

---

[a] FDA News Release: „FDA Approves Nonsteroidal Treatment for Duchenne Muscular Dystrophy" https://www.fda.gov/news-events/press-announcements/fda-approves-nonsteroidal-treatment-duchenne-muscular-dystrophy. Accessed April 04, 2024.

transition state.[16,78] Panobinostat, givinostat, and belinostat have a phenyl-based linker compared to vorinostat, while all four bear a hydroxamic acid as ZBG.[72,79]
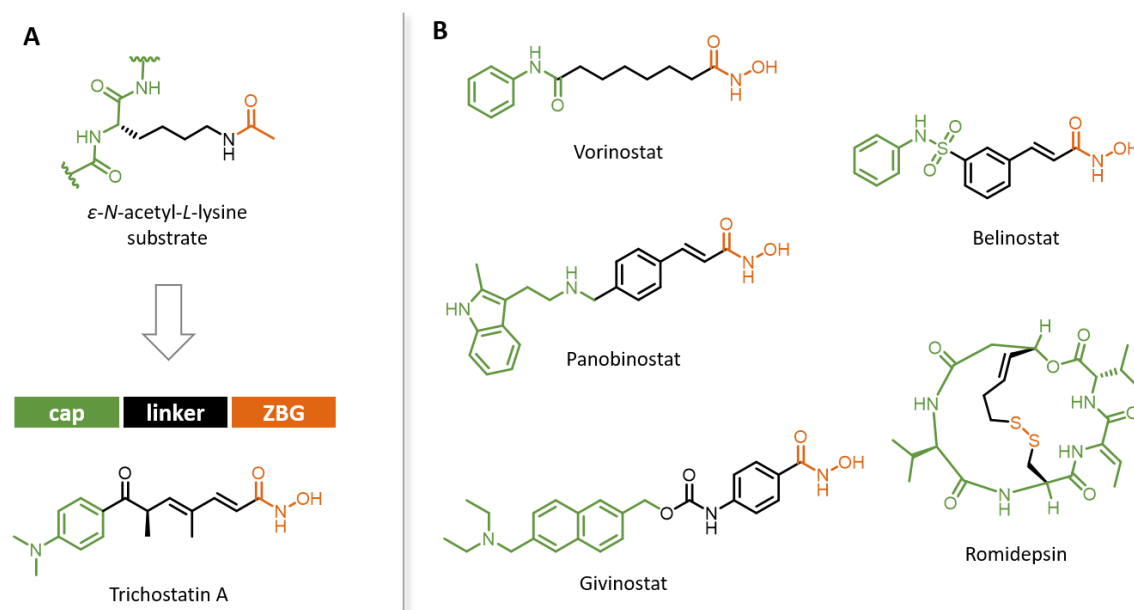
Figure 6. A) Pharmacophore model of typical HDAC inhibitors in relation to the natural peptidyl ε-*N*-acetyl-*L*-lysine substrate of HDACs using trichostatin A as example. **B**) Structures of the FDA approved HDAC inhibitors vorinostat, panobinostat, givinostat, belinostat, and romidepsin.

All five FDA-approved HDAC inhibitors are associated with severe side effects such as nausea, fatigue, diarrhea, and low blood counts.[80–82] This may be related to the poor selectivity profile of the inhibitors among the different HDAC isoforms, facilitating off-target interactions.[82,83] In addition, hydroxamic acids, which are frequently used as ZBG, are linked to mutagenic and genotoxic potential.[84] Hydroxamic acids can undergo the so called Lossen rearrangement, leading to toxic metabolites such as isocyanates.[66,84] It is therefore important to develop isoform selective HDAC inhibitors as well as to identify alternative ZBGs.

Meanwhile, only a few preferential or selective HDAC6 inhibitors are or have been studied in clinical trials.[b] For example, the hydroxamic acid HDAC inhibitor ricolinostat was investigated in a phase 2 clinical trial for painful diabetic peripheral neuropathy, multiple myeloma (NCT01323751), and in a phase 1 study for metastatic breast cancer (NCT02632071).[85,86] Citarinostat, also a hydroxamic acid-based HDAC inhibitor, was examined in a phase 1 clinical trial in combination with nivolumab for non-small cell lung cancer (NCT02635061), malignant myeloma (NCT02935790), and advanced solid tumors (NCT02551185).[87] In addition, CKD-504 (for Huntington disease, phase

---

[b] Data collected from the clinical trials database: https://clinicaltrials.gov. Accessed March 18, 2024.

1, NCT03713892)[c], CKD-506[88] (for rheumatoid arthritis, phase 2, NCT04204603), and CKD-510 (effect on healthy subjects, phase 1, NCT05526742)[c] were in clinical trials. However, the structure of CKD-510 has not been disclosed. The hydroxamic acid-based HDAC6 selective inhibitor KA2507[89] was in a clinical phase 2 trial for biliary tract cancer, and in a phase 1 study for solid tumors (NCT04186156). Furthermore, the dual LSD1/HDAC6 inhibitor JBI-802 is currently investigated in a phase 2 clinical trial in patients with metastatic or locally advanced solid tumors (NCT05268666).[c] Recently, a HDAC6 inhibitor with a new ZBG, the 2-(difluoromethyl)-1,3,4-oxadiazole (DFMO), entered phase 1 clinical trial for the treatment of heart failure with preserved ejection fraction (HFpEF).[90,91]

Ricolinostat (ACY 1215)

HDAC1: IC_{50} = 58 nM
HDAC6: IC_{50} = 4.8 nM
SI: 12

Citarinostat (ACY 241)

HDAC1: IC_{50} = 35 nM
HDAC6: IC_{50} = 2.6 nM
SI: 13
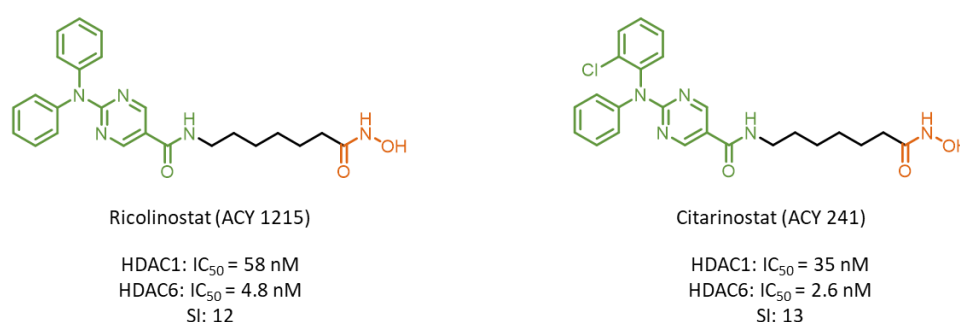
Figure 7. Structures and activity profiles of HDAC inhibitors ricolinostat and citarinostat. SI: selectivity index (IC_{50} HDAC1/ IC_{50} HDAC6).[92,93]

1.6 HDAC6 selective inhibitors

To achieve selectivity for HDAC6 over other HDAC isoforms, the most common approach is to utilize a branched ("T-shaped"), sterically demanding cap group.[64] The bulky cap group can interact with the HDAC6 surface at the entrance to the catalytic tunnel.[63] Such T-shaped inhibitors can also bear a relatively rigid cap group, compared to the flexible small cap of the I-shaped pan inhibitors. Additionally, attached to the cap, an aromatic linker can form π-π interactions with the F583 and F643 in the catalytic tunnel. Further, hydroxamic acids usually bind the zinc ion in a bidentate fashion, where the carbonyl oxygen and the N-O$^-$ coordinate the Zn^{2+}, forming a five-membered chelate complex. As an example, the HDAC6 inhibitor ricolinostat and its bidentate binding mode is shown in Figure 8A.[94] In comparison, the crystal structures of ACY 1083 and HPOB revealed an unusual monodentate binding mode for these selective HDAC6 inhibitors (see Figure 8B).[59] Through the bulky cap group and the shorter phenyl linker, the hydroxamic acid directly

---

[c] Data collected from the clinical trials database: https://clinicaltrials.gov. Accessed March 18, 2024.

coordinates the zinc only with the N-O⁻. The carbonyl oxygen forms a hydrogen bond with the water molecule bound to the metal ion.[94]
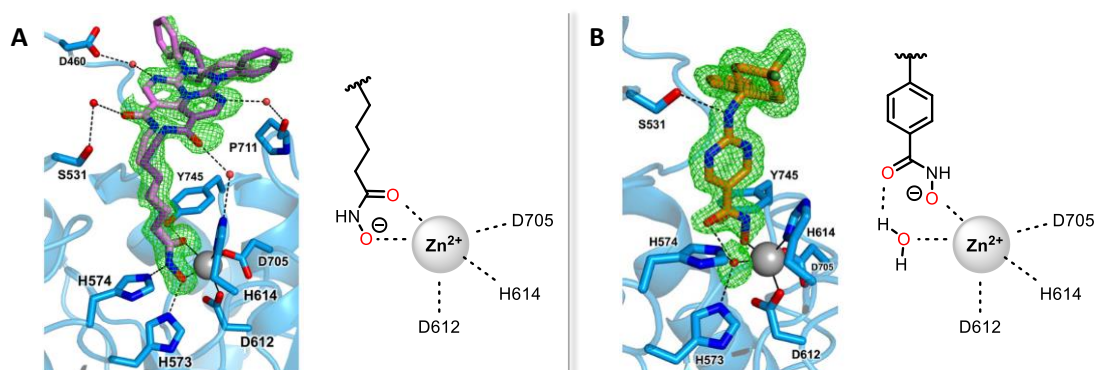
Figure 8. A) left: co-crystal structure of ricolinostat in HDAC6 zCD2; right: schematic representation of the bidentate binding mode. **B)** left: co-crystal structure of ACY 1083 in HDAC6 zCD2; right: schematic representation of the monodentate binding mode. The Zn^{2+} ion is displayed as a gray sphere; metal coordination and hydrogen bond interactions are indicated by dashed black lines. Reprinted with permission from Porter, N. J.; Mahendran, A.; Breslow, R. and Christianson, D. W. Unusual zinc-binding mode of HDAC6-selective hydroxamate inhibitors. Proc. Natl. Acad. Sci. **2017**, *114* (51), 13459-13464. Copyright 2017 National Academy of Sciences.

To address these structural criteria Butler et *al.* synthesized a series of compounds utilizing carbazoles and tetrahydro-carbolines as rigid and bulky cap groups attached to the hydroxamic acid ZBG by both alkylic and aromatic linkers.[95] They ended up with the highly selective HDAC6 inhibitor tubastatin A which has a tertiary amine in the tricyclic rigid cap group and a benzyl-based linker.[95] HDAC6 selectivity has also been achieved by branching an unselective urea-based HDAC

Tubastatin A

HDAC1: IC_{50} = 16.4 µM
HDAC6: IC_{50} = 0.015 µM
SI: 1093

Nexturastat A

HDAC1: IC_{50} = 3.02 µM
HDAC6: IC_{50} = 0.005 µM
SI: 604

ACY 1083

HDAC1: IC_{50} = 0.961 µM
HDAC6: IC_{50} = 0.004 µM
SI: 240

HPOB

HDAC1: IC_{50} = 2.9 µM
HDAC6: IC_{50} = 0.056 µM
SI: 52

NR160

HDAC1: IC_{50} = 5.18 µM
HDAC6: IC_{50} = 0.03 µM
SI: 172
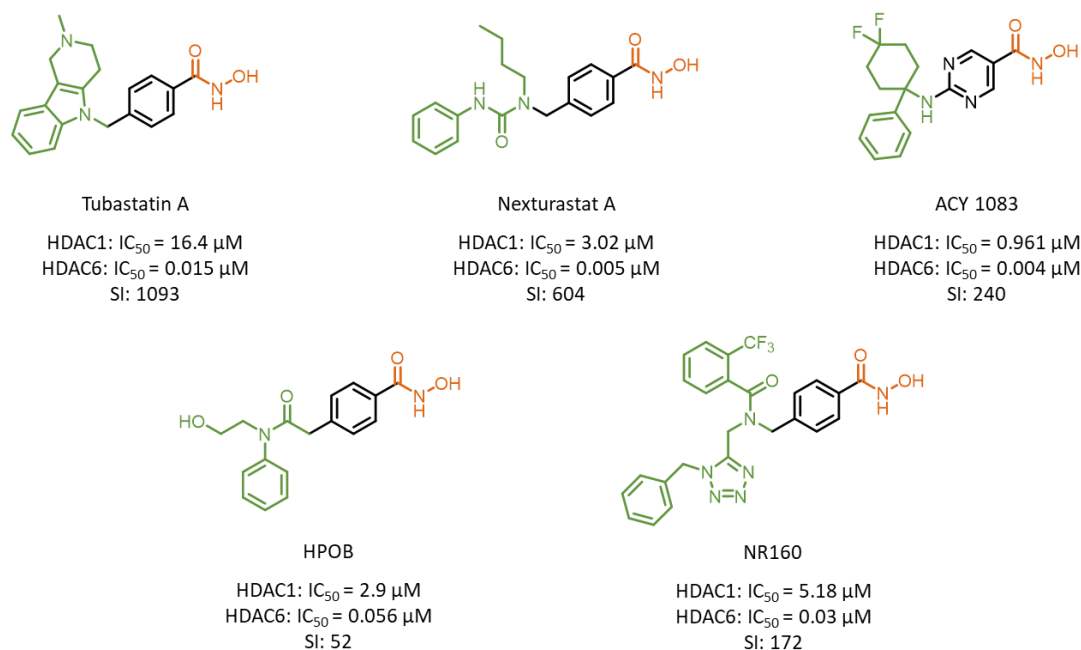
Figure 9. Selected hydroxamic acid-based HDAC6 inhibitors.[95–99] SI: selectivity index.

inhibitor, resulting in the highly potent HDAC6 inhibitor nexturastat A.[96] Other examples for selective HDAC6 inhibition using branched and rigid cap groups include ACY 1083[97] and HPOB.[98] Peptoid-based inhibitors possess bifurcated cap groups that improve HDAC6 selectivity, such as the peptoid analogue inhibitor NR160.[99,100]

Another approach to gain selectivity is to modify the ZBG. In particular, due to the genotoxic potential of hydroxamic acids, there is an urgent need for alternative ZBGs for applications beyond oncology.[84] In the case of HDAC6, the following ZBGs have been developed: mercaptoacetamides (**1**),[101] hydrazides (**2**),[102] 3-hydroxypyridine-2-thiones (3-HPTs, **3**),[103] trifluoromethyl-1,3,4-oxadiazoles (TFMOs),[104] and DFMOs[105–107] (see Figure 10). Compound **1** possesses a high selectivity index (SI) and showed increased tubulin acetylation *in vitro*.[101] Hydrazide **2** turned out to be a potent HDAC6 inhibitor with improved pharmacokinetics, while the 3-HPT derivative **3** showed no inhibition of HDAC1.[102,103] Recently, DFMOs have emerged as one of the most promising ZBG alternatives for selective HDAC6 inhibition. The DFMO-based HDAC6 inhibitor T-518 revealed therapeutic potential for the treatment of tauopathy in mice.[105] The change of the ZBG from DFMO **4** to TFMO **5** leads to a decrease in the inhibitory activity against HDAC6.[104] Both fluoroalkyoxadiazoles display high selectivity and potency for HDAC6, highlighting their potential as an alternative to hydroxamic acid-based selective HDAC6 inhibitors to overcome undesired side effects.

1
HDAC1: IC_{50} = 4.7 µM
HDAC6: IC_{50} = 0.0013 µM

2
HDAC1: IC_{50} = 1.53 µM
HDAC6: IC_{50} = 0.019 µM

3
HDAC1: IC_{50} = n.e.
HDAC6: IC_{50} = 0.3 µM

T-518
HDAC1: IC_{50} = n.e.
HDAC6: IC_{50} = 0.0046 µM

4
HDAC1: IC_{50} = n.d.
HDAC6: IC_{50} = 0.017 µM

5
HDAC1: IC_{50} = n.d.
HDAC6: IC_{50} = 0.033 µM
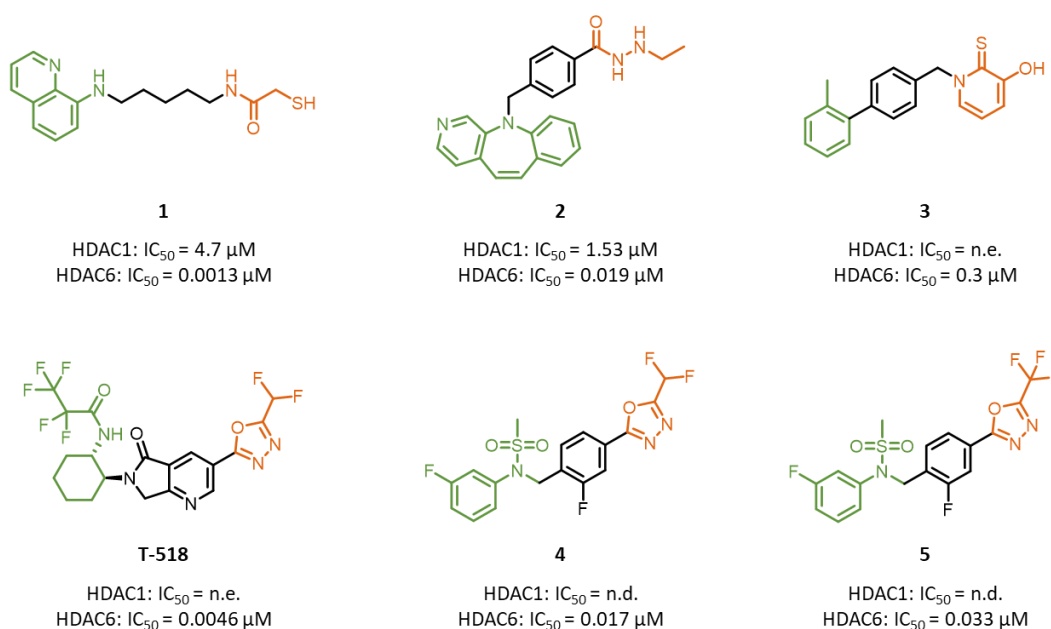
Figure 10. Selected alternative ZBGs for HDAC6. Top row: mercaptoacetamide **1**,[101] hydrazide **2**,[102] 3-HPT **3**;[103] bottom row: DFMOs T-518[105] and **4**, TFMO **5**.[104] n.e.: no effect; n.d.: not determined.

1.7 PROTACs

Hijacking the UPS for targeted protein degradation presents a promising alternative to the traditional small molecule inhibitor approach. Proteolysis targeting chimeras (PROTACs) are bifunctional molecules, which consist of a ligand capable of binding to the protein of interest (POI) and a ligand for an E3 ubiquitin ligase, both connected by a linker (Figure 11).[108] PROTACs redirect the UPS by bringing the POI and the ligase complex into close proximity promoting the transfer of ubiquitin to the POI, thereby marking it for degradation. After disengaging, the PROTAC molecule can be recycled and thus act in a catalytic mode of action.[109]

One advantage of PROTACs over traditional small molecule inhibitors is their catalytic mechanism which ensures a prolonged mode of action. In addition, they often exhibit increased selectivity by requiring the assembly of a ternary complex for precise ubiquitination of the target POI. Unlike small molecule inhibitors, PROTACs do not necessarily bind to the catalytic pocket of the POI, potentially enabling them to target previously inaccessible proteins. Moreover, the choice of specific E3 ligases might allows for tissue-specific degradation, further enhancing their selectivity.[110]
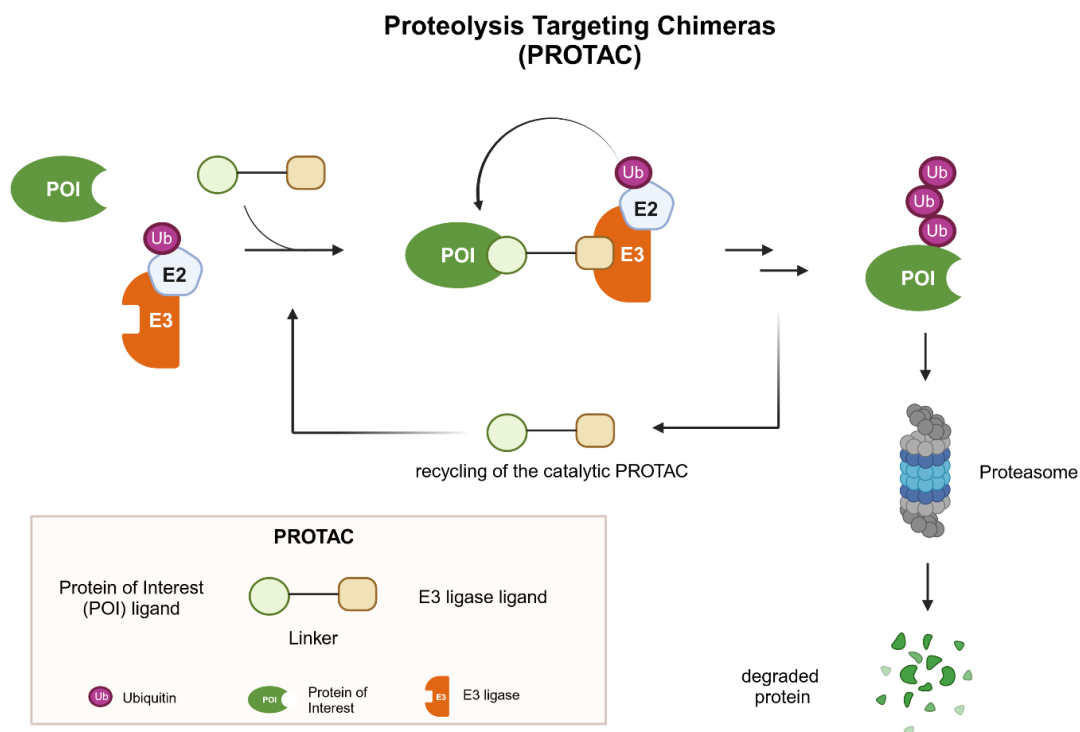
Figure 11. PROTAC mode of action. Adapted in a modified version from Fenglei et *al*. 2022.[111] Figure was created with Biorender.com.

However, PROTACs have drawbacks. As bivalent molecules, they often possess a high molecular weight, which can reduce cell permeability, tissue penetration, and oral bioavailability. Another concern is off-target protein degradation, either by degradation of a neighbouring protein within a protein complex or by recruitment of neosubstrates by the E3 ligase, leading to ubiquitination and degradation.[112,113] Furthermore, the "hook effect" is a challenge, as high concentrations of PROTACs can saturate the E3 ligase or the POI and prevent ternary complex formation. In addition, the PROTAC-protein complex can induce pharmacological responses other than degradation.[114]

Despite the 600 known E3 ligases in the human genome only a few have been successfully targeted by PROTACs so far.[115] The most common ones are cereblon (CRBN), von Hippel-Lindau (VHL), and inhibitor of apoptosis protein (IAP).[116] Thalidomide derivatives have been reported to bind CRBN, allowing the necessary E3 ligase recruitment for PROTACs.[117] Compounds targeting the VHL E3 ligase are based on a 4-hydroxyproline moiety.[118]

In 2018, Schiedel et *al.* reported the first PROTAC targeting sirtuine 2 (Sirt2), a NAD^+ dependent HDAC isoform, for proteasomal degradation (compound **6**, Figure 12).[119] Later in 2018, the first PROTAC for a Zn^{2+}-dependent HDAC was developed by Tang and co-workers.[120] They assembled the pan HDAC inhibitor crebinostat with pomalidomide, a CRBN recruiting ligase ligand, and a polyethylene glycol (PEG) linker. Unexpectedly, the degrader was able to selectively degrade HDAC6 in MCF-7 and MM.1S cells (compound **7**, Figure 12).[120] Since then, several approaches have been pursued to enable isoform selective degradation. PROTACs bearing the non-selective HDAC inhibitor dacinostat, assembled with different E3 ligase ligands showed different preferences towards HDAC isoforms. Interestingly, CRBN recruiting PROTACs displayed a preference for
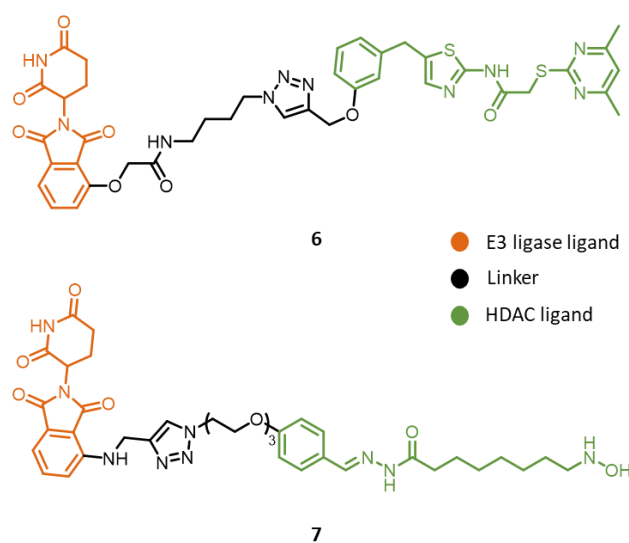
Figure 12. The first PROTACs targeting Sirt2 (6) and HDAC6 (7).[119,120]

degrading HDAC6 and 10, whereas VHL-based degraders showed a preference for HDAC3. When the POI ligand was changed to vorinostat, HDAC6 and 10 were degraded independently of the recruited E3 ligase.[121]

For the design of selective PROTACs there are several options to consider. The nature of the linker plays a crucial role in the formation of the ternary complex. Length, composition, and rigidity highly influence the degradation potential and have to be fine-tuned for each target. In addition to the linker and the E3 ligase recruiter, the POI ligand influences the selectivity profile of PROTACs. For instance, by incorporating the HDAC6 selective inhibitor nexturastat A, higher potency and selectivity towards HDAC6 could be achieved (compound **8**, Figure 13).[116,122] Nexturastat A was attached to the linker via different attachment points, resulting in PROTACs with single digit nanomolar half maximal degradation concentration (DC_{50}) values in MM.1S cells.[122] In addition, in cell viability assays, the PROTACs exhibited half maximal inhibitory concentrations of cell proliferation (GI_{50}) directly comparable to nexturastat A in the single digit micromolar range.[123] Furthermore, PROTAC **8** induces HDAC6 degradation within one hour of treatment.[122] Additionally, Figure 13 shows HDAC6 PROTACs with another HDAC6 selective ligand (compound **9**)[124] and the first selective HDAC6 PROTAC utilizing a VHL recruiting ligand (compound **10**)[125]. Compared to CRBN-based PROTACs, the VHL-based degrader **10** required a longer linker length to selectively degrade HDAC6.[125]
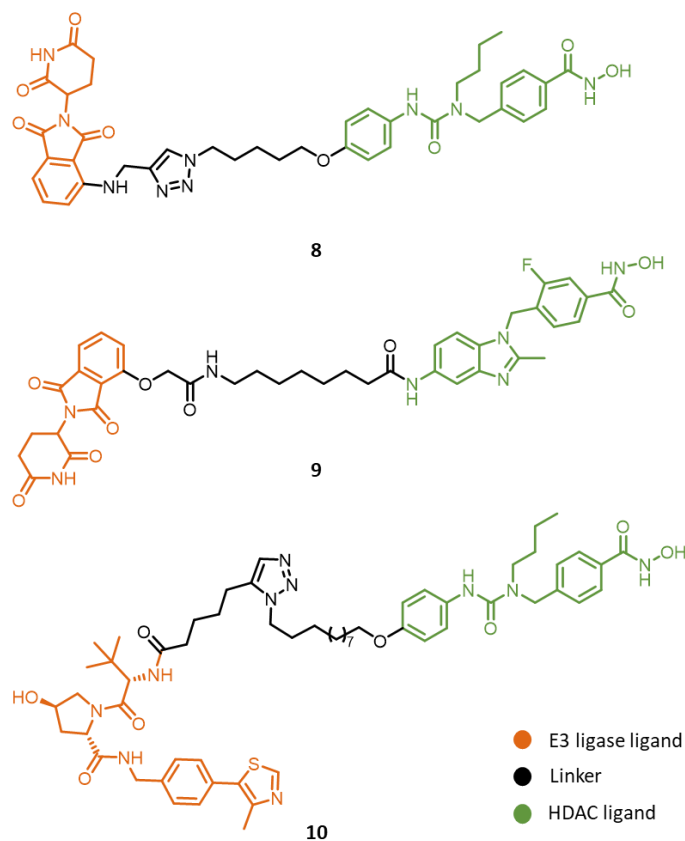
Figure 13. Selected HDAC6 PROTACs.[122,124,125]

1.8 Scope of thesis

HDAC6 is involved in various oncological and non-oncological conditions, including neurodegenerative diseases and rare disorders, such as Rett syndrome and Charcot-Marie-Tooth disease.[55,57,126] This makes it a valuable pharmaceutical target. To date, five non-selective HDAC inhibitors have been approved by the FDA, highlighting their potential for medical treatment.[72,d] However, the lack of selectivity might be associated with severe off-target effects. The use of isoform selective HDAC inhibitors could overcome these drawbacks.[127] One possibility to achieve selectivity towards HDAC6 is the incorporation of the recently emerging DFMO warhead.[105] The focus of this thesis is the development and elucidation of the mode of action of HDAC6 inhibitors and degraders bearing DFMOs as ZBGs.

Chapter 2 covers the development of the first non-hydroxamate HDAC6 degraders. For this purpose, PROTACs featuring a DFMO warhead for HDAC6 binding were designed. To evaluate linker preference, a set of PROTACs were synthesized utilizing PEG and alkyl chain linkers of different lengths. These linkers were connected via different attachment points at the *meta* and *para* position. The degraders were designed to recruit the well-studied E3 ligases CRBN and VHL. To assess the inhibitory activity of the PROTACs, the compounds were screened against HDAC1-4 and 6. The degradation efficacy of HDAC6 was determined by western blot experiments.

PROTACs recruiting CRBN:

1 *meta*; X: O
2 *meta*; X: CH$_2$
3 *para*; X: O

● E3 ligase ligand
● Linker
● HDAC6 ligand

PROTACs recruiting VHL:

4 *meta*; X: O
5 *meta*; X: CH$_2$
6 *para*; X: O
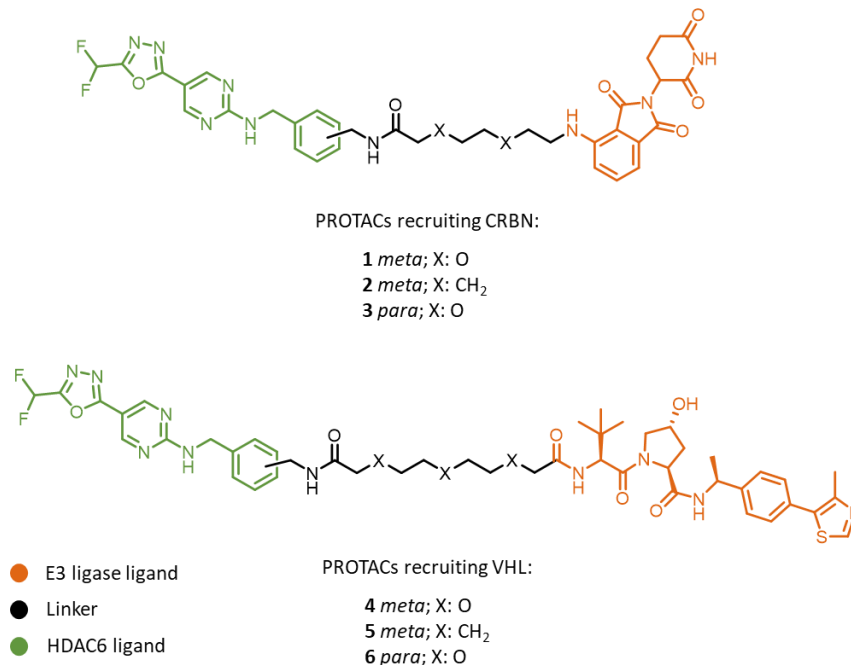
Figure 14. Overview of the designed non-hydroxamate HDAC6 degraders bearing a DFMO warhead. Numeration is referred to the publication.[128]

---

[d] FDA News Release: „FDA Approves Nonsteroidal Treatment for Duchenne Muscular Dystrophy" https://www.fda.gov/news-events/press-announcements/fda-approves-nonsteroidal-treatment-duchenne-muscular-dystrophy. Accessed April 04, 2024.

In addition, the most potent and efficient degraders from the CRBN and VHL set were further investigated in an in-depth biological evaluation.

Chapter 3 discusses the elucidation and development of DFMO derivatives as selective, mechanism-based, and essentially irreversible HDAC6 inhibitors. To this end, a series of different DFMO-based inhibitors were designed. To identify key structural requirements for selective HDAC6 inhibition, a fragment-based approach was used, including the synthesis of phenyl, pyridinyl and pyrimidinyl linkers attached to the ZBG (compounds **1**-**3**, Figure 15). Furthermore, *in vitro* assays were performed to evaluate the selectivity profile. Moreover, the fragments were extended to full-size inhibitors, including a compound with a pyrimidinyl linker (**6**). In addition, the DFMO was incorporated into established HDAC6 inhibitors such as nexturastat A (**9**) and peptoid-based inhibitors (**12**). The hit compound **6** was further investigated for its binding mechanism, including crystallographic experiments with the CD2 of zebrafish HDAC6, the analysis of association and dissociation properties as well as binding kinetic studies.
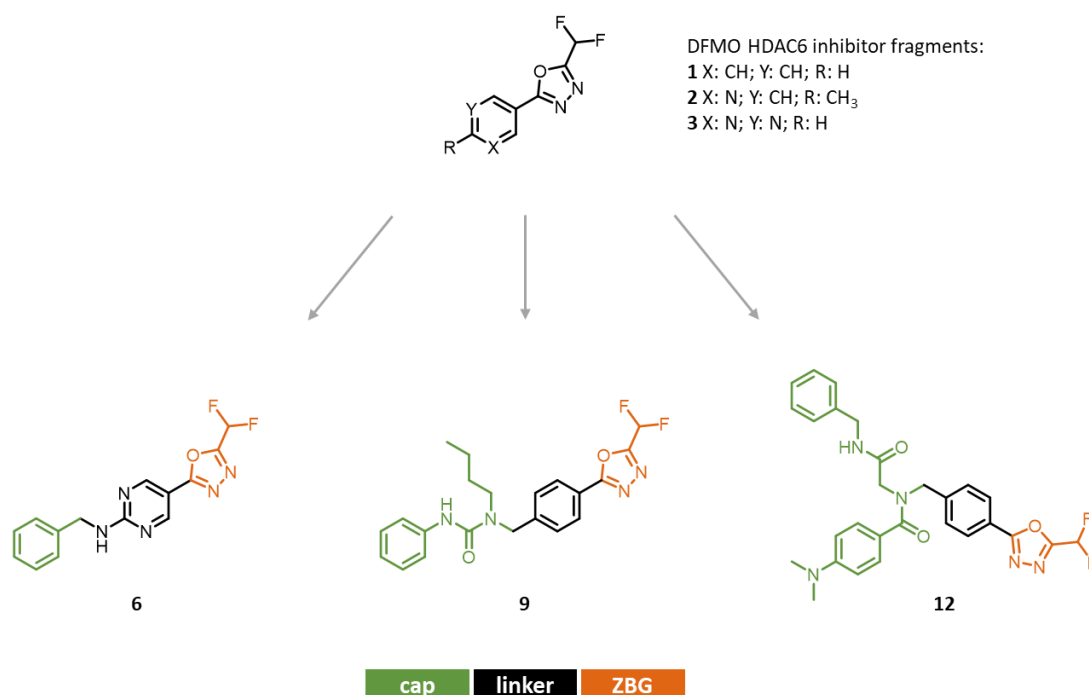
Figure 15. Overview of the designed DFMO fragments and full sized HDAC6 inhibitors. Numeration is referred to the publication.[106]

Chapter 4 is a viewpoint and summarizes the opportunities and challenges of selective HDAC6 modulation with DFMO-based inhibitors and degraders. The DFMO warhead has emerged as a promising alternative ZBG for HDAC6 inhibition.[107] This unique motif has been underrepresented in the scientific literature until recent years. First mentioned in a patent in 2017, the history and

development of DFMO-based compounds as highly selective HDAC6 inhibitors rapidly accelerated.[129] The aim of this viewpoint was to summarize the recent publications on the DFMO warhead for selective and potent HDAC6 inhibition and degradation. In detail, studies on the binding mechanism and pharmacokinetic profiles were assessed to highlight the advantages and drawbacks of this new class of selective HDAC6 inhibitors.

2 Development of the First Non-Hydroxamate Selective HDAC6 Degraders

Tim Keuler,* Beate König,* Nico Bückreiß,* Fabian B. Kraft, Philipp König, Linda Schäker-Hübner, Christian Steinebach, Gerd Bendas,# Michael Gütschow# and Finn K. Hansen#

* These authors contributed equally.

Shared senior authorship.

Please refer to Appendix I for the publication manuscript and supporting information.

2.1 Publication Summary

The strategic targeting of aberrant HDAC function, whether by the traditional small molecule inhibitors or targeted protein degradation (TPD), is emerging as a promising avenue for the treatment of cancer and other diseases beyond oncology.[127] The severe side effects of unselective HDAC inhibition prompted the pursuit of designing more selective HDAC inhibitors to reduce adverse effects.[130] HDAC6 stands out from other HDAC isoforms due to its unique structure and target specificity.[131]

Previously reported potent selective HDAC6 PROTACs have predominantly relied on a hydroxamic acid moiety as a ZBG to target the active site of HDAC6 CD2.[120–122,124] However, this class of compounds is susceptible to the formation of reactive isocyanate electrophiles due to Lossen rearrangements, leading to mutagenic and genotoxic effects.[84] Replacement of the hydroxamic acid as ZBG is highly appreciated and alternative inhibitors containing mercaptoacetamides or thiols have already been implemented.[132] Recent patent literature has introduced a pyrimidine-linked DFMO warhead as a potential HDAC6 selective scaffold, which served as a starting point for the design of non-hydroxamate HDAC6 PROTACs in this project.[133]

To evaluate the position of the exit vector, docking studies were performed, highlighting the solvent exposure of the *meta*-substituted ligand and the tendency of the acetyl group in the *para*-substituted derivative to interact with the amino acid residues T563 and M567 of the cavity. However, two DFMO based POI ligands with varying exit vectors were synthesized. This was achieved starting from the deprotection of *meta*- and *para*- mono-Boc-protected bis(aminomethyl)benzenes followed by the nucleophilic aromatic substitution of 2-

chloropyrimidinecarbonitrile. The respective carbonitriles were converted into tetrazoles and subsequently treated with difluoracetic anhydride to generate the DFMO moiety via a Huisgen reaction. Both POI ligands were connected to a CRBN and VHL recruiting ligand, resulting in the synthesis of six PROTACs with differing linkers.

Parameters such as experimental partition coefficient (elogD) and percentage of compound bound to human serum albumin were determined by high performance liquid chromatography (HPLC). Alkyl linker-based PROTACs exhibited higher lipophilicity and plasma protein binding than their respective PEG-based counterparts. *In vitro* assays revealed HDAC6 inhibition by each PROTAC with half maximal inhibitory concentration (IC_{50}) values ranging from 0.59 µM to 1.68 µM, while HDACs 1-4 were inhibited to less than 30% at a concentration of 30 µM.

Protein level analysis in MM.1S multiple myeloma cells after treatment with 1 µM of each PROTAC demonstrated a significant reduction in HDAC6 levels. The degradation selectivity profile of the identified hit compounds (PROTAC **1** and **4**) of the CRBN and VHL subset was confirmed through western blot analysis of HDAC1 and HDAC4 protein levels. Competition experiments with the HDAC inhibitor vorinostat and E3 ligase ligands pomalidomide or VH298, as well as pretreatment with the neddylation inhibitor MLN4924, supported the hypothesized ternary complex-dependent degradation via the UPS. Additionally, two tailored chemical negative controls were synthesized, which confirmed the proposed mechanism. These non-degrading control molecules were unable to adequately bind to the respective E3 ligase and therefore failed to promote HDAC6 degradation.

In conclusion, a set of six potent DFMO-based, selective HDAC6 PROTACs, targeting either the CRBN or the VHL E3 ligase, has been successfully developed. The two best degrading compounds underwent in-depth characterization, providing evidence for their selectivity profile and mode of action. These findings pave the way for the future development of non-hydroxamate PROTACs and contribute to a deeper understanding of the role of HDAC6 in different pharmacological pathways and diseases.

2.2 Author Contribution

All numbers are referred to the numeration within the publication. Within this project, I designed, synthesized and structurally characterized compounds **8**-**16**. Furthermore, I performed the enzymatic assays to determine the inhibitory activity of the PROTACs **1**-**6** against HDAC1-3 and 6. Apart from that, I contributed to the main text and the supporting information. Figure 1 and Scheme 1 of the main text and Figure S1 and Table S1 of the supporting information were prepared by myself.

3 Difluoromethyl-1,3,4-oxadiazoles Are Selective, Mechanism-Based, and Essentially Irreversible Inhibitors of Histone Deacetylase 6

Beate König,* Paris R. Watson,* Nina Reßing, Abigail D. Cragin, Linda Schäker-Hübner, David W. Christianson,[#] and Finn K. Hansen[#]

*These authors share the first authorship.

[#] Shared senior authorship.

Please refer to Appendix II for the publication manuscript and supporting information.

3.1 Publication Summary

HDACs are crucial epigenetic drug targets that modify histone modifications by removing acyl groups from lysine residues.[16] However, recent research has revealed a more complex substrate spectrum within the HDAC enzyme family.[16] There are four classes, with class I (HDACs 1, 2, 3 and 8) being the main regulator of the histone acylation status.[15] The class II enzymes can be further divided into the class IIa (HDACs 4, 5, 7, 9), which have a notable low catalytic activity, and into class IIb, consisting of HDAC6 and HDAC10. While HDAC6 is predominantly located in the cytosol and mainly regulates non-histone proteins, including cortactin,[35] the chaperone HSP90,[134] and Alzheimer-related tau,[61] HDAC10 is a polyamine deacetylase.[21,25] Class III HDAC enzymes are distinguished by their dependency from the cofactor NAD$^+$ and target a wide range of histone and non-histone proteins.[15] Class IV, represented by HDAC11, has an undefined biological role.[13]

The wide-ranging influence of HDACs on various diseases have prompted the development of HDAC inhibitors. They are generally designed based on the conserved active sites of the different isoforms, consisting of a ZBG, a cap group and an appropriate linker.[135] Unselective HDAC inhibitors, such as vorinostat, belinostat, panobinostat, and romidepsin, are FDA-approved anticancer drugs.[136] Despite limited anti-cancer potential when used in monotherapy, HDAC6 is emerging as an important target for combination therapies.[131,137,138] Further, it is being investigated for the use in non-oncological diseases such as neurodegenerative diseases,[61,126] rare disorders (e.g. Rett syndrome),[57] autoimmune diseases, idiopathic pulmonary fibrosis, and inflammasome-mediated diseases.[56,136,137]

However, the majority of selective HDAC6 inhibitors use hydroxamic acids as ZBG, which are associated with tolerability issues and off-target interactions.[84] The identification of alternative

ZBGs is crucial and so far, only a few surrogates have been developed, such as ethyl hydrazides and a non-hydroxamate compound with undisclosed structure in clinical phase II trials.[102,129] A promising HDAC6 selective binding motif is the DFMO group, which shows excellent inhibitory activity and selectivity.[133]

DFMO derivatives, such as SE-7552, exhibit selective HDAC6 inhibition and can overcome leptin resistance in obesity.[141] Incorporation of DFMO warheads into PROTACs have enabled remarkable HDAC6 selective degradation.[128] The aim of this publication was to elucidate the enigmatic binding mechanism of DFMOs inside HDAC6, which is responsible for the remarkable selectivity profile. To understand the structural requirements for selective HDAC6 inhibition, a fragment-based approach was used to investigate (hetero)aromatic linkers, leading to the identification of a pyrimidinyl derivative with the highest inhibitory potency against HDAC6.

Further explorations involved full-size HDAC inhibitors with a DFMO ZBG, benzyl or *para*-methoxy benzyl cap groups, and aminopyrimidinyl linkers. These compounds displayed submicromolar inhibitory activity against HDAC6 and no activity against HDAC1-4. Incorporation of a DFMO group as the ZBG into established HDAC6 inhibitors, such as nexturastat A and peptoid-based HDAC6 inhibitors, showed moderate inhibitory activity, indicating a distinct pharmacophore for DFMO-based HDAC6 inhibitors.

A X-ray crystal structure of compound **6** in complex with CD2 of HDAC6 revealed that **6** acts as a substrate analogue of HDAC6 and undergoes an enzyme catalyzed ring-opening reaction. The cocrystallized acylhydrazide fits the electron density map perfectly, providing insight into the extensive range of intermolecular interactions that stabilize the bound inhibitor. In detail, DFMOs act as selective, mechanism-based, and essentially irreversible inhibitors via a two-step slow-binding mechanism. The zinc-bound water attacks the sp2 carbon closest to the difluoromethyl moiety, leading to a ring opening of the oxadiazole and formation of a deprotonated difluoroacetylhydrazide as the active species, strongly coordinating the zinc ion. In addition, using HDAC6 mutants, the critical role of the histidines (H573/572) and tyrosine (Y745) in the ring-opening reaction and the second hydrolysis reaction to the corresponding hydrazide was confirmed.

In conclusion, DFMO-based HDAC6 inhibitors, particularly compound **6**, exhibit potent and selective inhibition through a unique binding mechanism. This involves an enzyme catalyzed ring-opening reaction yielding a deprotonated difluoroacetylhydrazide as the active species. Understanding the structural requirements and binding kinetics of these inhibitors might

contribute to the development of targeted therapies for various diseases and highlights the potential of HDAC6 as a drug target.

3.2 Author Contribution

All numbers are referred to the numeration within the publication. Within this project, I designed, synthesized and structurally characterized compounds **4**-**17**. Furthermore, I performed the enzymatic assays to determine the inhibitory activity of the inhibitors **6**, **7**, **9**, **10**, **12**, and **17** against HDAC1-4 and the inhibitors **6**, **7**, **9**, **10**, and **12-17** against HDAC6. Additionally, I evaluated in jump dilution and other kinetic experiments the binding mode of compound **6** and **17**. Apart from that, I contributed to the main text and the supporting information. Table 1, Scheme 1, Figure 4, Figure 5, and Figure 7 of the main text and Schemes S1-S4, and Figures S1-S6 of the supporting information, and the graphical abstract were prepared by myself.

4 2-(Difluoromethyl)-1,3,4-oxadiazoles: The Future of Selective Histone Deacetylase 6 Modulation?

Beate König and Finn K. Hansen

ACS Pharmacol. Transl. Sci. **2024**, *7* (3), 899-903.

Please refer to Appendix III for the publication manuscript.

4.1 Publication Summary

HDACs play crucial roles as epigenetic regulators and represent promising therapeutic targets for various diseases such as cancer, inflammation, and neurodegenerative disorders.[127] The HDAC family comprises four classes, with a total of 18 isoforms, subdivided on the basis of zinc ion dependence (classes I, II, and IV) and NAD^+-dependence (class III).[15] Class I includes HDAC1–3 and HDAC8, which are primarily located in the nucleus and catalyze histone deacylation.[142] Class II is subdivided into class IIa (HDAC4, 5, 7, 9) and IIb (HDAC6, 10), with IIa shuttling between the nucleus and cytoplasm and IIb located predominantly in the cytoplasm and acting on non-histone proteins.[16] The only member of class IV, HDAC11, is nuclear-centric.[15] Among HDACs, HDAC6 stands out due to its unique structural features, localization, and substrate range.[16] It possesses two independently active catalytic domains (CD1 and CD2) and a ubiquitin-binding zinc finger. HDAC6 influences various cellular processes such as cell motility, proliferation, apoptosis, and the aggresomal pathway.[127]

Due to the involvement in various pathophysiologies, HDAC6 is a promising target for drug development. Drug discovery efforts led to many HDAC inhibitors, which typically comprise a ZBG, a cap group, and a linker.[143] HDAC inhibitors approved by the FDA, such as vorinostat, belinostat, panobinostat, and romidepsin, lack isoform specificity, leading to significant side effects.[127,130] Recent efforts have focused on selective HDAC6 inhibition, using inhibitors with a bulky cap group, a phenyl or benzyl linker, and a hydroxamic acid as the ZBG.[143] However, concerns regarding mutagenic and genotoxic metabolites highlight the need for novel ZBGs.[84] The DFMO group has emerged as a promising alternative. This novel ZBG exhibits high isoform specificity and serves as a substrate analogue, making DFMO-based compounds mechanism-based, essentially irreversible inhibitors of HDAC6.[106]

The history of DFMO-based selective HDAC6 inhibitors dates back to a 2017 patent from Chong Kun Dang Pharmaceutical Corp.[129] In 2021, compound T-518 was published as an orally active, selective HDAC6 inhibitor revealing potential to treat Alzheimer´s disease.[105] Next, it was reported that the DFMO derivative SE-7552 demonstrates high HDAC6 selectivity and therapeutic potential in diseases such as multiple myeloma and obesity.[141,144] In addition, the DFMO warhead has been successfully incorporated into PROTACs for the selective degradation of HDAC6.[128]

Recent studies have provided insights into the crystal structures of DFMO-derived inhibitors in complex with HDAC6, shedding light on the slow- and tight-binding properties of the corresponding acylhydrazide as active species.[106,107] Further enzyme kinetic experiments revealed that the mechanism of action of DFMO involves an enzyme catalyzed ring-opening hydrolysis reaction, leading to the formation of a deprotonated difluoroacetylhydrazide as the active species.[106]

Despite the unparalleled selectivity of DFMO derivatives for HDAC6 over other isoforms, their pharmacokinetic profile was first investigated in 2023 in depth. The data by Ripa et *al*.[145] confirmed that DFMOs posses beneficial brain penetration and high oral bioavailability.[105] Despite challenges such as chemical stability, the potential of DFMO-based HDAC6 modulators remains promising due to their safety, efficacy, and selectivity.[145,146] These inhibitors show encouraging activity for the treatment of various diseases, including cancer, obesity, and neurodegenerative diseases, thereby making DFMOs compelling candidates for the development of HDAC6-targeted therapies.

In total, this viewpoint summarized the discovery and development of the enigmatic binding mode of DFMOs as potent and highly selective HDAC6 inhibitors. In addition, the opportunities and drawbacks regarding DFMO-based drugs for the treatment for HDAC6-driven diseases were highlighted.

4.2 Author Contribution

All numbers are referred to the numeration within the publication. Within this project, I collected and analyzed the data and contributed to the manuscript text. Figures 1-3 and the graphical abstract were prepared by myself.

5 Summary

HDAC6 is a unique member of the HDAC family and associated with various rare diseases, inflammatory processes, and neurodegenerative disorders, making it a valuable pharmaceutical target. To minimize off-target effects, it is desirable to selectively address only one of the 11 zinc-dependent HDAC isoforms. Currently, classical selective HDAC6 inhibitors consist of a bulky or branched cap group, a phenyl- or benzyl-based linker, and a hydroxamic acid as a ZBG. Due to the genotoxic properties of hydroxamic acids, there is an urgent need for alternative ZBGs. In addition to other alternative ZBGs such as mercaptoacetamides, hydrazides or 3-HPTs, the DFMO motif has emerged as a promising ZBG with an outstanding selectivity profile for HDAC6. This thesis presents three projects focusing on the development and elucidation of DFMOs as ZBGs for the selective inhibition and degradation of HDAC6.

The first project (Chapter 2) describes the development of the first non-hydroxamate selective HDAC6 degraders. In contrast to classical inhibition, PROTACs direct the POI to the ubiquitin proteasome system, thereby leading to its degradation. PROTACs are bifunctional molecules that recognize the POI and also hijacks an appropriate E3 ligase. By binding to the POI and the E3 ligase, a ternary complex is formed. Due to their close proximity, the E3-E2 ubiquitin complex is able to transfer ubiquitin to the POI. Over several steps, the POI gets polyubiquitinated and targeted for degradation by the proteasome. To this end, a set of PROTACs was designed and synthesized. In addition to the DFMO warhead for HDAC6 recognition, the degraders contain various PEG and alkyl chain linkers of different lengths that are linked to the inhibitor via two possible attachment points: *meta* and *para* position. The E3 ligase ligands were selected to recruit the well-studied E3 ubiquitin ligases CRBN and VHL. In total, six PROTACs were synthesized, characterized, and evaluated for their inhibitory activity against HDAC1-4 and 6. All degraders showed highly selective inhibition of HDAC6 with IC_{50} values ranging from 0.59 to 1.86 µM and were inactive against the HDAC isoforms 1-4. To investigate their degradation efficacy, western blot experiments were performed, confirming that all six PROTACs are capable of degrading HDAC6. The most efficient degraders of the CRBN and VHL sets were selected for further biological evaluations. The determination of the half maximal degrading concentration after 24 h revealed DC_{50} values in the low triple-digit nanomolar concentration range. Both degraders exhibited no toxicity in cell viability assays. To further confirm the HDAC6 selectivity, western blot experiments were conducted using a marker of reduced HDAC1-3 activity (acetylated histone H3) and a marker of reduced HDAC6 activity (acetylated α-tubulin). While the selected PROTACs did not impact the protein level of acetylated

histone H3, hyperacetylation of α-tubulin was observed, confirming HDAC6 selectivity of these degraders. To demonstrate that the degradation is dependent on the ternary complex formation, the CRBN ligand pomalidomide, the VHL ligand VH298, and the HDAC ligand vorinostat were included in the experimental setup. The western blot results showed that HDAC6 degradation only occurs when the corresponding E3 ligase and HDAC6 are not blocked by their respective ligands. This was further confirmed by negative controls, which are unable to bind the E3 ligase and therefore prevented HDAC6 degradation. Furthermore, rescue experiments were performed to demonstrate that HDAC6 degradation occurs via the proteasomal pathway. In conclusion, this project resulted in the design, synthesis, and evaluation of the first non-hydroxamate HDAC6 degraders using a DFMO warhead as ZBG. These selective HDAC6 degraders represent useful pharmacological tools to gain deeper insights into the function of HDAC6 in biological pathways and disorders.
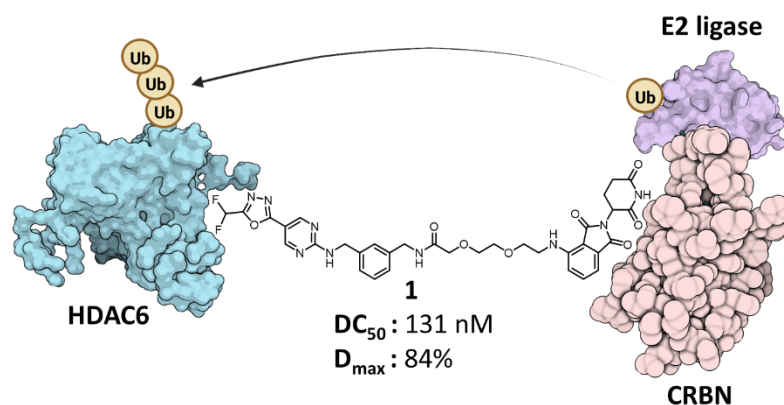
Figure 16. Schematic overview of the ternary complex formed by the first non-hydroxamate PROTAC based on a DFMO warhead as selective HDAC6 ZBG. Reproduced from Ref. 128 with permission from the Royal Society of Chemistry.

The second project (Chapter 3) elucidates DFMOs as selective, mechanism-based, and essentially irreversible inhibitors of HDAC6. A fragment-based approach was used to evaluate the influence of the linker moiety attached to the DFMO warhead as ZBG. Phenyl, pyridinyl, and pyrimidinyl linkers were designed, synthesized, and screened for their inhibition of HDAC6 and HDAC1-4. All fragments exhibited a more favorable inhibition against HDAC6, while HDAC1-4 were not inhibited. The pyrimidinyl derivative emerged as the most potent inhibitor of HDAC6. Based on these results, full-size inhibitors were designed utilizing the pyrimidinyl linker. In addition, the DFMO warhead was incorporated into established HDAC inhibitors, such as nexturastat A and peptoid-based HDAC6 inhibitors. While the most active full-size inhibitor compound **6** showed submicromolar inhibitory activity against HDAC6 (IC_{50} = 0.193 µM), the established HDAC inhibitor analogues only

displayed moderate activity against HDAC6. All inhibitors were inactive against the HDAC isoforms 1-4. These results suggest that the DFMO based inhibitors may bind via a different mode of action than the classical hydroxamic acid-based inhibitors, since the pharmacophores for selective HDAC6 inhibition, i.e. benzyl linker with bulky or branched cap group, cannot be applied for the design of DMFO-based inhibitors. To investigate the binding mechanism of the DMFO derivatives, compound **6** was selected for crystallographic experiments in the CD2 of zebrafish HDAC6. The crystal structure revealed that the oxadiazole undergoes an enzyme catalyzed ring-opening reaction, yielding an acylhydrazide as the active species. Further derivatives, i.e. methyl-1,3,4-oxadiazole, monofluoromethyl-1,3,4-oxadiazole, and trifluoromethyl-1,3,4-oxadiazole as well as the co-crystallized acylhydrazide as reference compound, were synthesized. To determine the structural features required for this mechanism. While the acylhydrazide and methyl analogues lacked inhibitory activity against HDAC6, the monofluoro derivative displayed weak inhibition and the trifluoro derivative exhibited notable inhibitory activity against HDAC6 in the submicromolar range (IC$_{50}$: 0.531 µM). To gain further insight into the binding mechanism, the difluoro and trifluoro derivatives were evaluated for their association and dissociation behavior. Various preincubation times in the enzymatic assay confirmed for both compounds slow-on binding properties. However, in jump dilution experiments, the DFMO derivative did not disengage from the enzyme, indicating tight-binding properties, while the trifluoro analogue revealed fast-off binding properties. This indicated that the two compounds bind via distinct modes of action. In order to prove this phenomenon, kinetic studies were performed, which revealed two different binding modes: a two-step slow-binding mechanism for DFMOs and a single-step slow-binding mechanism for the trifluoro derivative. Finally, the reaction mechanism for the enzyme catalyzed ring-opening reaction of DFMOs in HDAC6 was uncovered for the first time. The resulting anionic active acylhydrazide species strongly coordinates to the Zn^{2+} ion, leading to an essentially irreversible inhibition of HDAC6.
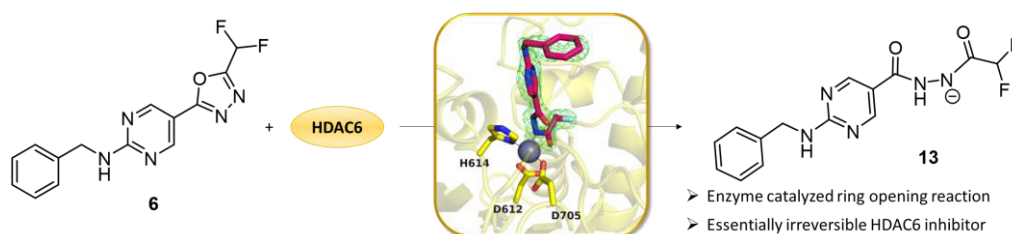
Figure 17. Overview of the enzyme catalyzed ring-opening reaction. Reprinted adapted with permission from König, B.; Watson, P. R.; Reßing, N.; Cragin, A. D.; Schäker-Hübner, L.; Christianson, D. W. and Hansen, F. H. Difluoromethyl-1,3,4-oxadiazoles Are Selective, Mechanism-Based, and Essentially Irreversible Inhibitors of Histone Deacetylase 6. *J. Med. Chem.* **2023**, *66* (19), 13821-13837. Copyright 2023 American Chemical Society.

The third project (chapter 4) discusses the future of selective HDAC6 modulation by DFMOs. To assess the opportunities and challenges of this promising new ZBG, the milestones of the discovery of the potent and selective HDAC6 inhibition by DFMOs were summarized (see Figure 18). Inhibitors utilizing a DFMO group as ZBG were first mentioned as selective HDAC6 inhibitors in a 2017 patent from Chong Kun Dang Pharmaceutical Corp. One of the first disclosures on DMFOs in the academic literature was in 2021 on the orally active and selective HDAC6 inhibitor T-518, which demonstrated therapeutic potential for the treatment of Alzheimer´s disease and tauopathy in mice. In addition, the first crystal structures of HDAC6 in complex with the respective inhibitors were disclosed in 2022 as well as the successful incorporation of the DFMO warhead into PROTACs for highly selective HDAC6 degradation. In 2023, various modes of action of DFMOs were proposed by academia and industry. Through a comprehensive study, this project was the first to validate the binding mechanisms of DFMOs, confirming that the enzyme catalyzed ring-opening reaction leads to the acylhydrazide as the active species. Furthermore, Ripa et *al.* published promising results on the pharmacokinetic profile of DFMOs in 2023. They reported no genotoxicity, high oral bioavailability, and low *in vivo* clearance. Overall, the exceptional selectivity of DMFO derivatives for HDAC6, together with its demonstrated efficacy against various diseases, such as obesity, multiple myeloma, and tauopathies, highlights the potential of DFMOs for drug development.
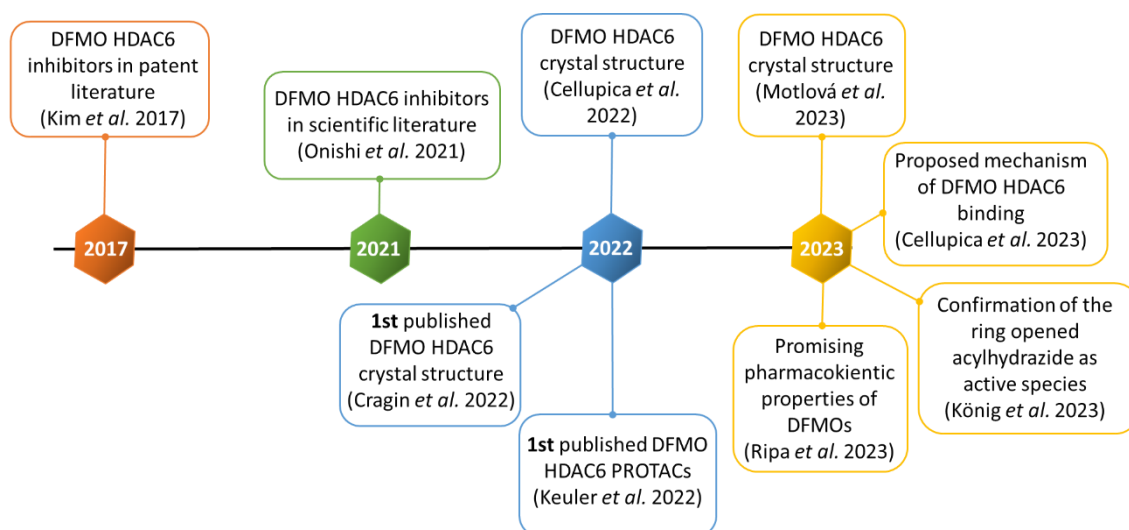
Figure 18. Overview of selected milestones of the discovery of DFMOs as highly selective and potent HDAC6 inhibitors.

In summary, this thesis provides new insights into the development of highly selective HDAC6 degraders and the elucidation of the enigmatic binding mechanism of outstanding selective HDAC6 inhibitors utilizing the DFMO group as promising ZBG. Finally, the milestones in the development of DFMO compounds for selective HDAC6 modulation were outlined, highlighting the potential of DFMOs as important drug candidates.

References

(1)   Waddington, C. H. Towards a Theoretical Biology. *Nature* **1968**, *218* (5141), 525–527. https://doi.org/10.1038/218525A0.

(2)   Dupont, C.; Armant, D. R.; Brenner, C. A. Epigenetics: Definition, Mechanisms and Clinical Perspective. *Semin. Reprod. Med.* **2009**, *27* (5), 351–357. https://doi.org/10.1055/s-0029-1237423.

(3)   Wu, C. T.; Morris, J. R. Genes, Genetics, and Epigenetics: A Correspondence. *Science* **2001**, *293* (5532), 1103–1105. https://doi.org/10.1126/science.293.5532.1103.

(4)   Kornberg, R. D.; Lorch, Y. Twenty-Five Years of the Nucleosome, Fundamental Particle of the Eukaryote Chromosome. *Cell* **1999**, *98* (3), 285–294. https://doi.org/10.1016/S0092-8674(00)81958-3.

(5)   Luger, K.; Mäder, A. W.; Richmond, R. K.; Sargent, D. F.; Richmond, T. J. Crystal Structure of the Nucleosome Core Particle at 2.8 A Resolution. *Nature* **1997**, *389* (6648), 251–260. https://doi.org/10.1038/38444.

(6)   Khorasanizadeh, S. The Nucleosome: From Genomic Organization to Genomic Regulation. *Cell* **2004**, *116* (2), 259–272. https://doi.org/10.1016/S0092-8674(04)00044-3.

(7)   Jenuwein, T.; Allis, C. D. Translating the Histone Code. *Science* **2001**, *293* (5532), 1074–1080. https://doi.org/10.1126/science.1063127.

(8)   Jones, P. A.; Issa, J. P. J.; Baylin, S. Targeting the Cancer Epigenome for Therapy. *Nat. Rev. Genet.* **2016**, *17* (10), 630–641. https://doi.org/10.1038/nrg.2016.93.

(9)   Spotswood, H. T.; Turner, B. M. An Increasingly Complex Code. *J. Clin. Invest.* **2002**, *110* (5), 577–582. https://doi.org/10.1172/jci16547.

(10)   Biel, M.; Wascholowski, V.; Giannis, A. Epigenetics - An Epicenter of Gene Regulation: Histones and Histone-Modifying Enzymes. *Angew. Chem. Int. Ed.* **2005**, *44* (21), 3186–3216. https://doi.org/10.1002/anie.200461346.

(11)   Arrowsmith, C. H.; Bountra, C.; Fish, P. V; Lee, K.; Schapira, M. Epigenetic Protein Families: A New Frontier for Drug Discovery. *Nat. Rev. Drug Discov.* **2012**, *11* (5), 384–400. https://doi.org/10.1038/nrd3674.

(12)   Biswas, S.; Rao, C. M. Epigenetic Tools (The Writers, The Readers and The Erasers) and Their Implications in Cancer Therapy. *Eur. J. Pharmacol.* **2018**, *837*, 8–24. https://doi.org/10.1016/j.ejphar.2018.08.021.

(13)   Roche, J.; Bertrand, P. Inside HDACs with More Selective HDAC Inhibitors. *Eur. J. Med. Chem.* **2016**, *121*, 451–483. https://doi.org/10.1016/j.ejmech.2016.05.047.

(14)   Taunton, J.; Hassig, C. A.; Schreiber, S. L. A Mammalian Histone Deacetylase Related to the Yeast Transcriptional Regulator Rpd3p. *Science* **1996**, *272* (5260), 408–411. https://doi.org/10.1126/science.272.5260.408.

(15)   Gregoretti, I. V.; Lee, Y. M.; Goodson, H. V. Molecular Evolution of the Histone Deacetylase Family: Functional Implications of Phylogenetic Analysis. *J. Mol. Biol.* **2004**, *338* (1), 17–31. https://doi.org/10.1016/j.jmb.2004.02.006.

(16)   Ho, T. C. S.; Chan, A. H. Y.; Ganesan, A. Thirty Years of HDAC Inhibitors: 2020 Insight and Hindsight. *J. Med. Chem.* **2020**, *63* (21), 12460–12484. https://doi.org/10.1021/acs.jmedchem.0c00830.

(17)   Wang, P.; Wang, Z.; Liu, J. Role of HDACs in Normal and Malignant Hematopoiesis. *Mol. Cancer* **2020**, *19* (1), 1–21. https://doi.org/10.1186/s12943-019-1127-7.

(18)   Verdin, E.; Dequiedt, F.; Kasler, H. G. Class II Histone Deacetylases: Versatile Regulators. *Trends Genet.* **2003**, *19* (5), 286–293. https://doi.org/10.1016/S0168-9525(03)00073-8.

(19)   Asfaha, Y.; Schrenk, C.; Alves Avelar, L. A.; Hamacher, A.; Pflieger, M.; Kassack, M. U.; Kurz, T. Recent Advances in Class IIa Histone Deacetylases Research. *Bioorg. Med. Chem.* **2019**, *27* (22), 115087. https://doi.org/10.1016/j.bmc.2019.115087.

(20)   Lahm, A.; Paolini, C.; Pallaoro, M.; Nardi, M. C.; Jones, P.; Neddermann, P.; Sambucini, S.; Bottomley, M. J.; Lo Surdo, P.; Carfí, A.; Koch, U.; De Francesco, R.; Steinkühler, C.; Gallinari, P. Unraveling the Hidden Catalytic Activity of Vertebrate Class IIa Histone Deacetylases. *Proc. Natl. Acad. Sci. USA* **2007**, *104* (44), 17335–17340. https://doi.org/10.1073/pnas.0706487104.

(21)   Hai, Y.; Shinsky, S. A.; Porter, N. J.; Christianson, D. W. Histone Deacetylase 10 Structure and Molecular Function as a Polyamine Deacetylase. *Nat. Commun.* **2017**, *8* (1), 15368. https://doi.org/10.1038/ncomms15368.

(22)   Verdel, A.; Khochbin, S. Identification of a New Family of Higher Eukaryotic Histone Deacetylases: Coordinate Expression of Differentiation-Dependent Chromatin Modifiers. *J.*

Biol. Chem. **1999**, *274* (4), 2440–2445. https://doi.org/10.1074/jbc.274.4.2440.

(23) Kutil, Z.; Skultetyova, L.; Rauh, D.; Meleshin, M.; Snajdr, I.; Novakova, Z.; Mikesova, J.; Pavlicek, J.; Hadzima, M.; Baranova, P.; Havlinova, B.; Majer, P.; Schutkowski, M.; Barinka, C. The Unraveling of Substrate Specificity of Histone Deacetylase 6 Domains Using Acetylome Peptide Microarrays and Peptide Libraries. *FASEB J.* **2019**, *33* (3), 4035–4045. https://doi.org/10.1096/fj.201801680R.

(24) Cohen, H. Y.; Lavu, S.; Bitterman, K. J.; Hekking, B.; Imahiyerobo, T. A.; Miller, C.; Frye, R.; Ploegh, H.; Kessler, B. M.; Sinclair, D. A. Acetylation of the C Terminus of Ku70 by CBP and PCAF Controls Bax-Mediated Apoptosis. *Mol. Cell* **2004**, *13* (5), 627–638. https://doi.org/10.1016/S1097-2765(04)00094-2.

(25) Hubbert, C.; Guardiola, A.; Shao, R.; Kawaguchi, Y.; Ito, A.; Nixon, A.; Yoshida, M.; Wang, X. F.; Yao, T. P. HDAC6 Is a Microtubule-Associated Deacetylase. *Nature* **2002**, *417* (6887), 455–458. https://doi.org/10.1038/417455a.

(26) Kovacs, J. J.; Murphy, P. J. M.; Gaillard, S.; Zhao, X.; Wu, J. T.; Nicchitta, C. V.; Yoshida, M.; Toft, D. O.; Pratt, W. B.; Yao, T. P. HDAC6 Regulates Hsp90 Acetylation and Chaperone-Dependent Activation of Glucocorticoid Receptor. *Mol. Cell* **2005**, *18* (5), 601–607. https://doi.org/10.1016/j.molcel.2005.04.021.

(27) Fan, S. J.; Huang, F. I.; Liou, J. P.; Yang, C. R. The Novel Histone Deacetylase 6 Inhibitor, MPT0G211, Ameliorates Tau Phosphorylation and Cognitive Deficits in an Alzheimer's Disease Model Article. *Cell Death Dis.* **2018**, *9* (6), 655. https://doi.org/10.1038/s41419-018-0688-5.

(28) Jiang, Y.; Liu, J.; Chen, D.; Yan, L.; Zheng, W. Sirtuin Inhibition: Strategies, Inhibitors, and Therapeutic Potential. *Trends Pharmacol. Sci.* **2017**, *38* (5), 459–472. https://doi.org/10.1016/j.tips.2017.01.009.

(29) Moreno-Yruela, C.; Galleano, I.; Madsen, A. S.; Olsen, C. A. Histone Deacetylase 11 Is an ε-N-Myristoyllysine Hydrolase. *Cell Chem. Biol.* **2018**, *25* (7), 849-856.e8. https://doi.org/10.1016/j.chembiol.2018.04.007.

(30) Kutil, Z.; Novakova, Z.; Meleshin, M.; Mikesova, J.; Schutkowski, M.; Barinka, C. Histone Deacetylase 11 Is a Fatty-Acid Deacylase. *ACS Chem. Biol.* **2018**, *13* (3), 685–693. https://doi.org/10.1021/acschembio.7b00942.

(31) Kaur, S.; Rajoria, P.; Chopra, M. HDAC6: A Unique HDAC Family Member as a Cancer Target.

Cell. Oncol. **2022**, *45* (5), 779–829. https://doi.org/10.1007/s13402-022-00704-6.

(32) Hubbert, C.; Guardiola, A.; Shao, R.; Kawaguchi, Y.; Ito, A.; Nixon, A.; Yoshida, M.; Wang, X. F.; Yao, T. P. HDAC6 Is a Microtubule-Associated Deacetylase. *Nature* **2002**, *417* (6887), 455–458. https://doi.org/10.1038/417455a.

(33) Matsuyama, A.; Shimazu, T.; Sumida, Y.; Saito, A.; Yoshimatsu, Y.; Seigneurin-Berny, D.; Osada, H.; Komatsu, Y.; Nishino, N.; Khochbin, S.; Horinouchi, S.; Yoshida, M. In Vivo Destabilization of Dynamic Microtubules by HDAC6-Mediated Deacetylation. *EMBO J.* **2002**, *21* (24), 6820–6831. https://doi.org/10.1093/emboj/cdf682.

(34) Zhang, Y.; Li, N.; Caron, C.; Matthias, G.; Hess, D.; Khochbin, S.; Matthias, P. HDAC-6 Interacts with and Deacetylates Tubulin and Microtubules in Vivo. *EMBO J.* **2003**, *22* (5), 1168–1179. https://doi.org/10.1093/emboj/cdg115.

(35) Zhang, X.; Yuan, Z.; Zhang, Y.; Yong, S.; Salas-Burgos, A.; Koomen, J.; Olashaw, N.; Parsons, J. T.; Yang, X. J.; Dent, S. R.; Yao, T. P.; Lane, W. S.; Seto, E. HDAC6 Modulates Cell Motility by Altering the Acetylation Level of Cortactin. *Mol. Cell* **2007**, *27* (2), 197–213. https://doi.org/10.1016/j.molcel.2007.05.033.

(36) Bryce, N. S.; Clark, E. S.; Leysath, J. L.; Currie, J. D.; Webb, D. J.; Weaver, A. M. Cortactin Promotes Cell Motility by Enhancing Lamellipodial Persistence. *Curr. Biol.* **2005**, *15* (14), 1276–1285. https://doi.org/10.1016/j.cub.2005.06.043.

(37) Ran, J.; Zhou, J. Targeted Inhibition of Histone Deacetylase 6 in Inflammatory Diseases. *Thorac. Cancer* **2019**, *10* (3), 405. https://doi.org/10.1111/1759-7714.12974.

(38) Kaluza, D.; Kroll, J.; Gesierich, S.; Yao, T. P.; Boon, R. A.; Hergenreider, E.; Tjwa, M.; Rössig, L.; Seto, E.; Augustin, H. G.; Zeiher, A. M.; Dimmeler, S.; Urbich, C. Class IIb HDAC6 Regulates Endothelial Cell Migration and Angiogenesis by Deacetylation of Cortactin. *EMBO J.* **2011**, *30* (20), 4142–4156. https://doi.org/10.1038/emboj.2011.298.

(39) Featherstone, C.; Jackson, S. P. Ku, a DNA Repair Protein with Multiple Cellular Functions? *Mutat. Res. - DNA Repair* **1999**, *434* (1), 3–15. https://doi.org/10.1016/S0921-8777(99)00006-3.

(40) Subramanian, C.; Jarzembowski, J. A.; Opipari, A. W.; Castle, V. P.; Kwok, R. P. S. HDAC6 Deacetylates Ku70 and Regulates Ku70-Bax Binding in Neuroblastoma. *Neoplasia* **2011**, *13* (8), 726. https://doi.org/10.1593/NEO.11558.

(41) Riolo, M. T.; Cooper, Z. A.; Holloway, M. P.; Cheng, Y.; Bianchi, C.; Yakirevich, E.; Ma, L.; Chin,

Y. E.; Altura, R. A. Histone Deacetylase 6 (HDAC6) Deacetylates Survivin for Its Nuclear Export in Breast Cancer. *J. Biol. Chem.* **2012**, *287* (14), 10885–10893. https://doi.org/10.1074/jbc.M111.308791.

(42) Wang, H.; Holloway, M. P.; Ma, L.; Cooper, Z. A.; Riolo, M.; Samkari, A.; Elenitoba-Johnson, K. S. J.; Chin, Y. E.; Altura, R. A. Acetylation Directs Survivin Nuclear Localization to Repress STAT3 Oncogenic Activity. *J. Biol. Chem.* **2010**, *285* (46), 36129–36137. https://doi.org/10.1074/jbc.M110.152777.

(43) Lee, J. Y. C.; Kuo, C. W.; Tsai, S. L.; Cheng, S. M.; Chen, S. H.; Chan, H. H.; Lin, C. H.; Lin, K. Y.; Li, C. F.; Kanwar, J. R.; Leung, E. Y.; Cheung, C. C. H.; Huang, W. J.; Wang, Y. C.; Cheung, C. H. A. Inhibition of HDAC3- and HDAC6-Promoted Survivin Expression Plays an Important Role in SAHA-Induced Autophagy and Viability Reduction in Breast Cancer Cells. *Front. Pharmacol.* **2016**, *7*, 81. https://doi.org/10.3389/fphar.2016.00081.

(44) Zhang, L.; Liu, N.; Xie, S.; He, X.; Tala; Zhou, J.; Liu, M.; Li, D. HDAC6 Regulates Neuroblastoma Cell Migration and May Play a Role in the Invasion Process. *Cancer Biol. Ther.* **2014**, *15* (11), 1561–1570. https://doi.org/10.4161/15384047.2014.956632.

(45) Lee, Y. S.; Lim, K. H.; Guo, X.; Kawaguchi, Y.; Gao, Y.; Barrientos, T.; Ordentlich, P.; Wang, X. F.; Counter, C. M.; Yao, T. P. The Cytoplasmic Deacetylase HDAC6 Is Required for Efficient Oncogenic Tumorigenesis. *Cancer Res.* **2008**, *68* (18), 7561–7569. https://doi.org/10.1158/0008-5472.CAN-08-0188.

(46) Lee, J. Y.; Koga, H.; Kawaguchi, Y.; Tang, W.; Wong, E.; Gao, Y. S.; Pandey, U. B.; Kaushik, S.; Tresse, E.; Lu, J.; Taylor, J. P.; Cuervo, A. M.; Yao, T. P. HDAC6 Controls Autophagosome Maturation Essential for Ubiquitin-Selective Quality-Control Autophagy. *EMBO J.* **2010**, *29* (5), 969–980. https://doi.org/10.1038/emboj.2009.405.

(47) Boyault, C.; Zhang, Y.; Fritah, S.; Caron, C.; Gilquin, B.; So, H. K.; Garrido, C.; Yao, T. P.; Vourc'h, C.; Matthias, P.; Khochbin, S. HDAC6 Controls Major Cell Response Pathways to Cytotoxic Accumulation of Protein Aggregates. *Genes Dev.* **2007**, *21* (17), 2172–2181. https://doi.org/10.1101/gad.436407.

(48) Kawaguchi, Y.; Kovacs, J. J.; McLaurin, A.; Vance, J. M.; Ito, A.; Yao, T. P. The Deacetylase HDAC6 Regulates Aggresome Formation and Cell Viability in Response to Misfolded Protein Stress. *Cell* **2003**, *115* (6), 727–738. https://doi.org/10.1016/S0092-8674(03)00939-5.

(49) Boyault, C.; Gilquin, B.; Zhang, Y.; Rybin, V.; Garman, E.; Meyer-Klaucke, W.; Matthias, P.;

Müller, C. W.; Khochbin, S. HDAC6-P97/VCP Controlled Polyubiquitin Chain Turnover. *EMBO J.* **2006**, *25* (14), 3357–3366. https://doi.org/10.1038/sj.emboj.7601210.

(50) Hideshima, T.; Richardson, P. G.; Anderson, K. C. Mechanism of Action of Proteasome Inhibitors and Deacetylase Inhibitors and the Biological Basis of Synergy in Multiple Myeloma. *Mol. Cancer Ther.* **2011**, *10* (11), 2034. https://doi.org/10.1158/1535-7163.MCT-11-0433.

(51) Iwata, A.; Riley, B. E.; Johnston, J. A.; Kopito, R. R. HDAC6 and Microtubules Are Required for Autophagic Degradation of Aggregated Huntingtin. *J. Biol. Chem.* **2005**, *280* (48), 40282–40292. https://doi.org/10.1074/jbc.M508786200.

(52) Olzmann, J. A.; Chin, L. S. Parkin-Mediated K63-Linked Polyubiquitination: A Signal for Targeting Misfolded Proteins to the Aggresome-Autophagy Pathway. *Autophagy* **2008**, *4* (1), 85–87. https://doi.org/10.4161/auto.5172.

(53) Sakamoto, K. M.; Aldana-Masangkay, G. I. The Role of HDAC6 in Cancer. *J. Biomed. Biotechnol.* **2011**, *2011*, 875824. https://doi.org/10.1155/2011/875824.

(54) Bali, P.; Pranpat, M.; Bradner, J.; Balasis, M.; Fiskus, W.; Guo, F.; Rocha, K.; Kumaraswamy, S.; Boyapalle, S.; Atadja, P.; Seto, E.; Bhalla, K. Inhibition of Histone Deacetylase 6 Acetylates and Disrupts the Chaperone Function of Heat Shock Protein 90: A Novel Basis for Antileukemia Activity of Histone Deacetylase Inhibitors. *J. Biol. Chem.* **2005**, *280* (29), 26729–26734. https://doi.org/10.1074/jbc.c500186200.

(55) Adalbert, R.; Kaieda, A.; Antoniou, C.; Loreto, A.; Yang, X.; Gilley, J.; Hoshino, T.; Uga, K.; Makhija, M. T.; Coleman, M. P. Novel HDAC6 Inhibitors Increase Tubulin Acetylation and Rescue Axonal Transport of Mitochondria in a Model of Charcot-Marie-Tooth Type 2F. *ACS Chem. Neurosci.* **2020**, *11*, 258–267. https://doi.org/10.1021/acschemneuro.9b00338.

(56) Campiani, G.; Cavella, C.; Osko, J. D.; Brindisi, M.; Relitti, N.; Brogi, S.; Saraswati, A. P.; Federico, S.; Chemi, G.; Maramai, S.; Carullo, G.; Jaeger, B.; Carleo, A.; Benedetti, R.; Sarno, F.; Lamponi, S.; Rottoli, P.; Bargagli, E.; Bertucci, C.; Tedesco, D.; Herp, D.; Senger, J.; Ruberti, G.; Saccoccia, F.; Saponara, S.; Gorelli, B.; Valoti, M.; Kennedy, B.; Sundaramurthi, H.; Butini, S.; Jung, M.; Roach, K. M.; Altucci, L.; Bradding, P.; Christianson, D. W.; Gemma, S.; Prasse, A. Harnessing the Role of HDAC6 in Idiopathic Pulmonary Fibrosis: Design, Synthesis, Structural Analysis, and Biological Evaluation of Potent Inhibitors. *J. Med. Chem.* **2021**, *64* (14), 9960–9988. https://doi.org/10.1021/acs.jmedchem.1c00184.

(57) Brindisi, M.; Saraswati, A. P.; Brogi, S.; Gemma, S.; Butini, S.; Campiani, G. Old but Gold: Tracking the New Guise of Histone Deacetylase 6 (HDAC6) Enzyme as a Biomarker and Therapeutic Target in Rare Diseases. *J. Med. Chem.* **2020**, *63* (1), 23–39. https://doi.org/10.1021/acs.jmedchem.9b00924.

(58) Chang, P.; Li, H.; Hu, H.; Li, Y.; Wang, T. The Role of HDAC6 in Autophagy and NLRP3 Inflammasome. *Front. Immunol.* **2021**, *12*, 763831. https://doi.org/10.3389/fimmu.2021.763831.

(59) Hai, Y.; Christianson, D. W. Histone Deacetylase 6 Structure and Molecular Basis of Catalysis and Inhibition. *Nat. Chem. Biol.* **2016**, *12* (9), 741–747. https://doi.org/10.1038/nchembio.2134.

(60) Miyake, Y.; Keusch, J. J.; Wang, L.; Saito, M.; Hess, D.; Wang, X.; Melancon, B. J.; Helquist, P.; Gut, H.; Matthias, P. Structural Insights into HDAC6 Tubulin Deacetylation and Its Selective Inhibition. *Nat. Chem. Biol.* **2016**, *12* (9), 748–754. https://doi.org/10.1038/nchembio.2140.

(61) Cohen, T. J.; Guo, J. L.; Hurtado, D. E.; Kwong, L. K.; Mills, I. P.; Trojanowski, J. Q.; Lee, V. M. Y. The Acetylation of Tau Inhibits Its Function and Promotes Pathological Tau Aggregation. *Nat. Commun.* **2011**, *2* (1), 252. https://doi.org/10.1038/ncomms1255.

(62) Osko, J. D.; Christianson, D. W. Structural Basis of Catalysis and Inhibition of HDAC6 CD1, the Enigmatic Catalytic Domain of Histone Deacetylase 6. *Biochemistry* **2019**, *58* (49), 4912–4924. https://doi.org/10.1021/acs.biochem.9b00934.

(63) Osko, J. D.; Porter, N. J.; Narayana Reddy, P. A.; Xiao, Y. C.; Rokka, J.; Jung, M.; Hooker, J. M.; Salvino, J. M.; Christianson, D. W. Exploring Structural Determinants of Inhibitor Affinity and Selectivity in Complexes with Histone Deacetylase 6. *J. Med. Chem.* **2020**, *63* (1), 295–308. https://doi.org/10.1021/acs.jmedchem.9b01540.

(64) Porter, N. J.; Osko, J. D.; Diedrich, D.; Kurz, T.; Hooker, J. M.; Hansen, F. K.; Christianson, D. W. Histone Deacetylase 6-Selective Inhibitors and the Influence of Capping Groups on Hydroxamate-Zinc Denticity. *J. Med. Chem.* **2018**, *61* (17), 8054–8060. https://doi.org/10.1021/acs.jmedchem.8b01013.

(65) Prejanò, M.; Vidossich, P.; Russo, N.; De Vivo, M.; Marino, T. Insights into the Catalytic Mechanism of Domains CD1 and CD2 in Histone Deacetylase 6 from Quantum Calculations. *ACS Catal.* **2021**, *11* (5), 3084–3093. https://doi.org/10.1021/acscatal.0c04729.

(66)   Porter, N. J.; Christianson, D. W. Structure, Mechanism, and Inhibition of the Zinc-Dependent Histone Deacetylases. *Curr. Opin. Struct. Biol.* **2019**, *59*, 9–18. https://doi.org/10.1016/j.sbi.2019.01.004.

(67)   Osko, J. D.; Christianson, D. W. Methods for the Expression, Purification, and Crystallization of Histone Deacetylase 6–Inhibitor Complexes. *Methods Enzymol.* **2019**, *626*, 447–474. https://doi.org/10.1016/bs.mie.2019.06.028.

(68)   Ferreira De Freitas, R.; Harding, R. J.; Franzoni, I.; Ravichandran, M.; Mann, M. K.; Ouyang, H.; Lautens, M.; Santhakumar, V.; Arrowsmith, C. H.; Schapira, M. Identification and Structure-Activity Relationship of HDAC6 Zinc-Finger Ubiquitin Binding Domain Inhibitors. *J. Med. Chem.* **2018**, *61* (10), 4517–4527. https://doi.org/10.1021/acs.jmedchem.8b00258.

(69)   Kawaguchi, Y.; Kovacs, J. J.; McLaurin, A.; Vance, J. M.; Ito, A.; Yao, T. P. The Deacetylase HDAC6 Regulates Aggresome Formation and Cell Viability in Response to Misfolded Protein Stress. *Cell* **2003**, *115* (6), 727–738. https://doi.org/10.1016/S0092-8674(03)00939-5.

(70)   Ouyang, H.; Ali, Y. O.; Ravichandran, M.; Dong, A.; Qiu, W.; MacKenzie, F.; Dhe-Paganon, S.; Arrowsmith, C. H.; Zhai, R. G. Protein Aggregates Are Recruited to Aggresome by Histone Deacetylase 6 via Unanchored Ubiquitin C Termini. *J. Biol. Chem.* **2012**, *287* (4), 2317–2327. https://doi.org/10.1074/jbc.M111.273730.

(71)   Yoshida, M.; Kijima, M.; Akita, M.; Beppu, T. Potent and Specific Inhibition of Mammalian Histone Deacetylase Both in Vivo and in Vitro by Trichostatin A*. *J. Biol. Chem.* **1990**, *265* (28), 17174–17179. https://doi.org/10.1016/S0021-9258(17)44885-X.

(72)   Cappellacci, L.; Perinelli, D. R.; Maggi, F.; Grifantini, M.; Petrelli, R. Recent Progress in Histone Deacetylase Inhibitors as Anticancer Agents. *Curr. Med. Chem.* **2020**, *27* (15), 2449–2493. https://doi.org/10.2174/0929867325666181016163110.

(73)   Finn, P. W.; Loza, E.; Carstensen, E. The Discovery and Development of Belinostat. In *Successful Drug Discovery*; John Wiley & Sons, Ltd, 2016; pp 31–57. https://doi.org/10.1002/9783527800315.ch3.

(74)   Atadja, P. Development of the Pan-DAC Inhibitor Panobinostat (LBH589): Successes and Challenges. *Cancer Lett.* **2009**, *280* (2), 233–241. https://doi.org/10.1016/j.canlet.2009.02.019.

(75)   San-Miguel, J. F.; Hungria, V. T. M.; Yoon, S. S.; Beksac, M.; Dimopoulos, M. A.; Elghandour, A.; Jedrzejczak, W. W.; Günther, A.; Nakorn, T. N.; Siritanaratkul, N.; Corradini, P.;

Chuncharunee, S.; Lee, J. J.; Schlossman, R. L.; Shelekhova, T.; Yong, K.; Tan, D.; Numbenjapon, T.; Cavenagh, J. D.; Hou, J.; LeBlanc, R.; Nahi, H.; Qiu, L.; Salwender, H.; Pulini, S.; Moreau, P.; Warzocha, K.; White, D.; Bladé, J.; Chen, W. M.; de la Rubia, J.; Gimsing, P.; Lonial, S.; Kaufman, J. L.; Ocio, E. M.; Veskovski, L.; Sohn, S. K.; Wang, M. C.; Lee, J. H.; Einsele, H.; Sopala, M.; Corrado, C.; Bengoudifa, B. R.; Binlich, F.; Richardson, P. G. Panobinostat plus Bortezomib and Dexamethasone versus Placebo plus Bortezomib and Dexamethasone in Patients with Relapsed or Relapsed and Refractory Multiple Myeloma: A Multicentre, Randomised, Double-Blind Phase 3 Trial. *Lancet Oncol.* **2014**, *15* (11), 1195–1206. https://doi.org/10.1016/S1470-2045(14)70440-1.

(76)   Shigematsu, N.; Ueda, H.; Takase, S.; Tanaka, H.; Yamamoto, K.; Tada, T. FR901228, a Novel Antitumor Bicyclic Depsipeptide Produced by Chromobacterium Violaceum No. 968 II. Structure Determination. *J. Antibiot.* **1994**, *47* (3), 311–314. https://doi.org/10.7164/antibiotics.47.311.

(77)   Foss, F.; Duvic, M.; Lerner, A.; Waksman, J.; Whittaker, S. Clinical Efficacy of Romidepsin in Tumor Stage and Folliculotropic Mycosis Fungoides. *Clin. Lymphoma, Myeloma Leuk.* **2016**, *16* (11), 637–643. https://doi.org/10.1016/j.clml.2016.08.009.

(78)   Jung, M.; Hoffmann, K.; Brosch, G.; Loidl, P. ANALOGUES OF TRICHOSTATIN A AND TRAPOXIN B AS HISTONE DEACETYLASE INHIBITORS. *Bioorg. Med. Chem. Lett.* **1997**, *7* (13), 1655–1658. https://doi.org/10.1016/S0960-894X(97)00284-9.

(79)   Marks, P. A.; Breslow, R. Dimethyl Sulfoxide to Vorinostat: Development of This Histone Deacetylase Inhibitor as an Anticancer Drug. *Nat. Biotechnol.* **2007**, *25* (1), 84–90. https://doi.org/10.1038/nbt1272.

(80)   O'connor, O. A. Clinical Experience with the Novel Histone Deacetylase Inhibitor Vorinostat (Suberoylanilide Hydroxamic Acid) in Patients with Relapsed Lymphoma. *Br. J. Cancer* **2006**, *95*, 7–12. https://doi.org/10.1038/sj.bjc.6603464.

(81)   Eleutherakis-Papaiakovou, E.; Kanellias, N.; Kastritis, E.; Gavriatopoulou, M.; Terpos, E.; Dimopoulos, M. A. Efficacy of Panobinostat for the Treatment of Multiple Myeloma. *J. Oncol.* **2020**, *2020*, 7131802. https://doi.org/10.1155/2020/7131802.

(82)   Van Veggel, M.; Westerman, E.; Hamberg, P. Clinical Pharmacokinetics and Pharmacodynamics of Panobinostat. *Clin. Pharmacokinet.* **2018**, *57* (1), 21–29. https://doi.org/10.1007/S40262-017-0565-X.

(83) Hogg, S. J.; Beavis, P. A.; Dawson, M. A.; Johnstone, R. W. Targeting the Epigenetic Regulation of Antitumour Immunity. *Nat. Rev. Drug Discov.* **2020**, *19* (11), 776–800. https://doi.org/10.1038/S41573-020-0077-5.

(84) Shen, S.; Kozikowski, A. P. Why Hydroxamates May Not Be the Best Histone Deacetylase Inhibitors - What Some May Have Forgotten or Would Rather Forget? *ChemMedChem* **2016**, *11* (1), 15–21. https://doi.org/10.1002/cmdc.201500486.

(85) Li, J.; Yu, M.; Fu, S.; Liu, D.; Tan, Y. Role of Selective Histone Deacetylase 6 Inhibitor ACY-1215 in Cancer and Other Human Diseases. *Front. Pharmacol.* **2022**, 13:907981. https://doi.org/10.3389/fphar.2022.907981.

(86) Jo, H.; Shim, K.; Jeoung, D. Targeting HDAC6 to Overcome Autophagy-Promoted Anti-Cancer Drug Resistance. *Int. J. Mol. Sci.* **2022**, *23* (17), 9592. https://doi.org/10.3390/ijms23179592.

(87) Awad, M. M.; Le Bruchec, Y.; Lu, B.; Ye, J.; Miller, J. A.; Lizotte, P. H.; Cavanaugh, M. E.; Rode, A. J.; Dumitru, C. D.; Spira, A. Selective Histone Deacetylase Inhibitor ACY-241 (Citarinostat) Plus Nivolumab in Advanced Non-Small Cell Lung Cancer: Results From a Phase Ib Study. *Front. Oncol.* **2021**, 11:696512. https://doi.org/10.3389/fonc.2021.696512.

(88) Park, J. K.; Jang, Y. J.; Oh, B. R.; Shin, J.; Bae, D.; Ha, N.; Choi, Y. Il; Youn, G. S.; Park, J.; Lee, E. Y.; Lee, E. B.; Song, Y. W. Therapeutic Potential of CKD-506, a Novel Selective Histone Deacetylase 6 Inhibitor, in a Murine Model of Rheumatoid Arthritis. *Arthritis Res. Ther.* **2020**, *22* (1), 176. https://doi.org/10.1186/s13075-020-02258-0.

(89) Tsimberidou, A. M.; Beer, P. A.; Cartwright, C. A.; Haymaker, C.; Vo, H. H.; Kiany, S.; Cecil, A. R. L.; Dow, J.; Haque, K.; Silva, F. A.; Coe, L.; Berryman, H.; Bone, E. A.; Nogueras-Gonzalez, G. M.; Vining, D.; McElwaine-Johnn, H.; Wistuba, I. I. Preclinical Development and First-in-Human Study of KA2507, a Selective and Potent Inhibitor of Histone Deacetylase 6, for Patients with Refractory Solid Tumors. *Clin. Cancer Res.* **2021**, *27* (13), 3584–3594. https://doi.org/10.1158/1078-0432.ccr-21-0238.

(90) Ranjbarvaziri, S.; Zeng, A.; Wu, I.; Greer-Short, A.; Farshidfar, F.; Budan, A.; Xu, E.; Shenwai, R.; Kozubov, M.; Li, C.; Van Pell, M.; Grafton, F.; MacKay, C. E.; Song, X.; Priest, J. R.; Argast, G.; Mandegar, M. A.; Hoey, T.; Yang, J. Targeting HDAC6 to Treat Heart Failure with Preserved Ejection Fraction in Mice. *Nat. Commun.* **2024**, *15*, 1352. https://doi.org/10.1038/s41467-024-45440-7.

(91)   Bexon, M.; Argast, G.; Robertson, L.; Hoey, T.; Vora, J.; Tingley, W.; Brown, F.; Schmelzer, K. Phase 1 Clinical Trial Of TN-301, A Highly Selective HDAC6 Inhibitor With Potential In HFPEF, Shows Target Engagement. *J. Card. Fail.* **2024**, *30* (1), 295. https://doi.org/10.1016/j.cardfail.2023.10.426.

(92)   Santo, L.; Hideshima, T.; Kung, A. L.; Tseng, J. C.; Tamang, D.; Yang, M.; Jarpe, M.; Van Duzer, J. H.; Mazitschek, R.; Ogier, W. C.; Cirstea, D.; Rodig, S.; Eda, H.; Scullen, T.; Canavese, M.; Bradner, J.; Anderson, K. C.; Jones, S. S.; Raje, N. Preclinical Activity, Pharmacodynamic, and Pharmacokinetic Properties of a Selective HDAC6 Inhibitor, ACY-1215, in Combination with Bortezomib in Multiple Myeloma. *Blood* **2012**, *119* (11), 2579. https://doi.org/10.1182/BLOOD-2011-10-387365.

(93)   Faridoon; Zha, Y. L.; Zhang, G.; Li, J. J. Medicinal Chemistry Insights into Non-Hydroxamate HDAC6 Selective Inhibitors. *Med. Chem. Res.* **2023**, *32* (1), 1–14. https://doi.org/10.1007/s00044-022-02987-8.

(94)   Porter, N. J.; Mahendran, A.; Breslow, R.; Christianson, D. W. Unusual Zinc-Binding Mode of HDAC6-Selective Hydroxamate Inhibitors. *Proc. Natl. Acad. Sci. USA* **2017**, *114* (51), 13459–13464. https://doi.org/10.1073/pnas.1718823114.

(95)   Butler, K. V.; Kalin, J.; Brochier, C.; Vistoli, G.; Langley, B.; Kozikowski, A. P. Rational Design and Simple Chemistry Yield a Superior, Neuroprotective HDAC6 Inhibitor, Tubastatin A. *J. Am. Chem. Soc.* **2010**, *132* (31), 10842–10846. https://doi.org/10.1021/ja102758v.

(96)   Bergman, J. A.; Woan, K.; Perez-Villarroel, P.; Villagra, A.; Sotomayor, E. M.; Kozikowski, A. P. Selective Histone Deacetylase 6 Inhibitors Bearing Substituted Urea Linkers Inhibit Melanoma Cell Growth. *J. Med. Chem.* **2012**, *55* (22), 9891–9899. https://doi.org/10.1021/jm301098e.

(97)   Gradilone, S. A.; LaRusso, N. F. TREATMENT OF POLYCYSTIC DISEASES WITH AN HDAC6 INHIBITOR. WO 2015/061684 A1, 2015.

(98)   Lee, J. H.; Mahendran, A.; Yao, Y.; Ngo, L.; Venta-Perez, G.; Choy, M. L.; Kim, N.; Ham, W. S.; Breslow, R.; Marks, P. A. Development of a Histone Deacetylase 6 Inhibitor and Its Biological Effects. *Proc. Natl. Acad. Sci. USA* **2013**, *110* (39), 15704–15709. https://doi.org/10.1073/pnas.1313893110.

(99)   Reßing, N.; Sönnichsen, M.; Osko, J. D.; Schöler, A.; Schliehe-Diecks, J.; Skerhut, A.; Borkhardt, A.; Hauer, J.; Kassack, M. U.; Christianson, D. W.; Bhatia, S.; Hansen, F. K.

Multicomponent Synthesis, Binding Mode, and Structure-Activity Relationship of Selective Histone Deacetylase 6 (HDAC6) Inhibitors with Bifurcated Capping Groups. *J. Med. Chem.* **2020**, *63* (18), 10339–10351. https://doi.org/10.1021/acs.jmedchem.9b01888.

(100) Reßing, N.; Schliehe-Diecks, J.; Watson, P. R.; Sönnichsen, M.; Cragin, A. D.; Schöler, A.; Yang, J.; Schäker-Hübner, L.; Borkhardt, A.; Christianson, D. W.; Bhatia, S.; Hansen, F. K. Development of Fluorinated Peptoid-Based Histone Deacetylase (HDAC) Inhibitors for Therapy-Resistant Acute Leukemia. *J. Med. Chem.* **2022**, *65* (22), 15457–15472. https://doi.org/10.1021/acs.jmedchem.2c01418.

(101) Segretti, M. C. F.; Vallerini, G. P.; Brochier, C.; Langley, B.; Wang, L.; Hancock, W. W.; Kozikowski, A. P. Thiol-Based Potent and Selective HDAC6 Inhibitors Promote Tubulin Acetylation and T-Regulatory Cell Suppressive Function. *ACS Med. Chem. Lett.* **2015**, *6* (11), 1156–1161. https://doi.org/https://doi.org/10.1021/acsmedchemlett.5b00303.

(102) Yue, K.; Sun, S.; Jia, G.; Qin, M.; Hou, X.; Chou, C. J.; Huang, C.; Li, X. First-in-Class Hydrazide-Based HDAC6 Selective Inhibitor with Potent Oral Anti-Inflammatory Activity by Attenuating NLRP3 Inflammasome Activation. *J. Med. Chem.* **2022**, *65* (18), 12140–12162. https://doi.org/10.1021/acs.jmedchem.2c00853.

(103) Patil, V.; Sodji, Q. H.; Kornacki, J. R.; Mrksich, M.; Oyelere, A. K. 3-Hydroxypyridin-2-Thione as Novel Zinc Binding Group for Selective Histone Deacetylase Inhibition. *J. Med. Chem.* **2013**, *56* (9), 3492–3506. https://doi.org/10.1021/jm301769u.

(104) Lee, J.; Han, Y.; Kim, Y.; Choi, D.; Min, J.; Bae, M.; Yang, H. 1,3,4-OXADIAZOLE SULFONAMIDE DERIVATIVE COMPOUNDS AS HISTONE DEACETYLASE 6 INHIBITOR; AND THE PHARMACEUTICAL COMPOSITION COMPRISING THE SAME. WO 2017/018803 A1, 2017.

(105) Onishi, T.; Maeda, R.; Terada, M.; Sato, S.; Fujii, T.; Ito, M.; Hashikami, K.; Kawamoto, T.; Tanaka, M. A Novel Orally Active HDAC6 Inhibitor T-518 Shows a Therapeutic Potential for Alzheimer's Disease and Tauopathy in Mice. *Sci. Rep.* **2021**, *11*, 15423. https://doi.org/10.1038/s41598-021-94923-w.

(106) König, B.; Watson, P. R.; Reßing, N.; Cragin, A. D.; Schäker-Hübner, L.; Christianson, D. W.; Hansen, F. K. Difluoromethyl-1,3,4-Oxadiazoles Are Selective, Mechanism-Based, and Essentially Irreversible Inhibitors of Histone Deacetylase 6. *J. Med. Chem.* **2023**, *66* (19), 13821–13837. https://doi.org/10.1021/acs.jmedchem.3c01345.

(107) Cellupica, E.; Caprini, G.; Cordella, P.; Cukier, C.; Fossati, G.; Marchini, M.; Rocchio, I.;

Sandrone, G.; Vanoni, M. A.; Vergani, B.; Źrubek, K.; Stevenazzi, A.; Steinkühler, C. Difluoromethyl-1,3,4-Oxadiazoles Are Slow-Binding Substrate Analog Inhibitors of Histone Deacetylase 6 with Unprecedented Isotype Selectivity. *J. Biol. Chem.* **2023**, *299* (1), 102800. https://doi.org/10.1016/j.jbc.2022.102800.

(108) Li, K.; Crews, C. M. PROTACs: Past, Present and Future. *Chemical Society Reviews*. The Royal Society of Chemistry June 20, 2022, pp 5214–5236. https://doi.org/10.1039/d2cs00193d.

(109) Nandi, D.; Tahiliani, P.; Kumar, A.; Chandu, D. The Ubiquitin-Proteasome System. *J. Biosci.* **2006**, *31*, 137–155. https://doi.org/10.1007/bf02705243.

(110) Khan, S.; He, Y.; Zhang, X.; Yuan, Y.; Pu, S.; Kong, Q.; Zheng, G.; Zhou, D. PROteolysis TArgeting Chimeras (PROTACs) as Emerging Anticancer Therapeutics. *Oncogene* **2020**, *39* (26), 4909–4924. https://doi.org/10.1038/s41388-020-1336-y.

(111) Li, F.; Hu, Q.; Zhang, X.; Sun, R.; Liu, Z.; Wu, S.; Tian, S.; Ma, X.; Dai, Z.; Yang, X.; Gao, S.; Bai, F. DeepPROTACs Is a Deep Learning-Based Targeted Degradation Predictor for PROTACs. *Nat. Commun. 2022 131* **2022**, *13* (1), 1–14. https://doi.org/10.1038/s41467-022-34807-3.

(112) Moreau, K.; Coen, M.; Zhang, A. X.; Pachl, F.; Castaldi, M. P.; Dahl, G.; Boyd, H.; Scott, C.; Newham, P. Proteolysis-Targeting Chimeras in Drug Development: A Safety Perspective. *Br. J. Pharmacol.* **2020**, *177* (8), 1709–1718. https://doi.org/10.1111/bph.15014.

(113) Békés, M.; Langley, D. R.; Crews, C. M. PROTAC Targeted Protein Degraders: The Past Is Prologue. *Nat. Rev. Drug Discov.* **2022**, *21* (3), 181–200. https://doi.org/10.1038/s41573-021-00371-6.

(114) Paiva, S. L.; Crews, C. M. Targeted Protein Degradation: Elements of PROTAC Design. *Curr. Opin. Chem. Biol.* **2019**, *50*, 111. https://doi.org/10.1016/j.cbpa.2019.02.022.

(115) Schneekloth, A. R.; Pucheault, M.; Tae, H. S.; Crews, C. M. Targeted Intracellular Protein Degradation Induced by a Small Molecule: En Route to Chemical Proteomics. *Bioorg. Med. Chem. Lett.* **2008**, *18* (22), 5904–5908. https://doi.org/10.1016/j.bmcl.2008.07.114.

(116) Patel, U.; Smalley, J. P.; Hodgkinson, J. T. PROTAC Chemical Probes for Histone Deacetylase Enzymes. *RSC Chem. Biol.* **2023**, *4* (9), 623–634. https://doi.org/10.1039/d3cb00105a.

(117) Ito, T.; Ando, H.; Suzuki, T.; Ogura, T.; Hotta, K.; Imamura, Y.; Yamaguchi, Y.; Handa, H. Identification of a Primary Target of Thalidomide Teratogenicity. *Science* **2010**, *327* (5971), 1345–1350. https://doi.org/10.1126/science.1177319.

(118) Diehl, C. J.; Ciulli, A. Discovery of Small Molecule Ligands for the von Hippel-Lindau (VHL) E3 Ligase and Their Use as Inhibitors and PROTAC Degraders. *Chem. Soc. Rev.* **2022**, *51* (19), 8216–8257. https://doi.org/10.1039/d2cs00387b.

(119) Schiedel, M.; Herp, D.; Hammelmann, S.; Swyter, S.; Lehotzky, A.; Robaa, D.; Oláh, J.; Ovádi, J.; Sippl, W.; Jung, M. Chemically Induced Degradation of Sirtuin 2 (Sirt2) by a Proteolysis Targeting Chimera (PROTAC) Based on Sirtuin Rearranging Ligands (SirReals). *J. Med. Chem.* **2018**, *61* (2), 482–491. https://doi.org/10.1021/acs.jmedchem.6b01872.

(120) Yang, K.; Song, Y.; Xie, H.; Wu, H.; Wu, Y. T.; Leisten, E. D.; Tang, W. Development of the First Small Molecule Histone Deacetylase 6 (HDAC6) Degraders. *Bioorg. Med. Chem. Lett.* **2018**, *28* (14), 2493–2497. https://doi.org/10.1016/j.bmcl.2018.05.057.

(121) Xiong, Y.; Donovan, K. A.; Eleuteri, N. A.; Kirmani, N.; Yue, H.; Razov, A.; Krupnick, N. M.; Nowak, R. P.; Fischer, E. S. Chemo-Proteomics Exploration of HDAC Degradability by Small Molecule Degraders. *Cell Chem. Biol.* **2021**, *28* (10), 1514–1527. https://doi.org/10.1016/j.chembiol.2021.07.002.

(122) Wu, H.; Yang, K.; Zhang, Z.; Leisten, E. D.; Li, Z.; Xie, H.; Liu, J.; Smith, K. A.; Novakova, Z.; Barinka, C.; Tang, W. Development of Multifunctional Histone Deacetylase 6 Degraders with Potent Antimyeloma Activity. *J. Med. Chem.* **2019**, *62* (15), 7042–7057. https://doi.org/10.1021/acs.jmedchem.9b00516.

(123) An, Z.; Lv, W.; Su, S.; Wu, W.; Rao, Y. Developing Potent PROTACs Tools for Selective Degradation of HDAC6 Protein. *Protein Cell* **2019**, *10* (8), 606–609. https://doi.org/10.1007/s13238-018-0602-z.

(124) Sinatra, L.; Yang, J.; Schliehe-Diecks, J.; Dienstbier, N.; Vogt, M.; Gebing, P.; Bachmann, L. M.; Sönnichsen, M.; Lenz, T.; Stühler, K.; Schöler, A.; Borkhardt, A.; Bhatia, S.; Hansen, F. K. Solid-Phase Synthesis of Cereblon-Recruiting Selective Histone Deacetylase 6 Degraders (HDAC6 PROTACs) with Antileukemic Activity. *J. Med. Chem.* **2022**, *65* (24), 16860–16878. https://doi.org/10.1021/acs.jmedchem.2C01659.

(125) Yang, K.; Wu, H.; Zhang, Z.; Leisten, E. D.; Nie, X.; Liu, B.; Wen, Z.; Zhang, J.; Cunningham, M. D.; Tang, W. Development of Selective Histone Deacetylase 6 (HDAC6) Degraders Recruiting von Hippel-Lindau (VHL) E3 Ubiquitin Ligase. *ACS Med. Chem. Lett.* **2020**, *11* (4), 575–581. https://doi.org/10.1021/acsmedchemlett.0c00046.

(126) Simões-Pires, C.; Zwick, V.; Nurisso, A.; Schenker, E.; Carrupt, P. A.; Cuendet, M. HDAC6 as a

Target for Neurodegenerative Diseases: What Makes It Different from the Other HDACs? *Mol. Neurodegener.* **2013**, *8* (1), 7. https://doi.org/10.1186/1750-1326-8-7.

(127) Jenke, R.; Reßing, N.; Hansen, F. K.; Aigner, A.; Büch, T. Anticancer Therapy with HDAC Inhibitors: Mechanism-Based Combination Strategies and Future Perspectives. *Cancers* **2021**, *13* (4), 634. https://doi.org/10.3390/cancers13040634.

(128) Keuler, T.; König, B.; Bückreiß, N.; Kraft, F. B.; König, P.; Schäker-Hübner, L.; Steinebach, C.; Bendas, G.; Gütschow, M.; Hansen, F. K. Development of the First Non-Hydroxamate Selective HDAC6 Degraders. *Chem. Commun.* **2022**, *58* (79), 11087–11090. https://doi.org/10.1039/d2cc03712b.

(129) Kim, Y.; Lee, C. S.; Oh, J. T.; Song, H.; Choi, J.; Lee, J. Oxadiazole Amine Derivative Compounds as Histone Deacetylase 6 Inhibitor, and the Pharmaceutical Composition Comprising the Same. WO 2017/065473 A1, 2017.

(130) Truong, N.; Goodis, C. C.; Cottingham, A. L.; Shaw, J. R.; Fletcher, S.; Pearson, R. M. Modified Suberoylanilide Hydroxamic Acid Reduced Drug-Associated Immune Cell Death and Organ Damage under Lipopolysaccharide Inflammatory Challenge. *ACS Pharmacol. Transl. Sci.* **2022**, *5* (11), 1128–1141. https://doi.org/10.1021/acsptsci.2c00119.

(131) Zhang, X.-H.; Qin-Ma; Wu, H.-P.; Khamis, M. Y.; Li, Y.-H.; Ma, L.-Y.; Liu, H.-M. A Review of Progress in Histone Deacetylase 6 Inhibitors Research: Structural Specificity and Functional Diversity. *J. Med. Chem.* **2021**, *64* (3), 1362–1391. https://doi.org/10.1021/acs.jmedchem.0c01782.

(132) Frühauf, A.; Meyer-Almes, F.-J. Non-Hydroxamate Zinc-Binding Groups as Warheads for Histone Deacetylases. *Molecules* **2021**, *26* (17), 5151. https://doi.org/10.1385/1-59259-153-1:123.

(133) Yates, C. M. Metalloenzyme Inhibitor Compounds. US 2018/0256572 A1, 2018.

(134) Karagöz, G. E.; Rüdiger, S. G. D. Hsp90 Interaction with Clients. *Trends Biochem. Sci.* **2015**, *40* (2), 117–125. https://doi.org/10.1016/j.tibs.2014.12.002.

(135) Bertrand, P. Inside HDAC with HDAC Inhibitors. *Eur. J. Med. Chem.* **2010**, *45* (6), 2095–2116. https://doi.org/10.1016/j.ejmech.2010.02.030.

(136) Kalin, J. H.; Bergman, J. A. Development and Therapeutic Implications of Selective Histone Deacetylase 6 Inhibitors. *J. Med. Chem.* **2013**, *56* (16), 6297–6313. https://doi.org/10.1021/jm4001659.

(137) Gaisina, I. N.; Tueckmantel, W.; Ugolkov, A.; Shen, S.; Hoffen, J.; Dubrovskyi, O.; Mazar, A.; Schoon, R. A.; Billadeau, D.; Kozikowski, A. P. Identification of HDAC6-Selective Inhibitors of Low Cancer Cell Cytotoxicity. *ChemMedChem* **2016**, *11* (1), 81–92. https://doi.org/10.1002/cmdc.201500456.

(138) Depetter, Y.; Geurs, S.; De Vreese, R.; Goethals, S.; Vandoorn, E.; Laevens, A.; Steenbrugge, J.; Meyer, E.; de Tullio, P.; Bracke, M.; D'hooghe, M.; De Wever, O. Selective Pharmacological Inhibitors of HDAC6 Reveal Biochemical Activity but Functional Tolerance in Cancer Models. *Int. J. Cancer* **2019**, *145* (3), 735–747. https://doi.org/10.1002/ijc.32169.

(139) Korfei, M.; Mahavadi, P.; Guenther, A. Targeting Histone Deacetylases in Idiopathic Pulmonary Fibrosis: A Future Therapeutic Option. *Cells* **2022**, *11* (10), 1626. https://doi.org/10.3390/cells11101626.

(140) Magupalli, V. G.; Negro, R.; Tian, Y.; Hauenstein, A. V; Caprio, G. Di; Skillern, W.; Deng, Q.; Orning, P.; Alam, H. B.; Maliga, Z.; Sharif, H.; Hu, J. J.; Evavold, C. L.; Kagan, J. C.; Schmidt, F. I.; Fitzgerald, K. A.; Kirchhausen, T.; Li, Y.; Wu, H. HDAC6 Mediates an Aggresome-like Mechanism for NLRP3 and Pyrin Inflammasome Activation. *Science* **2020**, *369* (6509), 8995. https://doi.org/10.1126/science.aas8995.

(141) Çakır, I.; Hadley, C. K.; Pan, P. L.; Bagchi, R. A.; Ghamari-Langroudi, M.; Porter, D. T.; Wang, Q.; Litt, M. J.; Jana, S.; Hagen, S.; Lee, P.; White, A.; Lin, J. D.; McKinsey, T. A.; Cone, R. D. Histone Deacetylase 6 Inhibition Restores Leptin Sensitivity and Reduces Obesity. *Nat. Metab.* **2022**, *4* (1), 44–59. https://doi.org/10.1038/s42255-021-00515-3.

(142) Cruz, D. L.; Pipalia, N.; Mao, S.; Gadi, D.; Liu, G.; Grigalunas, M.; O'Neill, M.; Quinn, T. R.; Kipper, A.; Ekebergh, A.; Dimmling, A.; Gartner, C.; Melancon, B. J.; Wagner, F. F.; Holson, E.; Helquist, P.; Wiest, O.; Maxfield, F. R. Inhibition of Histone Deacetylases 1, 2, and 3 Enhances Clearance of Cholesterol Accumulation in Niemann-Pick C1 Fibroblasts. *ACS Pharmacol. Transl. Sci.* **2021**, *4* (3), 1136–1148. https://doi.org/10.1021/acsptsci.1c00033.

(143) Osko, J. D.; Christianson, D. W. Structural Determinants of Affinity and Selectivity in the Binding of Inhibitors to Histone Deacetylase 6. *Bioorg. Med. Chem. Lett.* **2020**, *30* (8), 127023. https://doi.org/10.1016/j.bmcl.2020.127023.

(144) Holt, J. A.; Garvey, E. P.; Becherer, J. D.; Hoekstra, W. J.; Schotzinger, R. J.; Yates, C. M. SE-7552, a Highly Selective, Non-Hydroxamate Inhibitor of Histone Deacetylase-6 Blocks Multiple Myeloma Growth In Vivo. *Blood* **2018**, *132*, 3215. https://doi.org/10.1182/blood-2018-99-113066.

(145)   Ripa, L.; Sandmark, J.; Hughes, G.; Shamovsky, I.; Gunnarsson, A.; Johansson, J.; Llinas, A.; Collins, M.; Jung, B.; Nov, A.; Pemberton, N.; Mogemark, M.; Xiong, Y.; Li, Q.; Tångefjord, S.; Ek, M.; Åstrand, A. Selective and Bioavailable HDAC6 2-(Difluoromethyl)-1,3,4- Oxadiazole Substrate Inhibitors and Modeling of Their Bioactivation Mechanism. *J. Med. Chem.* **2023**, *66* (20), 14188–14207. https://doi.org/10.1021/acs.jmedchem.3c01269.

(146)   Ptacek, J.; Snajdr, I.; Schimer, J.; Kutil, Z.; Mikesova, J.; Baranova, P.; Havlinova, B.; Tueckmantel, W.; Majer, P.; Kozikowski, A.; Barinka, C. Selectivity of Hydroxamate- and Difluoromethyloxadiazole-Based Inhibitors of Histone Deacetylase 6 In Vitro and in Cells. *Int. J. Mol. Sci.* **2023**, *24* (5), 4720. https://doi.org/10.3390/ijms24054720.

Appendix

Appendix I. Publication I: Development of the first non-hydroxamate selective HDAC6 degraders

The following part contains the research article "Development of the first non-hydroxamate selective HDAC6 degraders", including the supporting information, as it was published in Chemical Communications by the Royal Society of Chemistry.

The article is reprinted with permission from:

Tim Keuler,* Beate König,* Nico Bückreiß,* Fabian B. Kraft, Philipp König, Linda Schäker-Hübner, Christian Steinebach, Gerd Bendas,[#] Michael Gütschow[#] and Finn K. Hansen[#]. Development of the first non-hydroxamate selective HDAC6 degraders. *Chem. Commun.* **2022**, *58*, 11087-11090.

*These authors share the first authorship.
[#] Shared senior authorship.

Check for updates

Development of the first non-hydroxamate selective HDAC6 degraders†

Tim Keuler,‡ Beate König,‡ Nico Bückreiß,‡ Fabian B. Kraft, Philipp König, Linda Schäker-Hübner, [ID] Christian Steinebach, [ID] Gerd Bendas, [ID]* Michael Gütschow [ID]* and Finn K. Hansen [ID]*

The targeted degradation of histone deacetylase 6 (HDAC6) by heterobifunctional degraders constitutes a promising approach to treat HDAC6-driven diseases. Previous HDAC6 selective degraders utilised a hydroxamic acid as a zinc-binding group (ZBG) which features mutagenic and genotoxic potential. Here we report the development of a new class of selective HDAC6 degraders based on a difluoromethyl-1,3,4-oxadiazole warhead as ZBG.

Histone deacetylases (HDACs) are considered important epigenetic drug targets for the therapy of haematological and solid cancers.[1] Four HDAC inhibitors (HDACi; vorinostat, romidepsin, belinostat, and panobinostat) have received regulatory approval from the FDA for treating T-cell lymphoma and multiple myeloma. However, all approved HDACi do not possess selectivity for a specific HDAC isoform.[1] Due to their lack of isoform-selectivity, such unselective HDACi often cause suffering from serious adverse effects.[1] Thus, to optimise the risk-benefit profile of HDACi, there is urgent need to develop isoform-specific HDACi.

HDAC6 is overexpressed in various cancer types and modulates the activity of several non-histone proteins such as α-tubulin, cortactin, and Hsp90.[2] Since the knockout of HDAC6 in mice did not produce significant defects, HDAC6 inhibitors are considered to exhibit improved safety profiles compared to pan-HDACi.[3] HDAC6 is structurally unique and comprises two active catalytic domains (CD1 and CD2) as well as a zinc finger functioning as a ubiquitin-binding domain (UBD). Classical HDAC6-selective inhibitors impede CD2 but do not interfere with enzymatic and non-enzymatic functions facilitated by CD1 or the UBD.[1] Hence, the chemical knockdown of HDAC6 may be superior to the sole inhibition of CD2.

Pharmaceutical Institute, University of Bonn, An der Immenburg 4, 53121, Bonn, Germany. E-mail: gbendas@uni-bonn.de, guetschow@uni-bonn.de, finn.hansen@uni-bonn.de

† Electronic supplementary information (ESI) available: Supplementary figures, schemes and tables, experimental procedures, ^{1}H NMR, ^{13}C NMR and MS data, docking protocols. See DOI: https://doi.org/10.1039/d2cc03712b
‡ These authors contributed equally.

Hijacking the ubiquitin-proteasome system (UPS) with proteolysis-targeting chimeras (PROTACs) is an emerging new therapeutic modality, which enables the targeted degradation of a protein of interest (POI). These heterobifunctional molecules consist of an E3 ligase ligand and a recognition motif for the POI connected by a suitable linker, thereby acting as proximity inducers.[4] The formation of a POI: PROTAC: E3 ligase ternary complex initiates the polyubiquitination of the POI, leading to its proteasomal degradation.[2] In 2018, Schiedel *et al.*[5] and Yang *et al.*[6] reported the first Sirt2 and HDAC6 PROTACs, respectively. Several selective HDAC6 degraders have been disclosed in the past years, including compounds based on the HDAC6 inhibitor nexturastat A and the pan-HDACi crebinostat.[6–10] All selective HDAC6 PROTACs reported so far contain a hydroxamate zinc-binding group (ZBG) which coordinates the zinc ion in the active site of HDAC6 CD2.[6–10] Although hydroxamic acids have been successfully utilised as ZBGs in approved HDACi as well as in numerous late-stage clinical candidates, they may transform *via* Lossen rearrangements into mutagenic and highly reactive electrophilic species such as isocyanates susceptible to react with naturally occurring nucleophiles.[11] To avoid such mutagenic and genotoxic potential, new ZBGs are desirable for HDAC PROTAC development.[11] Herein, we report the first non-hydroxamate, selective HDAC6 PROTACs that contain difluoromethyl-1,3,4-oxadiazole warheads as ZBGs.

Selective HDAC6 inhibitors typically consist of a hydroxamate ZBG connected to a short benzyl or 4-aminophenyl linker and a bulky, rigid cap group that confers isoform selectivity. A few alternative ZBGs, for example, mercaptoacetamides, thiols, and trifluoromethyl ketones enabled potent HDAC6 inhibition but exhibited lower selectivity than hydroxamic acids.[12] In 2018, Yates[13] disclosed a new type of highly potent HDAC6 selective inhibitors based on pyrimidine linkers and the 2-(difluoromethyl)-1,3,4-oxadiazole group as ZBG (for representative structures, see Fig. S1, ESI†). Inspired by this scaffold, we designed the *meta-* and *para-*connected HDAC6 ligands **I** and **II** (Fig. 1A) containing acetyl groups that mimic the PROTAC attachment points. Docking studies (Fig. S2, ESI†) to investigate their potential as POI ligands showed the acetyl group of the

Fig. 1 (A) HDAC6 ligands **I** and **II** with possible *meta* and *para* attachment points. (B) Docking pose of ligand **I** in the CD2 of HDAC6 (PDB: 5EDU).[14] The catalytic Zn^{2+}-ion is shown as gray sphere. (C) Designed *meta*- and *para*-connected HDAC6 PROTACs.

meta-substituted derivative **I** solvent-exposed (Fig. 1B), indicating an appropriate exit vector to assemble PROTACs. In turn, the predicted binding mode for the *para*-substituted analogue **II** suggests that the acetyl group binds in the proximity of Thr563 and Met567 (Fig. S3, ESI†). However, it seems sufficiently solvent-exposed. We thus decided to pursue both *meta*- and *para*-connected PROTACs and designed degraders that are capable of recruiting the well-studied E3 ubiquitin ligases cereblon (CRBN) and von Hippel-Lindau (VHL) (Fig. 1C).

For the synthesis of the required HDAC6 ligands (Scheme 1) the mono-Boc-protected bis(aminomethyl)benzenes **7** and **8** were converted to the orthogonally protected building blocks **9** and **10**. After Boc-deprotection, the nucleophilic aromatic substitution of 2-chloropyrimidine-5-carbonitrile afforded the carbonitrile intermediates **11** and **12**, which were subjected to the reaction with sodium azide to provide **13** and **14**. For the preparation of the desired HDAC6 ligands **15** and **16**, the tetrazoles **13** and **14** were reacted with difluoroacetic anhydride
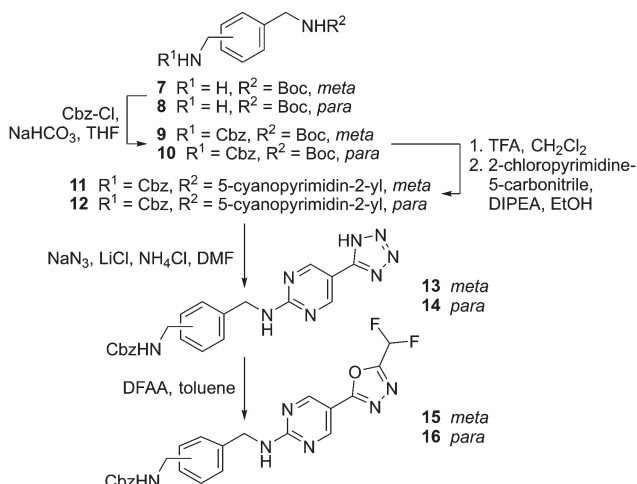
(DFAA) to generate the 2-(difluoromethyl)-1,3,4-oxadiazole group *via* a Huisgen 1,3,4-oxadiazole synthesis.[15]

The cereblon-based PROTAC precursors were obtained *via* the synthetic route depicted in Scheme 2. First, a PEG-containing precursor (**26**) with pomalidomide as a cereblon binding unit was prepared. For this purpose, 2-(2-aminoethoxy)ethanol (**17**) was Cbz-protected to **18**, which was elongated through *O*-alkylation with *tert*-butyl bromoacetate. The resulting orthogonally protected linker **19** underwent catalytic hydrogenolysis to give the primary amine **20**. This was employed in a nucleophilic substitution reaction with 4-fluorothalidomide (**25**) to yield **26**.[16] To evaluate the impact of compound polarity on degradation potency, we conceived the cereblon-based PROTAC precursor **27** with an alkylidene chain of equal length. Starting with 8-bromooctanoic acid (**21**), an esterification with *tert*-butanol and trifluoroacetic anhydride was performed,[17] leading to **22**, which was transformed into the azide **23**, followed by a Staudinger reaction. The amine **24** was then conjugated with 4-fluorothalidomide (**25**) to obtain the second cereblon-based PROTAC precursor **27**.

The preparation of the VHL-based PROTAC precursor **34** (Scheme 3) started with the *O*-alkylation of **28** to give **29**, followed by hydrogenolytic deprotection. The resulting alcohol **30** was oxidised with (diacetoxyiodo)benzene (BAIB) and TEMPO to the carboxylic acid **31**. The Boc-protected VHL ligand **33** was synthesised in a convergent approach (Scheme S1, ESI†).[18] Upon deprotection of **33**, it was linked to **31** in a uronium salt-mediated coupling to achieve the VHL-based PROTAC precursor **34**. The alkylidene precursor **35** was similarly obtained from unilaterally esterified undecanedioic acid **32**.

After hydrogenolytic deprotection of the HDAC6 ligands **15** and **16** and TFA-promoted deprotection of the PROTAC precursors **26**, **27**, **34** and **35**, respectively, the HDAC6 degraders **1–6** were finally assembled through amide coupling (Table 1). An overview of physicochemical properties (molecular weight, lipophilicity, plasma protein binding (PPB), number of rotatable bonds, polar surface area) to assess the drug-likeness of the degraders is provided in Table 1. Notably, introduction of oxygen atoms into the linker reduced both lipophilicity and plasma protein binding values.

Scheme 1 Synthesis of HDAC6 ligands with a 2-(difluoromethyl)-1,3,4-oxadiazole-based zinc-binding group.
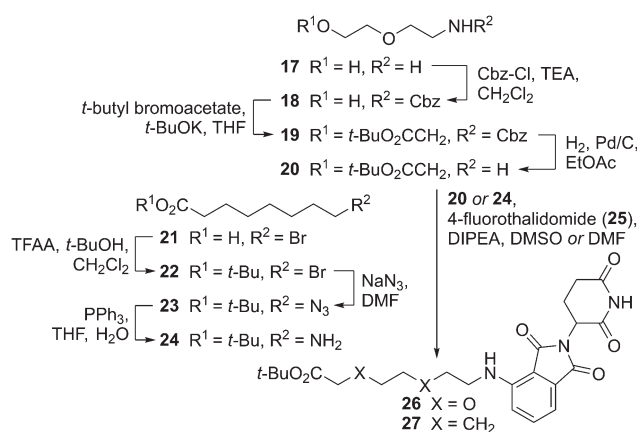
Scheme 2 Synthesis of precursors for cereblon-based PROTACs.

ChemComm

Communication
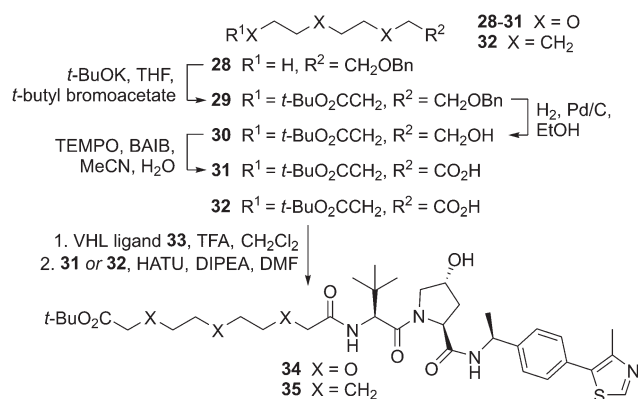
Scheme 3 Synthesis of precursors for VHL-based PROTACs.

PROTACs **1–6** were first assayed for their *in vitro* inhibitory activity against HDAC6 using ZMAL (Z-Lys(Ac)-AMC) as a fluorogenic substrate. The FDA-approved HDACi vorinostat was used as a positive control. All PROTACs demonstrated HDAC6 inhibitory properties with IC_{50} values ranging from 0.590 to 1.86 μM (Table 1). To analyse the selectivity profile of **1–6**, all PROTACs were further screened for their inhibitory potency at HDAC1–4. PROTACs **1–6** were inactive against HDAC1–4 ($IC_{50} > 30$ μM, Table S1, ESI†), thereby confirming their selectivity for HDAC6 over HDAC1–4.

In order to investigate whether the PROTACs **1–6** are capable of degrading HDAC6, we treated the multiple myeloma cell line MM.1S with 1 μM of each degrader for 24 hours. HDAC6 degradation was subsequently determined by western blot analysis. As summarised in Table 1 and Fig. 2A, all compounds demonstrated a pronounced degradation of HDAC6. The most substantial degradation was achieved by compound **1** from the CRBN-recruiting series, whereas compound **4** displayed the

highest reduction of HDAC6 levels among the VHL-recruiting PROTACs. Consequently, compounds **1** and **4** were selected for the following in-depth biological evaluation.

In the first step, MM.1S cells were incubated for 24 hours with several PROTAC concentrations to determine the half-degrading concentrations ($DC_{50,24h}$) of both degraders (Fig. S4, ESI†). Notably, albeit both compounds displayed only moderate inhibitory activity against HDAC6 (Table 1), **1** ($DC_{50,24h} = 131$ nM) and **4** ($DC_{50,24h} = 171$ nM) reduced HDAC6 levels with DC_{50} values in the low triple-digit nanomolar concentration range. Expectedly, **1** and **4** showed a hook effect at 10 μM (Fig. S5, ESI†). To exclude possible cytotoxic effects of the PROTACs, cell viability of MM.1S cells was detected by CellTiter-Glo 2.0 luminescent cell viability assay, confirming that neither **1** nor **4** caused any considerable reduction in cell viability (Fig. 2B). Additional experiments were conducted to investigate the selectivity profile of both PROTACs (Fig. 2C). To this end, HDAC1 was selected as a representative class I and HDAC4 as a representative class IIa isoform. Although both compounds degraded HDAC6 remarkably, they had no impact on HDAC1 and 4 levels. To further confirm the HDAC6 selectivity, western blot analyses of acetylated histone H3 (a marker of reduced HDAC1–3 activity) and acetylated α-tubulin (a marker of reduced HDAC6 activity) were performed. In good agreement with the results of the fluorogenic enzyme assay (Table S1, ESI†), the degraders **1** and **4** led to selective upregulation of acetyl-α-tubulin and caused no hyperacetylation of histone H3. Consequently, these results verify the potency and HDAC6 selectivity of both PROTACs.

To confirm that degradation of HDAC6 is mediated by ternary complex formation, MM.1S cells were pretreated with the CRBN-ligand pomalidomide or the VHL-ligand VH298, followed by the addition of the PROTACs. As expected, degradation of HDAC6 induced by **1** (CRBN-recruiting) was blocked by pomalidomide, while VH298 only prevented the degradation

Table 1 Final assembly of HDAC6-addressing PROTACs and overview on their biological activities and physicochemical properties

Cmpd	Aminomethyl position	X	HDAC6 IC_{50} (μM)	D_{max} [a] (%)	M_r (g mol^{-1})	$e \log D_{7.4}$ [b]	PPB (%) [c]	TPSA (Å^2) [d]	NRotB [e]
1	*meta*	O	0.643 ± 0.204	84	734	2.5	88	220	18
2	*meta*	CH$_2$	0.590 ± 0.133	17	730	3.3	95	201	18
3	*para*	O	1.86 ± 0.250	70	734	2.4	91	220	18
4	*meta*	O	0.686 ± 0.113	74	963	2.6	90	273	28
5	*meta*	CH$_2$	1.68 ± 0.255	43	957	3.3	95	246	28
6	*para*	O	1.59 ± 0.123	55	963	2.6	90	273	28

[a] D_{max}, maximal degradation. [b] Experimental distribution coefficient at pH 7.4. [c] Experimentally determined percentage of compound bound to human serum albumin. [d] Topological polar surface area. [e] Number of rotatable bonds.
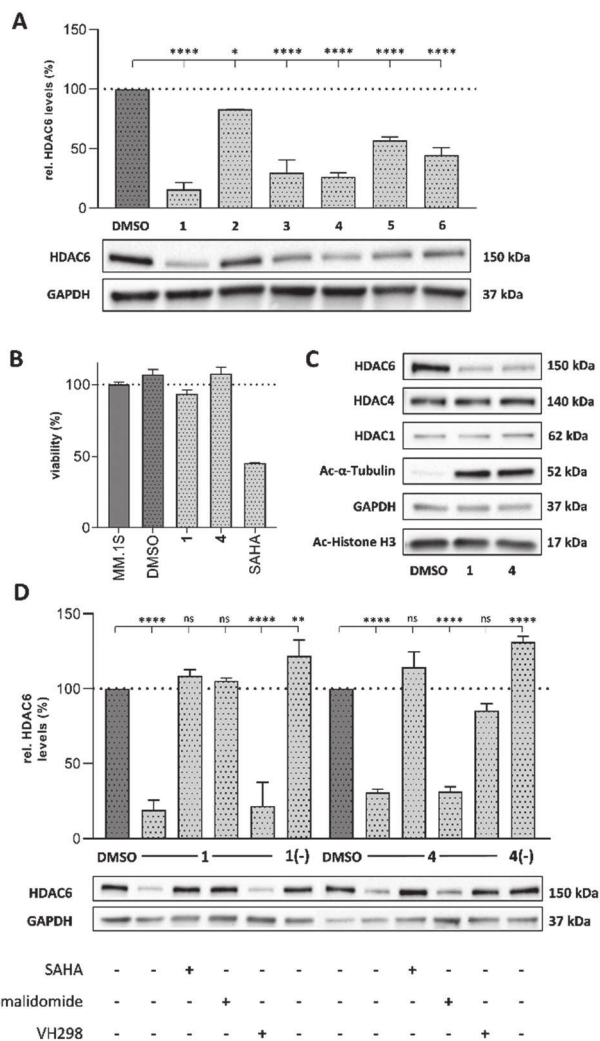
Fig. 2 Characterisation of non-hydroxamate HDAC6 PROTACs. (A) Western blot analysis of whole cell lysates of MM.1S cells after treatment with compounds **1–6** at 1 μM for 24 h or with vehicle control (DMSO). (B) Investigation of potential cytotoxicity mediated by PROTACs **1** and **4** at a concentration of 1 μM and after an incubation time of 72 h in MM.1S cells. SAHA (1 μM) was used as cytotoxic control. (C) Protein levels of HDAC1, HDAC4, HDAC6, acetyl-α-tubulin, acetyl-histone H3 and GAPDH were quantified by western blot analysis after an incubation of 24 h with respective PROTACs **1** and **4** (1 μM) in comparison to vehicle control (DMSO). (D) MM.1S cells were pre-treated with pomalidomide (10 μM), VH298 (10 μM), SAHA (1 μM) or vehicle control (DMSO) for 30 min and then treated for 24 h with 1 μM of **1** and **4**, respectively. Statistical analysis was performed by using one-way ANOVA followed by Dunnett's test. Statistical significance was indicated with asterisks (* = $p < 0.05$; ** = $p < 0.01$; *** = $p < 0.001$; **** = $p < 0.0001$).

activity of **4** (VHL-recruiting). Similarly, pretreatment with vorinostat (SAHA) rescued HDAC6 from degradation (Fig. 2D). To provide further evidence that HDAC6 degradation relied on ternary complex formation, we synthesised the non-degrading controls **1**(−) and **4**(−) by methylation of the glutarimide or by inversion of the stereochemistry at the hydroxyproline to

abolish the binding to the respective E3 ligase (see ESI† for structures and synthetic details). As illustrated in Fig. 2D, both control compounds showed no reduction in HDAC6 levels. Finally, rescue experiments with the NEDD8-activating enzyme inhibitor MLN4924 demonstrated that the degradation of HDAC6 occurs *via* the UPS (Fig. S6, ESI†).

In summary, we have designed, synthesised and evaluated the first non-hydroxamate HDAC6 degraders based on a difluoromethyl-1,3,4-oxadiazole warhead as ZBG. Western blot analysis demonstrated that the PROTACs **1** (CRBN-recruiting) and **4** (VHL-recruiting) are capable of degrading HDAC6 in a potent and selective manner. Considering the involvement of HDAC6 in various pathological conditions, the selective HDAC6 degraders reported in this work may be useful pharmacological tools to dissect the function of HDAC6 in cancer and non-oncological diseases.

Conflicts of interest

There are no conflicts to declare.

Notes and references

1 R. Jenke, N. Reßing, F. K. Hansen, A. Aigner and T. Büch, *Cancers*, 2021, **13**, 634.
2 F. Fischer, L. A. Alves Avelar, L. Murray and T. Kurz, *Future Med. Chem.*, 2021, **14**, 143–166.
3 Y. Zhang, S. Kwon, T. Yamaguchi, F. Cubizolles, S. Rousseaux, M. Kneissel, C. Cao, N. Li, H.-L. Cheng, K. Chua, D. Lombard, A. Mizeracki, G. Matthias, F. W. Alt, S. Khochbin and P. Matthias, *Mol. Cell. Biol.*, 2008, **28**, 1688–1701.
4 I. Sosič, A. Bricelj and C. Steinebach, *Chem. Soc. Rev.*, 2022, **51**, 3487–3534.
5 M. Schiedel, D. Herp, S. Hammelmann, S. Swyter, A. Lehotzky, D. Robaa, J. Oláh, J. Ovádi, W. Sippl and M. Jung, *J. Med. Chem.*, 2018, **61**, 482–491.
6 K. Yang, Y. Song, H. Xie, H. Wu, Y. T. Wu, E. D. Leisten and W. Tang, *Bioorg. Med. Chem. Lett.*, 2018, **28**, 2493–2497.
7 H. Wu, K. Yang, Z. Zhang, E. D. Leisten, Z. Li, H. Xie, J. Liu, K. A. Smith, Z. Novakova, C. Barinka and W. Tang, *J. Med. Chem.*, 2019, **62**, 7042–7057.
8 H. Yang, W. Lv, M. He, H. Deng, H. Li, W. Wu and Y. Rao, *Chem. Commun.*, 2019, **55**, 14848–14851.
9 L. Sinatra, J. J. Bandolik, M. Roatsch, M. Sönnichsen, C. T. Schoeder, A. Hamacher, A. Schöler, A. Borkhardt, J. Meiler, S. Bhatia, M. U. Kassack and F. K. Hansen, *Angew. Chem., Int. Ed.*, 2020, **59**, 22494–22499.
10 Y. Xiong, K. A. Donovan, N. A. Eleuteri, N. Kirmani, H. Yue, A. Razov, N. M. Krupnick, R. P. Nowak and E. S. Fischer, *Cell Chem. Biol.*, 2021, **28**, 1514–1527.
11 S. Shen and A. P. Kozikowski, *ChemMedChem*, 2016, **11**, 15–21.
12 A. Frühauf and F.-J. Meyer-Almes, *Molecules*, 2021, **26**, 5151.
13 C. M. Yates, US Pat., 2018/0256572 A1, 2018.
14 Y. Hai and D. W. Christianson, *Nat. Chem. Biol.*, 2016, **12**, 741–747.
15 R. Huisgen, J. Sauer and H. J. Sturm, *Angew. Chem.*, 1958, **70**, 272–273.
16 C. Steinebach, H. Kehm, S. Lindner, L. P. Vu, S. Köpff, Á. L. Mármol, C. Weiler, K. G. Wagner, M. Reichenzeller, J. Krönke and M. Gütschow, *Chem. Commun.*, 2019, **55**, 1821–1824.
17 C. Jacquot, C. M. McGinley, E. Plata, T. R. Holman and W. A. van der Donk, *Org. Biomol. Chem.*, 2008, **6**, 4242–4252.
18 M. Wang, J. Lu, M. Wang, C.-Y. Yang and S. Wang, *J. Med. Chem.*, 2020, **63**, 7510–7528.

<div align="center">

Supplementary Information

</div>

<div align="center">

Development of the first non-hydroxamate selective HDAC6 degraders

</div>

<div align="center">

Tim Keuler,[‡a] Beate König,[‡a] Nico Bückreiß,[‡a] Fabian B. Kraft,[a] Philipp König,[a] Linda Schäker-Hübner,[a] Christian Steinebach,[a] Gerd Bendas,[*a] Michael Gütschow[*a] and Finn K. Hansen[*a]

[a] Pharmaceutical Institute, University of Bonn, 53121 Bonn, Germany.

[‡] These authors contributed equally.

</div>

Content

1. Supplementary Figures, Schemes and Tables

2. Biological Experiments

3. Molecular Docking

4. Physicochemical Experiments

5. Chemical Experiments

1. Supplementary Figures, Schemes and Tables

cmpd 6

IC_{50} HDAC6 = 0.057 µM
IC_{50} HDAC1 > 30 µM

cmpd 9

IC_{50} HDAC6 = 0.038 µM
IC_{50} HDAC1 > 30 µM

cmpd 43

IC_{50} HDAC6 = 0.039 µM
IC_{50} HDAC1 > 30 µM

Figure S1. Selective HDAC6 inhibitors utilizing a 2-(difluoromethyl)-1,3,4-oxadiazole zinc-binding group. Structures and inhibition data taken from patent literature.[1]
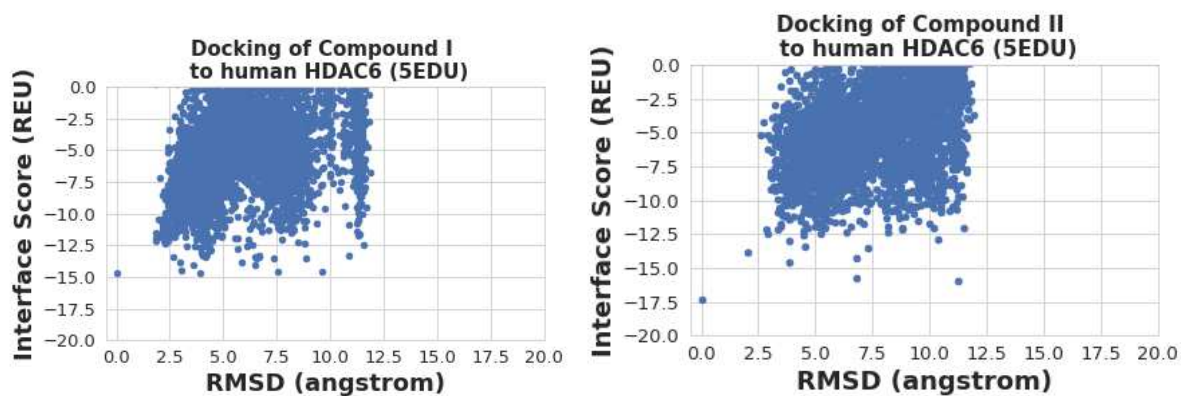
Figure S2. Ligand RMSD vs interface score plots for compound **I** and compound **II**. It was plotted against the models with the best scoring from their respective runs.
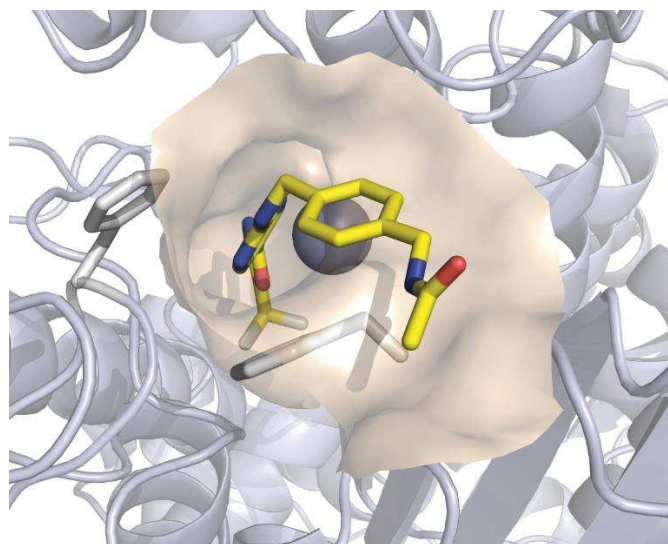
Figure S3. Docking pose of ligand **II** in the CD2 of HDAC6 (PDB: 5EDU).[2] The catalytic Zn^{2+}-ion is shown as gray sphere.
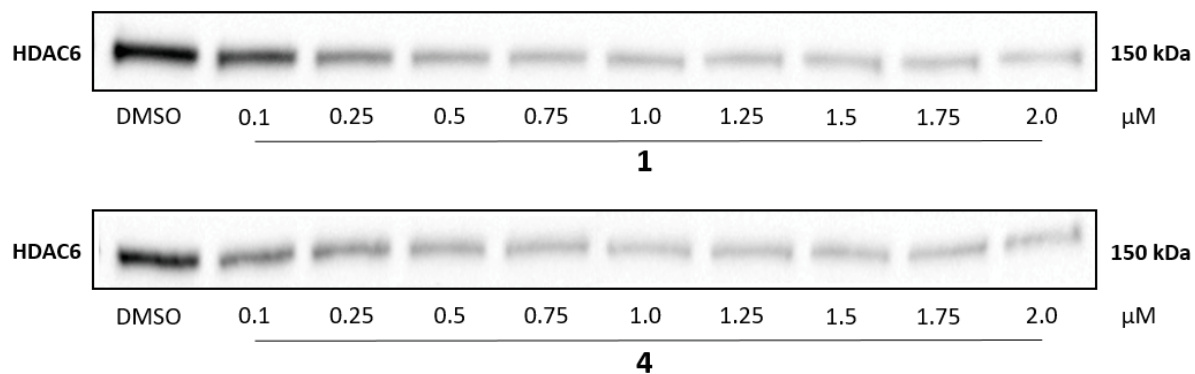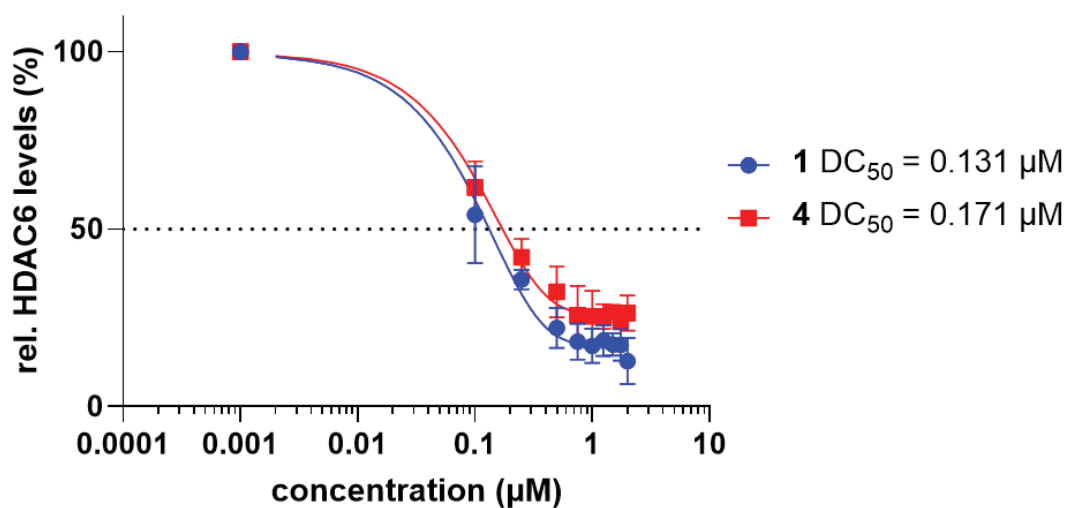
Figure S4. Determination of the half-degrading concentrations (DC_{50}) for PROTACss **1** and **4** in MM.1S cells. Multiple myeloma cells were incubated with several PROTAC concentrations ranging from 0.1 up to 2.0 µM.
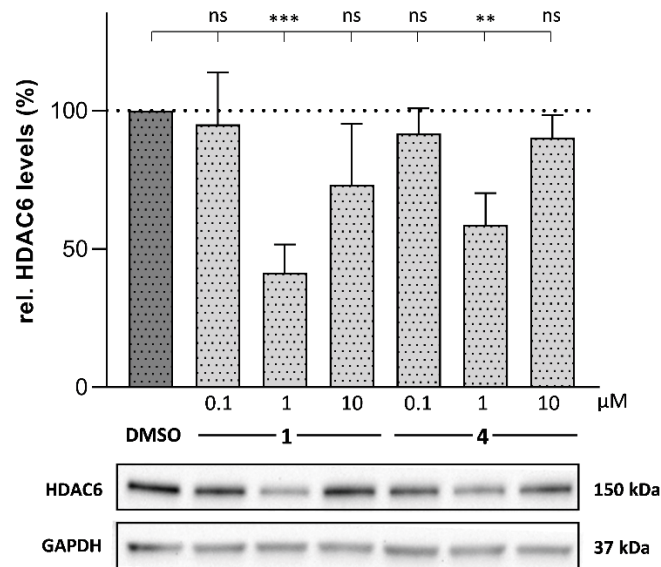
Figure S5. Investigation of concentration dependent degradation of HDAC6 induced by PROTACs **1** and **4**. Western blot analysis of MM.1S cells after treatment with compounds **1** and **4** at 0.1, 1 and 10 µM or with vehicle control (DMSO) for 6 h. At a concentration of 10 µM, a hook effect was observed for both compounds **1** and **4**. Statistical analysis was performed by using one-way ANOVA following Dunnett´s test. Statistical significance was indicated with asterisks (* = $p < 0.05$; ** = $p < 0.01$; *** = $p < 0.001$; **** = $p < 0.0001$).
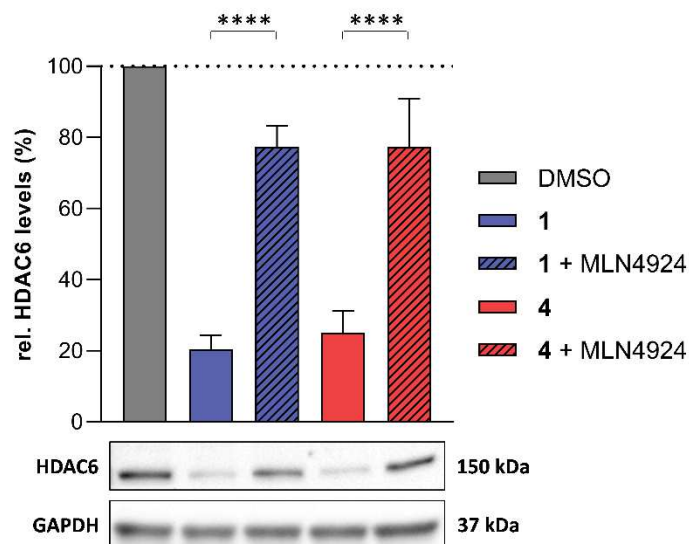
Figure S6. Elucidation of the involvement of the ubiquitin–proteasome system in the degradation of HDAC6 by western blot analysis. MM.1S cells were pre-treated with the NEDD8-activating enzyme inhibitor MLN4924 (1 µM) for 30 min and then treated for 24 h with 1 µM of **1** or **4**. DMSO was used as vehicle control. Statistical analysis was performed by using one-way ANOVA following Dunnett´s test. Statistical significance was indicated with asterisks (* = $p < 0.05$; ** = $p < 0.01$; *** = $p < 0.001$; **** = $p < 0.0001$).
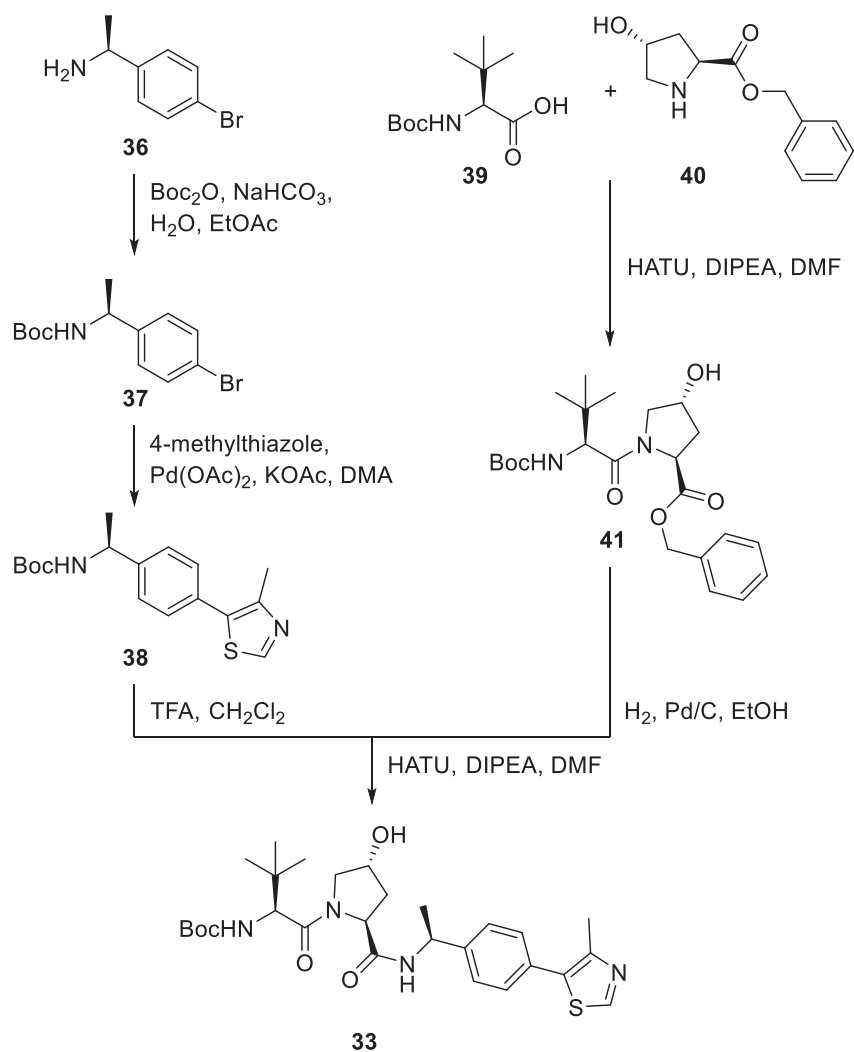
Scheme S1. Synthesis of the VHL ligand **33**.

Table S1. Inhibitory activities (IC_{50}) of PROTACs **1-6** against HDAC1-4 and HDAC6.

cmpd	IC_{50} (μM)				
	HDAC1	HDAC2	HDAC3	HDAC4	HDAC6
1	> 30[a]	> 30[a]	> 30[a]	> 30[a]	0.643 ± 0.204
2	> 30[a]	> 30[a]	> 30[a]	> 30[a]	0.590 ± 0.133
3	> 30[a]	> 30[a]	> 30[a]	> 30[a]	1.86 ± 0.250
4	> 30[a]	> 30[a]	> 30[a]	> 30[a]	0.686 ± 0.113
5	> 30[a]	> 30[a]	> 30[a]	> 30[a]	1.68 ± 0.255
6	> 30[a]	> 30[a]	> 30[a]	> 30[a]	1.59 ± 0.123
vorinostat	0.102 ± 0.003	0.150 ± 0.022	0.077 ± 0.006	> 30[a]	0.041 ± 0.004
TMP-269	n.d.	n.d.	n.d.	0.349 ± 0.059	n.d.

[a] < 30% inhibition at 30 μM; n.d.: not determined.

2. Biological Experiments

2.1. Inhibition Assay for HDAC1-4 and HDAC6

In vitro inhibitory activities against HDAC1-3 and HDAC6 were measured using a previously published protocol.[3] *In vitro* inhibitory activities against HDAC4 were measured using a previously published protocol with slight modifications.[4] For test compounds and controls, serial dilutions of the respective DMSO stock solution in assay buffer (50 mM Tris−HCl, pH 8.0, 137 mM NaCl, 2.7 mM KCl, 1.0 mM $MgCl_2 \cdot 6H_2O$, 0.1 mg/mL BSA) were prepared, and 5.0 μL of this serial dilution were transferred into OptiPlate-96 black microplates (PerkinElmer). In the case of HDAC1-3 and HDAC6, a volume of 35 μL of the fluorogenic substrate ZMAL (Z- Lys(Ac)-AMC,[5] 21.43 μM in assay buffer) and 10 μL enzyme solution were added. In the case of HDAC4, 35 μL of the fluorogenic substrate Boc-Lys(Tfa)-AMC (Bachem, Catalog# 4060676, 42.86 μM in assay buffer) were added, followed by 10 μL of enzyme solution. Human recombinant HDAC1 (BPS Bioscience, Catalog# 50051), HDAC2 (BPS Bioscience, Catalog# 50052), HDAC3/NcoR2 (BPS Bioscience, Catalog# 50003), HDAC4 (BPS Bioscience, Catalog# 50004), or HDAC6 (BPS Bioscience, Catalog# 50006) was applied. The total assay volume of 50 μL (HDAC6 max. 1% DMSO; HDAC1-4 max. 5% DMSO) was incubated at 37 °C for 90 min. Subsequently, 50 μL of trypsin (HDAC1-3 and HDAC6: 0.4 mg/mL; HDAC4: 1.0 mg/mL) in trypsin buffer (50 mM Tris−HCl, pH 8.0, 100 mM NaCl) was added, followed by additional 30 min of incubation at 37 °C. Fluorescence (excitation: 355 nm, emission: 460 nm) was measured using a FLUOstar OPTIMA microplate reader (BMG LABTECH). All compounds were tested at least twice in duplicates and the 50% inhibitory concentration (IC_{50}) was determined by plotting dose response curves and nonlinear regression with GraphPad Prism.

2.2. Cell Culture

The human multiple myeloma cell line MM.1S (CRL-2974) was obtained from ATCC (Manassas, VA, USA). MM.1S cells were cultivated in RPMI 1640 medium supplemented with 10% FBS, 100 IU/mL penicillin, 0.1 mg/mL streptomycin (PAN Biotech GmbH; Aidenbach, Germany) and 1 mM sodium pyruvate (ThermoFisher Scientific Inc.; Waltham, MA, USA) at 37 °C in a 5% CO_2 atmosphere. The semi-adherent cells were detached mechanically by using a cell scraper. The cell line was tested to exclude mycoplasma contamination every two weeks by qPCR.

2.3. Western Blot

MM.1S cells were seeded to cell culture flasks (75 cm²) and cultured for 96 h. Cells were then incubated for 24 h with the respective PROTACs at a concentration of 1 μM. In case of rescue experiments, cells were pre-incubated with the CRBN, VHL or HDAC6 ligands for 30 min before addition of the PROTACs. The next day, cell protein lysates were prepared from cells while incubating them at 4 °C on a shaker with cell extraction buffer (Life Technologies; Carlsbad, CA, USA) for 30 min. Lysed cells were afterwards centrifuged, the supernatant was collected and protein concentrations of the lysates

were quantified by a BCA protein assay kit (ThermoFisher Scientific Inc.). SDS-Page and western blots were conducted as described using stain-free gels.[6] After proteins were transferred to PVDF membranes, western blots were incubated with blocking solution (milk powder-solution 5%) for 1 h at room temperature. Subsequently, mouse anti-HDAC1, rabbit anti-HDAC4, rabbit anti-HDAC6, rabbit anti-acetyl-histone H3, rabbit anti-acetyl-α-tubulin (Cell Signaling Technology; Frankfurt am Main, Germany) or mouse anti-GAPDH (GeneTex; Irvine, USA) antibody solutions were added to membranes, depending on the respective target. Next, HRP-conjugated secondary anti-rabbit (R&D systems; Minneapolis, MN, USA) and anti-mouse (Santa Cruz Biotechnology; Heidelberg, Germany) antibodies were used to quantify the proteins of interest by means of a chemiluminescence reaction. For visualisation and analysis of the western blot, we used the Clarity Western ECL substrate chemiluminescence kit, a ChemiDoc XRS+ imaging acquiring system and Image Lab software v.5.2.1 from BioRad Laboratories GmbH (Munich, Germany). For normalization, stainfree protein normalization and GAPDH as loading control were used.

2.4. Cell Viability Assay

To exclude possible cytotoxic effects of the PROTACs, cell viability of MM.1S cells was determined by using CellTiter-Glo® 2.0 luminescent cell viability assay (Promega; Madison, WI, USA). Cells were seeded in 96-well plates (25.000 tumour cells/well) and incubated with PROTACs for 72 h at a concentration of 1 µM and 10 µM, respectively. FDA-approved HDACi vorinostat (SAHA) was used as a cytotoxic positive control at the same concentrations as PROTACs, and DPBS as a non-cytotoxic negative control. After incubation, 100 µL of CellTiter Glo 2.0 substrate were added to each well. In an ATP-dependent conversion of luciferin by a luciferase, conclusions can be drawn regarding the cytotoxic potential of the compounds. Luminescence readout is directly proportional to the number of viable cells.

2.5. Statistical Analysis

The results are shown as mean ± SD. Statistical analysis was performed by using one-way ANOVA following Dunnett´s test. Statistical significance was indicated with asterisks (* = $p < 0.05$; ** = $p < 0.01$; *** = $p < 0.001$; **** = $p < 0.0001$).

3. Molecular Docking

3.1. Procedure

The crystal structure of human HDAC6 (PDB: 5EDU)[2] was obtained from the Protein Data Bank (PDB, www.rcsb.org). Chain A, the maltose-binding periplasmic protein, and trichosatin A were deleted. All heteroatom records were removed, except for the metal ions (one zinc atom and two potassium atoms). The structure was optimized to the closest local energy minimum using RosettaRelax with coordinate constraints on the backbone and metal ion restraints.[7] Ligand input files for compound **I** and **II** were created with ChemDraw. An initial 3D conformer with hydrogen atoms was constructed in Chem3D and energetically minimized using the MM2 force field, followed by the production of an ensemble of 1000 low-energy conformers with BCL:ConformerGenerator.[8] One conformer was placed in the binding pocket of HDAC6. A constraint file was constructed to ensure binding of the amine of the linker to Ser453.[9] Ligand docking was performed with RosettaLigand for an initial 5000 models. Those models were clustered according to their similarity in their binding mode. The depicted models are the best scoring models from their respective runs.[10-12] Rosetta version 3.12 was used. The executed commands used throughout the modeling process are provided by the authors on demand.

4. Physicochemical Experiments

4.1. Molecular Descriptor Calculations

Predicted values for the topological polar surface area (TPSA) and the number of rotatable bonds were calculated using the web service www.swissadme.ch provided by the Swiss Institute of Bioinformatics.

4.2. HPLC-based Determinations of elog $D_{7.4}$

The determination of the $logD_{7.4}$ values was performed by a chromatographic method as described previously.[13,14] The system was calibrated by plotting the retention times of six different drugs (atenolol, metoprolol, labetalol, diltiazem, triphenylene, permethrin) *versus* their literature known $logD_{7.4}$ values to obtain a calibration line ($R^2 = 0.99$). Subsequently, the mean retention times of the analytes were taken to calculate their $logD_{7.4}$ values with aid of the calibration line.

4.3. Plasma Protein Binding Studies

Plasma protein binding (PPB) was estimated by correlating the logarithmic retention times of the analytes on a CHIRALPAK HSA 50 × 3 mm, 5 µm column with the literature known percentage PPB values (converted into logK values) of the following drugs, warfarin, ketoprofen, budesonide, nizatidine, indomethacin, acetylsalicylic acid, carbamazepine, piroxicam, nicardipine, and cimetidine (for details, see Valko *et al.*[15]). Samples were dissolved in MeCN/DMSO 9:1 to achieve a final concentration of 0.5 mg/mL. The mobile phase A was 50 mM ammonium acetate adjusted to pH 7.4 with aqueous ammonia, while mobile phase B was iPrOH. The flow rate was set to 1.0 mL/min, the UV detector was set to 254 nm, and the column temperature was kept at 30 °C. After injecting 3 µL of the sample, a linear gradient from 100% A to 30% iPrOH in 5.4 min was applied. From 5.4 to 18 min, 30% iPrOH was kept, followed by switching back to 100% A in 1.0 min and a re-equilibration time of 6 min. With the aid of the calibration line ($R^2 = 0.96$), the logK values of new substances were calculated and converted to their %PPB values.

5. Chemical Experiments

5.1. General Information

Chemicals were purchased from ABCR, Acros Organics, BLDpharm, Carl Roth, Fisher Scientific, Fluorochem, Sigma Aldrich, Tokyo Chemical Industry and VWR Chemicals. Thin layer chromatography was carried out with pre-coated silica gel (60 F_{254}) aluminum sheets from Merck. Detection was performed with UV light at 254 and 360 nm or with $AgNO_3$ or ninhydrin staining. Acros Organics silica gel 60 (70–230 mesh) was taken for preparative column chromatography. Preparative silica gel flash column chromatography was performed on an Interchim puriFlash XS520Plus with diode-array detection (DAD) from 200 to 400 nm. Uncorrected melting points were measured on a Büchi 510 oil bath apparatus or on a Büchi Melting Point M-565 apparatus. ESI-MS (LC-MS) analyses for compounds **1-6**, **18-48** and the chemical negative controls **1(-)** and **4(-)** respectively, were carried out on an API 2000 mass spectrometer coupled with an Agilent HPLC HP 1100 using an EC50/2 Nucleodur C18 Gravity 3 µm column or on an Agilent Infinity Lab LC/MSD-system coupled with an Agilent HPLC 1260 Infinity II using an EC50/2 Nucleodur C18 Gravity 3 µm column. The purity of synthesized compounds was determined by HPLC-DAD. HPLC measurements for compounds **15** and **16** were performed on a Thermo Fisher Scientific UltiMateTM 3000 UHPLC system with a Nucleodur 100-5 C18 column (250 × 4.6 mm, Macherey Nagel) with a flow rate of 1 mL/min and a temperature of 25 °C with an appropriate gradient. Detection was implemented by UV absorption measurement at a wavelength of λ = 254 nm. Bidest. H_2O (A) and MeCN (B) were used as eluents with an addition of 0.1% TFA for eluent A. Low resolution electrospray ionisation mass spectra (LRMS) were acquired with an Advion expression compact mass spectrometer coupled with an automated Advion TLC plate reader Plate Express. HR-ESI-MS spectra were recorded on a Bruker micrOTOF-Q mass spectrometer coupled with a HPLC Dionex UltiMate 3000 or a LTQ Orbitrap XL. NMR spectra were recorded on a Bruker Avance DRX 500 (500 MHz ^{1}H NMR, 126 MHz ^{13}C NMR) and a Bruker Avance III 600 (600 MHz ^{1}H NMR, 151 MHz ^{13}C NMR). Chemical shifts are given in parts per million (ppm) referring to the signal center using the solvent peaks for reference, DMSO-d_6 (2.49/39.7).

5.2. Preparation of Compounds

$$CbzHN \longrightarrow benzyl \longrightarrow NHBoc$$
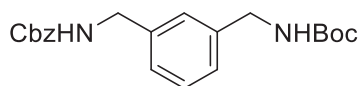
Benzyl (3-(((*tert*-butoxycarbonyl)amino)methyl)benzyl)carbamate (9). *tert*-Butyl (3-(aminomethyl)benzyl)carbamate (**7**, 803 mg, 3.40 mmol, 1.0 eq) was dissolved in THF (34 mL). NaHCO$_3$ (342 mg, 4.08 mmol, 1.2 eq) was added and the mixture was stirred at 0 °C. Subsequently, benzyl chloroformate (0.523 mL, 628 mg, 3.74 mmol, 1.1 eq) was added slowly and the reaction was allowed to stir for 12 h at room temperature. The mixture was quenched with water (60 mL) and extracted with EtOAc (3 × 60 mL). The combined organic layers were washed with brine (45 mL), dried over Na$_2$SO$_4$, filtered and concentrated under reduced pressure. The crude product was purified by silica gel column chromatography using cyclohexane/EtOAc (3+1), as eluent to yield **9** as a white solid (1.22 g, 3.31 mmol).

Yield 97%; mp. 99-102 °C; R_f = 0.34 (cyclohexane/EtOAc (3+1)); **^{1}H NMR** (600 MHz, DMSO-d_6) δ 1.38 (s, 9H), 4.09 (d, J = 6.2 Hz, 2H), 4.18 (d, J = 6.2 Hz, 2H), 5.03 (s, 2H), 7.07 – 7.13 (m, 3H), 7.24 (t, J = 7.5 Hz, 1H), 7.28 – 7.33 (m, 2H), 7.36 (d, J = 6.4 Hz, 4H), 7.78 (t, J = 6.2 Hz, 1H); **^{13}C NMR** (126 MHz, DMSO-d_6) δ 28.4, 43.5, 44.0, 65.5, 77.9, 125.5, 125.7, 127.8, 127.9, 128.3, 128.5, 137.3, 139.8, 140.4, 155.9, 156.5; **LRMS (ESI)** *m/z* [M+H]$^+$ calcd for C$_{21}$H$_{26}$N$_2$O$_4$ 371.2, found 371.1.
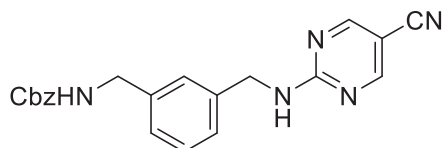
Benzyl (3-(((5-cyanopyrimidin-2-yl)amino)methyl)benzyl)carbamate (11). Benzyl (3-(((*tert*-butoxycarbonyl)amino)methyl)benzyl)carbamate (**9**, 1.22 g, 3.31 mmol, 1.0 eq) was dissolved in CH$_2$Cl$_2$ (26 mL), treated with TFA (7 mL) and stirred for 1 h at room temperature. After evaporation of the solvent, the resulting solid was dissolved in EtOH (11 mL), DIPEA (1.73 mL, 1.28 g, 9.93 mmol, 3.0 eq) and 2-chloropyrimidine-5-carbonitrile (924 mg, 6.62 mmol, 2.0 eq) were added and the reaction stirred at 80 °C for 24 h. The solvent was evaporated under reduced pressure, the residue was dissolved in EtOAc (200 mL), washed with brine (80 mL), dried over Na$_2$SO$_4$, filtered and concentrated under reduced pressure. The crude product was purified by silica gel column chromatography using cyclohexane/EtOAc (2+1) as eluent to afford **11** as a yellow solid (1.21 g, 3.26 mmol).

Yield 98%; mp. 122-128 °C; R_f = 0.26 (cyclohexane/EtOAc (2+1)); **^{1}H NMR** (600 MHz, DMSO-d_6) δ 4.18 (d, J = 6.2 Hz, 2H), 4.54 (d, J = 6.4 Hz, 2H), 5.03 (s, 2H), 7.13 (d, J = 7.6 Hz, 1H), 7.16 (d, J = 7.6 Hz, 1H), 7.19 (d, J = 1.8 Hz, 1H), 7.26 (t, J = 7.6 Hz, 1H), 7.29 – 7.40 (m, 5H), 7.79 (t, J = 6.2 Hz, 1H), 8.66 – 8.71 (m, 2H), 8.82 (t, J = 6.4 Hz, 1H); **^{13}C NMR** (151 MHz, DMSO-d_6) δ 43.9, 44.1, 65.5, 95.6, 117.2, 125.7, 125.8, 125.9, 127.9, 127.9, 128.4, 128.5, 137.3, 139.1, 140.0, 156.5, 161.6, 161.9; **LRMS (ESI)** *m/z* [M+H]$^+$ calcd for C$_{21}$H$_{19}$N$_5$O$_2$ 374.2, found 374.2.
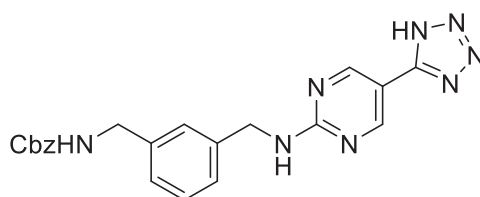
Benzyl (3-(((5-(1*H*-tetrazol-5-yl)pyrimidin-2-yl)amino)methyl)benzyl)carbamate (**13**). Benzyl (3-(((5-cyanopyrimidin-2-yl)amino)methyl)benzyl)carbamate (**11**, 205 mg, 0.550 mmol, 1.0 eq) was dissolved in DMF (2.2 mL). NaN$_3$ (71.5 mg, 1.1 mmol, 2.0 eq), NH$_4$Cl (38.5 mg, 0.720 mmol, 1.3 eq) and LiCl (11.8 mg, 0.280 mmol, 0.5 eq) were added and the reaction mixture was stirred at 100 °C for 18 h. After completion of the reaction, the mixture was quenched with ice water (8 mL) and acidified with 1 M HCl. The precipitated solid was filtered and washed with cold water to obtain the product **13** as a white solid (224 mg, 0.540 mmol).

Yield 98%; mp. 164-169 °C; **^{1}H NMR** (500 MHz, DMSO-d_6) δ 4.18 (d, J = 6.2 Hz, 2H), 4.57 (d, J = 5.9 Hz, 2H), 5.02 (s, 2H), 7.12 (d, J = 7.5 Hz, 1H), 7.18 – 7.25 (m, 3H), 7.25 – 7.39 (m, 5H), 7.78 (t, J = 6.3 Hz, 1H), 8.43 (t, J = 6.5 Hz, 1H), 8.88 (s, 2H); **^{13}C NMR** (126 MHz, DMSO-d_6) δ 44.0, 44.2, 65.5, 108.0, 125.6, 125.7, 125.9, 127.8, 127.9, 128.4, 128.5, 137.3, 139.8, 140.0, 156.5, 156.7, 157.0, 162.8; **LRMS (ESI)** *m/z* [M+H]$^+$ calcd for C$_{21}$H$_{20}$N$_8$O$_2$ 417.2, found 417.2.
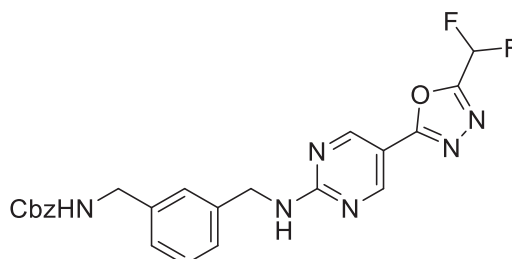
Benzyl (3-(((5-(5-(difluoromethyl)-1,3,4-oxadiazol-2-yl)pyrimidin-2-yl)amino)methyl)benzyl)-carbamate (**15**). Benzyl (3-(((5-(1*H*-tetrazol-5-yl)pyrimidin-2-yl)amino)methyl)benzyl)carbamate (**13**, 454 mg, 1.09 mmol, 1.0 eq) was dissolved in toluene (10 mL). Difluoroacetic anhydride (DFAA, 0.403 mL, 569 mg, 3.27 mmol, 3.0 eq) was added and it was stirred at 70 °C for 18 h. The reaction mixture was concentrated under reduced pressure and purified by silica gel flash column chromatography using a CH$_2$Cl$_2$/MeOH gradient (0% to 5% MeOH) as eluent to yield **15** as a white solid (234 mg, 0.502 mmol).

Yield 46%; mp. 148-152 °C; **^{1}H NMR** (600 MHz, DMSO-d_6) δ 4.17 (d, J = 6.2 Hz, 2H), 4.58 (d, J = 6.4 Hz, 2H), 5.01 (s, 2H), 7.12 (d, J = 7.5 Hz, 1H), 7.19 (d, J = 7.7 Hz, 1H), 7.21 – 7.39 (m, 7H), 7.51 (t, J = 51.4 Hz, 1H), 7.78 (t, J = 6.2 Hz, 1H), 8.71 (t, J = 6.4 Hz, 1H), 8.87 (s, 2H); **^{13}C NMR** (151 MHz, DMSO-d_6) δ 44.3, 44.5, 65.8, 106.8, 107.1 (t, J = 238.3 Hz), 126.1, 126.2, 128.2, 128.2, 128.8, 128.8, 137.6, 139.7, 140.3, 156.8, 157.5, 157.7, 158.0 (t, J = 28.9 Hz), 163.4, 163.6; **^{19}F NMR** (565 MHz, DMSO-d_6) δ -121.1, -121.2; **HRMS (ESI)** *m/z* [M+H]$^+$ calcd for C$_{23}$H$_{20}$F$_2$N$_6$O$_3$ 467.1638, found 467.1610; **HPLC** (95% H$_2$O 5 min, then to 95% MeCN in 5 min, then 100% MeCN to 20 min, 254 nm), t_R = 16.32 min, 99% purity.
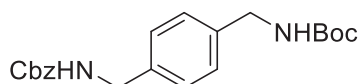
tert-Butyl **(4-((((benzyloxy)carbonyl)amino)methyl)benzyl)carbamate** **(10)**. 1-(N-Boc-aminomethyl)-4-(aminomethyl)benzene (**8**, 236 mg, 1.00 mmol, 1.0 eq.) was dissolved in THF (15 mL). $NaHCO_3$ (84.0 mg, 1.20 mmol, 1.2 eq) was added and the mixture was stirred at 0 °C. Subsequently, benzyl chloroformate (0.154 mL, 188 mg, 1.10 mmol, 1.1 eq) was added slowly and the reaction was allowed to stir for 12 h at room temperature. The mixture was quenched with water (20 mL) and extracted with EtOAc (3 × 20 mL). The combined organic layers were washed with brine (15 mL), dried over Na_2SO_4, filtered and concentrated under reduced pressure. The crude product was purified by silica gel column chromatography using cyclohexane/EtOAc (3+1), as eluent to yield **10** as a white solid (306 mg, 0.830 mmol).

Yield 83%; mp. 129-133 °C; R_f = 0.26 (cyclohexane/EtOAc (3+1)); **^{1}H NMR** (600 MHz, DMSO-d_6) δ 1.38 (s, 9H), 4.08 (d, J = 6.2 Hz, 2H), 4.16 (d, J = 6.2 Hz, 2H), 5.03 (s, 2H), 7.15 – 7.19 (m, 5H), 7.29 – 7.37 (m, 5H), 7.76 (t, J = 6.2 Hz, 1H); **^{13}C NMR** (151 MHz, DMSO-d_6) δ 28.4, 43.3, 43.8, 65.5, 77.9, 127.0, 127.1, 127.9, 127.9, 128.5, 137.3, 138.2, 138.9, 155.9, 156.5; **LRMS (ESI)** m/z [M+H]$^+$ calcd for $C_{21}H_{26}N_2O_4$ 371.2, found 371.1.
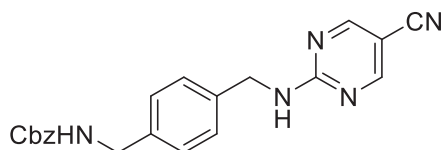
Benzyl **(4-(((5-cyanopyrimidin-2-yl)amino)methyl)benzyl)carbamate** **(12)**. *tert*-Butyl (4-((((benzyloxy)carbonyl)amino)methyl)benzyl)carbamate (**10**, 519 mg, 1.40 mmol, 1.0 eq) was dissolved in CH_2Cl_2 (11 mL), treated with TFA (3 mL) and stirred for 1 h at room temperarture. After evaporation of the solvent, the resulting solid was dissolved in EtOH (6 mL), DIPEA (0.730 mL, 542 mg, 4.20 mmol, 3.0 eq) and 2-chloropyrimidine-5-carbonitrile (390 mg, 2.80 mmol, 2.0 eq) were added and the reaction stirred at 80 °C for 24 h. The solvent was evaporated under reduced pressure, the residue was dissolved in EtOAc (100 mL), washed with brine (40 mL), dried over Na_2SO_4, filtered and concentrated under reduced pressure. The crude product was purified by silica gel column chromatography using cyclohexane/EtOAc (1+1) as eluent to afford **12** as a yellow solid (520 mg, 1.30 mmol).

Yield 92%; mp. 160-164 °C; R_f = 0.32 (cyclohexane/EtOAc (1+1)); **^{1}H NMR** (600 MHz, DMSO-d_6) δ 4.15 (d, J = 6.2 Hz, 2H), 4.51 (d, J = 6.3 Hz, 2H), 5.02 (s, 2H), 7.18 (d, J = 7.9 Hz, 2H), 7.22 (d, J = 8.1 Hz, 2H), 7.25 – 7.34 (m, 1H), 7.32 – 7.37 (m, 4H), 7.75 (t, J = 6.2 Hz, 1H), 8.66 (d, J = 3.0 Hz, 1H), 8.68 (d, J = 3.0 Hz, 1H), 8.78 (t, J = 6.4 Hz, 1H); **^{13}C NMR** (126 MHz, DMSO- d_6) δ 43.7, 43.9, 65.5, 95.5, 117.2, 127.2, 127.2, 127.8, 127.9, 128.5, 137.3, 137.6, 138.5, 156.5, 161.5, 161.8; **LRMS (ESI)** m/z [M+H]$^+$ calcd for $C_{21}H_{19}N_5O_2$ 374.2, found 374.2.
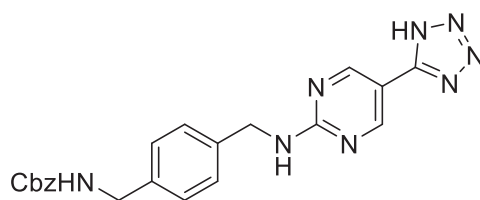
Benzyl (4-(((5-(1_H_-tetrazol-5-yl)pyrimidin-2-yl)amino)methyl)benzyl)carbamate (**14**). Benzyl (4-(((5-cyanopyrimidin-2-yl)amino)methyl)benzyl)carbamate (**12,** 281 mg, 0.750 mmol, 1.0 eq) was dissolved in DMF (3 mL). NaN_3 (97.5 mg, 1.50 mmol, 2.0 eq), NH_4Cl (52.4 mg, 0.980 mmol, 1.3 eq) and LiCl (16.0 mg, 0.380 mmol, 0.5 eq) were added and the reaction mixture was stirred at 100 °C for 18 h. After completion of the reaction, the mixture was quenched with ice water (9 mL) and acidified with 1 M HCl. The precipitated solid was filtered and washed with cold water to obtain the product **14** as a white solid (286 mg, 0.690 mmol).

Yield 92%; mp. 210-216 °C; **¹H NMR** (500 MHz, DMSO- d_6) δ 4.17 (d, J = 6.1 Hz, 2H), 4.56 (d, J = 6.3 Hz, 2H), 5.03 (s, 2H), 7.20 (d, J = 7.9 Hz, 2H), 7.24 – 7.32 (m, 4H), 7.31 – 7.39 (m, 3H), 7.76 (t, J = 6.3 Hz, 1H), 8.41 (t, J = 6.3 Hz, 1H), 8.85 (s, 2H); **¹³C NMR** (151 MHz, DMSO-d_6) δ 43.8, 44.0, 65.6, 108.1, 127.3, 127.3, 127.3, 128.0, 128.0, 128.6, 137.4, 138.3, 138.5, 156.6, 156.8, 157.1, 162.9; **LRMS (ESI)** m/z [M+H]$^+$ calcd for $C_{21}H_{20}N_8O_2$ 417.2, found 417.2.
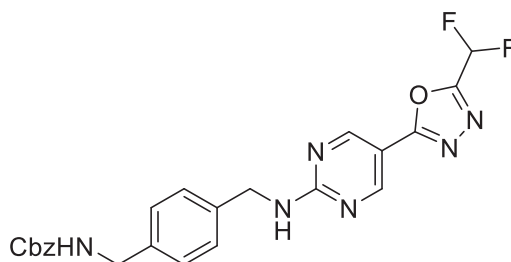
Benzyl (4-(((5-(5-(difluoromethyl)-1,3,4-oxadiazol-2-yl)pyrimidin-2-yl)amino)methyl)benzyl)-carbamate (**16**). Benzyl (4-(((5-(1_H_-tetrazol-5-yl)pyrimidin-2-yl)amino)methyl)benzyl)carbamate (**14,** 286 mg, 0.690 mmol, 1.0 eq) was dissolved in toluene (7 mL). Difluoroacetic anhydride (DFAA, 0.260 mL, 364 mg, 2.07 mmol, 3.0 eq) was added and it was stirred at 70 °C for 18 h. The reaction mixture was concentrated under reduced pressure and purified by silica gel flash column chromatography using a CH_2Cl_2/MeOH gradient (0% to 5% MeOH) as eluent to yield **16** as a white solid (236 mg, 0.506 mmol).

Yield 72%; mp. 174-177 °C; R_f = 0.46 (CH_2Cl_2/MeOH (19+1)); **¹H NMR** (500 MHz, DMSO-d_6) δ 4.17 (d, J = 6.2 Hz, 2H), 4.58 (d, J = 6.3 Hz, 2H), 5.03 (s, 2H), 7.20 (d, J = 7.9 Hz, 2H), 7.27 (d, J = 7.9 Hz, 2H), 7.28 – 7.39 (m, 5H), 7.50 (t, J = 51.6 Hz, 1H), 7.76 (t, J = 6.1 Hz, 1H), 8.70 (t, J = 6.4 Hz, 1H), 8.87 (s, 2H); **¹³C NMR** (126 MHz, DMSO-d_6) δ 43.7, 44.0, 65.5, 106.5, 106.7 (t, J(C,F) = 237.6 Hz), 127.2, 127.2, 127.8, 127.9, 128.5, 137.3, 137.9, 138.5, 156.5, 157.1, 157.3, 157.7 (t, J(C,F) = 29.4 Hz), 163.1, 163.3; **¹⁹F NMR** (565 MHz, DMSO-d_6) δ -121.1, -121.2; **HRMS (ESI)** m/z [M+H]$^+$ calcd for $C_{23}H_{20}F_2N_6O_3$ 467.1638, found 467.1635; **HPLC** (95% H_2O 5 min, then to 95% MeCN in 5 min, then 100% MeCN to 20 min, 254 nm), t_R = 12.77 min, 98% purity.
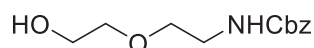
Compound **18** was synthesized as described.[16]
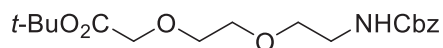
Compound **19** was synthesized as described.[16]
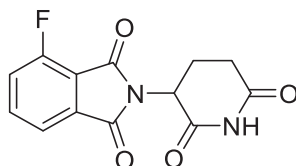
2-(2,6-Dioxopiperidin-3-yl)-4-fluoroisoindoline-1,3-dione (25). This compound was synthesized similar to a previously reported procedure.[17] 3-Fluorophthalic anhydride (1.24 g, 7.5 mmol) and 3-aminoglutarimide × HCl (0.82 g, 5 mmol) were put in a flask. A solution of sodium acetate (492 mg, 6 mmol) in glacial acetate (20 mL) was added and the reaction mixture was refluxed for 4 h. The reaction mixture was allowed to cool to room temperature and was then poured onto H_2O (100 mL). The precipitate was collected, washed with H_2O (3 × 5 mL) and petroleum ether (3 × 5 mL) and it was dried under high vacuum to yield **25** as a light purple solid (1.00 g, 3.62 mmol).

Yield 72%; R_f = 0.67 (petroleum ether/EtOAc (1+2)); mp. > 230 °C, lit.[17] mp. 236-238 °C; **^{1}H NMR** (600 MHz, DMSO-d_6) δ 2.04 – 2.10 (m, 1H), 2.51 – 2.57 (m, 1H), 2.58 – 2.64 (m, 1H), 2.85 – 2.93 (m, 1H), 5.15 (dd, J = 12.9, 5.4 Hz, 1H), 7.73 (d, J = 8.7 Hz, 1H), 7.79 (d, J = 7.3 Hz, 1H), 7.92 – 7.97 (m, 1H), 11.13 (s, 1H); **^{13}C NMR** (151 MHz, DMSO-d_6) δ 21.8 , 30.9 , 49.1 , 117.0 (d, ^2J (C,F) = 12.5 Hz), 120.0 (d, ^4J (C,F) = 2.8 Hz), 123.0 (d, ^2J (C, F) = 19.6 Hz), 133.4 , 138.0 (d, ^3J (C,F) = 7.7 Hz), 156.8 (d, ^1J (C,F) = 262.3 Hz), 163.9 , 166.1 (d, ^3J (C,F) = 2.6 Hz), 169.6, 172.7; **LC-MS (ESI)** (90% H_2O + 2 mM NH_4OAc to 100% MeCN in 10 min, then 100% MeCN to 20 min, DAD 220-500 nm), t_R = 6.99 min, 100% purity, m/z [M+H]$^+$ calcd for $C_{13}H_9FN_2O_4$ 277.1, found 277.0.
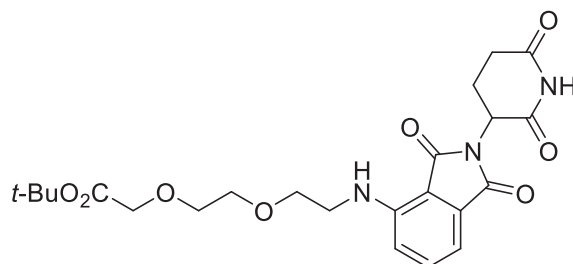
***tert*-Butyl 2-(2-(2-((2-(2,6-dioxopiperidin-3-yl)-1,3-dioxoisoindolin-4-yl)amino)ethoxy)ethoxy)-acetate (26).** This compound was synthesized similar to a previously reported procedure.[18] The orthogonally protected linker *tert*-butyl 3-oxo-1-phenyl-2,7,10-trioxa-4-azadodecan-12-oate (**19**, 1.06 g, 3 mmol) was dissolved in dry EtOAc (30 mL) and treated with 10% m/m Pd/C. The mixture was

stirred under H_2 (1 atm, balloon) for 18 h. The mixture was filtered through celite and the filtrate was concentrated. The residue, compound **20**, was taken up in dry DMSO (30 mL). DIPEA (0.78 g, 6 mmol) and 2-(2,6-dioxopiperidin-3-yl)-4-fluoroisoindoline-1,3-dione (**25**, 0.83 g, 3 mmol) were added. The reaction mixture was stirred at 90 °C for 18 h. It was allowed to cool to room temperature. Then it was poured onto half-saturated brine (300 mL) and it was extracted with EtOAc (2 × 150 mL). The combined organic layers were washed with 5% aqueous LiCl solution (150 mL) and brine (150 mL), dried over Na_2SO_4, filtered and concentrated. The crude product was purified by silica gel column chromatography using a gradient from petroleum ether/EtOAc (1+1) to petroleum ether/EtOAc (1+2) to yield **26** as a yellow solid (581 mg, 1.22 mmol).

Yield 41%; R_f = 0.20 (petroleum ether/EtOAc (1+1)); mp. 66-68 °C, lit.[17] mp. 66-68 °C; **¹H NMR** (600 MHz, DMSO-d_6) δ 1.41 (s, 9H), 2.00 – 2.05 (m, 1H), 2.52 – 2.63 (m, 2H), 2.84 – 2.92 (m, 1H), 3.47 (q, J = 5.6 Hz, 2H), 3.59 (s, 4H), 3.63 (t, J = 5.5 Hz, 2H), 3.97 (s, 2H), 5.05 (dd, J = 12.8, 5.4 Hz, 1H), 6.60 (t, J = 5.8 Hz, 1H), 7.04 (d, J = 7.0 Hz, 1H), 7.15 (d, J = 8.6 Hz, 1H), 7.58 (dd, J = 8.5, 7.1 Hz, 1H), 11.07 (s, 1H); **¹³C NMR** (151 MHz, DMSO-d_6) δ 22.1, 27.7, 31.0, 41.7, 48.5, 68.2, 68.9, 69.6, 69.9, 80.6, 109.2, 110.6, 117.4, 132.1, 136.2, 146.4, 167.3, 168.9, 169.3, 170.0, 172.7; **LC-MS (ESI)** (90% H_2O + 2 mM NH_4OAc to 100% MeOH + 2 mM NH_4OAc in 10 min, then 100% MeOH + 2 mM NH_4OAc to 20 min, DAD 220-500 nm), t_R = 10.19 min, 97% purity, m/z [M+H]$^+$ calcd for $C_{23}H_{29}N_3O_8$ 476.2, found 476.2.
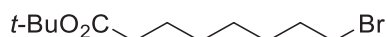
tert-Butyl 8-bromooctanoate (22). This compound was synthesized similar to a previously reported procedure.[19] 8-Bromooctanoic acid (**21**, 4.46 g, 20 mmol) was dissolved in dry CH_2Cl_2 (50 mL) and cooled to 0 °C under nitrogen. Trifluoroacetic anhydride (4.62 g, 22 mmol) was added dropwise at 0 °C and the mixture was allowed to stir for 2.5 h. *tert*-Butanol (5.19 g, 70 mmol) was added dropwise at 0 °C and the mixture was stirred for 1 h at 0 °C. It was allowed to warm to room temperature and was stirred for 16 h. The reaction was quenched by the addition of water (50 mL). The organic phase was separated and the aqueous layer was extracted with CH_2Cl_2 (2 × 50 mL). The combined organic layers were washed with brine (50 mL), dried over Na_2SO_4, filtered and concentrated. The crude product was purified by silica gel column chromatography using petroleum ether/EtOAc (39+1) as eluent to yield **22** as a colourless liquid (4.09 g, 14.6 mmol).

Yield 73%; R_f = 0.43 (petroleum ether/EtOAc (39+1)); **¹H NMR** (500 MHz, DMSO-d_6) δ 1.24 – 1.30 (m, 4H), 1.34 – 1.38 (m, 2H), 1.39 (s, 9H), 1.45 – 1.52 (m, 2H), 1.75 – 1.82 (m, 2H), 2.17 (t, J = 7.3 Hz, 2H), 3.52 (t, J = 6.7 Hz, 2H); **¹³C NMR** (126 MHz, DMSO-d_6) δ 24.4, 27.3, 27.7, 27.7, 28.1, 32.1, 34.7, 35.0, 79.3, 172.2; **LC-MS (ESI)** (90% H_2O + 2 mM NH_4OAc to 100% MeCN in 10 min, then 100% MeCN to 15 min), t_R = 9.35 min, m/z [M+NH$_4$]$^+$ calcd for $C_{12}H_{23}BrO_2$ 296.1, found 296.2.

$t\text{-BuO}_2\text{C}\diagdown\diagup\diagdown\diagup\diagdown\text{N}_3$
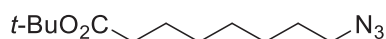
tert-Butyl 8-azidooctanoate (23). *tert*-Butyl 8-bromooctanoate (**22**, 4.05 g, 14.5 mmol) was dissolved in dry DMF (20 mL). Sodium azide (1.13 g, 17.4 mmol) was added in one portion. The reaction mixture was stirred at 80 °C for 24 h. The reaction mixture was concentrated under high vacuum. The residue was diluted with water (30 mL). The aqueous phase was extracted with Et$_2$O (3 × 50 mL). The combined organic layers were washed with brine (50 mL), dried over Na$_2$SO$_4$, filtered and concentrated to yield **23** as a colourless oil (3.31 g, 13.7 mmol).

Yield 94%; R_f = 0.41 (petroleum ether/EtOAc (39+1)); **^{1}H NMR** (500 MHz, DMSO-d_6) δ 1.23 – 1.33 (m, 6H), 1.39 (s, 9H), 1.44 – 1.56 (m, 4H), 2.17 (t, J = 7.3 Hz, 2H), 3.31 (t, J = 6.9 Hz, 2H); **^{13}C NMR** (126 MHz, DMSO-d_6) δ 24.4, 25.9, 27.7, 28.1, 28.1, 28.2, 34.7, 50.5, 79.2, 172.2.

$t\text{-BuO}_2\text{C}\diagdown\diagup\diagdown\diagup\diagdown\diagup\text{NH}_2$
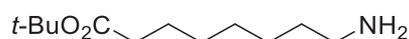
tert-Butyl 8-aminooctanoate (24). *tert*-Butyl 8-azidooctanoate (**23**, 3.26 g, 13.5 mmol) was dissolved in a mixture of THF (20 mL) and H$_2$O (10 mL). Triphenylphosphine (3.89 g, 14.9 mmol) was added in one portion and the reaction mixture was allowed to stir for 18 h at room temperature. The reaction mixture was diluted with H$_2$O (30 mL) and was extracted with CH$_2$Cl$_2$ (3 × 50 mL). The combined organic layers were dried over Na$_2$SO$_4$, filtered and concentrated. The crude product was purified by silica gel column chromatography using CH$_2$Cl$_2$ + 7 N NH$_3$ in MeOH (9+1) as eluent to yield **24** as a colourless liquid (2.47 g, 11.5 mmol).

Yield 85%; R_f = 0.22 (CH$_2$Cl$_2$/7 N NH$_3$ in MeOH (19+1)); **^{1}H NMR** (500 MHz, DMSO-d_6) δ 1.21 – 1.37 (m, 10H), 1.39 (s, 9H), 1.44 – 1.52 (m, 2H), 2.16 (t, J = 7.3 Hz, 2H), one signal (2H) is missing due to proton exchange; **^{13}C NMR** (126 MHz, DMSO-d_6) δ 24.5, 26.2, 27.7, 28.4, 28.6, 33.3, 34.7, 41.6, 79.2, 172.2; **LC-MS (ESI)** (90% H$_2$O + 2 mM NH$_4$OAc to 100% MeCN in 10 min, then 100% MeCN to 15 min), t_R = 5.12 min, m/z [M+H]$^+$ calcd for C$_{12}$H$_{25}$NO$_2$ 216.2, found 216.2, lit.[20] m/z [M+H]$^+$ found 216.2.
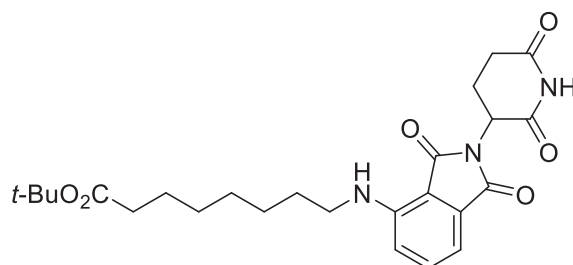
tert-Butyl 8-((2-(2,6-dioxopiperidin-3-yl)-1,3-dioxoisoindolin-4-yl)amino)octanoate (27). *tert*-Butyl 8-aminooctanoate (**24**, 646 mg, 3 mmol) was dissolved in dry DMF (10 mL). DIPEA (595 mg, 4.6 mmol) was added. 2-(2,6-Dioxopiperidin-3-yl)-4-fluoroisoindoline-1,3-dione (**25**, 635 mg, 2.3 mmol) was added and the mixture was stirred at 90 °C for 18 h. The organic layer was concentrated under high

vacuum. The residue was purified by silica gel column chromatography using petroleum ether/EtOAc (2+1) as eluent to yield **27** as a yellow solid (383 mg, 0.81 mmol).

Yield 27%; R_f = 0.24 (petroleum ether/EtOAc (2+1)); mp. 68-70 °C; **^{1}H NMR** (500 MHz, DMSO-d_6) δ 1.25 – 1.35 (m, 6H), 1.38 (s, 9H), 1.45 – 1.52 (m, 2H), 1.53 – 1.60 (m, 2H), 1.99 – 2.06 (m, 1H), 2.16 (t, J = 7.4 Hz, 2H), 2.53 – 2.62 (m, 2H), 2.83 – 2.93 (m, 1H), 5.04 (dd, J = 12.7, 5.4 Hz, 1H), 6.50 (t, J = 6.0 Hz, 1H), 7.02 (d, J = 7.0 Hz, 1H), 7.09 (d, J = 8.6 Hz, 1H), 7.57 (dd, J = 8.5, 7.2 Hz, 1H), 11.06 (s, 1H), one signal (2H) is obscured by the solvent signal; **^{13}C NMR** (126 MHz, DMSO-d_6) δ 22.1, 24.5, 26.1, 27.7, 28.3, 28.3, 28.6, 30.9, 34.7, 41.8, 48.5, 79.3, 109.0, 110.3, 117.1, 132.1, 136.2, 146.4, 167.2, 168.9, 170.0, 172.2, 172.7; **LC-MS (ESI)** (90% H_2O + 2 mM NH_4OAc to 100% MeCN in 10 min, then 100% MeCN to 15 min, DAD 220-600 nm), t_R = 8.46 min, 100% purity, m/z [M-H]$^-$ calcd for $C_{25}H_{33}N_3O_6$ 470.2, found 470.3.
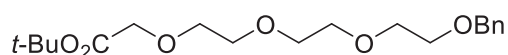
tert-Butyl 1-phenyl-2,5,8,11-tetraoxatridecan-13-oate (29). Potassium butoxide (1.18 g, 10.5 mmol) was dispersed in dry THF (60 mL) at 0 °C. 2-(2-(2-(Benzyloxy)ethoxy)ethoxy)ethan-1-ol (**28**, 2.40 g, 10 mmol) was added to the mixture. The solution was heated to 40 °C for 30 min. Afterwards the reaction was cooled to 0 °C. _tert_-Butyl 2-bromoacetate (1.95 g, 10 mmol) was added. The reaction mixture was stirred for 1 h at 0 °C. The mixture was allowed to warm to room temperature and was stirred for 18 h. The reaction mixture was partitioned between water (100 mL) and EtOAc (100 mL). The organic layer was separated. The aqueous phase was extracted with EtOAc (2 × 100 mL). The combined organic layers were washed with brine (100 mL), dried over Na_2SO_4, filtered and concentrated. The residue was purified by silica gel column chromatography using a gradient from petroleum ether/EtOAc (4+1) to petroleum ether/EtOAc (2+1) to yield **29** as a colourless oil (1.21 g, 3.41 mmol).

Yield 34%; R_f = 0.30 (petroleum ether/EtOAc (2+1)); **^{1}H NMR** (500 MHz, DMSO-d_6) δ 1.42 (s, 9H), 3.51 – 3.57 (m, 12H), 3.97 (s, 2H), 4.49 (s, 2H), 7.25 – 7.37 (m, 5H); **^{13}C NMR** (126 MHz, DMSO-d_6) δ 27.7, 68.1, 69.1, 69.7, 69.7, 69.8, 69.8, 72.0, 80.6, 127.3, 127.4, 128.1, 138.5, 169.3, one signal is missing due to overlapping peaks; **LC-MS (ESI)** (90% H_2O + 2 mM NH_4OAc to 100% MeOH + 2 mM NH_4OAc in 10 min, then 100% MeOH + 2 mM NH_4OAc to 20 min), t_R = 11.12 min, 90% purity, m/z [M+NH_4]$^+$ calcd for $C_{19}H_{30}O_6$ 372.2, found 372.2.
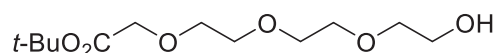
tert-Butyl 2-(2-(2-(2-hydroxyethoxy)ethoxy)ethoxy)acetate (30). This compound was synthesized similar to a previously reported procedure.[21] _tert_-Butyl 1-phenyl-2,5,8,11-tetraoxatridecan-13-oate (**29**, 1.24 g. 3.5 mmol) was dissolved in dry EtOH (10 mL) and treated with 10% m/m Pd/C under H_2 (1 atm, balloon) and was stirred for 18 h. The mixture was diluted with EtOAc (20 mL), filtered through celite and concentrated to yield **30** as a colourless oil.

Quantitative yield; R_f = 0.48 (CH$_2$Cl$_2$/MeOH (9+1)); **^{1}H NMR** (500 MHz, DMSO-d_6) δ 1.41 – 1.43 (m, 9H), 3.40 – 3.43 (m, 2H), 3.47 – 3.59 (m, 10H), 3.97 – 3.99 (m, 2H), 4.51 – 4.55 (m, 1H); **^{13}C NMR** (126 MHz, DMSO-d_6) δ 27.7, 60.2, 68.1, 69.7, 69.7, 69.7, 69.8, 72.3, 80.6, 169.3; **LC-MS (ESI)** (90% H$_2$O + 2 mM NH$_4$OAc to 100% MeOH + 2 mM NH$_4$OAc in 10 min, then 100% MeOH + 2 mM NH$_4$OAc to 20 min), t_R = 8.58 min, m/z [M+NH$_4$]$^+$ calcd for C$_{12}$H$_{24}$O$_6$ 282.2, found 282.2.

t-BuO$_2$C⌒O⌒⌒O⌒⌒O⌒CO$_2$H
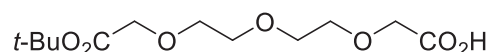
13,13-Dimethyl-11-oxo-3,6,9,12-tetraoxatetradecanoic acid (31). This compound was synthesized similar to a previously reported procedure.[21] *tert*-Butyl 2-(2-(2-(2-hydroxyethoxy)ethoxy)-ethoxy)acetate (**30**, 925 mg, 3.5 mmol) was dissolved in MeCN (6 mL) and water (6 mL). TEMPO (120 mg, 0.77 mmol) was added. (Diacetoxyiodo)benzene (2.48 g, 7.7 mmol) was added portionwise. The reaction mixture was stirred at room temperature for 16 h. It was quenched by the addition of saturated NaHCO$_3$ solution (85 mL) and the aqueous layer was washed with EtOAc (2 × 50 mL). The aqueous phase was acidified with 2 N HCl until pH~1. The mixture was then extracted with EtOAc (2 × 50 mL) and the combined organic layers were dried over Na$_2$SO$_4$, filtered and concentrated. The residue was purified by silica gel column chromatography using a gradient of CH$_2$Cl$_2$ to CH$_2$Cl$_2$/MeOH (19+1) to yield **31** as a colourless oil (460 mg, 1.65 mmol).

Yield 47%; R_f = 0.19 (CH$_2$Cl$_2$/MeOH (9+1)); **^{1}H NMR** (500 MHz, DMSO-d_6) δ 1.42 (s, 9H), 3.52 – 3.59 (m, 8H), 3.98 (s, 2H), 4.01 (s, 2H), one signal (1H) is missing due to proton exchange; **^{13}C NMR** (126 MHz, DMSO-d_6) δ 27.7, 67.6, 68.1, 69.6, 69.7, 69.8, 69.8, 80.6, 169.3, 171.6; **LC-MS (ESI)** (90% H$_2$O + 0,1% AcOH to 100% MeCN + 0,1% AcOH in 10 min, then 100% MeCN +0,1% AcOH to 20 min), t_R = 6.22 min, m/z [M+NH$_4$]$^+$ calcd for C$_{12}$H$_{22}$O$_7$ 296.2, found 296.2.

BocHN⌒(CH$_3$)⌒C$_6$H$_4$⌒Br
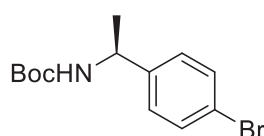
tert-Butyl (_S_)-(1-(4-bromophenyl)ethyl)carbamate (37). This compound was synthesized similar to a previously reported procedure.[22] (_S_)-1-(4-Bromophenyl)ethan-1-amine (**36**, 5.00 g, 25 mmol) and NaHCO$_3$ (1.58 g, 18.8 mmol) were dissolved in H$_2$O (15 mL) and EtOAc (10 mL) and cooled to 0 °C. Boc$_2$O (6.55 g, 30 mmol) was dissolved in EtOAc (3 mL) and was added dropwise. The reaction mixture was stirred for 2 h at 0 °C. The precipitate was collected, resuspended in H$_2$O/hexane (1+1) (25 mL), stirred for further 30 min and was again collected. The residue was washed with hexane (3 × 15 mL) and dried under high vacuum to yield **37** as a white solid (6.90 g, 23 mmol).

Yield 92%; mp. 141-143 °C; R_f = 0.71 (petroleum ether/EtOAc (4+1)); **^{1}H NMR** (600 MHz, DMSO-d_6) δ 1.27 (d, J = 7.0 Hz, 3H), 1.35 (s, 9H), 4.53 – 4.62 (m, 1H), 7.24 (d, J = 8.3 Hz, 2H), 7.39 (d, J = 8.2 Hz, 1H), 7.47 – 7.51 (m, 2H); **^{13}C NMR** (151 MHz, DMSO-d_6) δ 22.6, 28.2, 49.1, 77.7, 119.4, 128.1, 131.0, 144.9, 154.7; **LC-MS (ESI)** (90% H$_2$O + 2 mM NH4OAc to 100% MeCN in 10 min, then 100%

MeCN to 20 min, DAD 205-400 nm), t_R = 9.86 min, 100% purity, m/z [M+H]$^+$ calcd for $C_{13}H_{18}BrNO_2$ 302.1, found 302.0.
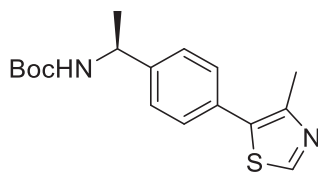
***tert*-Butyl (*S*)-(1-(4-(4-methylthiazol-5-yl)phenyl)ethyl)carbamate (38).** This compound was synthesized similar to a previously reported procedure.[22] *tert*-Butyl (*S*)-(1-(4-bromophenyl)ethyl)carbamate (**37**, 6.00 g, 20 mmol), Pd(OAc)$_2$ (45 mg, 0.2 mmol) and KOAc (3.93 g, 40 mmol) were dissolved in dry DMA (20 mL). 4-Methylthiazole (3.97 g, 40 mmol) was added and the mixture was heated to 130 °C under argon for 4 h. The mixture was allowed to cool to room temperature and was concentrated under high vacuum. The residue was diluted with water (80 mL) and was extracted with CH$_2$Cl$_2$ (3 × 80 mL). The combined organic layers were washed with brine (80 mL), dried over Na$_2$SO$_4$, filtered and concentrated. The residue was purified by silica gel column chromatography using petroleum ether/EtOAc (4+1) as eluent to yield **38** as a white solid (5.34 g, 16.8 mmol).

Yield 84%; mp. 124-126 °C; R_f = 0.15 (petroleum ether/EtOAc (4+1)); **^{1}H NMR** (500 MHz, DMSO-d_6) δ 1.33 (d, *J* = 7.0 Hz, 3H), 1.37 (s, 9H), 2.45 (s, 3H), 4.60 – 4.71 (m, 1H), 7.37 – 7.46 (m, 5H), 8.97 (s, 1H); **^{13}C NMR** (126 MHz, DMSO-d_6) δ 15.9, 22.7, 28.2, 49.2, 77.7, 126.3, 128.7, 129.6, 131.1, 145.3, 147.7, 151.3, 154.8; **LC-MS (ESI)** (90% H$_2$O + 2 mM NH$_4$OAc to 100% MeOH + 2 mM NH$_4$OAc in 10 min, then 100% MeOH + 2 mM NH$_4$OAc to 20 min, DAD 220-400 nm), t_R = 11.11 min, 96% purity, m/z [M+H]$^+$ calcd for $C_{17}H_{22}N_2O_2S$ 319.1, found 318.9.
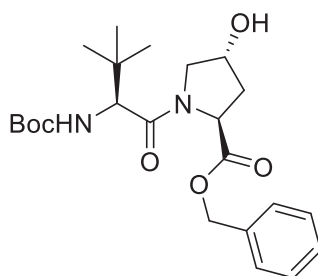
Benzyl (2*S*,4*R*)-1-((*S*)-2-((tert-butoxycarbonyl)amino)-3,3-dimethylbutanoyl)-4-hydroxy-pyrrolidine-2-carboxylate (41). Boc-Tle-OH (**39**, 4.63 g, 20 mmol) was dissolved in dry DMF (18 mL). HATU (8.03 g, 21.1 mmol) and DIPEA (9.05 g, 70 mmol) were added at 0°C and the mixture was stirred for 30 min under nitrogen. H-Hyp-OBzl×HCl (**40**, 5.15 g, 20 mmol) was dissolved in dry DMF (18 mL) and was added to the reaction mixture. The mixture was stirred under nitrogen at room temperature for 18 h. The reaction was quenched by the addition of H$_2$O (50 mL) and was extracted with EtOAc (3 × 50 mL). The combined organic layers were washed with saturated NaHCO$_3$ solution (50 mL) and brine (50 mL), dried over Na$_2$SO$_4$, filtered and concentrated. The residue was purified by

silica gel column chromatography using petroleum ether/EtOAc (1+1) as eluent to yield **41** as a white solid (5.91 g, 13.6 mmol).

Yield 68%; mp. 118-120 °C; R_f = 0.33 (petroleum ether/EtOAc (1+1)); **^{1}H NMR** (500 MHz, DMSO-d_6) δ 0.89 (s, 9H), 1.38 (s, 9H), 1.88 – 1.96 (m, 1H), 2.10 – 2.16 (m, 1H), 3.58 – 3.64 (m, 1H), 3.67 (dd, J = 10.6, 4.1 Hz, 1H), 4.15 (d, J = 9.4 Hz, 1H), 4.34 (br s, 1H), 4.42 (t, J = 8.3 Hz, 1H), 5.06 – 5.15 (m, 2H), 5.19 (d, J = 3.8 Hz, 1H), 6.47 (d, J = 9.4 Hz, 1H), 7.29 – 7.39 (m, 5H); **^{13}C NMR** (126 MHz, DMSO-d_6) δ 26.1, 28.1, 35.1, 37.2, 55.9, 57.7, 58.2, 65.8, 68.7, 78.1, 127.8, 127.9, 128.3, 135.8, 155.3, 170.1, 171.6; **LC-MS (ESI)** (90% H_2O + 2 mM NH_4OAc to 100% MeOH + 2 mM NH_4OAc in 10 min, then 100% MeOH + 2 mM NH_4OAc to 20 min, DAD 200-400 nm), t_R = 11.41 min, 100% purity, m/z [M+H]$^+$ calcd for $C_{23}H_{34}N_2O_6$ 435.2, found 435.4.
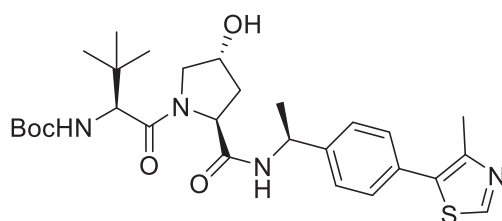
tert-Butyl ((_S_)-1-((2_S_,4_R_)-4-hydroxy-2-(((_S_)-1-(4-(4-methylthiazol-5-yl)phenyl)ethyl)carbamoyl)-pyrrolidin-1-yl)-3,3-dimethyl-1-oxobutan-2-yl)carbamate (33). This compound was synthesized similar to a previously reported procedure.[23] Benzyl (2_S_,4_R_)-1-((_S_)-2-((_tert_-butoxycarbonyl)amino)-3,3-dimethylbutanoyl)-4-hydroxypyrrolidine-2-carboxylate (**41**, 2.17 g, 5 mmol) was dissolved in dry EtOH (50 mL) and treated with 10% m/m Pd/C under H_2 (1 atm, balloon) for 18 h. The reaction mixture was filtered through celite and was concentrated to yield a white solid. _tert_-Butyl (_S_)-(1-(4-(4-methylthiazol-5-yl)phenyl)ethyl)carbamate (**38**, 1.59 g, 5 mmol) was dissolved in dry CH_2Cl_2 (15 mL) and TFA (5 mL) was added. The mixture was stirred for 2 h at room temperature. The mixture was concentrated under high vacuum. The obtained intermediate from the hydrogenolytic deprotection (2_S_,4_R_)-1-((_S_)-2-((_tert_-Butoxycarbonyl)amino)-3,3-dimethylbutanoyl)-4-hydroxy-pyrrolidine-2-carboxylic acid (1.72 g, 5 mmol) was dissolved in dry DMF (5 mL) and HATU (2.09 g, 5.5 mmol) and DIPEA (2.26 g, 17.5 mmol) were added. The concentrated residue of the TFA mediated deprotection was dissolved in dry DMF (5 mL) and was added to the reaction mixture. The reaction mixture was stirred at room temperature under argon for 18 h. The reaction was quenched by the addition of H_2O (25 mL) and was then extracted with EtOAc (3 × 50 mL). The combined organic layers were washed with brine (75 mL), dried over Na_2SO_4, filtered and concentrated. The residue was purified by silica gel column chromatography using EtOAc as eluent to yield **33** as a white solid (1.75 g, 3.21 mmol).

Yield 64%; mp. 208-210 °C; R_f = 0.29 (EtOAc); **^{1}H NMR** (600 MHz, DMSO-d_6) δ 0.93 (s, 9H), 1.36 – 1.40 (m, 12H), 1.75 – 1.82 (m, 1H), 2.00 – 2.05 (m, 1H), 2.45 (s, 3H), 3.52 – 3.63 (m, 2H), 4.14 (d, J = 9.3 Hz, 1H), 4.28 (br s, 1H), 4.45 (t, J = 8.0 Hz, 1H), 4.87 – 4.93 (m, 1H), 5.10 (d, J = 3.6 Hz, 1H), 6.37 (d, J = 9.3 Hz, 1H), 7.36 – 7.39 (m, 2H), 7.42 – 7.44 (m, 2H), 8.38 (d, J = 7.6 Hz, 1H), 8.98 (s, 1H); **^{13}C NMR** (151 MHz, DMSO-d_6) δ 15.9, 22.4, 26.3, 28.2, 35.3, 37.7, 47.7, 56.2, 58.4, 58.5, 68.8, 78.1, 126.3,

128.8, 129.6, 131.1, 144.7, 147.7, 151.4, 155.3, 169.7, 170.6; **LC-MS (ESI)** (90% H$_2$O + 2 mM NH$_4$OAc to 100% MeOH + 2 mM NH$_4$OAc in 10 min, then 100% MeOH + 2 mM NH$_4$OAc to 20 min, DAD 220-400 nm), t_R = 11.32 min, 97% purity, *m/z* [M+H]$^+$ calcd for C$_{28}$H$_{40}$N$_4$O$_5$S 545.3, found 545.1.
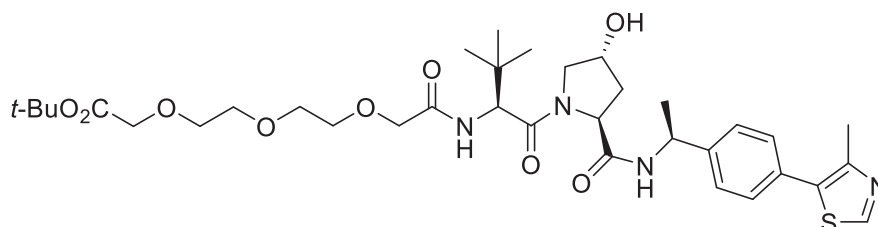
***tert*-Butyl (*S*)-13-((2*S*,4*R*)-4-hydroxy-2-(((*S*)-1-(4-(4-methylthiazol-5-yl)phenyl)ethyl)carbamoyl)-pyrrolidine-1-carbonyl)-14,14-dimethyl-11-oxo-3,6,9-trioxa-12-azapentadecanoate (34).** *tert*-Butyl ((*S*)-1-((2*S*,4*R*)-4-hydroxy-2-(((*S*)-1-(4-(4-methylthiazol-5-yl)phenyl)ethyl)carbamoyl)pyrrolidin-1-yl)-3,3-dimethyl-1-oxobutan-2-yl)carbamate (**33**, 872 mg, 1.6 mmol) was dissolved in dry CH$_2$Cl$_2$ (15 mL) and was treated with TFA (5 mL). The mixture was stirred for 2 h at room temperature. The mixture was concentrated under high vacuum. 13,13-Dimethyl-11-oxo-3,6,9,12-tetraoxatetradecanoic acid (**31**, 445 mg, 1.6 mmol) was dissolved in dry DMF (5 mL). HATU (669 mg, 1.76 mmol) and DIPEA (724 mg, 5.6 mmol) were added under argon. The deprotected VHL-ligand was dissolved in dry DMF (5 mL) and was added to the mixture, containing the activated acid compound. The reaction mixture was allowed to stir at room temperature under argon for 18 h. The reaction mixture was concentrated under high vacuum. The residue was diluted with water (25 mL) and was extracted with EtOAc (3 × 50 mL). The combined organic layers were washed with brine (75 mL), dried over Na$_2$SO$_4$, filtered and concentrated. The crude product was purified by silica gel column chromatography using CH$_2$Cl$_2$/MeOH (19+1) as eluent to yield **34** as a colourless resin (902 mg, 1.28 mmol).

Yield 80%; R_f = 0.24 (CH$_2$Cl$_2$/MeOH (19+1)); **¹H NMR** (600 MHz, DMSO-d_6) δ 0.94 (s, 9H), 1.38 (d, *J* = 7.0 Hz, 3H), 1.42 (s, 9H), 1.75 – 1.82 (m, 1H), 2.01 – 2.07 (m, 1H), 2.45 (s, 3H), 3.53 – 3.65 (m, 10H), 3.96 (d, *J* = 1.9 Hz, 2H), 3.98 (s, 2H), 4.28 (br s, 1H), 4.45 (t, *J* = 8.2 Hz, 1H), 4.55 (d, *J* = 9.5 Hz, 1H), 4.88 – 4.94 (m, 1H), 5.11 (d, *J* = 3.5 Hz, 1H), 7.34 – 7.39 (m, 3H), 7.41 – 7.46 (m, 2H), 8.41 (d, *J* = 7.7 Hz, 1H), 8.98 (s, 1H); **¹³C NMR** (151 MHz, DMSO-d_6) δ 15.9, 22.4, 26.2, 27.7, 35.7, 37.7, 47.7, 55.7, 56.5, 58.5, 68.1, 68.7, 69.5, 69.6, 69.7, 69.9, 70.4, 80.6, 126.3, 128.8, 129.7, 131.1, 144.7, 147.7, 151.4, 168.5, 169.0, 169.3, 170.4; **LC-MS (ESI)** (90% H$_2$O + 2 mM NH$_4$OAc to 100% MeOH + 2 mM NH$_4$OAc in 10 min, then 100% MeOH + 2 mM NH$_4$OAc to 20 min, DAD 220-400 nm), t_R = 11.47 min, 98% purity, *m/z* [M+H]$^+$ calcd for C$_{35}$H$_{52}$N$_4$O$_9$S 705.4, found 705.6.
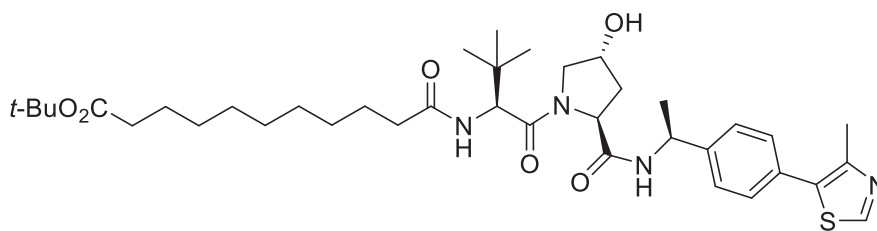
tert-Butyl 11-(((S)-1-((2S,4R)-4-hydroxy-2-(((S)-1-(4-(4-methylthiazol-5-yl)phenyl)ethyl)-carbamoyl)pyrrolidin-1-yl)-3,3-dimethyl-1-oxobutan-2-yl)amino)-11-oxoundecanoate (35). *tert*-Butyl ((S)-1-((2S,4R)-4-hydroxy-2-(((S)-1-(4-(4-methylthiazol-5-yl)phenyl)ethyl)carbamoyl)-pyrrolidin-1-yl)-3,3-dimethyl-1-oxobutan-2-yl)carbamate (**33**, 490 mg, 0.9 mmol) was dissolved in dry CH$_2$Cl$_2$ (5 mL) and was treated with TFA (5 mL). The mixture was stirred for 2 h at room temperature. The mixture was concentrated under high vacuum. 11-(*tert*-Butoxy)-11-oxoundecanoic acid (**32**, 245 mg, 0.9 mmol) was dissolved in dry DMF (5 mL). HATU (376 mg, 0.99 mmol) and DIPEA (407 mg, 3.15 mmol) were added under argon. The deprotected VHL ligand was dissolved in dry DMF (5 mL) and was added to the mixture containing the activated acid compound. The reaction mixture was allowed to stir at room temperature under argon for 3 h. The reaction mixture was concentrated under high vacuum. The residue was diluted with water (50 mL) and was extracted with CH$_2$Cl$_2$ (3 × 50 mL). The combined organic layers were washed with brine (50 mL), dried over Na$_2$SO$_4$, filtered and concentrated. The crude product was purified by silica gel column chromatography using CH$_2$Cl$_2$/MeOH (19+1) as eluent to yield **35** as a colourless resin (441 mg, 0.63 mmol).

Yield 70%; R_f = 0.28 (CH$_2$Cl$_2$/MeOH (9+1)); **^{1}H NMR** (600 MHz, DMSO-d_6) δ 0.93 (s, 9H), 1.22 – 1.25 (m, 10H), 1.37 – 1.39 (m, 12H), 1.43 – 1.51 (m, 4H), 1.77 – 1.83 (m, 1H), 1.97 – 2.03 (m, 1H), 2.06 – 2.13 (m, 1H), 2.14 – 2.18 (m, 2H), 2.21 – 2.28 (m, 1H), 2.45 (s, 3H), 3.57 – 3.64 (m, 2H), 4.26 – 4.30 (m, 1H), 4.42 (t, J = 8.0 Hz, 1H), 4.52 (d, J = 9.3 Hz, 1H), 4.89 – 4.95 (m, 1H), 5.07 (d, J = 3.5 Hz, 1H), 7.38 (d, J = 8.2 Hz, 2H), 7.43 (d, J = 8.2 Hz, 2H), 7.75 (d, J = 9.3 Hz, 1H), 8.34 (d, J = 7.8 Hz, 1H), 8.98 (s, 1H); **^{13}C NMR** (151 MHz, DMSO-d_6) δ 15.9, 22.4, 24.6, 25.4, 26.4, 27.7, 28.3, 28.6, 28.6, 28.7, 34.7, 34.9, 35.2, 37.7, 38.2, 47.7, 56.2, 56.3, 58.5, 68.7, 79.3, 126.4, 128.8, 129.7, 131.1, 144.6, 147.7, 151.4, 169.6, 170.6, 172.0, 172.3; **LC-MS (ESI)** (90% H$_2$O + 2 mM NH$_4$OAc to 100% MeCN in 10 min, then 100% MeCN to 15 min, DAD 220-600 nm), t_R = 8.48 min, 95% purity, *m/z* [M+H]$^+$ calcd for C$_{38}$H$_{58}$N$_4$O$_6$S 699.4, found 699.6.
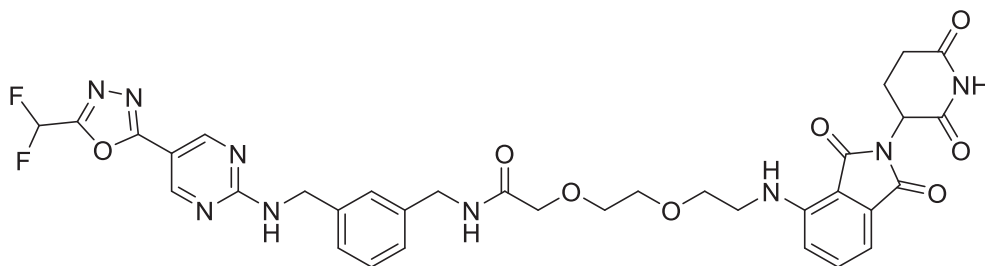
N-(3-(((5-(5-(Difluoromethyl)-1,3,4-oxadiazol-2-yl)pyrimidin-2-yl)amino)methyl)benzyl)-2-(2-(2-((2-(2,6-dioxopiperidin-3-yl)-1,3-dioxoisoindolin-4-yl)amino)ethoxy)ethoxy)acetamide (1). Benzyl (3-(((5-(5-(difluoromethyl)-1,3,4-oxadiazol-2-yl)pyrimidin-2-yl)amino)methyl)benzyl)carbamate (**15**, 117 mg, 0.25 mmol) was dissolved in a mixture of dry EtOH (10 mL) and dry EtOAc (5 mL). The mixture was treated with 10% m/m Pd/C under H_2 (1 atm, balloon) for 18 h. The mixture was filtered through celite and concentrated under high vacuum. *tert*-Butyl 2-(2-(2-((2-(2,6-dioxopiperidin-3-yl)-1,3-dioxoisoindolin-4-yl)amino)ethoxy)ethoxy)acetate (**26**, 119 mg, 0.25 mmol) was dissolved in dry CH_2Cl_2 (5 mL) and was treated with TFA (5 mL) for 2 h at room temperature. The mixture was concentrated under high vacuum. The deprotected acid compound was dissolved in dry DMF (5 mL). DIPEA (97 mg, 0.75 mmol) and HATU (105 mg, 0.28 mmol) were added under argon. The deprotected amine compound was dissolved in dry DMF (5 mL) and was added to the reaction mixture. The reaction mixture was allowed to stir at room temperature under argon for 2 h. The reaction mixture was concentrated under high vacuum. The crude product was purified by silica gel flash column chromatography using a CH_2Cl_2/MeOH gradient (0% to 4% MeOH) to yield **1** as a yellow solid (49 mg, 0.07 mmol).

Yield 27%; mp. 106-110 °C; R_f = 0.31 (CH_2Cl_2/MeOH (19+1)); **^{1}H NMR** (600 MHz, DMSO-d_6) δ 1.99 – 2.05 (m, 1H), 2.52 – 2.62 (m, 2H), 2.82 – 2.90 (m, 1H), 3.40 – 3.43 (m, 2H), 3.58 – 3.61 (m, 6H), 3.93 (s, 2H), 4.28 (d, J = 6.2 Hz, 2H), 4.57 (d, J = 6.3 Hz, 2H), 5.03 (dd, J = 12.8, 5.4 Hz, 1H), 6.56 (t, J = 5.9 Hz, 1H), 7.02 (d, J = 7.0 Hz, 1H), 7.08 – 7.13 (m, 2H), 7.16 – 7.26 (m, 3H), 7.51 (t, J = 51.3 Hz, 1H), 7.53 – 7.57 (m, 1H), 8.15 (t, J = 6.2 Hz, 1H), 8.70 (t, J = 6.4 Hz, 1H), 8.86 (s, 2H), 11.07 (s, 1H); **^{13}C NMR** (151 MHz, DMSO-d_6) δ 22.1, 31.0, 41.6, 41.6, 44.0, 48.5, 68.9, 69.4, 70.0, 70.3, 106.3, 106.5 (t, ^1J (C,F) = 238.6 Hz), 109.2, 110.6, 117.3, 125.5, 125.7, 125.9, 128.2, 132.0, 136.2, 139.2, 139.5, 146.3, 157.0, 157.1, 157.5 (t, ^2J (C,F) = 29.4 Hz), 162.9, 163.1, 167.2, 168.9, 169.2, 170.0, 172.7; **LC-MS (ESI)** (90% H_2O + 2 mM NH_4OAc to 100% MeCN in 10 min, then 100% MeCN to 15 min, DAD 200-600 nm), t_R = 5.84 min, 96% purity, m/z [M+H]$^+$ calcd for $C_{34}H_{33}F_2N_9O_8$ 734.2, found 734.4; **HRMS (ESI)** m/z [M+H]$^+$ calcd for $C_{34}H_{33}F_2N_9O_8$ 734.2493, found 734.2492.
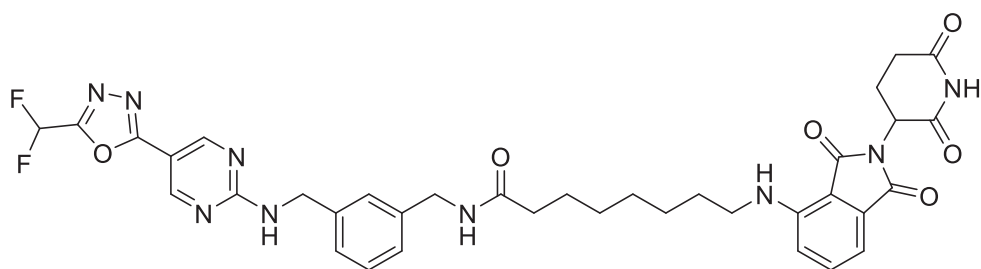
N-(3-(((5-(5-(Difluoromethyl)-1,3,4-oxadiazol-2-yl)pyrimidin-2-yl)amino)methyl)benzyl)-8-((2-(2,6-dioxopiperidin-3-yl)-1,3-dioxoisoindolin-4-yl)amino)octanamide (2). Benzyl (3-(((5-(5-(difluoromethyl)-1,3,4-oxadiazol-2-yl)pyrimidin-2-yl)amino)methyl)benzyl)carbamate (**15**, 93 mg, 0.2 mmol) was dissolved in dry THF (10 mL). The mixture was treated with 10% m/m Pd/C under H_2 (1 atm, balloon) for 18 h. The mixture was filtered through celite and concentrated under high vacuum. *tert*-Butyl 8-((2-(2,6-dioxopiperidin-3-yl)-1,3-dioxoisoindolin-4-yl)amino)octanoate (**27**, 94 mg, 0.2 mmol) was dissolved in dry CH_2Cl_2 (5 mL) and was treated with TFA (5 mL) for 2 h at room temperature. The mixture was concentrated under high vacuum. The deprotected acid compound was dissolved in dry DMF (5 mL). DIPEA (78 mg, 0.6 mmol) and HATU (84 mg, 0.22 mmol) were added under argon. The deprotected amine compound was dissolved in dry DMF (5 mL) and was added to the reaction mixture. The reaction mixture was allowed to stir at room temperature under argon for 2 h. The reaction mixture was concentrated under high vacuum. The crude product was purified by silica gel flash column chromatography using a CH_2Cl_2/MeOH gradient (0% to 4% MeOH) to yield **2** as a yellow solid (36 mg, 0.05 mmol).

Yield 25%; mp. 108-112 °C; R_f = 0.33 (CH_2Cl_2/MeOH (19+1)); **^{1}H NMR** (600 MHz, DMSO-d_6) δ 1.22 – 1.34 (m, 6H), 1.46 – 1.52 (m, 2H), 1.52 – 1.59 (m, 2H), 2.00 – 2.05 (m, 1H), 2.10 (t, J = 7.4 Hz, 2H), 2.52 – 2.62 (m, 2H), 2.84 – 2.91 (m, 1H), 3.25 – 3.30 (m, 2H), 4.22 (d, J = 5.9 Hz, 2H), 4.58 (d, J = 6.3 Hz, 2H), 5.04 (dd, J = 12.8, 5.4 Hz, 1H), 6.50 (t, J = 6.0 Hz, 1H), 7.01 (d, J = 7.0 Hz, 1H), 7.06 – 7.12 (m, 2H), 7.16 – 7.21 (m, 2H), 7.25 (t, J = 7.5 Hz, 1H), 7.52 (t, J = 51.3 Hz, 1H), 7.56 (dd, J = 8.5, 7.1 Hz, 1H), 8.24 (t, J = 6.1 Hz, 1H), 8.71 (t, J = 6.4 Hz, 1H), 8.87 (s, 2H), 11.07 (s, 1H); **^{13}C NMR** (151 MHz, DMSO-d_6) δ 22.1, 25.2, 26.2, 28.4, 28.6, 28.6, 31.0, 35.3, 41.8, 41.9, 44.0, 48.5, 106.3, 106.5 (t, ^1J (C,F) = 238.2 Hz), 109.0, 110.3, 117.1, 125.4, 125.7, 125.8, 128.2, 132.2, 136.2, 139.2, 139.9, 146.4, 157.0, 157.1, 157.5 (t, ^2J (C,F) = 29.5 Hz), 162.9, 163.1, 167.3, 168.9, 170.0, 172.0, 172.8; **LC-MS (ESI)** (90% H_2O + 2 mM NH_4OAc to 100% MeCN in 10 min, then 100% MeCN to 15 min, DAD 220-600 nm), t_R = 6.99 min, 98% purity, m/z [M+H]$^+$ calcd for $C_{36}H_{37}F_2N_9O_6$ 730.3, found 730.5; **HRMS (ESI)** m/z [M+H]$^+$ calcd for $C_{36}H_{37}F_2N_9O_6$ 730.2908, found 730.2907.
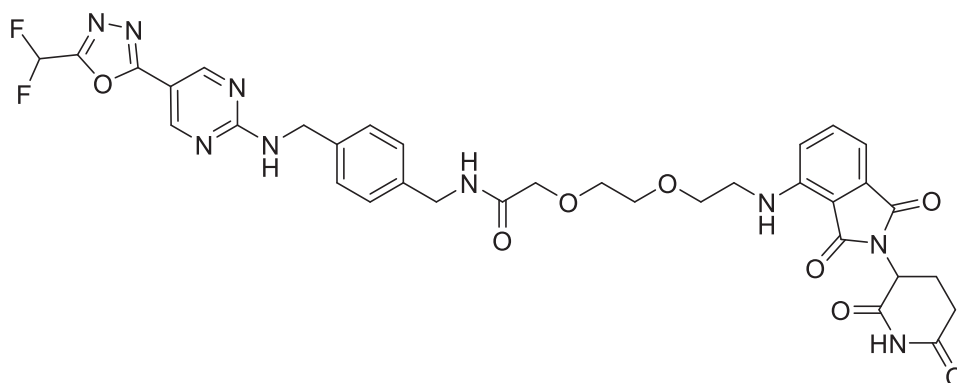
_N_-(4-(((5-(5-(Difluoromethyl)-1,3,4-oxadiazol-2-yl)pyrimidin-2-yl)amino)methyl)benzyl)-2-(2-(2-((2-(2,6-dioxopiperidin-3-yl)-1,3-dioxoisoindolin-4-yl)amino)ethoxy)ethoxy)acetamide (3). Benzyl (4-(((5-(5-(difluoromethyl)-1,3,4-oxadiazol-2-yl)pyrimidin-2-yl)amino)methyl)benzyl)carbamate (**16**, 117 mg, 0.25 mmol) was dissolved in a mixture of dry EtOAc (10 mL), dry EtOH (2 mL) and dry THF (2 mL). The mixture was treated with 10% m/m Pd/C under H_2 (1 atm, balloon) for 4 days. The mixture was filtered through celite and concentrated under high vacuum. _tert_-Butyl 2-(2-(2-((2-(2,6-dioxopiperidin-3-yl)-1,3-dioxoisoindolin-4-yl)amino)ethoxy)ethoxy)acetate (**26**, 119 mg, 0.25 mmol) was dissolved in dry CH_2Cl_2 (5 mL) and was treated with TFA (5 mL) for 2 h at room temperature. The mixture was concentrated under high vacuum. The deprotected acid compound was dissolved in dry DMF (5 mL). DIPEA (97 mg, 0.75 mmol) and HATU (105 mg, 0.28 mmol) were added under argon. The deprotected amine compound was dissolved in dry DMF (5 mL) and was added to the reaction mixture. The reaction mixture was allowed to stir at room temperature under argon for 2 h. The reaction mixture was concentrated under high vacuum. The crude product was purified by silica gel flash column chromatography using a CH_2Cl_2/MeOH gradient (0% to 6% MeOH) to yield **3** as a yellow solid (47 mg, 0.06 mmol).

Yield 26%; mp. 106-110 °C; R_f = 0.61 (CH_2Cl_2/MeOH (9+1)); **^{1}H NMR** (600 MHz, DMSO-d_6) δ 1.99 – 2.05 (m, 1H), 2.52 – 2.62 (m, 2H), 2.83 – 2.91 (m, 1H), 3.41 (q, _J_ = 5.6 Hz, 2H), 3.58 – 3.62 (m, 6H), 3.93 (s, 2H), 4.26 (d, _J_ = 6.1 Hz, 2H), 4.55 (d, _J_ = 6.3 Hz, 2H), 5.03 (dd, _J_ = 12.9, 5.5 Hz, 1H), 6.56 (t, _J_ = 5.9 Hz, 1H), 7.02 (d, _J_ = 7.1 Hz, 1H), 7.09 (d, _J_ = 8.6 Hz, 1H), 7.19 (d, _J_ = 8.0 Hz, 2H), 7.24 (d, _J_ = 7.9 Hz, 2H), 7.51 (t, _J_ = 51.4 Hz, 1H), 7.54 – 7.57 (m, 1H), 8.12 (t, _J_ = 6.2 Hz, 1H), 8.68 (t, _J_ = 6.4 Hz, 1H), 8.86 (s, 2H), 11.07 (s, 1H); **^{13}C NMR** (151 MHz, DMSO) δ 22.1, 30.9, 41.4, 41.6, 43.8, 48.5, 68.8, 69.4, 70.0, 70.3, 106.3, 106.5 (t, ^1J (C,F) = 238.7 Hz), 109.2, 110.6, 117.3, 127.0, 127.2, 132.0, 136.1, 137.7, 137.9, 146.3, 157.0, 157.1, 157.5 (t, ^2J (C,F) = 29.4 Hz), 162.9, 163.1, 167.2, 168.9, 169.1, 170.0, 172.7; **LC-MS (ESI)** (90% H_2O + 2 mM NH_4OAc to 100% MeCN in 10 min, then 100% MeCN to 15 min, DAD 200-600 nm), t_R= 6.01 min, 99% purity, _m/z_ [M+H]$^+$ calcd for $C_{34}H_{33}F_2N_9O_8$ 734.2, found 734.4; **HRMS (ESI)** m/z [M+H]$^+$ calcd for $C_{34}H_{33}F_2N_9O_8$ 734.2493, found 734.2482.

(2*S*,4*R*)-1-((*S*)-15-(*tert*-Butyl)-1-(3-(((5-(5-(difluoromethyl)-1,3,4-oxadiazol-2-yl)pyrimidin-2-yl)amino)methyl)phenyl)-3,13-dioxo-5,8,11-trioxa-2,14-diazahexadecan-16-oyl)-4-hydroxy-*N*-((*S*)-1-(4-(4-methylthiazol-5-yl)phenyl)ethyl)pyrrolidine-2-carboxamide (4). Benzyl (3-(((5-(5-(difluoromethyl)-1,3,4-oxadiazol-2-yl)pyrimidin-2-yl)amino)methyl)benzyl)carbamate (**15**, 117 mg, 0.25 mmol) was dissolved in dry THF (10 mL). The mixture was treated with 10% m/m Pd/C under H_2 (1 atm, balloon) for 18 h. The mixture was filtered through celite and was concentrated under high vacuum. *tert*-Butyl (*S*)-13-((2*S*,4*R*)-4-hydroxy-2-(((*S*)-1-(4-(4-methylthiazol-5-yl)phenyl)ethyl)-carbamoyl)pyrrolidine-1-carbonyl)-14,14-dimethyl-11-oxo-3,6,9-trioxa-12-azapentadecanoate (**34**, 176 mg, 0.25 mmol) was dissolved in dry CH_2Cl_2 (5 mL) and was treated with TFA (5 mL) for 2 h at room temperature. The mixture was concentrated under high vacuum. The deprotected acid compound was dissolved in dry DMF (5 mL). DIPEA (97 mg, 0.75 mmol) and HATU (105 mg, 0.28 mmol) were added under argon. The deprotected amine compound was dissolved in dry DMF (5 mL) and was added to the reaction mixture. The reaction mixture was allowed to stir at room temperature under argon for 2 h. The reaction mixture was concentrated under high vacuum. The crude product was purified by silica gel flash column chromatography using a CH_2Cl_2 /MeOH gradient (0% to 20% MeOH) to yield **4** as a white solid (117 mg, 0.12 mmol).

Yield 49%; mp. 88-92 °C; R_f = 0.30 (CH_2Cl_2/MeOH (9+1)); **^{1}H NMR** (600 MHz, DMSO-d_6) δ 0.93 (s, 9H), 1.37 (d, *J* = 7.0 Hz, 3H), 1.75 – 1.81 (m, 1H), 2.02 – 2.08 (m, 1H), 2.45 (s, 3H), 3.54 – 3.62 (m, 10H), 3.87 – 3.97 (m, 4H), 4.27 – 4.32 (m, 3H), 4.45 (t, *J* = 8.2 Hz, 1H), 4.54 (d, *J* = 9.6 Hz, 1H), 4.59 (d, *J* = 6.3 Hz, 2H), 4.87 – 4.93 (m, 1H), 5.11 (d, *J* = 3.5 Hz, 1H), 7.12 – 7.28 (m, 4H), 7.33 – 7.39 (m, 3H), 7.41 – 7.61 (m, 3H), 8.19 (t, *J* = 6.3 Hz, 1H), 8.41 (d, *J* = 7.6 Hz, 1H), 8.72 (t, *J* = 6.4 Hz, 1H), 8.87 (s, 2H), 8.97 (s, 1H); **^{13}C NMR** (151 MHz, DMSO-d_6) δ 15.9, 22.4, 26.2, 35.7, 37.7, 41.6, 44.0, 47.7, 55.7, 56.5, 58.5, 68.7, 69.6, 69.6, 70.0, 70.3, 70.4, 106.3, 106.6 (t, ^1J (C,F) = 238.8 Hz), 125.5, 125.8, 125.9, 126.3, 128.2, 128.8, 129.7, 131.1, 139.2, 139.5, 144.7, 147.7, 151.4, 157.0, 157.2, 157.5 (t, ^2J (C,F) = 29.3 Hz), 162.9, 163.1, 168.5, 169.0, 169.2, 170.4, one signal is missing due to overlapping signals; **LC-MS (ESI)** (90% H_2O + 2 mM NH_4OAc to 100% MeCN in 10 min, then 100% MeCN to 15 min, DAD 200-600 nm), t_R = 6.22 min, 96% purity, *m/z* [M+H]$^+$ calcd for $C_{46}H_{56}F_2N_{10}O_9S$ 963.4, found 963.5; **HRMS (ESI)** m/z [M+H]$^+$ calcd for $C_{46}H_{56}F_2N_{10}O_9S$ 963.3993, found 963.3990.
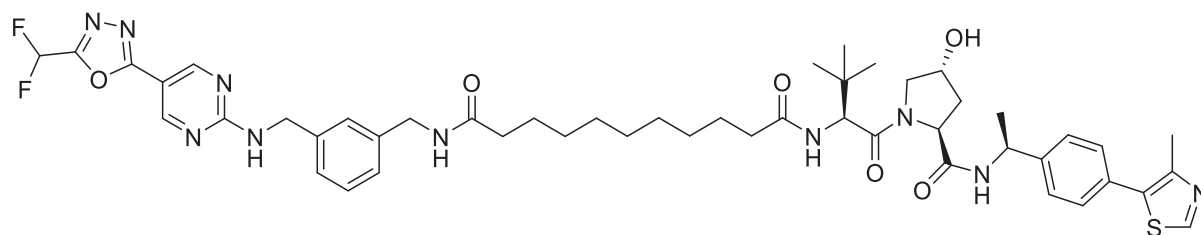
N^1-(3-(((5-(5-(Difluoromethyl)-1,3,4-oxadiazol-2-yl)pyrimidin-2-yl)amino)methyl)benzyl)-N^{11}-((S)-1-((2S,4R)-4-hydroxy-2-(((S)-1-(4-(4-methylthiazol-5-yl)phenyl)ethyl)carbamoyl)pyrrolidin-1-yl)-3,3-dimethyl-1-oxobutan-2-yl)undecanediamide (5). Benzyl (3-(((5-(5-(difluoromethyl)-1,3,4-oxadiazol-2-yl)pyrimidin-2-yl)amino)methyl)benzyl)carbamate (15, 70 mg, 0.15 mmol) was dissolved in dry THF (10 mL). The mixture was treated with 10% m/m Pd/C under H_2 (1 atm, balloon) for 18 h. The mixture was filtered through celite and concentrated under high vacuum. *tert*-Butyl 11-(((S)-1-((2S,4R)-4-hydroxy-2-(((S)-1-(4-(4-methylthiazol-5-yl)phenyl)ethyl)carbamoyl)pyrrolidin-1-yl)-3,3-dimethyl-1-oxobutan-2-yl)amino)-11-oxoundecanoate (35, 105 mg, 0.15 mmol) was dissolved in dry CH_2Cl_2 (5 mL) and was treated with TFA (5 mL) for 2 h at room temperature. The mixture was concentrated under high vacuum. The deprotected acid compound was dissolved in dry DMF (5 mL). DIPEA (58 mg, 0.45 mmol) and HATU (63 mg, 0.17 mmol) were added under argon. The deprotected amine compound was dissolved in dry DMF (5 mL) and was added to the reaction mixture. The reaction mixture was allowed to stir at room temperature under argon for 2 h. The reaction mixture was concentrated under high vacuum. The crude product was purified by silica gel flash column chromatography using a CH_2Cl_2/MeOH (0% to 20% MeOH) to yield 5 as a white solid (29 mg, 0.03 mmol).

Yield 20%; R_f = 0.32 (CH_2Cl_2/MeOH (9+1)); **^{1}H NMR** (500 MHz, DMSO-d_6) δ 0.92 (s, 9H), 1.21 (s, 10H), 1.37 (d, J = 7.0 Hz, 3H), 1.42 – 1.50 (m, 4H), 1.76 – 1.82 (m, 1H), 1.96 – 2.03 (m, 1H), 2.05 – 2.12 (m, 3H), 2.19 – 2.26 (m, 1H), 2.44 (s, 3H), 3.55 – 3.63 (m, 2H), 4.22 (d, J = 5.9 Hz, 2H), 4.25 – 4.29 (m, 1H), 4.42 (t, J = 8.0 Hz, 1H), 4.51 (d, J = 9.3 Hz, 1H), 4.58 (d, J = 6.3 Hz, 2H), 4.87 – 4.94 (m, 1H), 5.05 (d, J = 3.6 Hz, 1H), 7.10 (d, J = 7.4 Hz, 1H), 7.16 – 7.20 (m, 2H), 7.25 (t, J = 7.5 Hz, 1H), 7.35 – 7.38 (m, 2H), 7.40 – 7.62 (m, 3H), 7.72 (d, J = 9.3 Hz, 1H), 8.22 (t, J = 6.0 Hz, 1H), 8.32 (d, J = 7.8 Hz, 1H), 8.69 (t, J = 6.4 Hz, 1H), 8.86 (s, 2H), 8.96 (s, 1H); **^{13}C NMR** (126 MHz, DMSO-d_6) δ 15.9, 22.0, 22.3, 25.2, 25.4, 26.4, 28.6, 28.6, 28.7, 28.8, 34.9, 35.1, 35.3, 37.7, 41.9, 44.0, 47.6, 56.2, 56.3, 58.5, 68.7, 106.3, 106.5 (t, ^1J (C,F) = 238.9 Hz), 125.4, 125.6, 125.8, 126.3, 128.2, 128.8, 129.7, 131.1, 139.2, 139.9, 144.6, 147.7, 151.4, 156.9, 157.1, 157.5 (t, ^2J (C,F) = 29.3 Hz), 162.9, 163.1, 169.6, 170.6, 172.0, 172.0; **LC-MS (ESI)** (90% H_2O + 2 mM NH_4OAc to 100% MeCN in 10 min, then 100% MeCN to 15 min, DAD 200-600 nm), t_R = 7.17 min, 96% purity, m/z [M+H]$^+$ calcd for $C_{49}H_{62}F_2N_{10}O_6S$ 957.5, found 957.7; **HRMS (ESI)** m/z [M+H]$^+$ calcd for $C_{49}H_{62}F_2N_{10}O_6S$ 957.4615, found 957.4615.
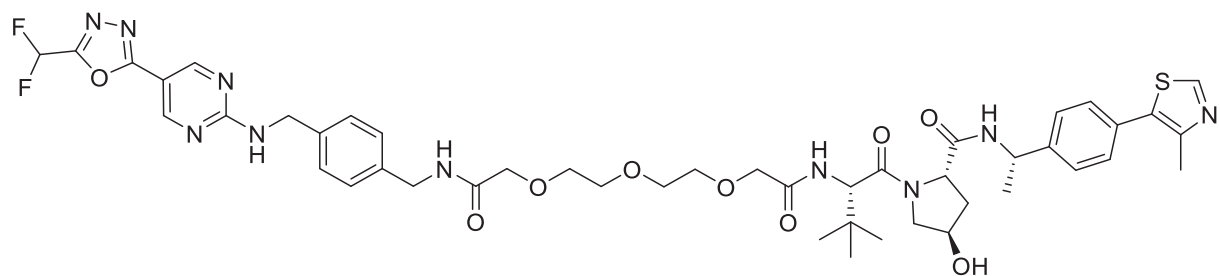
(2S,4R)-1-((S)-15-(*tert*-Butyl)-1-(4-(((5-(5-(difluoromethyl)-1,3,4-oxadiazol-2-yl)pyrimidin-2-yl)amino)methyl)phenyl)-3,13-dioxo-5,8,11-trioxa-2,14-diazahexadecan-16-oyl)-4-hydroxy-*N*-((S)-1-(4-(4-methylthiazol-5-yl)phenyl)ethyl)pyrrolidine-2-carboxamide (6). Benzyl (4-(((5-(5-(difluoromethyl)-1,3,4-oxadiazol-2-yl)pyrimidin-2-yl)amino)methyl)benzyl)carbamate (**16**, 93 mg, 0.2 mmol) was dissolved in dry THF (10 mL). The mixture was treated with 10% m/m Pd/C under H_2 (1 atm, balloon) for 18 h. The mixture was filtered through celite and concentrated under high vacuum. *tert*-Butyl (S)-13-((2S,4R)-4-hydroxy-2-(((S)-1-(4-(4-methylthiazol-5-yl)phenyl)ethyl)carbamoyl)-pyrrolidine-1-carbonyl)-14,14-dimethyl-11-oxo-3,6,9-trioxa-12-azapentadecanoate (**34**, 141 mg, 0.2 mmol) was dissolved in dry CH_2Cl_2 (5 mL) and was treated with TFA (5 mL) for 2 h at room temperature. The mixture was concentrated under high vacuum. The deprotected acid compound was dissolved in dry DMF (5 mL). DIPEA (78 mg, 0.6 mmol) and HATU (84 mg, 0.22 mmol) were added under argon. The deprotected amine compound was dissolved in dry DMF (5 mL) and was added to the reaction mixture. The reaction mixture was allowed to stir at room temperature under argon for 2 h. The reaction mixture was concentrated under high vacuum. The crude product was purified by silica gel flash column chromatography using a CH_2Cl_2/MeOH gradient (0% to 20% MeOH) to yield **6** as a white solid (52 mg, 0.05 mmol).

Yield 27%; mp. 88-92 °C; R_f = 0.30 (CH_2Cl_2/MeOH (9+1)); **^{1}H NMR** (600 MHz, DMSO-d_6) δ 0.93 (s, 9H), 1.37 (d, J = 7.0 Hz, 3H), 1.75 – 1.81 (m, 1H), 2.02 – 2.08 (m, 1H), 2.45 (s, 3H), 3.55 – 3.63 (m, 10H), 3.88 – 3.97 (m, 4H), 4.26 – 4.31 (m, 3H), 4.44 (t, J = 8.2 Hz, 1H), 4.54 (d, J = 9.5 Hz, 1H), 4.57 (d, J = 6.3 Hz, 2H), 4.87 – 4.94 (m, 1H), 5.11 (d, J = 3.5 Hz, 1H), 7.21 (d, J = 8.1 Hz, 2H), 7.27 (d, J = 8.3 Hz, 2H), 7.33 – 7.39 (m, 3H), 7.41 – 7.61 (m, 3H), 8.17 (t, J = 6.2 Hz, 1H), 8.41 (d, J = 7.7 Hz, 1H), 8.70 (t, J = 6.3 Hz, 1H), 8.87 (s, 2H), 8.97 (s, 1H); **^{13}C NMR** (151 MHz, DMSO) δ 15.9, 22.4, 26.2, 35.7, 37.7, 41.4, 43.8, 47.7, 55.7, 56.5, 58.5, 68.7, 69.5, 69.6, 69.6, 70.0, 70.3, 70.4, 106.3, 106.5 (t, ^1J (C,F) = 238.0 Hz), 126.3, 127.1, 127.3, 128.8, 129.7, 131.1, 137.7, 138.0, 144.7, 147.7, 151.4, 157.0, 157.1, 157.5 (t, ^2J (C,F) = 29.3 Hz), 162.9, 163.1, 168.5, 169.0, 169.2, 170.4; **LC-MS (ESI)** (90% H_2O + 2 mM NH_4OAc to 100% MeCN in 10 min, then 100% MeCN to 15 min, DAD 200-600 nm), t_R = 6.20 min, 97% purity, *m/z* [M+H]$^+$ calcd for $C_{46}H_{56}F_2N_{10}O_9S$ 963.4, found 963.7; **HRMS (ESI)** m/z [M+H]$^+$ calcd for $C_{46}H_{56}F_2N_{10}O_9S$ 963.3993, found 963.3991.
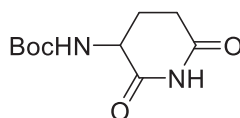
***tert*-Butyl (2,6-dioxopiperidin-3-yl)carbamate (42).** This compound was synthesized similar to a previously reported procedure.[17] Boc-Gln-OH (4.93 g, 20 mmol) was dissolved in dry THF (75 mL). 1,1'-Carbonyldiimidazole (3.89 g, 24 mmol) and DMAP (0.005 g) were added. The reaction mixture was refluxed for 10 h. The mixture was concentrated and the residue was taken up in EtOAc (300 mL). The organic layer was washed with H_2O (75 mL) and brine (75 mL). The organic layer was dried over Na_2SO_4 and loaded onto a pad of silica gel. The product was eluted with EtOAc. The solvent was evaporated to yield **42** as a white solid (3.08 g, 13.5 mmol).

Yield 68%; mp. 192-194 °C, lit.[24] mp. 193.7-194.4 °C; R_f = 0.31 (petroleum ether/EtOAc (1+1)); **¹H NMR** (500 MHz, DMSO-d_6) δ 1.40 (s, 9H), 1.86 – 1.99 (m, 2H), 2.44 – 2.49 (m, 1H), 2.66 – 2.75 (m, 1H), 4.17 – 4.28 (m, 1H), 7.09 (d, J = 8.5 Hz, 1H), 10.70 (s, 1H); **¹³C NMR** (126 MHz, DMSO-d_6) δ 24.4, 28.1, 30.9, 50.4, 78.1, 155.4, 172.4, 172.9; **LC-MS (ESI)** (90% H_2O + 2 mM NH_4OAc to 100% MeCN in 10 min, then 100% MeCN to 15 min, t_R = 3.02 min, *m/z* [M-H]⁻ calcd for $C_{10}H_{16}N_2O_4$ 227.1, found 227.0.
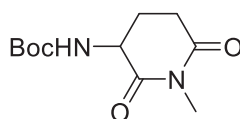
***tert*-Butyl (1-methyl-2,6-dioxopiperidin-3-yl)carbamate (43).** This compound was synthesized similar to a previously reported procedure.[17] *tert*-Butyl (2,6-dioxopiperidin-3-yl)carbamate (**42**, 2.97 g, 13 mmol) was dissolved in dry DMF (30 mL). K_2CO_3 (3.59 g, 26 mmol) and iodomethane (1.85 g, 13 mmol) were added. The reaction mixture was sonicated for 2 h. The mixture was concentrated under high vacuum. The residue was taken up in EtOAc (15 mL). The organic layer was washed with 1 N NaOH (2 × 40 mL), H_2O (40 mL) and brine (40 mL). The organic layer was dried over Na_2SO_4, filtered and concentrated. The crude product was purified by silica gel column chromatography using petroleum ether/EtOAc (2+1) as eluent to yield **43** as a white solid (1.55 g, 6.40 mmol).

Yield 49%; mp. 86-88 °C, lit.[17] mp. 84-86 °C; R_f = 0.41 (petroleum ether/EtOAc (2+1)); **¹H NMR** (500 MHz, DMSO-d_6) δ 1.40 (s, 9H), 1.85 – 2.00 (m, 2H), 2.60 – 2.68 (m, 1H), 2.75 – 2.84 (m, 1H), 2.97 (s, 3H), 4.22 – 4.37 (m, 1H), 7.16 (d, J = 8.6 Hz, 1H); **¹³C NMR** (126 MHz, DMSO) δ 23.5, 26.4, 28.1, 31.1, 50.9, 78.1, 155.4, 172.0, 172.2; **LC-MS (ESI)** (90% H_2O + 2 mM NH_4OAc to 100% MeCN in 10 min, then 100% MeCN to 15 min), t_R = 4.05 min, *m/z* [M-H]⁻ calcd for $C_{11}H_{18}N_2O_4$ 241.1, found 241.1.
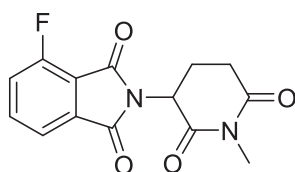
4-Fluoro-2-(1-methyl-2,6-dioxopiperidin-3-yl)isoindoline-1,3-dione (44). This compound was synthesized similar to a previously reported procedure.[17] 3-Fluorophthalic anhydride (1.28 g, 9 mmol) and *tert*-butyl (1-methyl-2,6-dioxopiperidin-3-yl)carbamate (**43**, 1.45 g, 6 mmol) were put in a flask. A solution of sodium acetate (995 mg, 7.2 mmol) in glacial acetate (20 mL) was added and the reaction mixture was refluxed for 6 h. The reaction mixture was allowed to cool to room temperature and was then poured onto H_2O (100 mL). The precipitate was collected, washed with H_2O (3 × 5 mL) and petroleum ether (3 × 5 mL) and it was dried under high vacuum to yield **44** as a light purple solid (1.30 g, 4.48 mmol).

Yield 75%; mp. 200-202 °C, lit.[17] mp. 196-198 °C; R_f = 0.23 (petroleum ether/EtOAc (2+1)); **^{1}H NMR** (500 MHz, DMSO-d_6) δ 2.05 – 2.12 (m, 1H), 2.52 – 2.59 (m, 1H), 2.74 – 2.81 (m, 1H), 2.91 – 3.00 (m, 1H), 3.03 (s, 3H), 5.22 (dd, J = 13.1, 5.4 Hz, 1H), 7.74 (t, J = 8.9 Hz, 1H), 7.79 (d, J = 7.3 Hz, 1H), 7.92 – 7.98 (m, 1H); **^{13}C NMR** (126 MHz, DMSO-d_6) δ 21.0, 26.6, 31.0, 49.6, 117.0 (d, ^2J (C, F) = 12.6 Hz), 120.0 (d, ^4J (C,F) = 3.0 Hz), 123.0 (d, ^2J (C, F) = 19.6 Hz), 133.4, 138.0 (d, ^3J (C,F) = 7.7 Hz), 156.8 (d, ^1J (C,F) = 262.4 Hz), 163.9, 166.0 (d, ^3J (C,F) = 2.9 Hz), 169.3, 171.6; **LC-MS (ESI)** (90% H_2O + 2 mM NH_4OAc to 100% MeCN in 10 min, then 100% MeCN to 15 min, DAD 220-600 nm), t_R = 4.51 min, 100% purity, *m/z* [M+H]$^+$ calcd for $C_{14}H_{11}FN_2O_4$ 291.1, found 291.0.
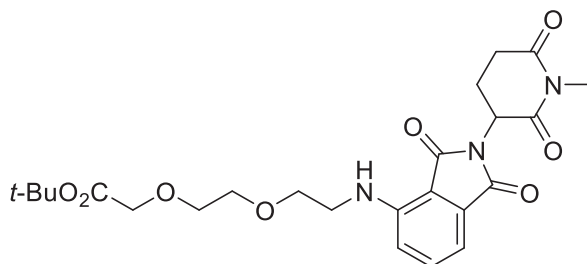
tert-Butyl 2-(2-(2-((2-(1-methyl-2,6-dioxopiperidin-3-yl)-1,3-dioxoisoindolin-4-yl)amino)ethoxy)-ethoxy)acetate (45). The orthogonally protected linker *tert*-butyl 3-oxo-1-phenyl-2,7,10-trioxa-4-azadodecan-12-oate (**19**, 1.06 g, 3 mmol) was dissolved in dry EtOAc (30 mL) and treated with 10% m/m Pd/C. The reaction mixture was stirred under H_2 (1 atm, balloon) for 18 h. The mixture was filtered through celite and the filtrate was concentrated. The residue was redissolved in dry DMSO (30 mL) and DIPEA (0.776 g, 6 mmol) and 4-fluoro-2-(1-methyl-2,6-dioxopiperidin-3-yl)isoindoline-1,3-dione (**44**, 871 mg, 3 mmol) were added. The reaction mixture was stirred at 90 °C for 18 h. The reaction mixture was allowed to cool to room temperature. Then it was poured onto half-saturated brine (300 mL) and it was extracted with EtOAc (2 × 150 mL). The combined organic layers were washed with 5% aqueous LiCl solution (150 mL) and brine (150 mL), dried over Na_2SO_4, filtered and concentrated. The crude

product was purified by silica gel column chromatography using a gradient from petroleum ether/EtOAc (1+1) to petroleum ether/EtOAc (1+2) to yield **45** as a yellowish-green resin (665 mg, 1.36 mmol).

Yield 45%; R_f = 0.33 (petroleum ether/EtOAc (1+1)); **¹H NMR** (500 MHz, DMSO-d_6) δ 1.41 (s, 9H), 2.01 – 2.08 (m, 1H), 2.51 – 2.59 (m, 1H), 2.72 – 2.79 (m, 1H), 2.90 – 2.99 (m, 1H), 3.02 (s, 3H), 3.47 (q, J = 5.6 Hz, 2H), 3.57 – 3.60 (m, 4H), 3.63 (t, J = 5.4 Hz, 2H), 3.97 (s, 2H), 5.12 (dd, J = 13.0, 5.4 Hz, 1H), 6.60 (t, J = 5.9 Hz, 1H), 7.04 (d, J = 7.0 Hz, 1H), 7.15 (d, J = 8.5 Hz, 1H), 7.59 (dd, J = 8.5, 7.1 Hz, 1H); **¹³C NMR** (126 MHz, DMSO-d_6) δ 21.3, 26.5, 27.7, 31.1, 41.7, 49.1, 68.2, 68.8, 69.6, 69.9, 80.6, 109.2, 110.6, 117.4, 132.0, 136.2, 146.4, 167.2, 168.9, 169.3, 169.7, 171.7; **LC-MS (ESI)** (90% H₂O + 2 mM NH₄OAc to 100% MeCN in 10 min, then 100% MeCN to 15 min, DAD 220-600 nm), t_R = 6.83 min, 99% purity, *m/z* [M-H]⁻ calcd for C₂₄H₃₁N₃O₈ 488.2, found 488.2.
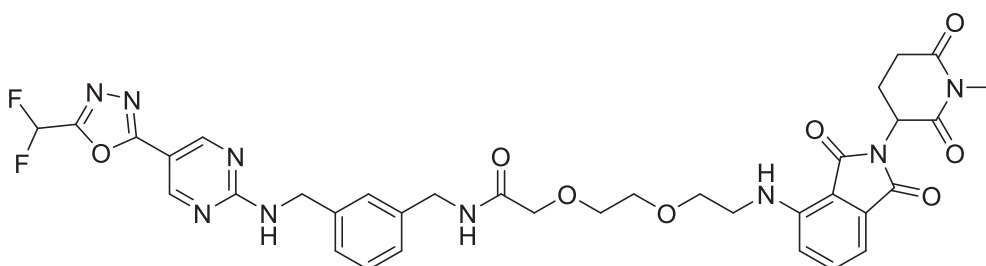
***N*-(3-((((5-(5-(Difluoromethyl)-1,3,4-oxadiazol-2-yl)pyrimidin-2-yl)amino)methyl)benzyl)-2-(2-(2-((2-(1-methyl-2,6-dioxopiperidin-3-yl)-1,3-dioxoisoindolin-4-yl)amino)ethoxy)ethoxy)acetamide (1(-)).** Benzyl (3-((((5-(5-(difluoromethyl)-1,3,4-oxadiazol-2-yl)pyrimidin-2-yl)amino)methyl)benzyl)-carbamate (**15**, 93 mg, 0.2 mmol) was dissolved in dry THF (10 mL) and was treated with 10% m/m Pd/C under H₂ (1 atm, balloon) for 18 h. The mixture was filtered through celite and concentrated under high vacuum. *tert*-Butyl 2-(2-(2-((2-(1-methyl-2,6-dioxopiperidin-3-yl)-1,3-dioxoisoindolin-4-yl)amino)ethoxy)ethoxy)acetate (**45**, 98 mg, 0.2 mmol) was dissolved in dry CH₂Cl₂ (5 mL) and was treated with TFA (5 mL) for 2 h at room temperature. The mixture was concentrated under high vacuum. The deprotected acid compound was dissolved in dry DMF (5 mL). DIPEA (78 mg, 0.6 mmol) and HATU (84 mg, 0.22 mmol) were added under argon. The deprotected amine compound was dissolved in dry DMF (5 mL) and was added. The reaction mixture was allowed to stir at room temperature under argon for 18 h. The mixture was concentrated under high vacuum. The crude product was purified by silica gel flash column chromatography using a CH₂Cl₂/MeOH gradient (0% to 4% MeOH) to yield **1(-)** as a yellow solid (72 mg, 0.096 mmol).

Yield 48%; mp. 82-88 °C; R_f = 0.24 (CH₂Cl₂/MeOH (19+1)); **¹H NMR** (600 MHz, DMSO-d_6) δ 2.00 – 2.06 (m, 1H), 2.51 – 2.57 (m, 1H), 2.72 – 2.77 (m, 1H), 2.88 – 2.96 (m, 1H), 3.01 (s, 3H), 3.41 (q, J = 5.6 Hz, 2H), 3.58 – 3.61 (m, 6H), 3.92 (s, 2H), 4.28 (d, J = 6.2 Hz, 2H), 4.57 (d, J = 6.3 Hz, 2H), 5.10 (dd, J = 13.0, 5.4 Hz, 1H), 6.56 (t, J = 5.9 Hz, 1H), 7.02 (d, J = 7.0 Hz, 1H), 7.08 – 7.13 (m, 2H), 7.16 – 7.26 (m, 3H), 7.51 (t, J = 51.3 Hz, 1H), 7.56 (dd, J = 8.6, 7.1 Hz, 1H), 8.15 (t, J = 6.2 Hz, 1H), 8.70 (t, J = 6.4 Hz, 1H), 8.86 (s, 2H); **¹³C NMR** (151 MHz, DMSO-d_6) δ 21.3, 26.6, 31.1, 41.6, 41.6, 44.0, 49.1, 68.8, 69.4, 70.0, 70.3, 106.3, 106.5 (t, ^1J (C,F) = 238.3 Hz), 109.2, 110.7, 117.4, 125.5, 125.7,

125.9, 128.2, 132.0, 136.2, 139.2, 139.5, 146.3, 157.0, 157.1, 157.5 (t, ^2J (C,F) = 29.3 Hz), 162.9, 163.1, 167.2, 168.9, 169.2, 169.8, 171.7; **LC-MS (ESI)** (90% H_2O + 2 mM NH_4OAc to 100% MeCN in 10 min, then 100% MeCN to 15 min, DAD 220-600 nm), t_R= 6.34 min, 99% purity, *m/z* [M+H]$^+$ calcd for $C_{35}H_{35}F_2N_9O_8$ 748.3, found 748.5; **HRMS (ESI)** *m/z* [M+H]$^+$ calcd for $C_{35}H_{35}F_2N_9O_8$ 748.2649, found 748.2649.
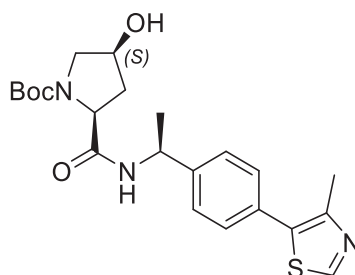
***tert*-Butyl** **(2*S*,4*S*)-4-hydroxy-2-((((*S*)-1-(4-(4-methylthiazol-5-yl)phenyl)ethyl)carbamoyl)-pyrrolidine-1-carboxylate (46).** *tert*-Butyl (*S*)-(1-(4-(4-methylthiazol-5-yl)phenyl)ethyl)carbamate (**38**, 1.27 g, 4 mmol) was dissolved in dry CH_2Cl_2 (5 mL) and was treated with TFA (5 mL) for 2 h at room temperature. The mixture was concentrated under high vacuum. (2*S*,4*S*)-1-(*tert*-Butoxycarbonyl)-4-hydroxypyrrolidine-2-carboxylic acid (925 mg, 4 mmol) was dissolved in dry DMF (10 mL). DIPEA (1.81 g, 14 mmol) and HATU (1.67 g, 4.4 mmol) were added under argon. The deprotected amine compound was dissolved in dry DMF (10 mL) and was added to the reaction mixture. The reaction mixture was stirred under argon for 4 h. The reaction mixture was concentrated under high vacuum. The residue was diluted with water (50 mL) and was extracted with EtOAc (3 × 50 mL). The combined organic layers were washed with saturated $NaHCO_3$ solution (50 mL) and brine (50 mL). The organic phase was dried over Na_2SO_4, filtered and concentrated. The crude product was purified by silica gel column chromatography using CH_2Cl_2/MeOH (19+1) as eluent to yield **46** as a white solid (449 mg, 1.04 mmol).

Yield 26%; mp. 62-64 °C; R_f = 0.28 (CH_2Cl_2/MeOH (19+1)); **^{1}H NMR** (600 MHz, DMSO-d_6) δ 1.32 (s, 6H), 1.37 – 1.43 (m, 6H), 1.64 – 1.70 (m, 1H), 2.28 – 2.37 (m, 1H), 2.45 (s, 3H), 3.15 – 3.24 (m, 1H), 3.46 – 3.50 (m, 1H), 4.10 – 4.18 (m, 2H), 4.93 – 5.03 (m, 1H), 5.14 – 5.22 (m, 1H), 7.38 – 7.47 (m, 4H), 8.30 and 8.39 (each d, *J* = 7.5 Hz, *J* = 7.8 Hz, 1H, major and minor rotamer), 8.98 (s, 1H); **^{13}C NMR** (151 MHz, DMSO-d_6) δ 15.9, 21.8, 27.9, 38.6, 47.5, 54.4, 58.8, 68.0, 78.7, 126.5, 128.8, 129.9, 131.0, 144.1, 147.8, 151.5, 153.3, 172.1; **LC-MS (ESI)** (90% H_2O + 2 mM NH_4OAc to 100% MeCN in 10 min, then 100% MeCN to 15 min, DAD 220-600 nm), t_R = 5.69 min, 96% purity, *m/z* [M-H]$^-$ calcd for $C_{22}H_{29}N_3O_4S$ 430.2, found 430.2.
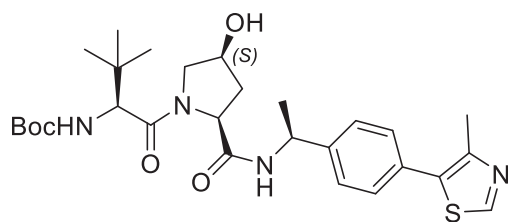
tert-Butyl ((_S_)-1-((2_S_,4_S_)-4-hydroxy-2-(((_S_)-1-(4-(4-methylthiazol-5-yl)phenyl)ethyl)carbamoyl)-pyrrolidin-1-yl)-3,3-dimethyl-1-oxobutan-2-yl)carbamate (47). _tert_-Butyl (2_S_,4_S_)-4-hydroxy-2-(((_S_)-1-(4-(4-methylthiazol-5-yl)phenyl)ethyl)carbamoyl)pyrrolidine-1-carboxylate (**46**, 432 mg, 1 mmol) was dissolved in dry CH₂Cl₂ (5 mL) and was treated with TFA (5 mL) for 2 h. The mixture was concentrated under high vacuum. Boc-Tle-OH (**39**, 231 mg, 1 mmol) was dissolved in dry DMF (5 mL). HATU (418 mg, 1.1 mmol) and DIPEA (452 mg, 3.5 mmol) were added under argon. The deprotected amine compound was dissolved in dry DMF (5 mL) and was added to the reaction mixture. The reaction mixture was stirred for 18 h under argon. The mixture was concentrated under high vacuum. The crude product was purified by silica gel column chromatography using EtOAc as eluent to yield **47** as a white solid (339 mg, 0.62 mmol).

Yield 62%; mp. 100-102 °C; R_f = 0.24 (CH₂Cl₂ + MeOH (19+1)); **¹H NMR** (500 MHz, DMSO-d_6) δ 0.95 (s, 9H), 1.36 – 1.40 (m, 12H), 1.62 – 1.68 (m, 1H), 2.29 – 2.36 (m, 1H), 2.46 (s, 3H), 3.38 (dd, _J_ = 10.1, 5.3 Hz, 1H), 3.81 – 3.90 (m, 1H), 4.10 (d, _J_ = 8.7 Hz, 1H), 4.17 – 4.24 (m, 1H), 4.36 (dd, _J_ = 8.8, 6.0 Hz, 1H), 4.88 – 4.96 (m, 1H), 5.31 (d, _J_ = 6.7 Hz, 1H), 6.51 (d, _J_ = 8.8 Hz, 1H), 7.37 – 7.40 (m, 2H), 7.42 – 7.45 (m, 2H), 8.33 (d, _J_ = 7.6 Hz, 1H), 8.98 (s, 1H); **¹³C NMR** (126 MHz, DMSO-d_6) δ 15.9, 22.2, 26.3, 28.1, 34.7, 36.7, 47.8, 55.4, 58.4, 58.6, 69.0, 78.1, 126.3, 128.8, 129.7, 131.0, 144.3, 147.7, 151.4, 155.5, 170.1, 171.0; **LC-MS (ESI)** (90% H₂O + 2 mM NH₄OAc to 100% MeCN in 10 min, then 100% MeCN to 15 min, DAD 220-600 nm), t_R = 6.55 min, 95% purity, _m/z_ [M+H]⁺ calcd for C₂₈H₄₀N₄O₅S 545.3, found 545.5.
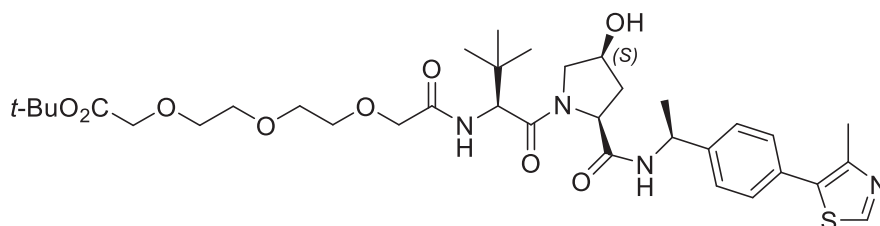
tert-Butyl (_S_)-13-((2_S_,4_S_)-4-hydroxy-2-(((_S_)-1-(4-(4-methylthiazol-5-yl)phenyl)ethyl)carbamoyl)-pyrrolidine-1-carbonyl)-14,14-dimethyl-11-oxo-3,6,9-trioxa-12-azapentadecanoate (48). _tert_-Butyl ((_S_)-1-((2_S_,4_S_)-4-hydroxy-2-(((_S_)-1-(4-(4-methylthiazol-5-yl)phenyl)ethyl)carbamoyl)pyrrolidin-1-yl)-3,3-dimethyl-1-oxobutan-2-yl)carbamate (**47**, 327 mg, 0.6 mmol) was dissolved in dry CH₂Cl₂ (5 mL) and was treated with TFA (5 mL). The mixture was stirred for 2 h at room temperature. The mixture was concentrated under high vacuum. 13,13-Dimethyl-11-oxo-3,6,9,12-tetraoxatetradecanoic acid (**31**, 167 mg, 0.6 mmol) was dissolved in dry DMF (5 mL). HATU (251 mg, 0.66 mmol) and DIPEA (271 mg, 2.1 mmol) were added under argon. The deprotected (-)VHL-ligand was dissolved in dry DMF (5

mL) and was added to the mixture, containing the activated acid compound. The reaction mixture was stirred at room temperature under argon for 18 h. The mixture was concentrated under high vacuum. The crude product was purified by silica gel column chromatography using CH$_2$Cl$_2$/MeOH (19+1) as eluent to yield **48** as a white solid (267 mg, 0.38 mmol).

Yield 63%; R_f = 0.18 (CH$_2$Cl$_2$/MeOH (19+1)); **^{1}H NMR** (600 MHz, DMSO-d_6) δ 0.95 (s, 9H), 1.38 (d, J = 7.0 Hz, 3H), 1.42 (s, 9H), 1.62 – 1.67 (m, 1H), 2.30 – 2.36 (m, 1H), 2.46 (s, 3H), 3.40 (dd, J = 10.1, 5.4 Hz, 1H), 3.55 – 3.62 (m, 8H), 3.86 (dd, J = 10.1, 5.7 Hz, 1H), 3.95 (d, J = 4.2 Hz, 2H), 3.97 (s, 2H), 4.18 – 4.24 (m, 1H), 4.35 (dd, J = 8.7, 6.3 Hz, 1H), 4.50 (d, J = 9.2 Hz, 1H), 4.90 – 4.96 (m, 1H), 5.32 (d, J = 6.7 Hz, 1H), 7.35 – 7.40 (m, 3H), 7.42 – 7.46 (m, 2H), 8.37 (d, J = 7.7 Hz, 1H), 8.98 (s, 1H); **^{13}C NMR** (151 MHz, DMSO) δ 15.9, 22.2, 26.2, 27.7, 35.1, 36.8, 47.8, 55.5, 55.8, 58.5, 68.1, 68.9, 69.5, 69.7, 69.9, 70.4, 80.6, 126.4, 128.8, 129.8, 131.1, 144.3, 147.8, 151.4, 168.8, 169.3, 169.3, 170.9, one signal is missing due to overlapping signals; **LC-MS (ESI)** (90% H$_2$O + 2 mM NH$_4$OAc to 100% MeCN in 10 min, then 100% MeCN to 15 min, DAD 220-600 nm), t_R = 6.55 min, 99% purity, m/z [M+H]$^+$ calcd for C$_{35}$H$_{52}$N$_4$O$_9$S 705.4, found 705.6.

(2S,4S)-1-((S)-15-($tert$-Butyl)-1-(3-(((5-(5-(difluoromethyl)-1,3,4-oxadiazol-2-yl)pyrimidin-2-yl)amino)methyl)phenyl)-3,13-dioxo-5,8,11-trioxa-2,14-diazahexadecan-16-oyl)-4-hydroxy-N-((S)-1-(4-(4-methylthiazol-5-yl)phenyl)ethyl)pyrrolidine-2-carboxamide (4(-)). Benzyl (3-(((5-(5-(difluoromethyl)-1,3,4-oxadiazol-2-yl)pyrimidin-2-yl)amino)methyl)benzyl)carbamate (**15**, 70 mg, 0.15 mmol) was dissolved in dry THF (10 mL). The mixture was treated with 10% m/m Pd/C under H$_2$ (1 atm, balloon) for 18 h. The mixture was filtered through celite and concentrated under high vacuum. $tert$-Butyl (S)-13-((2S,4S)-4-hydroxy-2-(((S)-1-(4-(4-methylthiazol-5-yl)phenyl)ethyl)carbamoyl)-pyrrolidine-1-carbonyl)-14,14-dimethyl-11-oxo-3,6,9-trioxa-12-azapentadecanoate (**48**, 106 mg, 0.15 mmol) was dissolved in dry CH$_2$Cl$_2$ (5 mL) and was treated with TFA (5 mL) for 2 h at room temperature. The mixture was concentrated under high vacuum. The deprotected acid compound was dissolved in dry DMF (5 mL). DIPEA (58 mg, 0.45 mmol) and HATU (63 mg, 0.165 mmol) were added under argon. The deprotected amine compound was dissolved in dry DMF (5 mL) and was added to the reaction mixture. The reaction mixture was allowed to stir at room temperature under argon for 18 h. The reaction mixture was concentrated under high vacuum. The crude product was purified by silica gel flash column chromatography using a CH$_2$Cl$_2$/MeOH gradient (0% to 20% MeOH) to yield **4(-)** as a white solid (71 mg, 0.074 mmol).

Yield 49%; mp. 80-86 °C; R_f = 0.49 (CH$_2$Cl$_2$/MeOH (9+1)); **^{1}H NMR** (600 MHz, DMSO-d_6) δ 0.94 (s, 9H), 1.37 (d, J = 6.9 Hz, 3H), 1.61 – 1.67 (m, 1H), 2.28 – 2.35 (m, 1H), 2.45 (s, 3H), 3.39 (dd, J = 10.1, 5.4 Hz, 1H), 3.53 – 3.62 (m, 8H), 3.85 (dd, J = 10.2, 5.7 Hz, 1H), 3.88 – 3.96 (m, 4H), 4.17 – 4.23 (m, 1H), 4.29 (d, J = 6.2 Hz, 2H), 4.34 (dd, J = 8.7, 6.3 Hz, 1H), 4.50 (d, J = 9.3 Hz, 1H), 4.59 (d, J = 6.4 Hz, 2H), 4.89 – 4.95 (m, 1H), 5.31 (d, J = 6.7 Hz, 1H), 7.11 – 7.28 (m, 4H), 7.35 – 7.40 (m, 3H), 7.42 – 7.61 (m, 3H), 8.19 (t, J = 6.3 Hz, 1H), 8.37 (d, J = 7.6 Hz, 1H), 8.72 (t, J = 6.4 Hz, 1H), 8.87 (s, 2H), 8.97 (s, 1H); **^{13}C NMR** (151 MHz, DMSO-d_6) δ 15.9, 22.2, 26.2, 35.2, 36.8, 41.6, 44.0, 47.8, 55.5, 55.8, 58.5, 68.9, 69.5, 69.6, 70.0, 70.3, 70.3, 106.3, 106.6 (t, ^1J(C,F) = 238.3 Hz), 125.5, 125.8, 125.9, 126.4, 128.2, 128.8, 129.8, 131.0, 139.2, 139.5, 144.3, 147.8, 151.4, 157.0, 157.2, 157.5 (t, ^2J(C,F) = 29.3 Hz), 162.9, 163.1, 168.8, 169.2, 169.3, 170.9, one signal is missing due to overlapping signals; **LC-MS (ESI)** (90% H$_2$O + 2 mM NH$_4$OAc to 100% MeCN in 10 min, then 100% MeCN to 15 min, DAD 220-600 nm), t_R = 6.34 min, 97% purity, m/z [M+H]$^+$ calcd for C$_{46}$H$_{56}$F$_2$N$_{10}$O$_9$S 963.4, found 963.7; **HRMS (ESI)** m/z [M+H]$^+$ calcd for C$_{46}$H$_{56}$F$_2$N$_{10}$O$_9$S 963.3993, found 963.3991.

5.3. NMR Data

¹H NMR spectrum of **9** (600 MHz, DMSO-d_6)

¹³C NMR spectrum of **9** (126 MHz, DMSO-d_6)

¹H NMR spectrum of **11** (600 MHz, DMSO-*d₆*)

¹³C NMR spectrum of **11** (151 MHz, DMSO-*d₆*)

^{1}H NMR spectrum of **13** (500 MHz, DMSO-*d$_6$*)
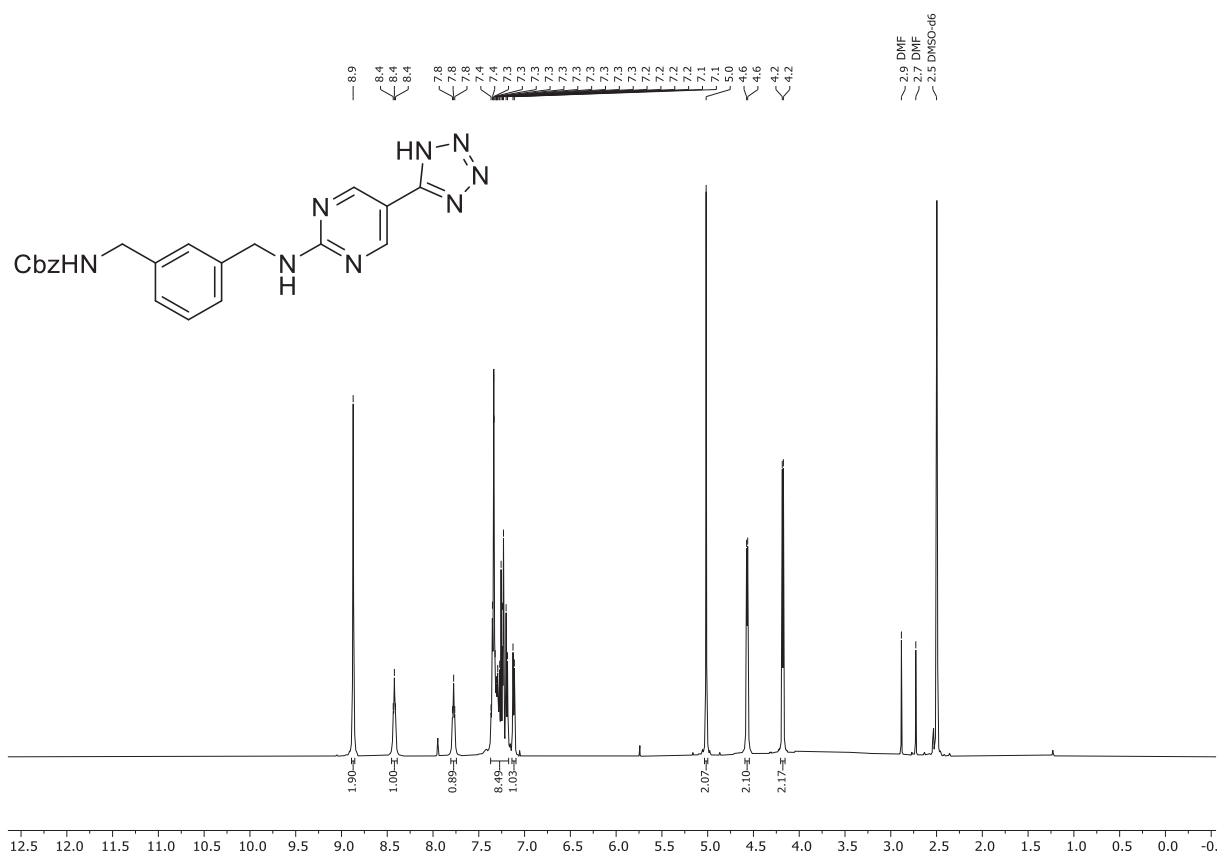
^{13}C NMR spectrum of **13** (126 MHz, DMSO-*d$_6$*)

¹H NMR spectrum of **15** (600 MHz, DMSO-d_6)

¹³C NMR spectrum of **15** (151 MHz, DMSO-d_6)
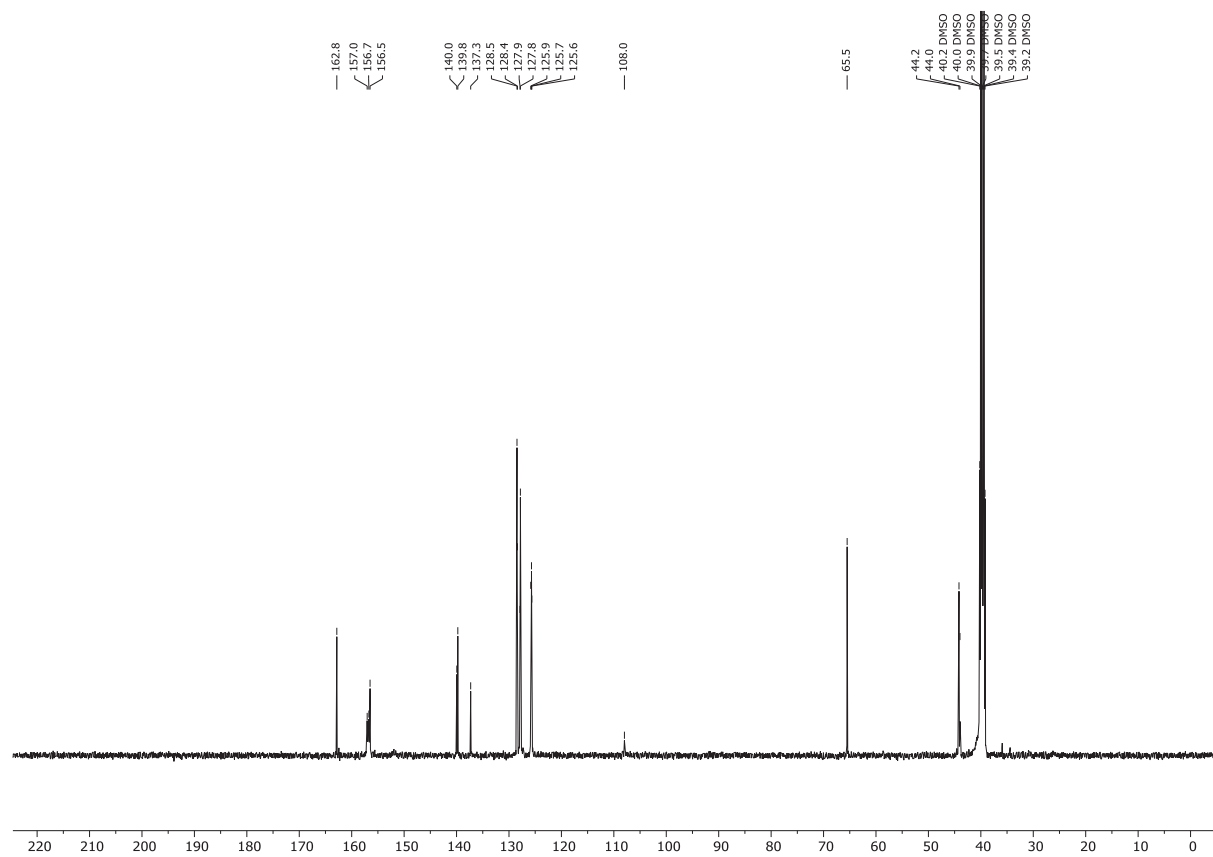
¹⁹F NMR spectrum of **15** (565 MHz, DMSO-*d₆*)

-121.1
-121.2

-112.5 -113.5 -114.5 -115.5 -116.5 -117.5 -118.5 -119.5 -120.5 -121.5 -122.5 -123.5 -124.5 -125.5 -126.5

¹H NMR spectrum of **10** (600 MHz, DMSO-*d₆*)

¹H NMR spectrum of **10** (600 MHz, DMSO-*d₆*)

CbzHN, NHBoc structure

7.8 7.8 7.8 7.4 7.4 7.4 7.3 7.3 7.3 7.3 7.3 7.3 7.2 7.2 7.2
5.0
4.2 4.2 4.1 4.1
2.5 DMSO-d6
1.4

0.89 5.49 4.52   2.08   2.09 1.94   8.76

12.0 11.5 11.0 10.5 10.0 9.5 9.0 8.5 8.0 7.5 7.0 6.5 6.0 5.5 5.0 4.5 4.0 3.5 3.0 2.5 2.0 1.5 1.0 0.5 0.0 -0
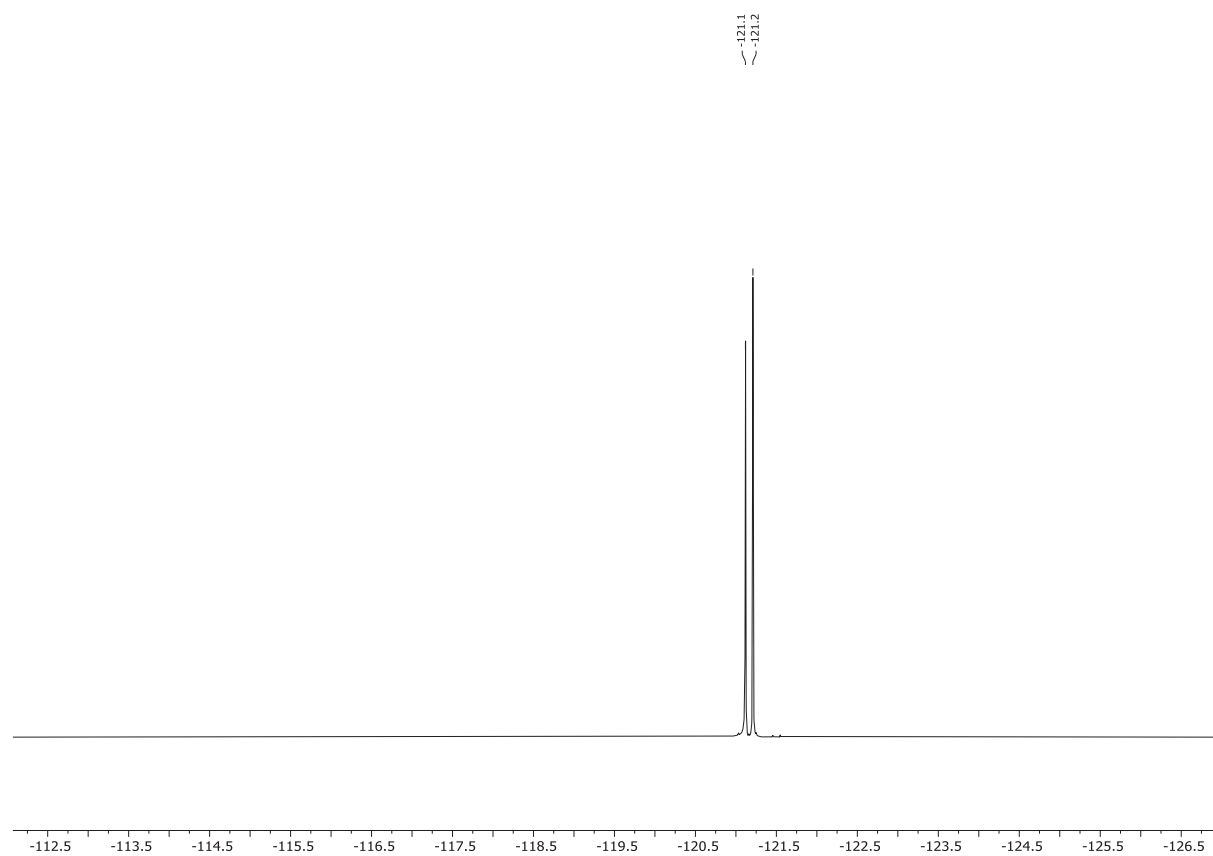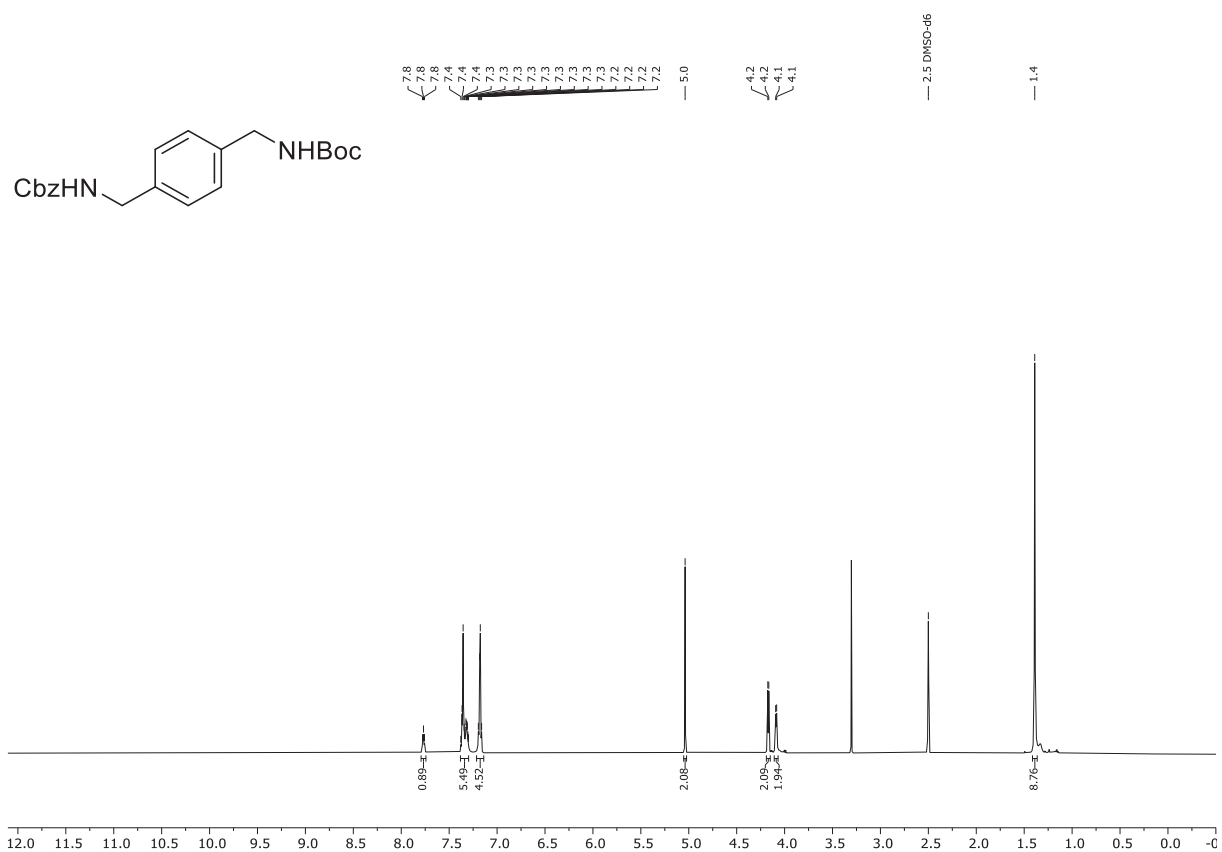
¹³C NMR spectrum of **10** (151 MHz, DMSO-*d₆*)

156.5 155.9
138.9 138.2 137.3 128.5 127.9 127.1 127.0
77.9
65.5
43.8 43.3 40.1 DMSO 40.0 DMSO 39.8 DMSO 39.7 DMSO 39.6 DMSO 39.4 DMSO 39.3 DMSO 28.4

230 220 210 200 190 180 170 160 150 140 130 120 110 100 90 80 70 60 50 40 30 20 10 0

^{1}H NMR spectrum of 12 (600 MHz, DMSO-d_6)

^{13}C NMR spectrum of 12 (126 MHz, DMSO-d_6)
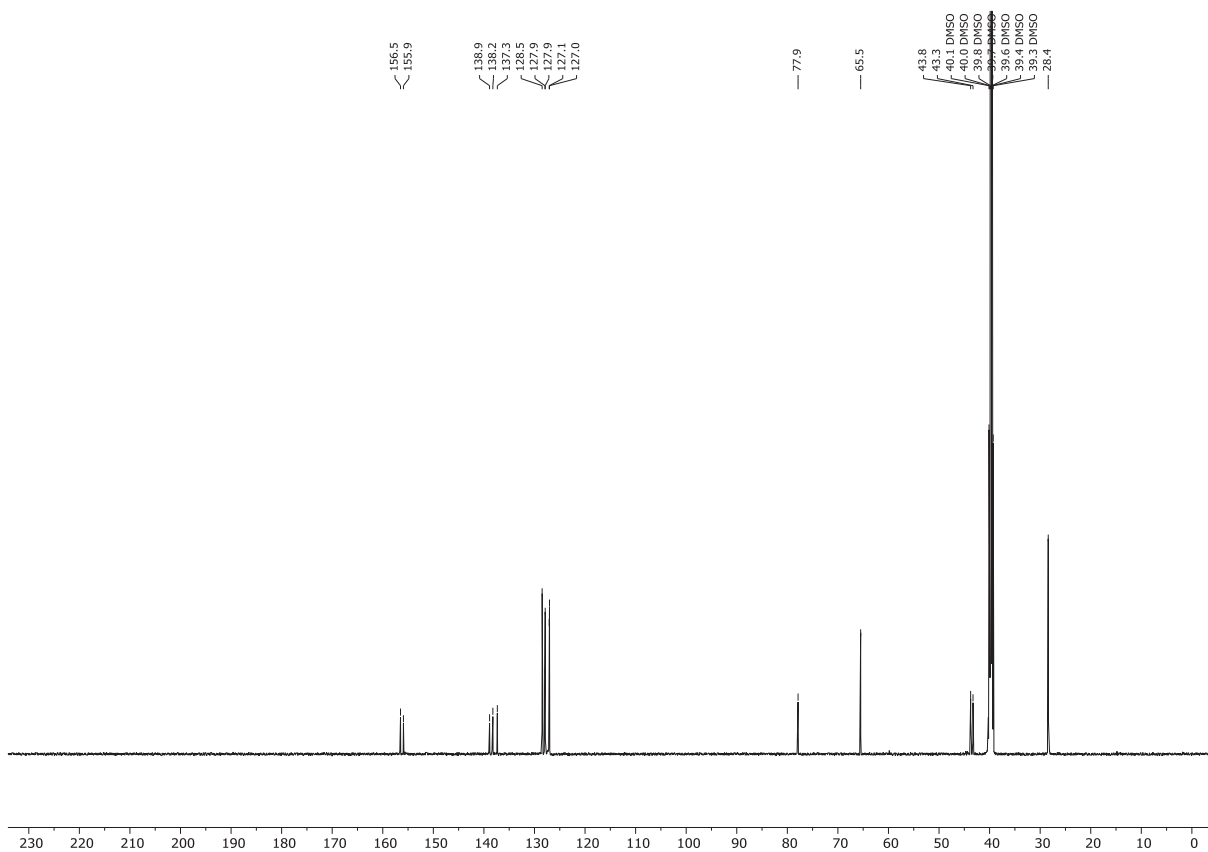
¹H NMR spectrum of **14** (500 MHz, DMSO-*d₆*)
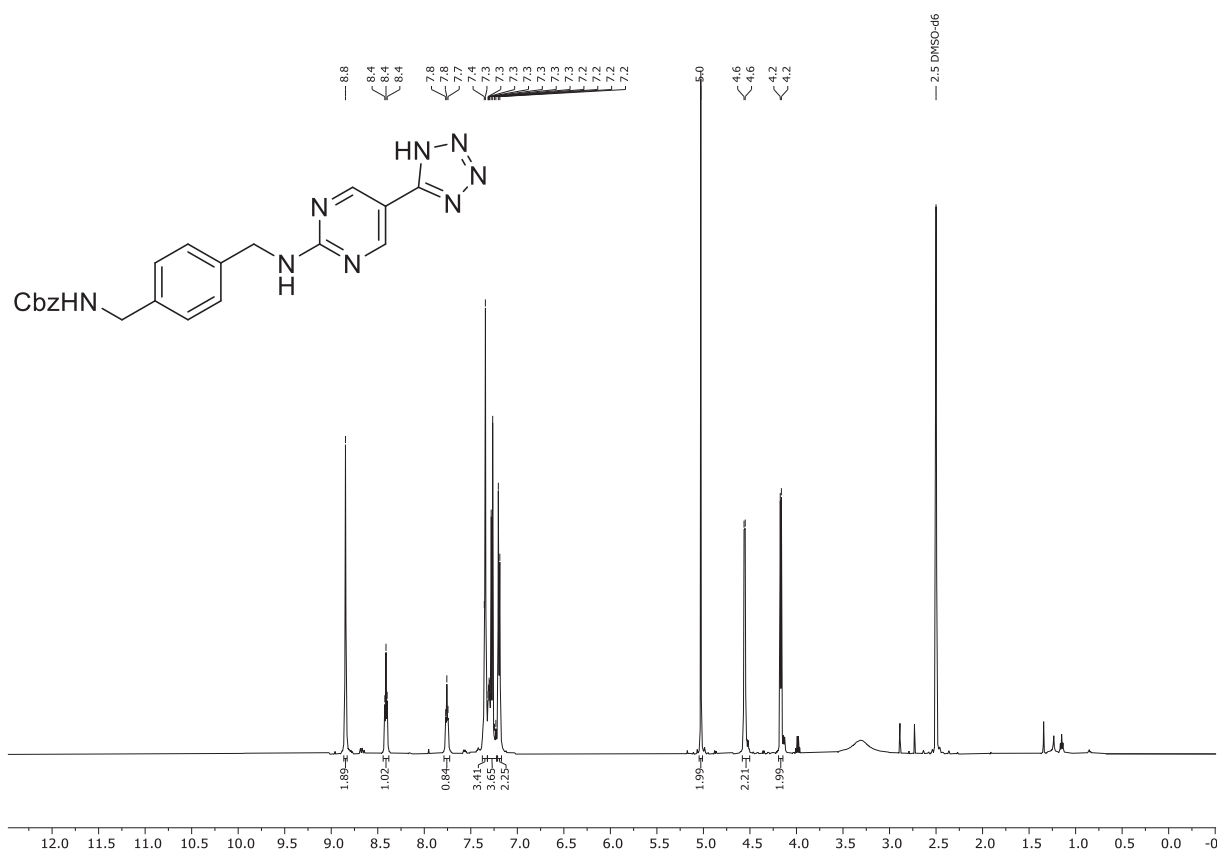
¹³C NMR spectrum of **14** (151 MHz, DMSO-*d₆*)
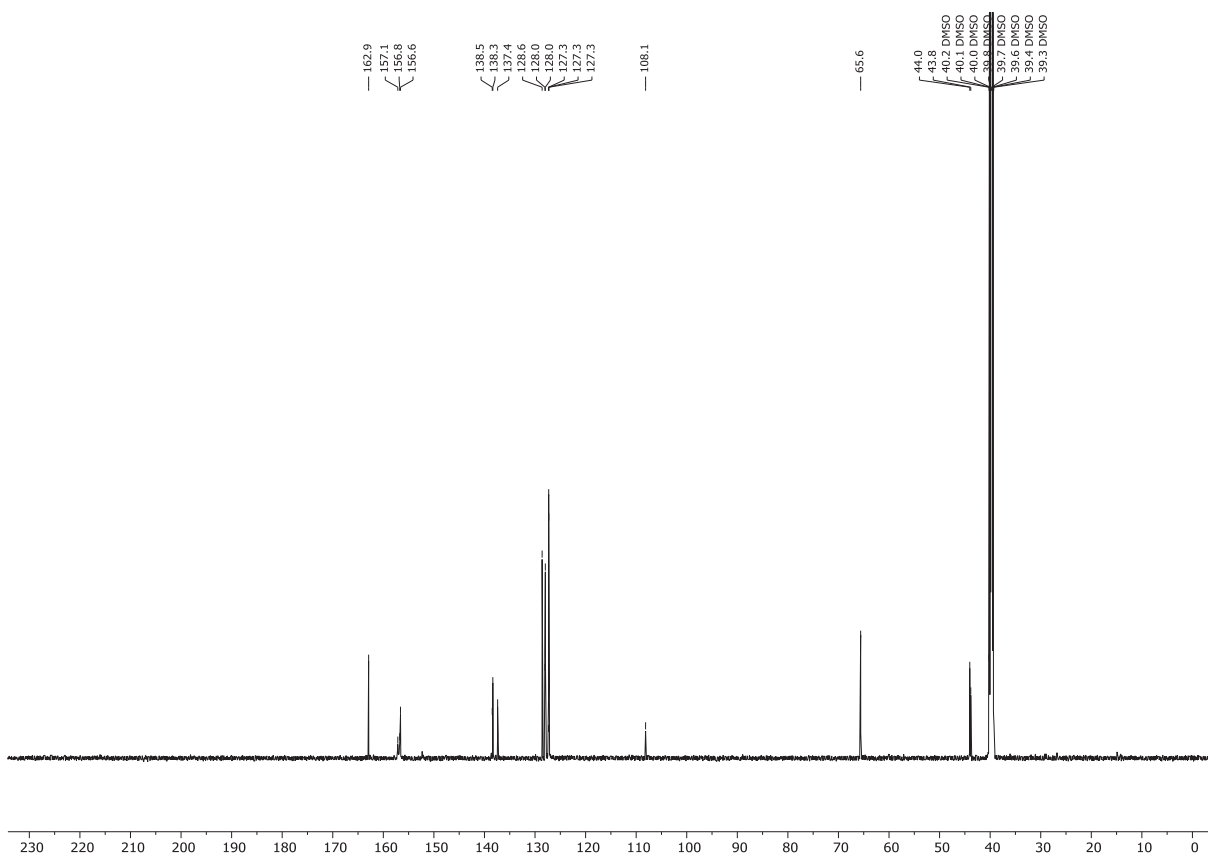
¹H NMR spectrum of **16** (500 MHz, DMSO-*d₆*)
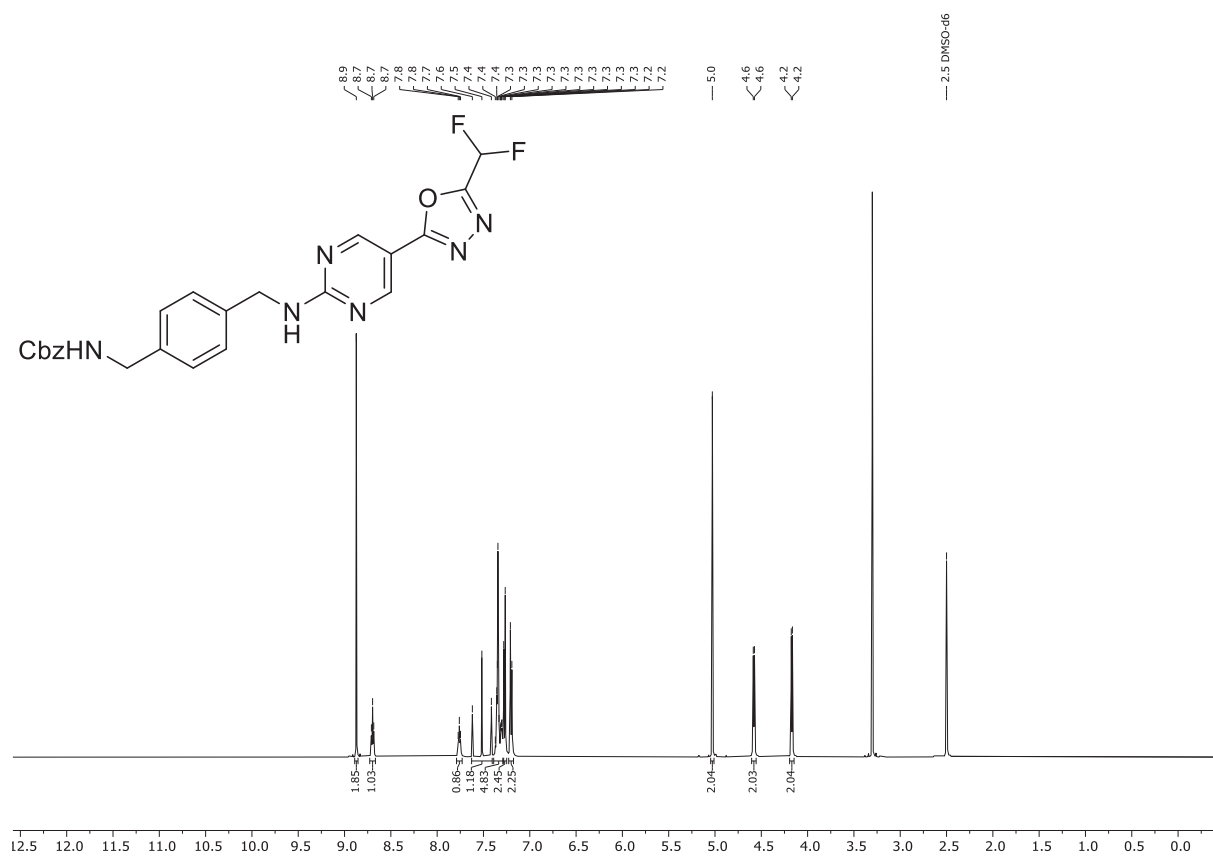
¹³C NMR spectrum of **16** (126 MHz, DMSO-*d₆*)
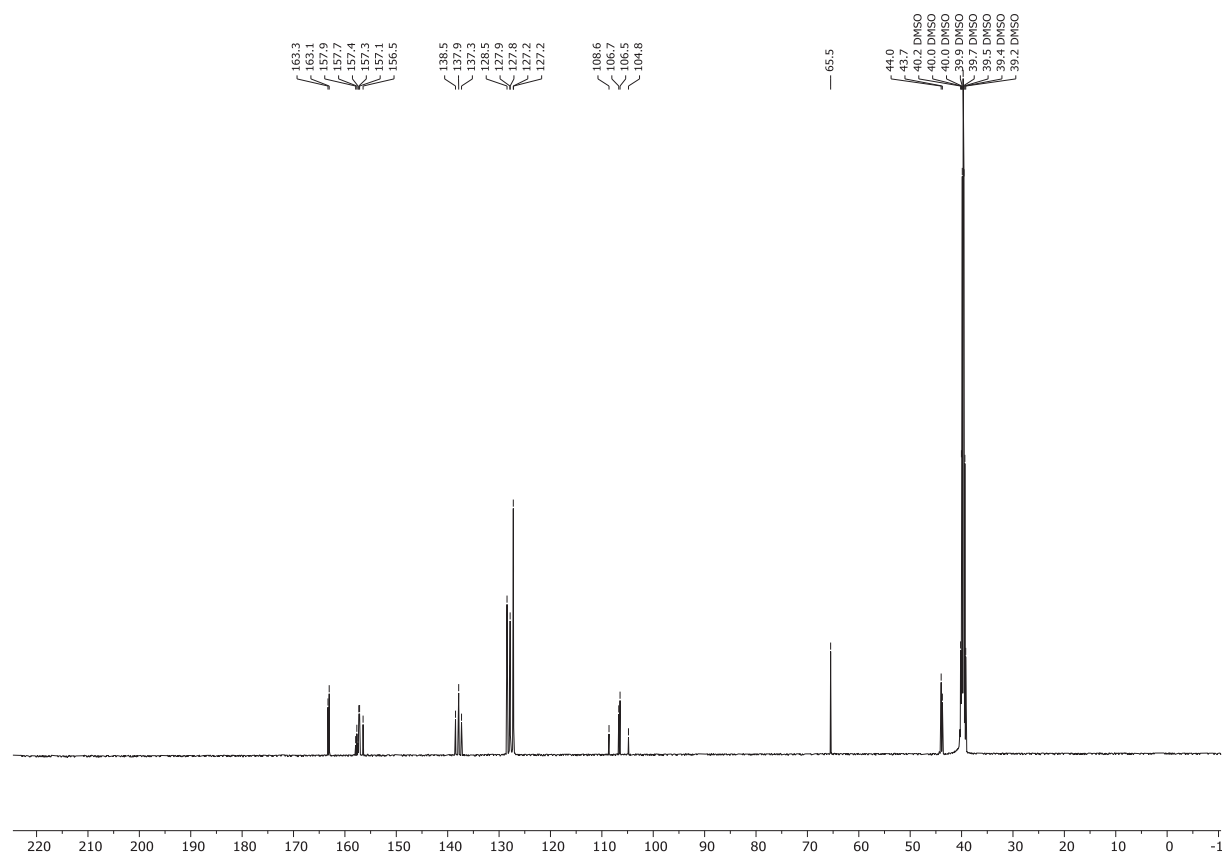
¹⁹F NMR spectrum of **16** (565 MHz, DMSO-*d₆*)

-121.1
-121.2

10   0   -10   -20   -30   -40   -50   -60   -70   -80   -90   -100   -110   -120   -130   -140   -150   -160   -170   -180   -190   -200   -210

¹H NMR spectrum of **25** (600 MHz, DMSO-*d*₆)

¹³C NMR spectrum of **25** (151 MHz, DMSO-*d*₆)
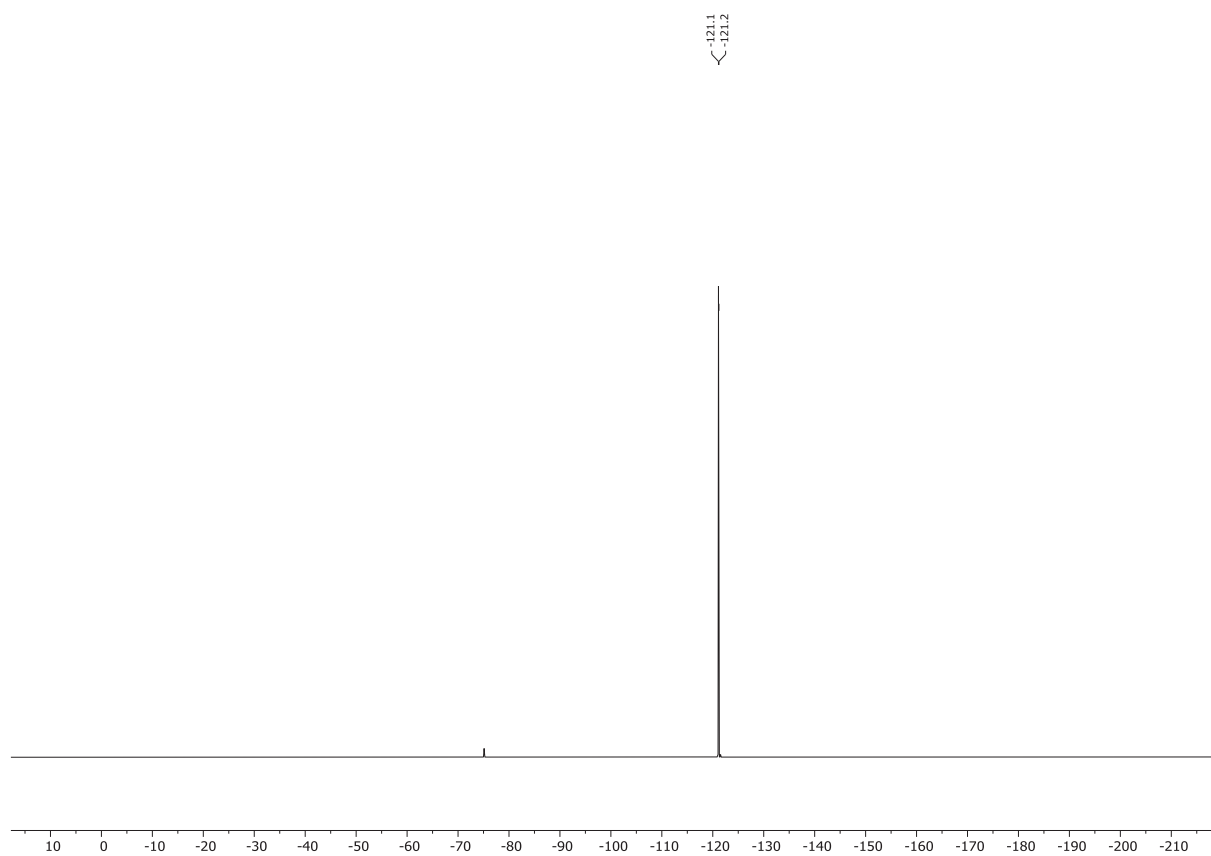
¹H NMR spectrum of **26** (600 MHz, DMSO-d_6)
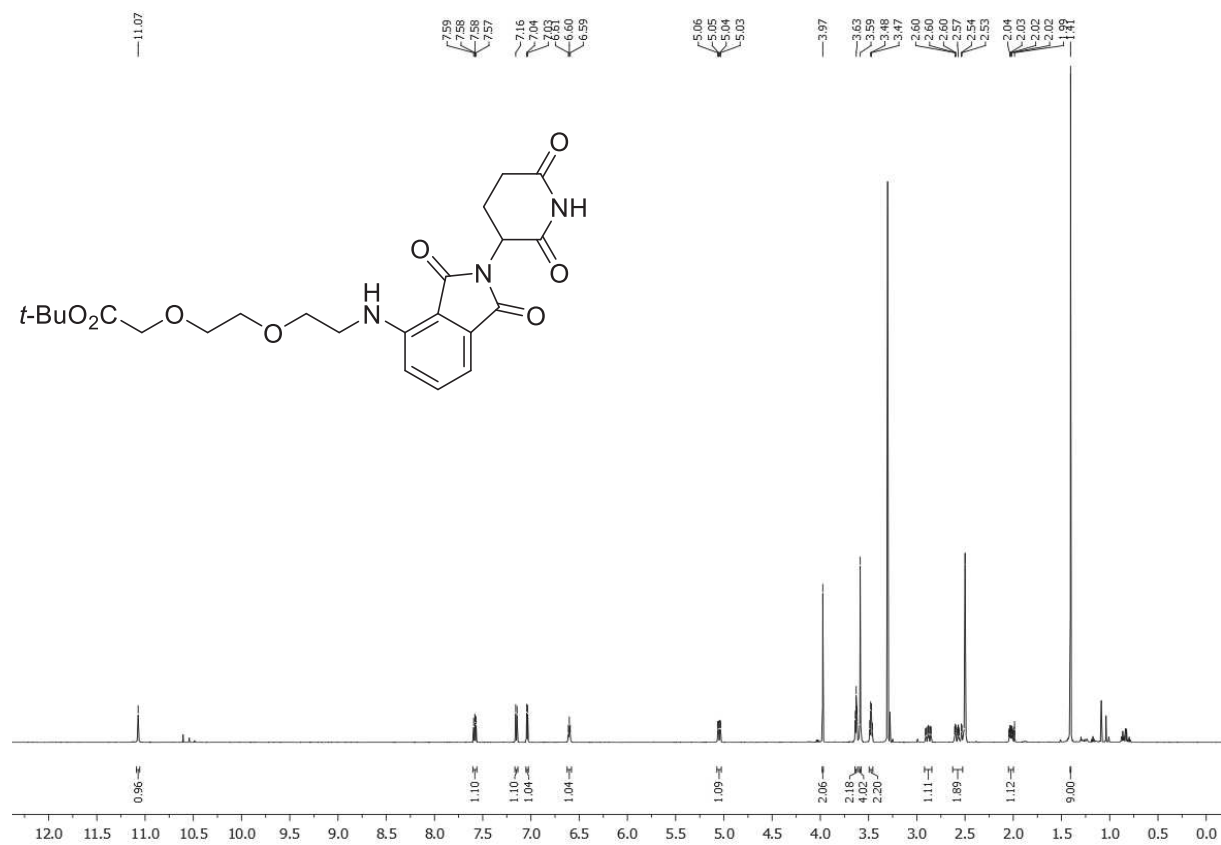
¹³C NMR spectrum of **26** (151 MHz, DMSO-d_6)
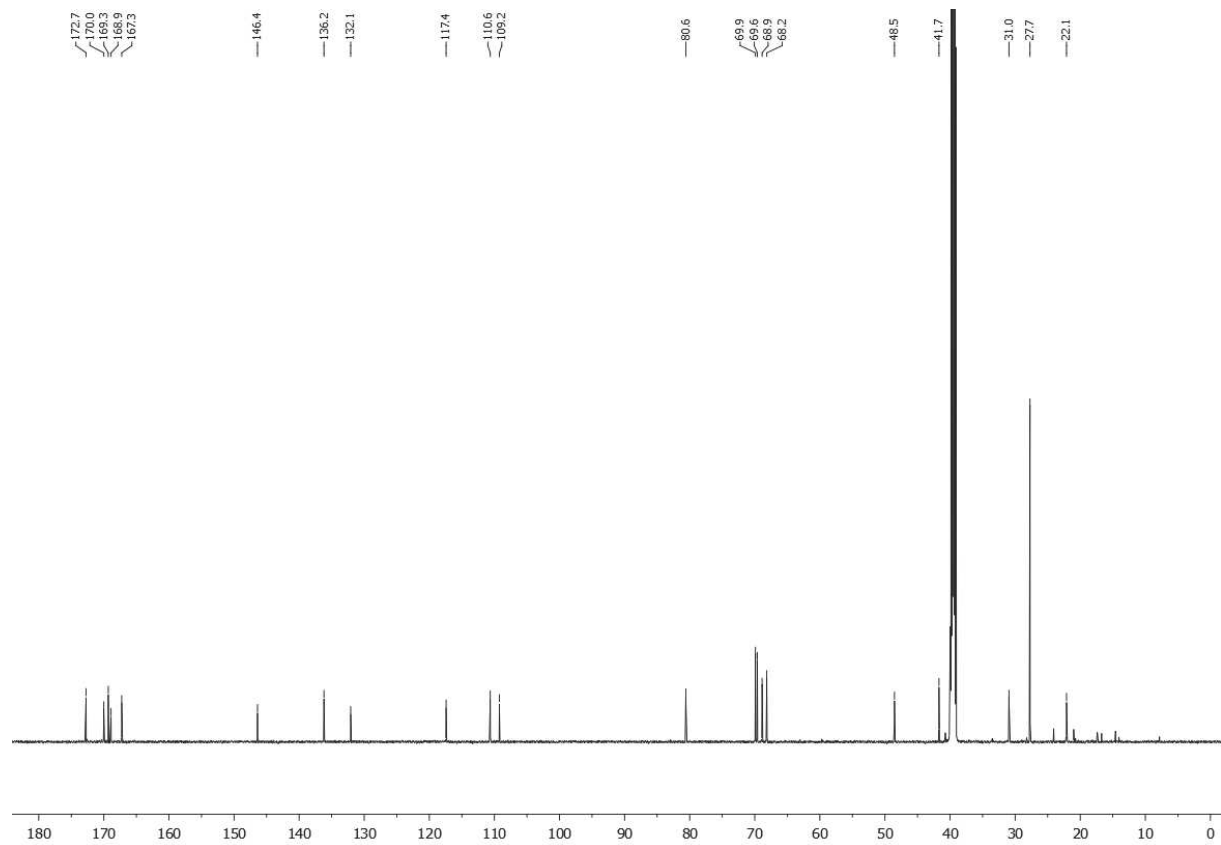
¹H NMR spectrum of **22** (500 MHz, DMSO-d_6)

3.53
3.52
3.50

2.18
2.17
2.15

1.80
1.79
1.78
1.77
1.48
1.39
1.37
1.35
1.28
1.27
1.27
1.26

t-BuO₂C⟍⟍⟍⟍⟍⟍Br

2.00

1.96
2.07
2.21
9.08
1.98
4.04

12.0 11.5 11.0 10.5 10.0 9.5 9.0 8.5 8.0 7.5 7.0 6.5 6.0 5.5 5.0 4.5 4.0 3.5 3.0 2.5 2.0 1.5 1.0 0.5 0.0
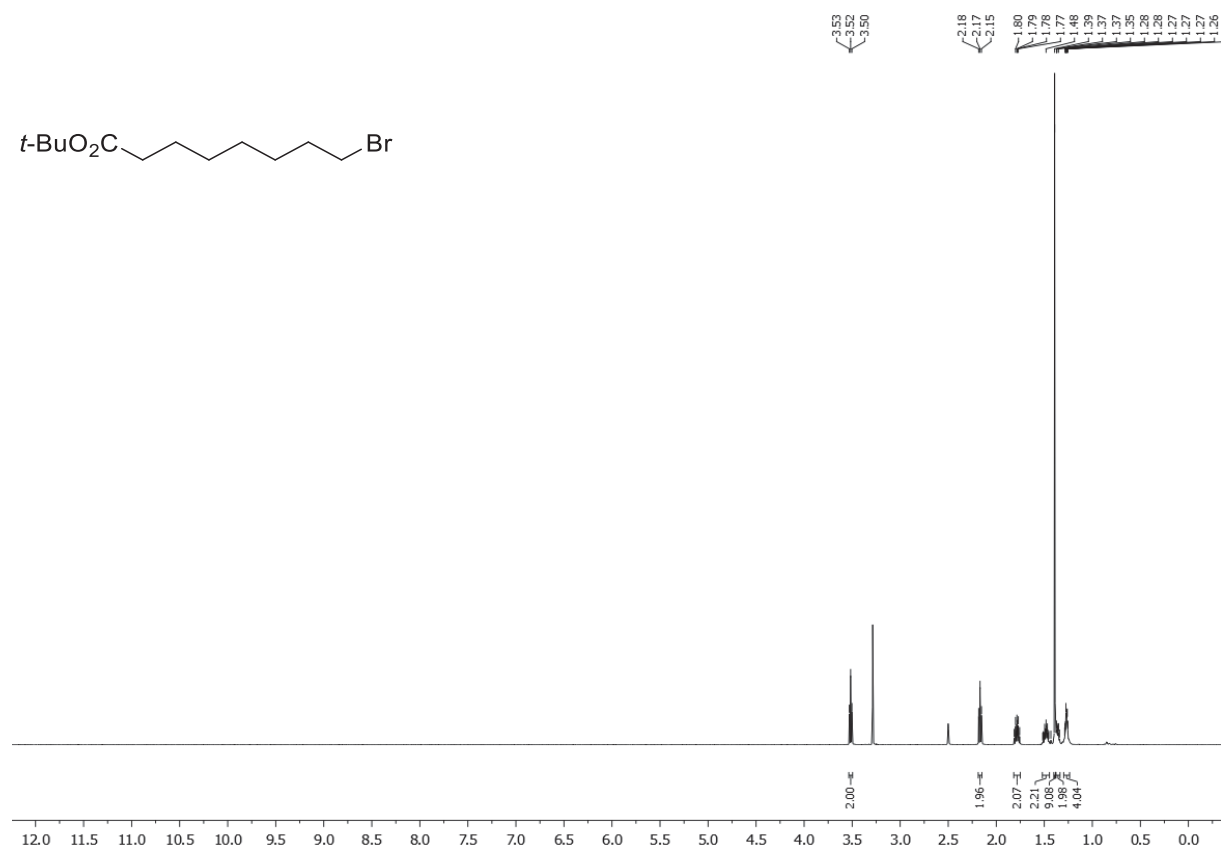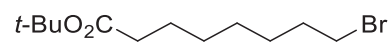
¹³C NMR spectrum of **22** (126 MHz, DMSO-d_6)

172.2

79.3

35.0
34.7
32.1
28.1
27.7
27.7
27.3
24.4

180 170 160 150 140 130 120 110 100 90 80 70 60 50 40 30 20 10 0

S50
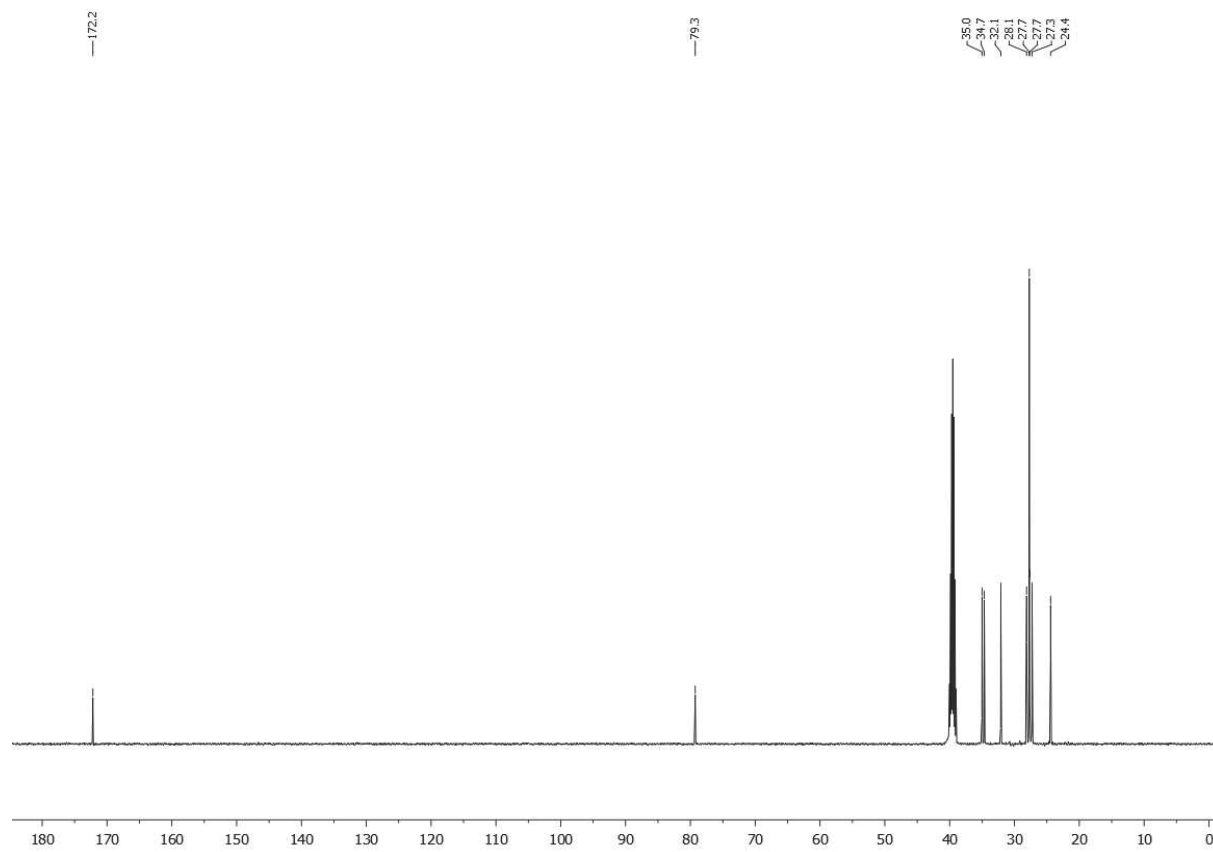
¹H NMR spectrum of **23** (500 MHz, DMSO-d_6)

3.32
3.31
3.29

2.18
2.17
2.15

1.52
1.51
1.48
1.39
1.29
1.28
1.28
1.28
1.27
1.27
1.27
1.26
1.26

t-BuO₂C⌒⌒⌒⌒⌒N₃

1.96

1.99

4.10
9.00
6.34

12.5 12.0 11.5 11.0 10.5 10.0 9.5 9.0 8.5 8.0 7.5 7.0 6.5 6.0 5.5 5.0 4.5 4.0 3.5 3.0 2.5 2.0 1.5 1.0 0.5 0.0
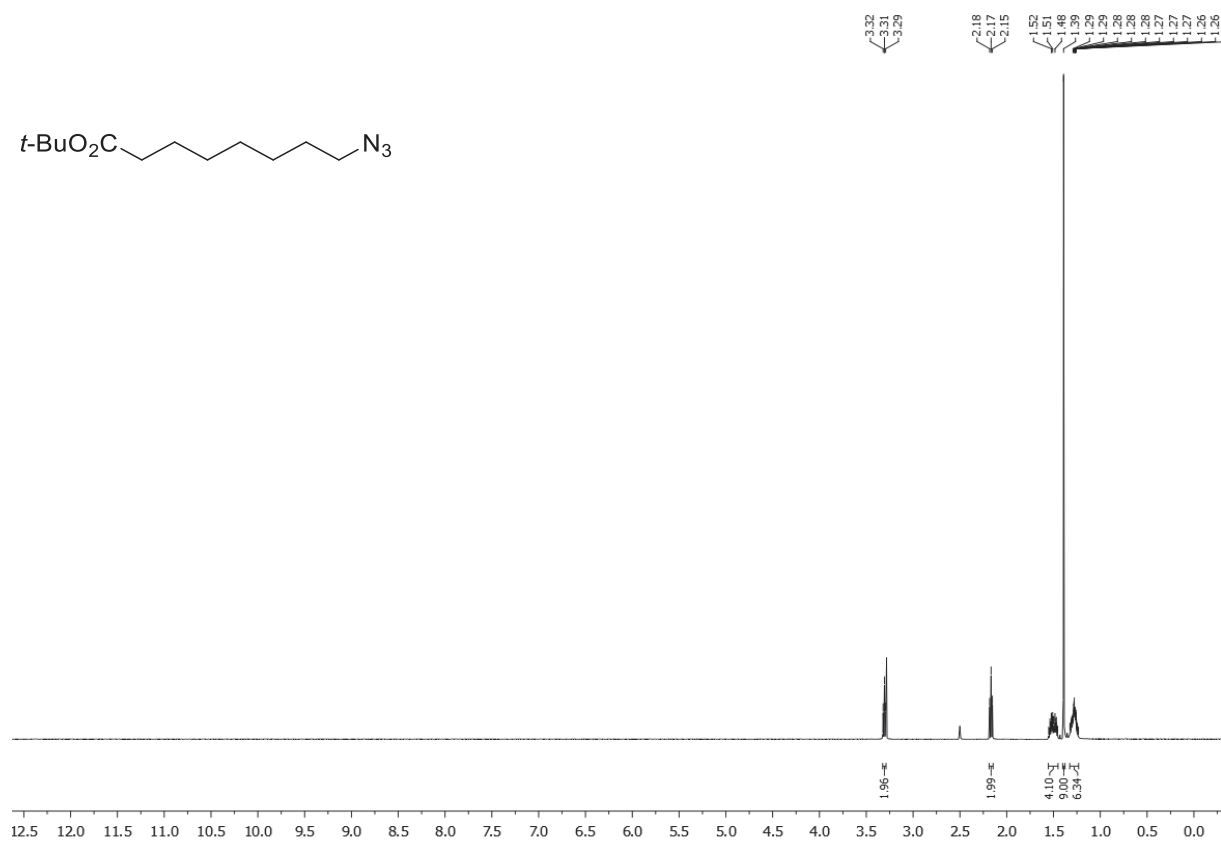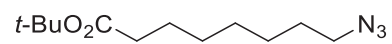
¹³C NMR spectrum of **23** (126 MHz, DMSO-d_6)

172.2

79.2

50.5

34.7
28.2
28.1
28.1
27.7
25.9
24.4

180 170 160 150 140 130 120 110 100 90 80 70 60 50 40 30 20 10 0

S51
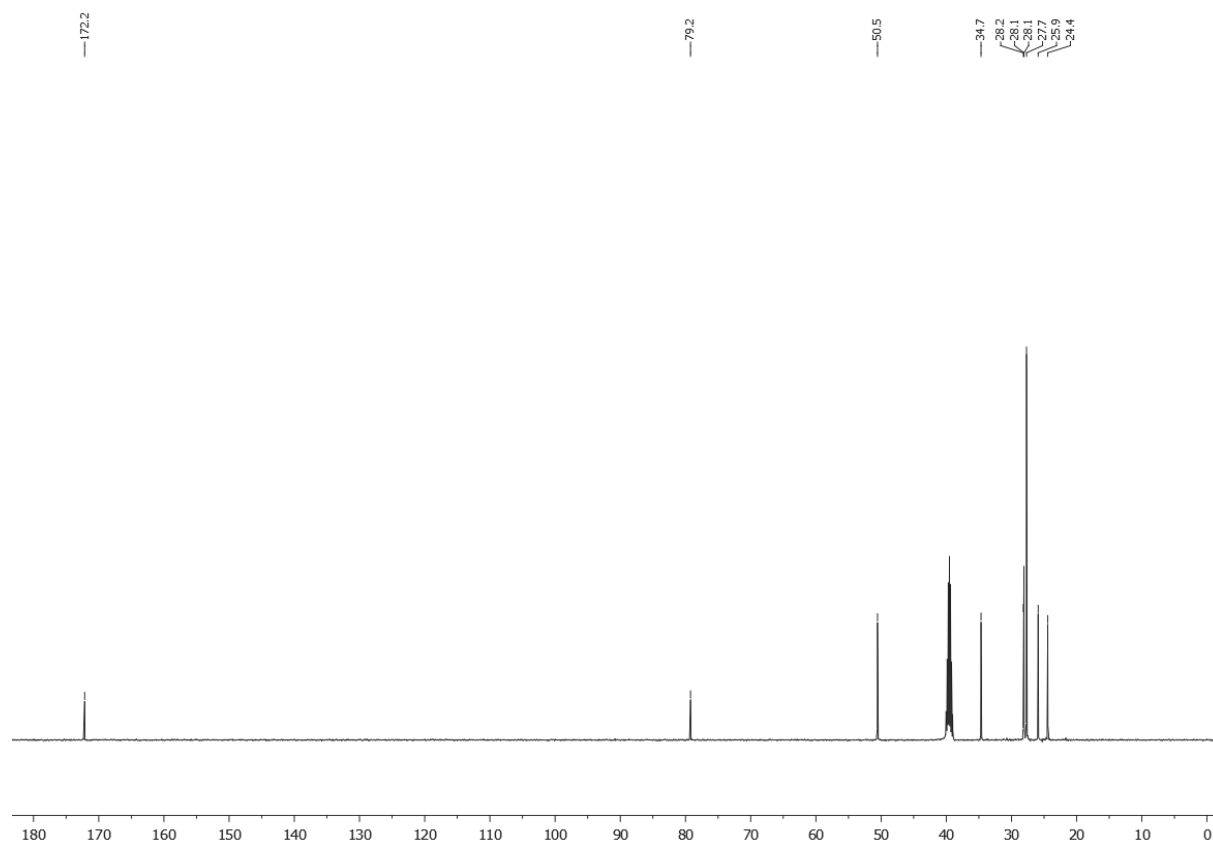
¹H NMR spectrum of **24** (500 MHz, DMSO-d_6)

2.17, 2.16, 2.14
1.49, 1.48, 1.47, 1.46, 1.39, 1.33, 1.31, 1.30, 1.27, 1.26, 1.25, 1.24

$t\text{-BuO}_2\text{C}$⌇⌇⌇NH_2

2.20

2.47, 9.08, 9.74

| 12.0 | 11.5 | 11.0 | 10.5 | 10.0 | 9.5 | 9.0 | 8.5 | 8.0 | 7.5 | 7.0 | 6.5 | 6.0 | 5.5 | 5.0 | 4.5 | 4.0 | 3.5 | 3.0 | 2.5 | 2.0 | 1.5 | 1.0 | 0.5 | 0.0 |
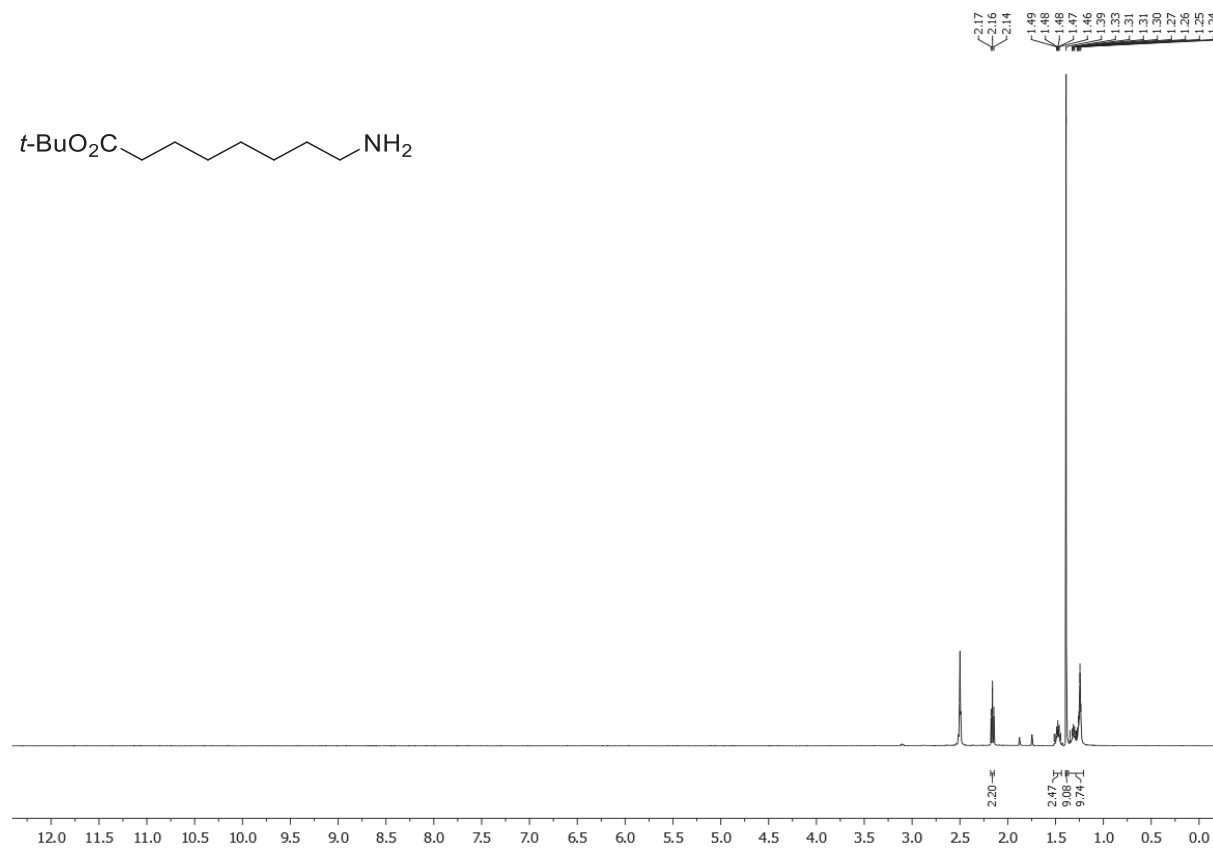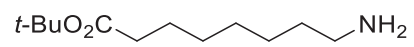
¹³C NMR spectrum of **24** (126 MHz, DMSO-d_6)

172.2

79.2

41.6

34.7, 33.3, 28.6, 28.4, 27.7, 26.2, 24.5

| 180 | 170 | 160 | 150 | 140 | 130 | 120 | 110 | 100 | 90 | 80 | 70 | 60 | 50 | 40 | 30 | 20 | 10 | 0 |

S52
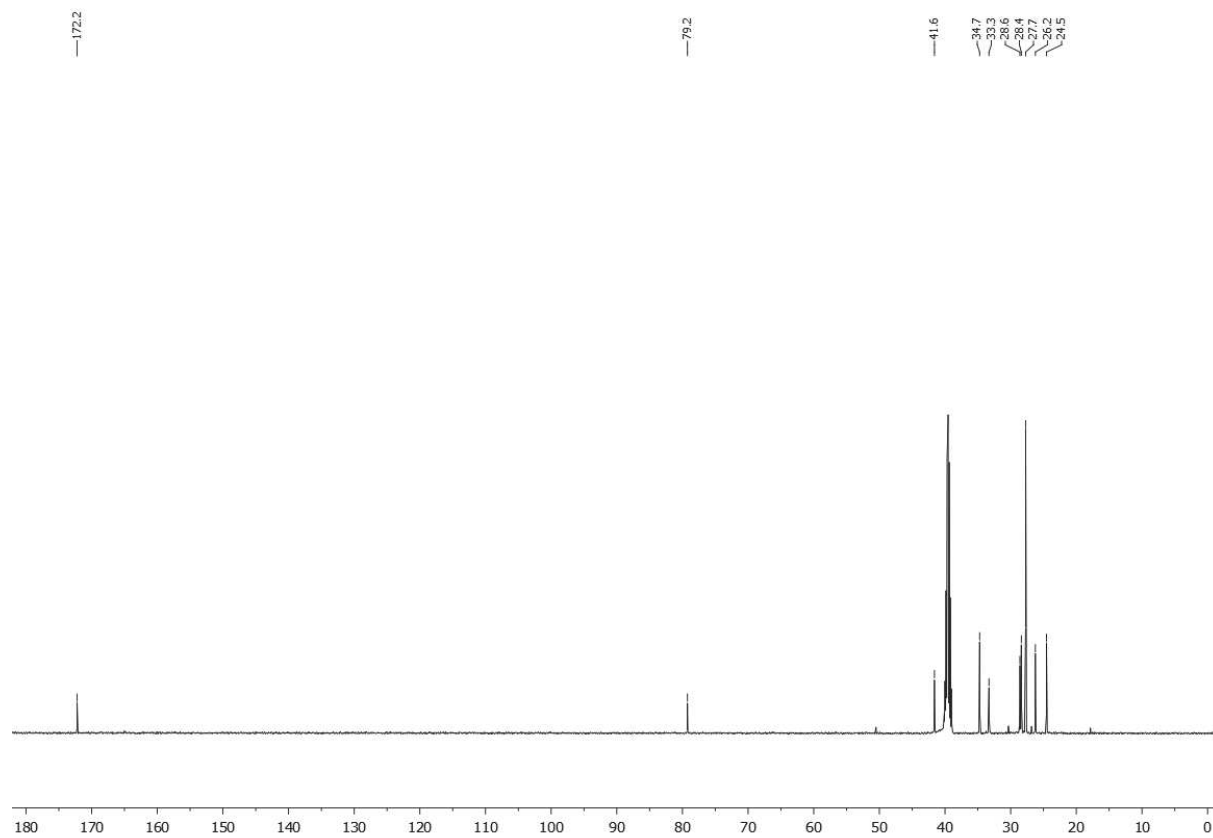
¹H NMR spectrum of **27** (500 MHz, DMSO-d_6)
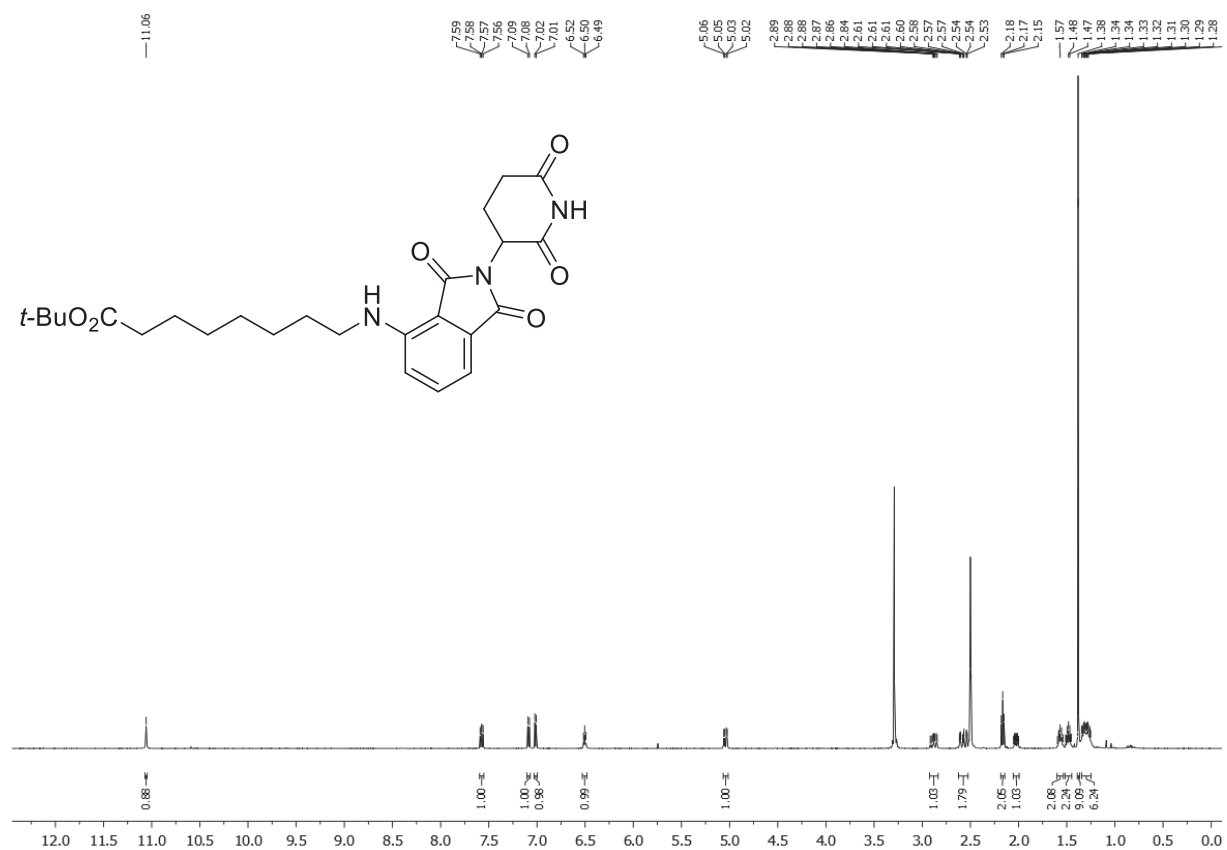
¹³C NMR spectrum of **27** (126 MHz, DMSO-d_6)

S53
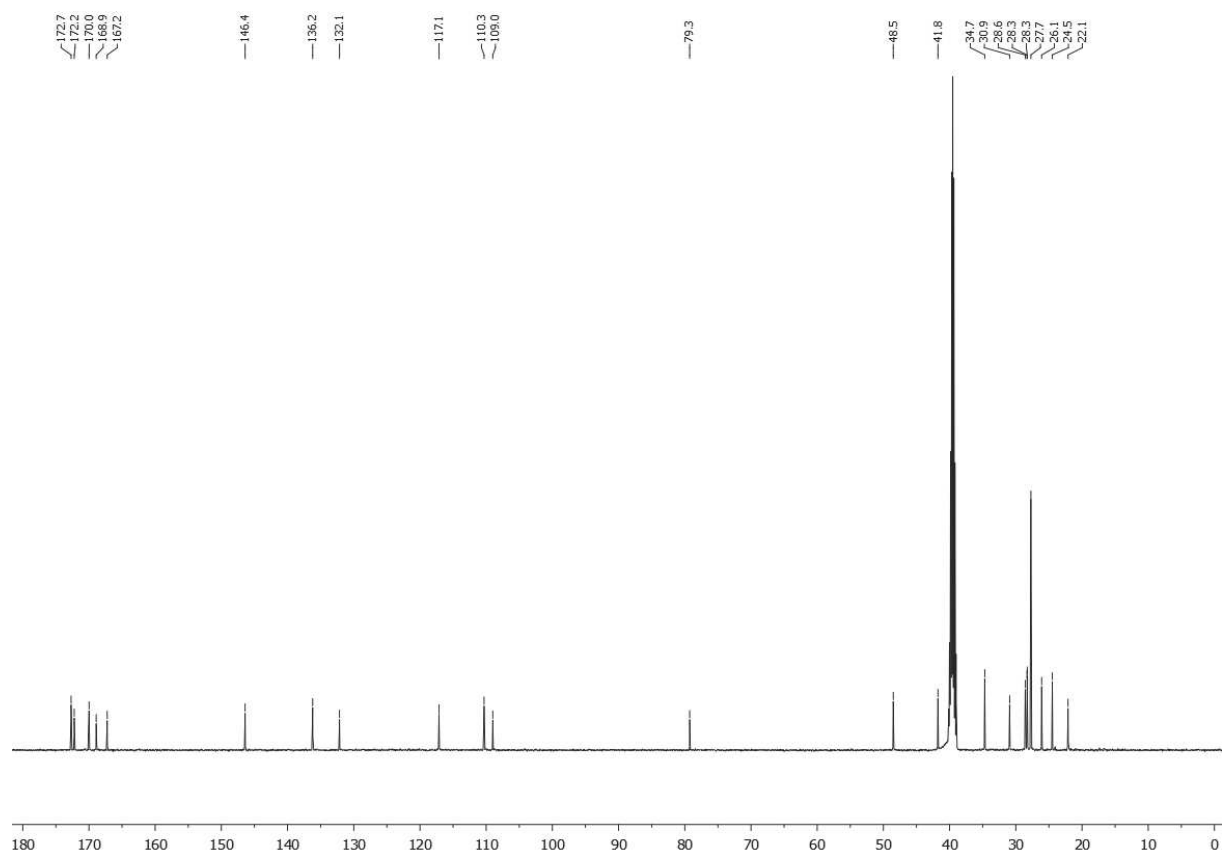
¹H NMR spectrum of **29** (500 MHz, DMSO-*d₆*)

t-BuO$_2$C $\diagup\!\!\!\diagdown$ O $\diagup\!\!\!\diagdown$ O $\diagup\!\!\!\diagdown$ O $\diagup\!\!\!\diagdown$ OBn

7.37, 7.36, 7.36, 7.35, 7.35, 7.34, 7.33, 7.32, 7.32, 7.31, 7.31, 7.30, 7.29, 7.29, 7.28, 7.28, 7.28, 7.27, 7.27, 7.26, 7.26

4.49

3.97, 3.57, 3.57, 3.57, 3.56, 3.56, 3.55, 3.55, 3.54, 3.54, 3.53, 3.53, 3.53, 3.52, 3.52

1.42

5.09   1.84   1.75   12.32   9.00

12.0 11.5 11.0 10.5 10.0 9.5 9.0 8.5 8.0 7.5 7.0 6.5 6.0 5.5 5.0 4.5 4.0 3.5 3.0 2.5 2.0 1.5 1.0 0.5 0.0
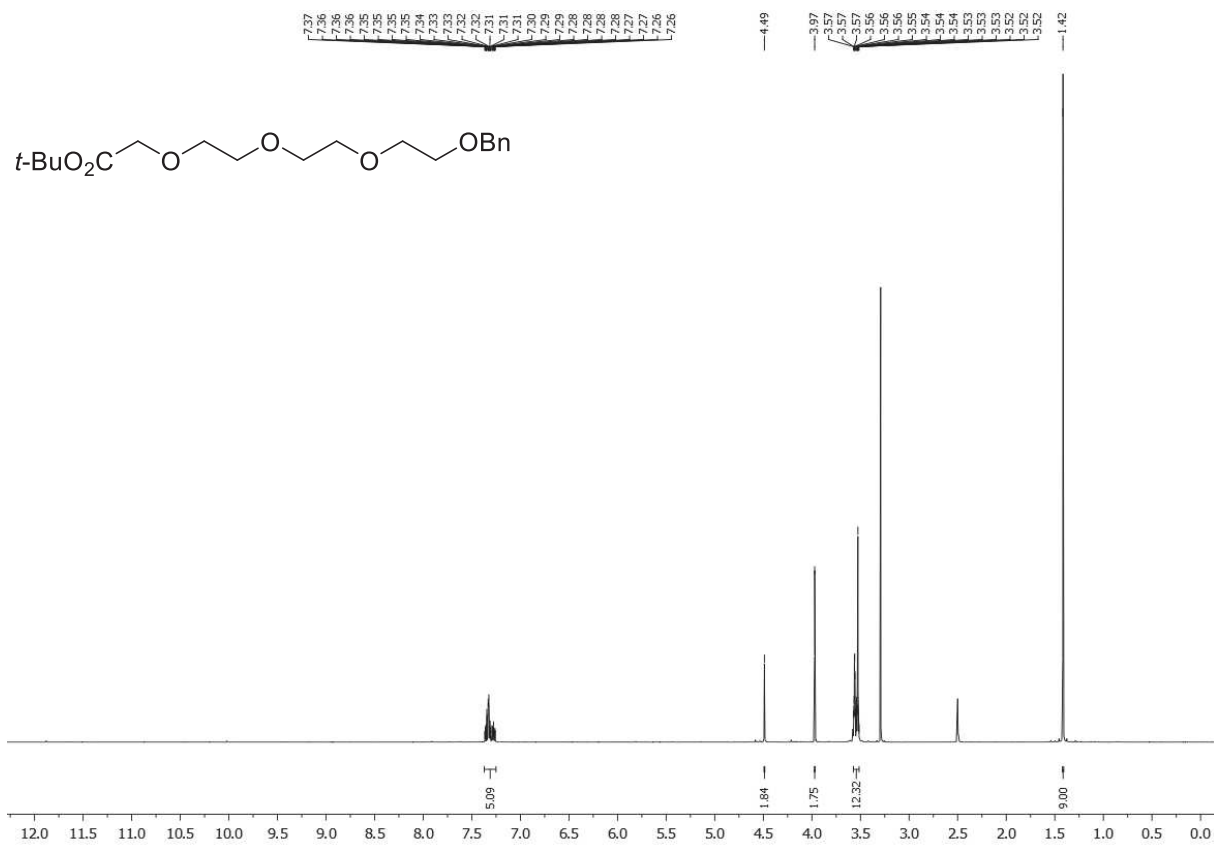
¹³C NMR spectrum of **29** (126 MHz, DMSO-*d₆*)

169.3   138.5   128.1, 127.4, 127.3   80.6   72.0, 69.8, 69.7, 69.7, 69.1, 68.1   27.7

180 170 160 150 140 130 120 110 100 90 80 70 60 50 40 30 20 10 0

S54
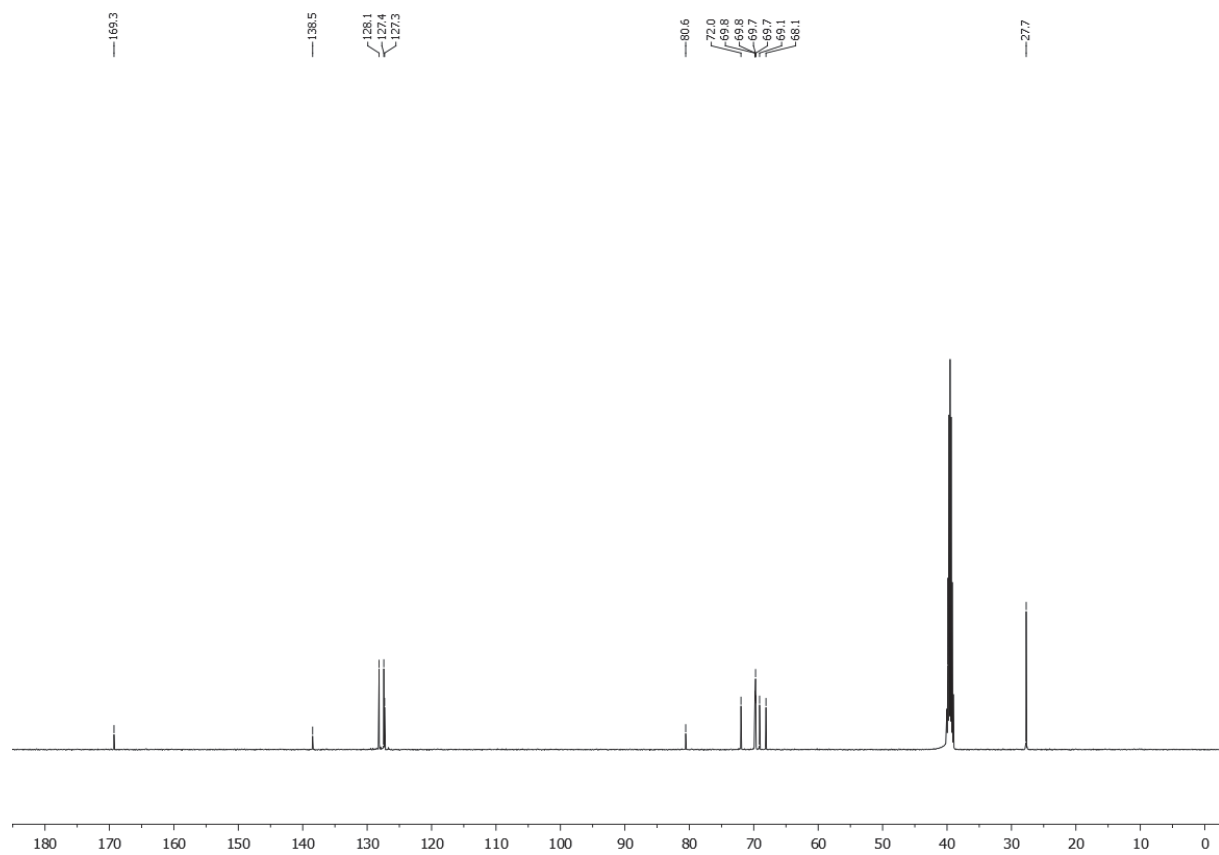
^{1}H NMR spectrum of **30** (500 MHz, DMSO-d_6)

4.54
4.54
4.53
4.53
4.52
4.52
3.98
3.98
3.58
3.57
3.57
3.56
3.56
3.54
3.54
3.53
3.53
3.52
3.49
3.48
3.43
1.42
1.42
1.42
1.42

t-BuO₂C〜〜O〜〜O〜〜O〜〜OH

0.95
1.84
10.39
1.95
8.91

12.0 11.5 11.0 10.5 10.0 9.5 9.0 8.5 8.0 7.5 7.0 6.5 6.0 5.5 5.0 4.5 4.0 3.5 3.0 2.5 2.0 1.5 1.0 0.5 0.0
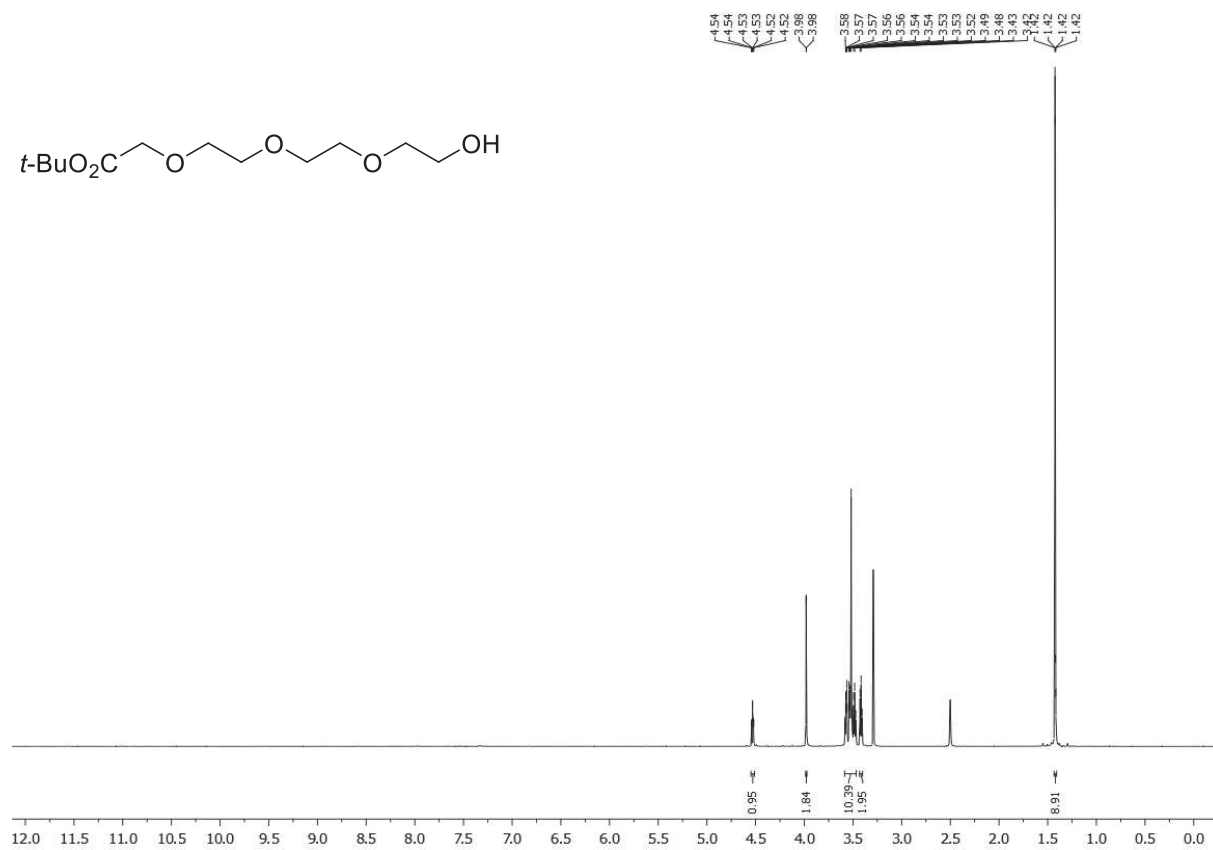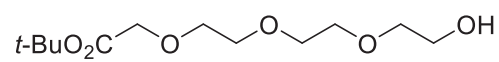
^{13}C NMR spectrum of **30** (126 MHz, DMSO-d_6)

169.3
80.6
72.3
69.8
69.7
69.7
69.7
68.1
60.2
27.7

180 170 160 150 140 130 120 110 100 90 80 70 60 50 40 30 20 10 0

S55
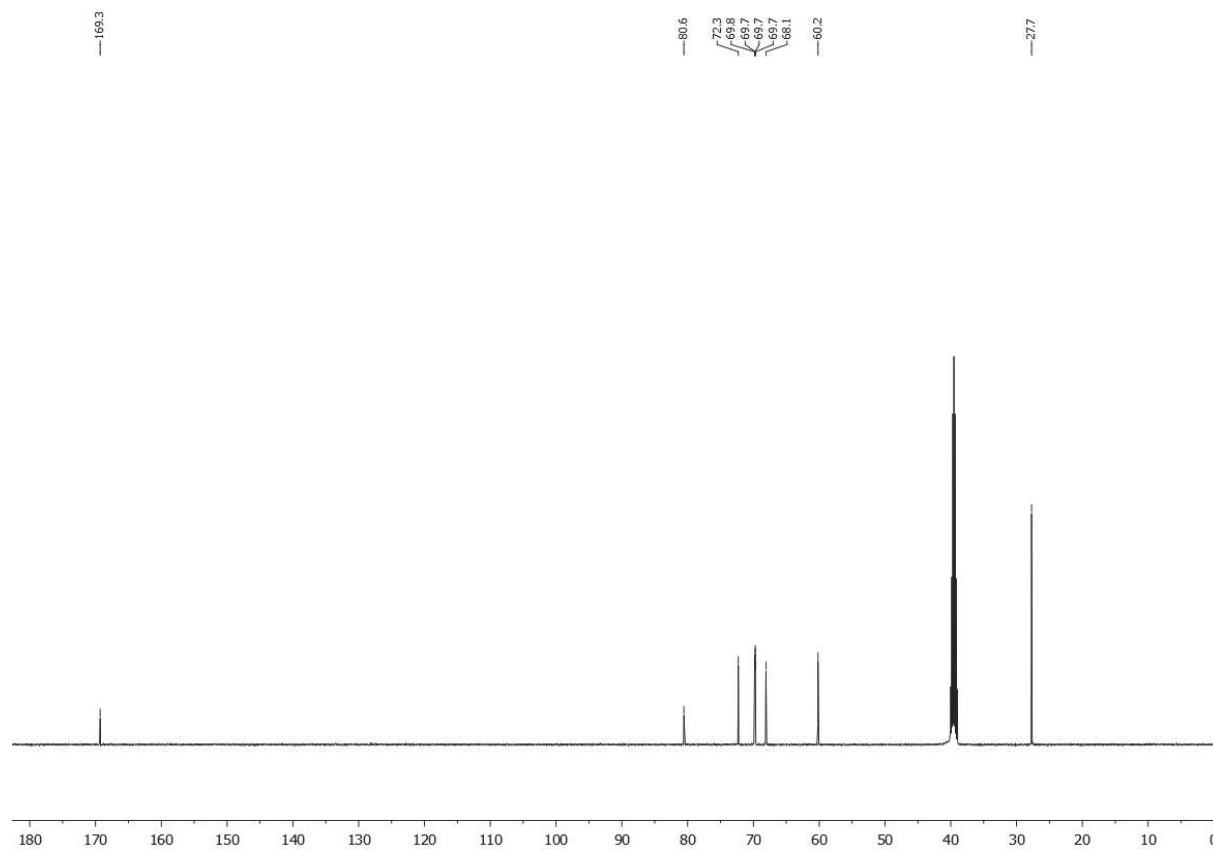
¹H NMR spectrum of **31** (500 MHz, DMSO-d_6)

t-BuO₂C$\diagup$O$\diagup\diagup$O$\diagup\diagup$O$\diagup$CO₂H

4.01
3.98
3.59
3.59
3.58
3.57
3.57
3.57
3.56
3.55
3.54
3.54
3.53
3.53
3.52
1.42

1.73
1.94
8.25
9.00

12.0 11.5 11.0 10.5 10.0 9.5 9.0 8.5 8.0 7.5 7.0 6.5 6.0 5.5 5.0 4.5 4.0 3.5 3.0 2.5 2.0 1.5 1.0 0.5 0.0
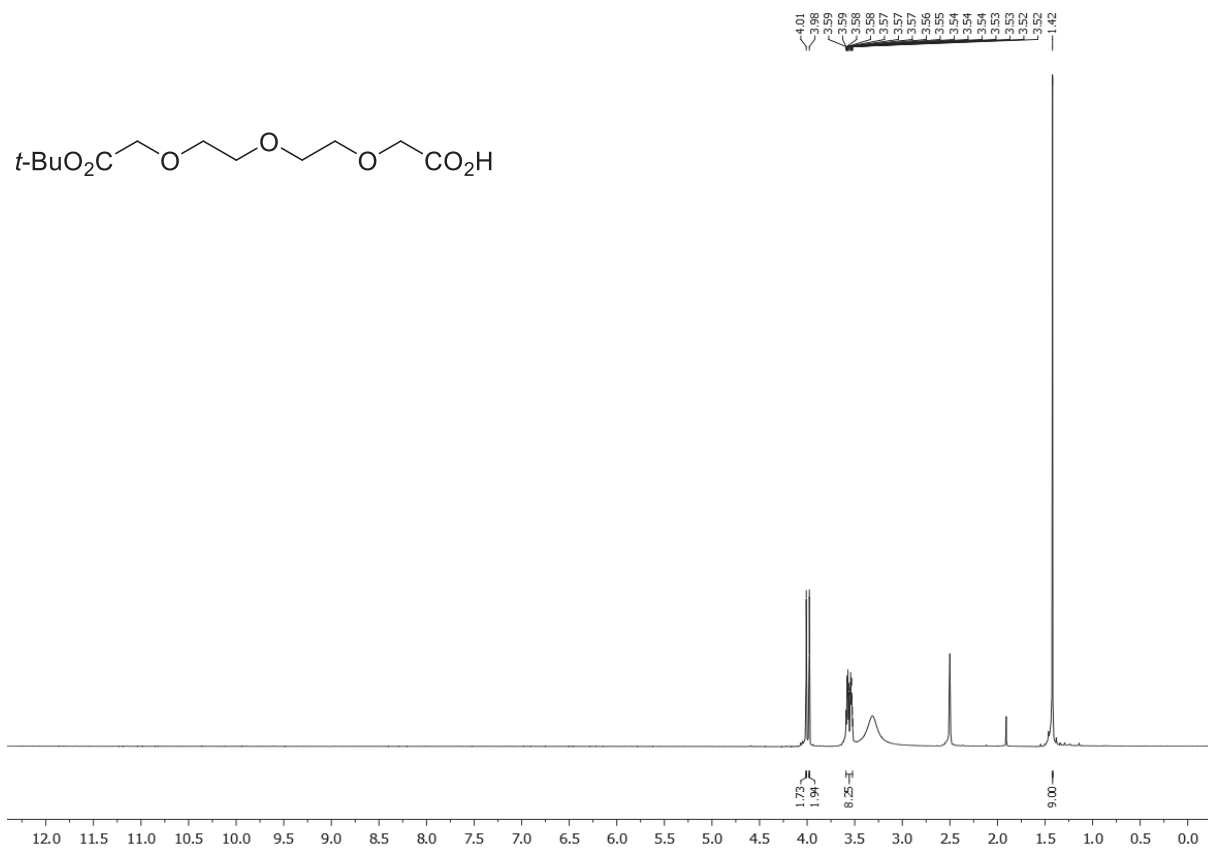
¹³C NMR spectrum of **31** (126 MHz, DMSO-d_6)

171.6
169.3

80.6

69.8
69.8
69.7
69.6
68.1
67.6

27.7

180 170 160 150 140 130 120 110 100 90 80 70 60 50 40 30 20 10 0

S56
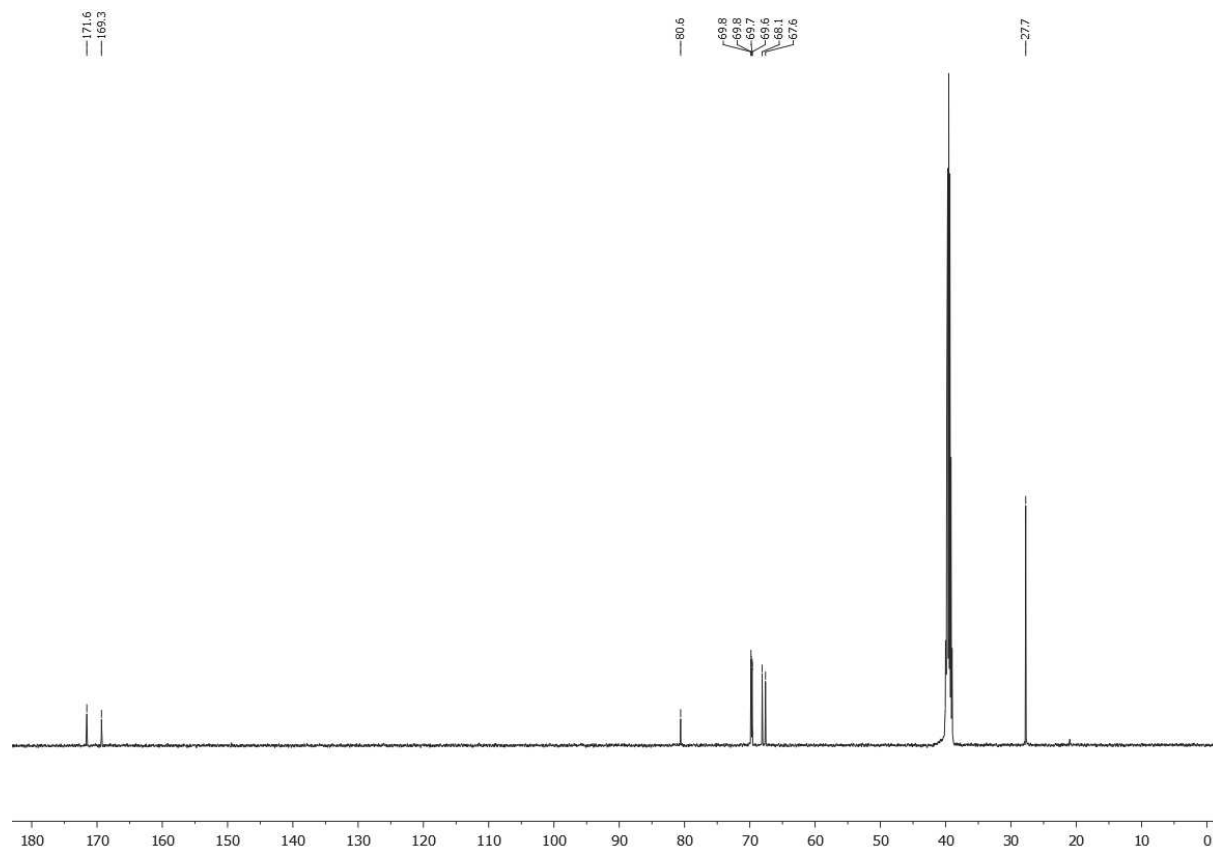
¹H NMR spectrum of **37** (600 MHz, DMSO-*d₆*)
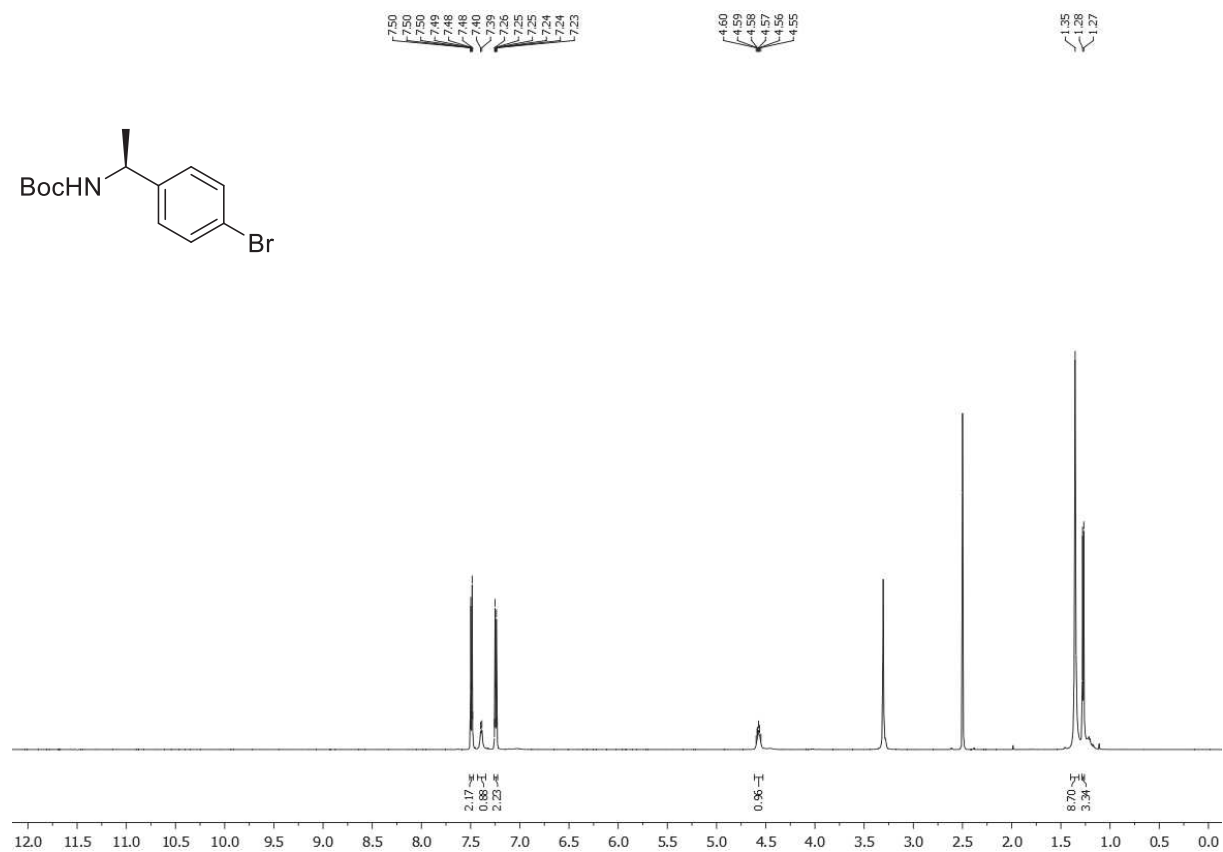
¹³C NMR spectrum of **37** (151 MHz, DMSO-*d₆*)

S57
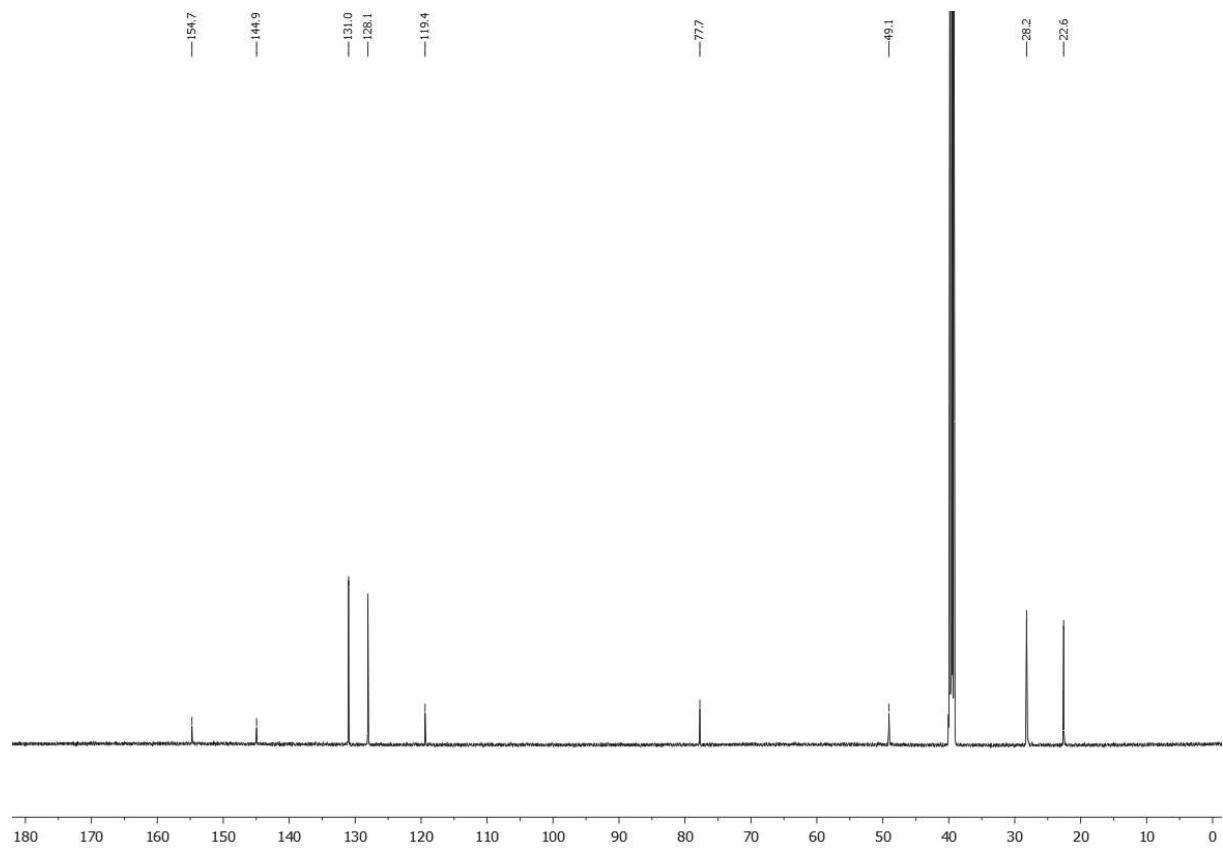
¹H NMR spectrum of **38** (500 MHz, DMSO-*d*₆)
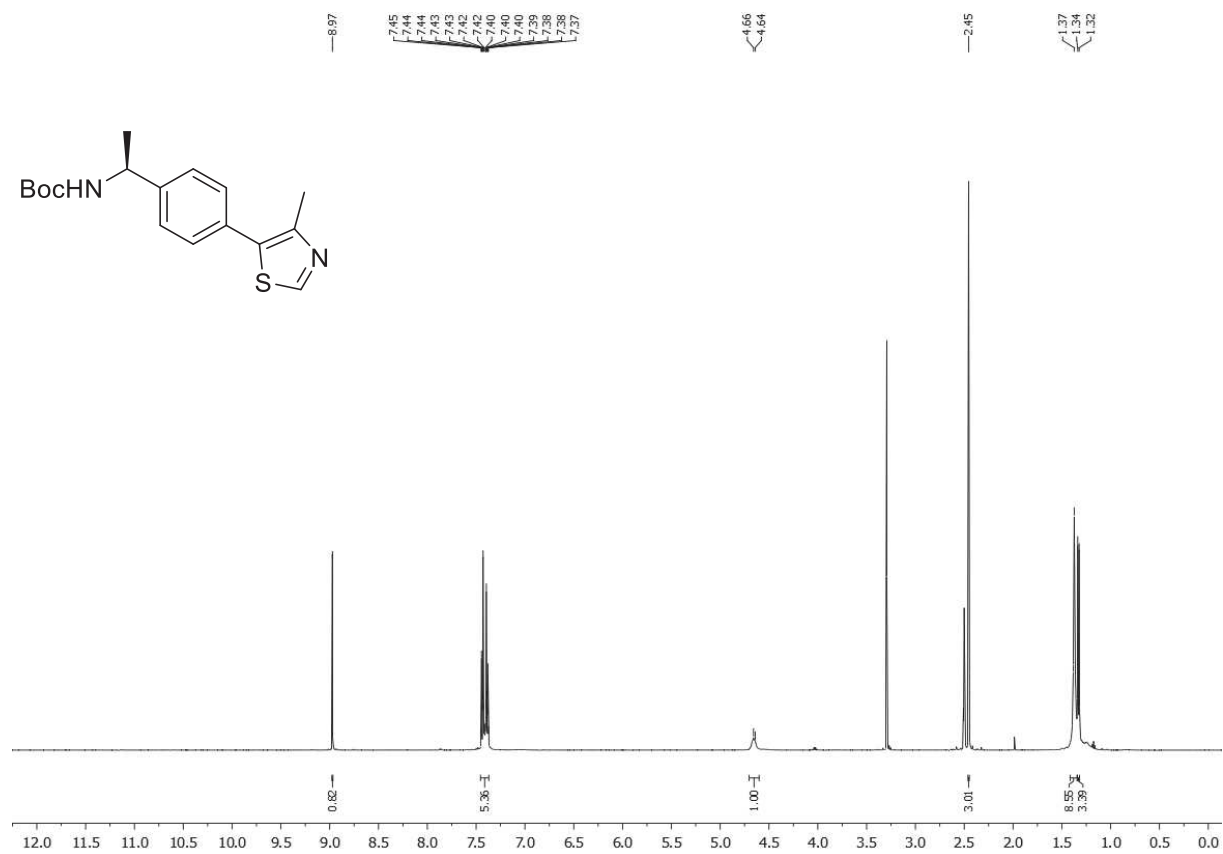
¹³C NMR spectrum of **38** (126 MHz, DMSO-*d*₆)
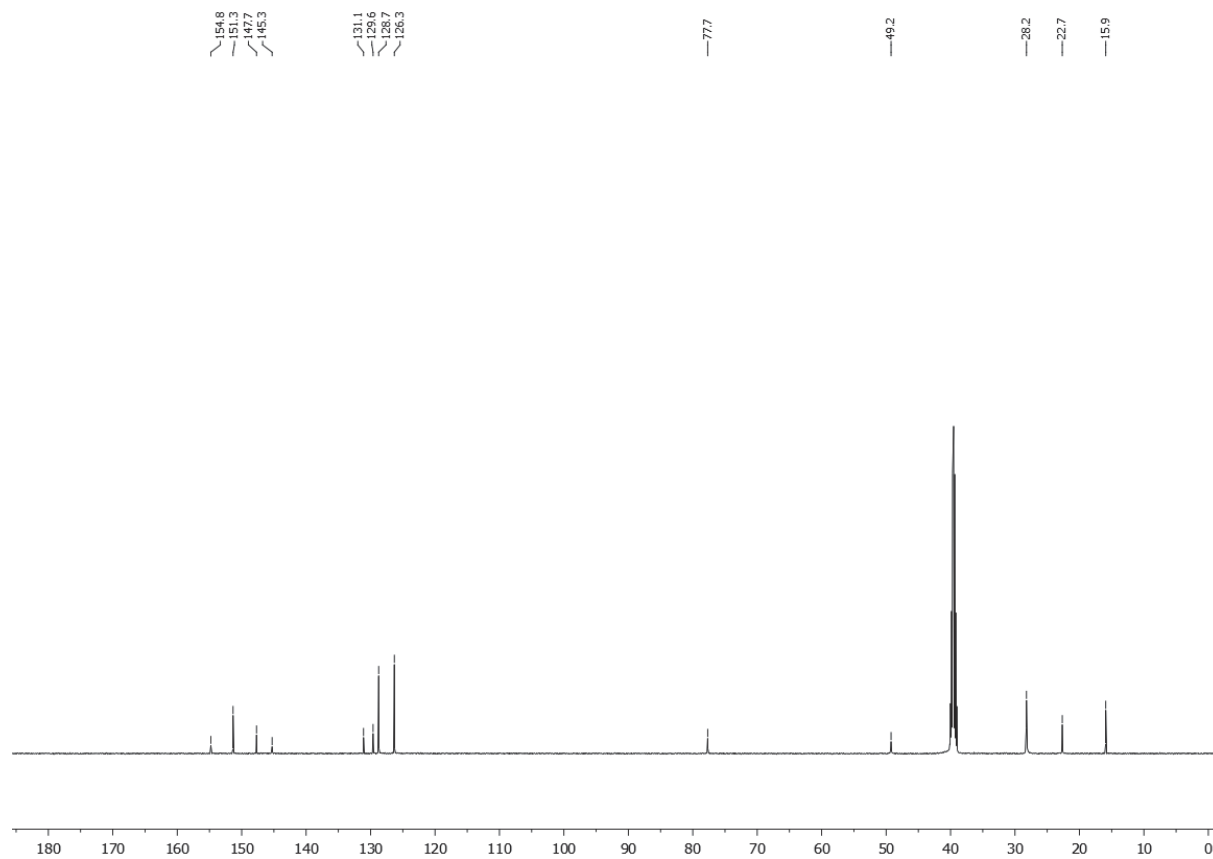
¹H NMR spectrum of **41** (500 MHz, DMSO-*d₆*)
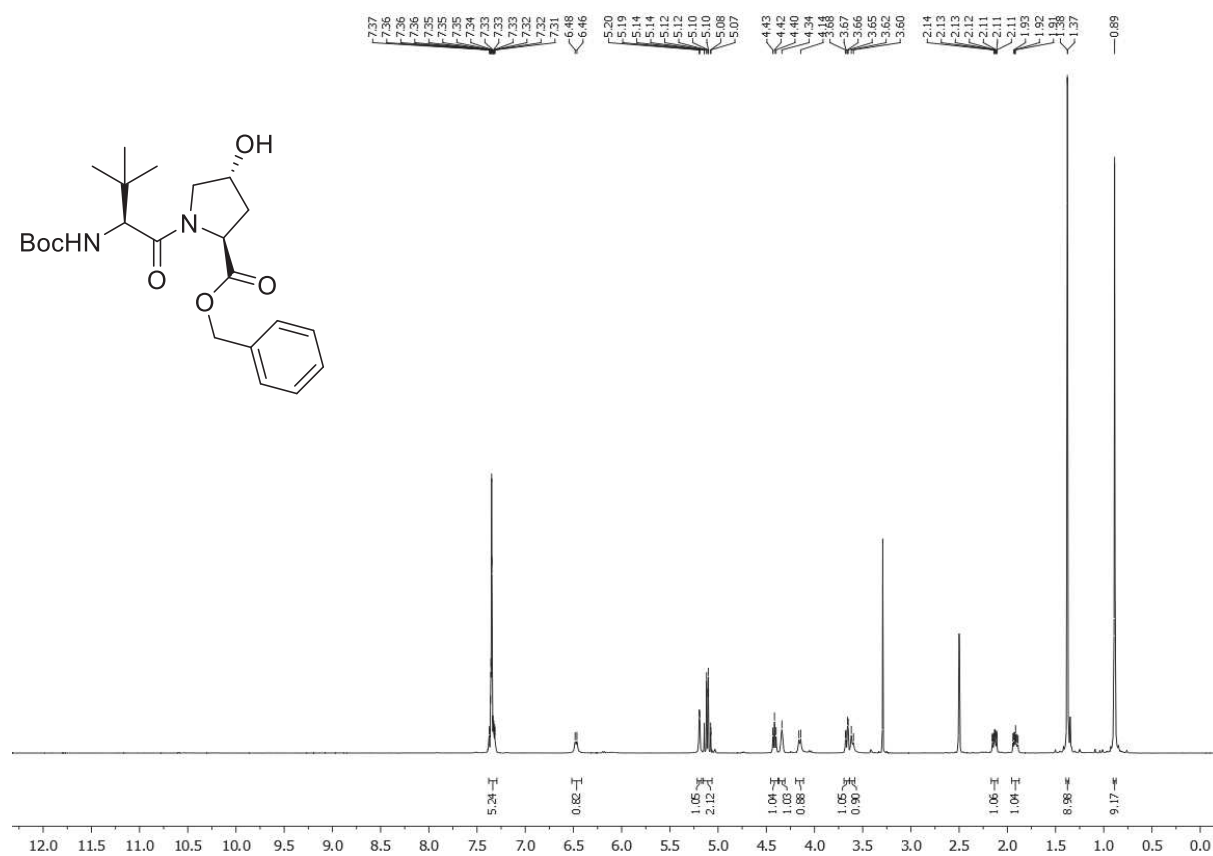
¹³C NMR spectrum of **41** (126 MHz, DMSO-*d₆*)
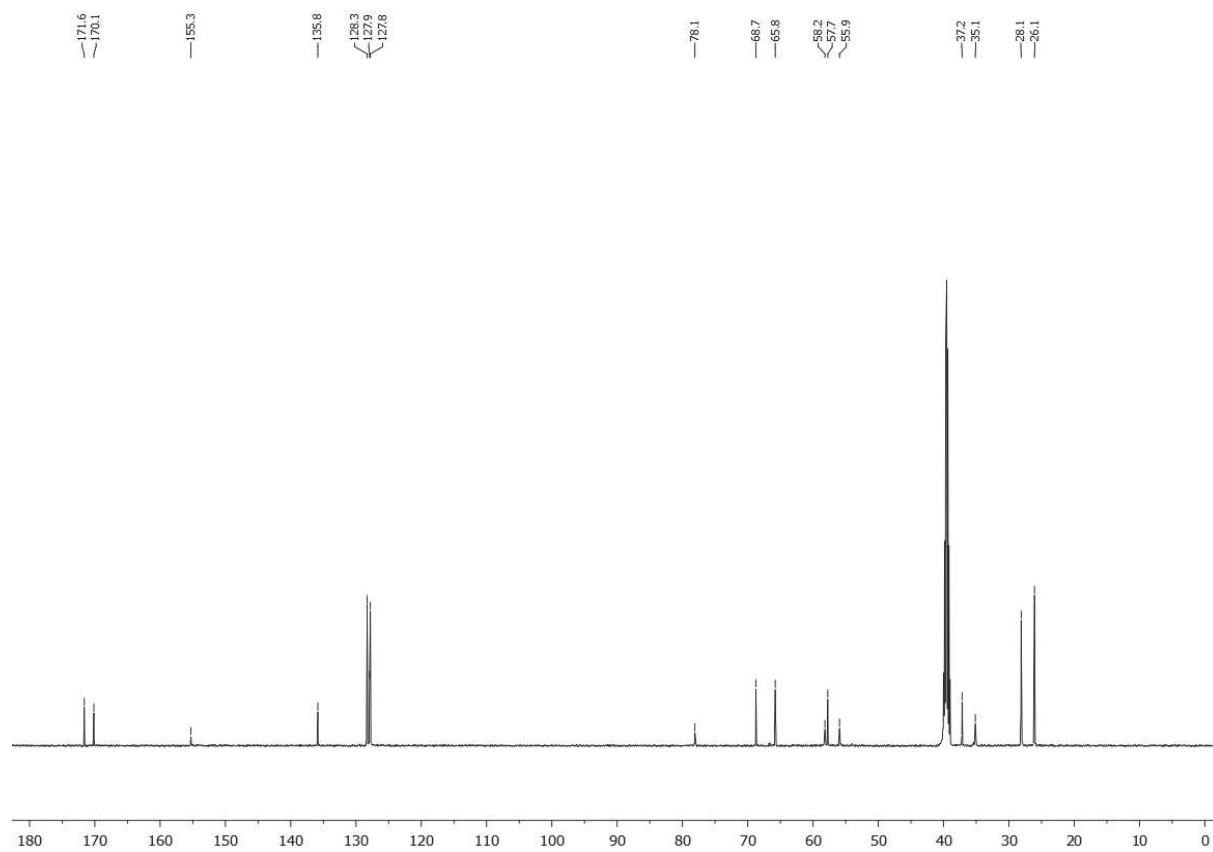
¹H NMR spectrum of **33** (600 MHz, DMSO-d_6)
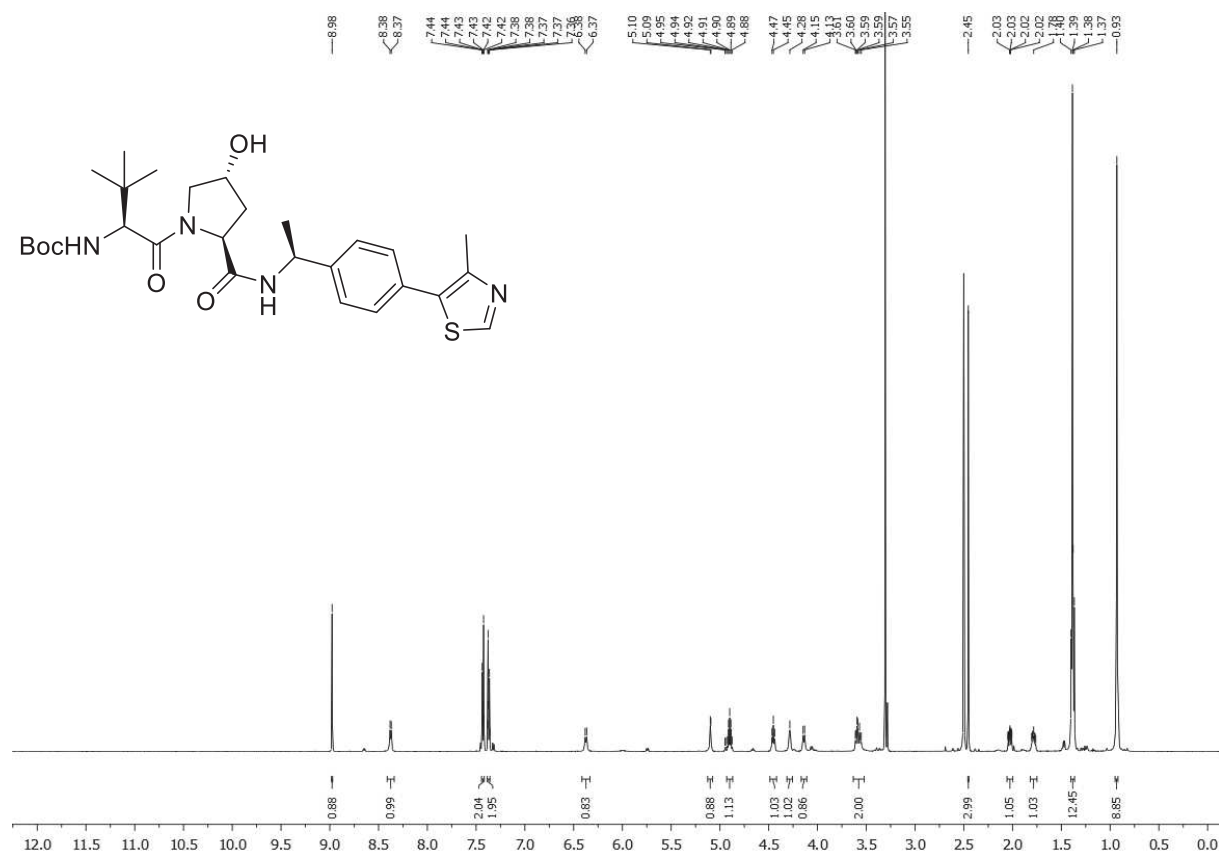
¹³C NMR spectrum of **33** (151 MHz, DMSO-d_6)
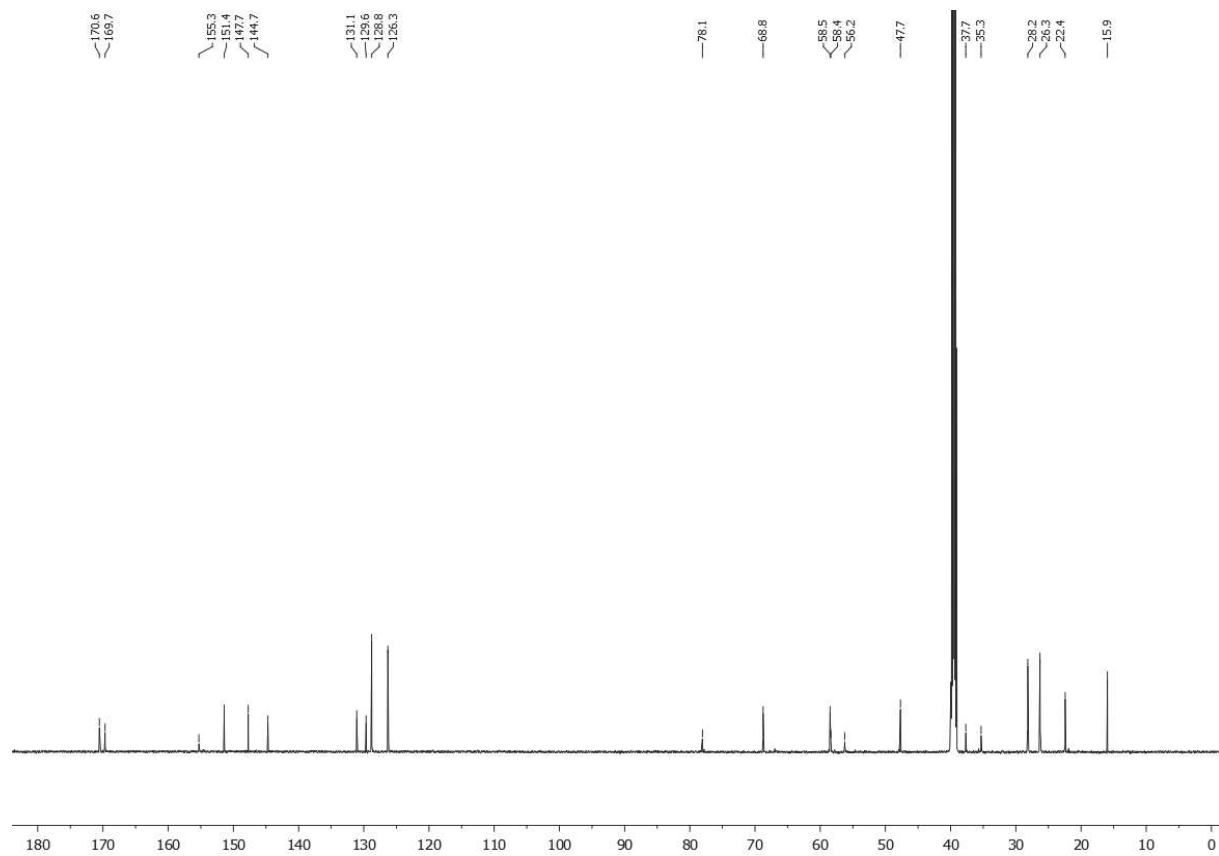
¹H NMR spectrum of **34** (600 MHz, DMSO-*d*₆)
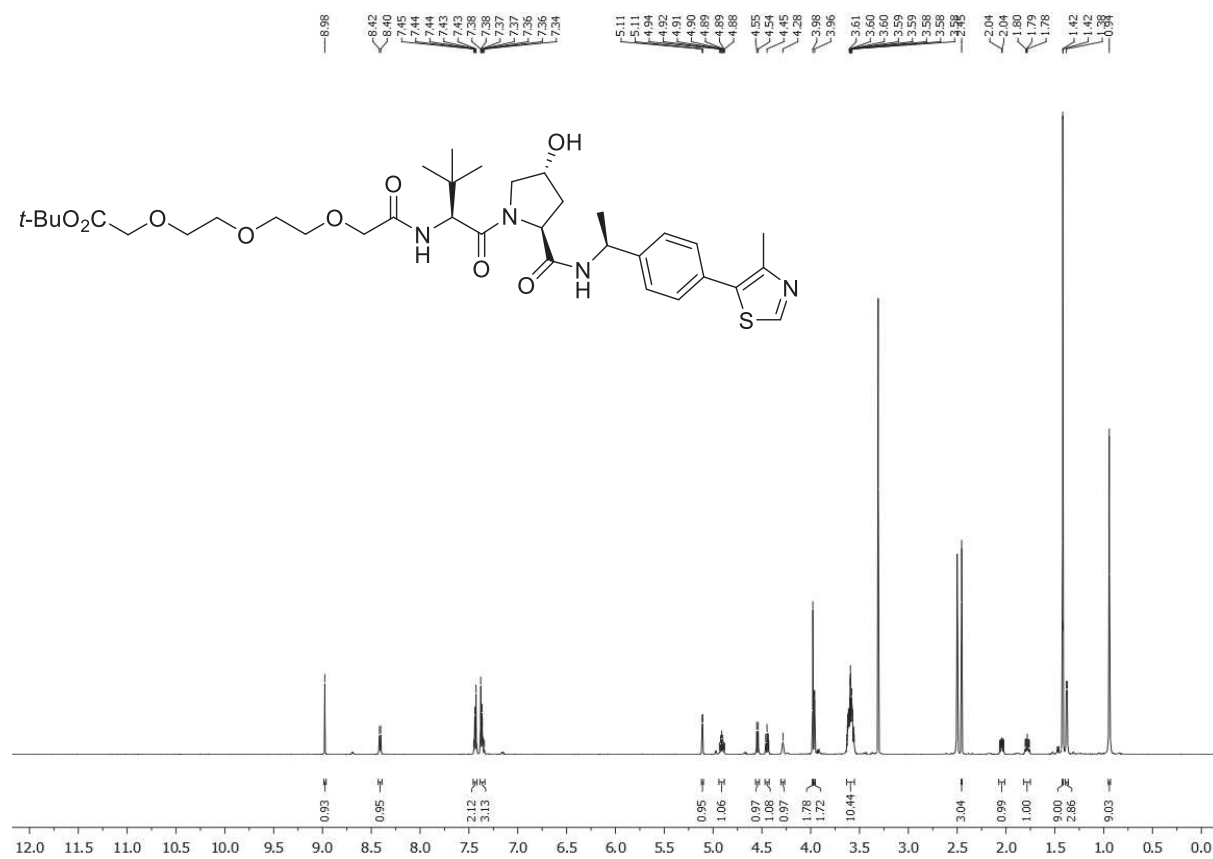
¹³C NMR spectrum of **34** (151 MHz, DMSO-*d*₆)
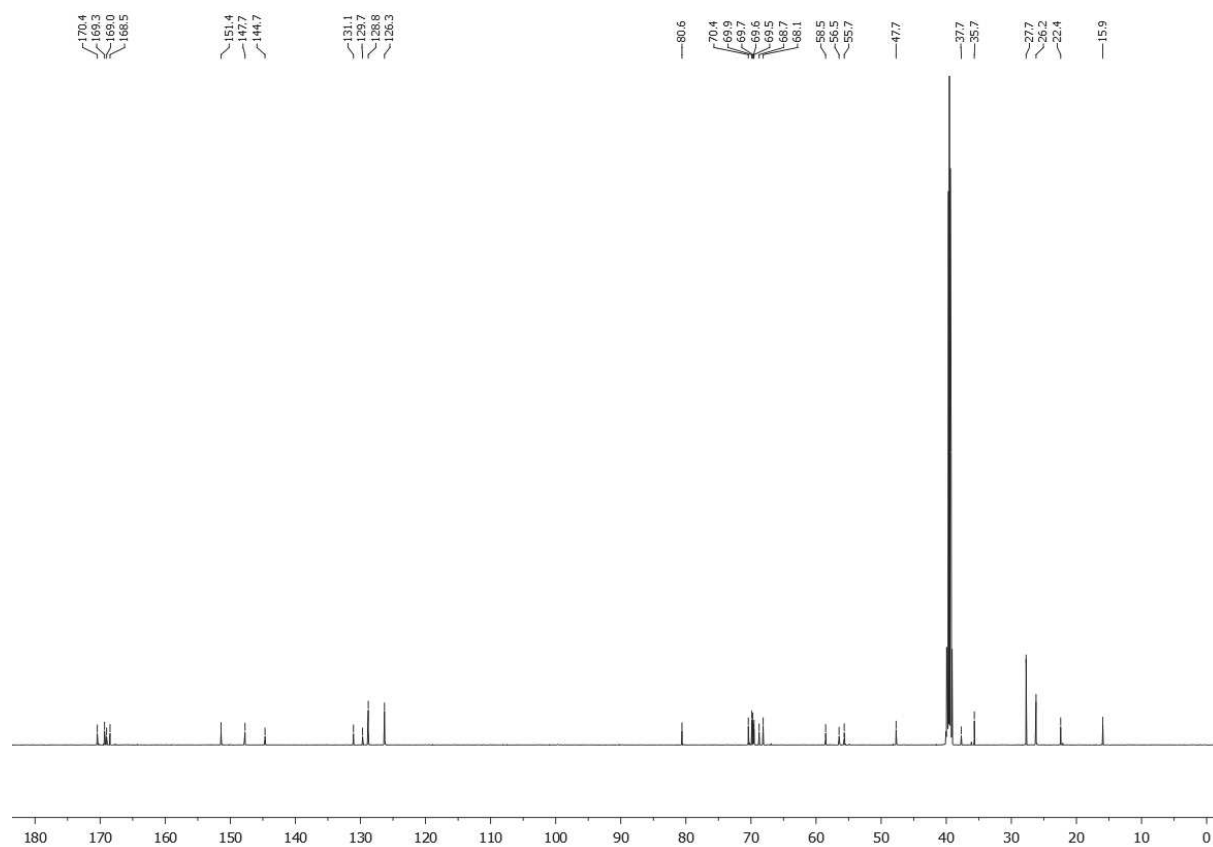
^{1}H NMR spectrum of **35** (600 MHz, DMSO-d_6)
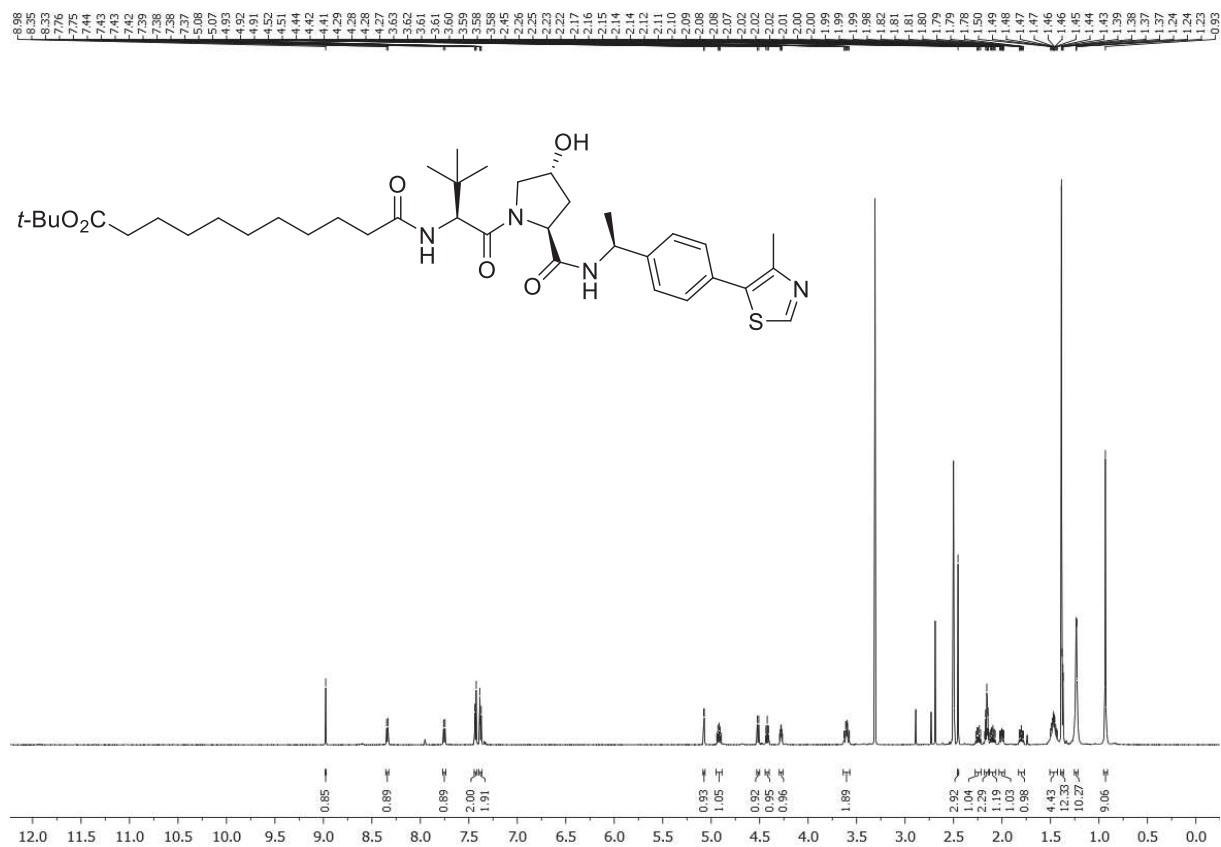
^{13}C NMR spectrum of **35** (151 MHz, DMSO-d_6)
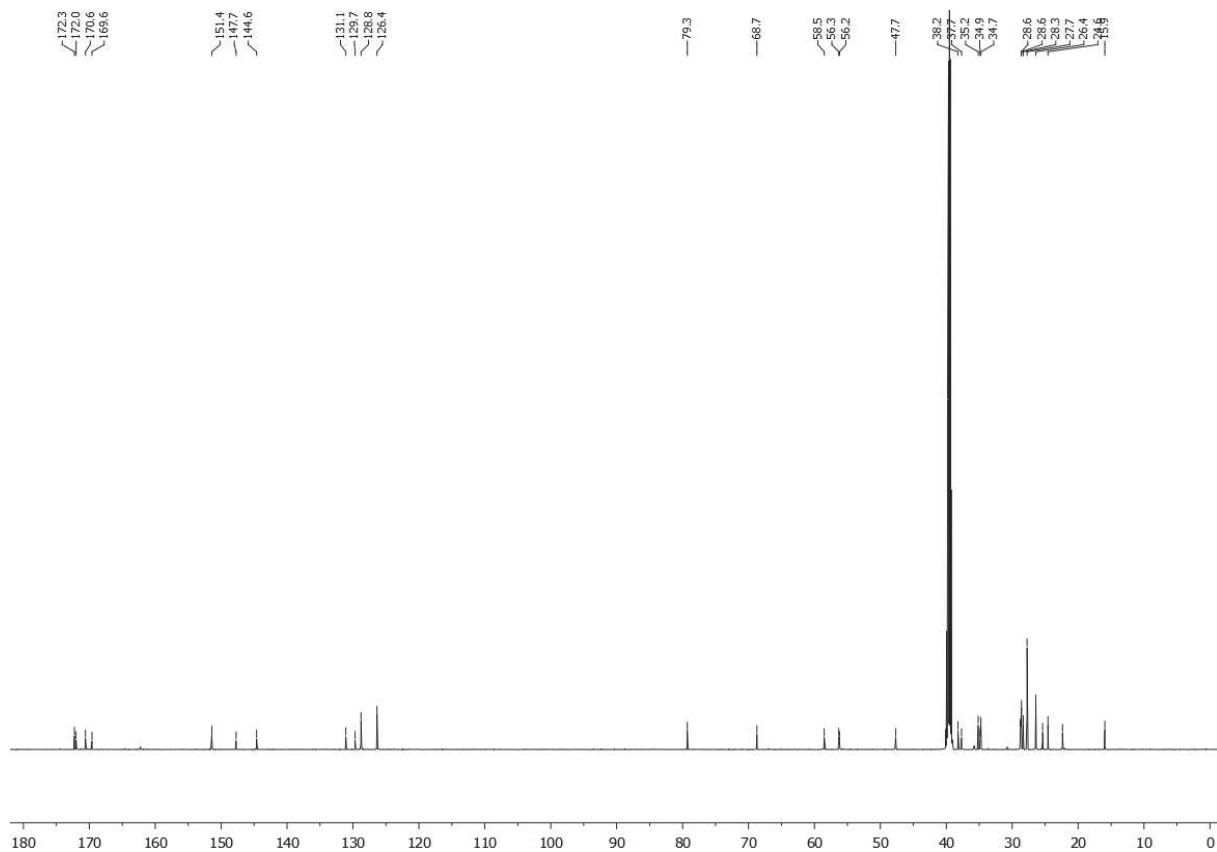
¹H NMR spectrum of **1** (600 MHz, DMSO-*d₆*)

¹³C NMR spectrum of **1** (151 MHz, DMSO-*d₆*)

S63
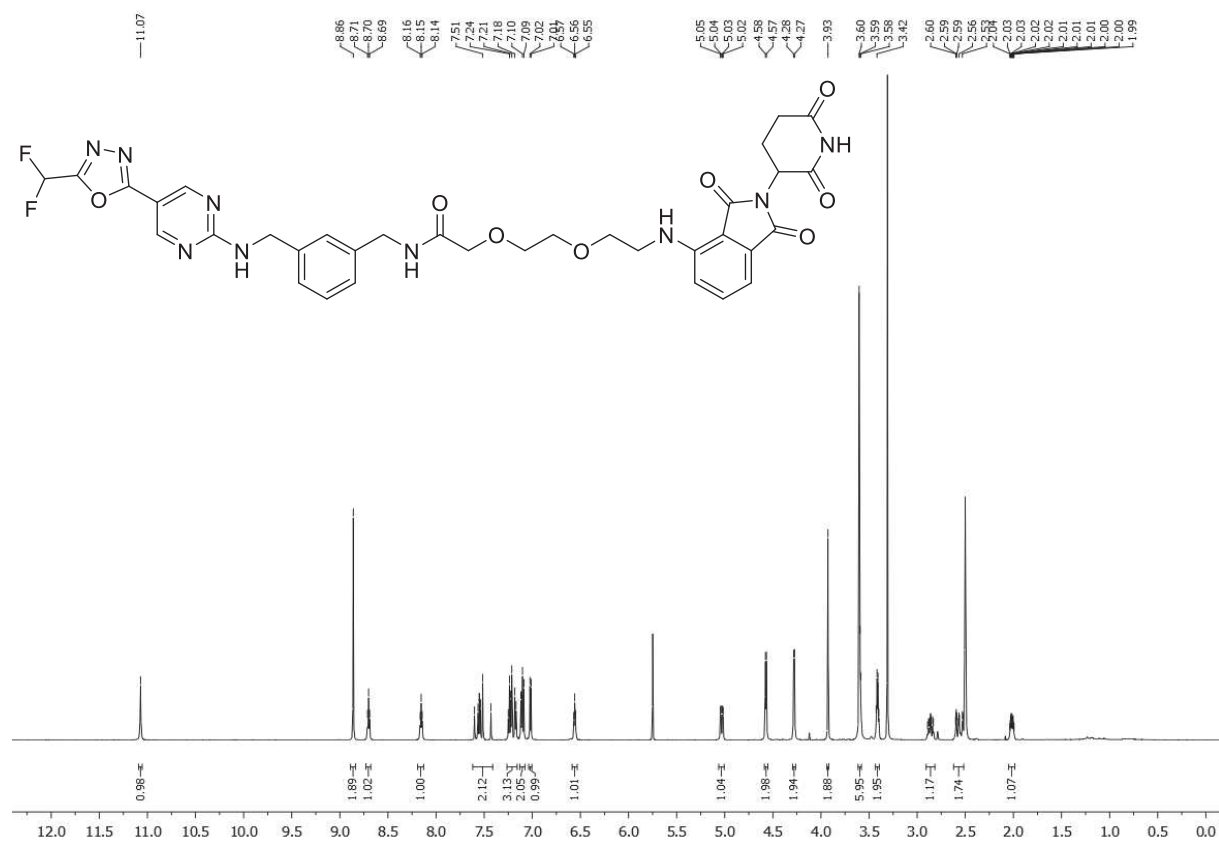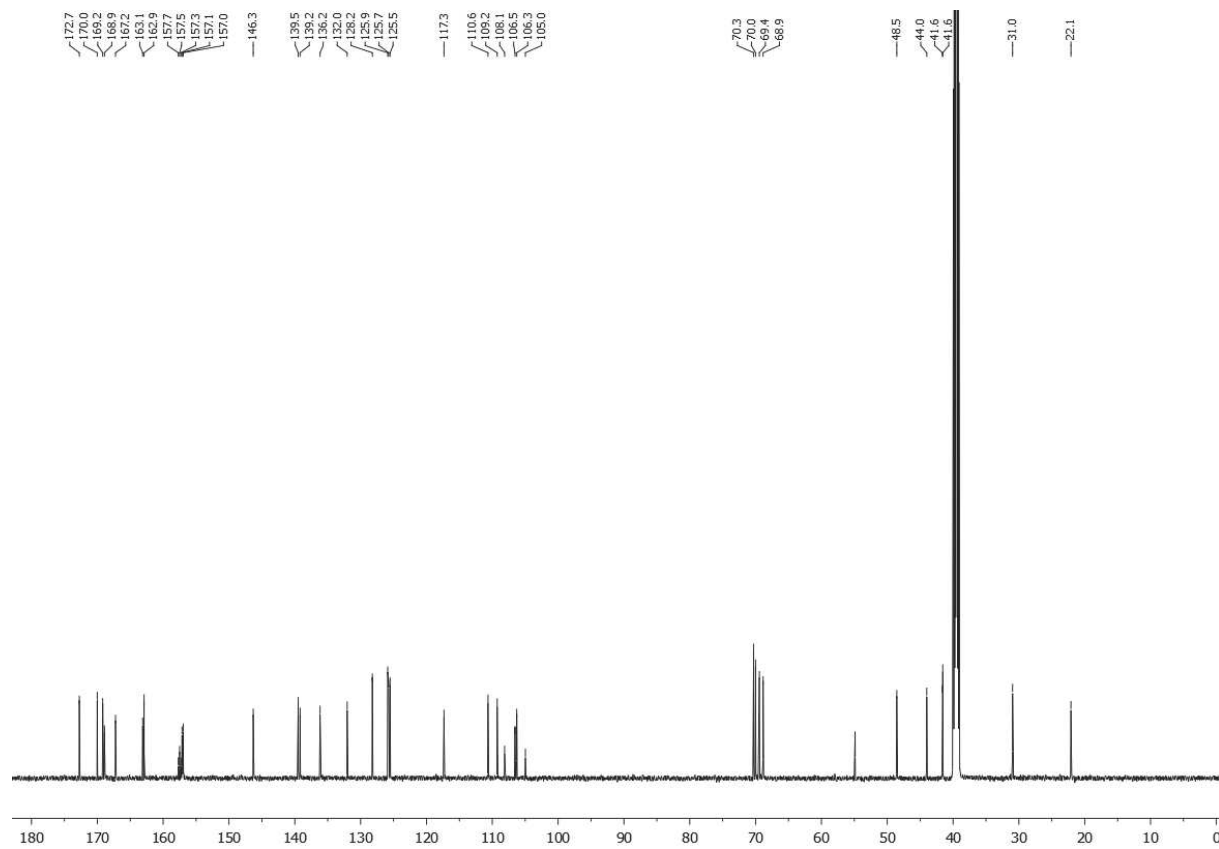
¹H NMR spectrum of **2** (600 MHz, DMSO-*d₆*)

¹³C NMR spectrum of **2** (151 MHz, DMSO-*d₆*)
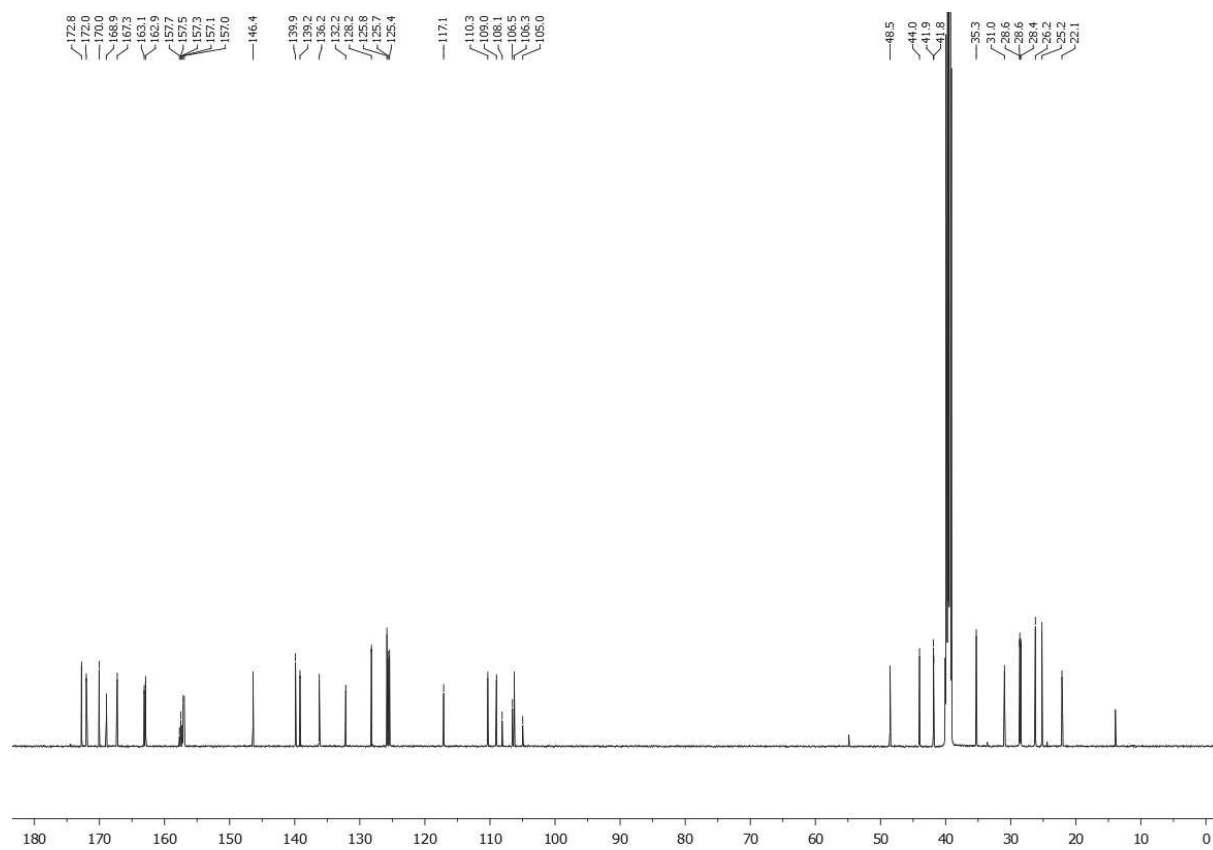
¹H NMR spectrum of **3** (600 MHz, DMSO-*d₆*)
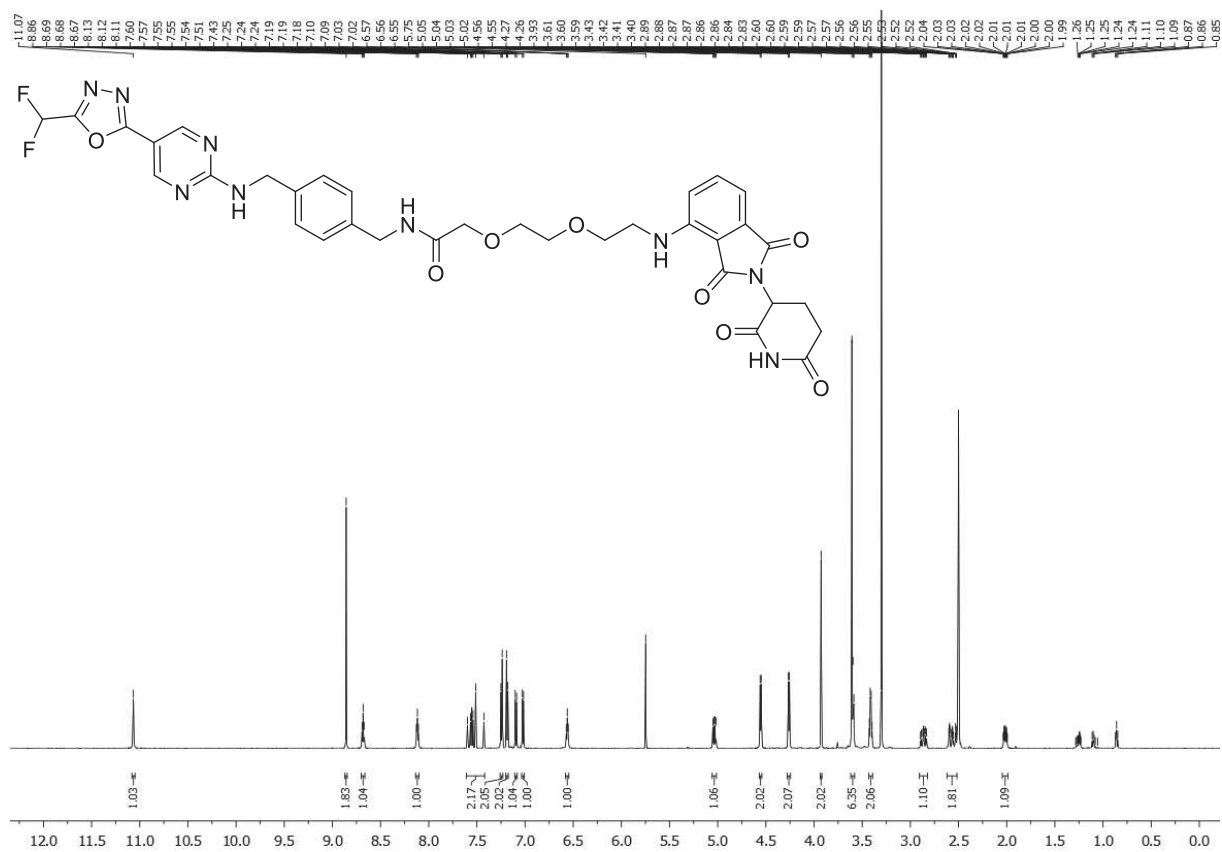
¹³C NMR spectrum of **3** (151 MHz, DMSO-*d₆*)
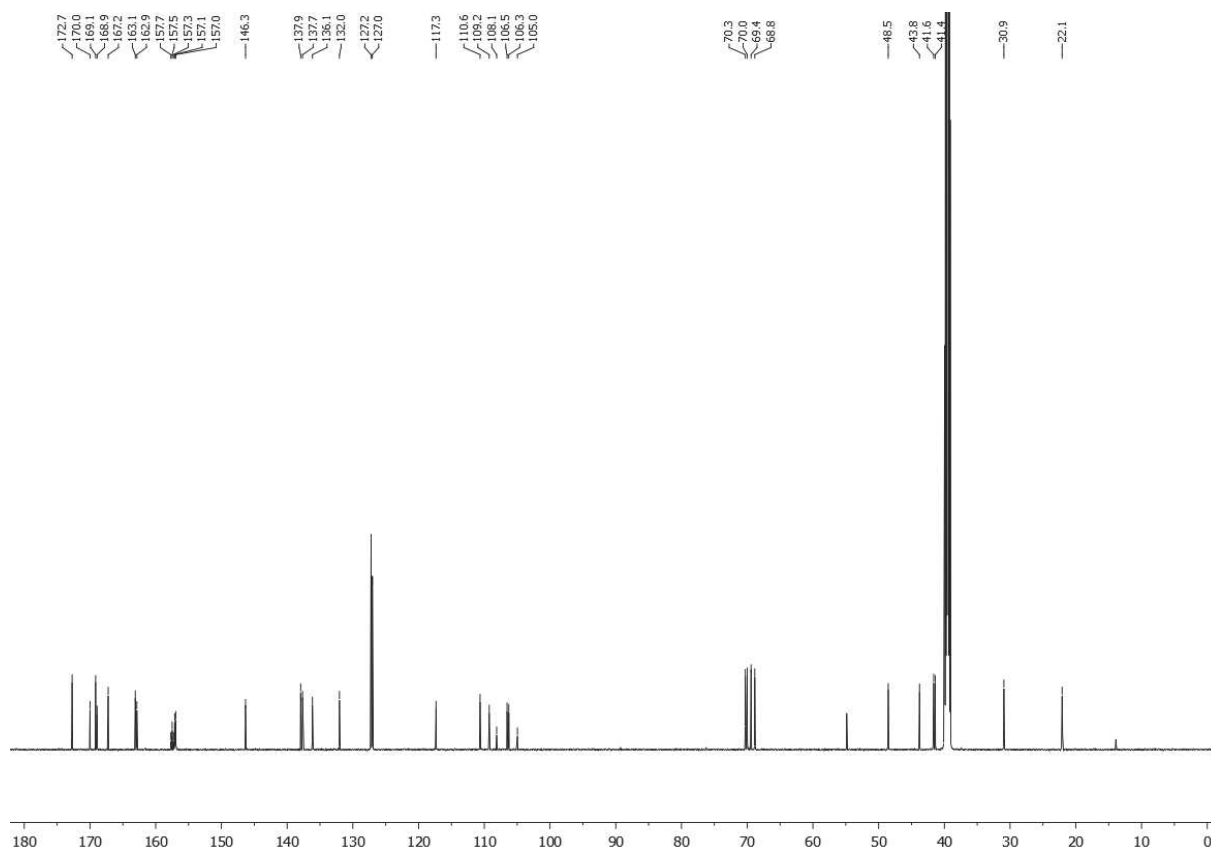
^{1}H NMR spectrum of **4** (600 MHz, DMSO-d_6)
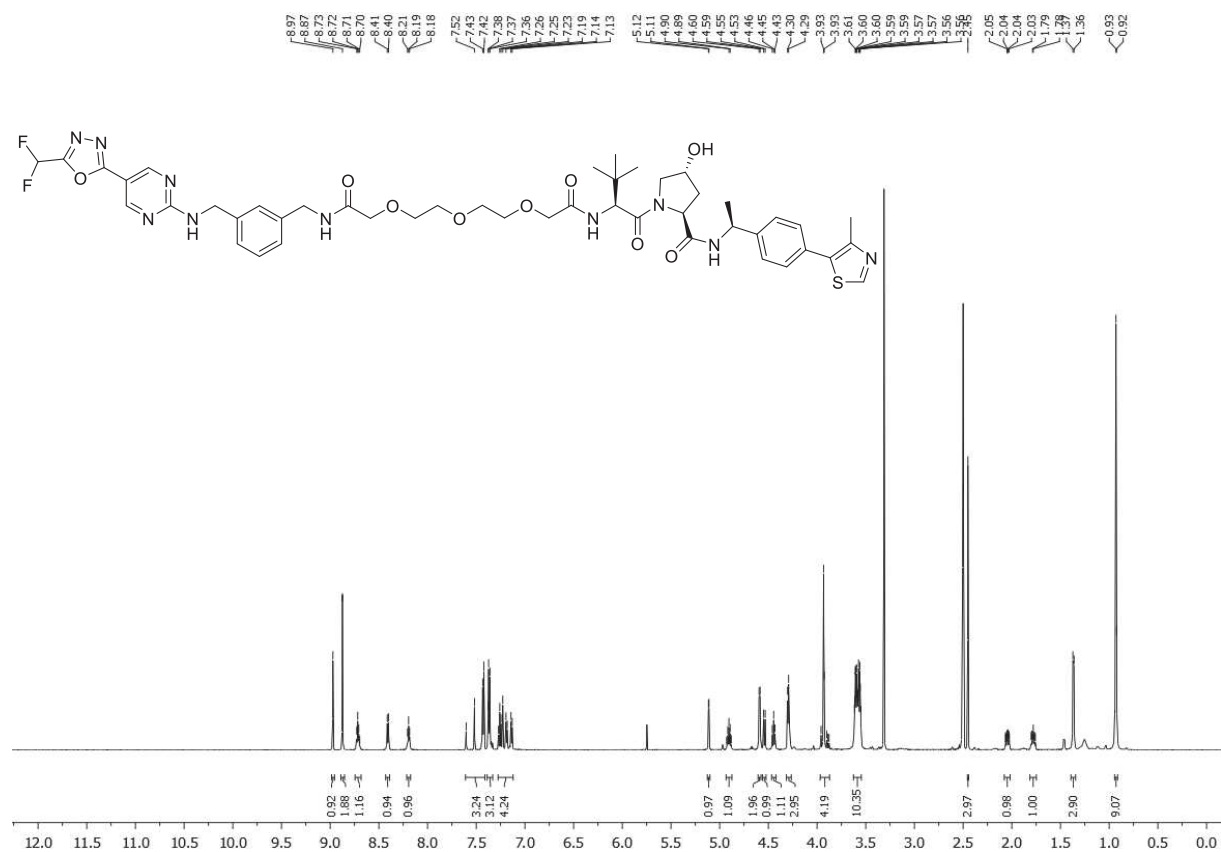
^{13}C NMR spectrum of **4** (151 MHz, DMSO-d_6)
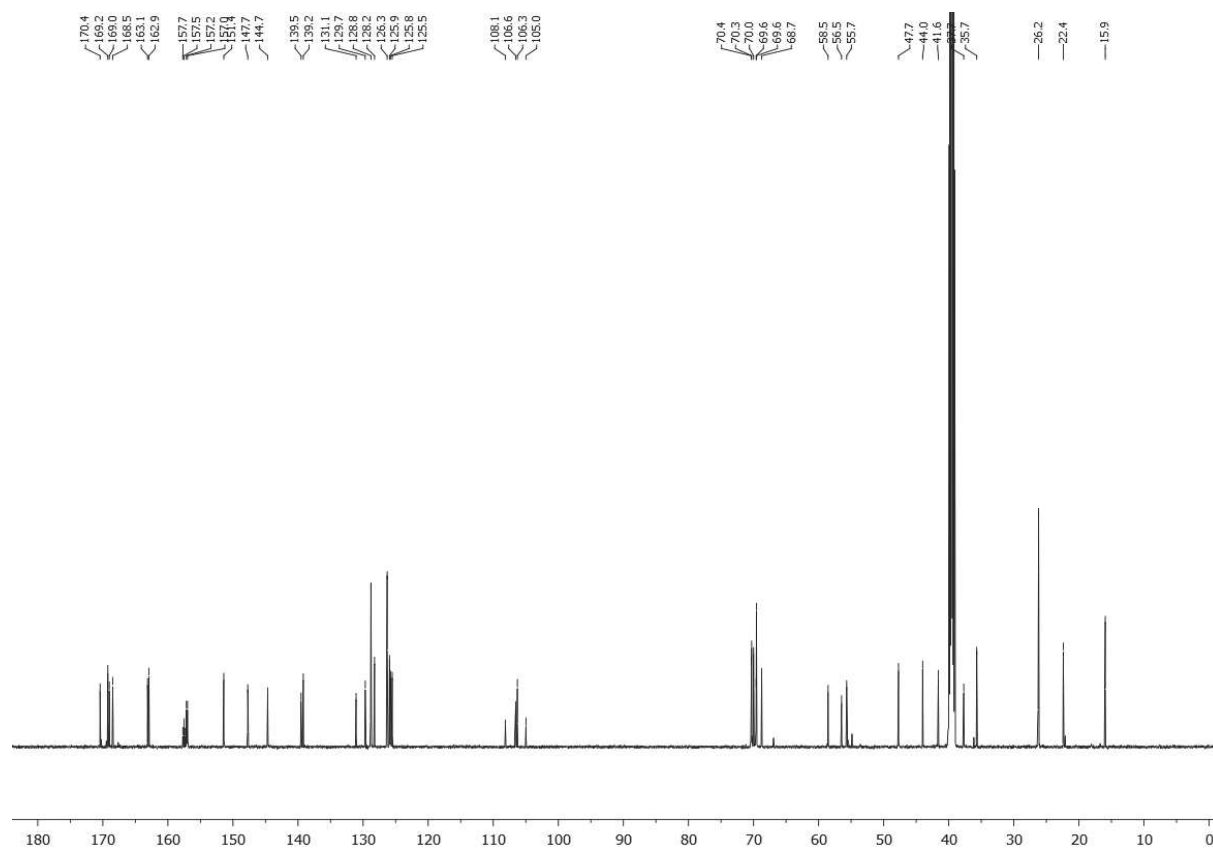
¹H NMR spectrum of **5** (500 MHz, DMSO-*d*₆)

¹³C NMR spectrum of **5** (126 MHz, DMSO-*d*₆)

S67

¹H NMR spectrum of **6** (600 MHz, DMSO-*d*₆)

¹³C NMR spectrum of **6** (151 MHz, DMSO-*d*₆)
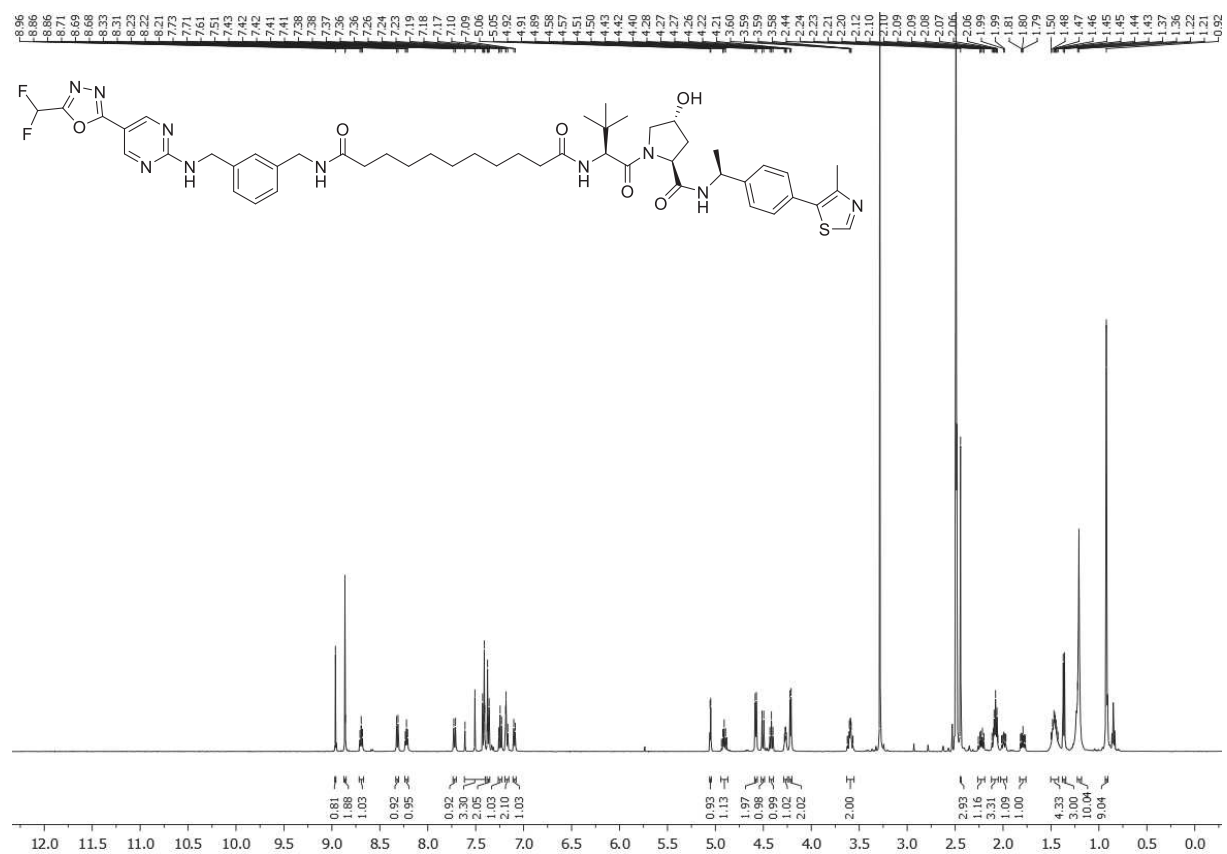
¹H NMR spectrum of **42** (500 MHz, DMSO-*d₆*)
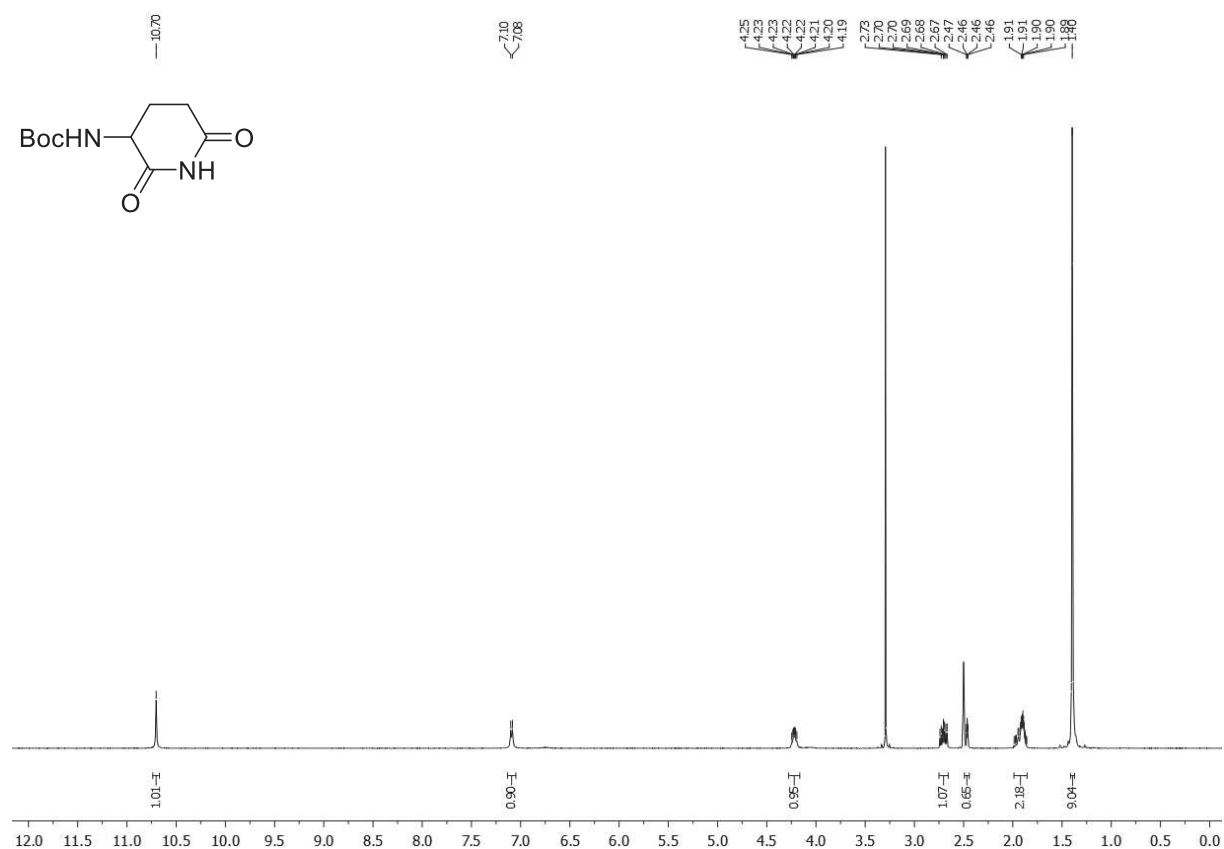
¹³C NMR spectrum of **42** (126 MHz, DMSO-*d₆*)
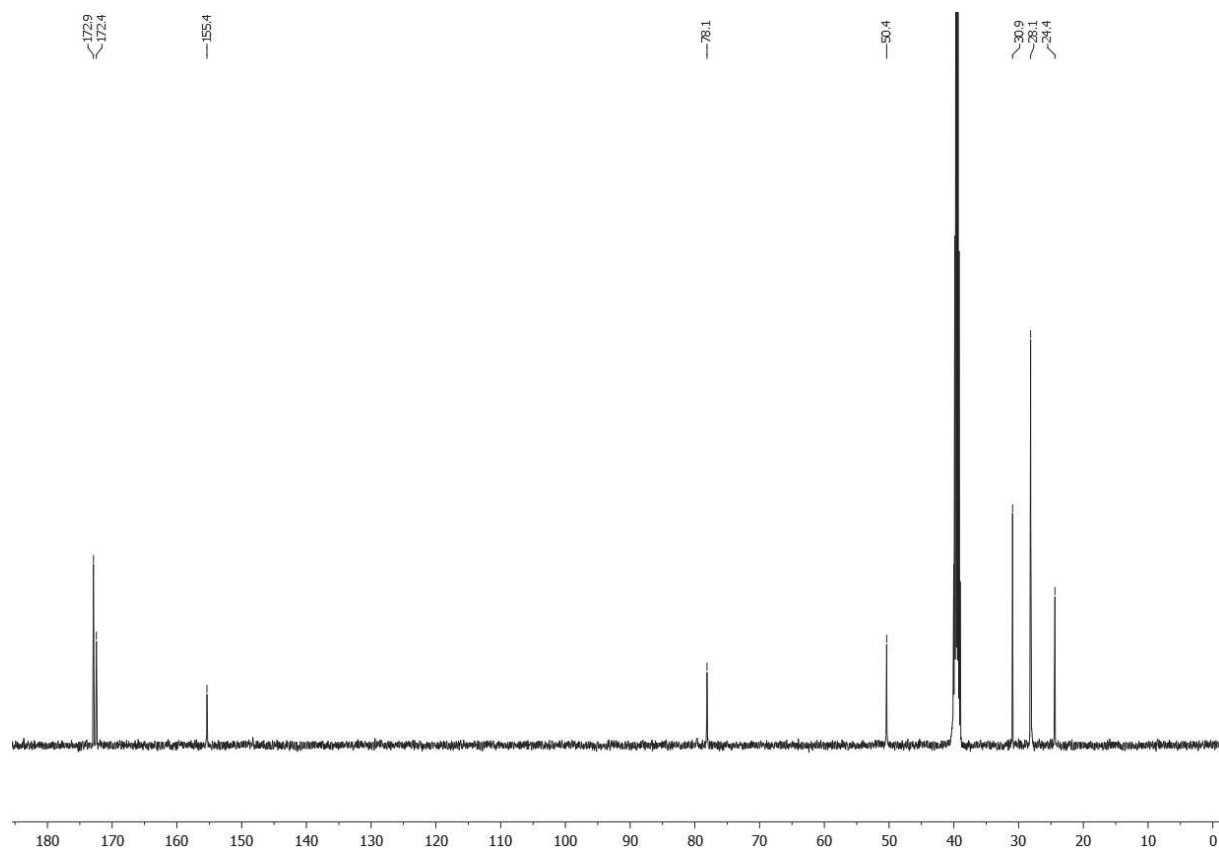
¹H NMR spectrum of **43** (500 MHz, DMSO-d_6)
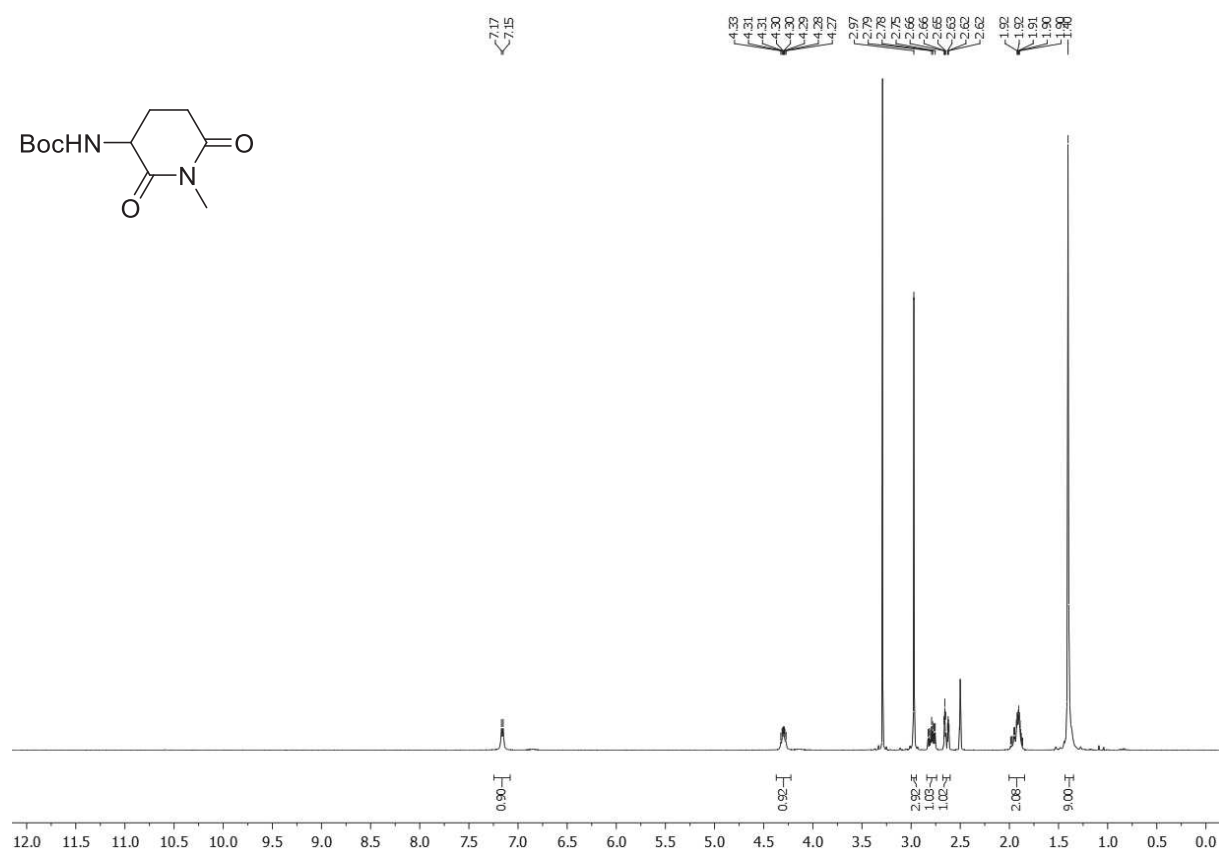
¹³C NMR spectrum of **43** (126 MHz, DMSO-d_6)
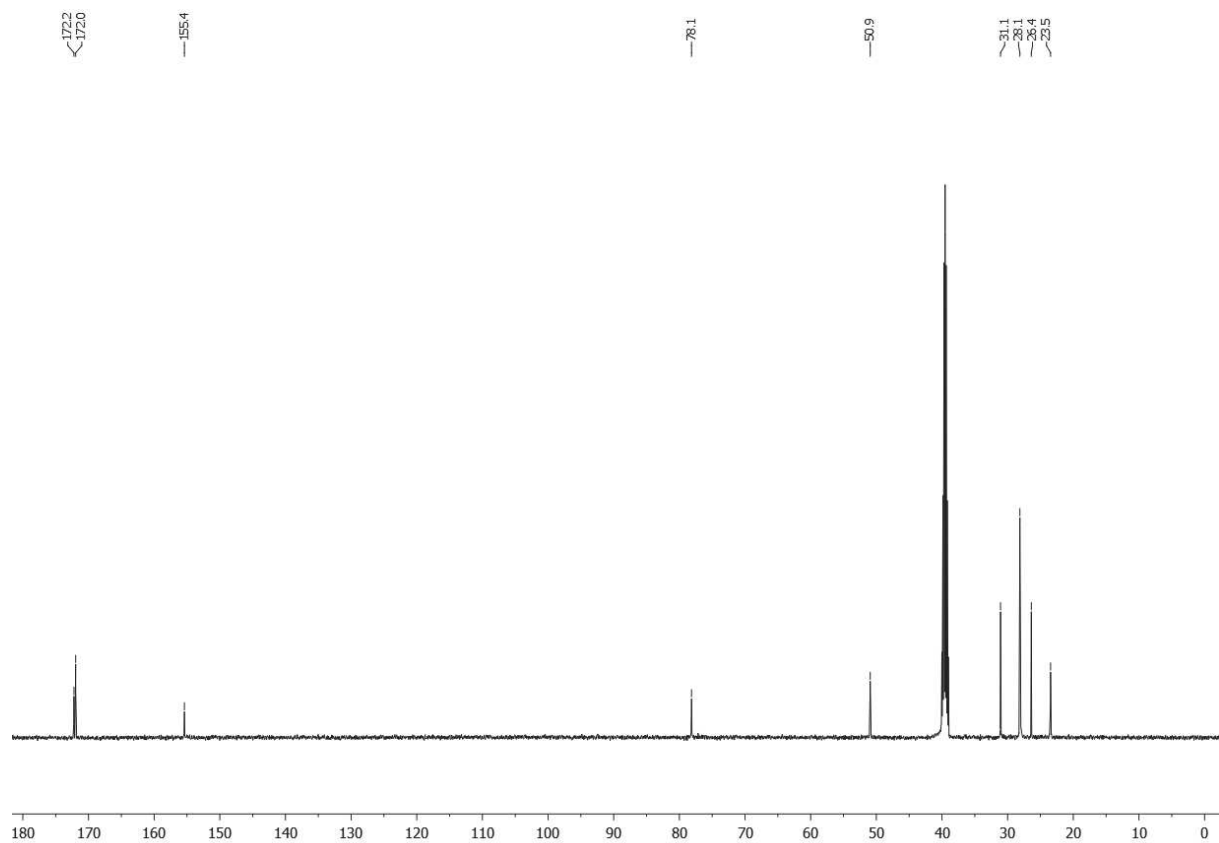
¹H NMR spectrum of **44** (500 MHz, DMSO-*d*₆)
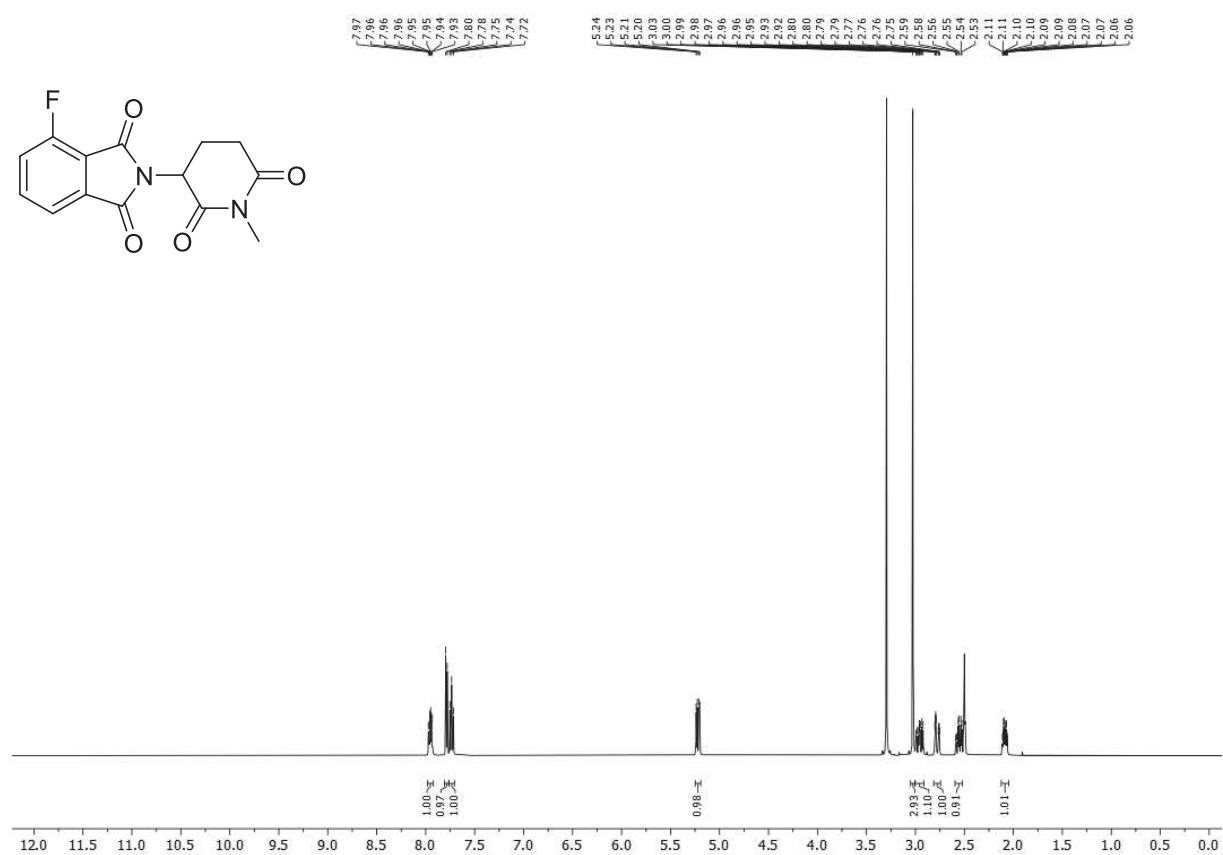
¹³C NMR spectrum of **44** (126 MHz, DMSO-*d*₆)
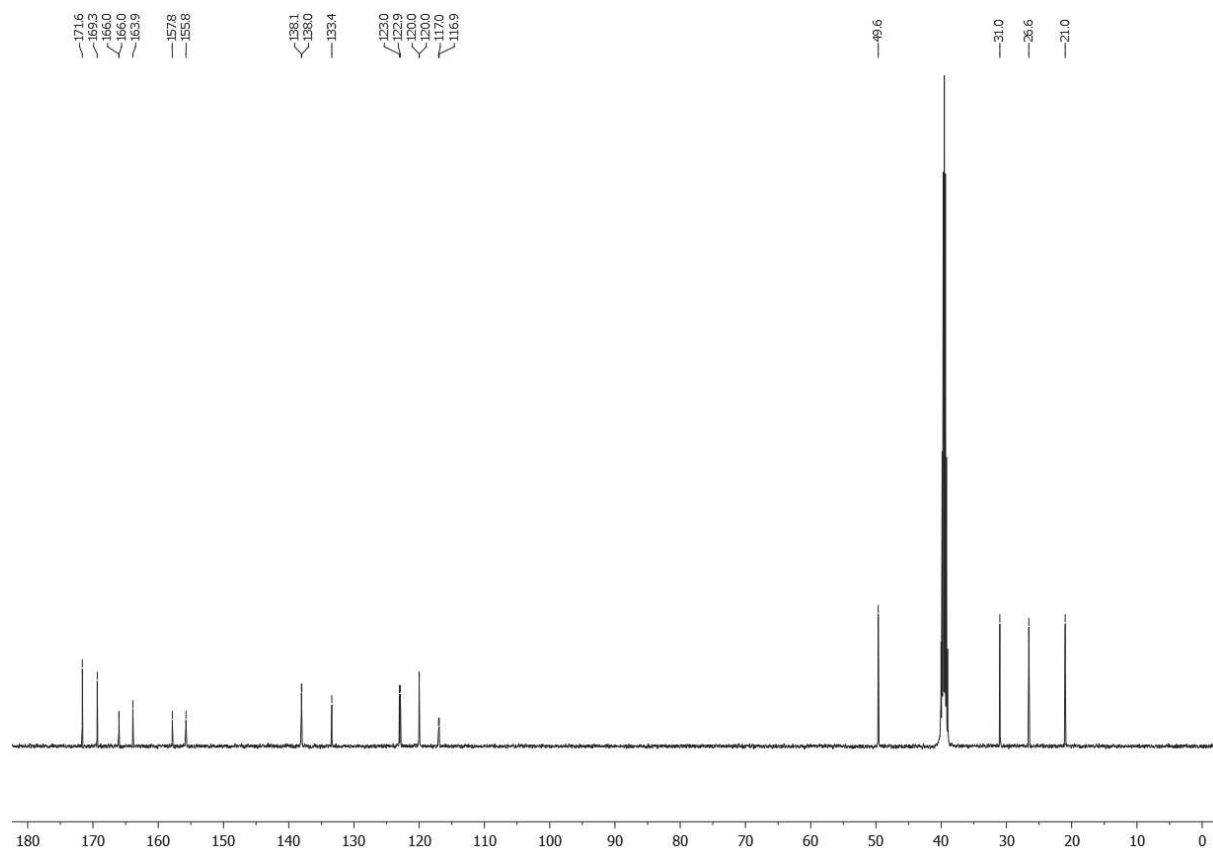
¹H NMR spectrum of **45** (500 MHz, DMSO-*d*₆)

¹³C NMR spectrum of **45** (126 MHz, DMSO-*d*₆)

S72
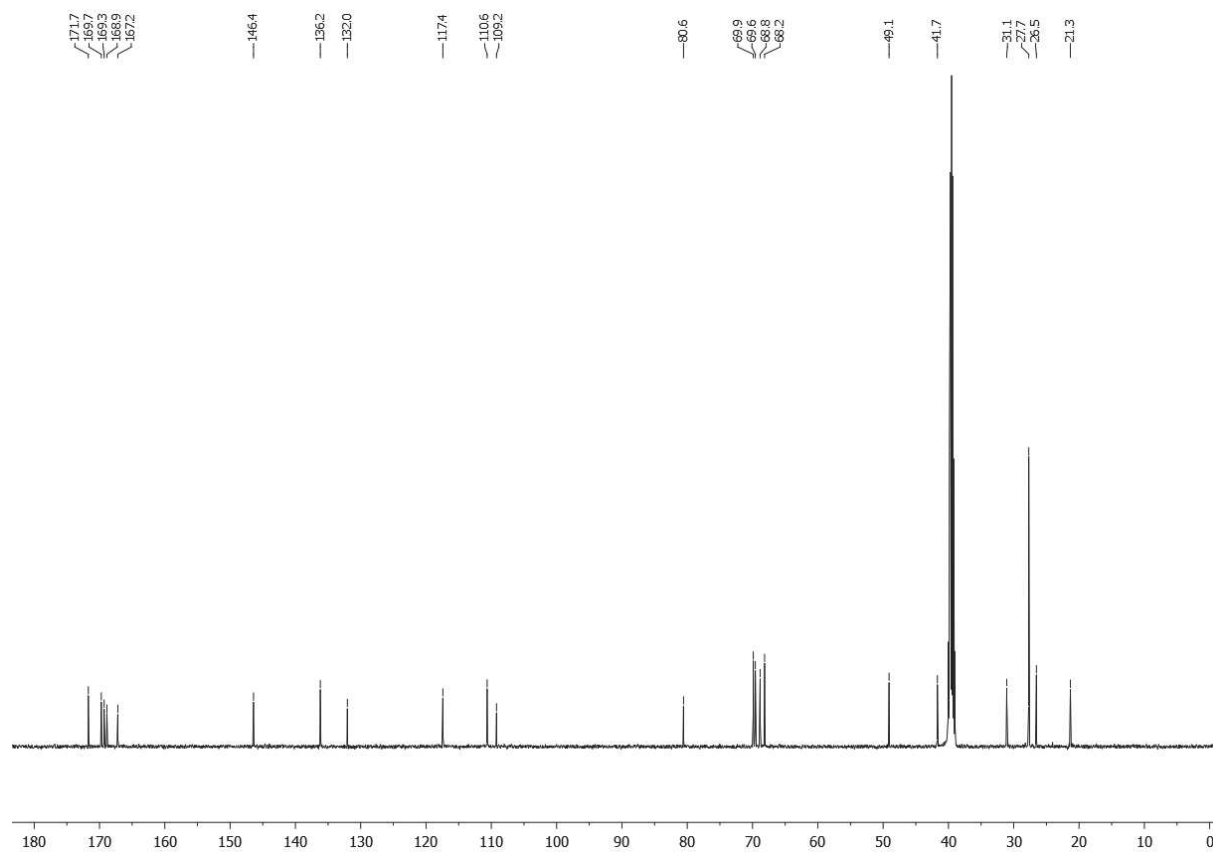
¹H NMR spectrum of **1(-)** (600 MHz, DMSO-*d₆*)
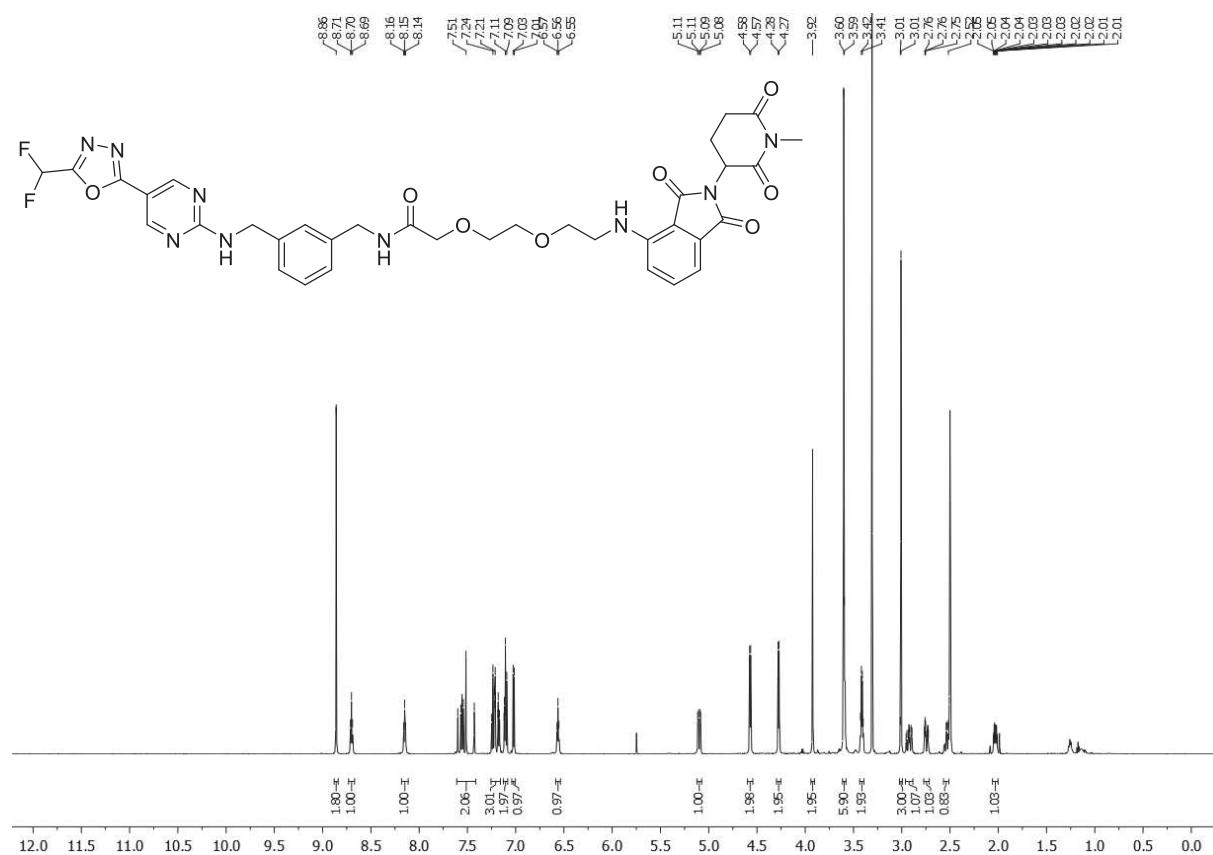
¹³C NMR spectrum of **1(-)** (151 MHz, DMSO-*d₆*)
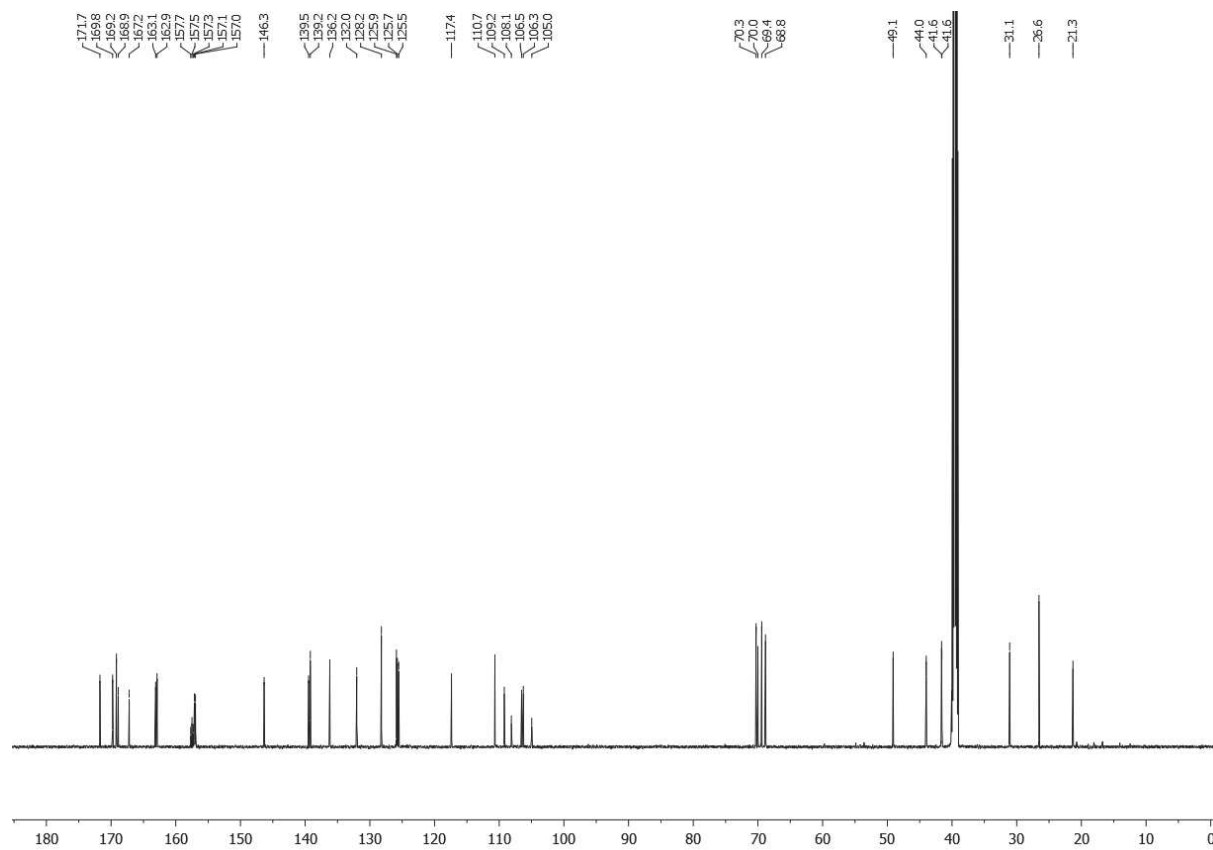
¹H NMR spectrum of **46** (600 MHz, DMSO-*d₆*)
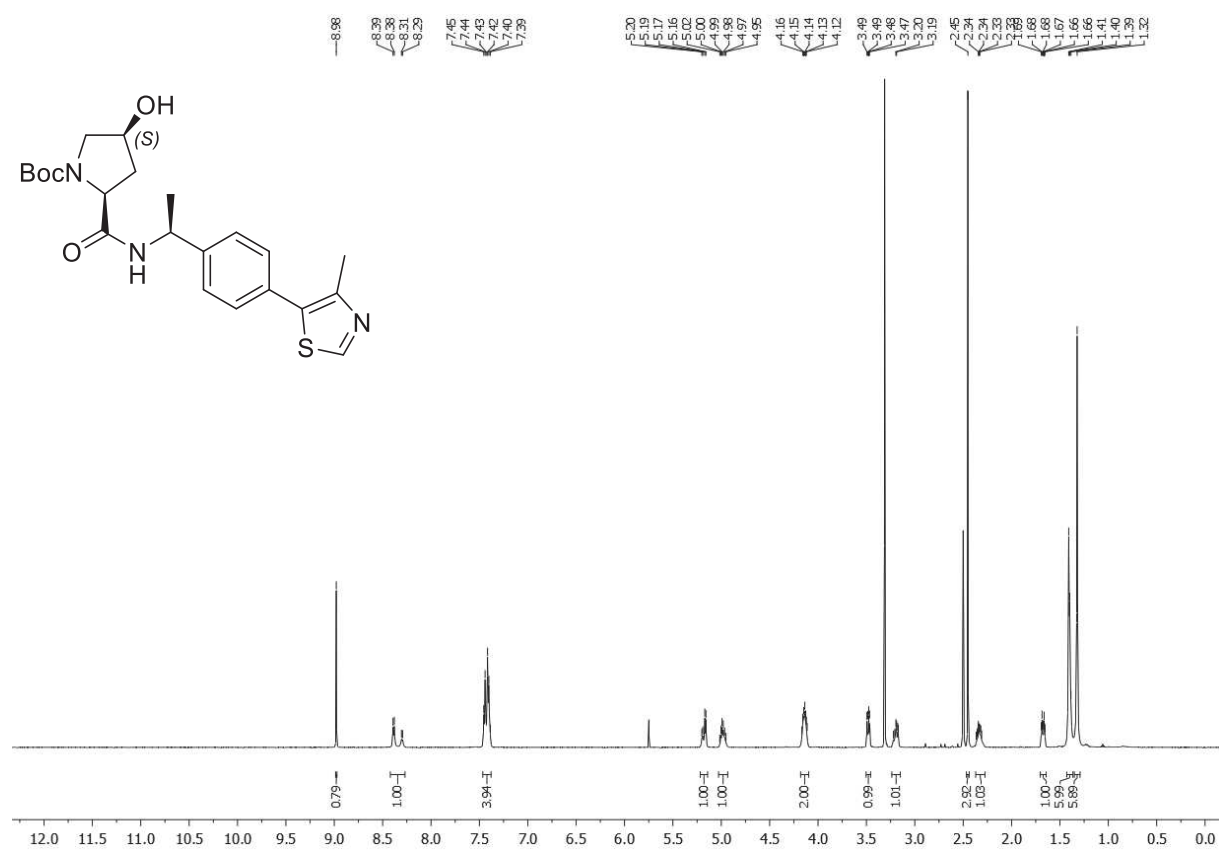
¹³C NMR spectrum of **46** (151 MHz, DMSO-*d₆*)

¹H NMR spectrum of **47** (500 MHz, DMSO-*d*₆)

¹³C NMR spectrum of **47** (126 MHz, DMSO-*d*₆)
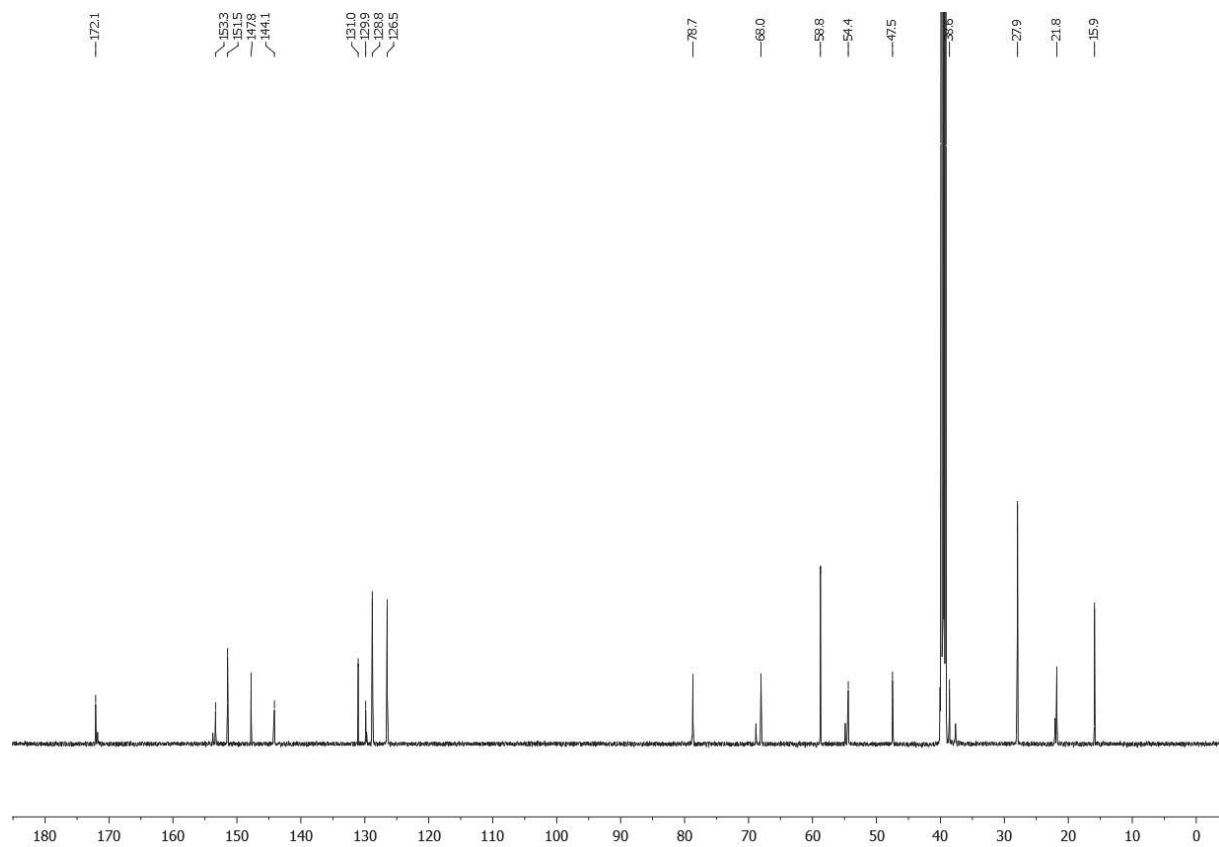
¹H NMR spectrum of **48** (600 MHz, DMSO-*d*₆)
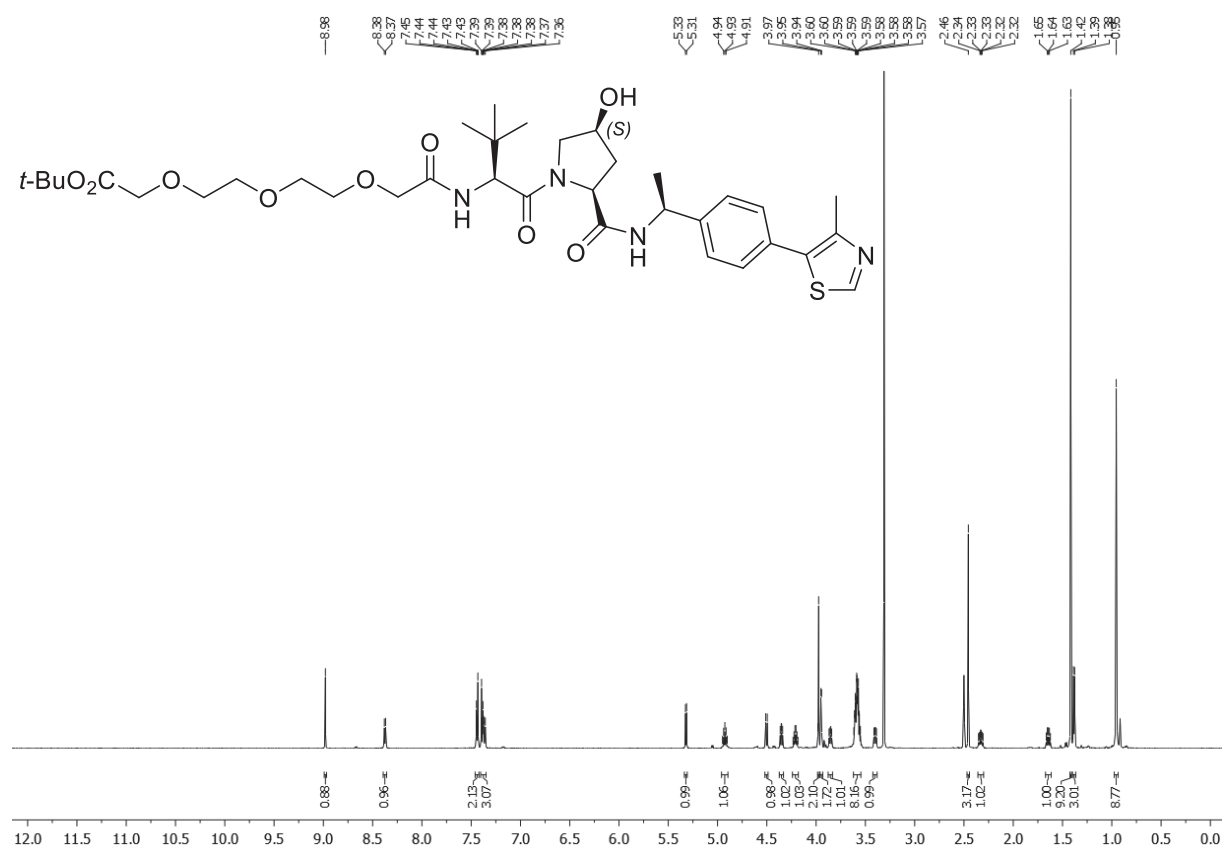
¹³C NMR spectrum of **48** (151 MHz, DMSO-*d*₆)

¹H NMR spectrum of **4(-)** (600 MHz, DMSO-*d*₆)

¹³C NMR spectrum of **4(-)** (151 MHz, DMSO-*d*₆)

S77
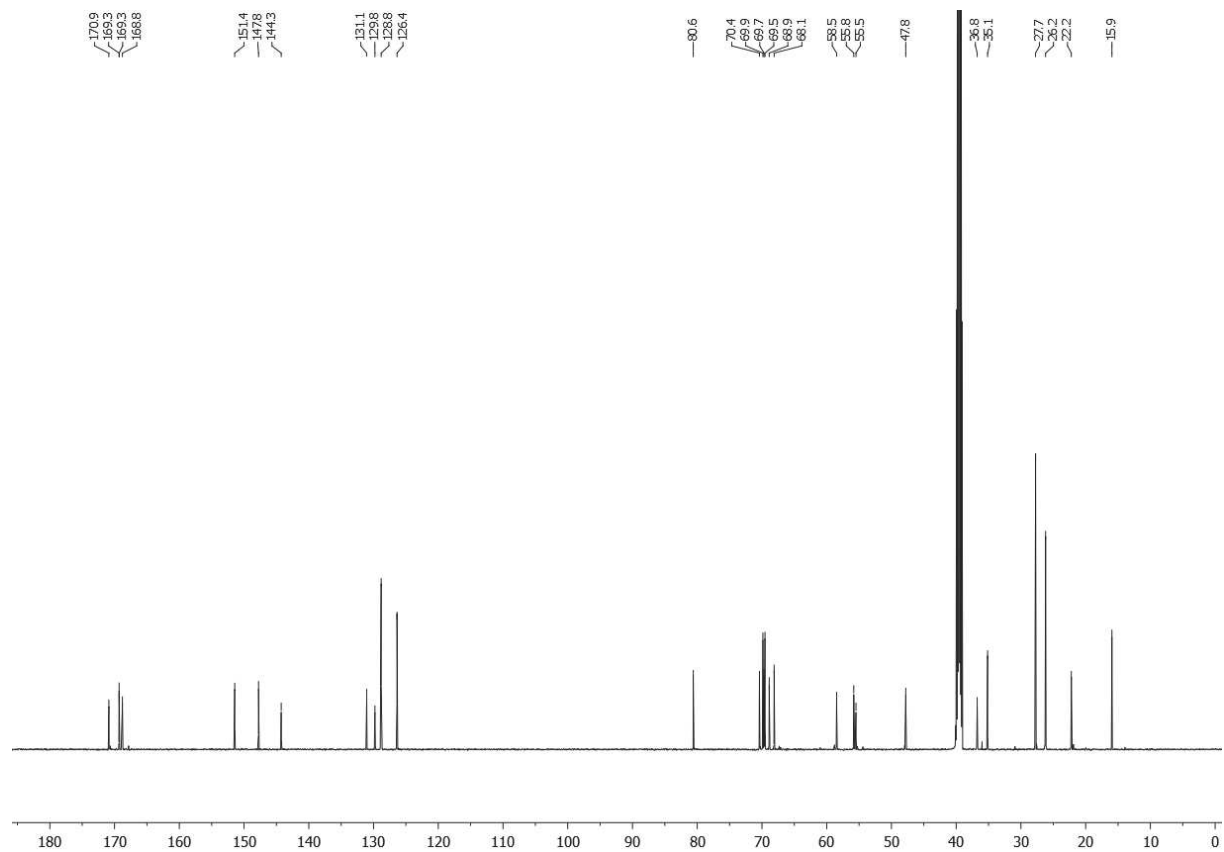
6. References

1   C. M. Yates, US Pat., 2018/0256572 A1, 2018.

2   Y. Hai and D. W. Christianson, *Nat. Chem. Biol.*, 2016, **12**, 741–747.

3   L. Schäker-Hübner, R. Warstat, H. Ahlert, P. Mishra, F. B. Kraft, J. Schliehe-Diecks, A. Schöler, A. Borkhardt, B. Breit, S. Bhatia, M. Hügle, S. Günther and F. K. Hansen, *J. Med. Chem.*, 2021, **64**, 14620–14646.

4   Y. Asfaha, C. Schrenk, L. A. Alves Avelar, F. Lange, C. Wang, J. J. Bandolik, A. Hamacher, M. U. Kassack and T. Kurz, *Bioorg. Med. Chem.*, 2020, **28**, 115108.

5   B. Heltweg, F. Dequiedt, E. Verdin and M. Jung, *Anal. Biochem.*, 2003, **319**, 42–48.

6   M. B. Piva, B. Jakubzig and G. Bendas, *Cancers*, 2017, **9**, 125.

7   L. G. Nivón, R. Moretti and D. Baker, *PLoS One*, 2013, **8**, e59004.

8   S. Kothiwale, J. L. Mendenhall and J. Meiler, *J. Cheminform.*, 2015, **7**, 1–15.

9   M. K. Mackwitz, A. Hamacher, J. D. Osko, J. Held, A. Schöler, D. W. Christianson, M. U. Kassack and F. K. Hansen, *Org. Lett.*, 2018, **20**, 3255–3258.

10 J. Meiler and D. Baker, *Proteins*, 2006, **65**, 538–548.

11 K. W. Kaufmann and J. Meiler, *PLoS One*, 2012, **7**, e50769.

12 S. DeLuca, K. Khar and J. Meiler, *PLoS One*, 2015, **10**, 1–19.

13 C. Steinebach, Y. L. Ng, I. Sosic, C. S. Lee, S. Chen, S. Lindner, L. P. Vu, A. Bricelj, R. Haschemi, M. Monschke, E. Steinwarz, K. G. Wagner, G. Bendas, J. Luo, M. Gütschow and J. Krönke, *Chem. Sci.*, 2020, **11**, 3474–3486.

14 E. H. Kerns, L. Di, S. Petusky, T. Kleintop, D. Huryn, O. McConnell and G. Carter, *J. Chromatogr. B*, 2003, **791**, 381–388.

15 K. Valko, S. Nunhuck, C. Bevan, M. H. Abraham and D. P. Reynolds, *J. Pharm. Sci.*, 2003, **92**, 2236–2248.

16 T. Keuler, K. Gatterdam, A. Akbal, M. Lovotti, M. Marleaux, M. Geyer, E. Latz and M. Gütschow, *Front. Chem.*, 2021, **9**, 642273.

17 C. Steinebach, S. Lindner, N. D. Udeshi, D. C. Mani, H. Kehm, S. Köpff, S. A. Carr, M. Gütschow and J. Krönke; *ACS Chem. Biol.*, 2018, **13**, 2771–2782.

18 C. Steinebach, H. Kehm, S. Lindner, L. P. Vu, S. Köpff, Á. L. Mármol, C. Weiler, K. G. Wagner, M. Reichenzeller, J. Krönke and M. Gütschow, *Chem. Commun.*, 2019, **55**, 1821–1824.

19 C. Jacquot, C. M. McGinley, E. Plata, T. R. Holman and W. A. van der Donk, *Org. Biomol. Chem.*, 2008, **6**, 4242–4252.

20 N. Butkevich, G. Lukinavičius, E. D'Este and S. W. Hell, *J. Am. Chem. Soc.*, 2017, **139**, 12378–12381.

21 M. Girardini, C. Maniaci, S. J. Hughes, A. Testa and A. Ciulli, *Bioorg. Med. Chem.*, 2019, **27**, 2466–2479.

22 K. Raina, J. Lu, Y. Qian, M. Altieri, D. Gordon, A. M. Rossi, J. Wang, X. Chen, H. Dong, K. Siu, J. D. Winkler, A. P. Crew, C. M. Crews and K. G. Coleman, *Proc. Natl. Acad. Sci. USA*, 2016, **113**, 7124–7129.

23 M. Wang, J. Lu, M. Wang, C. Yang and S. Wang, *J. Med. Chem.*, 2020, **63**, 7510–7528.

24   C. Contino-Pépin, A. Parat, C. Patinote, W. A. Roscoe, S. J. Karlik and B. Pucci, *ChemMedChem*, 2010, **5**, 2057–2064.

Appendix II. Publication II: Difluoromethyl-1,3,4-oxadiazoles Are Selective, Mechanism-Based, and Essentially Irreversible Inhibitors of Histone Deacetylase 6

The following part contains the research article "Difluoromethyl-1,3,4-oxadiazoles Are Selective, Mechanism-Based, and Essentially Irreversible Inhibitors of Histone Deacetylase 6", including the supporting information, as it was published in the Journal of Medicinal Chemistry by the American Chemical Society.

The article is reprinted with permission from:

Beate König,* Paris R. Watson,* Nina Reßing, Abigail D. Cragin, Linda Schäker-Hübner, David W. Christianson,[#] and Finn K. Hansen.[#] Difluoromethyl-1,3,4-oxadiazoles Are Selective, Mechanism-Based, and Essentially Irreversible Inhibitors of Histone Deacetylase 6. *J. Med. Chem.* **2023**, *66* (19), 13821-13837.

*These authors share the first authorship.
[#] Shared senior authorship.

Copyright 2023, American Chemical Society.

Difluoromethyl-1,3,4-oxadiazoles Are Selective, Mechanism-Based, and Essentially Irreversible Inhibitors of Histone Deacetylase 6

Beate König,[#] Paris R. Watson,[#] Nina Reßing, Abigail D. Cragin, Linda Schäker-Hübner, David W. Christianson,* and Finn K. Hansen*

Read Online

ACCESS | Metrics & More | Article Recommendations | SI Supporting Information
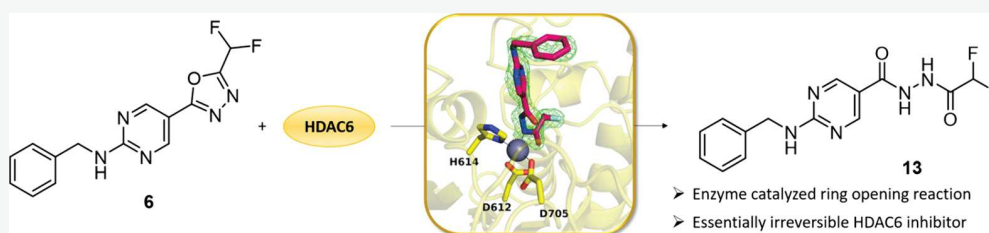
ABSTRACT: Histone deacetylase 6 (HDAC6) is an important drug target in oncological and non-oncological diseases. Most available HDAC6 inhibitors (HDAC6i) utilize hydroxamic acids as a zinc-binding group, which limits therapeutic opportunities due to its genotoxic potential. Recently, difluoromethyl-1,3,4-oxadiazoles (DFMOs) were reported as potent and selective HDAC6i but their mode of inhibition remained enigmatic. Herein, we report that DFMOs act as mechanism-based and essentially irreversible HDAC6i. Biochemical data confirm that DFMO **6** is a tight-binding HDAC6i capable of inhibiting HDAC6 via a two-step slow-binding mechanism. Crystallographic and mechanistic experiments suggest that the attack of **6** by the zinc-bound water at the sp^2 carbon closest to the difluoromethyl moiety followed by a subsequent ring opening of the oxadiazole yields deprotonated difluoroacetylhydrazide **13** as active species. The strong anionic zinc coordination of **13** and the binding of the difluoromethyl moiety in the P571 pocket finally result in an essentially irreversible inhibition of HDAC6.

INTRODUCTION

Histone deacetylases (HDACs) are epigenetic drug targets that have originally been assumed to modify histone modifications by removing acetyl groups from lysine residues. Meanwhile, however, it has turned out that the substrate spectrum of the enzyme family is more complex.[1] In agreement with the usual division into four classes, it is now clear that only class I HDACs (HDACs 1, 2, 3, and 8) actually regulate histones.[1] Class III HDACs differ from the other zinc-dependent isoforms by the fact that they are NAD$^+$-dependent, whereas class IV consists of no more than one isoform, HDAC11, whose biological role is yet unclear.[2,3] A more versatile class of HDACs is class II with class IIa enzymes (HDACs 4, 5, 7, 9) playing a crucial role in gene expression, despite their poor deacetylase qualities.[1,4−6] Class IIb, on the other hand, includes HDAC6 and the polyamine deacetylase HDAC10, which are both mainly located in the cytosol.[1,7,8] Tailored to fit the highly conserved active sites of the different isoforms, HDAC inhibitors (HDACi) typically consist of a zinc-binding group (ZBG), a variably sized cap group, and a suitable linker connecting the two units.[9] In contrast to unselective or class I-specific HDAC inhibition by HDACi such as vorinostat, belinostat, panobinostat, and romidepsin, which have been introduced as FDA-approved anticancer drugs in the past two decades, HDAC6 inhibition has no effect on histones and is thus presumed to cause less severe adverse effects.[10,11] Originally considered to be a tubulin deacetylase, HDAC6 has since been found to regulate a range of other proteins as well, most notably cortactin, the Alzheimer-related tau, and the chaperone Hsp90.[7,12−15] Serving this particular range of substrates, HDAC6 regulation has been investigated as a promising treatment option for non-oncological conditions, for example neurodegenerative diseases,[13,14,16,17] several rare disorders, like Rett syndrome and Charcot−Marie−Tooth disease,[18,19] autoimmune diseases, and other chronic conditions including idiopathic pulmonary fibrosis and inflammasome-mediated disorders.[20−22] Through enabling aggresome formation, HDAC6 is further involved in cellular protein degradation, which makes it a prominent target for synergistic drug combination approaches with proteasome inhibitors.[23−25] On the clinical level, this synergism is already being addressed by the combination of bortezomib, dexamethasone, and the pan-HDACi panobinostat for the treatment of multiple

Table 1. Inhibitory Activities of the Synthesized Difluoromethyl-1,3,4-oxadiazoles against HDAC6 and the Control Isoforms HDAC1-4[a]

1: X = CH; Y = CH; R = H
2: X = N; Y = CH; R = CH₃
3: X = N; Y = N; R = H

6: R = H
7: R = OCH₃

9: R= NH-phenyl
10: R= phenyl

12
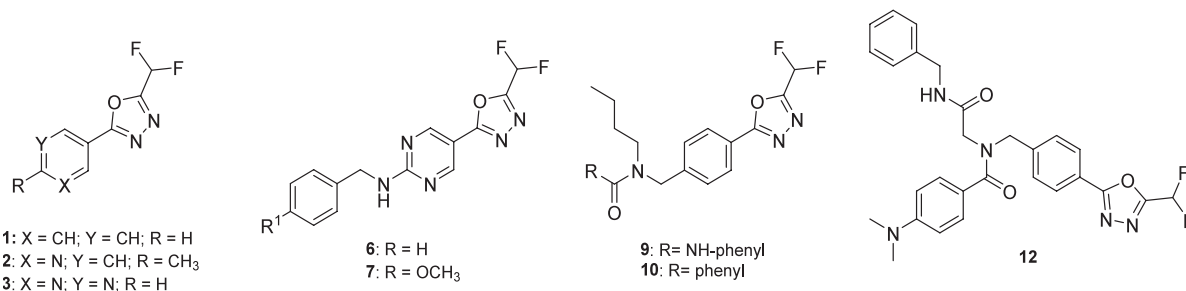
Cpd	HDAC6	HDAC1	HDAC2	HDAC3	HDAC4
1	n. e.	n. e.	n. e.	n. e.	n. e.
2	39%	n. e.	n. e.	n. e.	n. e.
3	56%	n. e.	n. e.	n. e.	n. e.
6	$0.193 \pm 0.006 \ \mu M$	n. e.	n. e.	n. e.	n. e.
7	$0.337 \pm 0.026 \ \mu M$	n. e.	n. e.	n. e.	n. e.
9	76%	n. e.	n. e.	n. e.	n. e.
10	75%	n. e.	n. e.	n. e.	n. e.
12	27%	n. e.	n. e.	n. e.	n. e.
vorinostat	$0.039 \pm 0.005 \ \mu M$	$0.128 \pm 0.009 \ \mu M$	$0.158 \pm 0.033 \ \mu M$	$0.079 \pm 0.016 \ \mu M$	n. d.
TMP-269	n. d.	n. d.	n. d.	n. d.	$0.753 \pm 0.010 \ \mu M$

[a]IC$_{50}$ values [μM, mean $\pm$ SD] or percent inhibition at 10 μM; n. e.: no effect = <15% inhibition at 10 μM; n. d.: not determined. Preincubation of HDAC1−4 or 6 and inhibitor: 1 h at 25 °C.

myeloma while further combination studies using the HDAC6-preferential inhibitor ricolinostat are ongoing.[26] Other promising targets for synergistic activities with HDAC6i that are currently being investigated include BET proteins,[27,28] topoisomerases,[29] lysine-specific demethylase 1 (LSD1),[30−33] and Hsp90.[34−38] In consequence, and despite having limited clinical anticancer potential on its own, HDAC6 has turned out to be a prominent drug target for combination therapies but only few of the many selective HDAC6i presented so far have yet entered clinical trials.[39−42] One major limitation in this regard seems to be the fact that most HDAC6i incorporate hydroxamate ZBGs, which affect the drug's tolerability and overall performance by promoting off-target interactions and the appearance of toxic metabolites. In fact, hydroxamate groups have long been suspected of releasing hydroxylamine or undergoing the Lossen rearrangement yielding isocyanates under physiological conditions.[11,43] Given that both species are highly mutagenic and thus unsuitable for long-term therapy, there is an urgent need for alternative ZBGs, but even after several years of intensive research, there are only few candidates with pleasing chelating properties and low toxicity levels.[44] Besides ethyl hydrazides[45] and several non-hydroxamate compounds of yet undisclosed structures that are currently in phase II trials, the most promising HDAC6-selective binding motif seems to be the difluoromethyl-1,3,4-oxadiazole (DFMO) group that has been discovered by Kim et al.[46] According to their study, the DFMO group exhibited excellent HDAC6 inhibition in the low nanomolar concentration range with a high selectivity over HDAC1.[46] Despite frequently appearing in patents,[46−50] this ZBG is relatively underrepresented in research manuscripts. However, in 2022, the DFMO derivative SE-7552 was used as a selective HDAC6 inhibitor to overcome leptin resistance in obesity.[51] In the same year, we successfully incorporated the DFMO warhead into proteolysis-targeting chimeras (PROTACs) to selectively degrade HDAC6.[52] However, the mechanism by which

DFMOs inhibit or degrade HDAC6 remained enigmatic. In a conference abstract published in 2022, we disclosed that a DFMO derivative underwent an enzyme-catalyzed ring-opening reaction, resulting in an acylhydrazide that was cocrystallized in an extended conformation within the active site of HDAC6.[53] More recently, Barinka and co-workers[54] conducted a comparative assessment of a hydroxamate-based HDAC6 inhibitor and its corresponding DFMO analogue. Biochemical and cell-based assays unequivocally demonstrated the superior potency and selectivity of the DFMO ZBG.[54] Similarly, the high HDAC6 selectivity of DFMOs compared to related hydroxamic acid-derived HDAC6i was confirmed in a recent patent.[55]

In 2023, Steinkühler and co-workers[56] reported the structure of the HDAC6 complex with a hydrazide inhibitor resulting from a double hydrolysis of a related oxadiazole inhibitor. The authors speculated that the crystallized hydrazide may not be solely responsible for the remarkable HDAC6 inhibition observed. Instead, they proposed the existence of a high-affinity intermediate that forms a tight and long-lived enzyme−inhibitor complex. This intermediate may take the form of a closed hydrated intermediate or a protonated acylhydrazide, both of which were proposed as possible active species. However, the nature of the active species could not be conclusively confirmed.[56]

Herein, we report the full experimental details of our 2022 conference abstract[53] demonstrating that DFMOs act as selective, mechanism-based, and essentially irreversible inactivators capable of inhibiting HDAC6 via a two-step slow-binding mechanism. Our findings reveal that the zinc-bound water attacks the sp² carbon nearest to the difluoromethyl moiety of the DFMO group followed by a subsequent ring opening of the oxadiazole, thereby yielding a deprotonated difluoroacetylhydrazide as active species.

Scheme 1. Synthesis of HDAC6 inhibitors 6, 7, 9, 10, and 12[a]
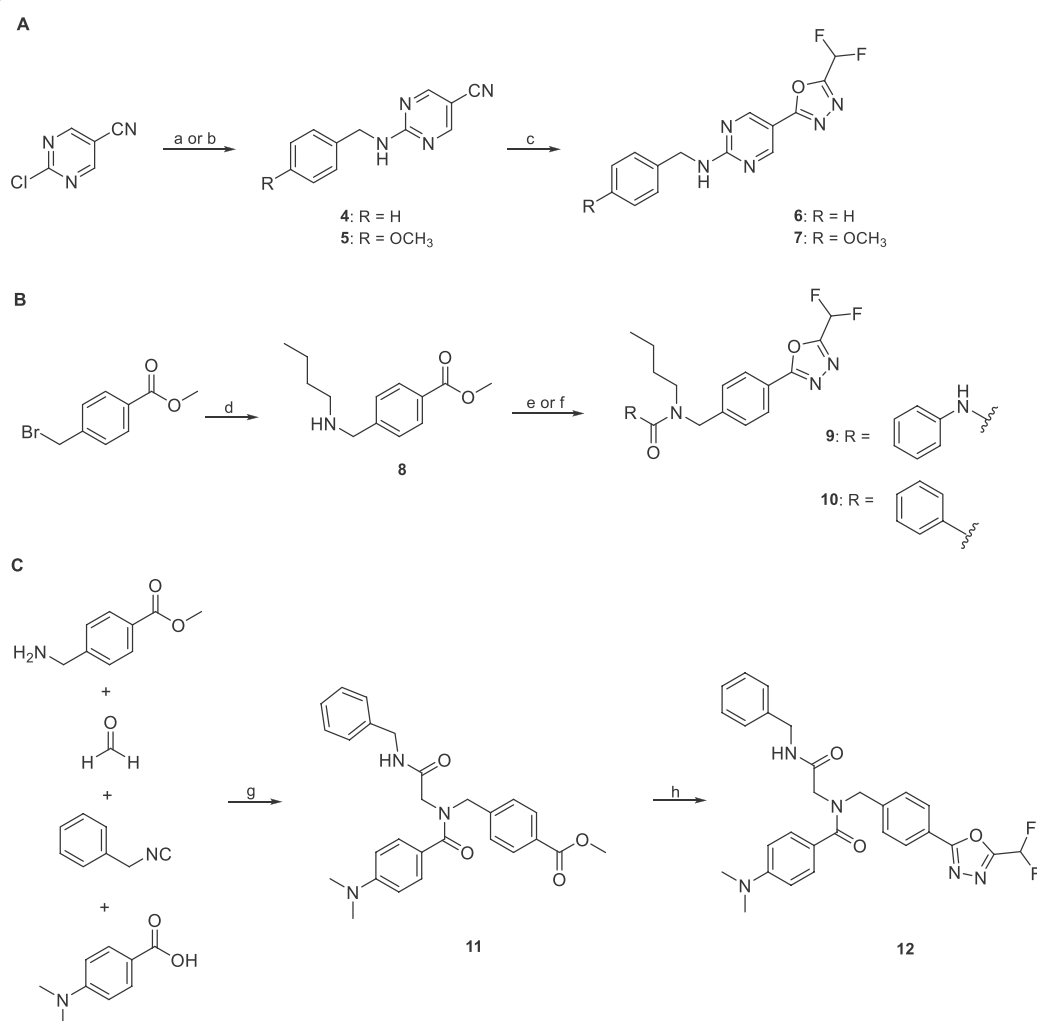
[a]Reagents and conditions: (a) Benzylamine, DIPEA, EtOH, 90 °C, 18 h (4); (b) 4-methoxybenzylamine, DIPEA, EtOH, 90 °C, 18 h (5); (c) i: NaN₃, NH₄Cl, LiCl·H₂O, DMF, 100 °C, 18 h; ii: DFAA, 70 °C, 18 h; (d) n-butylamine, THF, rt., 3 h; (e) i: phenyl phenylcarbamate, TEA, THF, 66 °C, 2 h; ii: hydrazine monohydrate, MeOH, 70 °C, 3 h; iii: DFAA, DMF, 70 °C, 1 h; iv: Burgess reagent, THF, 60 °C, 18 h (9); (f) i: benzoyl chloride, CH₂Cl₂, rt., 2 h; ii: hydrazine monohydrate, MeOH, 70 °C, 3 h; iii: DFAA, DMF, 70 °C, 1 h; iv: Burgess reagent, THF, 60 °C, 18 h (10); (g) TEA, MeOH, rt., 72 h; (h) i: hydrazine monohydrate, MeOH, 70 °C, 3 h; ii: DFAA, TEA, DMF, 70 °C, 1 h; iii: Burgess reagent, TEA, THF, 60 °C, 18 h.

■ RESULTS AND DISCUSSION

Design, Synthesis, and HDAC Inhibition of Difluoromethyloxadiazole-Based HDAC6 Inhibitors. To identify key structural requirements for selective HDAC6 inhibition by DFMO-derived inhibitors, we decided to pursue a fragment-based approach. In the first step, to investigate the influence of the (hetero)aromatic linker, HDAC6i fragments containing phenyl (1), pyridinyl (2), and pyrimidinyl (3) linkers attached to the DFMO ZBG were included in the design and synthesis of initial prototypic compounds. For the synthesis of fragments 1, 2, and 3, the respective carbonitriles were transformed into the corresponding tetrazoles by the treatment with sodium azide, followed by the reaction with difluoroacetic anhydride (DFAA) to generate the DFMO group via a Huisgen 1,3,4-oxadiazole synthesis (see Scheme S1, Supporting Information).[57] The three synthesized fragments were screened for their inhibition of HDAC6 and HDAC1−4 using biochemical HDAC inhibition assays. The pyrimidinyl derivative 3

displayed the highest inhibitory potency against HDAC6, while all fragments were inactive against the control isoforms HDAC1−4 (Table 1).

Due to the initial activity of the pyrimidinyl fragment 3, we designed full-sized HDACi including a benzyl as well as a para-methoxy benzyl cap group, an aminopyrimidinyl linker, and the DFMO ZBG. To obtain 6 and 7, the respective benzylamines were subjected to a nucleophilic aromatic substitution reaction with 2-chloropyrimidine-5-carbonitrile. The resulting carbonitrile intermediates were converted into the corresponding DFMO derivatives as described above (Scheme 1A). In subsequent HDAC inhibition assays, we observed submicromolar inhibitory activities against HDAC6 for both full-sized HDAC6i (6 and 7), with IC₅₀ values of 0.193 and 0.337 μM, respectively, and no activity against HDAC1−4 (Table 1).

Additionally, the DFMO ZBG was introduced in potent well-established HDAC6i such as nexturastat A and our previously published peptoid-based HDAC6i.[58,59] For the synthesis of the nexturastat derivatives (9, 10), n-butylamine
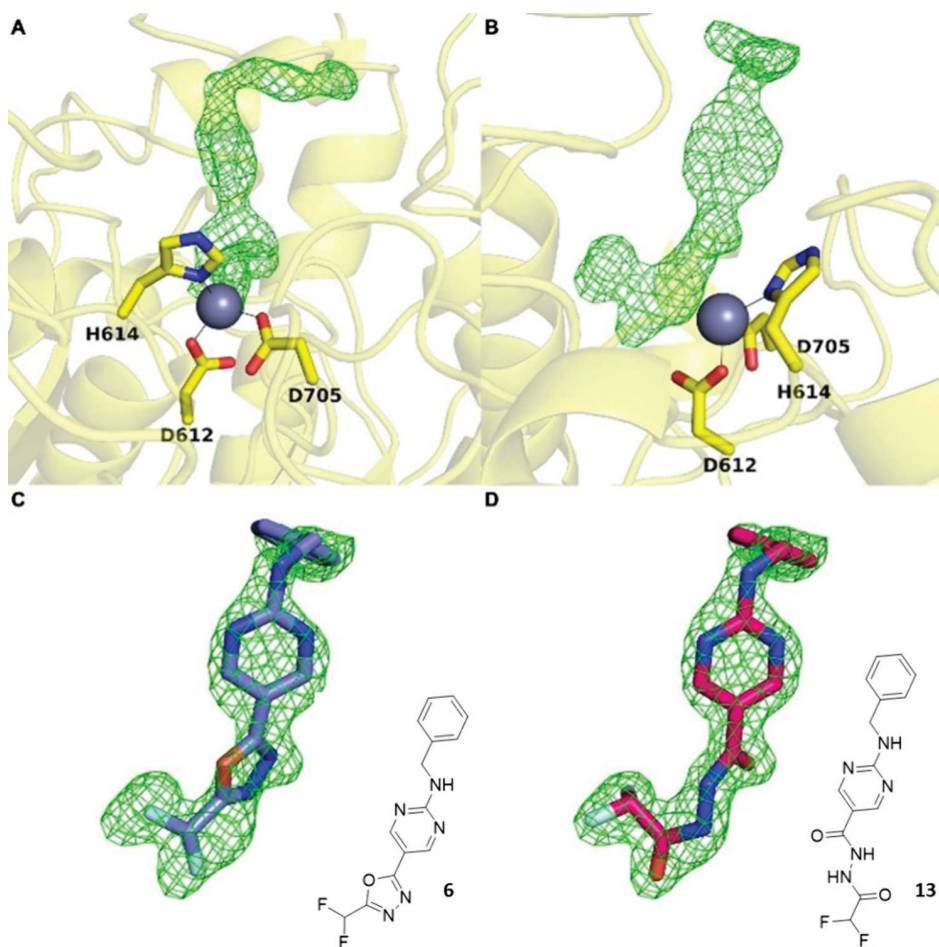
Figure 1. Initial $|F_o|-|F_c|$ map (two orientations (A) and (B)) calculated from X-ray diffraction data collected from crystals of HDAC6 cocrystallized with inhibitor **6** reveals strong, unbiased electron density for the bound inhibitor in the active site. Surprisingly, this difference density could not be fit satisfactorily with intact oxadiazole **6** (C); instead, it could be fit perfectly with acylhydrazide **13** resulting from hydrolysis and ring opening of the oxadiazole (D).

was alkylated with methyl 4-(bromomethyl)benzoate. Next, the resulting intermediate **8** was treated with phenyl phenylcarbamate or benzoyl chloride to provide the corresponding urea and carboxamide derivatives. The respective products were subjected to a hydrazinolysis followed by a difluoroacetylation reaction with DFAA. The resulting acylhydrazides were converted into the desired DFMO ZBG via a dehydrative cyclization reaction using Burgess reagent (Scheme 1B). The peptoid derivative (**12**) was synthesized starting from an Ugi four-component reaction.[59,60] The formation of the DFMO moiety was accomplished in three steps from methyl ester intermediate **11** via the hydrazinolysis, difluoroacetylation, and dehydrative cyclization sequence described above (Scheme 1C). Interestingly, the nexturastat A analogues **9** and **10** and the peptoid-based HDACi **12** displayed only moderate inhibitory activity against HDAC6 and were inactive against HDAC1−4. The typical structural features of selective hydroxamate-based HDAC6i include a benzyl linker in combination with a bulky or branched cap group.[61] Our results for the DFMO derivatives **9**, **10**, and **12** indicate that this HDAC6 pharmacophore cannot be directly translated to DFMO-based HDAC6i. A possible explanation for this phenomenon could be a different binding mode in the active site of HDAC6. Due to the highest HDAC6 inhibitory activity in this set of compounds, we selected **6** for elucidating its

binding mode in the second catalytic domain 2 (CD2) of *Danio rerio* (zebrafish) HDAC6.

Compound 6 Is a Substrate Analogue of HDAC6 that Undergoes an Enzyme-Catalyzed Ring-Opening Reaction. Oxadiazole **6** was cocrystallized with HDAC6, and crystals diffracted X-rays to 2.00 Å resolution. The initial electron density map of the enzyme−inhibitor complex was phased by molecular replacement using the structure of the unliganded enzyme (PDB: 5EEM)[62] as a search probe for rotation and translation function calculations. After a molecular replacement solution was achieved and initial rounds of crystallographic structure refinement were completed, we attempted to fit oxadiazole **6** into strong $|F_o|-|F_c|$ difference electron density in the active site (Figure 1A,B). Surprisingly, the intact oxadiazole would not fit satisfactorily in this electron density map (Figure 1C). After studying the electron density map and considering the possible reactivity of the oxadiazole moiety, we concluded that the oxadiazole ring had undergone nucleophilic attack by the zinc-bound water to yield a ring-opened form—acylhydrazide **13**—which fits the initial, unbiased electron density map perfectly (Figure 1D). The structure of the HDAC6−**13** complex was refined to convergence with R/R_{free} = 0.185/0.223.

A Polder omit map of the final enzyme−inhibitor complex is shown in Figure 2A. Inhibitor binding does not trigger any
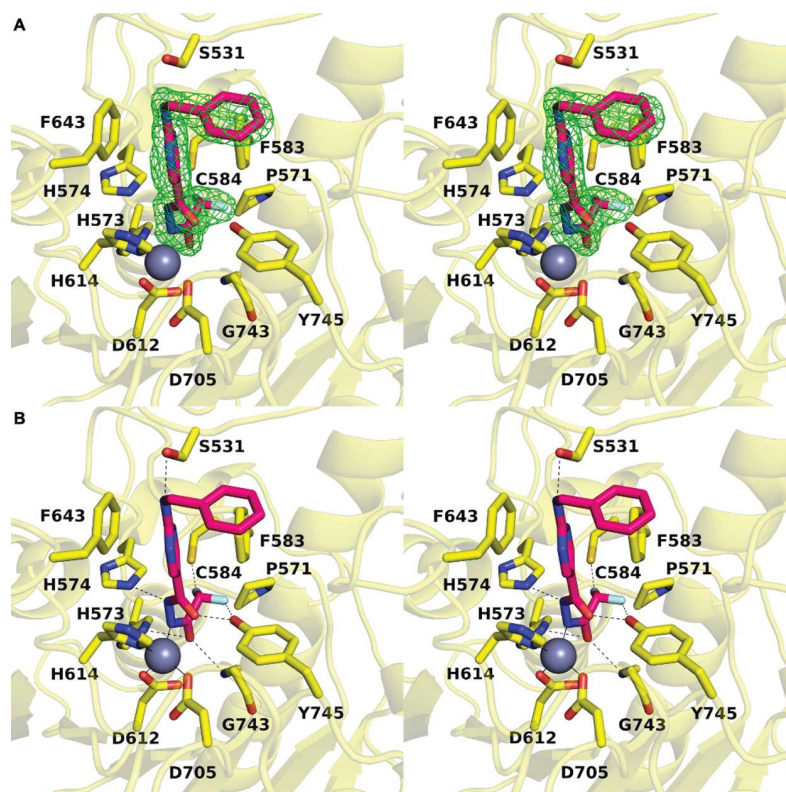
Figure 2. (A) Stereoview of the Polder omit map of **13** contoured at 3σ (PDB 8GD4). (B) Stereoview highlighting intermolecular interactions in the enzyme−inhibitor complex in the active site of HDAC6. The catalytic zinc ion is shown as a gray sphere; metal coordination and hydrogen bond interactions are shown as solid and dashed black lines, respectively (PDB: 8GD4).
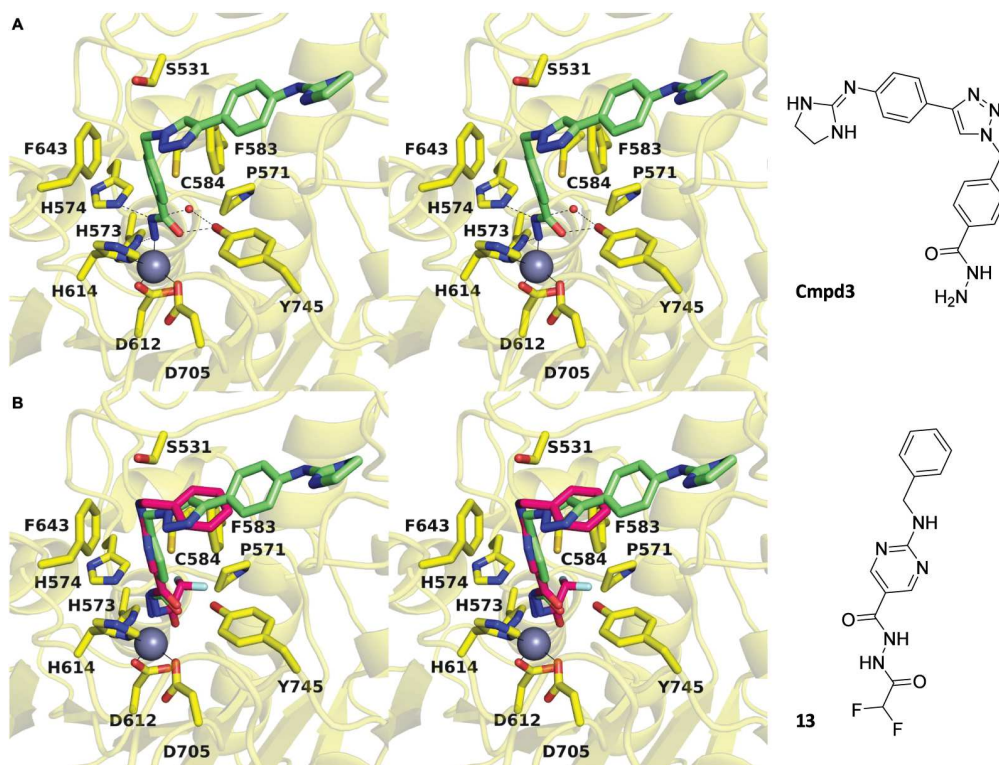
Figure 3. (A) Stereoview of the oxadiazole-derived hydrazide inhibitor Cmpd3 bound in the active site of HDAC6 (PDB: 8A8Z). (B) Overlay of the oxadiazole-derived acylhydrazide **13** and hydrazide inhibitor Cmpd3 bound in the active site of HDAC6.
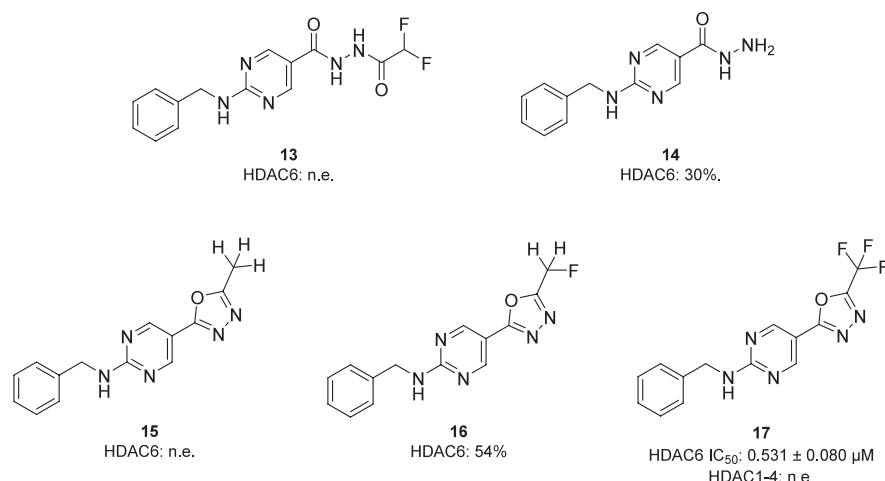
Figure 4. Structures of the acylhydrazide (**13**), hydrazide (**14**), methyl-1,3,4-oxadiazole (**15**), monofluoromethyl-1,3,4-oxadiazole (**16**), and trifluoromethyl-1,3,4-oxadiazole (**17**) analogues. Inhibitory activities of prepared compounds against HDAC1–4 and HDAC6; IC$_{50}$ [μM, mean $\pm$ SD] or percent inhibition at 10 μM; n.e.: no effect = <15% inhibition at 10 μM.

major structural changes in the protein, and the root-mean-square deviation is 0.177 Å for 315 Cα atoms between the inhibitor-bound and unliganded enzymes (PDB: 5EEM). Interestingly, the structure reveals an extensive array of intermolecular interactions that stabilize the bound inhibitor (Figure 2B). Key among these interactions is coordination of an acylhydrazide nitrogen to the catalytic zinc ion (N•••Zn^{2+} distance = 2.0 Å). This interaction requires deprotonation of the acylhydrazide NH group closest to the difluoromethyl group to form a nitrogen anion—this could result directly from the mechanism of ring opening, or it could result from deprotonation of the neutral acylhydrazide (as discussed later).

The bound inhibitor makes numerous hydrogen bond interactions with active site residues. One carbonyl group of the acylhydrazide forms hydrogen bonds with H574 and the backbone NH group of G743, and the other carbonyl group forms a hydrogen bond with Y745. Interestingly, both C−F groups engage in hydrogen bond interactions: one C−F group forms a hydrogen bond with C584, and the other forms a hydrogen bond with Y745. Finally, the benzylamino NH group forms a hydrogen bond with S531 and both aromatic rings of the inhibitor engage in offset-stacked and edge-to-face aromatic interactions with F583 and F643.

Overlay of the structure of the HDAC6 complex with acylhydrazide **13** and the recently reported structure of the HDAC6 complex with the hydrazide Cmpd3 resulting from hydrolysis of another oxadiazole inhibitor (ITF5924, PDB: 8A8Z)[56] reveals slight shifts of 0.9 Å in the orientation of the ZBG and the aromatic linker region; unlike the situation for zinc coordination by an amide NH group, the primary amino group of the hydrazide does not have to be deprotonated to coordinate to zinc (Figure 3). Other differences between the binding of acylhydrazide and hydrazide inhibitors include the hydrogen bond with catalytic tyrosine Y745, which at 2.1 Å is 0.4 Å shorter in the complex with the hydrazide (making this a very short hydrogen bond), and the binding of a water molecule in the P571 pocket.

DFMOs Are Mechanism-Based and Essentially Irreversible HDAC6 Inhibitors. The enzyme-catalyzed ring-opening reaction observed for **6** in the presence of HDAC6 prompted us to investigate the structural requirements for this unique mode of action in detail. To this end, we synthesized

the cocrystallized acylhydrazide **13** as a reference compound as well as the corresponding methyl-1,3,4-oxadiazole (**15**), monofluoromethyl-1,3,4-oxadiazole (**16**), and trifluoromethyl-1,3,4-oxadiazole (**17**) analogues of **6** (Figure 4; see Schemes S3 and S4 for synthetic details, Supporting Information). Furthermore, due to the crystal structure reported by Steinkühler et al.,[56] we synthesized hydrazide **14** (Figure 4, see Scheme S4 for synthetic details, Supporting Information). The subsequent HDAC6 inhibition assays revealed that the protonated acylhydrazide **13** and the methyl-1,3,4-oxadiazole derivative **15** displayed only very weak inhibitory properties with less than 15% inhibition at the highest concentration tested (10 μM). Furthermore, hydrazide **14** and monofluoromethyl-1,3,4-oxadiazole **16** showed only weak HDAC6 inhibitory activity with 30 and 54% inhibition at 10 μM. These results suggest that the oxadiazole C=N bond is insufficiently activated for nucleophilic attack in methyl- and monofluoromethyl-oxadiazoles **15** and **16** to yield a zinc-bound nitranion comparable to deprotonated **13**. The low inhibitory potency of **13** itself suggests that there is a higher energetic barrier for deprotonation to yield a zinc-bound nitranion compared with the hydrolysis of oxadiazole **6**, which would directly yield a zinc-bound nitranion. The nitranion makes a strong charge−charge interaction with zinc, whereas the amino group of **14** would make a weaker dipole−charge interaction once deprotonated. This may account for the weaker inhibitory potency observed for **14**.

In contrast, trifluoromethyl-1,3,4-oxadiazole (TFMO) **17** displayed submicromolar HDAC6 inhibitory activity against HDAC6 (IC$_{50}$: 0.531 μM) and no inhibition of the four control isoforms HDAC1−4. Consequently, we focused on difluoromethyl-1,3,4-oxadiazole **6** and trifluoromethyl-1,3,4-oxadiazole **17** in our in-depth evaluation of the binding kinetics. Most hydroxamates are HDACi with fast-on and fast-off binding kinetics, while HDACi with alternative ZBGs such as aminoanilides and alkyl hydrazides are often slow- and tight-binding inhibitors.[45,63,64] To investigate whether **6** and **17** display slow-on binding properties, we performed HDAC6 inhibition assays with different preincubation times using vorinostat as control; the results are summarized in Figure 5A. As expected, the HDAC6 inhibition by vorinostat did not depend on the preincubation time. In contrast, the observed
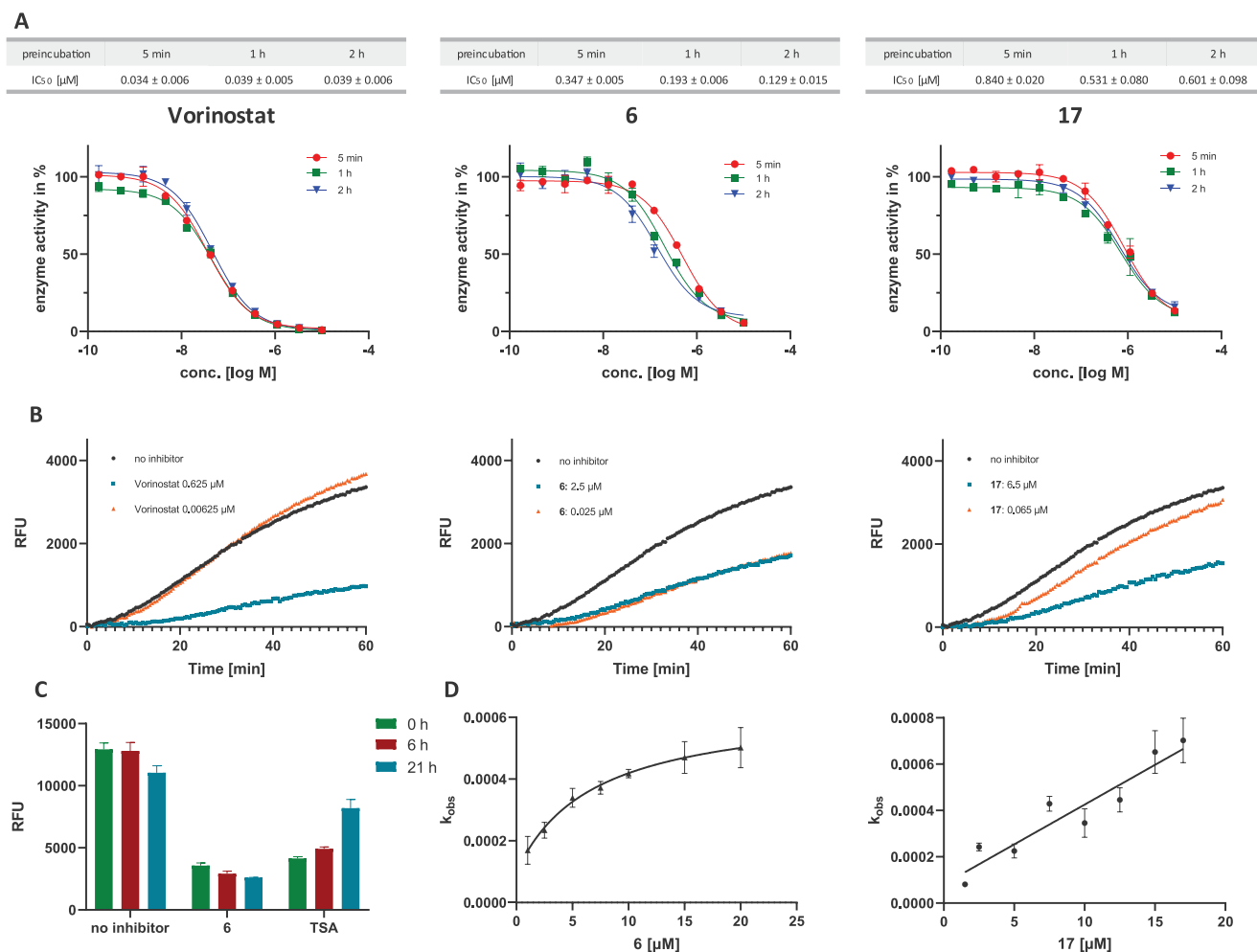
Figure 5. Analysis of the association and dissociation behavior of **6** and **17** at HDAC6. (A) Representative dose−response curves and IC_{50} values of vorinostat (left, control), **6** (middle), and **17** (right) after preincubation with HDAC6 for 5, 60, and 120 min. (B) Progression curves of 100-fold jump dilution experiments with vorinostat (left, control), **6** (middle), and **17** (right) at HDAC6. Inhibitor concentrations are indicated on the left. Fluorescence of cleaved AMC is measured in relative fluorescence units (RFU). (C) Recovered HDAC6 activity from samples incubated with DMSO, **6**, and trichostatin A (TSA, control) after dialysis against 10.000-fold excess fresh buffer. (D) The apparent first-order rate constant k_{obs} (mean ± SD) was plotted against the corresponding inhibitor concentrations $[I]$. The resulting curves were fitted into eq 2 or 3 (see Supporting Information). (Left) **6**: the hyperbolic relationship between k_{obs} and $[I]$ indicates slow-binding, "induced-fit" mechanism II; (right) **17**: the linear relationship between k_{obs} and $[I]$ indicates slow-binding mechanism I.[63]

concentration−effect curves of **6** and thus the IC_{50} values were highly dependent on the preincubation time (5 min IC_{50}: 0.347 μM; 1 h IC_{50}: 0.193 μM; 2 h IC_{50}: 0.129 μM), thereby indicating a slow-binding profile. Similarly, **17** also showed a substantial decrease in the HDAC6 IC_{50} values upon preincubation (5 min IC_{50}: 0.840 μM; 1 h IC_{50}: 0.531 μM; 2 h IC_{50}: 0.601 μM).

To determine whether **6** and **17** are tight-binding inhibitors of HDAC6, we analyzed the dissociation behavior of both compounds by 100-fold jump dilution experiments using vorinostat as control. Briefly, HDAC6 in assay buffer was incubated with an excess of the respective inhibitor (at least 10-fold IC_{50}) or with blank (DMSO 1%) for 1 h at room temperature. Subsequently, this mixture was diluted 100-fold either with the respective inhibitor at the original concentration or with the assay buffer. The substrate (Z-Lys(Ac)-AMC (ZMAL)) and trypsin were added to all samples, and the time-dependent in situ AMC release was monitored continuously following our previously reported protocol.[63] In the

case of the 100-fold jump dilution of vorinostat (Figure 5B, left), HDAC6 regained full deacetylase activity compared to blank (DMSO 1%), which is in excellent agreement with the fast-on/fast-off binding behavior of vorinostat. Conversely, the HDAC6 activity could not be restored after 100-fold dilution of **6** (Figure 5B, middle), hence indicating that **6** or the ring-opened deprotonated acylhydrazide **13** disengages very slowly from HDAC6. Dialysis experiments with 10,000-fold excess of buffer over 21 h confirmed the tight-binding properties of **6** (Figure 5C), suggesting that the unique binding mode of **6** leads to essentially irreversible inhibition of HDAC6. In contrast, the deacetylase activity of HDAC6 was nearly completely restored after the 100-fold jump dilution of **17** (Figure 5B, right). These results indicate that the closely related analogues **6** (tight-binding, essentially irreversible inhibitor) and **17** (fast-off binding properties) differ in their dissociation behavior and might therefore act via different modes of action.

The trifluoromethyl analogue **17** similarly undergoes HDAC6-catalyzed ring opening based on LC-MS analysis of the product mixture resulting from incubation with HDAC6 (see Figures S3 and S4, Supporting Information). However, in contrast with DFMO analogue **6**, jump dilution experiments with **17** revealed that it binds to HDAC6 reversibly. The crystal structure of the HDAC6−**13** complex shows that the difluoromethyl moiety binds in a small pocket defined in part by P571. We hypothesize that the trifluoromethyl group of **17** is sufficiently larger than the difluoromethyl group of **13** so as to destabilize binding of the trifluoromethyl group in the P571 pocket, which results in reversible rather than irreversible inhibition. Substitution of the CHF_2 group of **13** with a CF_3 group to generate a model of **17** bound in the HDAC6 active site suggests a steric clash as well as an unfavorable electrostatic interaction between the C−F group and the backbone carbonyl of G582 (Figure 6).
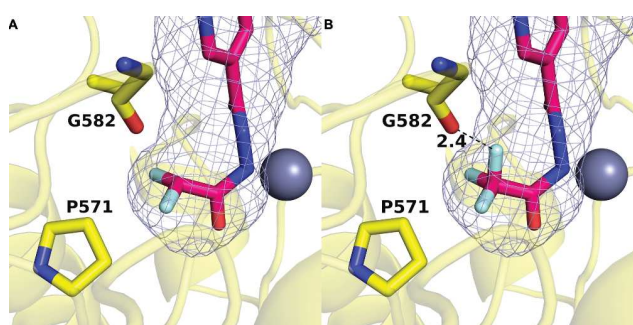
Figure 6. (A) Binding pocket of HDAC6 in purple mesh generated by GetCleft showing the orientation of the difluoromethyl group determined in the crystal structure of the complex with **13** (PDB: 8GD4). (B) Substitution of the CHF_2 group with a CF_3 group yields a model of the complex with hydrolyzed **17** in the ring-opened form. The additional fluorine atom results in a clash with the backbone carbonyl of G582.

Quantitative LC-MS experiments were conducted with compounds **6** and **17** (see Figure S3, Supporting Information), revealing that both compounds can undergo a second hydrolysis reaction, thereby resulting in the formation of hydrazide **14**. Notably, the concentration of the generated hydrazide differs by a factor of 2. When HDAC6 was incubated with 100 μM of **6**, 9 μM of **14** was produced while **17** yielded 18 μM of **14**. The second hydrolysis reaction from the respective acylhydrazide to hydrazide **14** requires the restoration of the Zn^{2+} coordination sphere by the entry of a

second water molecule. The fast-off binding kinetics of **17** may facilitate the entry of a second water molecule, potentially explaining the increased concentration of **14** when HDAC6 is incubated with **17**.

To confirm the hypothesis of different binding mechanisms for the difluoromethyl and trifluoromethyl analogues, we performed HDAC6 kinetic studies. Our preincubation experiments demonstrated that **6** and **17** are slow-binding inhibitors of HDAC6. The most common types of slow-binding mechanisms are "simple slow-binding" (mechanism I) and "induced-fit" (mechanism II) (see Figure S1, Supporting Information).[63,65] While mechanism I represents a single-step slow-binding mode of inhibition, mechanism II is characterized as a two-step slow-binding inhibition mode.[63,65] The slow-binding mechanisms I and II can be distinguished by their respective relationships between the rate constant for the onset of inhibition (k_{obs}) and the inhibitor concentration.[63,65] To determine the binding mechanism of **6** and **17** at HDAC6, we utilized the *Progression Method*[63,65] and measured a series of progression curves using fixed concentrations of enzyme, substrate, and different inhibitor concentrations. Subsequently, the generated data were fitted into eq 1 (see Supporting Information) to calculate the k_{obs} values for the different inhibitor concentrations. The resulting k_{obs} vs inhibitor concentration plots are depicted in Figure 5D. In the case of **6**, we observed a hyperbolic relationship between k_{obs} and the inhibitor concentration (Figure 5D, left), suggesting that **6** inhibits HDAC6 via the slow-binding "induced-fit" mechanism II. For **17**, the relationship between inhibitor concentration and k_{obs} was linear (Figure 5D, right), indicating binding via the single-step slow-binding mechanism I. As discussed above, DFMO **6** is hydrolyzed by HDAC6 and afterward essentially trapped in the active site in a small pocket defined in part by P571 while trifluoromethyl analogue **17** is hydrolyzed and dissociates fast out of the enzyme. These differences might explain the different slow-binding mechanisms observed for **6** and **17**.

Proposed Reaction Mechanism. DFMO **6** is an essentially irreversible inhibitor of HDAC6, even though deprotonated **13** does not form a covalent bond with any residues in the enzyme active site. We have determined that the generation of deprotonated acylhydrazide **13** requires the enzyme, since **6** does not undergo hydrolysis in the absence of enzyme to yield **13**. This implicates the reactive zinc-bound water molecule as the nucleophile for oxadiazole hydrolysis. Moreover, a mass shift of 2 is observed by mass spectrometry for acylhydrazide **13** when HDAC6 is incubated with **6** in
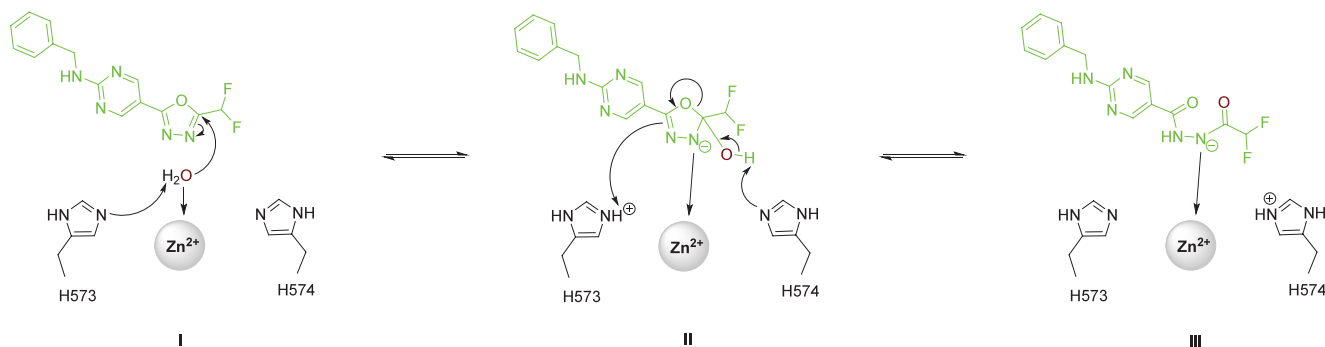
Figure 7. Proposed reaction mechanism of Zn^{2+}-catalyzed ring-opening reaction of DFMO compound **6**.

$H_2{}^{18}O$ instead of $H_2{}^{16}O$. Subsequent hydrolysis of the ^{18}O-labeled acylhydrazide yields hydrazide **14** without the ^{18}O label, as determined by mass spectrometry (see Figure S5, Supporting Information). These results indicate that the ^{18}O label was contained in the second hydrolysis product, difluoroacetate, which further implies that the initial nucleophilic attack of zinc-bound water at oxadiazole **6** occurs exclusively at the C=N bond closest to the difluoromethyl moiety. This result supports our proposed reaction mechanism depicted in Figure 7, in which the described C=N bond undergoes nucleophilic attack by the zinc-bound water molecule to form a tetrahedral intermediate. Electron rearrangement results in the ring opening of the oxadiazole, directly forming the deprotonated acylhydrazide. The negatively charged nitrogen can strongly coordinate to the zinc ion, supporting the assumption for essential irreversible inhibition. Due to the crucial strong anionic zinc coordination, the proposed mechanism is in agreement with our results, that the synthetic acylhydrazide **13**, bearing a protonated nitrogen, does not show any inhibitory activity. In other words, it is easier to generate the nitrogen anion of **13** through oxadiazole hydrolysis, captured and stabilized by Zn^{2+} coordination during the ring-opening mechanism, rather than by direct deprotonation of synthetic **13**. While this manuscript was under review, a similar mechanism for the generation of zinc-bound **13** was proposed on the basis of computational chemistry calculations.[66]

The histidine dyad H573/H574 plays a crucial role as a proton shuttle in the deacetylation of native acetyllysine peptide substrates of HDAC6 and, presumably, in the enzyme-catalyzed ring-opening reaction of DFMOs/TFMOs.[62] Furthermore, recent reports by Steinkühler and co-workers[56] as well as Barinka and co-workers[54] highlighted the importance of Y745 for the kinetics of the second hydrolysis reaction. Both groups observed a significant increased conversion rate into the respective hydrazide derivative when Y745 was mutated into phenylalanine. To gain further insights into the reaction mechanism, we prepared H573A, H574A, and Y745F mutants of HDAC6 and conducted quantitative LC-MS analysis after incubation of wild-type HDAC6 and the respective mutants with DFMO **6** and TFMO **17** (see Figure S6, Supporting Information). For the histidine mutants H573A and H574A, we observed a notable reduction in the formation of acylhydrazides **13** and **20**. In addition, both mutants were unable to hydrolyze **6** and **17** to hydrazide **14**. These results clearly confirm the critical role of the histidine dyad H573/H574 in the ring-opening reaction of DFMOs and TFMOs as well as the second hydrolysis reaction to the corresponding hydrazide. When incubating the Y745F mutant of HDAC6 with **6** and **17**, we observed an increased formation of hydrazide **14** compared to the wild type. In fact, in the case of incubation with TFMO **17**, the hydrazide was detected as the main reaction product. Our crystal structure of the HDAC6–**13** complex revealed that one carbonyl group and one C–F group of deprotonated **13** form hydrogen bonds with Y745 (Figure 2). Due to the absence of two important hydrogen bonds with Y745, deprotonated **13** may disengage from the catalytic center of the Y745F mutant, thereby facilitating a second hydrolysis reaction after the restoration of the Zn^{2+} coordination sphere by the entry of a second water molecule. Based on our crystallographic data (Figure 2) and LC-MS experiments with wild type and Y745F HDAC6 (see Figure S6, Supporting Information), we conclude that Y745 is critically important for the binding mode of deprotonated **13** and significantly contributes to the essentially irreversible binding of this active species.

CONCLUSIONS

In summary, we have characterized the DFMO derivative **6** as a potent and selective HDAC6 inhibitor. In IC_{50} shift experiments with various preincubation times, compound **6** showed slow-on binding properties with decreasing IC_{50} values. By analysis of the slow-binding characteristics, we found that **6** inhibits HDAC6 via a two-step slow-binding mechanism. To investigate the dissociation characteristics, we performed jump dilution experiments that revealed an essentially irreversible binding mode of DFMO **6** to its target. Additional dialysis experiments further confirmed the tight-binding properties of **6**. The trifluoromethyl analogue **17**, on the other hand, acts as a slow-binding inhibitor following a single-step slow-binding mechanism. In contrast to **6**, compound **17** was observed to disengage from the enzyme with fast-off binding properties in jump dilution assays, thus confirming that the two derivatives act via different modes of inhibition.

Steinkühler et al. recently reported the structure of the HDAC6 complex with a hydrazide inhibitor resulting from hydrolysis of a related oxadiazole inhibitor.[56] The authors postulated that the remarkable HDAC6 inhibition is not solely attributed to the crystallized hydrazide but rather to a high-affinity intermediate that forms a stable and long-lasting enzyme–inhibitor complex.[56] They suggested a closed hydrated intermediate and a protonated acylhydrazide as potential active species.[56] Using our crystallographic and mechanistic data, we are now able to confirm that DFMOs serve as substrate analogues and therefore as mechanism-based inhibitors undergoing an HDAC6-catalyzed ring-opening reaction, which is initiated by the attack of the zinc-bound water at the sp^2 carbon closest to the difluoromethyl moiety. Ultimately, this leads to the formation of the deprotonated acylhydrazide **13** as the active species. The analysis of the resulting HDAC6–**13** complex reveals an extensive array of intermolecular interactions that stabilize the bound inhibitor, particularly the strong anionic zinc coordination of **13** in combination with the binding of the difluoromethyl moiety in the P571 pocket. These structural features contribute to an exceptionally tight enzyme–inhibitor complex, thereby leading to an essentially irreversible inhibition of HDAC6.

EXPERIMENTAL SECTION

Chemistry. Chemicals were obtained from abcr GmbH, Acros Organics, BLDpharm, Carbolution Chemicals, Carl Roth, Fluorochem, Sigma-Aldrich, TCI Chemicals, or VWR and used without further purification. Technical-grade solvents were distilled prior to use. For all HPLC purposes, acetonitrile in HPLC-grade quality (HiPerSolv CHROMANORM, VWR) was used. Water was purified with a PURELAB Flex (ELGA VEOLIA). Air-sensitive reactions were carried out under an argon atmosphere utilizing standard Schlenk techniques. Thin-layer chromatography (TLC) was carried out on prefabricated plates (silica gel 60, F254, Merck). Components were visualized either by irradiation with ultraviolet light (254 or 366 nm) or by staining appropriately. Column chromatography was carried out on silica gel (NORMASIL 60, 40−63 μm, VWR or MACHEREY-Nagel silica gel 60, 40−63 μm). Mixtures of two or more solvents are specified as "solvent A"/"solvent B" (67/33, v/v), meaning that 100 mL of the respective mixture consists of 67 mL of "solvent A" and 33 mL of "solvent B". Preparative silica gel flash column chromatography

was performed on an Interchim puriFlash XS 520 Plus with diode-array detection (DAD) from 200 to 400 nm. The uncorrected melting points were determined using a Büchi Melting Point M-565 apparatus or Barnstead Electrothermal 9100 apparatus. *Nuclear magnetic resonance spectroscopy (NMR):* Proton (^{1}H), carbon (^{13}C), and fluorine (^{19}F) NMR spectra were recorded either on a Bruker Avance DRX 500 (500 MHz ^{1}H NMR, 126 MHz ^{13}C NMR), a Bruker Avance III 600 (600 MHz ^{1}H NMR, 151 MHz ^{13}C NMR), a Bruker Avance III HD 400 (400 MHz ^{1}H NMR, 101 MHz ^{13}C NMR, 377 MHz ^{19}F NMR), a Varian/Agilent MERCURYplus-400 (400 MHz ^{1}H NMR, 101 MHz ^{13}C NMR, 376 MHz ^{19}F NMR), or a Varian/Agilent MERCURYplus-300 (300 MHz ^{1}H, 75 MHz ^{13}C NMR, 282 MHz NMR ^{19}F NMR). The chemical shifts are given in parts per million (ppm). Deuterated chloroform (CDCl$_3$) and deuterated dimethyl sulfoxide (DMSO-d_6) were used as solvents. The residual solvent signal (CDCl$_3$: ^{1}H NMR: 7.26 ppm, ^{13}C NMR: 77.1 ppm; DMSO-d_6: ^{1}H NMR: 2.50 ppm, ^{13}C NMR: 39.52 ppm) was used for calibration. The multiplicity of each signal is reported as singlet (s), doublet (d), triplet (t), quartet (q), pentet (p), multiplet (m), or combinations thereof. Multiplicities and coupling constants are reported as measured and might disagree with the expected values. ^{19}F NMR spectra were recorded proton-decoupled if not stated otherwise. *Mass spectrometry:* High-resolution electrospray ionization mass spectra (HRMS-ESI) were acquired with either a Bruker Daltonics GmbH micrOTOF coupled to an LC Packings UltiMate HPLC system and controlled by micrOTOFControl3.4 and HyStar 3.2-LC/MS, a Bruker Daltonics GmbH ESI-qTOF Impact II coupled to a Dionex UltiMate 3000 UHPLC system and controlled by micrOTOFControl 4.0 and HyStar 3.2-LC/MS, a Bruker micrOTOF-Q mass spectrometer coupled with a HPLC Dionex UltiMate 3000, or an LTQ Orbitrap XL. Low-resolution electrospray ionization mass spectra (LRMS ESI) were acquired either with an Advion expression compact mass spectrometer (CMS) coupled with an automated TLC plate reader Plate Express (Advion), an API 2000 mass spectrometer coupled with an Agilent HPLC HP 1100 using an EC 50/2 NUCLEODUR C18 Gravity 3 μm column, or an Agilent Infinity Lab LC/MSD-system coupled with an Agilent HPLC 1260 Infinity II using an EC50/2 NUCLEODUR C18 Gravity 3 μm column. *High-performance liquid chromatography (HPLC):* For analytical purposes, HPLC measurements were performed on a Thermo Fisher Scientific UltiMate 3000 UHPLC system with a NUCLEODUR 100−5 C18 (250 × 4.6 mm, MACHEREY Nagel), using a flow rate of 1 mL/min and a temperature of 25 °C with an appropriate gradient. Detection was implemented by UV absorption measurement at a wavelength of λ = 220 nm and λ = 250 nm. Bidest. H$_2$O (A) and MeCN (B) were used as eluents with an addition of 0.1% TFA for eluent A. For preparative purposes, an AZURA Prep. 500/1000 gradient system with a NUCLEODUR 110−5 C18 HTec (150 × 32 mm, MACHEREY Nagel) column was used with a flow rate of 20 mL/min and an appropriate gradient. Detection was implemented by UV absorption measurement at a wavelength of λ = 220 nm and λ = 250 nm. Bidest. H$_2$O (A) and MeCN (B) were used as eluents with an addition of 0.1% TFA for eluent A. *Purity:* The purity of all final compounds was 95% or higher. Purity was determined via HPLC at 250 nm using the protocols described above, if not stated otherwise.

General Procedure A. The respective carbonitrile (1.0 equiv), NaN$_3$ (2.0 equiv), NH$_4$Cl (2.0 equiv), and LiCl (0.8 equiv) were suspended in DMF (2 mL, 1 M), and the resulting mixture was subjected to microwave irradiation at 150 W and 100 °C under vigorous stirring for 24 h. The reaction mixture was then filtered over a 5 cm layer of silica (CH$_2$Cl$_2$/MeOH, 9/1, v/v). Upon removal of the solvent under reduced pressure, the crude tetrazole intermediate was dissolved in CH$_2$Cl$_2$ (30 mL) and DFAA (6.1 equiv) was added dropwise at 0 °C. The resulting solution was allowed to warm to RT and stirred for 24 h. After completion of the reaction, the mixture was diluted with CH$_2$Cl$_2$ (30 mL) and washed with 1 M NaOH (2 × 10 mL), water (1 × 10 mL), and brine (1 × 10 mL). Drying of the organic layer over Na$_2$SO$_4$, and subsequent evaporation of the solvent afforded the desired product.

General Procedure B. The respective methyl ester (1.0 equiv) was dissolved in MeOH (0.2 M). Hydrazine monohydrate (10.0 equiv) was added, and the reaction mixture was stirred at 70 °C for 3 h. After completion of the reaction, the solvent was removed under reduced pressure. The crude product was used directly in the next step. The resulting hydrazide (1.0 equiv) was dissolved in DMF (0.1 M). DFAA (1.3 equiv) and Et$_3$N (2.0 equiv) were added, and the reaction mixture was stirred at 70 °C for 1 h. The mixture was concentrated under reduced pressure and used without further purification in the next reaction. The resulting difluoromethylacylhydrazide (1.0 equiv) was taken up in dry THF (0.1 M). Et$_3$N (3.0 equiv) and Burgess reagent (3.0 equiv) were added, and the reaction mixture was stirred at 60 °C for 18 h. The solvent was removed under reduced pressure, and the crude was purified by preparative HPLC.

General Procedure C. The respective carbonitrile (1.0 equiv) was dissolved in DMF (0.25 M). NaN$_3$ (2.0 equiv), NH$_4$Cl (1.3 equiv), and LiCl (0.5 equiv) were added, and the reaction mixture was stirred at 100 °C for 18 h. After completion of the reaction, the mixture was quenched with ice water (8 mL) and acidified with 1 M HCl to pH = 2. The precipitated solid was filtered and washed with cold water. The tetrazole product was used without further purification in the next step. The tetrazole derivative (1.0 equiv) was dissolved in toluene (0.05 M). DFAA (3.0 equiv) was added, and the solution was stirred at 70 °C for 18 h. The reaction mixture was concentrated under reduced pressure and purified by preparative HPLC.

2-(Difluoromethyl)-5-phenyl-1,3,4-oxadiazole (1). Benzonitrile (206 mg, 2.00 mmol, 1.0 equiv), NaN$_3$ (260 mg, 4.00 mmol, 2.0 equiv), NH$_4$Cl (213 mg, 4.00 mmol, 2.0 equiv), and LiCl (66 mg, 1.56 mmol, 0.8 equiv) were suspended in DMF (2 mL), and the resulting mixture was subjected to microwave irradiation at 150 W and 100 °C under vigorous stirring for 24 h. After evaporation of the solvent, the mixture was dissolved in 1 M NaOH (20 mL) and washed with EtOAc (2 × 10 mL) to remove excess benzonitrile. The aqueous layer was acidified using 10% HCl (pH 4) and extracted with CH$_2$Cl$_2$ (3 × 50 mL). The combined organic layers were dried over MgSO$_4$ and concentrated under reduced pressure. The intermediate 5-phenyl-1*H*-tetrazole was obtained as a white solid (216 mg, 1.47 mmol) and used without analytical characterization for the next reaction step. A solution of 5-phenyl-1*H*-tetrazole (180 mg, 1.22 mmol, 1.0 equiv) in CH$_2$Cl$_2$ (18 mL) was cooled to 0 °C, and DFAA (0.75 mL, 6.10 mmol, 5.0 equiv) was added dropwise. The resulting solution was allowed to warm to RT and stirred for 24 h before water (20 mL) was added. The mixture was extracted with CH$_2$Cl$_2$ (3 × 30 mL), and the combined organic layers were washed with brine (10 mL) and dried over MgSO$_4$. Removal of the solvent under reduced pressure and recrystallization from EtOAc (2 mL) and petrol ether (20 mL) afforded the desired product **1** as a white solid (193 mg, 0.98 mmol). Yield: 81%; mp 101−105 °C; ^{1}H NMR (300 MHz, CDCl$_3$): δ 8.19−8.07 (m, 2H), 7.67−7.46 (m, 3H), 6.92 (t, *J* (H, F) = 51.7 Hz, 1H); ^{13}C NMR (101 MHz, CDCl$_3$): δ 166.3, 158.3 (t, ^2J (C, F) = 28.8 Hz), 132.9, 129.4, 127.6, 122.8, 106.0 (t, ^1J (C, F) = 240.9 Hz; ^{19}F NMR (377 MHz, CDCl$_3$) δ −127.0, −127.1; HRMS (ESI) *m/z* [M + H]$^+$ calcd for C$_9$H$_7$F$_2$N$_2$O$^+$ 197.0521, found 197.0516; HPLC (95% H$_2$O 1 min, and then to 95% MeCN in 7 min, and then 100% MeCN to 17 min, 254 nm), t_R = 8.86 min, 95% purity.

2-(Difluoromethyl)-5-(6-methylpyridin-3-yl)-1,3,4-oxadiazole (2). The product was synthesized according to general procedure B, using methyl 6-methylnicotinate (453 mg, 3.00 mmol, 1.0 equiv) as starting material. The reaction mixture was purified by silica gel column chromatography (DCM/MeOH, 97/3, v/v) to afford **2** as yellow oil (146 mg, 0.70 mmol). Yield: 23%; R_f = 0.58 (DCM/MeOH, 95/5, v/v); ^{1}H NMR (600 MHz, DMSO-d_6) δ 9.08 (d, *J* = 2.3 Hz, 1H), 8.31 (dd, *J* = 8.1, 2.3 Hz, 1H), 7.56 (t, *J* (H, F) = 51.4 Hz, 1H), 7.53 (d, *J* = 8.2 Hz, 1H), 2.59 (s, 3H); ^{13}C NMR (151 MHz, DMSO-d_6) δ 164.0, 162.8, 158.6 (t, ^2J (C, F) = 29.2 Hz), 147.3, 135.0, 123.9, 116.6, 106.7 (t, ^1J (C, F) = 238.8 Hz), 24.4; ^{19}F NMR (565 MHz, DMSO-d_6) δ −121.5, −121.6; HRMS (ESI) *m/z* [M + H]$^+$ calcd for C$_9$H$_8$F$_2$N$_3$O$^+$ 212.0630, found 212.0620; HPLC (95% H$_2$O 5 min,

and then to 95% MeCN in 5 min, and then 100% MeCN to 20 min, 254 nm), t_R = 10.98 min, 95% purity.

2-(Difluoromethyl)-5-(pyrimidin-5-yl)-1,3,4-oxadiazole **(3)**. Synthesis according to general procedure A starting from 5-cyanopyrimidine (208 mg, 2.00 mmol, 1.0 equiv) afforded **3** as a yellow solid (80 mg, 0.41 mmol). Yield: 20%; mp. 104−107 °C; ^{1}H NMR (400 MHz, CDCl$_3$): δ 9.49−9.40 (m, 3H), 6.97 (t, J (H, F) = 51.6 Hz, 1H); ^{13}C NMR (75 MHz, CDCl$_3$): δ 162.1, 161.5, 159.2 (t, ^2J (C, F) = 29.3 Hz), 155.4, 118.4, 105.7 (t, ^1J (C, F) = 241.9 Hz); ^{19}F NMR (377 MHz, CDCl$_3$) δ −119.2, −119.3. HRMS (ESI) m/z [M + H]$^+$ calcd for C$_7$H$_5$F$_2$N$_4$O$^+$ 199.0426, found 199.0425; HPLC (95% H$_2$O 1 min, and then to 95% MeCN in 7 min, and then 100% MeCN to 17 min, 254 nm), t_R = 6.59 min, 97% purity.

2-(Benzylamino)pyrimidine-5-carbonitrile **(4)**. Benzylamine (0.328 mL, 3.00 mmol, 1.0 equiv) and 2-chlorpyrimidine-5-carbonitrile (837 mg, 6.00 mmol, 2.0 equiv) were dissolved in EtOH (4 mL, 0.3 M). DIPEA (1.56 mL, 6.00 mmol, 3.0 equiv) was added, and the reaction mixture was stirred at 90 °C for 18 h. After completion of the reaction, the solvent was removed under reduced pressure. EtOAc was added, and the organic phase was washed with brine, dried over Na$_2$SO$_4$, filtered, and evaporated. The crude was purified by a silica gel column using a cyclohexane/EtOAc gradient (16% to 25% EtOAc) to obtain the desired product as a yellow solid (598 mg, 2.85 mmol). Yield: 95%; mp 170−172 °C; R_f = 0.5 (cyclohexane/EtOAc, 3/1, v/v); ^{1}H NMR (600 MHz, DMSO-d_6) δ 8.80 (t, J = 6.4 Hz, 1H), 8.71−8.65 (m, 2H), 7.33−7.29 (m, 1H), 7.31−7.25 (m, 3H), 7.25−7.19 (m, 1H), 4.55 (d, J = 6.4 Hz, 2H); ^{13}C NMR (151 MHz, DMSO-d_6) δ 161.9, 161.6, 139.1, 128.5, 127.2, 127.0, 117.2, 95.6, 44.1; LRMS (ESI) m/z [M + H]$^+$ calcd for C$_{12}$H$_{11}$N$_4$$^+$ 211.1, found 210.9.

2-[(4-Methoxybenzyl)amino]pyrimidine-5-carbonitrile **(5)**. 4-Methoxybenzylamine (0.235 mL, 1.80 mmol, 1.0 equiv) and 2-chlorpyrimidine-5-carbonitrile (502 mg, 3.60 mmol, 2.0 equiv) were dissolved in EtOH (6 mL, 0.3 M). DIPEA (0.943 mL, 5.40 mmol, 3.0 equiv) was added, and the reaction mixture was stirred at 90 °C for 18 h. After completion of the reaction, the solvent was removed under reduced pressure. EtOAc was added, and the organic phase was washed with brine, dried over Na$_2$SO$_4$, filtered, and evaporated. The crude was purified by a silica gel column using a cyclohexane/EtOAc gradient (16% to 25% EtOAc) to obtain the desired product as a yellow solid (455 mg, 1.70 mmol). Yield: 94%; mp 177−178 °C; R_f = 0.18 (cyclohexane/EtOAc, 3/1, v/v); ^{1}H NMR (600 MHz, CDCl$_3$) δ 8.53 (d, J = 2.9 Hz, 1H), 8.18−8.14 (m, 1H), 7.26−7.21 (m, 2H), 6.90−6.85 (m, 2H), 6.42 (s, 1H), 4.56 (d, J = 5.6 Hz, 2H), 3.79 (s, 3H); ^{13}C NMR (151 MHz, CDCl$_3$) δ 161.6, 161.4, 160.6, 159.4, 129.2, 129.2, 116.3, 114.2, 97.0, 55.3, 45.2; LRMS (ESI) m/z [M + H]$^+$ calcd for C$_{13}$H$_{13}$N$_4$O$^+$ 241.1, found 240.9.

N-Benzyl-5-[5-(difluoromethyl)-1,3,4-oxadiazol-2-yl]pyrimidin-2-amine **(6)**. The product was synthesized according to general procedure C, using **4** (55 mg, 0.26 mmol, 1.0 equiv) as starting material. The crude was purified by silica gel column chromatography (cyclohexane/EtOAc, 4/1, v/v) to afford **6** as a white solid (31 mg, 0.10 mmol). Yield: 38%; mp 174−176 °C; R_f = 0.28 (cyclohexane/EtOAc, 3/1, v/v); ^{1}H NMR (600 MHz, DMSO-d_6) δ 8.87 (s, 2H), 8.71 (t, J = 6.4 Hz, 1H), 7.51 (t, J (H, F) = 51.4 Hz, 1H), 7.34−7.28 (m, 4H), 7.26−7.19 (m, 1H), 4.60 (d, J = 6.4 Hz, 2H); ^{13}C NMR (151 MHz, DMSO-d_6) δ 163.3, 163.1, 157.7 (t, ^2J (C, F) = 29.2 Hz), 157.3, 157.2, 139.3, 128.5, 127.2, 127.0, 106.7, 106.5 (t, ^1J (C, F) = 237.4 Hz), 44.2; ^{19}F NMR (565 MHz, DMSO-d_6) δ −121.1, −121.2; HRMS (ESI) m/z [M + H]$^+$ calcd for C$_{14}$H$_{12}$F$_2$N$_5$O$^+$ 304.1004, found 304.0995; HPLC (95% H$_2$O 5 min, and then to 95% MeCN in 5 min, and then 100% MeCN to 20 min, 254 nm), t_R = 12.71 min, 99% purity.

5-[5-(Difluoromethyl)-1,3,4-oxadiazol-2-yl]-N-(4-methoxybenzyl)pyrimidin-2-amine **(7)**. The product was synthesized according to general procedure C, using **5** (336 mg, 1.40 mmol, 1.0 equiv) as starting material. Purification by RP flash column chromatography using a water/ACN gradient (5 to 95% ACN) yielding **7** as a white solid (225 mg, 0.70 mmol). Yield: 50%; mp 165−166 °C; ^{1}H NMR (600 MHz, DMSO-d_6) δ 8.89−8.83 (m, 2H), 8.65 (t, J = 6.4 Hz, 1H),

7.51 (t, J (H, F) = 51.4 Hz, 1H), 7.27−7.22 (m, 2H), 6.89−6.84 (m, 2H), 4.52 (d, J = 6.3 Hz, 2H), 3.71 (s, 3H); ^{13}C NMR (151 MHz, DMSO-d_6) δ 163.3, 163.0, 157.7 (t, ^2J (C, F) = 29.2 Hz), 157.3, 157.2, 131.2, 128.7, 113.9, 107.5 (t, ^1J (C, F) = 238.4 Hz), 106.4, 55.2, 43.7; ^{19}F NMR (565 MHz, DMSO-d_6) δ −121.1, −121.2; HRMS (ESI) m/z [M + H]$^+$ calcd for C$_{15}$H$_{14}$F$_2$N$_5$O$_2$$^+$ 334.1110, found 334.1113; HPLC (95% H$_2$O 5 min, and then to 95% MeCN in 5 min, and then 100% MeCN to 20 min, 254 nm), t_R = 12.66 min, 98% purity.

Methyl 4-[(Butylamino)methyl]benzoate **(8)**. Methyl 4-(bromomethyl)benzoate (263 mg, 1.15 mmol, 1.0 equiv) and butylamine (0.568 mL, 5.75 mmol, 5.0 equiv) were dissolved in THF (3 mL, 0.4 M), and the reaction was stirred at room temperature for 1 h. After completion of the reaction, the mixture was diluted with NaHCO$_3$ (30 mL) and extracted with DCM (3 × 30 mL), dried over Na$_2$SO$_4$, and filtered and the solvent was removed under reduced pressure. The crude product was purified by silica gel column chromatography (DCM/MeOH, 95/5, v/v) to afford **8** as a colorless oil (221 mg, 1.00 mmol). Yield: 87%; R_f = 0.28 (DCM/MeOH, 95/5, v/v); ^{1}H NMR (600 MHz, DMSO-d_6) δ 7.92−7.87 (m, 2H), 7.48−7.44 (m, 2H), 3.83 (s, 3H), 3.75 (s, 2H), 2.47 (t, J = 7.3 Hz, 2H), 1.40 (dq, J = 8.6, 7.0 Hz, 2H), 1.34−1.24 (m, 2H), 0.84 (t, J = 7.3 Hz, 3H); N$\underline{H}$-proton was not detectable; ^{13}C NMR (151 MHz, DMSO-d_6) δ 166.4, 146.9, 129.2, 128.2, 128.1, 52.7, 52.1, 48.5, 31.7, 20.1, 14.0; LRMS (ESI) m/z [M + H]$^+$ calcd for C$_{13}$H$_{20}$NO$_2$$^+$ 222.1, found 222.1.

1-Butyl-1-{4-[5-(difluoromethyl)-1,3,4-oxadiazol-2-yl]benzyl}-3-phenylurea **(9)**. The product was synthesized according to general procedure B, using **19** (340 mg, 1.00 mmol, 1.0 equiv) as starting material, affording **9** as a white lyophilized solid (29 mg, 0.071 mmol). Yield: 9%; ^{1}H NMR (600 MHz, DMSO-d_6) δ 8.38 (s, 1H), 8.06−8.02 (m, 2H), 7.53 (t, J (H, F) = 51.4 Hz, 1H), 7.51 (d, J = 8.1 Hz, 2H), 7.45 (dd, J = 8.2, 6.9 Hz, 2H), 7.25−7.19 (m, 2H), 6.96−6.90 (m, 1H), 4.68 (s, 2H), 3.36−3.32 (m, 2H), 1.49 (p, J = 7.5 Hz, 2H), 1.26 (h, J = 7.4 Hz, 2H), 0.86 (t, J = 7.4 Hz, 3H); ^{13}C NMR (151 MHz, DMSO-d_6) δ 165.4, 158.4 (t, ^2J (C, F) = 29.5 Hz), 155.4, 144.7, 140.6, 128.4, 128.3, 127.4, 122.0, 121.1, 120.3, 106.8 (t, ^1J (C, F) = 238.3 Hz), 49.4, 46.5, 30.2, 19.6, 13.9; ^{19}F NMR (565 MHz, DMSO-d_6) δ −121.4, −121.5; HRMS (ESI) m/z [M + H]$^+$ calcd for C$_{21}$H$_{23}$F$_2$N$_4$O$_2$$^+$ 401.1784, found 401.1791; HPLC (95% H$_2$O 5 min, then to 95% MeCN in 5 min, then 100% MeCN to 20 min, 254 nm), t_R = 17.05 min, 96% purity.

N-Butyl-N-{4-[5-(difluoromethyl)-1,3,4-oxadiazol-2-yl]benzyl}-benzamide **(10)**. **8** (211 mg, 1.00 mmol, 1.0 equiv) was dissolved in DCM (2.5 mL, final concentration 0.2 M). Benzoyl chloride (280 mg, 2 mmol, 2 equiv) was separately dissolved in DCM (2.5 mL) and added dropwise over 10 min to the reaction. The mixture was stirred at room temperature for 2 h. After completion, the reaction was quenched by the addition of water (10 mL) and extracted with DCM (3 × 10 mL), dried over Na$_2$SO$_4$, and filtered, and the solvent was removed under reduced pressure. The crude intermediate methyl 4-((N-butylbenzamido)methyl)benzoate was purified by silica gel column chromatography (cyclohexane/EtOAc, 3/1, v/v) to afford a yellow oil (187 mg, 0.57 mmol). This intermediate was used without analytical characterization for the next reaction step. **10** was synthesized in the next steps according to general procedure B using methyl 4-((N-butylbenzamido)methyl)benzoate (187 mg, 0.57 mmol, 1.0 equiv) as starting material, affording **10** as a white lyophilized solid (32 mg, 0.084 mmol). Yield: 15%; ^{1}H NMR (600 MHz, CDCl$_3$, mixture of 2 rotamers in 0.6:0.4 ratio) δ 8.11 (d, J = 7.8 Hz, 2H), 7.54 (d, J = 7.8 Hz, 1H), 7.42 (d, J = 19.2 Hz, 6H), 6.92 (t, J (H, F) = 51.7 Hz, 1H), 4.93−4.79 (m, 1.2H), 4.68−4.54 (m, 0.8H), 3.55−3.43 (m, 0.8H), 3.28−3.13 (m, 1.2H), 1.75−1.58 (m, 0.8H), 1.55−1.44 (m, 1.2H), 1.42−1.31 (m, 0.8H), 1.16−1.06 (m, 1.2H), 1.01−0.90 (m, 1.2H), 0.79−0.67 (m, 1.8H); ^{13}C NMR (151 MHz, CDCl$_3$, mixture of 2 rotamers) δ 172.5, 166.0, 158.3, 158.2 (t, ^2J (C, F) = 29.1 Hz), 142.9, 142.6, 136.0, 129.7, 128.7, 128.6, 127.9, 127.6, 126.5, 121.7, 115.7, 113.8, 105.8 (t, ^1J (C, F) = 240.9 Hz), 52.4, 48.7, 47.6, 45.0, 30.4, 29.1, 20.2, 19.6, 13.8, 13.5; ^{19}F NMR (565 MHz, CDCl$_3$) δ −120.0, −120.1; HRMS (ESI) m/z [M + H]$^+$ calcd

for $C_{21}H_{22}F_2N_3O_2^+$ 386.1675, found 386.1674; HPLC (95% H_2O 5 min, and then to 95% MeCN in 5 min, and then 100% MeCN to 20 min, 254 nm), t_R = 13.40 min, 98% purity.

Methyl 4-({N-[2-(Benzylamino)-2-oxoethyl]-4-(dimethylamino)-benzamido}methyl)benzoate (11). Compound **11** was synthesized as described.[59]

N-[2-(Benzylamino)-2-oxoethyl]-N-{4-[5-(difluoromethyl)-1,3,4-oxadiazol-2-yl]benzyl}-4-(dimethylamino)benzamide (12). The product was synthesized according to general procedure B, using **11** (135 mg, 0.30 mmol, 1.0 equiv) as starting material, affording **12** as a white lyophilized solid (13.7 mg, 0.026 mmol). Yield: 9%; ^1H NMR (600 MHz, DMSO-d_6) δ 8.44 (t, J = 5.9 Hz, 1H), 8.04 (d, J = 8.0 Hz, 2H), 7.59 (t, J (H, F) = 51.7 Hz, 1H), 7.55 (d, J = 7.8 Hz, 2H), 7.35–7.29 (m, 4H), 7.24 (t, J = 7.3 Hz, 3H), 6.65 (d, J = 8.5 Hz, 2H), 4.73 (s, 2H), 4.30 (d, J = 5.9 Hz, 2H), 3.94 (s, 2H), 2.93 (s, 6H); ^{13}C NMR (151 MHz, DMSO-d_6) δ 172.0, 168.3, 165.4, 158.4 (t, ^2J (C, F) = 29.5 Hz), 151.4, 143.1, 139.4, 128.8, 128.4, 127.4, 127.0, 121.3, 111.2, 106.8 (t, ^1J (C, F) = 238.3 Hz), 42.3; ^{19}F NMR (565 MHz, DMSO-d_6) δ −121.4, −121.5; HRMS (ESI) m/z [M + H]$^+$ calcd for $C_{28}H_{28}F_2N_5O_3^+$ 520.2155, found 520.2075; HPLC (95% H_2O 5 min, then to 95% MeCN in 5 min, then 100% MeCN to 20 min, 254 nm), t_R = 15.29 min, 99% purity.

2-(Benzylamino)-N′-(2,2-difluoroacetyl)pyrimidine-5-carbohy-drazide (13). **18** (371 mg, 1.50 mmol, 1.0 equiv) was dissolved in MeOH (10 mL, 0.2 M). Hydrazine monohydrate (0.75 mL, 10.00 mmol, 10.0 equiv) was added, and the reaction mixture was stirred at 70 °C for 3 h. After completion of the reaction, the solvent was removed under reduced pressure. The crude was used directly in the next step. The resulting hydrazide (1.0 equiv) was dissolved in DMF (15 mL, 0.1 M). DFAA (0.205 mL, 1.65 mmol, 1.1 equiv) was added, and it was stirred at 70 °C for 1 h. The solvent was removed under reduced pressure, and the crude was purified by preparative HPLC to afford **13** as a white lyophilized solid (82 mg, 0.26 mmol). Yield: 17%; ^1H NMR (600 MHz, DMSO-d_6) δ 10.90 (s, 1H), 10.45 (s, 1H), 8.73 (s, 2H), 8.45 (t, J = 6.4 Hz, 1H), 7.31 (d, J = 4.8 Hz, 4H), 7.26–7.20 (m, 1H), 6.42 (t, J (H, F) = 53.0 Hz, 1H), 4.58 (d, J = 6.4 Hz, 2H); ^{13}C NMR (151 MHz, DMSO-d_6) δ 163.3, 163.1, 161.7 (t, ^2J (C, F) = 25.8 Hz), 158.4, 158.0, 139.7, 128.4, 127.2, 126.9, 114.6, 108.3 (t, ^1J (C, F) = 246.6 Hz), 44.2; ^{19}F NMR (565 MHz, DMSO-d_6) δ −127.1, −127.2; HRMS (ESI) m/z [M + H]$^+$ calcd for $C_{14}H_{14}F_2N_5O_2^+$ 322.1110, found 322.1110; HPLC (95% H_2O 5 min, and then to 95% MeCN in 5 min, and then 100% MeCN to 20 min, 254 nm), t_R = 11.28 min, 98% purity.

2-(Benzylamino)pyrimidine-5-carbohydrazide (14). **18** (243 mg, 1.00 mmol, 1.0 equiv) was dissolved in MeOH (5 mL, 0.2 M). Hydrazine monohydrate (1.00 mL, 10.00 mmol, 10.0 equiv) was added, and the reaction mixture was stirred at 70 °C for 3 h. After completion of the reaction, the solvent was removed under reduced pressure and the crude product was purified by preparative HPLC to afford **14** as a yellow lyophilized solid (203 mg, 0.83 mmol). Yield: 83%; ^1H NMR (600 MHz, DMSO-d_6) δ 9.53 (s, 1H), 8.65 (s, 2H), 8.24 (t, J = 6.4 Hz, 1H), 7.31–7.27 (m, 4H), 7.24–7.18 (m, 1H), 4.54 (d, J = 6.4 Hz, 2H), 4.38 (s, 2H).; ^{13}C NMR (151 MHz, DMSO-d_6) δ 163.9, 163.0, 157.8, 157.3, 139.9, 128.4, 127.2, 126.8, 115.8, 44.1; HRMS (ESI) m/z [M + H]$^+$ calcd for $C_{12}H_{14}N_5O^+$ 244.1193, found 244.1186; HPLC (95% H_2O 5 min, and then to 95% MeCN in 5 min, and then 100% MeCN to 20 min, 254 nm), t_R = 10.56 min, 96% purity.

N-Benzyl-5-(5-methyl-1,3,4-oxadiazol-2-yl)pyrimidin-2-amine (15). **4** (105 mg, 0.50 mmol, 1.0 equiv) was dissolved in DMF (0.25 M). NaN$_3$ (65 mg, 1.00 mmol, 2.0 equiv), NH$_4$Cl (35 mg, 0.65 mmol, 1.3 equiv), and LiCl (11 mg, 0.25 mmol, 0.5 equiv) were added, and the reaction mixture was stirred at 100 °C for 18 h. After completion of the reaction, the mixture was quenched with ice water (4 mL) and acidified with 1 M HCl. The precipitated solid was filtered and washed with cold water. The tetrazole product was used without further purification in the next step. The tetrazole derivative (126 mg, 0.50 mmol, 1.0 equiv) was dissolved in toluene (0.05 M). Acetic anhydride (6 mL, 63 mmol, 126.0 equiv) was added, and it was stirred at 70 °C for 18 h. The reaction mixture was concentrated

under reduced pressure and conducted without purification in the next reaction step. The mixture was dissolved (MeOH/H$_2$O, 0.15 M, 1/1, v/v), K$_2$CO$_3$ (207 mg, 1.50 mmol, 3.0 equiv) was added, and the reaction mixture was stirred at room temperature for 12 h. The crude product was concentrated under reduced pressure and purified by RP flash column chromatography using a water/ACN gradient (5% to 95% ACN) yielding **15** as a white solid (72 mg, 0.27 mmol). Yield: 54%; mp 189–192 °C; ^1H NMR (500 MHz, DMSO-d_6) δ 8.78 (s, 2H), 8.53 (t, J = 6.3 Hz, 1H), 7.34–7.26 (m, 4H), 7.26–7.18 (m, 1H), 4.58 (d, J = 6.3 Hz, 2H), 2.53 (s, 3H); ^{13}C NMR (126 MHz, DMSO-d_6) δ 163.1, 162.9, 161.5, 156.6, 156.2, 139.5, 128.4, 127.2, 126.9, 107.6, 44.2, 10.6; HRMS (ESI) m/z [M + H]$^+$ calcd for $C_{14}H_{14}N_5O^+$ 268.1193, found 268.1189; HPLC (95% H_2O 5 min, then to 95% MeCN in 5 min, then 100% MeCN to 20 min, 254 nm), t_R = 12.29 min, 96% purity.

N-Benzyl-5-(5-(fluoromethyl)-1,3,4-oxadiazol-2-yl)pyrimidin-2-amine (16). Synthesis according to general procedure A starting from **14** (100 mg, 0.41 mmol, 1.0 equiv), using monofluoroacetic acid (0.028 mL, 0.49 mmol, 1.2 equiv) to afford **16** as a white lyophilized solid (4.6 mg, 0.016 mmol). Yield: 4%; ^1H NMR (500 MHz, DMSO-d_6): δ 8.85 (s, 2H), 8.64 (t, J = 6.4 Hz, 1H), 7.34–7.27 (m, 4H), 7.27–7.18 (m, 1H), 5.71 (d, J = 46.7 Hz, 2H), 4.60 (d, J = 6.2 Hz, 2H); ^{13}C NMR (126 MHz, DMSO-d_6): δ 163.0, 162.9, 160.9 (d, ^2J (C, F) = 19.5 Hz), 157.1, 156.8, 139.4, 128.4, 127.2, 127.0, 107.0, 73.6 (d, ^1J (C, F) = 165.3 Hz), 44.2; ^{19}F NMR (471 MHz, DMSO-d_6) δ −74.2. HRMS (ESI) m/z [M + H]$^+$ calcd for $C_{14}H_{13}FN_5O^+$ 286.1099, found 286.1101; HPLC (95% H_2O 1 min, then to 95% MeCN in 7 min, then 100% MeCN to 17 min, 254 nm), t_R = 12.44 min, 96% purity.

N-Benzyl-5-[5-(trifluoromethyl)-1,3,4-oxadiazol-2-yl]pyrimidin-2-amine (17). The product was synthesized according to general procedure C, using **4** (105 mg, 0.50 mmol, 1.0 equiv) and trifluoroacetic anhydride (TFAA, 0.139 mL, 1.00 mmol, 2.0 equiv) as starting material. The crude was purified by silica gel column chromatography (cyclohexane/EtOAc, 4/1, v/v) to afford **17** as a white solid (88 mg, 0.27 mmol). Yield: 54%; mp 185–187 °C; R_f = 0.4 (cyclohexane/EtOAc, 4/1, v/v); ^1H NMR (600 MHz, DMSO-d_6) δ 8.89 (d, J = 1.5 Hz, 2H), 8.78 (t, J = 6.4 Hz, 1H), 7.34–7.28 (m, 4H), 7.23 (ddd, J = 8.6, 5.3, 3.3 Hz, 1H), 4.61 (d, J = 6.2 Hz, 2H); ^{13}C NMR (151 MHz, DMSO-d_6) δ 164.2, 163.2, 157.6, 157.5, 153.4 (q, ^2J (C, F) = 43.8 Hz), 139.3, 128.5, 127.3, 127.0, 117.4 (q, ^1J (C, F) = 270.3 Hz), 106.1, 44.2; ^{19}F NMR (565 MHz, DMSO-d_6) δ −65.0; HRMS (ESI) m/z [M + H]$^+$ calcd for $C_{14}H_{11}F_3N_5O^+$ 322.0910, found 322.0481; HPLC (95% H_2O 5 min, then to 95% MeCN in 5 min, then 100% MeCN to 20 min, 254 nm), t_R = 13.21 min, 97% purity.

Methyl 2-(Benzylamino)pyrimidine-5-carboxylate (18). Benzylamine (0.220 mL, 2.00 mmol, 1.0 equiv) and methyl 2-chlorpyrimidin-5-carboxylate (345 mg, 2.00 mmol, 1.0 equiv) were dissolved in EtOH (10 mL, 0.2 M). DIPEA (0.524 mL, 3.00 mmol, 1.5 equiv) was added, and the reaction mixture was stirred at 80 °C for 18 h. After completion of the reaction, the solvent was removed under reduced pressure. EtOAc was added, and the organic phase was washed with brine, dried over Na$_2$SO$_4$, filtered, and evaporated. The product was obtained as a yellow solid (371 mg, 1.50 mmol) and used without further purification. Yield: 76%; mp 151–153 °C; ^1H NMR (600 MHz, DMSO-d_6) δ 8.74 (d, J = 3.1 Hz, 2H), 8.61 (t, J = 6.4 Hz, 1H), 7.32–7.29 (m, 4H), 7.25–7.21 (m, 1H), 4.58 (d, J = 6.4 Hz, 2H), 3.78 (s, 3H); ^{13}C NMR (151 MHz, DMSO-d_6) δ 164.7, 163.5, 159.8, 159.8, 139.4, 128.4, 127.2, 126.9, 112.6, 51.7, 44.2; LRMS (ESI) m/z [M + H]$^+$ calcd for $C_{13}H_{14}N_3O_2^+$ 244.1, found 243.9.

Methyl 4-[(1-Butyl-3-phenylureido)methyl]benzoate (19). Phenyl phenylcarbamate (149 mg, 0.70 mmol, 1.0 equiv) and **8** (197 mg, 0.84 mmol, 1.2 equiv) were dissolved in THF (7 mL, 0.1 M). Et$_3$N (0.195 mL, 1.40 mmol, 2.0 equiv) was added, and the reaction mixture was stirred at 60 °C for 2 h. The reaction was allowed to cool down to room temperature and quenched by the addition of water (10 mL). The mixture was extracted with EtOAc (3 × 5 mL). The combined organic layers were washed with brine, dried over Na$_2$SO$_4$, and filtered, and the solvent was removed under reduced pressure.

Table 2. Primers for zCD2 Mutagenesis

primer	sequence	annealing temperature
Y745F Fwd	5′-GGAAGGCGGTTTTAACCTGACCA-3′	63 °C
Y745F Rev	5′-AGGATAATCAGCACACGAC-3′	
H573A Fwd	5′-TCCGCCGGGCGCGCACGCAGAAAAAGATACCGC-3′	72 °C
H574A Rev	5′-CGCACGATGGCCACCGCA-3′	

The crude product was purified by silica gel column chromatography (cyclohexane/EtOAc, 3/1, *v/v*) to afford **19** as colorless oil (207 mg, 0.60 mmol). Yield: 87%; R_f = 0.36 (cyclohexane/EtOAc, 3/1, *v/v*); ^{1}H NMR (600 MHz, CDCl₃) δ 8.05−7.98 (m, 2H), 7.36 (d, *J* = 8.2 Hz, 2H), 7.31−7.27 (m, 2H), 7.25−7.22 (m, 2H), 7.00 (tt, *J* = 7.1, 1.3 Hz, 1H), 6.29 (s, 1H), 4.61 (s, 2H), 3.90 (s, 3H), 3.34−3.30 (m, 2H), 1.65−1.56 (m, 2H), 1.35 (h, *J* = 7.4 Hz, 2H), 0.92 (t, *J* = 7.3 Hz, 3H); ^{13}C NMR (151 MHz, CDCl₃) δ 166.8, 155.3, 143.1, 138.8, 130.2, 129.5, 129.5, 128.9, 127.1, 123.2, 119.9, 52.1, 50.5, 47.8, 30.5, 20.2, 13.8; LRMS (ESI) *m/z* [M + H]⁺ calcd for $C_{20}H_{25}N_2O_3^+$ 341.2, found 341.2.

Biological Experiments. *HDAC Inhibition Assays. Preincubation Assay for HDAC1−4 and HDAC6.* In vitro inhibitory activity assays against HDAC1−3 and HDAC6 were performed using a modified protocol based on our previously published assays.[63] *In vitro* inhibitory activities against HDAC4 were measured using a previously published protocol with slight modifications.[67] For compounds and controls, threefold serial dilutions of the respective DMSO-stock solution in assay buffer (50 mM Tris−HCl, pH 8.0, 137 mM NaCl, 2.7 mM KCl, 1.0 mM MgCl₂•6 H₂O, 5 mg/mL BSA) were prepared and 5.0 μL of this serial dilution was transferred into OptiPlate-96 black microplates (PerkinElmer). Then, 25 μL of assay buffer and 10 μL of enzyme solution (human recombinant HDAC1 (BPS Bioscience, Catalog no. 50051); HDAC2 (BPS Bioscience, Catalog no. 50052); HDAC3/NcoR2 (BPS Bioscience, Catalog no. 50003); HDAC4 (BPS Bioscience, Catalog no. 50004); HDAC6 (BPS Bioscience, Catalog no. 50006)) were added. The enzyme and inhibitor were preincubated at 25 °C for 60 min. Afterward, the fluorogenic substrate ZMAL (Z-Lys(Ac)-AMC;[68] 10 μL; 75 μM in assay buffer) was added. In the case of HDAC4, the fluorogenic substrate Boc-Lys(Tfa)-AMC (Bachem, Catalog no. 4060676, 10 μL; 42.86 μM in assay buffer) was added. The total assay volume (50 μL, max. 1% DMSO) was incubated at 37 °C for 90 min. Subsequently, 50 μL of trypsin solution (0.4 mg/mL trypsin in buffer: 50 mM Tris−HCl, pH 8.0, 100 mM NaCl) was added, followed by an additional 30 min of incubation at 37 °C. Fluorescence (excitation: 355 nm, emission: 460 nm) was measured using a FLUOstar OPTIMA microplate reader (BMG Labtech). Compounds were tested at least twice in duplicates; the 50% inhibitory concentration (IC₅₀) was determined by plotting normalized dose−response curves using nonlinear regression (Prism 8).

IC₅₀-Shift Experiments at HDAC6. For IC₅₀-shift experiments, we used the preincubation assay for HDAC6 as stated above and varied the preincubation period as follows: the enzyme and the respective inhibitor dilutions were preincubated at 25 °C for 5 to 120 min. Afterward, the assay protocol was continued, as stated above. Compounds were tested at least twice in duplicates.

Determination of Binding Kinetics via the Progression Method.[63,65] HDAC6 deacetylase activity was evaluated at varying inhibitor concentrations. Appropriate inhibitor concentrations were chosen based on the previously determined IC₅₀ values. To ensure substrate excess during the experiment, the substrate concentration was set to five times K_M. K_M was determined using a series of substrate concentrations (see Figure S2, Supporting Information). The respective steady-state velocities were plotted against the corresponding substrate concentrations [*S*] and fitted to the Michaelis−Menten equation (K_M HDAC6 = 19.27 μM). For the progression curves, the enzyme was incubated with the fluorogenic substrate and inhibitor in assay buffer (50 μL; 50 mM Tris−HCl, pH 8.0, 137 mM NaCl, 2.7 mM KCl, 1.0 mM MgCl₂•6 H₂O, 5 mg/mL BSA) and 50 μL of trypsin solution (40 ng/μL; buffer: 50 mM Tris−HCl, pH 8.0, 100

mM NaCl). The total assay volume (100 μL) contained the following final concentrations: HDAC6 (Lot no.: 220419-GC; 220 pg/μL), ZMAL (93.0 μM), and trypsin (20 ng/μL). In situ AMC release was monitored continuously by fluorescence readings (excitation: 360 nm, emission: 460 nm; TECAN Spark multimode microplate reader) recorded every 0.5 min for 45 min at 37 °C. The relationship between AMC concentration and relative fluorescence units (RFU) was determined, and the measured RFU were transformed into the respective AMC concentration in μM. The data of each progression curve were fitted to obtain the apparent first-order rate constant k_{obs} (eq 1, see Supporting Information). The apparent first-order rate constants k_{obs} were replotted against the corresponding inhibitor concentrations [*I*], and the curves were either fitted into eq 2 or eq 3 (see Supporting Information). Compounds were tested in triplicates. Data were fitted to the relevant equations using Prism 8.

100-Fold Jump Dilution Experiments. HDAC6 (22 ng/μL) in assay buffer (50 mM Tris−HCl, pH 8.0, 137 mM NaCl, 2.7 mM KCl, 1.0 mM MgCl₂•6 H₂O, 5 mg/mL BSA) was incubated with an inhibitor concentrate (at least 10-fold IC₅₀) or blank (DMSO 1%) for 1 h at room temperature. Afterward, this "incubation mix" was diluted 100-fold either in the presence of the respective inhibitors at their original concentrations or solely with assay buffer. The substrate ZMAL (25 μL; 372 μM in assay buffer) and trypsin (50 μL; 40 ng/μL; buffer: 50 mM Tris−HCl, pH 8.0, 100 mM NaCl) were added to all samples. The total assay volume (100 μL) contained the following final concentrations: HDAC6 (Lot no.: 220419-GC; 220 pg/μL), ZMAL (93 μM), and trypsin (20 ng/μL). The time-dependent in situ AMC release was monitored continuously by fluorescence readings (excitation: 360 nm, emission: 460 nm; TECAN Spark multimode microplate reader) recorded every 0.5 min for 60 min at 37 °C. Compounds were tested in triplicates.

LC-MS Experiments. *General Information. D. rerio* HDAC6 catalytic domain 2 (zCD2) was expressed and purified as previously described, with the modification of 0 mM imidazole in buffer A.[69]

zCD2 Mutagenesis. Two mutants were generated of zCD2, Y745F and H573A, which were prepared using the Q5 Site-Directed Mutagenesis Kit (New England Biolabs) with the addition of 5% DMSO. PCR primer sequences and annealing temperatures were generated using NEBaseChanger and are listed in Table 2. Following sequence confirmation, the plasmids were transformed into BL21-(DE3) cells expressed and purified by the same method as wild-type zCD2. Mutant H574A was generated previously, expressed, and then purified by the same method as wild-type zCD2.[62]

LC-MS to Study Oxadiazole Hydrolysis. To study the zHDAC6 CD2-catalyzed ring-opening reaction of **6** to yield **13**, 50 μM enzyme in size exclusion buffer (50 mM HEPES (pH 7.5), 100 mM KCl, 1 mM TCEP, 5% glycerol (*v/v*)) was incubated with 100 μM inhibitor overnight, total volume 100 μL. Control experiments were also performed with 100 μM inhibitor in size exclusion buffer only, to prove that the ring-opening reaction only occurs in the presence of enzyme. Following overnight incubation, protein was precipitated using 100 μL of methanol followed by filtering through a 22 μm GV Durapore filter. A 2 μL aliquot was injected over a C₁₈ reverse-phase column on a Waters Acquity UPLC-MS using a 2 min gradient of 95:5 H₂O:MeCN to 5:95 H₂O:MeCN. Mass spectra were analyzed using Mestrenova.

LC-MS to Determine $H_2^{18}O$ Incorporation. To ascertain the utilization of $H_2^{18}O$ in the zHDAC6 CD2-catalyzed hydrolysis of **6** to yield **13**, 100 μL samples of 50 μM enzyme in size exclusion buffer (50 mM HEPES (pH 7.5), 100 mM KCl, 1 mM TCEP, 5% glycerol (*v/v*)) were dialyzed against size exclusion buffer lacking glycerol

overnight (50 mM HEPES (pH 7.5), 100 mM KCl, 1 mM TCEP). Samples were then lyophilized for 2 h before being resolubilized in 100 μL buffer including 100 μM inhibitor in $H_2^{16}O$ and $H_2^{18}O$. Samples were then incubated overnight and subject to LC-MS analysis, as described above.

Irreversibility of Inhibition. To determine the irreversibility of binding, 300 μL samples of 1 μM of zCD2 were incubated with 100 μM inhibitor for 1 h before being subject to dialysis. Initial measurements of inhibition were made through the standard discontinuous assay using the commercially available HDAC substrate RHKK(Ac)-AMC. A 25 μL sample was taken from dialysis and incubated with 25 μL of 250 μM substrate for 30 min. Following this, 50 μL of developer solution was added consisting of 1 μM trypsin to cleave the AMC group and 10 μM TSA to stop the reaction. Fluorescence of the AMC group was measured using an Infinite M1000Pro plate reader at excitation 360 nM and emission 460 nM.

Samples were dialyzed against 3 L of size exclusion buffer [50 mM HEPES (pH 7.5), 100 mM KCl, 5% glycerol (v/v), and 1 mM TCEP] supplemented with 0.25% DMSO (v/v) at 4 °C. The samples were taken at 6 h post incubation and subjected to the standard discontinuous assay as above. The remaining 200 μL was subjected to dialysis overnight in 2 L of size exclusion buffer supplemented with 0.25% DMSO (v/v) and a sample taken at 21 h before being measured as described above. The experiment was performed in triplicates.

X-ray Crystallography. Crystal Structure Determination. The zHDAC6 CD2−**6** complex was crystallized by the sitting-drop vapor diffusion method. A 100 nL drop of protein solution [10 mg/mL HDAC6 CD2, 50 mM 4-(2-hydroxyethyl)-1-piperazineethanesulfonic acid (HEPES) (pH 7.5), 100 mM KCl, 5% glycerol (v/v), 1 mM tris(2-carboxyethyl)phosphine (TCEP), and 2 mM **6**] was combined with 100 nL of precipitant solution [0.04 M citric acid, 0.06 M bis-Tris propane (pH 5.0), 16% (w/v) polyethylene glycol 3350] and equilibrated against 80 μL of precipitant solution in the well reservoir at 4 °C. Plate-like crystals formed within 24 h and were harvested after 48 h. Crystals were flash-cooled in mother liquor supplemented with 20% ethylene glycol prior to data collection.

X-ray diffraction data were collected on the NSLS-II AMX beamline at Brookhaven National Laboratory.[70] Data were indexed and scaled on the AMX automated fast-dp pipeline. The electron density map was phased from these data by molecular replacement using the program Phaser and the structure of unliganded HDAC6 CD2 less water molecules (PDB: 5EEM).[62] Atomic coordinates were built and manipulated in Coot[71] and refined using Phenix.[72]

The Patterson map calculated for these data revealed a substantial peak (49.4% of the origin peak height), indicating severe translational noncrystallographic symmetry. Therefore, we indexed and scaled the data in space group P1 using iMosflm and Aimless to validate the space group.[73,74] These data were phased with Phaser,[75] and the program Zanuda[76] was used to validate the space group ($P2_12_12_1$) and crystallographic origin with two molecules in the asymmetric unit.

Upon discovering that **6** had undergone hydrolysis to yield **13** in the enzyme active site, the atomic coordinates of **13** were built into the electron density map during the later stages of refinement. All data collection and refinement statistics are recorded in Table S1.

PAINS Analysis. We filtered all compounds for pan-assay interference compounds (PAINS) using the online filter http://zinc15.docking.org/patterns/home/.[77]

■ ASSOCIATED CONTENT

⒮ Supporting Information

The Supporting Information is available free of charge at https://pubs.acs.org/doi/10.1021/acs.jmedchem.3c01345.

> Synthesis of HDAC6 inhibitor fragments; synthesis of the acylhydrazide **13**; synthesis of the trifluoromethyl-1,3,4-oxadiazole (**17**) and methyl-1,3,4-oxadiazole (**15**) analogues; synthesis of hydrazide **14** and monofluoromethyl-1,3,4-oxadiazole **16**; representative examples of

different kinetic mechanisms of enzyme inhibition; Michaelis−Menten constant K_M determination for HDAC6 using a series of substrate concentrations; quantified hydrolysis products from LC-UV-MS analysis after overnight incubation of the respective compound (100 μM) with HDAC6; representative UV and related mass traces from two independent LC-UV-MS experiments; representative UV and related mass traces of LC-UV-MS experiments; quantified hydrolysis products from LC-UV-MS analysis after overnight incubation of the respective compound (100 μM) with various HDAC6 mutants; equations; data collection and refinement statistics; NMR data of synthesized compounds; and HPLC chromatograms (PDF)

Molecular strings formula (CSV)

Accession Codes

The atomic coordinates and crystallographic structure factors of the HDAC6-**13** complex have been deposited in the Protein Data Bank (www.rcsb.org) with accession code 8GD4. The authors will release the atomic coordinates upon article publication.

■ AUTHOR INFORMATION

Corresponding Authors

David W. Christianson − *Roy and Diana Vagelos Laboratories, Department of Chemistry, University of Pennsylvania, Philadelphia, Pennsylvania 19104-6323, United States;* ⓞ orcid.org/0000-0002-0194-5212; Phone: (+1) 215 898 5714; Email: chris@sas.upenn.edu

Finn K. Hansen − *Department of Pharmaceutical and Cell Biological Chemistry, Pharmaceutical Institute, University of Bonn, Bonn 53121, Germany;* ⓞ orcid.org/0000-0001-9765-5975; Phone: (+49) 228 73 5213; Email: finn.hansen@uni-bonn.de

Authors

Beate König − *Department of Pharmaceutical and Cell Biological Chemistry, Pharmaceutical Institute, University of Bonn, Bonn 53121, Germany; Roy and Diana Vagelos Laboratories, Department of Chemistry, University of Pennsylvania, Philadelphia, Pennsylvania 19104-6323, United States*

Paris R. Watson − *Roy and Diana Vagelos Laboratories, Department of Chemistry, University of Pennsylvania, Philadelphia, Pennsylvania 19104-6323, United States*

Nina Reßing − *Department of Pharmaceutical and Cell Biological Chemistry, Pharmaceutical Institute, University of Bonn, Bonn 53121, Germany*

Abigail D. Cragin − *Roy and Diana Vagelos Laboratories, Department of Chemistry, University of Pennsylvania, Philadelphia, Pennsylvania 19104-6323, United States;* ⓞ orcid.org/0000-0002-4805-9760

Linda Schäker-Hübner − *Department of Pharmaceutical and Cell Biological Chemistry, Pharmaceutical Institute, University of Bonn, Bonn 53121, Germany*

Complete contact information is available at: https://pubs.acs.org/10.1021/acs.jmedchem.3c01345

Author Contributions

■ ABBREVIATIONS

CDCl$_3$, chloroform-*d*; DFMO, difluoromethyl-1,3,4-oxadiazole; DMSO, dimethyl sulfoxide; DCM, dichloromethane; EtOAc, ethyl acetate; HDAC, histone deacetylase; HDACi, histone deacetylase inhibitor; MeOH, methanol; min, minutes; RT, room temperature; TFA, trifluoroacetic acid; TFMO, trifluoromethyl-1,3,4-oxadiazole.

■ REFERENCES

(1) Ho, T. C. S.; Chan, A. H. Y.; Ganesan, A. Thirty Years of HDAC Inhibitors: 2020 Insight and Hindsight. *J. Med. Chem.* **2020**, *63*, 12460−12484.

(2) Gregoretti, I. V.; Lee, Y. M.; Goodson, H. V. Molecular Evolution of the Histone deacetylase Family: Functional Implications of Phylogenetic Analysis. *J. Mol. Biol.* **2004**, *338*, 17−31.

(3) Roche, J.; Bertrand, P. Inside HDACs with More Selective HDAC Inhibitors. *Eur. J. Med. Chem.* **2016**, *121*, 451−483.

(4) Wang, P.; Wang, Z.; Liu, J. Role of HDACs in Normal and Malignant Hematopoiesis. *Mol. Cancer* **2020**, *19*, 1−21.

(5) Mielcarek, M.; Zielonka, D.; Carnemolla, A.; Marcinkowski, J. T.; Guidez, F. HDAC4 as a Potential Therapeutic Target in Neurodegenerative Diseases: A Summary of Recent Achievements. *Front. Cell. Neurosci.* **2015**, *9*, 1−9.

(6) Parra, M.; Verdin, E. Regulatory Signal Transduction Pathways for Class IIa Histone Deacetylases. *Curr. Opin. Pharmacol.* **2010**, *10*, 454−460.

(7) Hubbert, C.; Guardiola, A.; Shao, R.; Kawaguchi, Y.; Ito, A.; Nixon, A.; Yoshida, M.; Wang, X. F.; Yao, T. P. HDAC6 Is a Microtubule-Associated deacetylase. *Nature* **2002**, *417*, 455−458.

(8) Hai, Y.; Shinsky, S. A.; Porter, N. J.; Christianson, D. W. Histone deacetylase 10 Structure and Molecular Function as a Polyamine deacetylase. *Nat. Commun.* **2017**, *8*, 1−9.

(9) Bertrand, P. Inside HDAC with HDAC Inhibitors. *Eur. J. Med. Chem.* **2010**, *45*, 2095−2116.

(10) Kalin, J. H.; Bergman, J. A. Development and Therapeutic Implications of Selective Histone deacetylase 6 Inhibitors. *J. Med. Chem.* **2013**, *56*, 6297−6313.

(11) Shen, S.; Kozikowski, A. P. Why hydroxamates May Not Be the Best Histone deacetylase Inhibitors - What Some May Have Forgotten or Would Rather Forget? *ChemMedChem* **2016**, *11*, 15−21.

(12) Zhang, X.; Yuan, Z.; Zhang, Y.; Yong, S.; Salas-Burgos, A.; Koomen, J.; Olashaw, N.; Parsons, J. T.; Yang, X.; Dent, S. R.; Yao, T.; Lane, W. S.; Seto, E. HDAC6 Modulates Cell Motility by Altering the Acetylation Level of cortactin. *Mol. Cell. Biol.* **2007**, *27*, 197−213.

(13) Cohen, T. J.; Guo, J. L.; Hurtado, D. E.; Kwong, L. K.; Mills, I. P.; Trojanowski, J. Q.; Lee, V. M. Y. The Acetylation of Tau Inhibits Its Function and Promotes Pathological Tau Aggregation. *Nat. Commun.* **2011**, *2*, 252.

(14) Ding, H.; Dolan, P. J.; Johnson, G. V. W. Histone deacetylase 6 Interacts with the Microtubule-Associated Protein Tau. *J. Neurochem.* **2008**, *106*, 2119−2130.

(15) Karagöz, G. E.; Rüdiger, S. G. D. Hsp90 Interaction with Clients. *Trends Biochem. Sci.* **2015**, *40*, 117−125.

(16) Simões-Pires, C.; Zwick, V.; Nurisso, A.; Schenker, E.; Carrupt, P. A.; Cuendet, M. HDAC6 as a Target for Neurodegenerative Diseases: What Makes It Different from the Other HDACs? *Mol. Neurodegen.* **2013**, *8*, 7.

(17) Dompierre, J. P.; Godin, J. D.; Charrin, B. C.; Cordelières, F. P.; King, S. J.; Humbert, S.; Saudou, F. Histone deacetylase 6 Inhibition Compensates for the Transport Deficit in Huntington's Disease by Increasing Tubulin Acetylation. *J. Neurosci.* **2007**, *27*, 3571−3583.

(18) Brindisi, M.; Saraswati, A. P.; Brogi, S.; Gemma, S.; Butini, S.; Campiani, G. Old but Gold: Tracking the New Guise of Histone deacetylase 6 (HDAC6) Enzyme as a Biomarker and Therapeutic Target in Rare Diseases. *J. Med. Chem.* **2020**, *63*, 23−39.

(19) Adalbert, R.; Kaieda, A.; Antoniou, C.; Loreto, A.; Yang, X.; Gilley, J.; Hoshino, T.; Uga, K.; Makhija, M. T.; Coleman, M. P. Novel HDAC6 Inhibitors Increase Tubulin Acetylation and Rescue Axonal Transport of Mitochondria in a Model of Charcot-Marie-Tooth Type 2F. *ACS Chem. Neurosci.* **2020**, *11*, 258−267.

(20) Korfei, M.; Mahavadi, P.; Guenther, A. Targeting Histone Deacetylases in Idiopathic Pulmonary Fibrosis: A Future Therapeutic Option. *Cells* **2022**, *11*, 1626−1645.

(21) Campiani, G.; Cavella, C.; Osko, J. D.; Brindisi, M.; Relitti, N.; Brogi, S.; Saraswati, A. P.; Federico, S.; Chemi, G.; Maramai, S.; Carullo, G.; Jaeger, B.; Carleo, A.; Benedetti, R.; Sarno, F.; Lamponi, S.; Rottoli, P.; Bargagli, E.; Bertucci, C.; Tedesco, D.; Herp, D.; Senger, J.; Ruberti, G.; Saccoccia, F.; Saponara, S.; Gorelli, B.; Valoti, M.; Kennedy, B.; Sundaramurthi, H.; Butini, S.; Jung, M.; Roach, K. M.; Altucci, L.; Bradding, P.; Christianson, D. W.; Gemma, S.; Prasse, A. Harnessing the Role of HDAC6 in Idiopathic Pulmonary Fibrosis: Design, Synthesis, Structural Analysis, and Biological Evaluation of Potent Inhibitors. *J. Med. Chem.* **2021**, *64*, 9960−9988.

(22) Magupalli, V. G.; Negro, R.; Tian, Y.; Hauenstein, A. V.; Di Caprio, G.; Skillern, W.; Deng, Q.; Orning, P.; Alam, H. B.; Maliga, Z.; Sharif, H.; Hu, J. J.; Evavold, C. L.; Kagan, J. C.; Schmidt, F. I.; Fitzgerald, K. A.; Kirchhausen, T.; Li, Y.; Wu, H. HDAC6 Mediates an Aggresome-like Mechanism for NLRP3 and Pyrin Inflammasome Activation. *Science* **2020**, *369*, No. eaas8995.

(23) Hideshima, T.; Bradner, J. E.; Wong, J.; Chauhan, D.; Richardson, P.; Schreiber, S. L.; Anderson, K. C. Small-Molecule Inhibition of Proteasome and Aggresome Function Induces Synergistic Antitumor Activity in Multiple Myeloma. *Proc. Natl. Acad. Sci. U. S. A.* **2005**, *102*, 8567−8572.

(24) Hideshima, T.; Richardson, P. G.; Anderson, K. C. Mechanism of Action of Proteasome Inhibitors and deacetylase Inhibitors and the Biological Basis of Synergy in Multiple Myeloma. *Mol. Cancer Ther.* **2011**, *10*, 2034−2042.

(25) Bhatia, S.; Krieger, V.; Groll, M.; Osko, J. D.; Reßing, N.; Ahlert, H.; Borkhardt, A.; Kurz, T.; Christianson, D. W.; Hauer, J.; Hansen, F. K. Discovery of the First-in-Class Dual Histone deacetylase-Proteasome Inhibitor. *J. Med. Chem.* **2018**, *61*, 10299−10309.

(26) Vogl, D. T.; Raje, N.; Jagannath, S.; Richardson, P.; Hari, P.; Orlowski, R.; Supko, J. G.; Tamang, D.; Yang, M.; Jones, S. S.; Wheeler, C.; Markelewicz, R. J.; Lonial, S. Ricolinostat, the First Selective Histone deacetylase 6 Inhibitor, in Combination with

Bortezomib and Dexamethasone for Relapsed or Refractory Multiple Myeloma. *Clin. Cancer Res.* 2017, 23, 3307−3315.

(27) Atkinson, S. J.; Soden, P. E.; Angell, D. C.; Bantscheff, M.; Chung, C. w.; Giblin, K. A.; Smithers, N.; Furze, R. C.; Gordon, L.; Drewes, G.; Rioja, I.; Witherington, J.; Parr, N. J.; Prinjha, R. K. The Structure Based Design of Dual HDAC/BET Inhibitors as Novel Epigenetic Probes. *Med. Chem. Commun.* 2014, 18, 342−351.

(28) Tang, F.; Yang, Z.; Tan, Y.; Li, Y. Super-Enhancer Function and Its Application in Cancer Targeted Therapy. *npj Precis. Oncol.* 2020, 4, 1−7.

(29) Guerrant, W.; Patil, V.; Canzoneri, J. C.; Oyelere, A. K. Dual Targeting of Histone deacetylase and Topoisomerase II with Novel Bifunctional Inhibitors. *J. Med. Chem.* 2012, 55, 1465−1477.

(30) Zhijun, H.; Shusheng, W.; Han, M.; Jianping, L.; Li-sen, Q.; Dechun, L. Pre-Clinical Characterization of 4SC-202, a Novel Class I HDAC Inhibitor, against Colorectal Cancer Cells. *Tumor Biol.* 2016, 37, 10257−10267.

(31) Kalin, J. H.; Wu, M.; Gomez, A. V.; Song, Y.; Das, J.; Hayward, D.; Adejola, N.; Wu, M.; Panova, I.; Chung, H. J.; Kim, E.; Roberts, H. J.; Roberts, J. M.; Prusevich, P.; Jeliazkov, J. R.; Roy Burman, S. S.; Fairall, L.; Milano, C.; Eroglu, A.; Proby, C. M.; Dinkova-Kostova, A. T.; Hancock, W. W.; Gray, J. J.; Bradner, J. E.; Valente, S.; Mai, A.; Anders, N. M.; Rudek, M. A.; Hu, Y.; Ryu, B.; Schwabe, J. W. R.; Mattevi, A.; Alani, R. M.; Cole, P. A. Targeting the CoREST Complex with Dual Histone deacetylase and demethylase Inhibitors. *Nat. Commun.* 2018, 9, 53.

(32) Morera, L.; Lübbert, M.; Jung, M. Targeting Histone Methyltransferases and Demethylases in Clinical Trials for Cancer Therapy. *Clin. Epigenet.* 2016, 8, 16.

(33) Wobser, M.; Weber, A.; Glunz, A.; Tauch, S.; Seitz, K.; Butelmann, T.; Hesbacher, S.; Goebeler, M.; Bartz, R.; Kohlhof, H.; Schrama, D.; Houben, R. Elucidating the Mechanism of Action of Domatinostat (4SC-202) in Cutaneous T Cell Lymphoma Cells. *J. Hematol. Oncol.* 2019, 12, 1−16.

(34) Ojha, R.; Huang, H. L.; HuangFu, W. C.; Wu, Y. W.; Nepali, K.; Lai, M. J.; Su, C. J.; Sung, T. Y.; Chen, Y. L.; Pan, S. L.; Liou, J. P. 1-Aroylindoline-Hydroxamic Acids as Anticancer Agents, Inhibitors of HSP90 and HDAC. *Eur. J. Med. Chem.* 2018, 150, 667−677.

(35) Mehndiratta, S.; Lin, M. H.; Wu, Y. W.; Chen, C. H.; Wu, T. Y.; Chuang, K. H.; Chao, M. W.; Chen, Y. Y.; Pan, S. L.; Chen, M. C.; Liou, J. P. N-Alkyl-Hydroxybenzoyl Anilide hydroxamates as Dual Inhibitors of HDAC and HSP90, Downregulating IFN-γ Induced PD-L1 Expression. *Eur. J. Med. Chem.* 2020, 185, No. 111725.

(36) Liu, T.; Wan, Y.; Xiao, Y.; Xia, C.; Duan, G. Dual-Target Inhibitors Based on HDACs: Novel Antitumor Agents for Cancer Therapy. *J. Med. Chem.* 2020, 63, 8977−9002.

(37) de Lera, A. R.; Ganesan, A. Two-Hit Wonders: The Expanding Universe of Multitargeting Epigenetic Agents. *Curr. Opin. Chem. Biol.* 2020, 57, 135−154.

(38) He, S.; Dong, G.; Li, Y.; Wu, S.; Wang, W.; Sheng, C. Potent Dual BET/HDAC Inhibitors for Efficient Treatment of Pancreatic Cancer. *Angew. Chem., Int. Ed.* 2020, 59, 3028−3032.

(39) Gaisina, I. N.; Tueckmantel, W.; Ugolkov, A.; Shen, S.; Hoffen, J.; Dubrovskyi, O.; Mazar, A.; Schoon, R. A.; Billadeau, D.; Kozikowski, A. P. Identification of HDAC6-Selective Inhibitors of Low Cancer Cell Cytotoxicity. *ChemMedChem* 2016, 11, 81−92.

(40) Depetter, Y.; Geurs, S.; De Vreese, R.; Goethals, S.; Vandoorn, E.; Laevens, A.; Steenbrugge, J.; Meyer, E.; de Tullio, P.; Bracke, M.; D'hooghe, M.; De Wever, O. Selective Pharmacological Inhibitors of HDAC6 Reveal Biochemical Activity but Functional Tolerance in Cancer Models. *Int. J. Cancer* 2019, 145, 735−747.

(41) Zhang, X.-H.; Qin-Ma; Wu, H.-P.; Khamis, M. Y.; Li, Y.-H.; Ma, L.-Y.; Liu, H.-M. A Review of Progress in Histone deacetylase 6 Inhibitors Research: Structural Specificity and Functional Diversity. *J. Med. Chem.* 2021, 64, 1362−1391.

(42) Jenke, R.; Reßing, N.; Hansen, F. K.; Aigner, A.; Büch, T. Anticancer Therapy with HDAC Inhibitors: Mechanism-Based Combination Strategies and Future Perspectives. *Cancers.* 2021, 13, 634.

(43) Wang, C. Y.; Lee, L. H. Mutagenicity and Antibacterial Activity of Hydroxamic Acids. *Antimicrob. Agents Chemother.* 1977, 11, 753−755.

(44) Zhang, L.; Zhang, J.; Jiang, Q.; Zhang, L.; Song, W. Zinc Binding Groups for Histone deacetylase Inhibitors. *J. Enzyme Inhib. Med. Chem.* 2018, 33, 714−721.

(45) Yue, K.; Sun, S.; Jia, G.; Qin, M.; Hou, X.; Chou, C. J.; Huang, C.; Li, X. First-in-Class Hydrazide-Based HDAC6 Selective Inhibitor with Potent Oral Anti-Inflammatory Activity by Attenuating NLRP3 Inflammasome Activation. *J. Med. Chem.* 2022, 65, 12140−12162.

(46) Kim, Y.; Lee, C. S.; Oh, J. T.; Song, H.; Choi, J.; Lee, J. Oxadiazole Amine Derivative Compounds as Histone deacetylase 6 Inhibitor, and the Pharmaceutical Composition Comprising the Same. WO 2017/065473 A1, 2017.

(47) Lee, J.; Han, Y.; Kim, Y.; Min, J.; Bae, M.; Kim, D.; Jin, S.; Kyung, J. 1,3,4-Oxadiazole Sulfamide Derivative Compounds as Histone deacetylase 6 Inhibitor, and the Pharmaceutical Composition Comprising the Same. WO 2017/018805 A1, 2017.

(48) Ito, M.; Sugiyama, H.; Kubo, O.; Kikuchi, F.; Yasu, T.; Kakegawa, K.; Ikeda, Z.; Miyazaki, T.; Arikawa, Y.; Okawa, T.; Yonemori, J.; Toita, A.; Kojima, T.; Asano, Y.; Sato, A.; Maezaki, H.; Sasaki, S.; Kokubo, H.; Homma, M.; Sasaki, M.; Imadea, Y. Heterocyclic Compound. WO 2019/027054 A1, 2019.

(49) Lee, C. K.; Ko, M. S.; Yun, S. H.; Kim, H. M. 1,3,4-Oxadiazole Derivative Compounds as Histone deacetylase 6 Inhibitor, and the Pharmaceutical Composition Comprising the Same. WO 2021/210857 A1, 2021.

(50) Mandegar, M. A.; Patel, S.; Ding, P.; Bhatt, U.; Holan, M.; Lee, J.; Li, Y.; Medina, J.; Nerurkar, A.; Seidl, F.; Sperandino, D.; Widjaja, T. Fluoroalkyl-Oxadiazoles and Uses Thereof. WO 2021/127643 A1, 2021.

(51) Çakır, I.; Hadley, C. K.; Pan, P. L.; Bagchi, R. A.; Ghamari-Langroudi, M.; Porter, D. T.; Wang, Q.; Litt, M. J.; Jana, S.; Hagen, S.; Lee, P.; White, A.; Lin, J. D.; McKinsey, T. A.; Cone, R. D. Histone deacetylase 6 Inhibition Restores Leptin Sensitivity and Reduces Obesity. *Nat. Metab.* 2022, 4, 44−59.

(52) Keuler, T.; König, B.; Bückreiß, N.; Kraft, F. B.; König, P.; Schäker-Hübner, L.; Steinebach, C.; Bendas, G.; Gütschow, M.; Hansen, F. K. Development of the First Non-hydroxamate Selective HDAC6 Degraders. *Chem. Commun.* 2022, 58, 11087−11090.

(53) Cragin, A.; Watson, P. R.; König, B.; Hansen, F. K.; Christianson, D. W. A Novel Zinc Binding Group for HDAC6 Inhibition. *FASEB J.* 2022, 36, DOI: DOI: 10.1096/fasebj.2022.36.S1.R3604.

(54) Ptacek, J.; Snajdr, I.; Schimer, J.; Kutil, Z.; Mikesova, J.; Baranova, P.; Havlinova, B.; Tueckmantel, W.; Majer, P.; Kozikowski, A.; Barinka, C. Selectivity of Hydroxamate- and Difluoromethyloxadiazole-Based Inhibitors of Histone deacetylase 6. In Vitro and in Cells. *Int. J. Mol. Sci.* 2023, 24. 4720.

(55) Yates, C. M. Metalloenzyme Inhibitor Compounds. US 2018/0256572 A1, 2018.

(56) Cellupica, E.; Caprini, G.; Cordella, P.; Cukier, C.; Fossati, G.; Marchini, M.; Rocchio, I.; Sandrone, G.; Vanoni, M. A.; Vergani, B.; Źrubek, K.; Stevenazzi, A.; Steinkühler, C. Difluoromethyl-1,3,4-Oxadiazoles Are Slow-Binding Substrate Analog Inhibitors of Histone deacetylase 6 with Unprecedented Isotype Selectivity. *J. Biol. Chem.* 2023, 299, No. 102800.

(57) Huisgen, R.; Sauer, J.; Sturm, H. J. Acylierung 5-Substituierter tetrazole zu 1.3.4-Oxdiazolen. *Angew. Chem.* 1958, 70, 272−273.

(58) Bergman, J. A.; Woan, K.; Perez-Villarroel, P.; Villagra, A.; Sotomayor, E. M.; Kozikowski, A. P. Selective Histone deacetylase 6 Inhibitors Bearing Substituted Urea Linkers Inhibit Melanoma Cell Growth. *J. Med. Chem.* 2012, 55, 9891−9899.

(59) Krieger, V.; Hamacher, A.; Cao, F.; Stenzel, K.; Gertzen, C. G. W.; Schäker-Hübner, L.; Kurz, T.; Gohlke, H.; Dekker, F. J.; Kassack, M. U.; Hansen, F. K. Synthesis of Peptoid-Based Class I-Selective Histone deacetylase Inhibitors with Chemosensizing Properties. *J. Med. Chem.* 2019, 62, 11260−11279.

(60) Diedrich, D.; Hamacher, A.; Gertzen, C. G. W.; Alves Avelar, L. A.; Reiss, G. J.; Kurz, T.; Gohlke, H.; Kassack, M. U.; Hansen, F. K. Rational Design and Diversity-Oriented Synthesis of Peptoid-Based Selective HDAC6 Inhibitors. *Chem. Commun.* 2016, *52*, 3219−3222.

(61) Sippl, W.; Melesina, J.; Simoben, C. V.; Bülbül, E. F.; Praetorius, L.; Robaa, D. Strategies to Design Selective Histone deacetylase Inhibitors. *ChemMedChem.* 2021, *16*, 1336−1359.

(62) Hai, Y.; Christianson, D. W. Histone deacetylase 6 Structure and Molecular Basis of Catalysis and Inhibition. *Nat. Chem. Biol.* 2016, *12*, 741−747.

(63) Schäker-Hübner, L.; Haschemi, R.; Büch, T.; Kraft, F. B.; Brumme, B.; Schöler, A.; Jenke, R.; Meiler, J.; Aigner, A.; Bendas, G.; Hansen, F. K. Balancing Histone deacetylase (HDAC) Inhibition and Drug-Likeness: Biological and Physicochemical Evaluation of Class I Selective HDAC Inhibitors. *ChemMedChem* 2022, *17*, No. e202100755.

(64) Jiang, Y.; Xu, J.; Yue, K.; Huang, C.; Qin, M.; Chi, D.; Yu, Q.; Zhu, Y.; Hou, X.; Xu, T.; Li, M.; Chou, C. J.; Li, X. Potent Hydrazide-Based HDAC Inhibitors with a Superior Pharmacokinetic Profile for Efficient Treatment of Acute Myeloid Leukemia in Vivo. *J. Med. Chem.* 2022, *65*, 285−302.

(65) Copeland, R. A. *Evaluation of Enzyme Inhibitors - A Guide for Medical Chemists and Pharmacologists*, 2nd ed.; John Wiley and Sons, Inc., Hoboken: NJ, 2013.

(66) Motlová, L.; Snajdr, I.; Kutil, Z.; Andris, E.; Ptacek, J.; Novotna, A.; Novakova, Z.; Havlinova, B.; Tueckmantel, W.; Draberova, H.; Majer, P.; Schutkowski, M.; Kozikowski, A.; Rulisek, L.; Barinka, C. Comprehensive Mechanistic View of the Hydrolysis of Oxadiazole-Based Inhibitors by Histone deacetylase 6 (HDAC6). *ACS Chem. Biol.* 2023, *18*, 1594−1610.

(67) Reßing, N.; Schliehe-Diecks, J.; Watson, P. R.; Sönnichsen, M.; Cragin, A. D.; Schöler, A.; Yang, J.; Schäker-Hübner, L.; Borkhardt, A.; Christianson, D. W.; Bhatia, S.; Hansen, F. K. Development of Fluorinated Peptoid-Based Histone deacetylase (HDAC) Inhibitors for Therapy-Resistant Acute Leukemia. *J. Med. Chem.* 2022, *65*, 15457−15472.

(68) Kraft, F. B.; Hanl, M.; Feller, F.; Schäker-Hübner, L.; Hansen, F. K. Photocaged Histone deacetylase Inhibitors as Prodrugs in Targeted Cancer Therapy. *Pharmaceuticals* 2023, *16*, 356.

(69) Osko, J. D.; Christianson, D. W. Methods for the Expression, Purification, and Crystallization of Histone deacetylase 6−Inhibitor Complexes. *Methods Enzymol.* 2019, *626*, 447−474.

(70) Schneider, D. K.; Soares, A. S.; Lazo, E. O.; Kreitler, D. F.; Qian, K.; Fuchs, M. R.; Bhogadi, D. K.; Antonelli, S.; Myers, S. S.; Martins, B. S.; Skinner, J. M.; Aishima, J.; Bernstein, H. J.; Langdon, T.; Lara, J.; Petkus, R.; Cowan, M.; Flaks, L.; Smith, T.; Shea-McCarthy, G.; Idir, M.; Huang, L.; Chubar, O.; Sweet, R. M.; Berman, L. E.; McSweeney, S.; Jakoncic, J. AMX - the Highly Automated Macromolecular Crystallography (17-ID-1) Beamline at the NSLS-II. *J. Synchrotron Radiat.* 2022, *29*, 1480−1494.

(71) Emsley, P.; Lohkamp, B.; Scott, W. G.; Cowtan, K. Features and Development of Coot. *Acta Crystallogr. Sect. D* 2010, *66*, 486−501.

(72) Adams, P. D.; Afonine, P. V.; Bunkóczi, G.; Chen, V. B.; Davis, I. W.; Echols, N.; Headd, J. J.; Hung, L.-W.; Kapral, G. J.; Grosse-Kunstleve, R. W.; McCoy, A. J.; Moriarty, N. W.; Oeffner, R.; Read, R. J.; Richardson, D. C.; Richardson, J. S.; Terwilliger, T. C.; Zwart, P. H. Phenix: A Comprehensive Python-Based System for Macromolecular Structure Solution. *Acta Crystallogr. Sect. D* 2010, *66*, 213−221.

(73) Battye, T. G. G.; Kontogiannis, L.; Johnson, O.; Powell, H. R.; Leslie, A. G. W. iMosflm: A New Graphical Interface for Diffraction-Image Processing with MOSFLM. *Acta Crystallogr. Sect. D* 2011, *67*, 271−281.

(74) Evans, P. R.; Murshudov, G. N. How Good Are My Data and What Is the Resolution? *Acta Crystallogr. Sect. D* 2013, *69*, 1204−1214.

(75) McCoy, A. J.; Grosse-Kunstleve, R. W.; Adams, P. D.; Winn, M. D.; Storoni, L. C.; Read, R. J. Phaser Crystallographic Software. *J. Appl. Crystallogr.* 2007, *40*, 658−674.

(76) Lebedev, A. A.; Isupov, M. N. Space-Group and Origin Ambiguity in Macromolecular Structures with Pseudo-Symmetry and Its Treatment with the Program Zanuda. *Acta Crystallogr. Sect. D* 2014, *70*, 2430−2443.

(77) Baell, J. B.; Holloway, G. A. New Substructure Filters for Removal of Pan Assay Interference Compounds (PAINS) from Screening Libraries and for Their Exclusion in Bioassays. *J. Med. Chem.* 2010, *53*, 2719−2740.

Supporting Information

Difluoromethyl-1,3,4-oxadiazoles Are Selective, Mechanism-Based, and Essentially Irreversible inhibitors of Histone Deacetylase 6

Beate König,[1,2] Paris R. Watson,[2] Nina Reßing,[1] Abigail D. Cragin,[2] Linda Schäker-Hübner,[1] David W. Christianson[*2] and Finn K. Hansen[*1]

[1] Department of Pharmaceutical and Cell Biological Chemistry, Pharmaceutical Institute, University of Bonn, 53121 Bonn, Germany.

[2] Roy and Diana Vagelos Laboratories, Department of Chemistry, University of Pennsylvania, 231 South 34th Street, Philadelphia, Pennsylvania 19104-6323, United States.

Corresponding authors:
F.K.H.: E-Mail, finn.hansen@uni-bonn.de
D.W.C: E-Mail: chris@sas.upenn.edu

Content

1 Supplementary Schemes, Figures, Equations and Tables
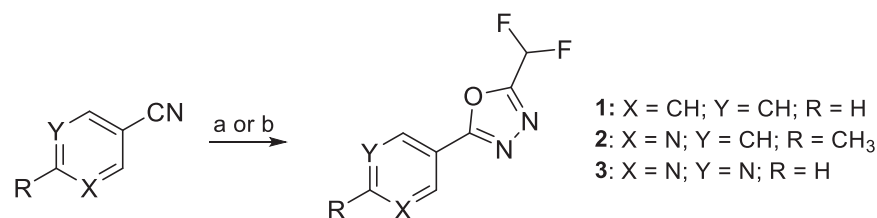
Scheme S1. Synthesis of HDAC6 inhibitor fragments. a) i: NaN₃, NH₄Cl, LiCl·H₂O, DMF, 100 °C, 150 W, 24 h; ii: DFAA, DCM, rt., 24 h (**1**, **3**); b) i: NaN₃, NH₄Cl, LiCl, DMF, 100 °C, 18 h; ii: difluoroacetic anhydride (DFAA), toluene, 70 °C, 18 h (**2**).
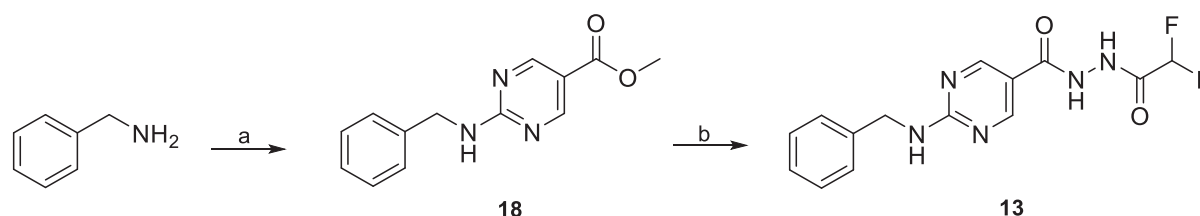
Scheme S2. Synthesis of the acylhydrazide **13**. a) Methyl 2-chlorpyrimidine-5-carboxylate, DIPEA, EtOH, 90 °C, 18 h; b) i: hydrazine monohydrate, MeOH, 70 °C, 3 h; ii: DFAA, DMF, 70 °C, 1 h.

15: R = H
17: R = F
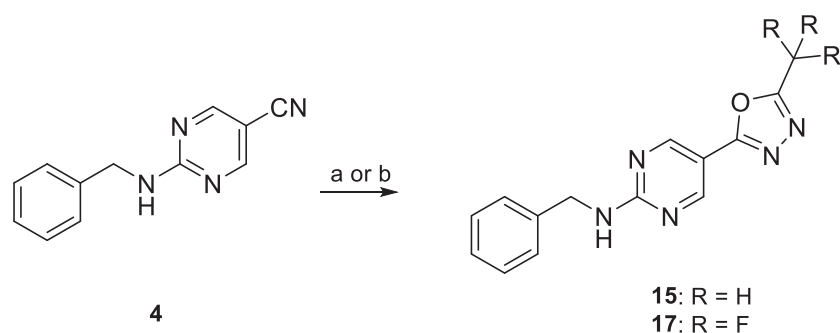
Scheme S3. Synthesis of the trifluoromethyl-1,3,4-oxadiazole (**17**) and methyl-1,3,4-oxadiazole (**15**) analogs. a) i: NaN₃, NH₄Cl, LiCl, DMF, 100 °C, 18 h; ii: trifluoroacetic anhydride, toluene, 70 °C, 18 h (**14**); b) i: NaN₃, NH₄Cl, LiCl, DMF, 100 °C, 18 h; ii: acetic anhydride, toluene, 70 °C, 18 h; iii: K₂CO₃, MeOH/H₂O (**15**).
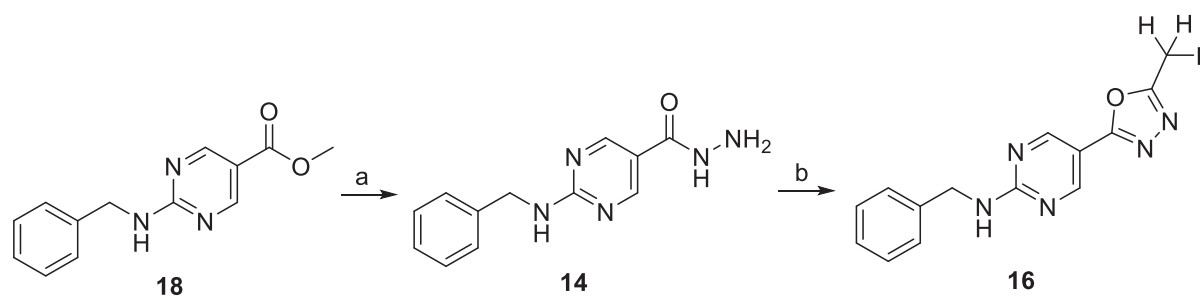
Scheme S4. Synthesis of hydrazide **14** and monofluoromethyl-1,3,4-oxadiazole **16**. a) hydrazine monohydrate, MeOH, 70 °C, 3 h; b) i: monofluroacetic acid, DMF, 70 °C, 3 h; ii: Burgess reagent, THF, 60 °C, 18 h.
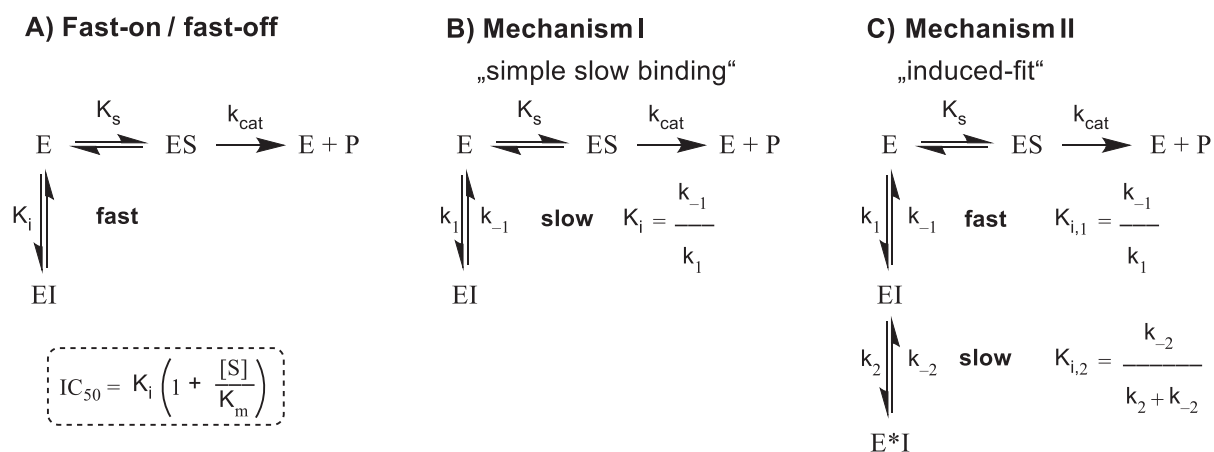
Figure S1. Representative examples of different kinetic mechanisms of enzyme inhibition, including the relationships between the respective association and dissociation rate constants (e. g., k_1 & k_{-1}) and the related equilibrium dissociation constant K_i. **A)** Fast-on/fast-off binding kinetics. For competitive fast-on/fast-off inhibitors the half maximum inhibitory concentration (IC$_{50}$) and the K_i are directly related by the Cheng-Prusoff equation[1]; **B)** slow-binding Mechanism I: single-step slow binding, k_1 & k_{-1} are inherently slow; **C)** slow-binding Mechanism II: two-step slow binding. Initially, inhibitor and enzyme form an encounter complex [EI] that subsequently slowly undergoes isomerization to a binary enzyme inhibitor complex [E*I].[2]
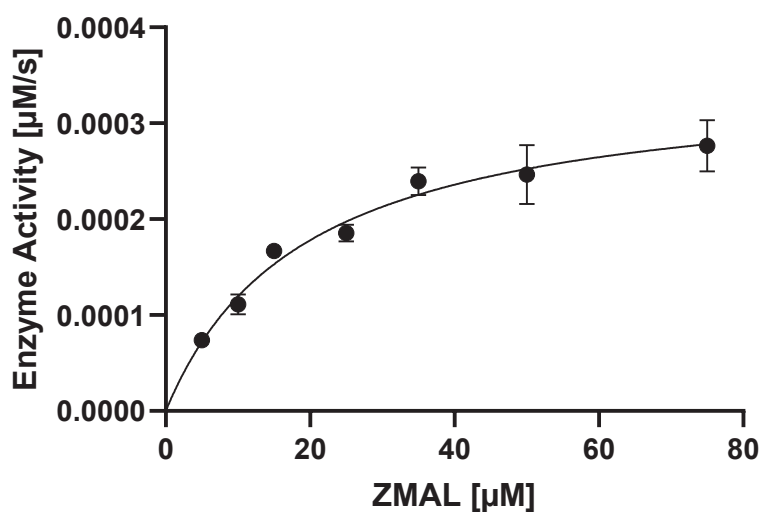
Figure S2. Michaelis-Menten constant K_M determination for HDAC6 using a series of substrate concentrations. Steady-state velocities [$\mu M \cdot s^{-1}$] (mean ± SD) were plotted against the corresponding substrate concentrations [μM] and fitted to the Michaelis-Menten equation yielding the Michaelis-Menten constant: K_M HDAC6 = 19.27 μM. Experiment was performed in triplicates.
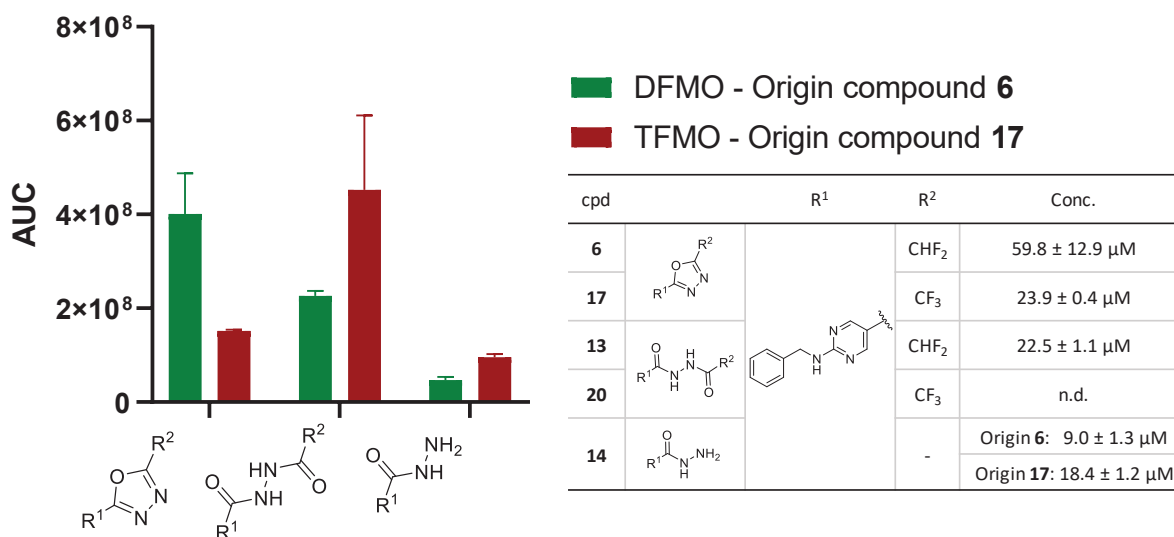
Figure S3. Quantified hydrolysis products from LC-UV-MS analysis after over night incubation of the respective compound (100 μM) with HDAC6. Experiments were performed in triplicates. AUC: area under the curve; DFMO: difluoromethyl-1,3,4-oxadiazole; TFMO: trifluoromethyl-1,3,4-oxadiazole. n.d.: not determined.

S4
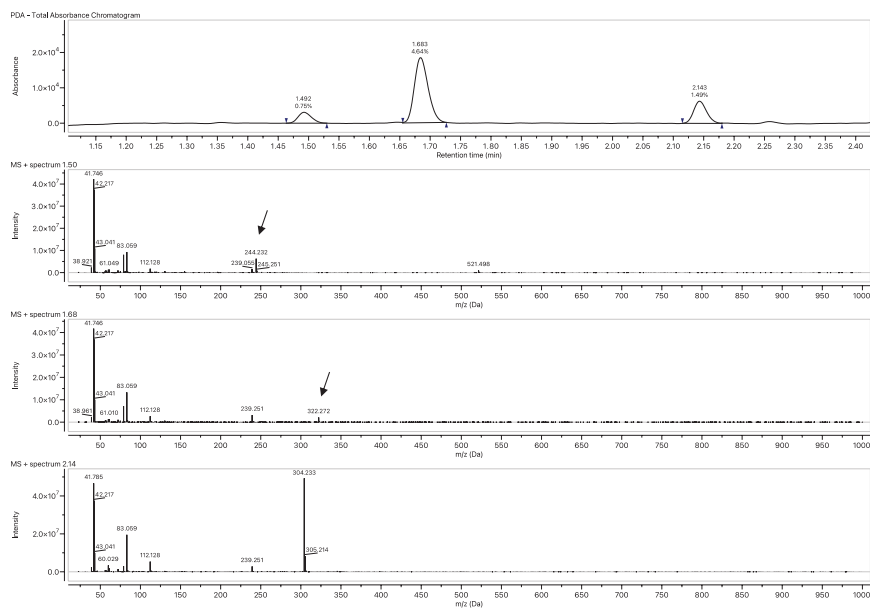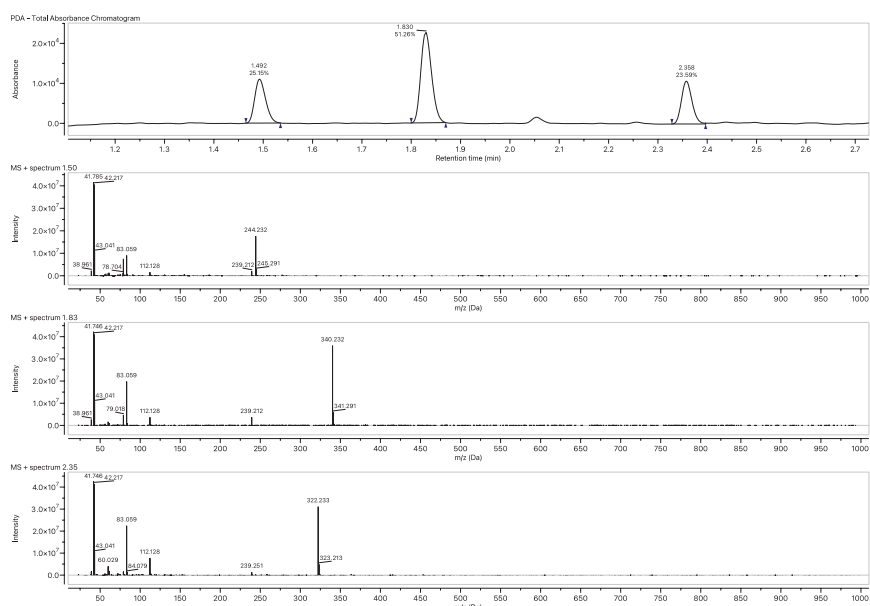
Figure S4. Representative UV and related mass traces from two independent LC-UV-MS experiments. **A**: Compound **6** was incubated with HDAC6 overnight; **B**: Compound **17** was incubated with HDAC6 overnight; x axis: retention time in mins (chromatogram), m/z ration (mass spectras), y axis: intensity in Absorbance Units (AU). Experiments were performed in triplicates.

A

14: [M+H]⁺: 244.28

13: [M+H]⁺: 322.30

6: [M+H]⁺: 304.28

B

14: [M+H]⁺: 244.28

13: [M+H]⁺: 324.30

6: [M+H]⁺: 304.28
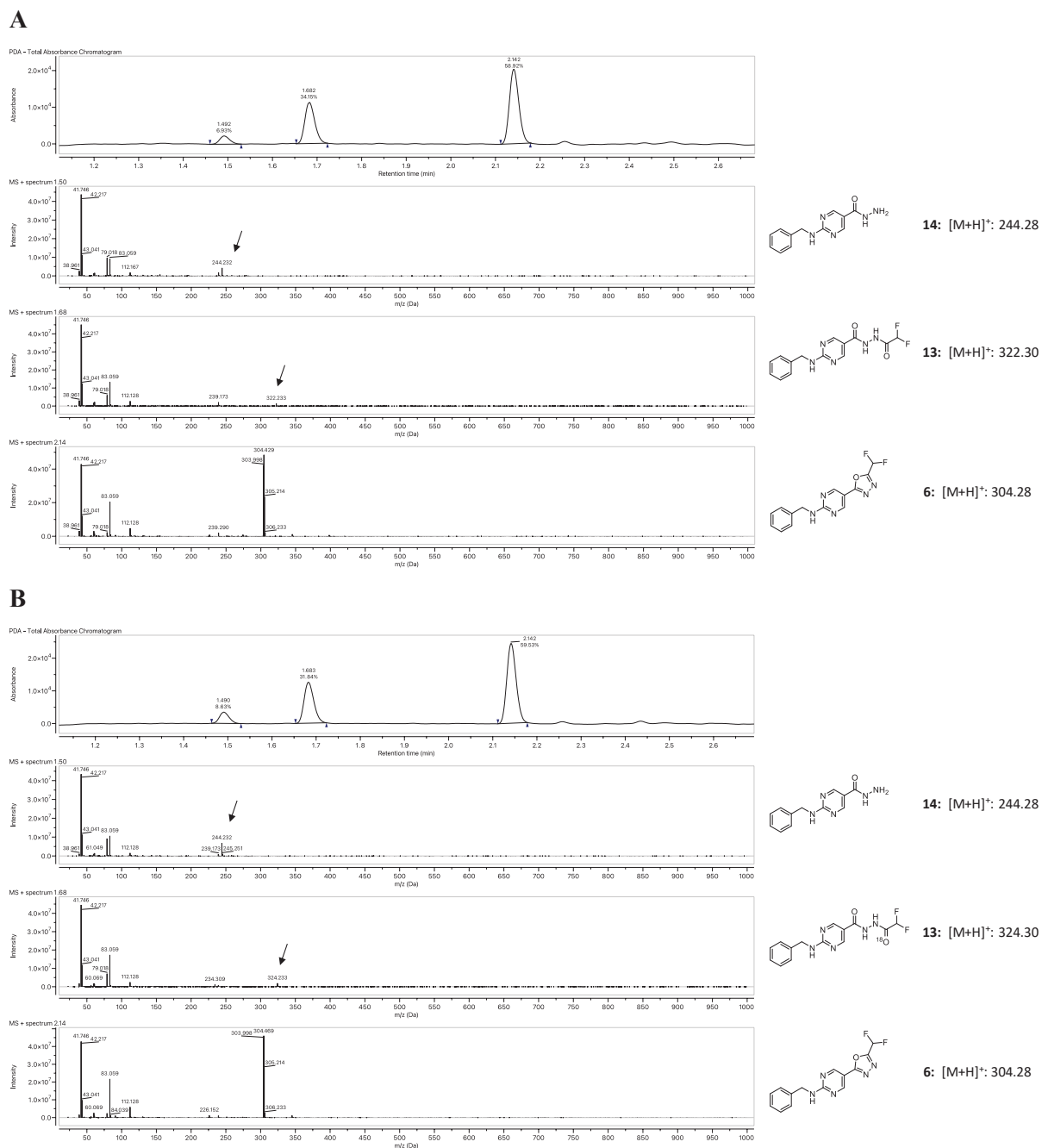
Figure S5. Representative UV and related mass traces of LC-UV-MS experiments. **A**: Compound **6** was incubated with HDAC6 overnight in $H_2^{16}O$ water; **B**: Compound **6** incubated with HDAC6 overnight in $H_2^{18}O$ water; x axis: retention time in mins (chromatogram), m/z ration (mass spectras), y axis: intensity in Absorbance Units (AU). Experiments were performed in triplicates.

A

Compound 6 with HDAC6 variants

HDAC6	Hydrolysis products from compound 6	
	Acylhydrazide **13**	Hydrazide **14**
WT	22.5 ± 1.11 μM	9.0 ± 1.3 μM
H573A	10.2 ± 3.2 μM	n.o.
H574A	6.9 ± 2.3 μM	n.o.
Y745F	14.9 ± 1.9 μM	26.2 ± 6.8 μM

B

Compound 17 with HDAC6 variants

HDAC6	Hydrolysis products from compound 17	
	Acylhydrazide **20**	Hydrazide **14**
WT	n.d.	18.6 μM ± 1.2 μM
H573A	n.d.	n.o.
H574A	n.d.	n.o.
Y745F	n.d.	64.4 ± 8.9 μM
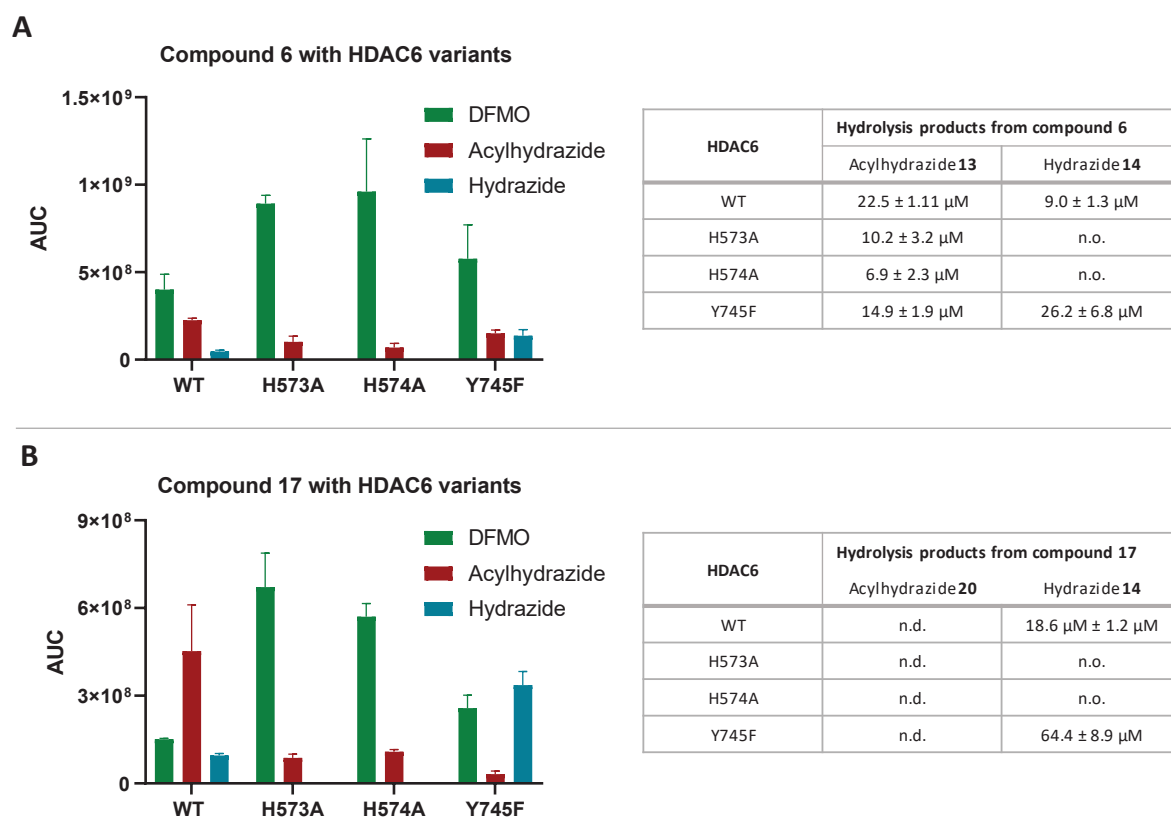
Figure S6. Quantified hydrolysis products from LC-UV-MS analysis after over night incubation of the respective compound (100 μM) with various HDAC6 mutants (wild-type (WT), H573A, H574A, Y745F). Y-axis: AUC – area under the curve. Experiments were performed in triplicates. n.d.: not determined; n.o.: not observed.

$$[P] = v_{ss}t + \frac{v_{in} - v_{ss}}{k_{obs}}\left(1 - e^{-k_{obs}t}\right) \qquad \text{(Eq. 1)}$$

Equation 1. Time-dependent product formation for inhibitors showing slow-binding Mechanism I&II. [P]: amount of generated AMC; v_{ss}: steady-state velocity (product formation); t: time; v_{in}: initial velocity (product formation); k_{obs}: apparent first-order rate constant for the conversion from v_{in} to v_{ss}.

$$k_{obs} = k_{-1} + k_1\left(1 + \frac{[S]}{K_M}\right)[I] \qquad \text{(Eq. 2)}$$

Equation 2. The single-step slow-binding Mechanism I results in a linear relationship between k_{obs} and inhibitor concentration. k_{-1}: dissociation rate constant; k_1: association rate constant; [S]: substrate concentration; K_M: Michelis-Menten constant; [I]: inhibitor concentration.

$$k_{obs} = k_{-2} + \frac{k_2}{[I] + K_{i,1}\left(1 + \frac{[S]}{K_M}\right)}[I] \qquad \text{(Eq. 3)}$$

Equation 3. The two-step slow-binding Mechanism II results in a hyperbolic relationship between k_{obs} and inhibitor concentration. k_{-2}: secondary dissociation rate constant; k_2: secondary association rate constant; $K_{i,1}$: equilibrium dissociation constant of the enzyme inhibitor encounter complex [EI].

Table S1: Data collection and refinement statistics[a]

	HDAC6 CD2–**13** Complex
Space group	$P2_12_12_1$
a,b,c (Å)	74.60, 92.30, 96.60
α, β, γ (°)	90.00, 90.00, 90.00
R_{merge}[b]	0.210 (0.706)
R_{pim}[c]	0.084(0.289)
$CC_{1/2}$[d]	0.993(0.851)
Redundancy	1.9
Completeness (%)	99.5(94.3)
I/σ	7.3(2.5)
Refinement	
Resolution (Å)	36.216–2.00 (2.07–2.00)
No. reflections	90179 (8857)
R_{work}/R_{free}[e]	0.185/0.223 (0.228/0.0.266)
Number of Atoms[f]	
Protein	5469
Ligand	52
Solvent	424
Average B factors (Å^2)	
Protein	15
Ligand	20
Solvent	20
RMS Deviations	
Bond lengths (Å)	0.03
Bond angles (°)	1.4
Ramachandran Plot[g]	
Favored	97.01
Allowed	2.99
Outliers	0.00

[a]Values in parentheses refer to the highest-resolution shell of data.

[b]$R_{merge} = \sum_h \sum_i |I_{i,h} - \langle I \rangle_h| / \sum_h \sum_i I_{i,h}$, where $\langle I \rangle_h$ is the average intensity calculated for reflection h from i replicate measurements.

[c]$R_{p.i.m.} = (\sum_h (1/(N-1))^{1/2} \sum_i |I_{i,h} - \langle I \rangle_h|) / \sum_h \sum_i I_{i,h}$, where N is the number of reflections and $\langle I \rangle_h$ is the average intensity calculated for reflection h from replicate measurements.

[d]Pearson correlation coefficient between random half-datasets.

[e]$R_{work} = \sum ||F_o| - |F_c|| / \sum |F_o|$ for reflections contained in the working set. $|F_o|$ and $|F_c|$ are the observed and calculated structure factor amplitudes, respectively. R_{free} is calculated using the same expression for reflections contained in the test set held aside during refinement.

[f]Per asymmetric unit.

[g]Calculated with MolProbity.

2 NMR Data of synthesized compounds

¹**H NMR** spectrum of **1** (300 MHz, CDCl₃)
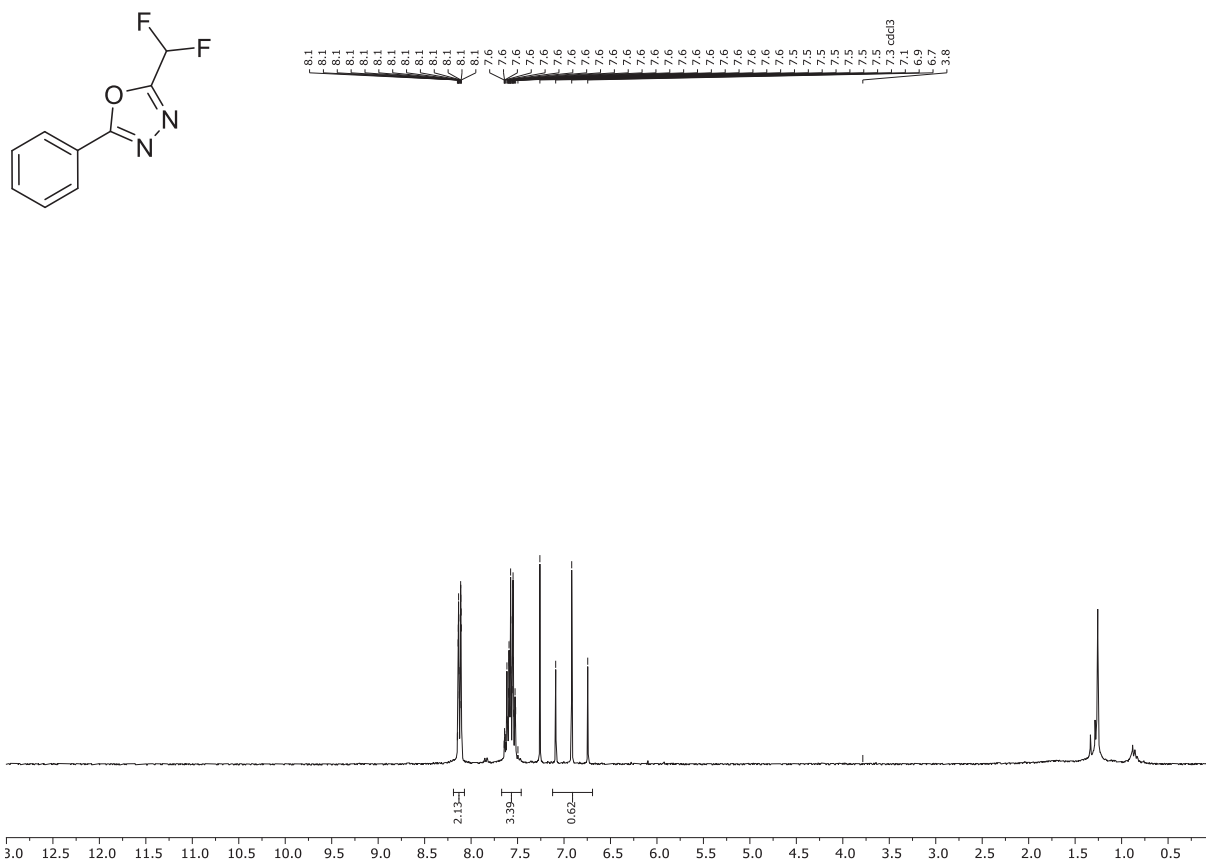
¹³**C NMR** spectrum of **1** (101 MHz, CDCl₃)
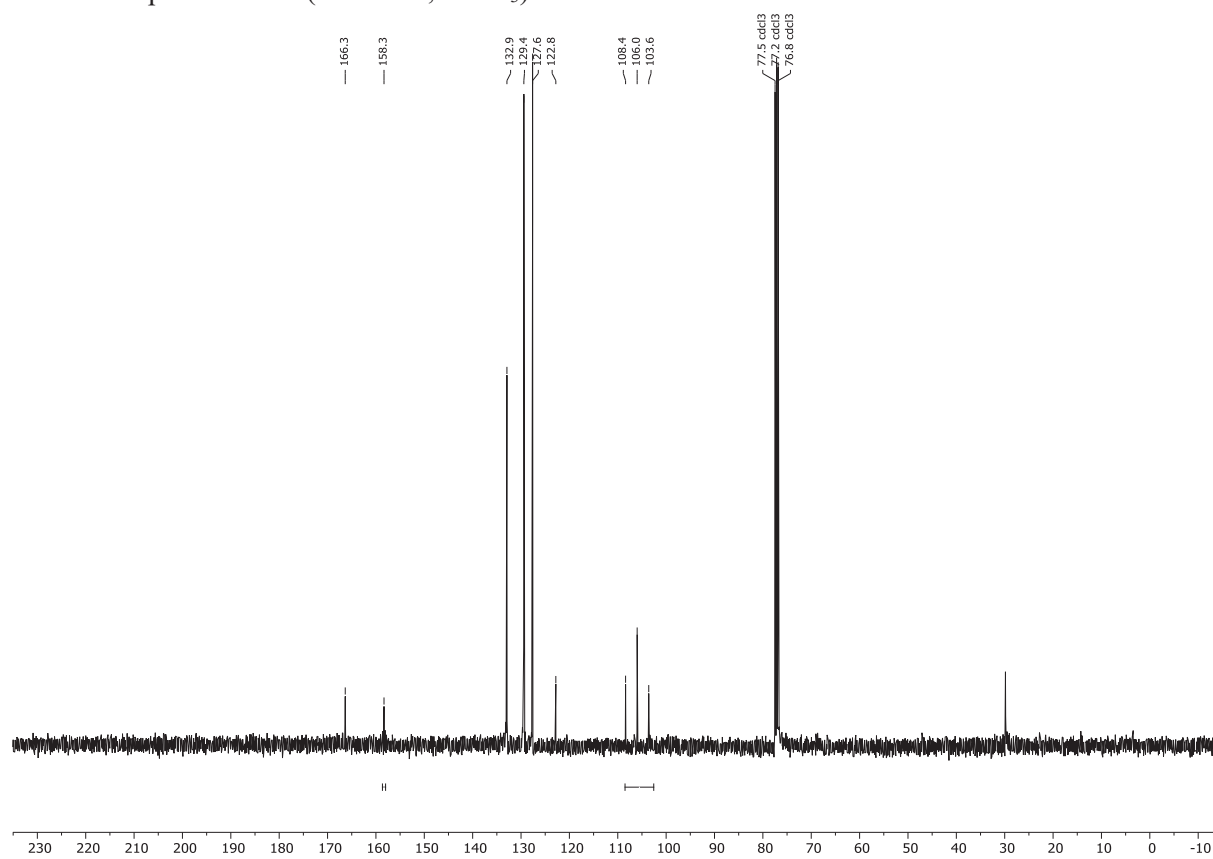
¹⁹F NMR spectrum of **1** (377 MHz, CDCl₃)

-127.0
-127.1

70 60 50 40 30 20 10 0 -10 -20 -30 -40 -50 -60 -70 -80 -90 -100 -110 -120 -130 -140 -150 -160 -170 -180 -190 -200 -210 -220 -230 -240 -250 -260 -270

¹H NMR spectrum of **2** (600 MHz, DMSO-d_6)

9.1
9.1
8.3
8.3
8.3
7.6
7.6
7.5
7.5
7.5
— 3.3 H2O
2.6
2.5 DMSO
2.5 DMSO
2.5 DMSO
2.5 DMSO-d6
2.5 DMSO
2.5 DMSO

0.96
1.08
0.99
1.08
3.00

3.0 12.5 12.0 11.5 11.0 10.5 10.0 9.5 9.0 8.5 8.0 7.5 7.0 6.5 6.0 5.5 5.0 4.5 4.0 3.5 3.0 2.5 2.0 1.5 1.0 0.5 0

¹³C NMR spectrum of **2** (151 MHz, DMSO-d_6)

164.0
162.8
158.8
158.6
158.4
— 147.3
— 135.0
— 123.9
— 116.6
108.3
106.7
105.1
40.1 DMSO
40.0 DMSO
39.8 DMSO
39.7 DMSO
39.6 DMSO
39.4 DMSO
39.3 DMSO
— 24.4

230 220 210 200 190 180 170 160 150 140 130 120 110 100 90 80 70 60 50 40 30 20 10 0

¹⁹F NMR spectrum of **2** (565 MHz, DMSO-*d*₆)

10   0   -10   -20   -30   -40   -50   -60   -70   -80   -90   -100   -110   -120   -130   -140   -150   -160   -170   -180   -190   -200   -210
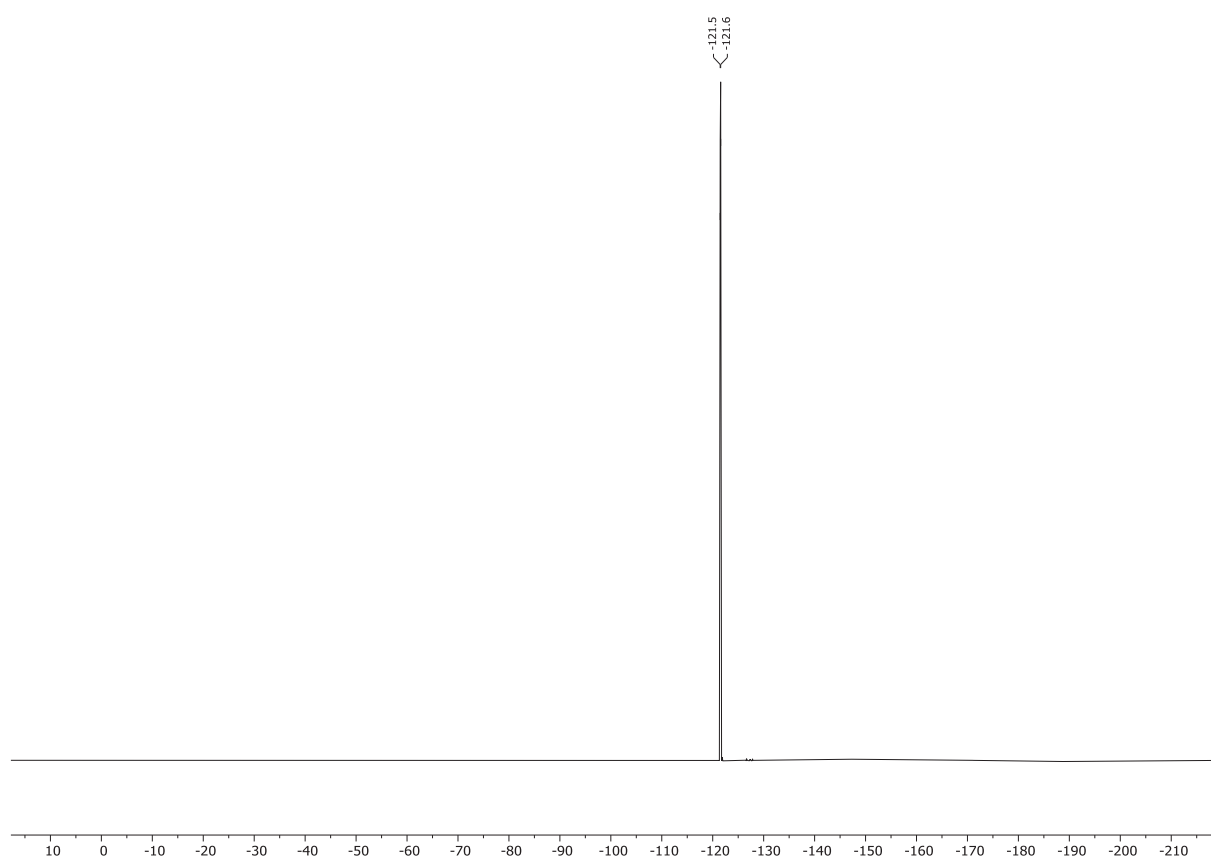
¹H NMR spectrum of **3** (400 MHz, CDCl₃)
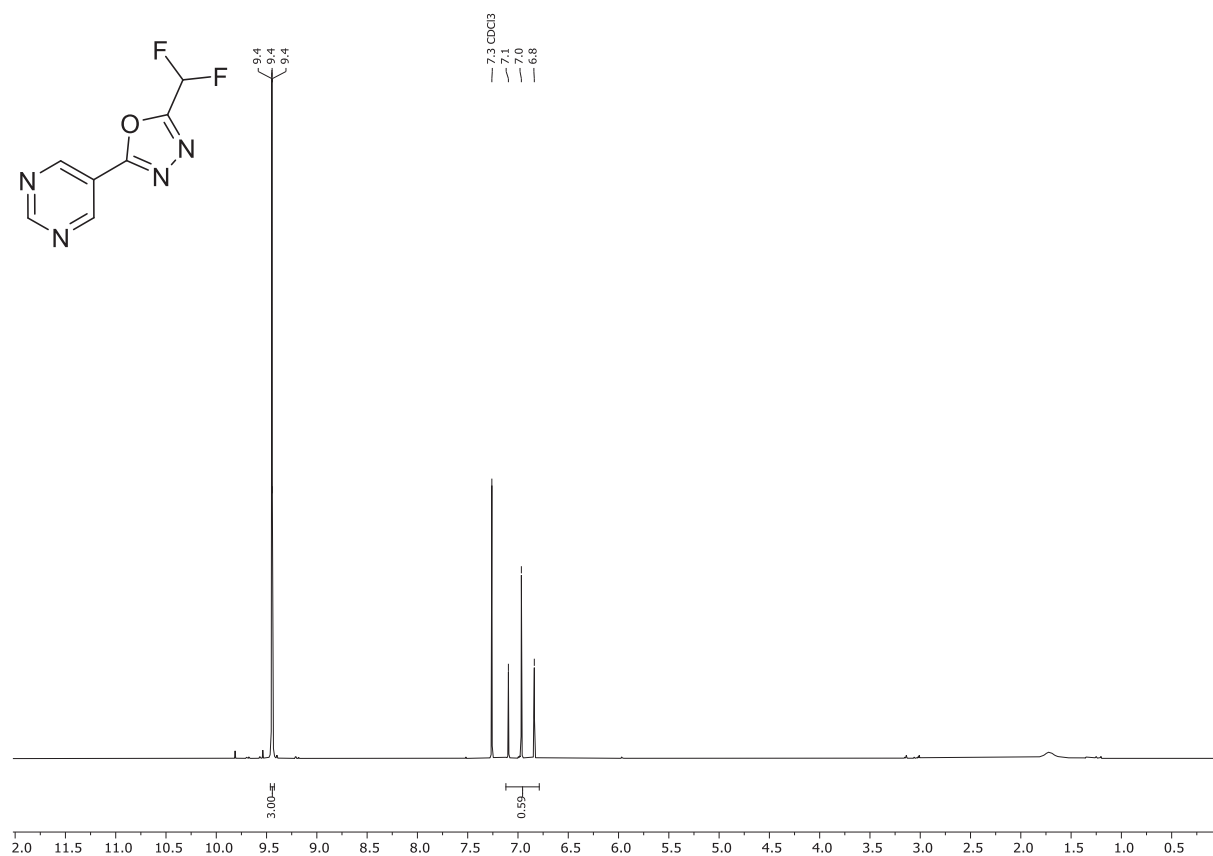
¹³C NMR spectrum of **3** (75 MHz, CDCl₃)
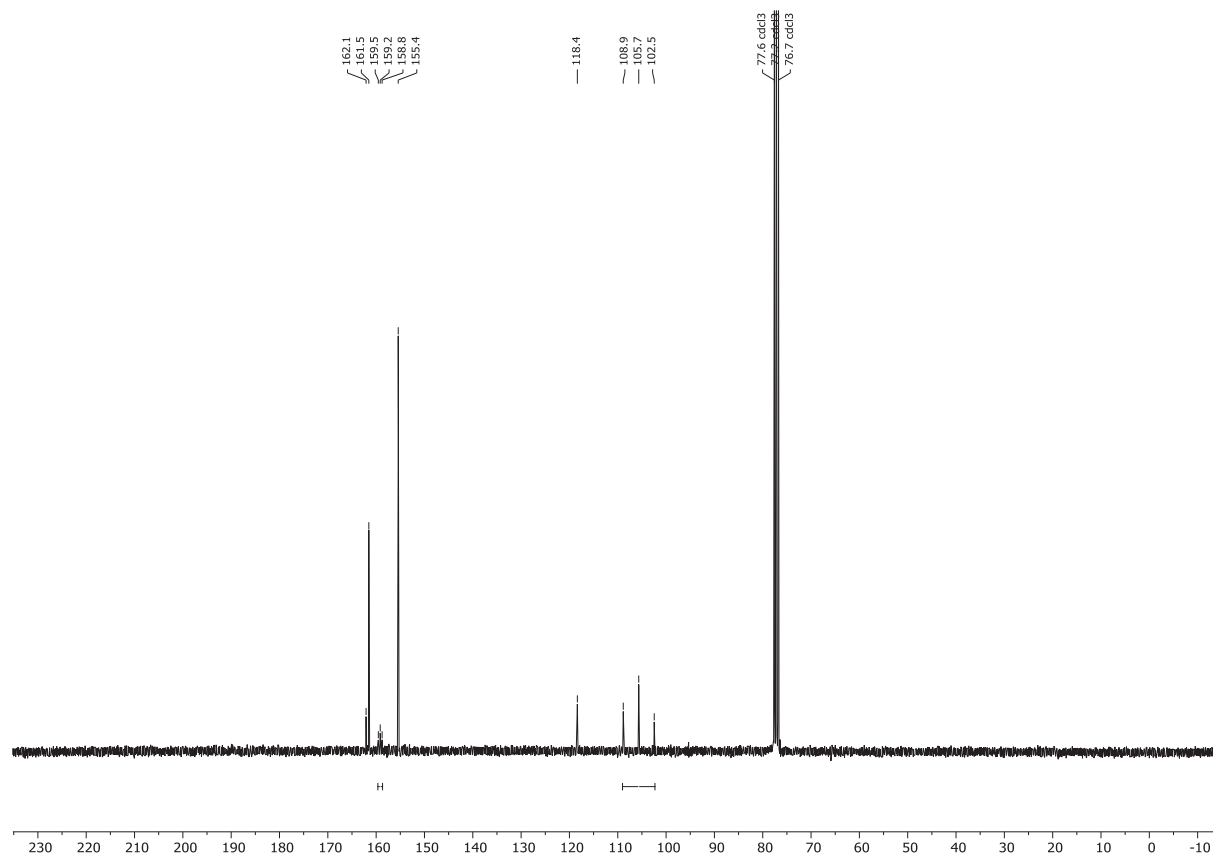
¹⁹F NMR spectrum of **3** (377 MHz, CDCl₃)

¹H NMR spectrum of **4** (600 MHz, DMSO-d_6)

¹³C NMR spectrum of **4** (151 MHz, DMSO-d_6)
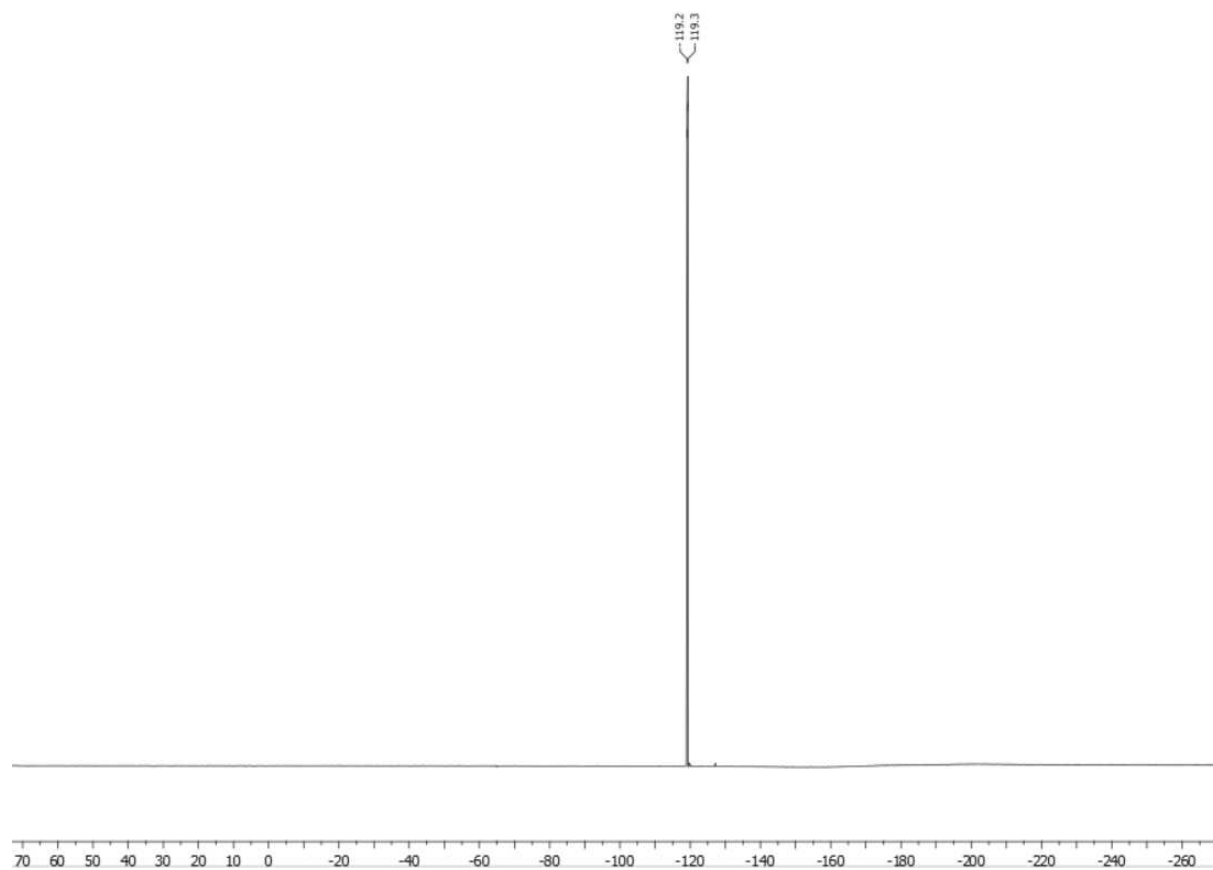
¹H NMR spectrum of **5** (600 MHz, CDCl₃)
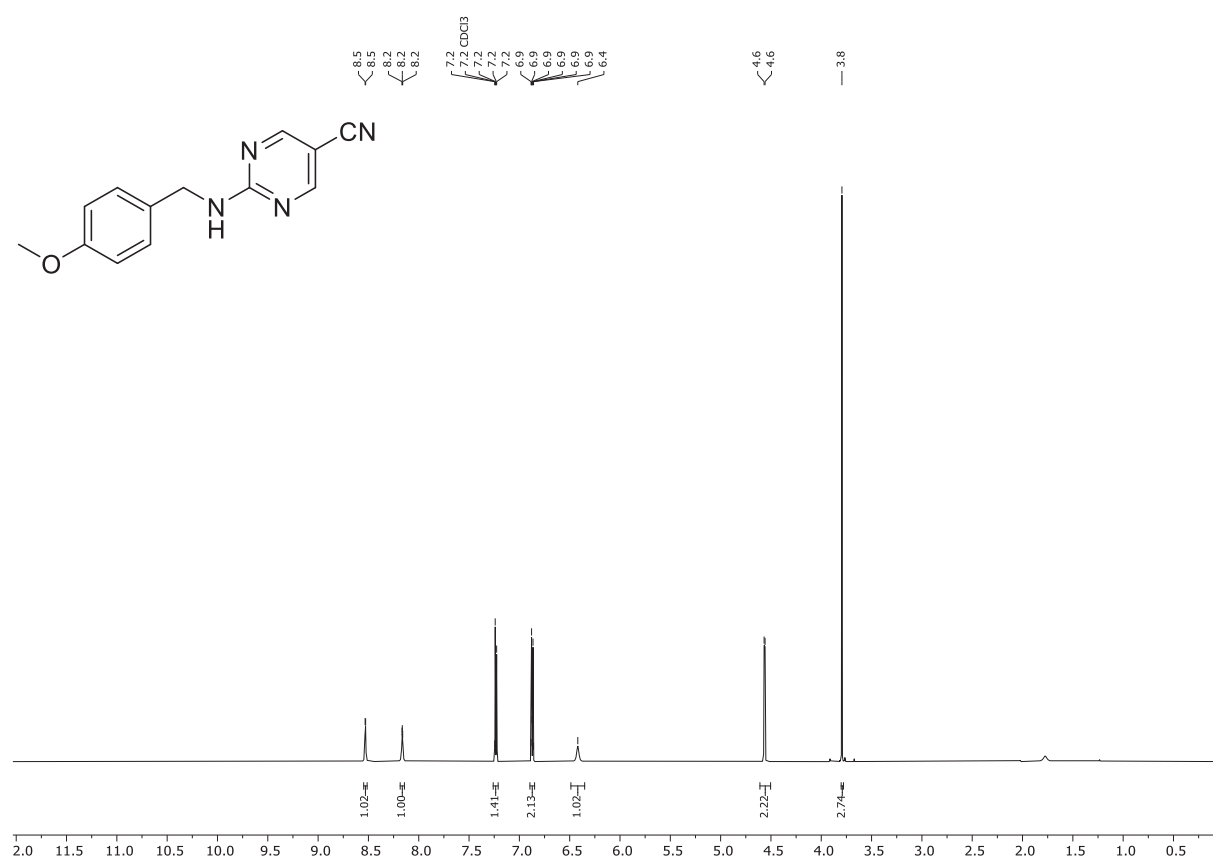
¹³C NMR spectrum of **5** (151 MHz, CDCl₃)
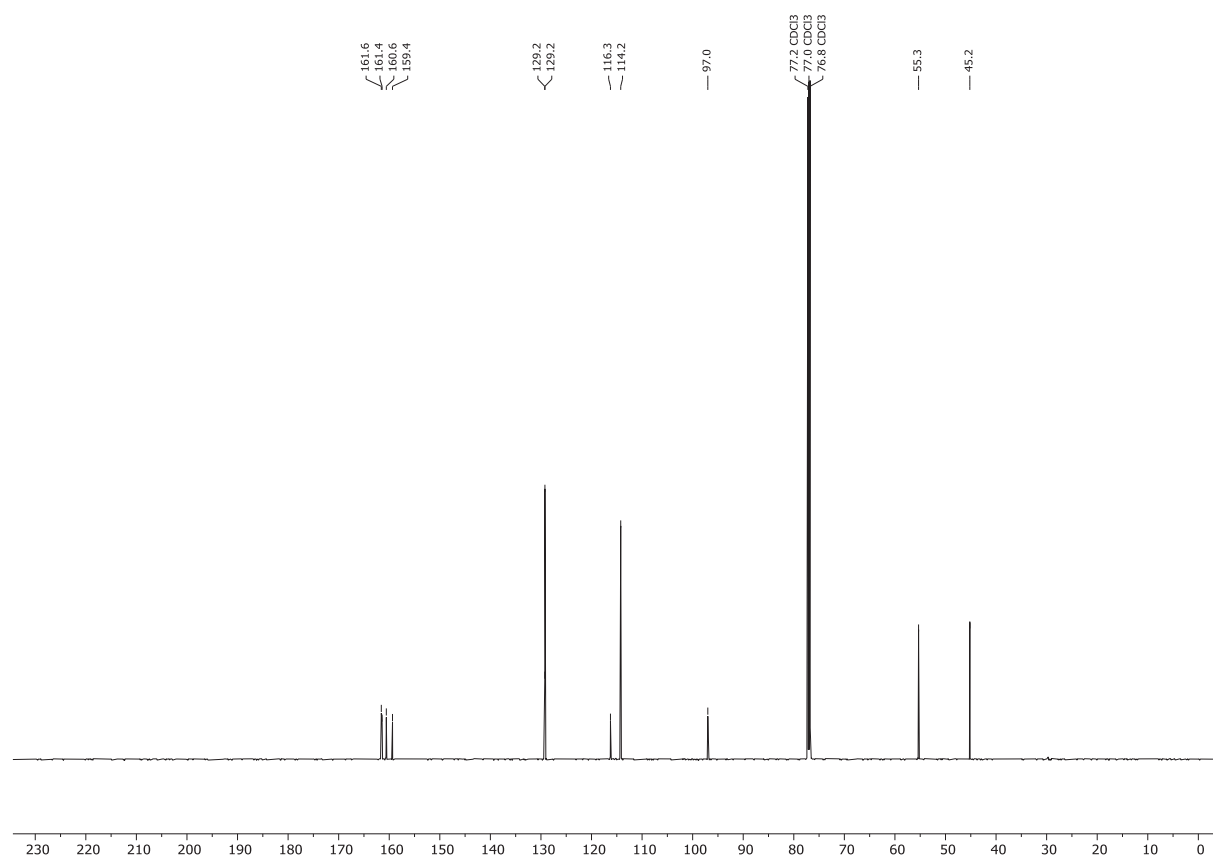
¹H NMR spectrum of **6** (600 MHz, DMSO-*d*₆)
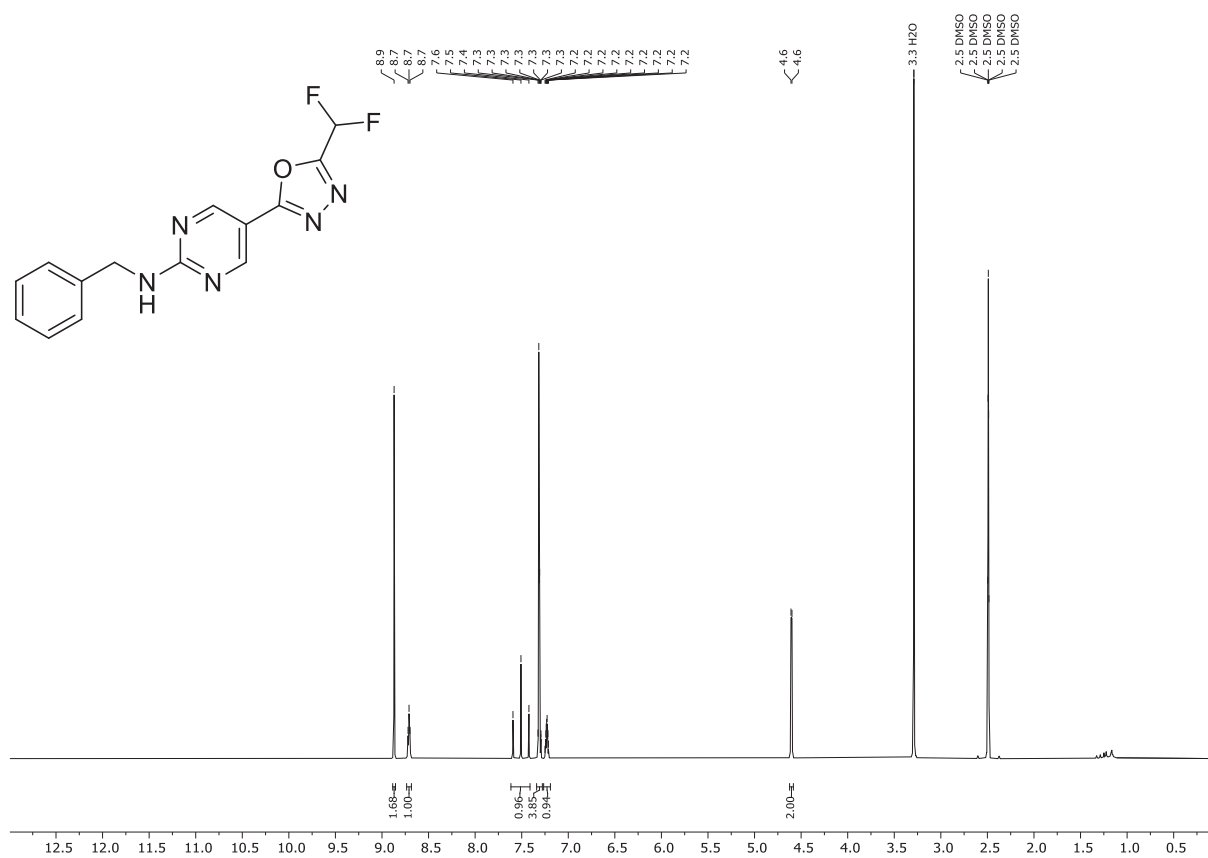
¹³C NMR spectrum of **6** (151 MHz, DMSO-*d*₆)
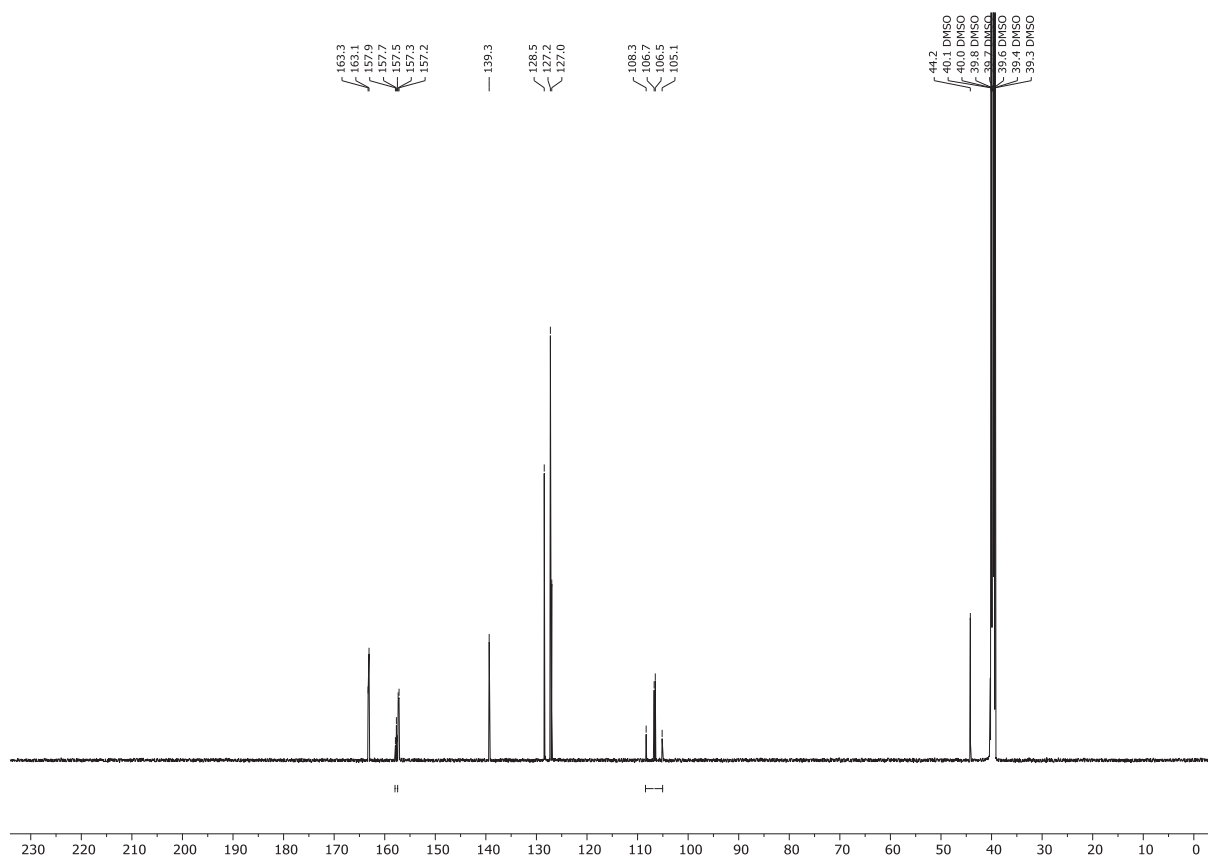
¹⁹F NMR spectrum of **6** (565 MHz, DMSO-d_6)
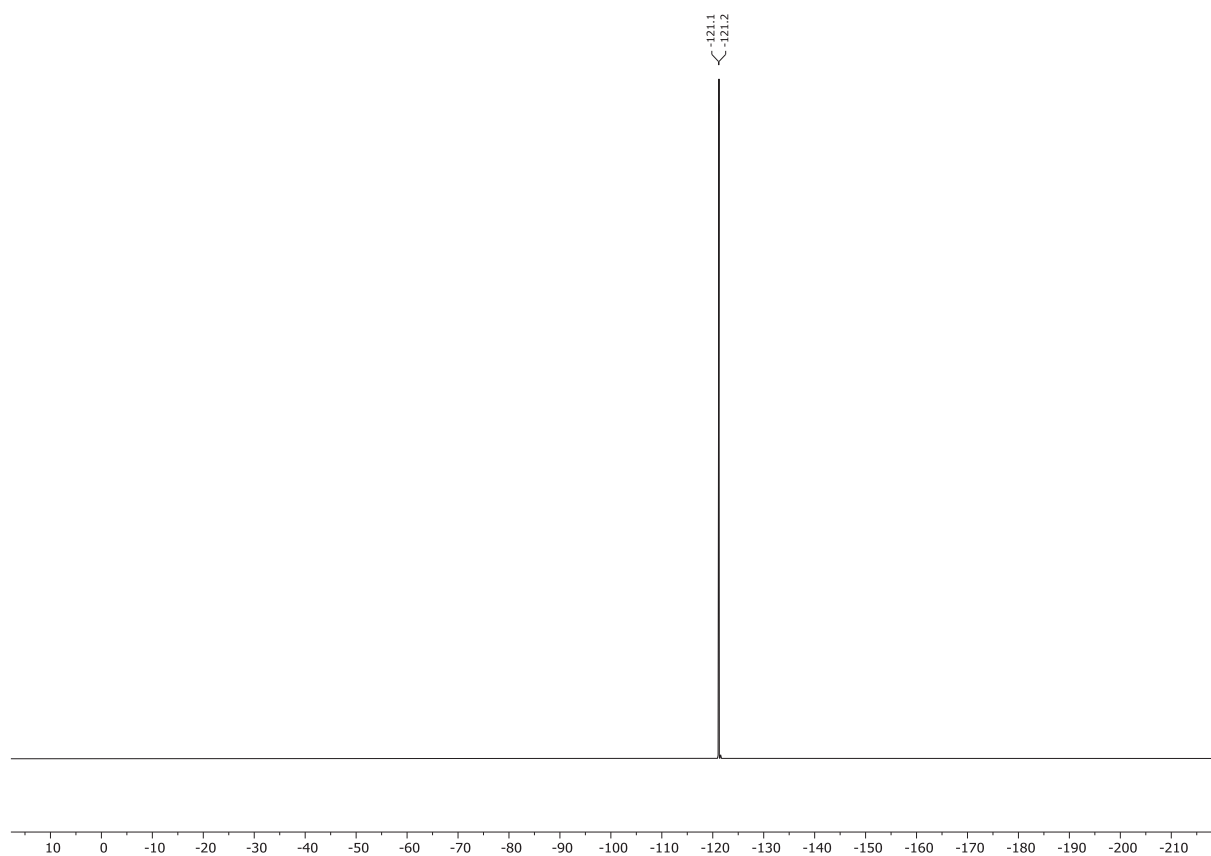
¹H NMR spectrum of **7** (600 MHz, DMSO-d_6)
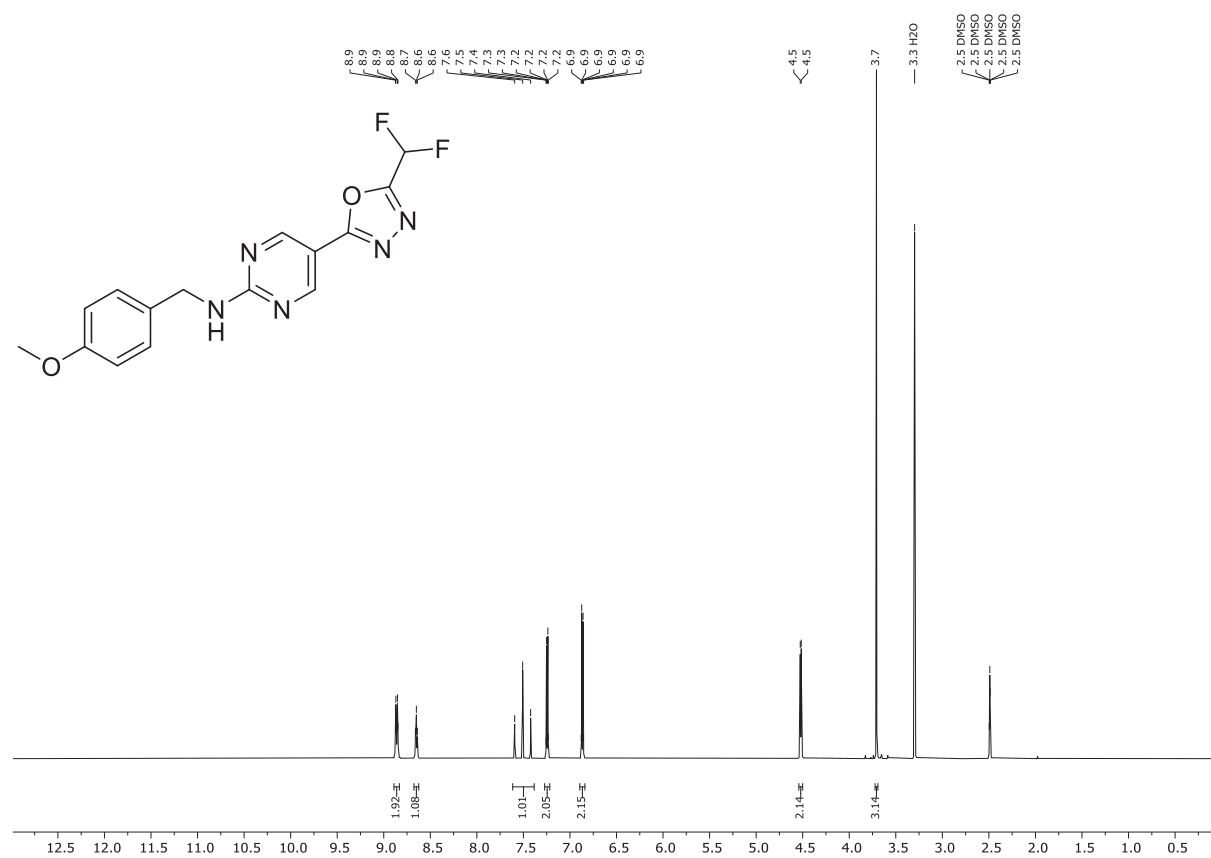
¹³C NMR spectrum of **7** (151 MHz, DMSO-d_6)
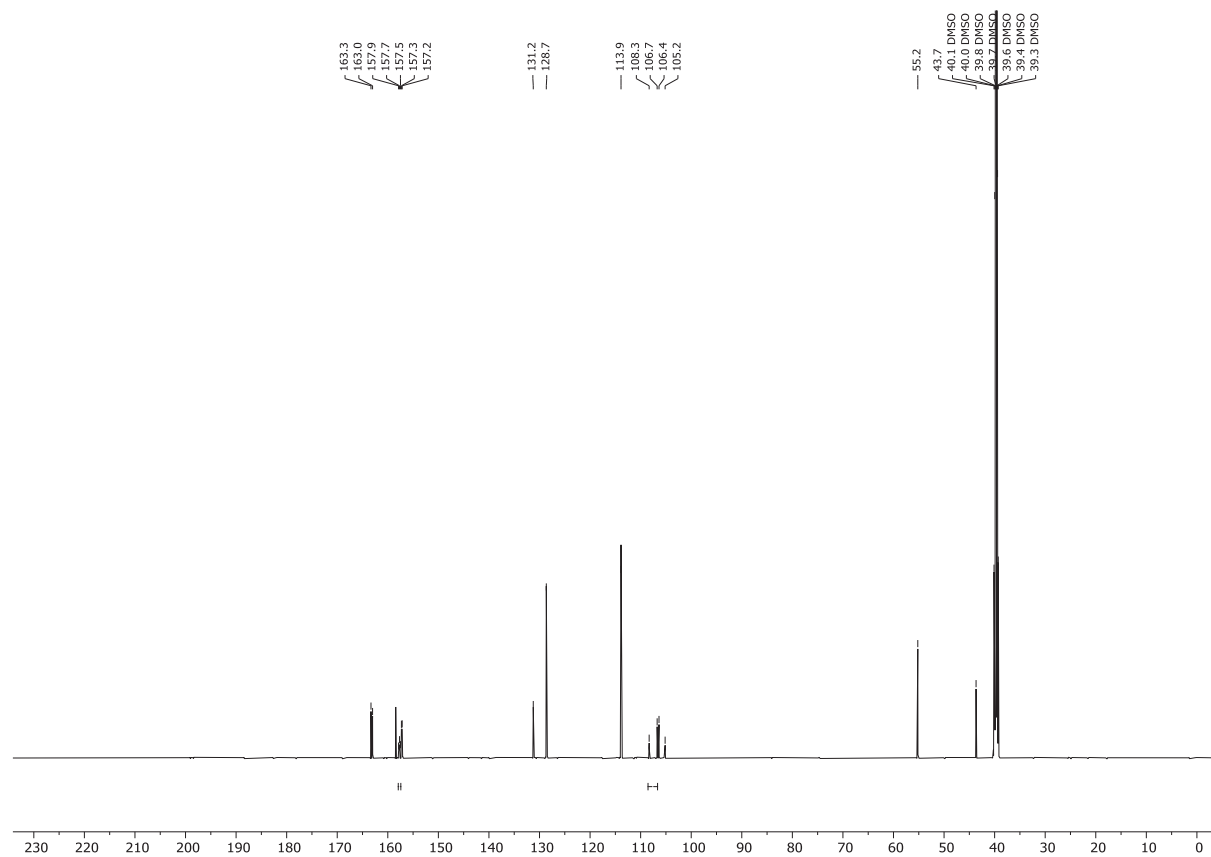
¹⁹F NMR spectrum of **7** (565 MHz, DMSO-*d*₆)

-121.1
-121.2

10 0 -10 -20 -30 -40 -50 -60 -70 -80 -90 -100 -110 -120 -130 -140 -150 -160 -170 -180 -190 -200 -210
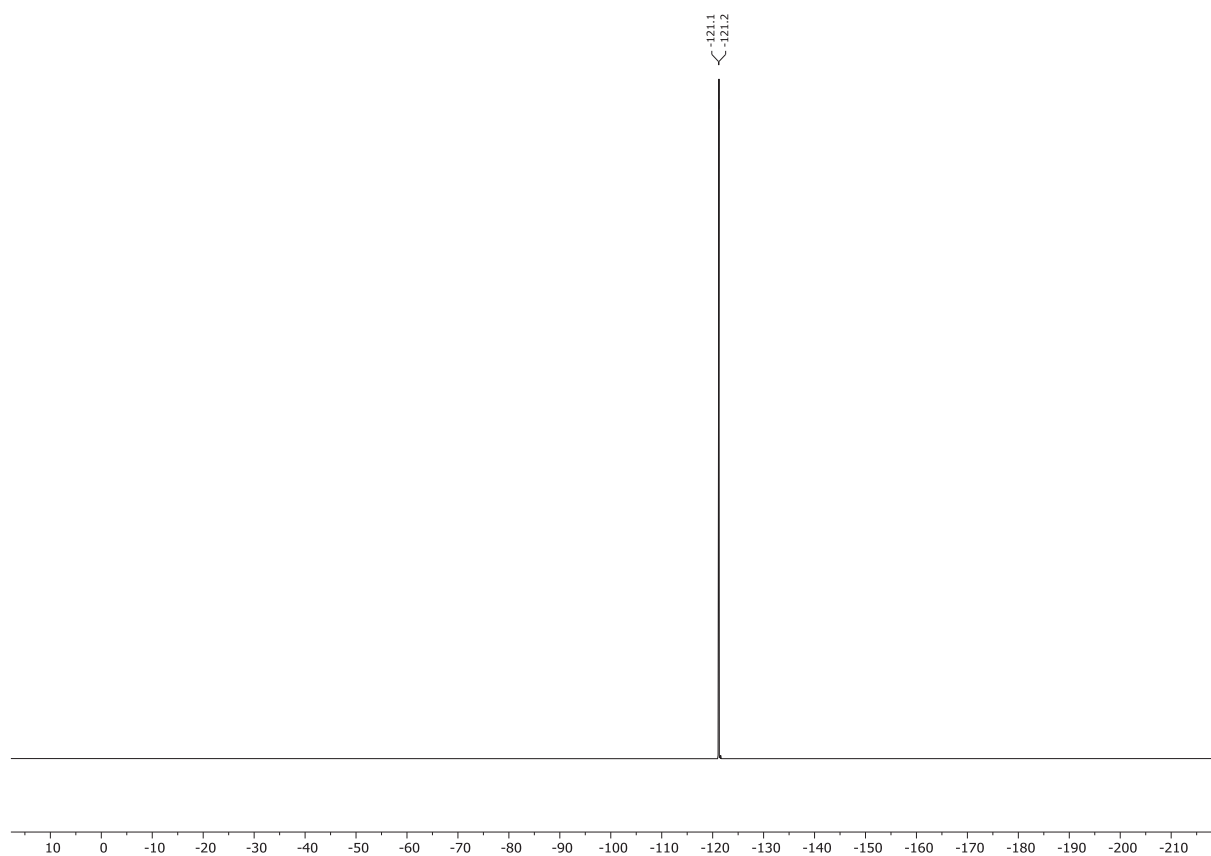
¹H NMR spectrum of **8** (600 MHz, DMSO-d_6)
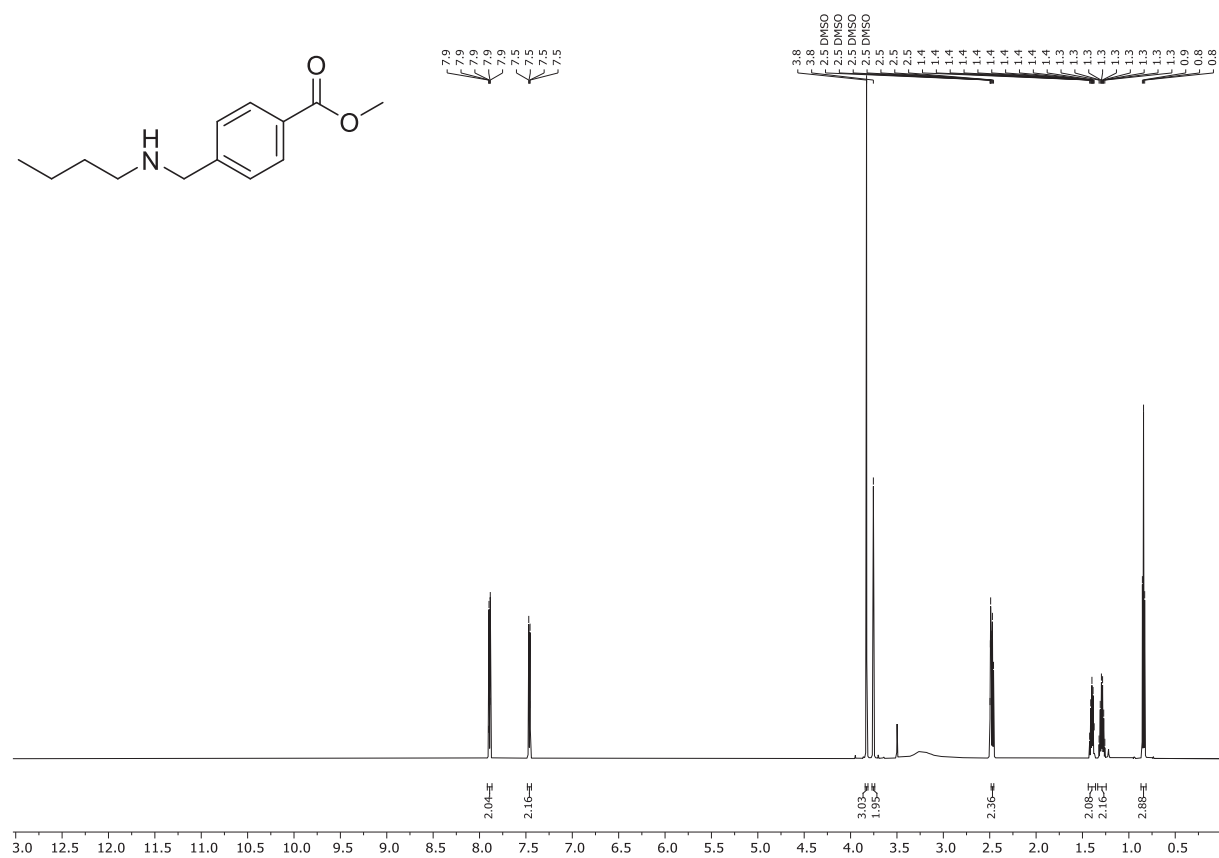
¹³C NMR spectrum of **8** (151 MHz, DMSO-d_6)

¹H NMR spectrum of 9 (600 MHz, DMSO-*d₆*)

¹H NMR spectrum of **9** (600 MHz, DMSO-*d₆*)

¹³C NMR spectrum of **9** (151 MHz, DMSO-*d₆*)
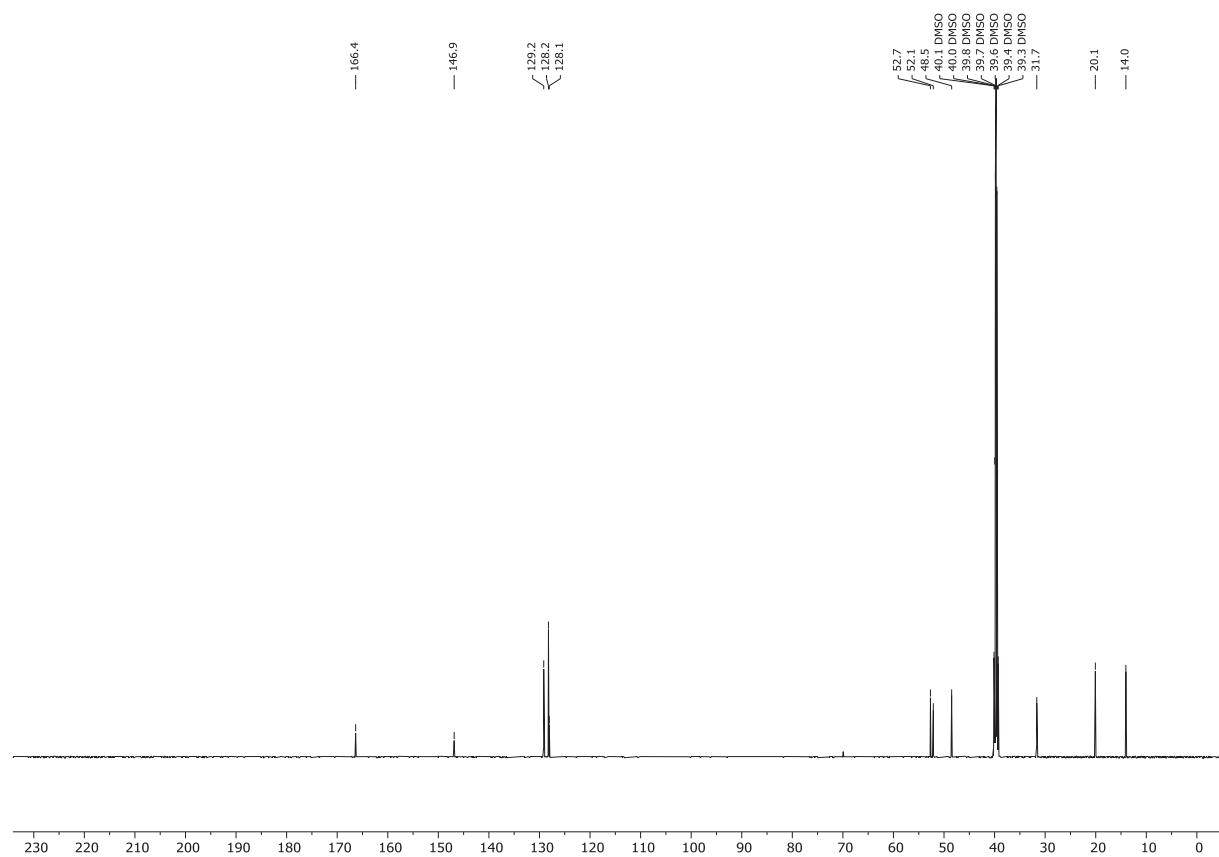
¹⁹F NMR spectrum of **9** (565 MHz, DMSO-*d*₆)
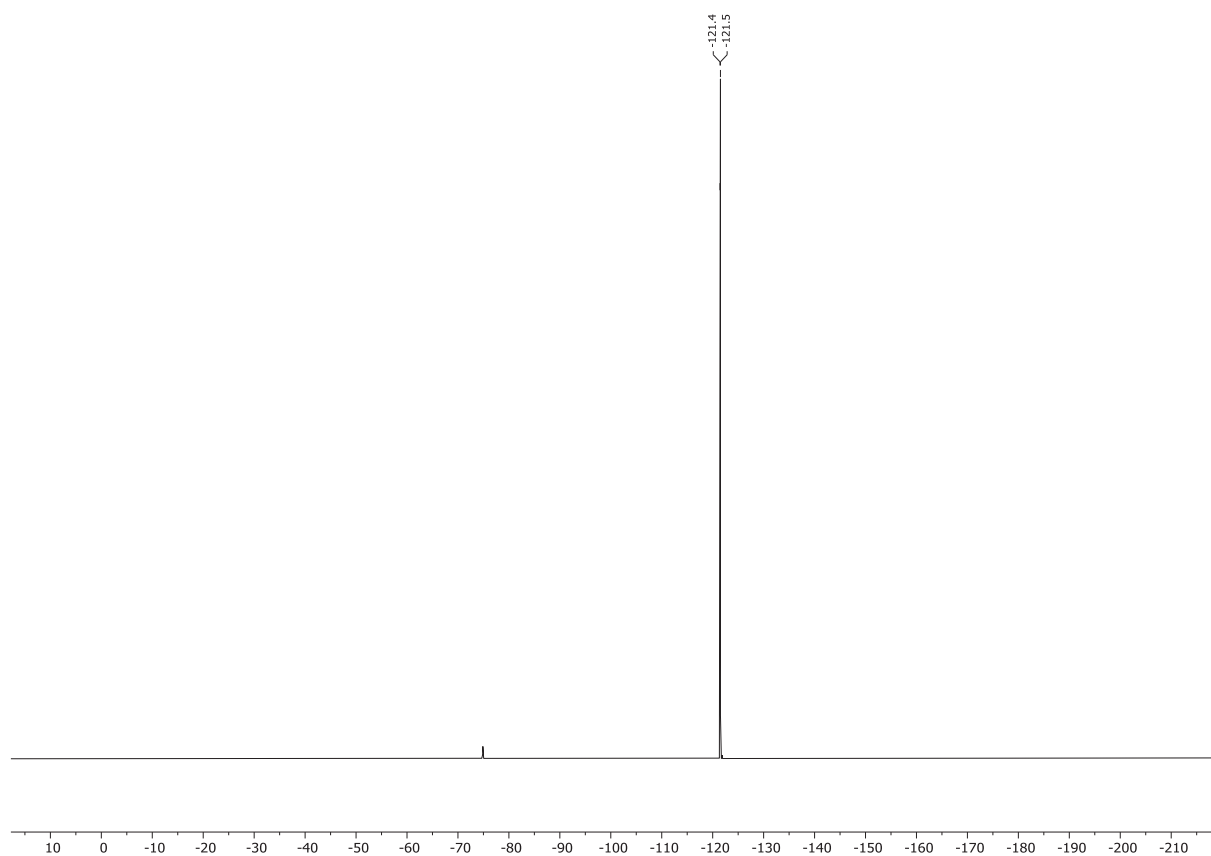
¹H NMR spectrum of **10** (600 MHz, CDCl₃)
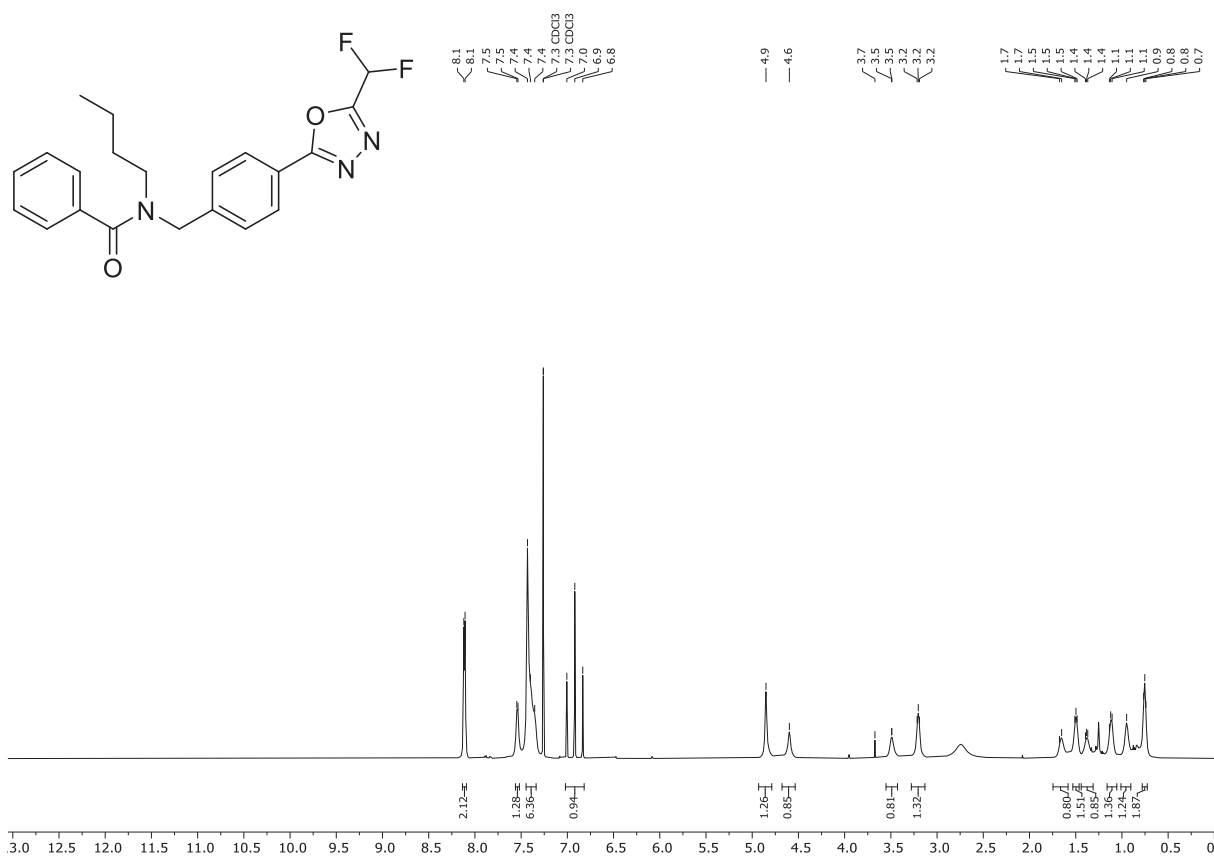
¹³C NMR spectrum of **10** (151 MHz, CDCl₃)
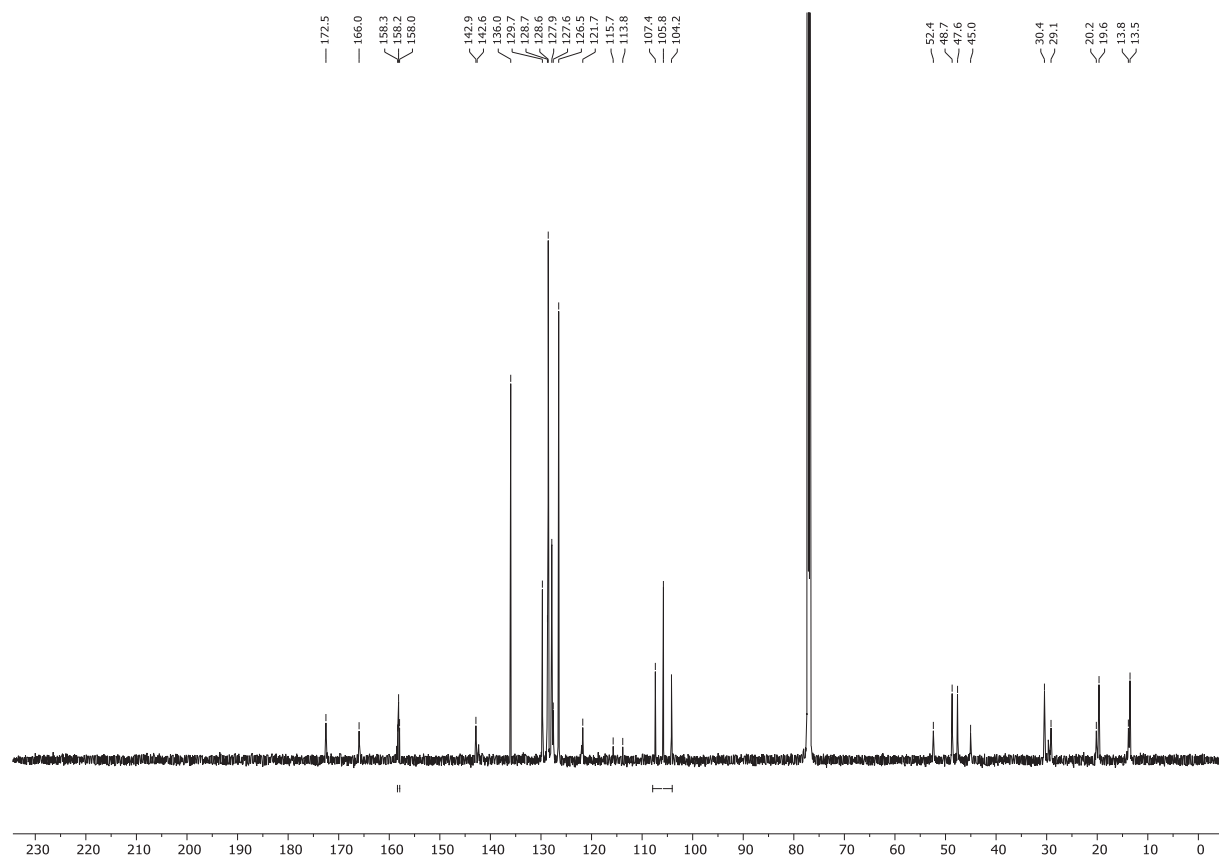
¹⁹F NMR spectrum of **10** (565 MHz, CDCl₃)

TFA

—77.0

-120.0
-120.1

10   0   -10 -20 -30 -40 -50 -60 -70 -80 -90 -100 -110 -120 -130 -140 -150 -160 -170 -180 -190 -200 -210

¹H NMR spectrum of **12** (600 MHz, DMSO-d_6)

¹³C NMR spectrum of **12** (151 MHz, DMSO-d_6)
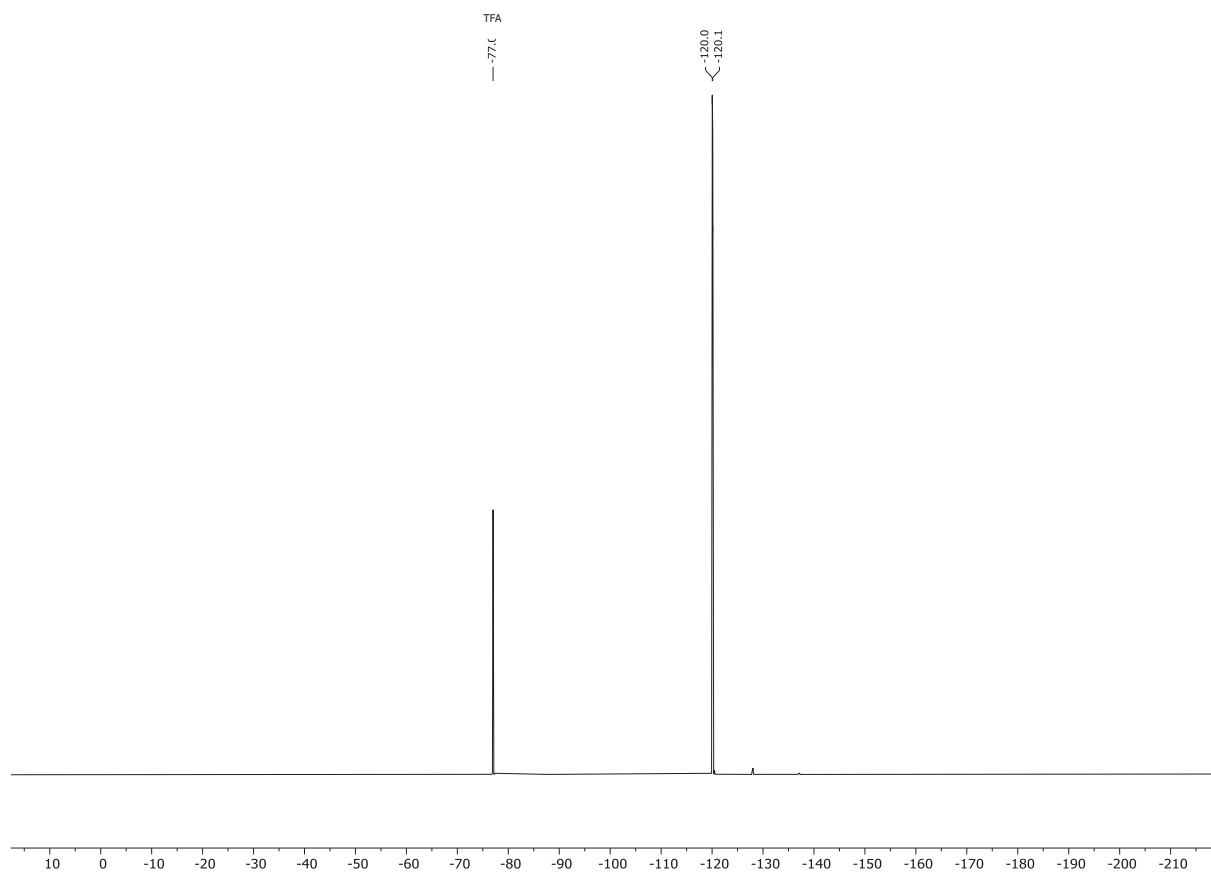
¹⁹F NMR spectrum of **12** (565 MHz, DMSO-*d*₆)
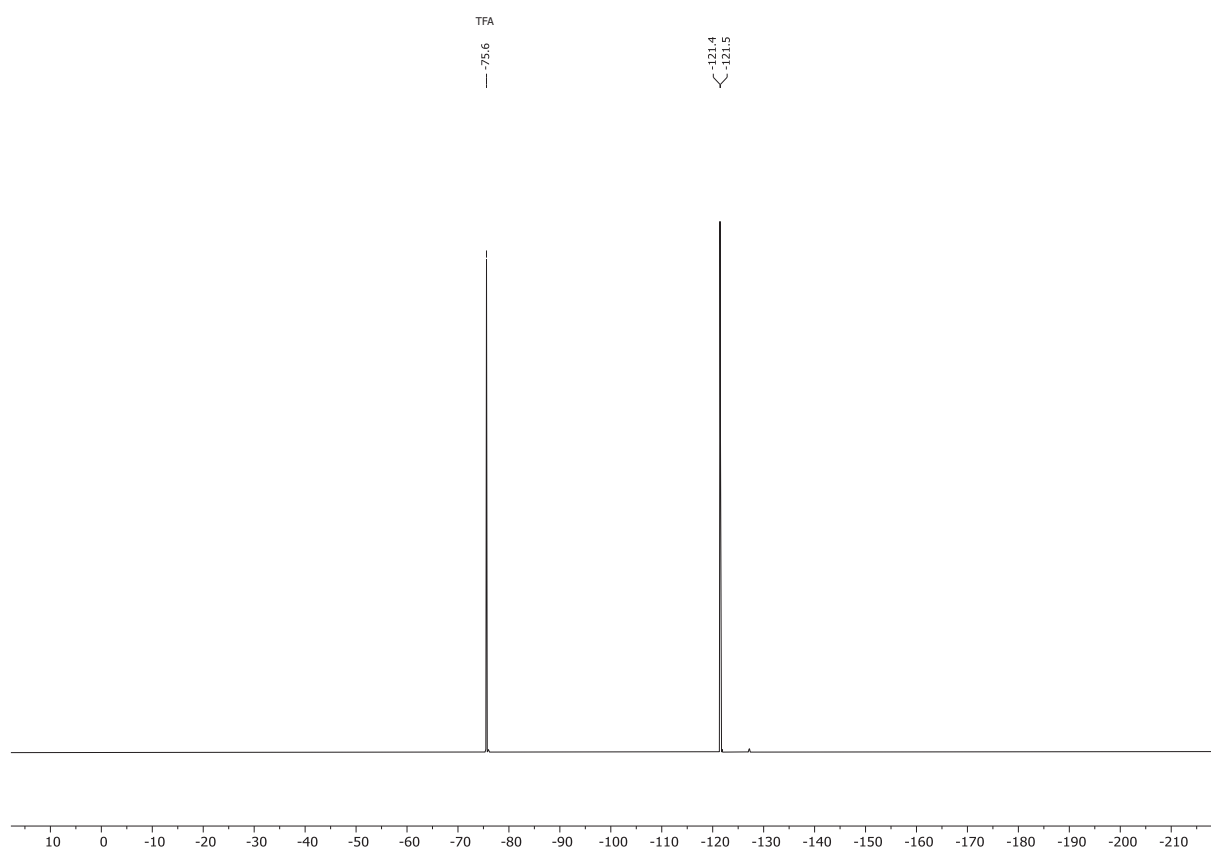
¹H NMR spectrum of **13** (600 MHz, DMSO-*d*₆)
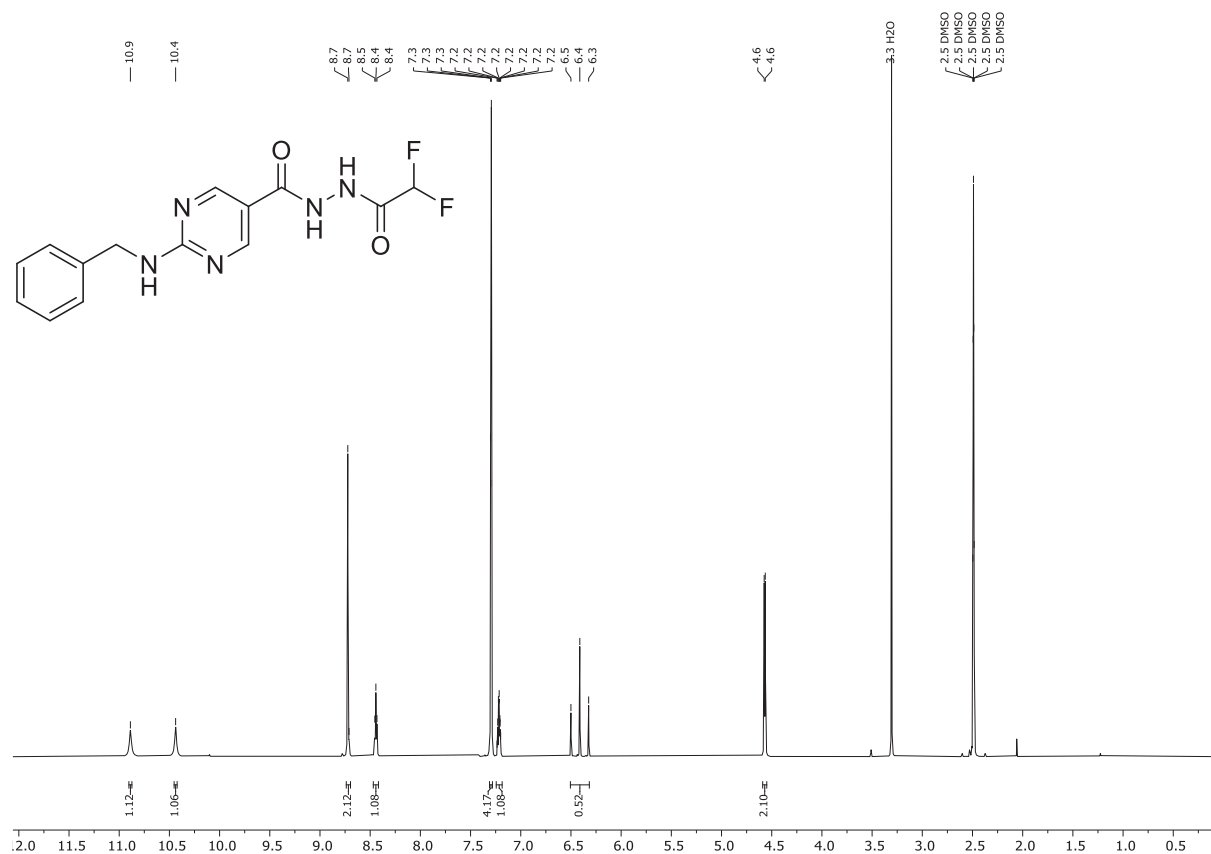
¹³C NMR spectrum of **13** (151 MHz, DMSO-*d*₆)
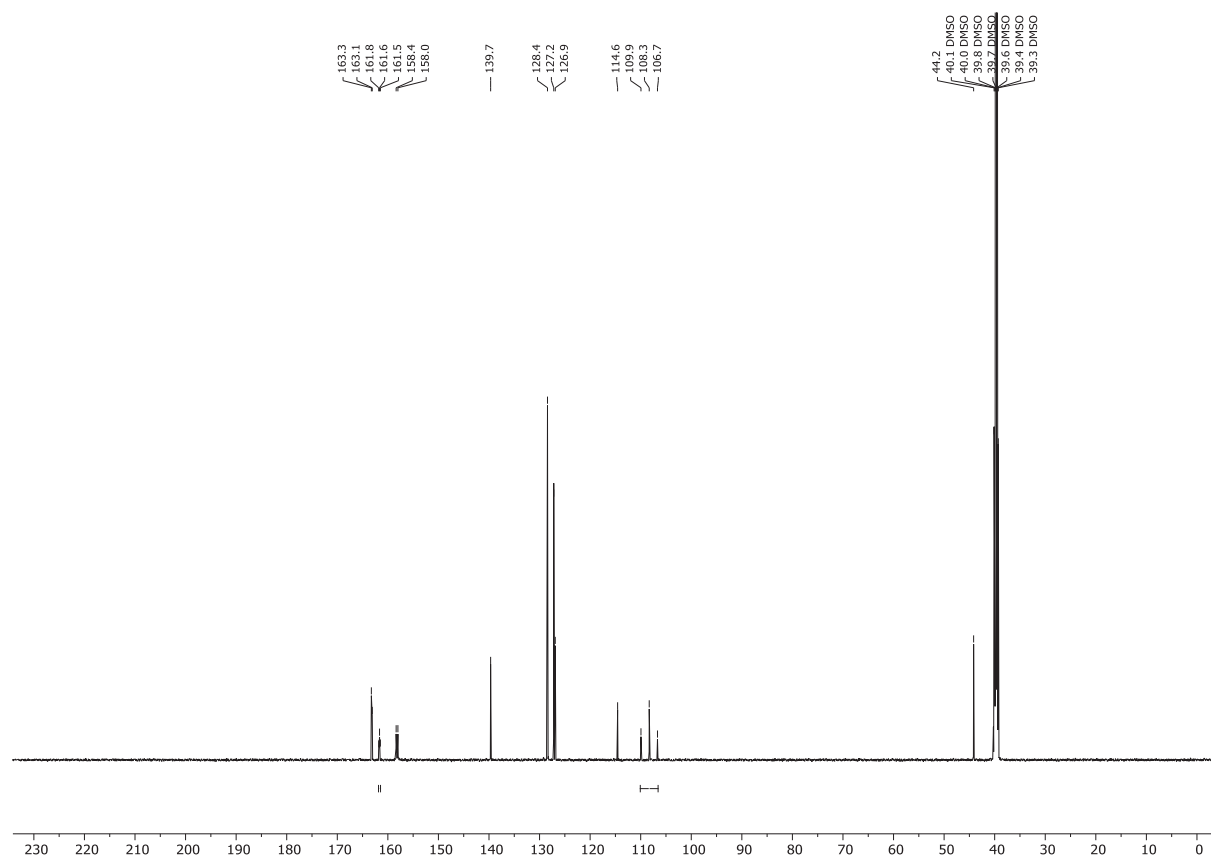
¹⁹F NMR spectrum of **13** (565 MHz, DMSO-*d*₆)

-127.1
-127.2

10 0 -10 -20 -30 -40 -50 -60 -70 -80 -90 -100 -110 -120 -130 -140 -150 -160 -170 -180 -190 -200 -210
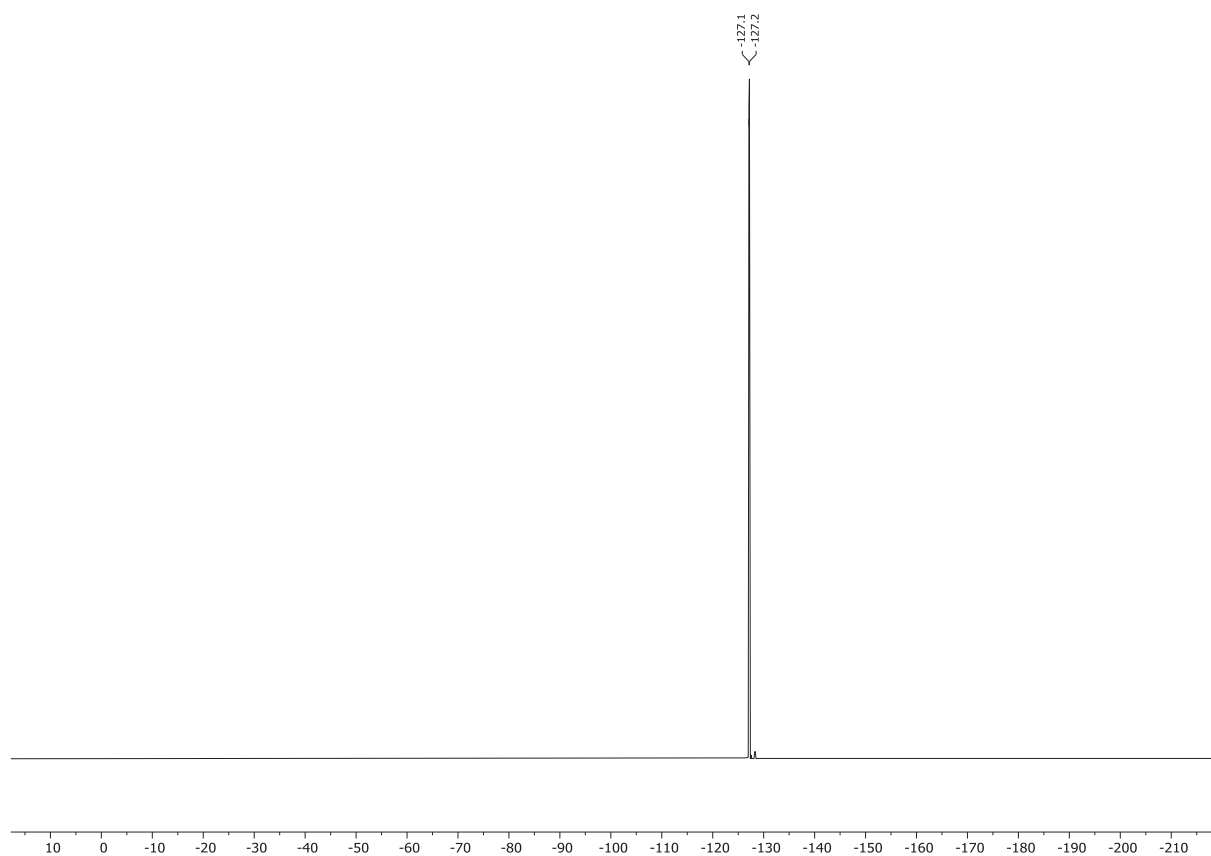
¹H NMR spectrum of **14** (600 MHz, DMSO-d_6)

¹³C NMR spectrum of **14** (151 MHz, DMSO-d_6)
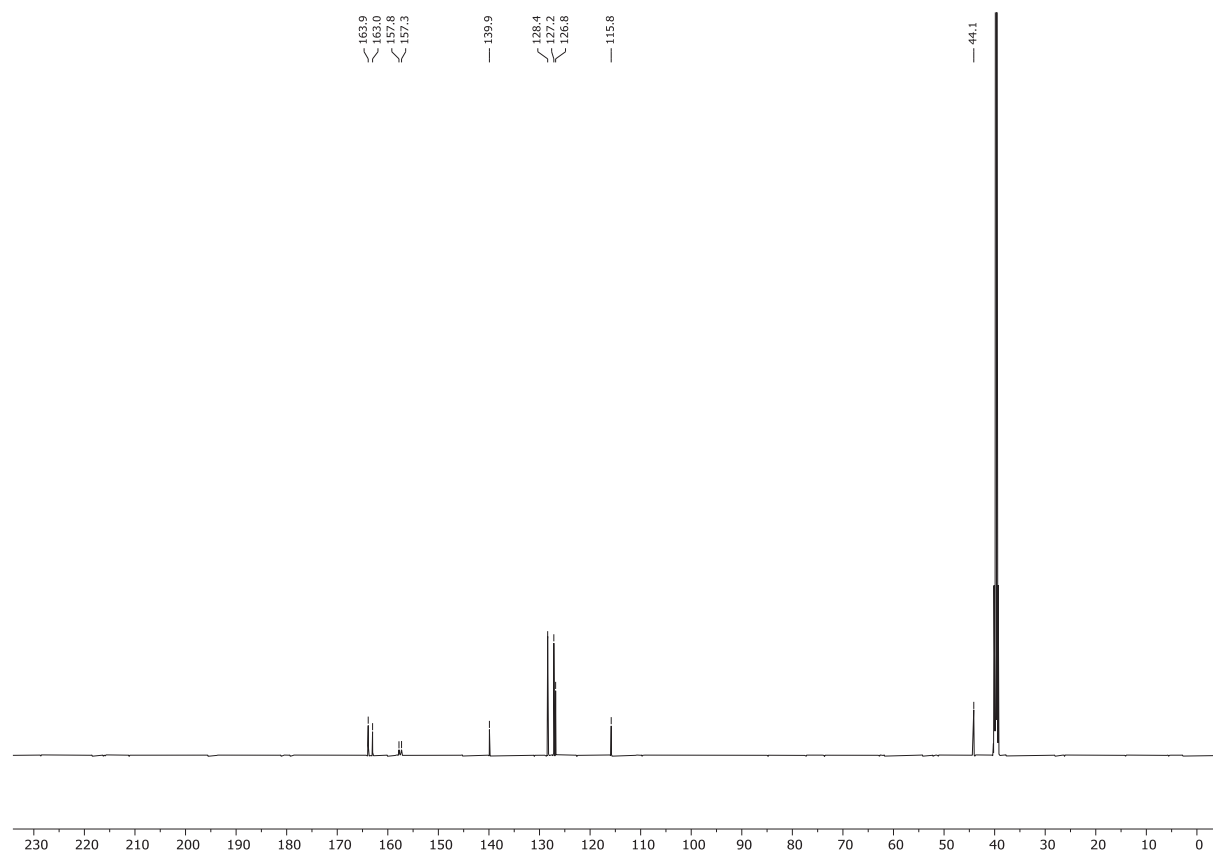
¹H NMR spectrum of **15** (600 MHz, DMSO-*d₆*)

¹³C NMR spectrum of **15** (126 MHz, DMSO-*d₆*)

¹H NMR spectrum of **16** (500 MHz, DMSO-*d*₆)

¹³C NMR spectrum of **16** (126 MHz, DMSO-*d*₆)

S33
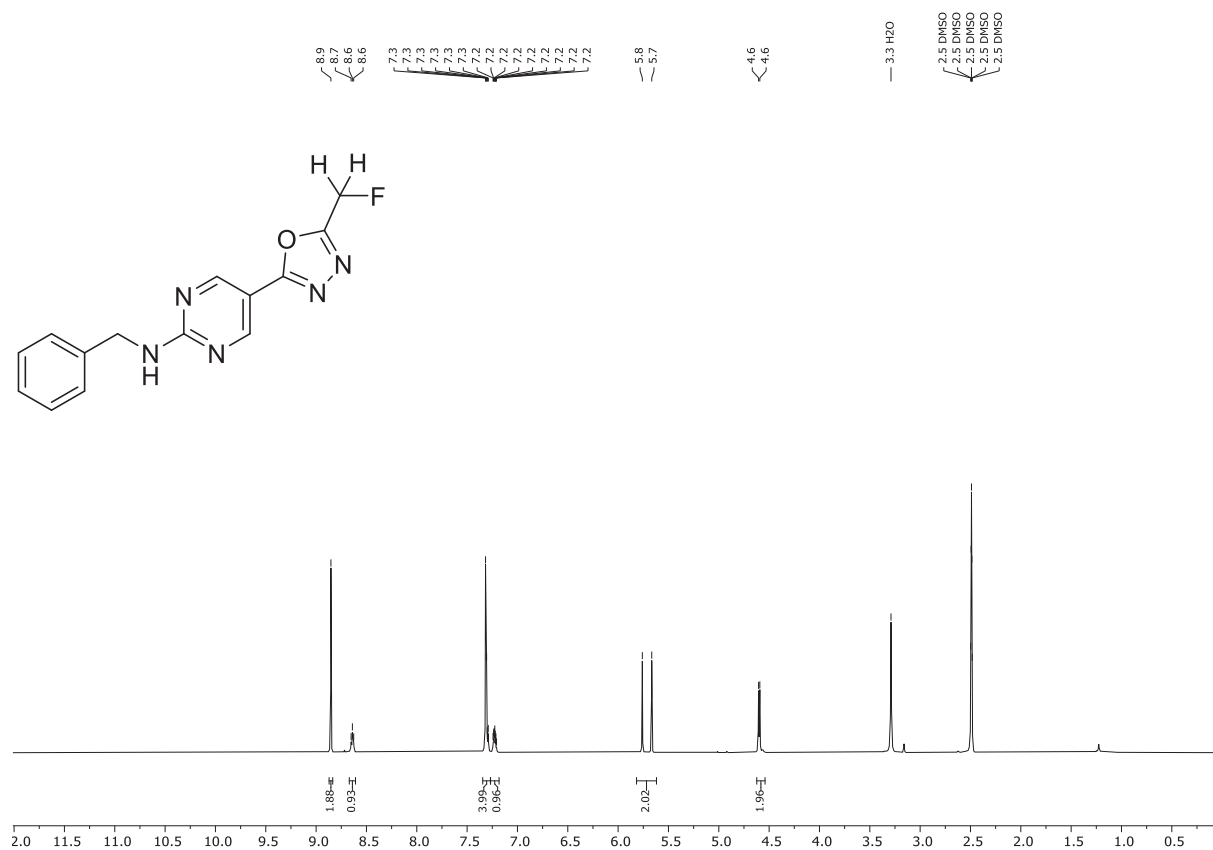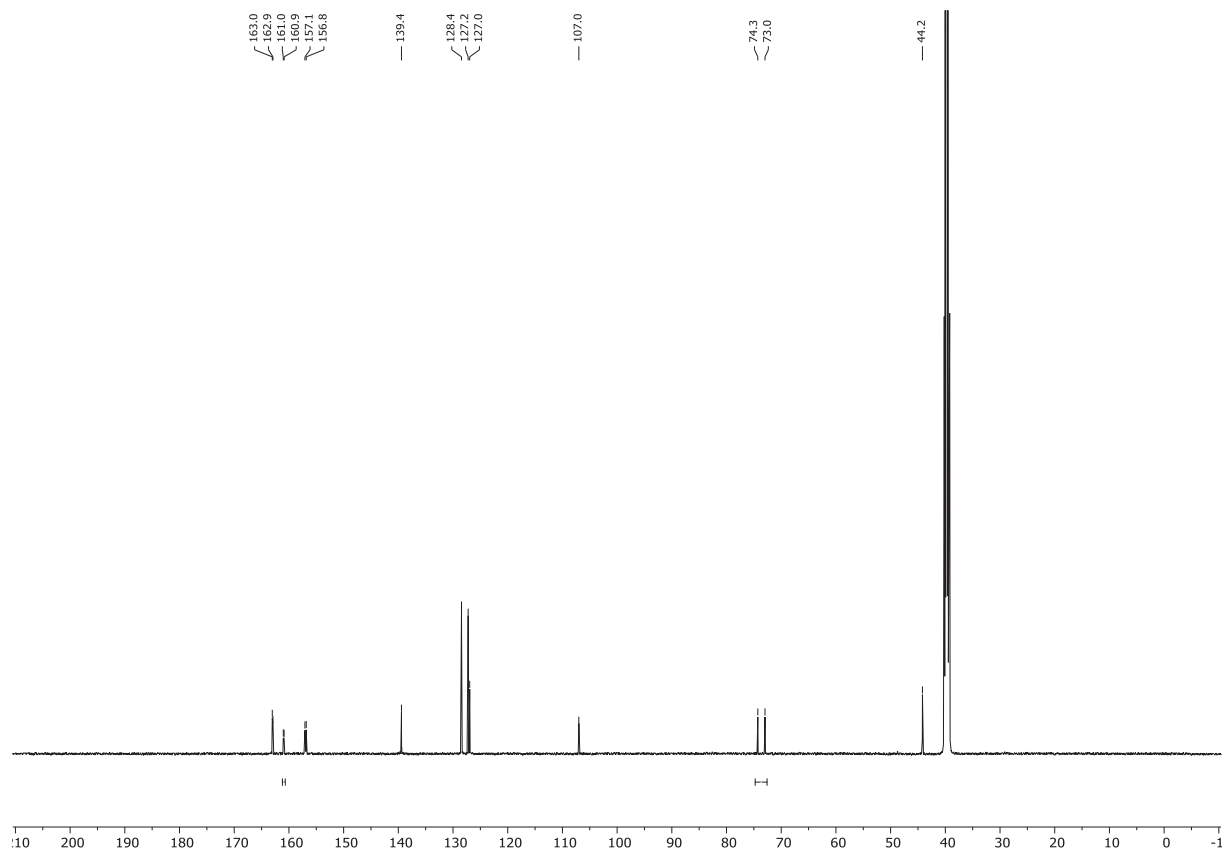
^{19}F NMR spectrum of **16** (471 MHz, DMSO-d_6)

— −74.2

60   50   40   30   20   10   0   -10   -20   -30   -40   -50   -60   -70   -80   -90   -100   -110   -120   -130   -140   -150   -160   -17
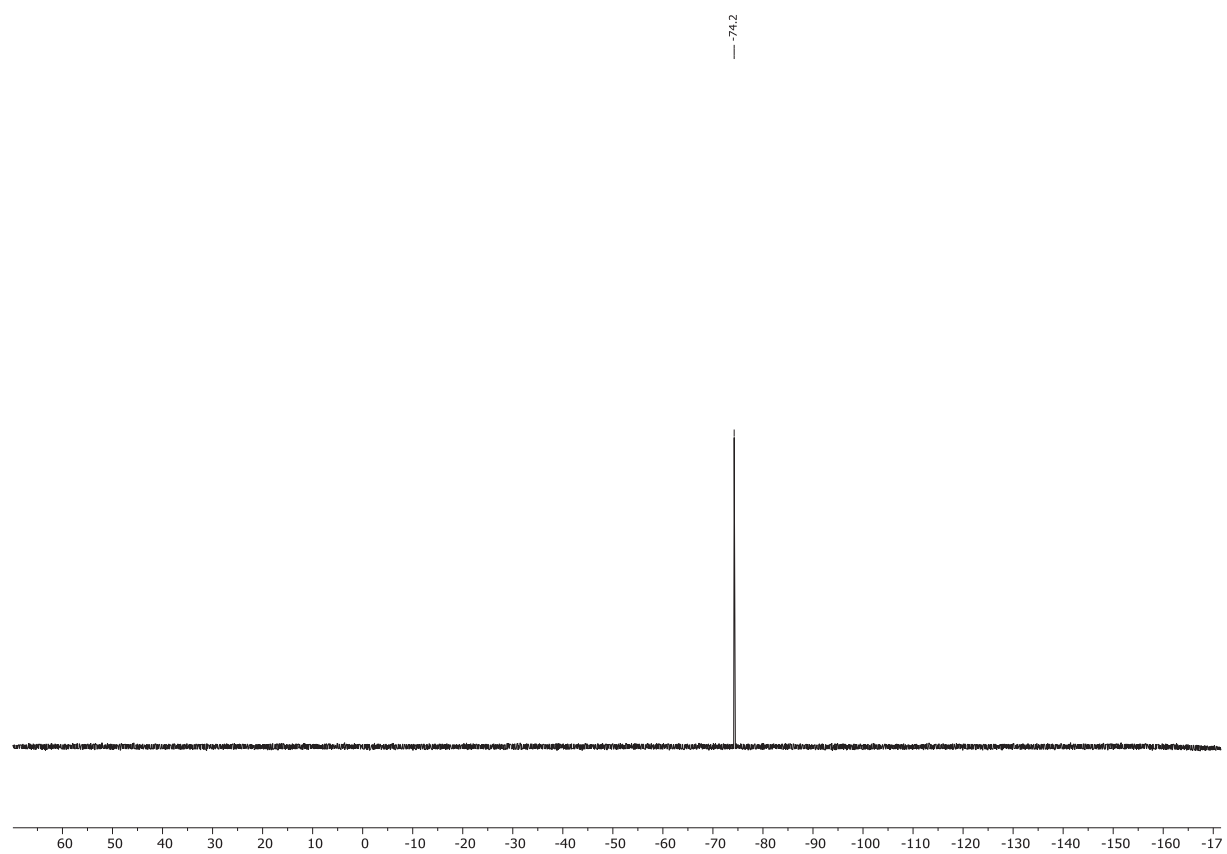
¹H NMR spectrum of **17** (600 MHz, DMSO-*d*₆)
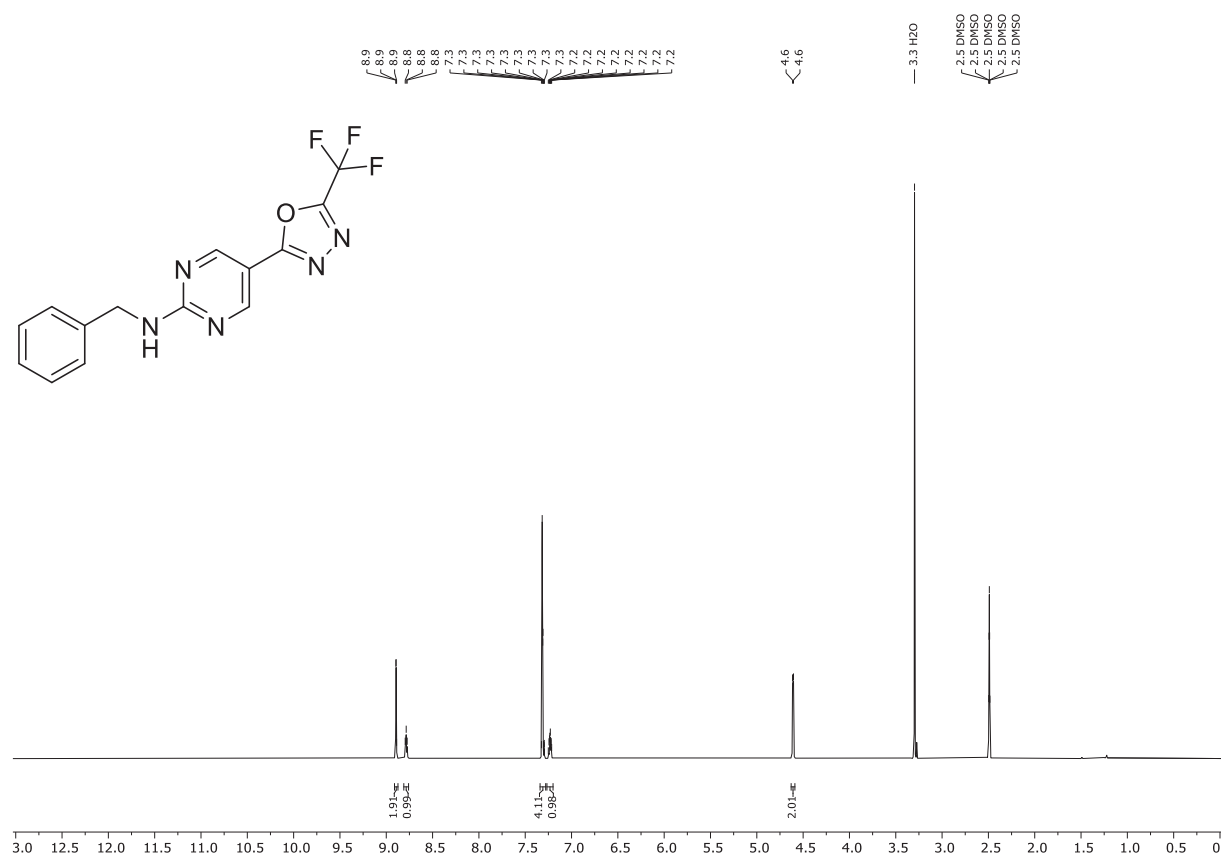
¹³C NMR spectrum of **17** (151 MHz, DMSO-*d*₆)
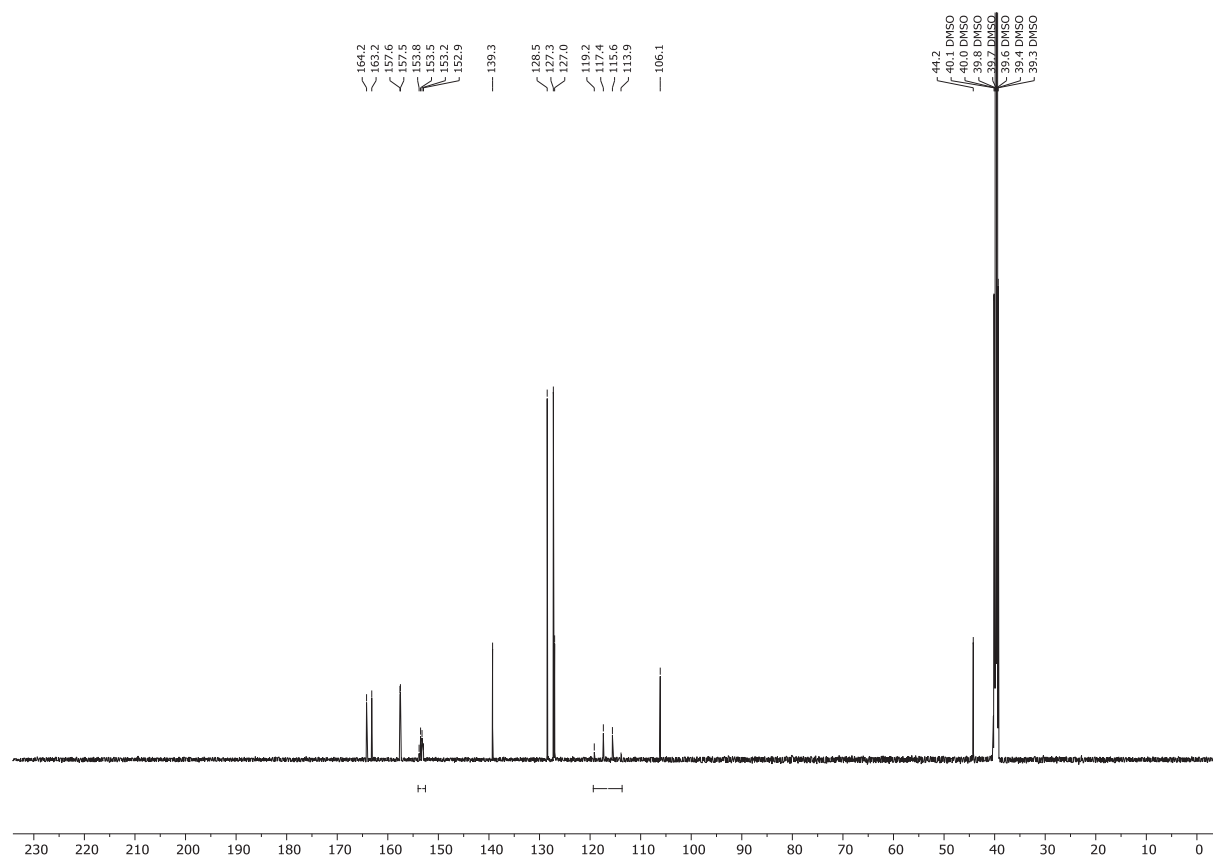
¹⁹F NMR spectrum of **17** (565 MHz, DMSO-*d*₆)

—-65.0

10 0 -10 -20 -30 -40 -50 -60 -70 -80 -90 -100 -110 -120 -130 -140 -150 -160 -170 -180 -190 -200 -210

¹H NMR spectrum of **18** (600 MHz, DMSO-d_6)

¹³C NMR spectrum of **18** (151 MHz, DMSO-d_6)
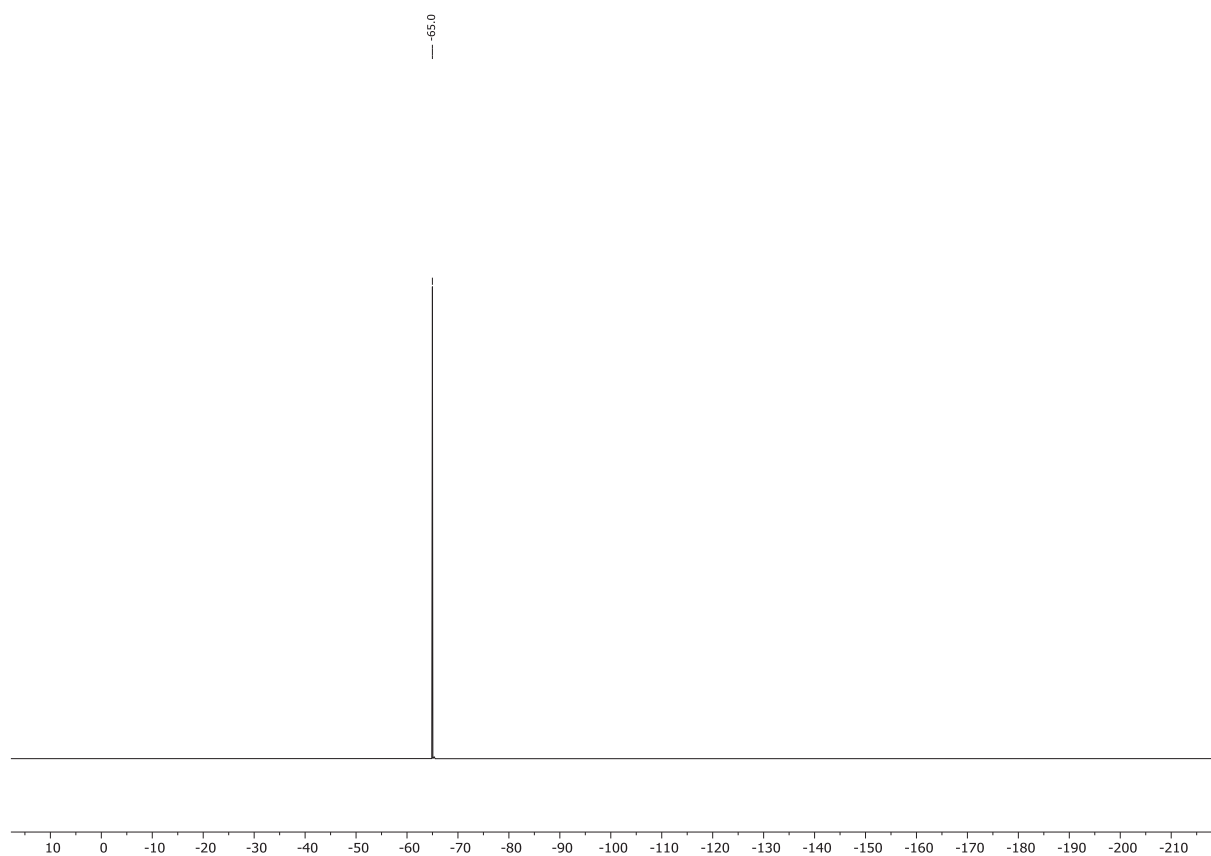
¹H NMR spectrum of **19** (600 MHz, CDCl₃)
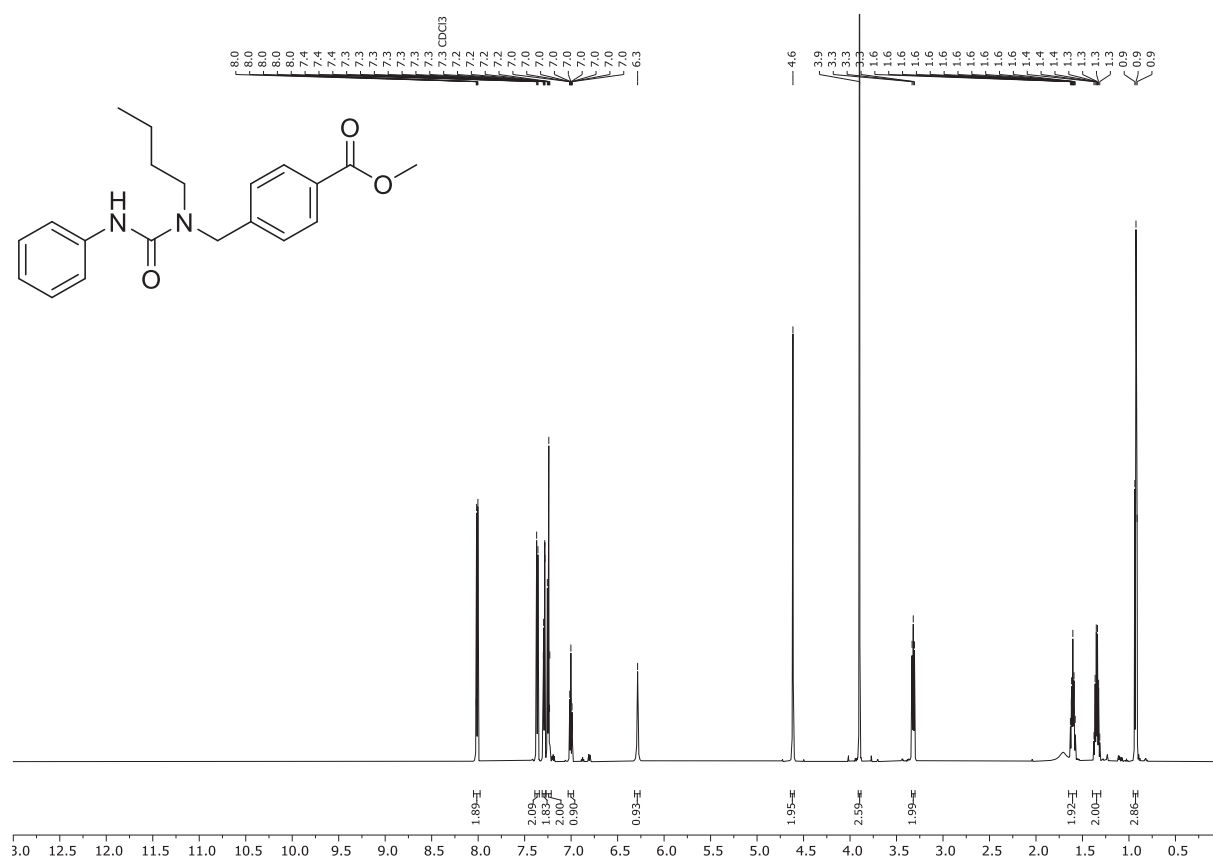
¹³C NMR spectrum of **19** (151 MHz, CDCl₃)
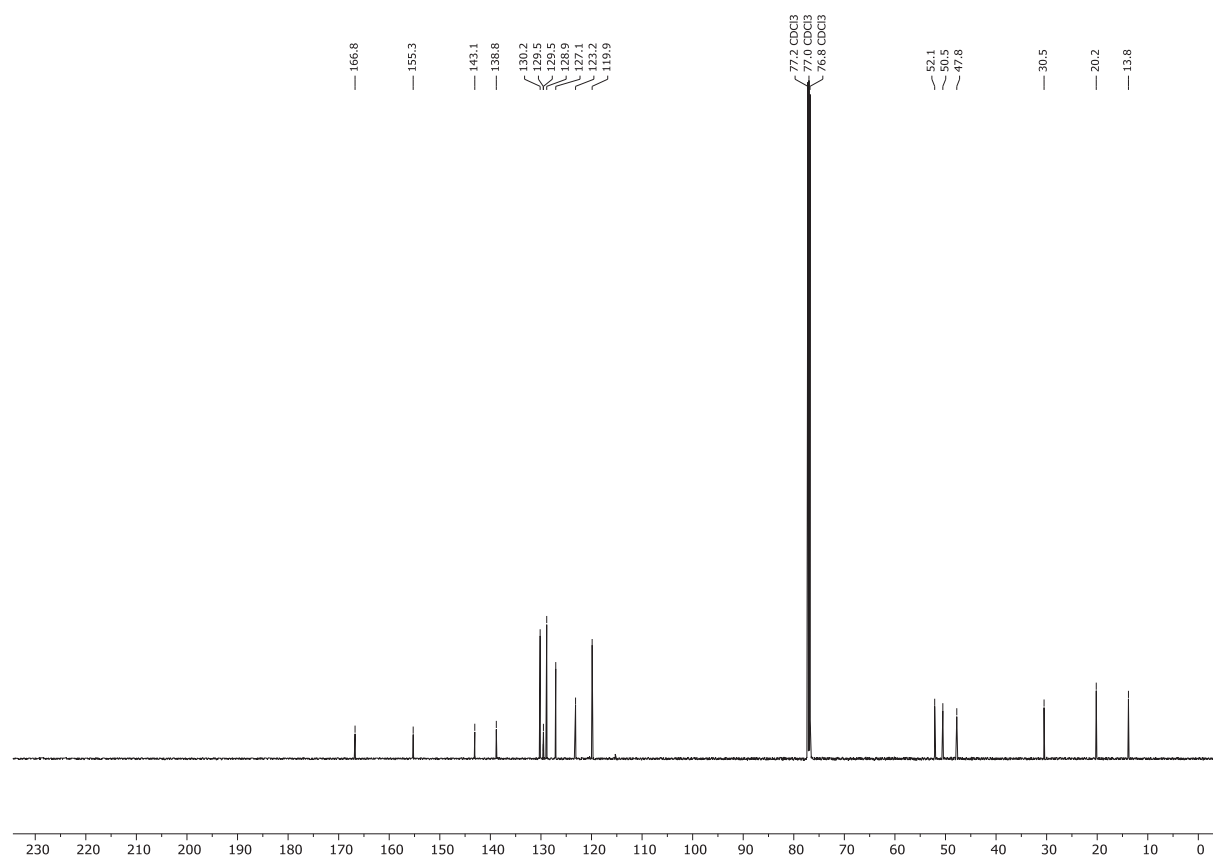
3 HPLC Chromatograms

HPLC chromatogram of **6**.

No.	Peak Name	Retention Time min	Area mAU*min	Height mAU	Relative Area %	Relative Height %	Amount n.a.
1		11,277	0,104	1,336	0,14	0,12	n.a.
2		11,840	0,055	0,610	0,07	0,05	n.a.
3		12,287	0,197	2,193	0,26	0,20	n.a.
4		12,460	0,063	1,000	0,08	0,09	n.a.
5		12,707	74,825	1114,514	99,27	99,44	n.a.
6		13,780	0,127	1,122	0,17	0,10	n.a.
Total:			75,372	1120,775	100,00	100,00	

HPLC chromatogram of **9**.

No.	Peak Name	Retention Time min	Area mAU*min	Height mAU	Relative Area %	Relative Height %	Amount n.a.
1		16,917	0,383	6,653	0,16	0,23	n.a.
2		17,047	229,074	2744,890	95,72	95,88	n.a.
3		17,193	3,848	51,276	1,61	1,79	n.a.
4		17,343	5,999	60,125	2,51	2,10	n.a.
Total:			239,304	2862,945	100,00	100,00	

HPLC chromatogram of **10**.

No.	Peak Name	Retention Time min	Area mAU*min	Height mAU	Relative Area %	Relative Height %	Amount n.a.
1		11,730	0,188	1,976	0,20	0,14	n.a.
2		11,980	1,382	16,316	1,46	1,16	n.a.
3		12,463	0,056	0,399	0,06	0,03	n.a.
4		13,107	0,361	4,111	0,38	0,29	n.a.
5		13,403	92,416	1380,661	97,84	98,33	n.a.
6		14,470	0,051	0,618	0,05	0,04	n.a.
Total:			94,454	1404,081	100,00	100,00	

HPLC chromatogram of **12**.

No.	Peak Name	Retention Time min	Area mAU*min	Height mAU	Relative Area %	Relative Height %	Amount n.a.
1		13,640	0,109	1,534	0,07	0,08	n.a.
2		14,130	0,139	1,959	0,09	0,10	n.a.
3		14,583	0,060	0,785	0,04	0,04	n.a.
4		14,830	0,088	1,154	0,06	0,06	n.a.
5		15,297	150,362	1964,865	99,55	99,54	n.a.
6		15,603	0,083	1,056	0,05	0,05	n.a.
7		17,183	0,150	1,757	0,10	0,09	n.a.
8		18,217	0,052	0,787	0,03	0,04	n.a.
Total:			151,042	1973,896	100,00	100,00	

HPLC chromatogram of **13**.

No.	Peak Name	Retention Time min	Area mAU*min	Height mAU	Relative Area %	Relative Height %	Amount n.a.
1		10,540	0,760	6,097	0,45	0,26	n.a.
2		10,790	0,628	9,940	0,38	0,42	n.a.
3		11,097	0,229	3,264	0,14	0,14	n.a.
4		11,283	163,658	2332,505	97,92	98,18	n.a.
5		11,437	1,170	13,436	0,70	0,57	n.a.
6		11,610	0,689	10,437	0,41	0,44	n.a.
Total:			167,134	2375,678	100,00	100,00	

HPLC chromatogram of **14**.

No.	Peak Name	Retention Time min	Area mAU*min	Height mAU	Relative Area %	Relative Height %	Amount n.a.
1		9,773	0,904	2,965	0,87	0,22	n.a.
2		10,557	99,659	1283,046	95,85	96,64	n.a.
3		11,627	0,416	4,202	0,40	0,32	n.a.
4		12,260	0,582	7,570	0,56	0,57	n.a.
5		12,787	2,415	29,840	2,32	2,25	n.a.
Total:			103,977	1327,622	100,00	100,00	

HPLC chromatogram of **15**.

No.	Peak Name	Retention Time min	Area mAU*min	Height mAU	Relative Area %	Relative Height %	Amount n.a.
1		9,770	1,128	2,972	3,40	0,72	n.a.
2		12,290	31,769	405,888	95,71	98,56	n.a.
3		14,100	0,295	2,959	0,89	0,72	n.a.
Total:			33,191	411,819	100,00	100,00	

HPLC chromatogram of **16**.

No.	Peak Name	Retention Time min	Area mAU*min	Height mAU	Relative Area %	Relative Height %	Amount n.a.
1		9,827	0,241	1,164	0,18	0,06	n.a.
2		10,570	0,493	2,484	0,36	0,13	n.a.
3		10,997	1,181	16,517	0,87	0,90	n.a.
4		11,317	0,282	2,511	0,21	0,14	n.a.
5		11,670	0,056	0,587	0,04	0,03	n.a.
6		11,833	0,077	1,249	0,06	0,07	n.a.
7		12,040	0,506	3,387	0,37	0,18	n.a.
8		12,290	1,301	17,316	0,95	0,94	n.a.
9		12,443	132,078	1794,888	96,72	97,36	n.a.
10		12,630	0,075	0,679	0,06	0,04	n.a.
11		13,187	0,169	1,286	0,12	0,07	n.a.
12		13,540	0,097	1,498	0,07	0,08	n.a.
Total:			136,557	1843,567	100,00	100,00	

HPLC chromatogram of **17**.

No.	Peak Name	Retention Time min	Area mAU*min	Height mAU	Relative Area %	Relative Height %	Amount n.a.
1		10,560	0,283	2,011	0,63	0,29	n.a.
2		11,617	0,096	1,234	0,21	0,18	n.a.
3		12,403	0,079	0,833	0,18	0,12	n.a.
4		12,567	0,149	2,399	0,33	0,34	n.a.
5		13,213	43,425	687,496	97,30	97,94	n.a.
6		13,543	0,125	1,441	0,28	0,21	n.a.
7		14,127	0,473	6,510	1,06	0,93	n.a.
Total:			44,629	701,925	100,00	100,00	

4 References

(1)   Yung-Chi, C.; Prusoff, W. H. Relationship between the Inhibition Constant (KI) and the Concentration of Inhibitor which causes 50 per cent Inhibition (I50) of an Enzymatic Reaction. *Biochem. Pharmacol.* **1973**, *22*, 3099–3108.

(2)   Schäker-Hübner, L.; Haschemi, R.; Büch, T.; Kraft, F. B.; Brumme, B.; Schöler, A.; Jenke, R.; Meiler, J.; Aigner, A.; Bendas, G.; Hansen, F. K. Balancing Histone Deacetylase (HDAC) Inhibition and Drug-Likeness: Biological and Physicochemical Evaluation of Class I Selective HDAC Inhibitors. *ChemMedChem* **2022**, *17*, e202100755.

Appendix III. Publication III: 2 (Difluoromethyl)-1,3,4-oxadiazoles: The Future of Selective Histone Deacetylase 6 Modulation?

The following part contains the viewpoint article "2 (Difluoromethyl)-1,3,4-oxadiazoles: The Future of Selective Histone Deacetylase 6 Modulation?" as it was published in ACS Pharmacological & Translational Science.

The article is reprinted with permission from:

Beate König and Finn K. Hansen. 2 (Difluoromethyl)-1,3,4-oxadiazoles: The Future of Selective Histone Deacetylase 6 Modulation? *ACS Pharmacol. Transl. Sci.* **2024**, *7* (3), 899-903.

2-(Difluoromethyl)-1,3,4-oxadiazoles: The Future of Selective Histone Deacetylase 6 Modulation?

Beate König and Finn K. Hansen*

Read Online

ACCESS | Metrics & More | Article Recommendations

- Exceptional high HDAC6 selectivity
- Slow- and tight-binding properties
- Enzyme-catalyzed ring opening reaction
- Deprotonated difluoroacetylhydrazide as active species
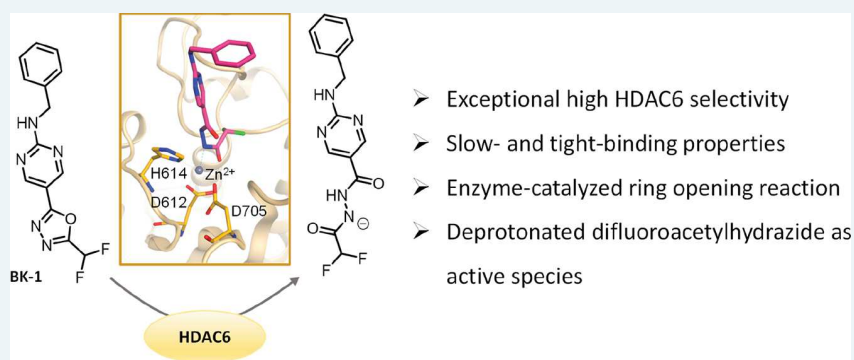
ABSTRACT: Histone deacetylase 6 (HDAC6) is an important target for the treatment of oncological and non-oncological diseases. Established HDAC6 inhibitors feature a hydroxamic acid as a zinc-binding group (ZBG) and thus possess mutagenic and genotoxic potential. Recently, the 2-(difluoromethyl)-1,3,4-oxadiazole (DFMO) group emerged as a novel ZBG. In this Viewpoint, we summarize the discovery of the mode of action of DFMOs. Additionally, we discuss opportunities and challenges in the journey toward the clinical development of DFMO-based drugs for the treatment of HDAC6-driven diseases.

KEYWORDS: Histone deacetylase, HDAC6, epigenetics, difluoromethyl-1,3,4-oxadiazole, zinc-binding group

Histone deacetylases (HDACs) play a pivotal role as epigenetic regulators, thereby holding significant promise as therapeutic targets for a range of conditions, including cancer, inflammation, and neurodegenerative diseases.[1] The HDAC family is divided into four classes with a total of 18 isoforms.[1] Classes I, II, and IV are Zn^{2+}-dependent, whereas class III enzymes, also known as sirtuins, are NAD^+-dependent.[2] Class I consists of HDAC1−3 and HDAC8, which are mostly located in the nucleus and mainly catalyze the deacylation of lysine side chains of histones.[3,4] Class II is further subdivided into class IIa, consisting of HDAC4, 5, 7, and 9, and class IIb, containing HDAC6 and 10.[5] While class IIa HDACs shuttle between the nucleus and the cytoplasm, their counterparts in class IIb are primarily located in the cytoplasm and deacetylate lysine side chains of non-histone proteins or, in the case of HDAC10, polyamines such as spermidine as their primary substrates.[1,6] Further, the only member of class IV, HDAC11, is mainly located in the nucleus.[2]

HDAC6 stands out among HDAC isoforms due to its distinct structural features, localization, and substrate range.[5] Notably, HDAC6 features two independently active catalytic domains (CD1 and CD2) and a zinc finger serving as an ubiquitin-binding domain.[1,7] Initially identified as a tubulin

deacetylase, HDAC6 also catalyzes the deacetylation of various other proteins.[8] Moreover, it plays a pivotal role in modulating cortactin,[9] the Alzheimer-related tau protein,[10] and the chaperone HSP90.[1,11] Consequently, HDAC6 is crucial for various cellular processes (see Figure 1 for representative examples), including cell motility, proliferation, apoptosis, and the aggresomal pathway, thereby making it a valuable target for drug development.[1]

Commonly, HDAC inhibitors (HDACi) consist of a zinc-binding group (ZBG) binding to the Zn^{2+} ion in the catalytic site, a cap group for protein surface interactions, and a linker connecting these two moieties.[12] The non-selective HDACi vorinostat, belinostat, panobinostat, and romidepsin (see Figure 2A), previously approved by the U.S. Food and Drug Administration (FDA), lack selectivity across HDAC isoforms.[1,13] This may lead to severe side effects and off-target
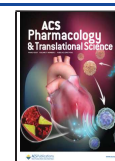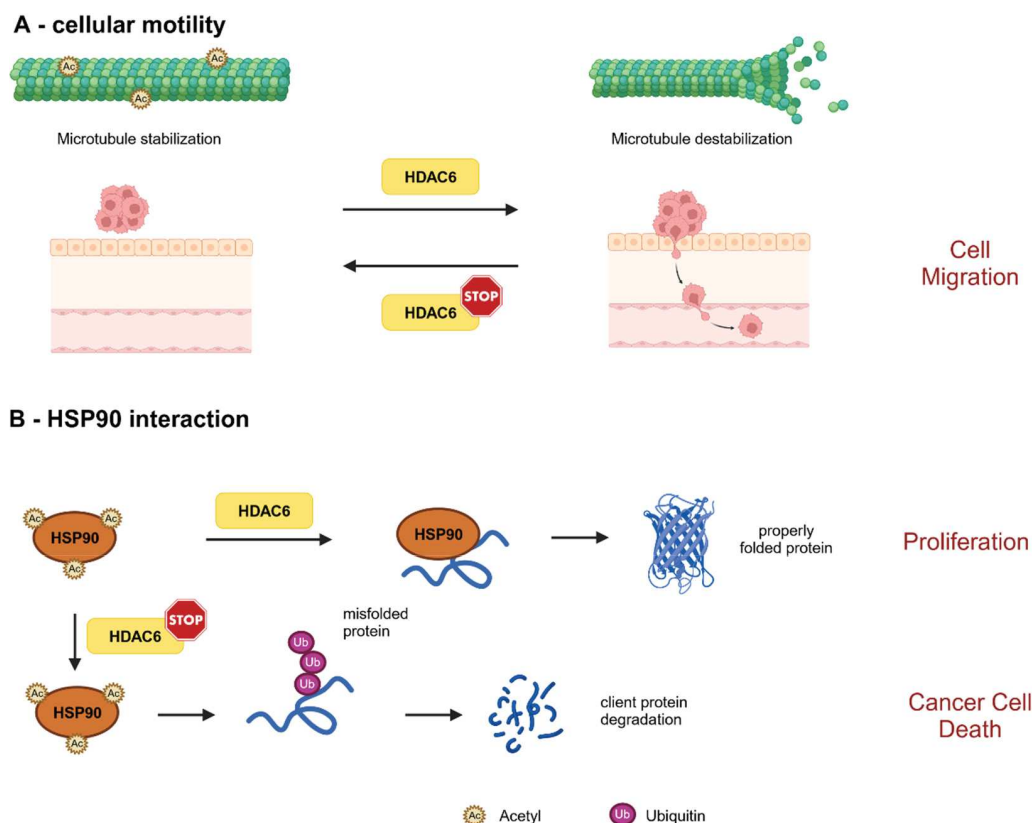
Figure 1. HDAC6 interactions in specific cellular pathways. (A) HDAC6 inhibition induces α-tubulin acetylation and microtubule stabilization and diminishes cancer cell migration. (B) HDAC6 inhibition leads to HSP90 hyperacetylation, accumulation of misfolded protein, and degradation of HSP90 client proteins. (Figure created with BioRender.com.)

interactions.[13] In recent years, selective HDAC6 inhibition was primarily achieved by utilizing HDACi with a bulky cap group, a phenyl or benzyl linker, and a hydroxamic acid as ZBG (Figure 2B), which provided T-shaped inhibitors capable of engaging the unique and relatively wide L1 loop pocket exclusively present in HDAC6.[12] However, the potential of hydroxamic acids for generating mutagenic and genotoxic metabolites, through either Lossen rearrangement or hydroxylamine release, underscores the urgent need to identify novel ZBGs.[14] Recently, the 2-(difluoromethyl)-1,3,4-oxadiazole (DFMO) group has emerged as a promising alternative to hydroxamic acids; for selected DFMO-based HDAC6 inhibitors see Figure 2C.[15−19] These novel inhibitors are gaining their high isoform specificity by serving as substrate analogs and thus mechanism-based inhibitors of HDAC6. In this Viewpoint, we summarize the discovery of the unique mode of action of DFMOs as potent and selective HDAC6 inhibitors. Furthermore, we discuss our views on opportunities and challenges concerning the clinical development of DFMO-based drugs for the treatment of HDAC6-driven diseases.

HISTORY OF DFMO-BASED SELECTIVE HDAC6 INHIBITORS AND DEGRADERS

The DFMO group was first introduced as a ZBG for selective HDAC6 inhibition in a 2017 patent by Chong Kun Dang Pharmaceutical Corp.[21] Despite its frequent appearance in patents, this ZBG is relatively underrepresented in research manuscripts. However, in 2021, Onishi et al.[20] disclosed that the DFMO-based selective HDAC6 inhibitor T-518 (Figure 2C) demonstrated therapeutic potential to treat Alzheimer's disease and tauopathy in mice after oral administration. The high HDAC6 selectivity was confirmed at both the biochemical and cellular levels.[20] Furthermore, T-518 showed an encouraging pharmacokinetic profile and favorable brain penetration.[20] Shortly later, the hydroxamate tubastatin A (Figure 2B) and the DFMO derivative SE-7552 (Figure 2C), a compound first mentioned in a conference abstract as a non-hydroxamate HDAC6 inhibitor capable of blocking multiple myeloma growth *in vivo*,[22] were used by Cone and co-workers as selective HDAC6 inhibitors to overcome leptin resistance in obesity.[16] Notably, they could show that SE-7552 acts as an anti-obesity agent in diet-induced obese mice.[16] In the next step, our group successfully incorporated the DFMO warhead into proteolysis-targeting chimeras (PROTACs) for the selective degradation of HDAC6.[23] However, the mechanism by which DFMOs inhibit or degrade HDAC6 remained enigmatic.

In a 2022 conference abstract, the Christianson group, in collaboration with us, disclosed that the DFMO derivative BK-1 (Figure 2C) underwent an enzyme-catalyzed ring-opening reaction.[24] This process led to the formation of an acylhydrazide, which was subsequently co-crystallized in an extended conformation within the active site of HDAC6.[24] In 2023, Steinkühler and colleagues elucidated the HDAC6 complex structure with a hydrazide inhibitor derived from the twofold hydrolysis of the DFMO inhibitor ITF5924 (Figure 2C).[17] The authors speculated that the crystallized hydrazide, though identified, may not be responsible for the observed profound HDAC6 inhibition, suggesting that the hydrazide might not represent the primary active species.[17] Instead, the
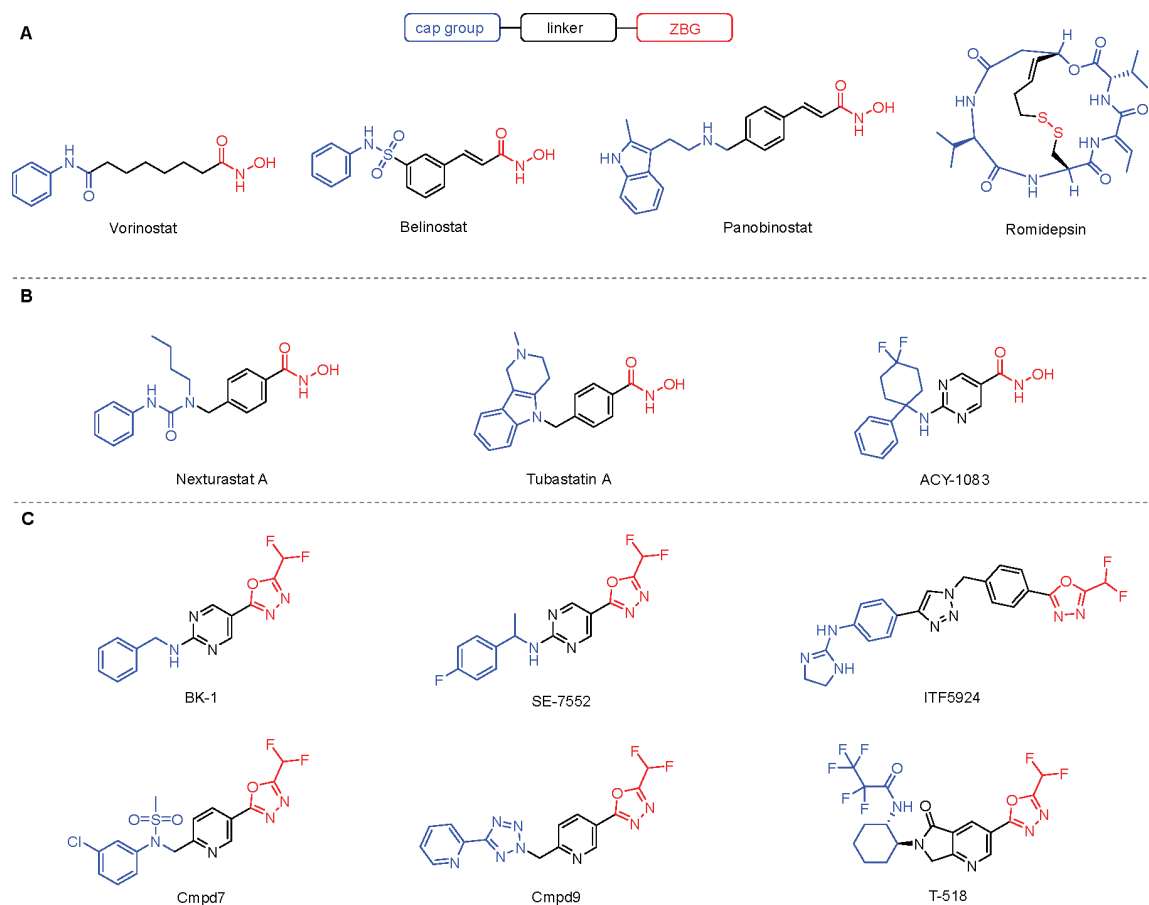
Figure 2. (A) FDA-approved HDAC inhibitors. (B) Selected hydroxamate-based HDAC6 inhibitors. (C) Selected DFMO-based selective HDAC6 inhibitors: BK-1,[15] SE-7552,[16] ITF5924,[17] Cmpd7,[18] Cmpd9,[19] and T-518.[20]
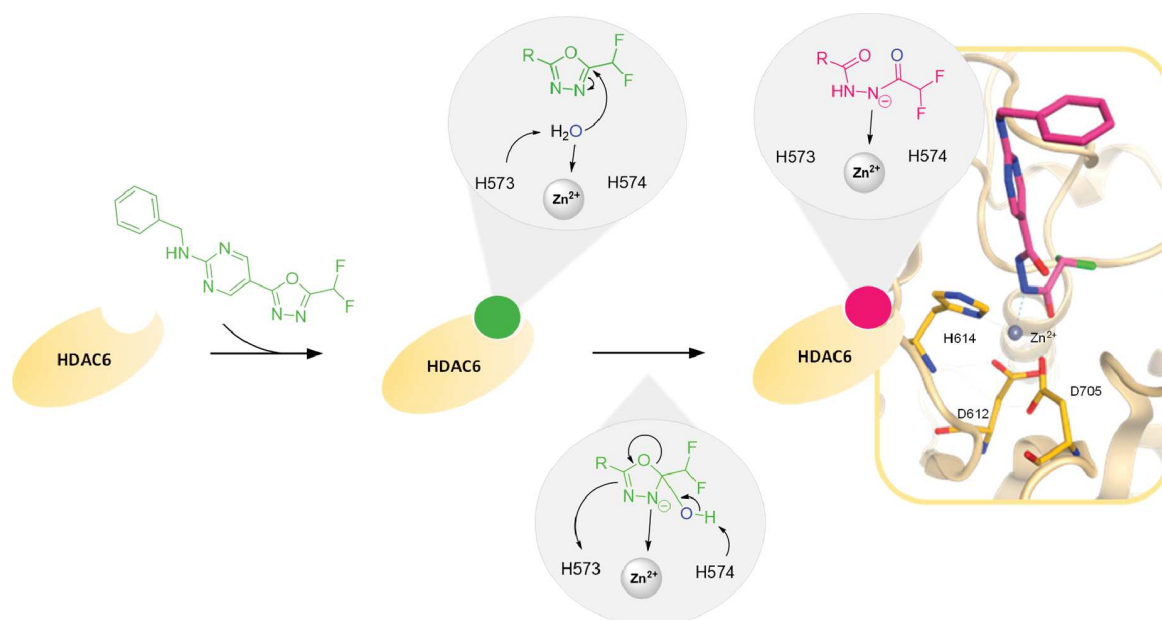
Figure 3. Schematic representation of the enzyme-catalyzed ring-opening reaction of inhibitor BK-1 by HDAC6 (based on PDB ID 8GD4).

authors postulated the presence of a high-affinity intermediate, forming a durable tight-binding enzyme−inhibitor complex.[17] This intermediate may appear as a closed hydrated form or a protonated acylhydrazide; both options were suggested as

potential active species.[17] Almost in parallel, based on crystallographic and mechanistic experiments, the Christianson and Hansen groups disclosed the full experimental details of their initial conference contribution,[24] confirming that the

DFMO warhead undergoes an enzyme-catalyzed ring-opening reaction, resulting in a deprotonated difluoroacetylhydrazide as active species (Figure 3).[15] The strong anionic zinc coordination of the deprotonated difluoroacetylhydrazide and the binding of the difluoromethyl moiety in the P571 pocket of the CD2 of HDAC6 finally results in an essentially irreversible inhibition of the enzyme.[15] The tight-binding properties of the active species were confirmed by jump-dilution and dialysis experiments.[15] Overall, there is now clear evidence that DFMOs act as mechanism-based, slow- and tight-binding HDAC6 inhibitors.[15]

Also in 2023, Barinka and co-workers performed a systematic comparison of the DFMO Cmpd7 (Figure 2C) and its corresponding hydroxamic acid analog, thereby clearly supporting the observation that DFMOs are new ZBGs with unparalleled selectivity for HDAC6 over all other HDAC isoforms.[18] Additionally, a comprehensive mechanistic analysis of the hydrolysis of Cmpd7 provided additional evidence that DFMOs can undergo an enzyme-catalyzed ring-opening reaction to a difluoroacetylhydrazide as well as a significantly slower second hydrolytic step to the corresponding unsubstituted hydrazide.[25] Another thorough biochemical evaluation of ITF5924 further confirmed the slow- and tight-binding properties of DFMOs.[26] Similarly, Ripa et al.[19] investigated the bioactivation of DFMOs and confirmed once more that this class of compound acts as a substrate analog of acetyl-lysine. Their crystallization attempts of the DFMO Cmpd9 (Figure 2C) confirmed that the DFMO was degraded to the corresponding hydrazide.[19] Furthermore, the authors showed that DFMOs are stable at pH = 7 but chemically unstable at acidic and basic pH values.[19] In addition, Cmpd9 showed a promising *in vitro* safety profile with no activity in a panel of cardiovascular ion channels and was negative for *in vitro* micronuclei, thereby indicating that this DFMO derivative possesses neither cardiovascular toxicity nor genotoxicity.[19] Importantly, this study also disclosed a high oral bioavailability and low *in vivo* clearance of DFMO-based selective HDAC6 inhibitors.[19]

CONCLUSION AND FUTURE OUTLOOK

DFMO-based HDAC6 inhibitors did not appear in the scientific literature until recently. However, in the past few years, several publications on the HDAC6 selectivity and mode of action appeared. While the first papers did not address the mode of action of DFMOs, recent work from both academic groups and industry has confirmed that DFMOs act as substrate analogs and thus are mechanism-based inhibitors of HDAC6. Currently, there are several HDAC6-selective inhibitors with undisclosed structures in clinical trials. This raises the question of whether DFMO-based HDAC6 inhibitors have already progressed to the clinical stage. However, there are several challenges ahead to obtain regulatory approval. The chemical stability of DFMO derivatives is the most obvious challenge during their clinical development.[19] The limited stability at acidic and basic pH values arises from the electrophilicity of the oxadiazole ring. While it might be possible to optimize the stability further by fine-tuning the substitution in the 2- and 5-positions of the 1,3,4-oxadiazole ring, it is rather unlikely to mitigate the stability issues completely, because the electrophilicity is required for the mode of action relying on being a substrate analog capable of undergoing the essential ring-opening reaction. Nevertheless, DFMOs are stable at pH = 7, and

suitable formulations have been developed for various acid-labile drugs, including blockbusters such as proton pump inhibitors.

Besides that, the mode of action of DFMOs might not be perfectly suitable for the incorporation of this warhead into PROTACs. One major advantage of PROTACs is their catalytic mode of action. In the case of DFMO-based HDAC6 PROTACs, the oxadiazole ring will undergo ring-opening during the first degradation cycle, and the degrader will presumably be released as a hydrazide featuring a reduced ability to engage HDAC6. However, Steinkühler and co-workers reported that the corresponding hydrazide obtained from ring-opening of ITF5924 followed by a second hydrolytic step is capable of inhibiting HDAC6 with nanomolar potency.[17] Three co-crystal structures of degraded DFMOs (PDB IDs 8CJ7, 8BJK, and 8A8Z) provide further evidence that the resulting final hydrolysis products, the respective hydrazides, can reengage HDAC6, albeit presumably with somewhat lower degradation efficiency.[17,19,25] Nevertheless, the first DFMO-based PROTACs reduced HDAC6 levels with DC_{50} values in the low triple-digit nanomolar concentration range, thus suggesting that DFMOs are suitable for the development of non-hydroxamate HDAC6 degraders.[23]

Despite the challenges ahead, there are compelling reasons to be optimistic that DFMOs can succeed in clinical trials. These include favorable pharmacokinetic profiles and efficient brain penetration, along with high oral bioavailability and low *in vivo* clearance. Notably, DFMOs exhibit no cardiovascular toxicity or genotoxicity, providing additional evidence for their potential safety and efficacy in clinical applications.[19] Moreover, these inhibitors showcase an outstanding selectivity profile within the HDAC family and beyond, positioning DFMOs as highly promising candidates for the treatment of cancer and other HDAC6-related diseases.[18,20] Additionally, the proven *in vivo* efficacy against diverse conditions such as multiple myeloma,[22] obesity,[16] and tauopathies[20] underscores the significant potential of DFMOs. To conclude, the future could be bright for DFMO-based HDAC6 modulators.

AUTHOR INFORMATION

Corresponding Author

Finn K. Hansen — *Department of Pharmaceutical and Cell Biological Chemistry, Pharmaceutical Institute, University of Bonn, 53121 Bonn, Germany;* ⊙ orcid.org/0000-0001-9765-5975; Phone: (+49) 228 73 5213; Email: finn.hansen@uni-bonn.de

Author

Beate König — *Department of Pharmaceutical and Cell Biological Chemistry, Pharmaceutical Institute, University of Bonn, 53121 Bonn, Germany*

Complete contact information is available at:
https://pubs.acs.org/10.1021/acsptsci.4c00031

Notes

ABBREVIATIONS

CD, catalytic domain; DFMO(s), 2-(difluoromethyl)-1,3,4-oxadiazole(s); FDA, U.S. Food and Drug Administration; HDAC(s), histone deacetylase(s); HSP90, heat shock protein 90; NAD^+, nicotinamide adenine dinucleotide; PROTAC(s),

proteolysis targeting chimera(s); ZBG(s), zinc-binding group(s)

■ REFERENCES

(1) Jenke, R.; Reßing, N.; Hansen, F. K.; Aigner, A.; Büch, T. Anticancer Therapy with HDAC Inhibitors: Mechanism-Based Combination Strategies and Future Perspectives. *Cancers* **2021**, *13* (4), 634.

(2) Gregoretti, I. V.; Lee, Y. M.; Goodson, H. V. Molecular Evolution of the Histone Deacetylase Family: Functional Implications of Phylogenetic Analysis. *J. Mol. Biol.* **2004**, *338* (1), 17–31.

(3) Roche, J.; Bertrand, P. Inside HDACs with More Selective HDAC Inhibitors. *Eur. J. Med. Chem.* **2016**, *121*, 451–483.

(4) Cruz, D. L.; Pipalia, N.; Mao, S.; Gadi, D.; Liu, G.; Grigalunas, M.; O'Neill, M.; Quinn, T. R.; Kipper, A.; Ekebergh, A.; Dimmling, A.; Gartner, C.; Melancon, B. J.; Wagner, F. F.; Holson, E.; Helquist, P.; Wiest, O.; Maxfield, F. R. Inhibition of Histone Deacetylases 1, 2, and 3 Enhances Clearance of Cholesterol Accumulation in Niemann-Pick C1 Fibroblasts. *ACS Pharmacol. Transl. Sci.* **2021**, *4* (3), 1136–1148.

(5) Ho, T. C. S.; Chan, A. H. Y.; Ganesan, A. Thirty Years of HDAC Inhibitors: 2020 Insight and Hindsight. *J. Med. Chem.* **2020**, *63* (21), 12460–12484.

(6) Hai, Y.; Shinsky, S. A.; Porter, N. J.; Christianson, D. W. Histone Deacetylase 10 Structure and Molecular Function as a Polyamine Deacetylase. *Nat. Commun.* **2017**, *8*, 15368.

(7) Duda, J. M.; Thomas, S. N. Interactions of Histone Deacetylase 6 with DNA Damage Repair Factors Strengthen Its Utility as a Combination Drug Target in High-Grade Serous Ovarian Cancer. *ACS Pharmacol. Transl. Sci.* **2023**, *6* (12), 1924–1933.

(8) Vogelmann, A.; Jung, M.; Hansen, F. K.; Schiedel, M. Comparison of Cellular Target Engagement Methods for the Tubulin Deacetylases Sirt2 and HDAC6: NanoBRET, CETSA, Tubulin Acetylation, and PROTACs. *ACS Pharmacol. Transl. Sci.* **2022**, *5* (2), 138–140.

(9) Zhang, X.; Yuan, Z.; Zhang, Y.; Yong, S.; Salas-burgos, A.; Koomen, J.; Olashaw, N.; Parsons, J. T.; Yang, X.; Dent, S. R.; Yao, T.; Lane, W. S.; Seto, E. HDAC6 Modulates Cell Motility by Altering the Acetylation Level of Cortactin. *Mol. Cell. Biol.* **2007**, *27* (2), 197–213.

(10) Cohen, T. J.; Guo, J. L.; Hurtado, D. E.; Kwong, L. K.; Mills, I. P.; Trojanowski, J. Q.; Lee, V. M. Y. The Acetylation of Tau Inhibits Its Function and Promotes Pathological Tau Aggregation. *Nat. Commun.* **2011**, *2* (1), 252.

(11) Karagöz, G. E.; Rüdiger, S. G. D. Hsp90 Interaction with Clients. *Trends Biochem. Sci.* **2015**, *40* (2), 117–125.

(12) Osko, J. D.; Christianson, D. W. Structural Determinants of Affinity and Selectivity in the Binding of Inhibitors to Histone Deacetylase 6. *Bioorg. Med. Chem. Lett.* **2020**, *30* (8), 127023.

(13) Truong, N.; Goodis, C. C.; Cottingham, A. L.; Shaw, J. R.; Fletcher, S.; Pearson, R. M. Modified Suberoylanilide Hydroxamic Acid Reduced Drug-Associated Immune Cell Death and Organ Damage under Lipopolysaccharide Inflammatory Challenge. *ACS Pharmacol. Transl. Sci.* **2022**, *5* (11), 1128–1141.

(14) Shen, S.; Kozikowski, A. P. Why Hydroxamates May Not Be the Best Histone Deacetylase Inhibitors - What Some May Have Forgotten or Would Rather Forget? *ChemMedChem.* **2016**, *11* (1), 15–21.

(15) König, B.; Watson, P. R.; Reßing, N.; Cragin, A. D.; Schäker-Hübner, L.; Christianson, D. W.; Hansen, F. K. Difluoromethyl-1,3,4-Oxadiazoles Are Selective, Mechanism-Based, and Essentially Irreversible Inhibitors of Histone Deacetylase 6. *J. Med. Chem.* **2023**, *66* (19), 13821–13837.

(16) Çakır, I.; Hadley, C. K.; Pan, P. L.; Bagchi, R. A.; Ghamari-Langroudi, M.; Porter, D. T.; Wang, Q.; Litt, M. J.; Jana, S.; Hagen, S.; Lee, P.; White, A.; Lin, J. D.; McKinsey, T. A.; Cone, R. D. Histone Deacetylase 6 Inhibition Restores Leptin Sensitivity and Reduces Obesity. *Nat. Metab.* **2022**, *4* (1), 44–59.

(17) Cellupica, E.; Caprini, G.; Cordella, P.; Cukier, C.; Fossati, G.; Marchini, M.; Rocchio, I.; Sandrone, G.; Vanoni, M. A.; Vergani, B.; Źrubek, K.; Stevenazzi, A.; Steinkühler, C. Difluoromethyl-1,3,4-Oxadiazoles Are Slow-Binding Substrate Analog Inhibitors of Histone Deacetylase 6 with Unprecedented Isotype Selectivity. *J. Biol. Chem.* **2023**, *299* (1), 102800.

(18) Ptacek, J.; Snajdr, I.; Schimer, J.; Kutil, Z.; Mikesova, J.; Baranova, P.; Havlinova, B.; Tueckmantel, W.; Majer, P.; Kozikowski, A.; Barinka, C. Selectivity of Hydroxamate- and Difluoromethyloxadiazole-Based Inhibitors of Histone Deacetylase 6 In Vitro and in Cells. *Int. J. Mol. Sci.* **2023**, *24* (5), 4720.

(19) Ripa, L.; Sandmark, J.; Hughes, G.; Shamovsky, I.; Gunnarsson, A.; Johansson, J.; Llinas, A.; Collins, M.; Jung, B.; Noven, A.; Pemberton, N.; Mogemark, M.; Xiong, Y.; Li, Q.; Tangefjord, S.; Ek, M.; Astrand, A. Selective and Bioavailable HDAC6 2-(Difluoromethyl)-1,3,4- Oxadiazole Substrate Inhibitors and Modeling of Their Bioactivation Mechanism. *J. Med. Chem.* **2023**, *66* (20), 14188–14207.

(20) Onishi, T.; Maeda, R.; Terada, M.; Sato, S.; Fujii, T.; Ito, M.; Hashikami, K.; Kawamoto, T.; Tanaka, M. A Novel Orally Active HDAC6 Inhibitor T-518 Shows a Therapeutic Potential for Alzheimer's Disease and Tauopathy in Mice. *Sci. Rep.* **2021**, *11* (1), 15423.

(21) Kim, Y.; Lee, C. S.; Oh, J. T.; Song, H.; Choi, J.; Lee, J. *Oxadiazole Amine Derivative Compounds as Histone Deacetylase 6 Inhibitor, and the Pharmaceutical Composition Comprising the Same.* WO 2017/065473 A1, 2017.

(22) Holt, J. A.; Garvey, E. P.; Becherer, J. D.; Hoekstra, W. J.; Schotzinger, R. J.; Yates, C. M. SE-7552, a Highly Selective, Non-Hydroxamate Inhibitor of Histone Deacetylase-6 Blocks Multiple Myeloma Growth In Vivo. *Blood* **2018**, *132*, 3215.

(23) Keuler, T.; König, B.; Bückreiß, N.; Kraft, F. B.; König, P.; Schäker-Hübner, L.; Steinebach, C.; Bendas, G.; Gütschow, M.; Hansen, F. K. Development of the First Non-Hydroxamate Selective HDAC6 Degraders. *Chem. Commun.* **2022**, *58* (79), 11087–11090.

(24) Cragin, A.; Watson, P. R.; König, B.; Hansen, F. K.; Christianson, D. W. A Novel Zinc Binding Group for HDAC6 Inhibition. *FASEB J.* **2022**, *36* (S1), R3604.

(25) Motlová, L.; Snajdr, I.; Kutil, Z.; Andris, E.; Ptacek, J.; Novotna, A.; Novakova, Z.; Havlinova, B.; Tueckmantel, W.; Draberova, H.; Majer, P.; Schutkowski, M.; Kozikowski, A.; Rulisek, L.; Barinka, C. Comprehensive Mechanistic View of the Hydrolysis of Oxadiazole-Based Inhibitors by Histone Deacetylase 6 (HDAC6). *ACS Chem. Biol.* **2023**, *18* (7), 1594–1610.

(26) Cellupica, E.; Caprini, G.; Fossati, G.; Mirdita, D.; Cordella, P.; Marchini, M.; Rocchio, I.; Sandrone, G.; Stevenazzi, A.; Vergani, B.; Steinkühler, C.; Vanoni, M. A. The Importance of the "Time Factor" for the Evaluation of Inhibition Mechanisms: The Case of Selected HDAC6 Inhibitors. *Biology* **2023**, *12*, 1049.

Danksagung

Zuallererst möchte ich mich bei meinem Doktorvater Prof. Finn Hansen bedanken für die Aufnahme in den Arbeitskreis und die Überlassung der sehr spannenden und doch auch herausfordernden Projekte. Danke für das entgegengebrachte Vertrauen, die konstruktiven, fachlichen Diskussionen und die stets engagierte Betreuung. Des Weiteren möchte ich mich für die Ermöglichung meines Forschungsaufenthalts in Philly bedanken, dies trifft natürlich ebenfalls auf Prof. David Christianson zu, der mich sehr freundlich in sein Labor aufgenommen hat.

Außerdem gilt mein Dank Prof. Gerd Bendas für die Übernahme des Zweitgutachtens, sowie den weiteren Mitgliedern der Prüfungskommission Frau Prof. Evi Kostenis und Herrn Prof. Matthias Geyer.

Als Nächstes möchte ich allen Kooperationspartnern aus den Arbeitskreisen von Prof. Michael Gütschow, Prof. Gerd Bendas und Prof. David Christianson meinen Dank aussprechen für die stets erfolgreiche Zusammenarbeit zur Umsetzung der interdisziplinären Projekte. Besonders möchte ich mich bei meinen Koautor*innen bedanken, Dr. Tim Keuler, Nico Bückreiß und Dr. Paris Watson.

Marion Schneider und Christine Bous danke ich für die zuverlässige Zusammenarbeit im Rahmen der Aufnahme zahlreicher NMR Spektren und Hilfestellung zur Strukturaufklärung. Iris Jusen und Dieter Baumert danke ich für die immerwährende Unterstützung zu allen Belangen innerhalb des Instituts, sowie eure immer fröhliche Art.

Mein herzlicher Dank geht an alle Mitglieder des Arbeitskreises Hansen. Darüber hinaus möchte ich mich bei meinem langjährigen Laborkollegen Fabian Kraft bedanken, insbesondere für die Unterstützung beim Aufbau des Arbeitskreises am neuen Standort, die Renovierung der Labore, sowie deine unermüdliche Motivation über Rückschläge hinwegzusehen. Des Weiteren gilt mein Dank Daniel Stopper, Felix Feller, Dr. Kathrin Tan und Dr. Linda Schäker-Hübner für die freundschaftliche Atmosphäre, die Rückendeckung und Euer stets offenes Ohr.

Außerdem möchte ich mich bei allen bedanken, die direkt oder indirekt zum Gelingen dieser Arbeit beigetragen und mich in dieser Zeit begleitet und unterstützt haben. Mein größter Dank wird meinen Eltern zuteil für Eure immerwährende Unterstützung, Euer vollkommenes Vertrauen und Eure ständige Bereitschaft in allen Lebenslagen an meiner Seite zu stehen.